Multimetallic Azole and Carbene Complexes in Supramolecular Chemistry and Catalysis

Jonathan Michael Fowler

Submitted in accordance with the requirements for the degree of
Doctor of Philosophy

The University of Leeds
School of Chemistry

May, 2018

References for jointly authored publications:

1. N.J. Cookson, J.M. Fowler, D.P. Martin, J. Fisher, J.J. Henkelis, T.K. Ronson, F.L. Thorp-Greenwood, C.E. Willans, M.J. Hardie*, *Supramol. Chem.*, 2018, **4**, 255; Metallo-cryptophane cages from cis-linked and trans-linked strategies.

The work described within this publication is presented in Chapter 2 of this thesis. L2 was prepared and fully characterised by the candidate. Crystals of [$Pd_3L_2Cl_6$] were grown and the structure solved by the candidate. Solution state studies on the cage were carried out by D.P. Martin. Other ligands and assemblies in this publication were prepared and characterised by Dr. N.J. Cookson and Dr. F.L. Thorp-Greenwood, and are not included in this thesis. Prof. M.J. Hardie was the primary investigator.

2. J.M. Fowler, F.L. Thorp-Greenwood, S.L. Warriner, C.E. Willans, M.J. Hardie*, *Chem. Commun.*, 2016, **52**, 8699; $M_{12}L_8$ metallo-supramolecular cube with cyclotriguaiacylene-type ligand: spontaneous resolution of cube and its constituent host ligand.

The work described within this publication is presented in Chapter 3 of this thesis. All compounds were prepared and characterised by the candidate. One crystal structure was solved by Dr. F.L. Thorp-Greenwood. Direct-injection mass spectra of cages were carried out by Dr. S.L. Warriner. Dr. C.E. Willans and Prof. M.J. Hardie were primary investigators.

Acknowledgements

First and foremost, I would like to thank my supervisors Prof. Michaele Hardie and Dr. Charlotte Willans for giving me this opportunity. I've learnt so much about such wide branches of chemistry during this PhD project and I'm extremely grateful for all the support and guidance you have both given me over the past three and a half years. Michaele, it has been an absolute pleasure to work on such an enjoyable project and I've gained so many valuable skills in the process. Charlotte, you've always been in my corner despite the fact I'm from the 'wrong' side of the Pennines.

Next I would like to thank the many technical members of staff in Leeds, especially Dr. Chris Pask for making sense of horrendously disordered solvent molecules in crystal structures. Our trips to Diamond *via* Leicester Forest East M1 services will also live long in the memory! I also have to thank Ms. Tanya Marinko-Covell for running CHN samples before your retirement, and for being the most talkative person I will ever meet.

I wouldn't be where I am now without past and present members of the Hardie group. Firstly Flo for making the office such a friendly place to work from day one of my PhD and Vikki for showing me the ropes, as well as the early morning coffee trips. Hayder, your ability to put the whole office in a food coma with generous servings of Iraqi food is unrivalled. Next I would like to thank Samwell Tarly, your eternal pessimism, love of bland food and disdain for the most menial of things (hot drinks) always put a smile on my face. Ed 'the Eagle' Bohill, where do I start? Your alternative views on the theory of evolution and the numerous Westerosi discussions made you a pleasure to work with. I would also like to acknowledge all the MChem students over the past four years for your infectious enthusiasm, particularly Dave Martin for your endeavour throughout the project I gave you.

Special thanks go to the Willans group. Firstly Mike for your limitless knowledge and outrageous drunkenness. I have to thank Jordan for a thoroughly entertaining three years sitting next to you in the office, despite being the loudest person I know and constantly moving my glovebox samples out of reach. Your infamous carborane-mediated demolition of a fume cupboard will also not be

Abstract

The development of tritopic azole ligands tethered to the cyclotriveratrylene (CTV) molecular host is described within this thesis. The assembly of tripodal pyridyl-CTV ligands with metal precursors has led to the discovery of a diverse range of metallo-supramolecular assemblies, but comparable ligands incorporating five-membered ring counterparts are considerably less developed. New azole ligands could potentially coordinate to metals at different bite angles compared to the established pyridyl systems, leading to the assembly of previously inaccessible architectures. Furthermore, azoles, in particular 1,3-diazoles, are precursors to organometallic N-heterocyclic carbene (NHC) complexes. The fusion of NHC ligands and CTV cavitands has not previously been investigated.

A tritopic benzimidazole ligand was prepared, which assembles with [Pd(Cl)$_2$(MeCN)$_2$] to yield a rare *trans*-linked metallocryptophane as an alternative to the more commonly encountered architectures requiring a *cis*-protected Pd(II) precursor. Additionally, the coordination of an oxazole ligand was investigated, leading to the assembly of 1D polymer chains.

The assembly of a 4-thiazolyl ligand with AgBF$_4$ and AgReO$_4$ led to the assembly of the first CTV-type coordination cubes, with chiral self sorting upon coordination to Ag(I) and spontaneous resolution of crystals being exhibited. In addition to cubic cages, 2D and 3D coordination polymers were also accessible upon coordination to Ag(I).

The first metal-NHC complexes on a CTV scaffold were also prepared, with Ir(III) and Ru(II) complexes being examined as catalysts in the transfer hydrogenation of acetophenone, suggesting that in the case of Ru(II), intermolecular cooperativity may be exhibited.

Trinuclear Pd(II)-NHC complexes were targeted, and examined as catalysts in the regioselective Suzuki-Miyaura reaction of 2,4-dibromopyridine and 4-methoxybenzeneboronic acid. Catalysts displayed high activities over a short period of time, preparing traces of the 'favoured' *o*-coupled product and significant quantities of *para*- and *bis*-coupled products, potentially *via* two pathways.

Table of Contents

List of Tables

List of Figures

Chapter 3:

List of Schemes

List of Abbreviations

asu	Asymmetric unit
BAr$^F_4$	*Tetrakis*[3,5-*bis*(trifluoromethyl)phenyl]borate
BET	Brunauer-Emmett-Teller
BINAP	2,2'-Bis(diphenylphosphino)-1,1'-binaphthyl
COD	1,5-Cyclooctadiene
COSY	Correlation spectroscopy
Cp	Cyclopentadienyl
Cp*	1,2,3,4,5-Pentamethylcyclopentadienyl
CTC	Cyclotricatechylene
CTG	Cyclotriguaiacylene
CTV	Cyclotriveratrylene
DCM	Dichloromethane
DEA	Diethylamine
DEPT	Distortionless enhancement by polarisation transfer
DFT	Density functional theory
Dipp	2,6-Diisopropylphenyl
DMAC	*N,N'*-Dimethylacetamide
DMF	*N,N'*-Dimethylformamide
DMSO	Dimethylsulfoxide
DNA	Deoxyribonucleic acid
dppe	1,2-diphenylphosphinoethane
EDX	Energy-dispersive X-ray spectroscopy
ee	Enantiomeric excess
ESI	Electrospray ionisation
FTIR	Fourier transform infrared spectroscopy
HMBC	Heteronuclear multiple bond correlation
HMQC	Heteronuclear multiple quantum correlation

HPLC	High performance liquid chromatography
HRMS	High resolution mass spectrometry
HSAB	Hard and soft (Lewis) acid and base
IPA	Isopropanol
J	NMR coupling constant
L	Ligand
Mes	Mesityl (1,3,5-trimethylphenyl)
MOF	Metal organic framework
nbe	Norbornene
NHC	N-heterocyclic carbene
NMP	*N*-methylpyrrolidone
NMR	Nuclear magnetic resonance
NOESY	Nuclear Overhauser effect spectroscopy
PEPPSI	Pyridine enhanced precatalyst preparation stabilisation and initiation
PXRD	Powder X-ray diffraction
ROESY	Rotating-frame nuclear Overhauser effect spectroscopy
RNA	Ribonucleic acid
rt	Room temperature
SCXRD	Single crystal X-ray diffraction
SEM	Scanning electron microscopy
TBTQ	Tribenzotriquinacene
TGA	Thermogravimetric analysis
TH	Transfer hydrogenation
TOF	Turnover frequency
TON	Turnover number
tren	*tris*(2-Aminoethyl)amine
VT	Variable temperature
ZIF	Zeolitic imidazolate framework
χ_P	Pauling electronegativity

Chapter 1
Introduction

1.1 Supramolecular Chemistry

The term 'supramolecular chemistry' was first coined by Johannes Diederick van der Waals in 1873, when he proposed molecules close in space must interact with one another.[1] In 1894, Fished suggested the lock and key mechanism when researching the enzymatic cleavage of polysaccharides.[2] The lock and key mechanism involves the selective fitting of a guest within the active site of a biological host molecule, often an enzyme, which were later understood to be through intermolecular interactions such as hydrogen bonding and π-π stacking.

The field of supramolecular chemistry focuses on 'chemistry beyond the molecule', a term coined by Jean-Marie Lehn, a recipient of the 1987 Nobel Prize in chemistry.[3] The basis of supramolecular chemistry is molecular self-assembly, which involves the spontaneous arrangement of covalently bound molecular subunits into ordered arrays through reversible interactions, such as hydrogen bonding, halogen bonding and metal coordination. Self-assembly is a dynamic process and in equilibrium, allowing systems to self-correct as the thermodynamic minimum is reached, which is not an instantaneous process. Supramolecular chemistry has since developed into a multidisciplinary field, hugely impacting both biological and physical sciences. Life itself cannot function without supramolecular chemistry, with examples including the complementary hydrogen bonds between DNA nucleotides,[4] facilitating the assembly of the double helix structure, and the folding of enzymes through hydrogen bonding, and π-π stacking and disulfide links formed between cysteine residues. The extent of supramolecular interactions in biological systems led to Nadrian Seeman inventing the field of DNA nanotechnology.[5] The development and influence of supramolecular chemistry have developed in tandem with the establishment and improvement of analytical instrumentation, for example synchrotron sources for X-ray diffraction, which have led to a number of critical discoveries.

Research on macrocycles by Lehn, Cram and Pedersen directed the field of supramolecular chemistry, with Pedersen discovering the cation-templated synthesis

of crown ethers.[6, 7] Changing the metal cation selected based on ionic radii led to the templation of different sized crown-ethers through the Williamson ether synthesis. Addition of Li^+ led to the smaller 12-crown-4 being isolated, whilst K^+ templates the cyclisation of 18-crown-6. Crown ethers are also excellent receptors for cationic species, with oxygen atoms of the macrocycle coordinating to the relevant cation. The recognition properties of crown ethers and the 3D cryptand hosts developed by Lehn and co-workers have greatly influenced the field of metallo-supramolecular chemistry.[8, 9]

1.1.1 Metallo-supramolecular chemistry

Metal coordination to multitopic ligands is a powerful tool for supramolecular chemists, and well-defined polyhedra. The combination of a transition metal centre, whose geometries are often well-defined by crystal field effects, and a carefully designed multitopic ligand can lead to the assembly of architectures with high fidelity. Lehn and co-workers have demonstrated this by combining poly-2,2'-bipyridine ligands with Cu(I), which has a propensity to yield tetrahedral complexes. This particular combination led to the assembly of a dinuclear $[Cu_2L_2]^{2+}$ double helicate complex.[10] Additionally, coordination of octahedral Ni(II) cations to similar poly-2,2'-bipyridine ligands led to the assembly of triple helicates.[11] Self-recognition properties of helicates were demonstrated in the same article, and upon employing poly-2,2'bipyridines of different lengths, alongside both Cu(I) and Ni(II) salts, only the homoleptic, homonuclear double or triple helicates were observed as products. The same ligand class assembled with $FeCl_2$ to surprisingly yield a $[Fe_5L_5(Cl)]^{9+}$ circular helicate ensemble whose assembly was anion-templated.[12] Using modern-day organometallic chemistry, Leigh and co-workers used alkene metathesis chemistry to link a circular helicate analogue into a pentafoil knot (figure 1.1, right).[13]

Employing two ditopic units with specific geometries allows for the assembly of 2D shapes.[14] A key example is Fujita's archetypal $[Pd_4L_4]^{8+}$ molecular square (figure 1.1, left), which combined a *cis*-protected Pd(II) subunit and the rigid ditopic ligand 4,4'-bipyridine.[15] The ethylenediamine ligand forced the incoming 4,4'-bipyridine ligands to coordinate *cis*- with respect to one another, leading to the assembly of a square as the thermodynamic product. By changing the geometry of

the ligand and/or metal subunits, shapes such as triangles[16] and hexagons[17] can also be accessed.
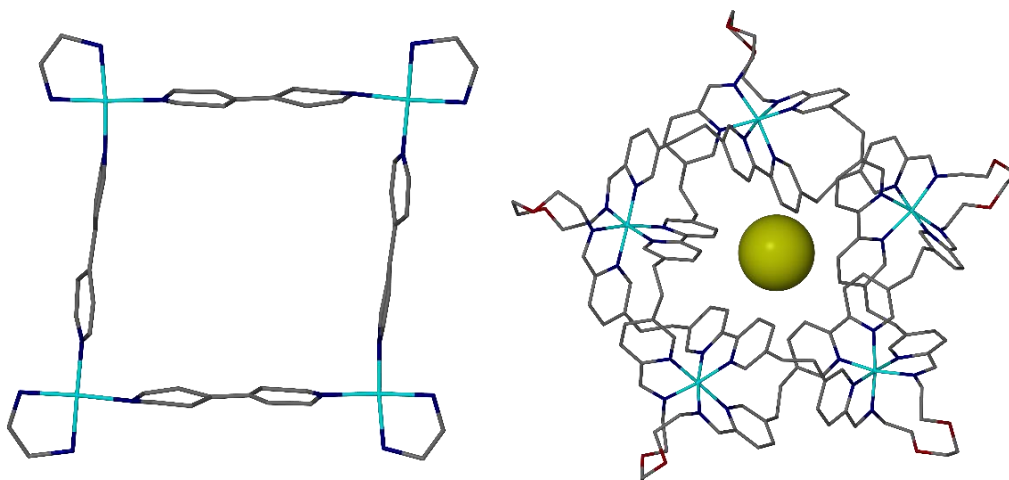
Figure 1.1 Left: Fujita's molecular square. Right: Leigh's pentafoil knot.[13, 15]

The combination of ditopic and tritopic components leads to the assembly of 3D polyhedra. Raymond and co-workers have prepared $[Ga_4L_6(NEt_4^+)]^{11-}$ and the analogous Fe^{3+} tetrahedra from linear *bis*-catecholate and octahedral Ga^{3+} cations (figure 1.2, left).[18] The same class of complex is capable of encapsulating highly reactive cationic phosphine-acetone adducts in aqueous media.[19] Nitschke and co-workers have prepared a family of cationic $[M_4L_6]^{n+}$ tetrahedra, which can be prepared in a one-pot synthesis through subcomponent self-assembly.[20] Many ligands prepared in this group revolve around the condensation of 2-formylpyridine and amines in the presence of a metal centre, yielding a bidentate pyridylimine ligand.[21] The same group demonstrated the encapsulation of white phosphorus within a tetrahedral cage, rendering it indefinitely stable in aqueous media (figure 1.2, right).[22] The authors stated that P_4 was unable to be oxidised because the products were too large to fit within the cavity. The addition of benzene led to the release of white phosphorus from the cage. The encapsulation of white phosphorus, and yellow arsenic (As_4) has also recently been achieved by Wu and co-workers within an anionic tetrahedral cage.[23]
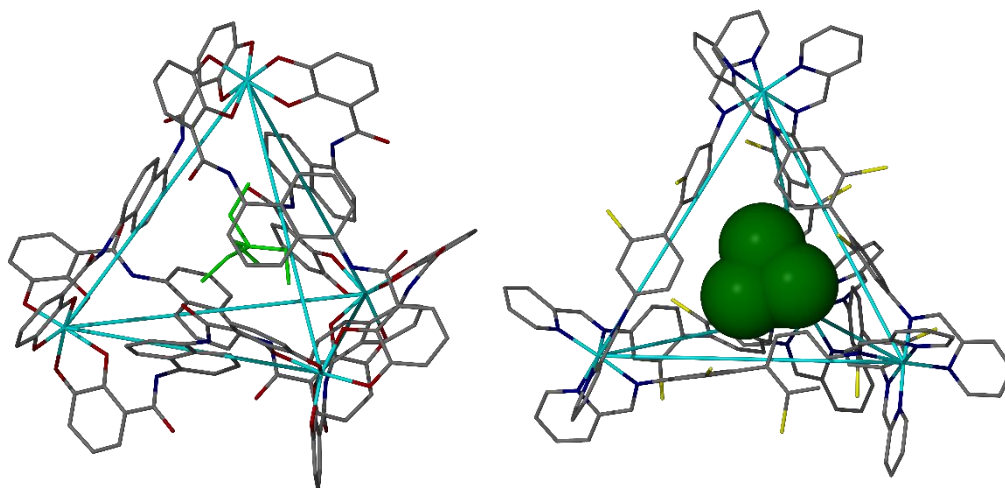
Figure 1.2 Left: Raymond's [Ga$_4$L$_6$]$^{11-}$ tetrahedron.[18] Triethylammonium guest is shown in green. Right: Nitschke's [Fe$_4$L$_6$]$^{8+}$ tetrahedron encapsulating white phosphorus.[22] One position of the P$_4$ guest is shown as space-filling and only the S of SO$_3$ groups shown for clarity.

Larger platonic solids are also accessible, such as metallo-cubes, which typically arise through the edge-directed assembly of a facially-protected octahedral metal with linear linkers such as 4,4'-bipyridine, as demonstrated by Thomas and co-workers when reporting a [Ru$_8$L$_{12}$] cube.[24] Nitschke and co-workers intricately prepared a [Fe$_8$Pt$_6$L$_{24}$]$^{28+}$ heterobimetallic cube by combining subcomponent self-assembly with molecular panelling.[25, 26] Square-planar Pt(II) ions reside in the centre of each face coordinated to four ligands, making a square-shaped [PdL$_4$] fragment. Bidentate pyridylimine groups terminate each of the ligands coordinating to Pt^{2+}, and concomitantly, three coordinate to octahedral Fe(II) centres on each vertex of the cube (figure 1.3, left).

Molecular panelling is an approach Fujita and co-workers have made great strides in, and assemblies are face-directed.[27] By treating ligands as 2D geometric panels such as triangles or squares, they can be linked together roughly orthogonally by square planar metals to give rise to 3D polyhedra. The first example reported in this group was the assembly of a triangular ligand with a *cis*-protected Pd(II) tecton into a [Pd$_6$L$_4$]$^{12+}$ octahedron.[28] The precursor [Pd(en)(NO$_3$)$_2$] was employed as a tecton because it possesses a bidentate ethylenediamine (en) ligand which forces two oncoming ligands to coordinate *cis*- to one another about the square planar Pd(II) centre. Alternating faces of the octahedron were occupied by ligands, and the cage behaved as a receptor to adamantanecarboxylates (figure 1.3, right). Derivatives of

Fujita's octahedral cages have proven to be effective host molecules towards a range of substrates, including tetrabenzylsilane[29] and *cis*-azobenzene, with no evidence of the azobenzene moiety isomerising to yield the *trans*-isomer in solution.[30]
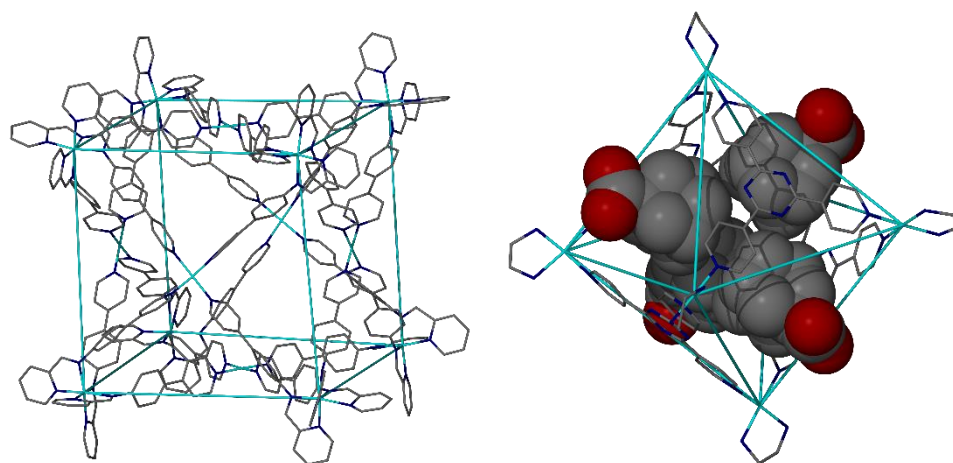
Figure 1.3 Left: Nitschke's $[Fe_8Pt_6L_{24}]^{28+}$ cube.[26] Right: Fujita's catalytically active $[Pd_6L_4]^{12+}$ octahedron.[31] Adamantanecarboxylate guests shown in space-filling.

In contrast to Platonic solids, which are regular polyhedra with congruent faces, Archimedean solids are semi-regular 3D polyhedra, and contain two or more polygons as faces in the assembly. Archimedean solids are much rarer than their Platonic counterparts. Fujita has more recently reported the assembly of much larger Archimedean solids by employing $[Pd(MeCN)_4](BF_4)_2$ and slightly bent ditopic ligands. The unprotected Pd(II) centre can coordinate to four ligands, facilitating the assembly of 3D polyhedra with bent ligand systems. Fujita has elegantly demonstrated that slightly altering the bite angle between the *m*-pyridyl donors of his ligand, by substituting the phenyl group of 1,3-di(4-pyridyl)benzene for 2,5-furan, 2,5-thiophene or 2,5-selenophene interior can drastically alter the polyhedron obtained post-assembly, accessing $M_{12}L_{24}$ cuboctahedra (figure 1.4, left),[32] $M_{24}L_{48}$ rhombicuboctahedra,[33], $M_{30}L_{60}$ icosidodecahedra,[34] with the largest assembly to date in his group being a $M_{48}L_{96}$ polyhedron comprising of trigonal and tetragonal faces.[35] In addition to Fujita's Archimedean assemblies, Stang,[14, 17, 36] Newkome[37] (figure 1.4, right) and Ward[38] have made invaluable contributions with their discoveries of truncated tetrahedra, cuboctahedra and truncated octahedra through metal coordination and hydrogen bonds.
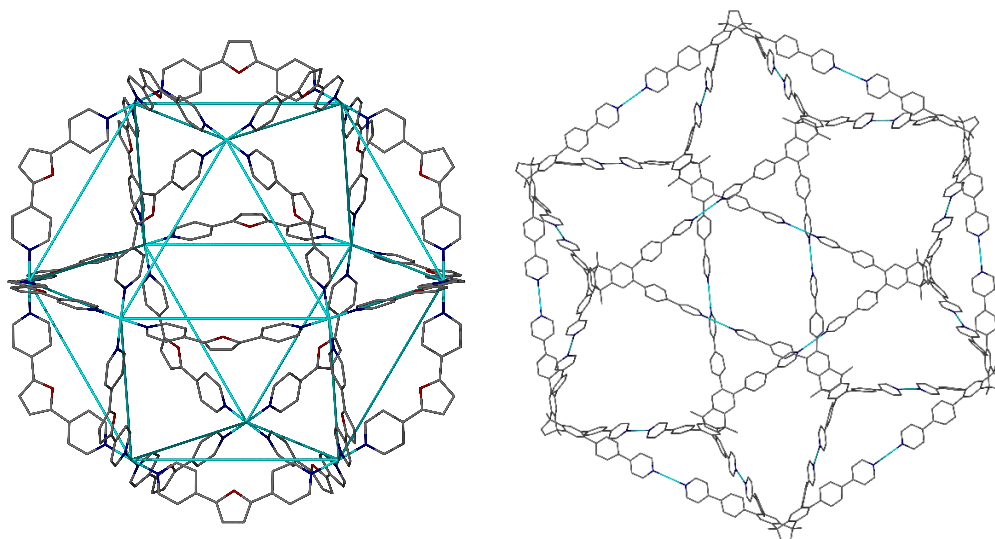
Figure 1.4 Left: Fujita's cuboctahedron. Right: Newkome's cuboctahedron.[32, 37]

1.1.2 Cavitands

A number of bowl-shaped molecules with internal cavities exist, and have been coined as cavitands by Cram.[39] The most commonly encountered cavitands are derivatives of calix[4]arene. A common precursor in calix[4]arene chemistry is ^{t}butylcalix[4]arene, whose synthesis is straightforward upon condensation of 4-^{t}butylphenol and formaldehyde under basic conditions.[40-42] Removal of the *tert*-butyl group under Lewis acidic conditions is facile, and replacement with a range of ligand groups is possible. The hydroxyl groups on the lower-rim partake in hydrogen bonding interactions with one another, thus adopting a cone conformation, although introducing steric bulk to the methylene bridges can disrupt and overcome the propensity to form hydrogen bonds, leading to partial cone conformations prevailing.[43]

Calix[n]arenes display rich and varied coordination chemistry. Coordination of metals to the lower-rim hydroxyl groups is established,[44, 45] as well as through ligand functionality introduced to the calix[4]arene upper-rim. Key assemblies include Kobayashi and Fukazawa's [M$_4$L$_2$] cages bearing pyridyl donors[46, 47] and de Mendoza's carboxylate-functionalised calix[4]arene and calix[5]arene scaffolds, which coordinate equatorially around uranyl cations with hexagonal bipyramidal geometries, affording $[(UO_2)_8(L)_6]^{8-}$ octahedral and $[(UO_2)_{20}(L)_{12}]^{20-}$ icosahedral cages respectively (figure 1.5).[48]
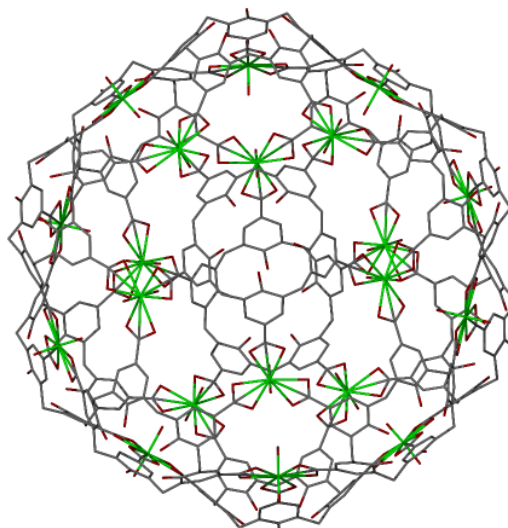
Figure 1.5 De Mendoza's $[(UO_2)_{20}(L)_{12}]^{20-}$ icosoahedron.[48]

1.1.3 Cyclotriveratrylene

Cyclotriveratrylene (CTV) is a rigid C_3-symmetric cavitand with a shallow hydrophobic cavity (figure 1.6, left). The interior of the bowl is electron-rich and CTV has been utilised as a molecular host to fullerenes.[49, 50] The structure of CTV was realised in 1965 by Lindsey,[51] but first discovered by Robinson in 1915 who mistook it for the dimer.[52] A number of CTV derivatives are known, including the *hexakis*-hydroxyl derivative cyclotricatechylene (CTC), which is accessible *via* the complete demethylation of CTV. Robson and co-workers elegantly demonstrated the ability of CTC to form clam-like structures and encapsulate anions of different sizes within the electron-rich cavity by dissociation of hydrogen bonds about the dimer.[53] CTC has also been employed as a C_3-symmetric dioxolene ligand,[54] and also as a portion of the monomer in a polymer of intrinsic microporosity.[55] Arguably the most synthetically useful derivative is the *tris*-hydroxyl analogue cyclotriguaiacylene (CTG) (figure 1.6, right), which can be functionalised through straightforward means by reaction with an alkyl halide or acid halide under basic conditions to give rise to a range of compounds bearing ligand groups for metal coordination[56] or for applications such as Hg(II) detection in aqueous media.[57]
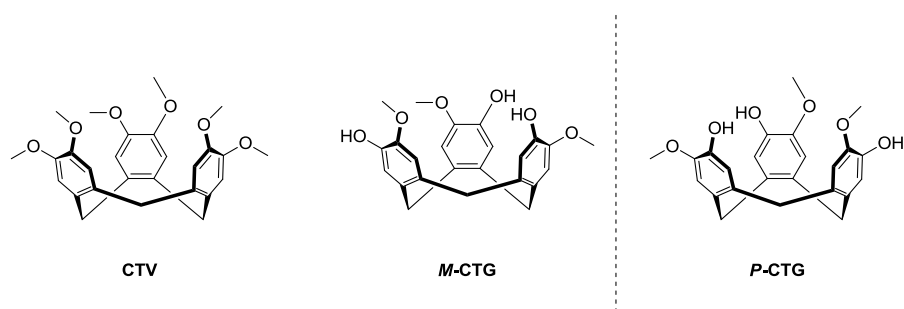
Figure 1.6 Left: Cyclotriveratrylene (CTV). Right: helical enantiomers of cyclotriguaiacylene (CTG).

Like all CTV derivatives, CTG exists predominantly in the crown-conformation. Additionally, CTG possesses helical chirality about the upper-rim and enantiomers can be separated through chiral HPLC techniques. Racemisation occurs after *ca.* one month at 20 °C, *via* the unfavourable saddle conformation, although this is accelerated at higher temperatures and varies depending on functionality introduced to the cavitand (figure 1.7).[58, 59] Interconversion between enantiomers is slow and cannot be measured on the NMR timescale due to the high energy barrier for inversion *via* the saddle conformation. Chiral self-sorting can occur upon metal coordination.[60] The favourable crown-conformation contains two doublets corresponding to the *endo-* and *exo-* protons of the lower rim at δ = 5.0-4.6 and 3.9-3.6 ppm, with geminal coupling between the two doublets observed at roughly 14 Hz.

Crown (*P*-isomer)   Saddle   Crown (*M*-isomer)
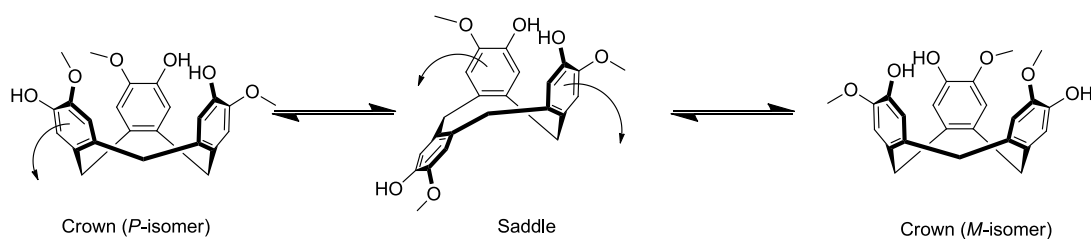
Figure 1.7 Racemisation of CTG *via* the saddle conformation.

The concave nature of the CTV bowl makes it an ideal capping group for molecular cages, the simplest of which are known as cryptophanes, where two CTV units typically adopt a head-to-head arrangement and are linked together by a range of spacer units.[8, 61] Both CTV units in a cryptophane possess helical chirality, therefore the cryptophanes are typically isolated as diastereomers, termed the *syn*-diastereomer and *anti*-diastereomer which are of different symmetries.[62, 63] The *syn*-cryptophane comprises two CTV units of opposite handedness, whereas the *anti*-cryptophanes contain two CTV units of the same handedness and are therefore

chiral. Whilst the vast majority of cryptophanes have the 'out-out' conformation, Holman and co-workers isolated a rare example of an 'imploded' cryptophane upon thermal release of guest, led to one CTV cap taking up the unfavourable saddle conformation and the capsule collapsing.[64] Addition of THF guest reinflates the cryptophane.

Cryptophanes have proven to behave as reversible hosts to a range of small neutral molecules including bromochlorofluoromethane,[65] methane,[66] aminoxy radicals,[67] ammonium cations[68] and also xenon (figure 1.8, left).[69, 70] The electron-rich nature of the CTV-bowl leads to cryptophanes being poor receptors for anions. Holman and co-workers have however addressed this by furnishing each CTV arene face with d^6 metal arene and Cp complexes (Fe(II), Ru(II) and Ir(III)) in a sandwich motif, causing a significant increase in π-acidity within the cavity and facilitating the binding of anions within the CTV core and also cryptophanes.[71-74]

In addition to cryptophanes bearing organic linkers, coordination chemistry can be utilised to link two derivatised CTV-type ligands through three metal centres. This was first demonstrated by Shinkai and co-workers in 2001, who assembled a C_3-symmetric pyridyl CTV ligand with *cis*-protected Pd(II) tectons to yield chiral *anti*-metallo-cryptophanes.[75] Further investigations by Chambron and co-workers led to the stereoselective assembly of chiral *anti*-isomers.[76] The same group also employed a mixture of two CTV-type ligands and self-recognition led to only homoleptic cryptophanes being isolated. Hardie and co-workers have extensively studied *cis*-protected metallo-cryptophanes, reporting chiral Ir(III) isomers,[77] in addition to achiral [Pd$_3$(*bis*-NHC)$_3$(L)$_2$] *syn*-cryptophane cages (figure 1.8, right).[78] Further investigations into metallated cryptophanes have notably revealed the assembly of a catenated metallo-cryptophane,[79] and a soft coordination polymer derived from organic cryptophanes bearing a carboxylic acid ligand on the equator.[80]

As well as metallo-cryptophanes, a host of larger cages have been reported. Upon mixing Pd(NO$_3$)$_2$ and the *tris*-isonicotinoylcyclotriveratrylene ligand, a [Pd$_6$L$_8$]$^{12+}$ stellated octahedron assembles (figure 1.9, left). Each CTV ligand occupies one face of an octahedron and the CTV lower-rim stellates from the centre of each face.[82] The same cages have been proven to encapsulate sodium alkyl sulfates in solution,[83] and can be disassembled and reassembled in solution.[84] In addition to using [Pd(NO$_3$)$_2$] as a precursor for the assembly of stellated octahedra,

Hardie and co-workers reacted the chelating $[Pd(en)(NO_3)_2]$ with the same isonicotinoyl ligand, and a $[Pd_3(en)_3(L)_2]$ metallo-cryptophane was the initial product. However, this proved to be metastable and rearranged in solution to yield the $[Pd_6L_8]^{12+}$ stellated octahedron and $[Pd(en)_2]^{2+}$ as byproduct.[78]
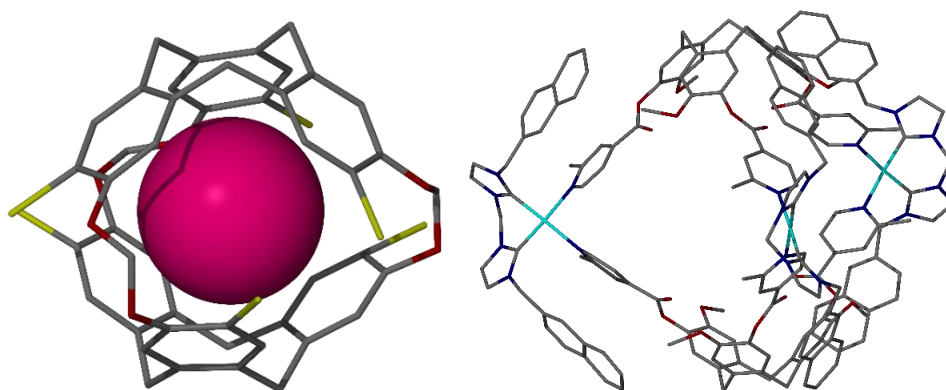
Figure 1.8 Left: Holman's organic cryptophane bearing a Xe guest molecule (pink sphere).[81] Right: Hardie's $[Pd_3(L)_2(bis\text{-}NHC)_3]^{6+}$ metallo-cryptophane.[78]

Further examples of CTV-type metallo-cages include tetrahedral assemblies. Hardie and co-workers have reported two different types of $[Ag_4L_4]^{4+}$ tetrahedra. One is built upon the amino- derivative of cyclotriguaiacylene, the base of each bowl behaves as the cornerpiece of the assembly and each Ag(I) centre is tetrahedral, interacting with three ligands and one acetonitrile molecule.[85-87] The second class of reported $[Ag_4L_4]^{4+}$ tetrahedron is based on a quinoline-functionalised CTV ligand, one arm on each host is non-coordinating, and the Ag(I) centres are linear 2-coordinate.[88] Robson and co-workers have reported the assembly of $[Cu_6(CTC)_4]^{12-}$ and $[(VO)_6(CTC)_4]^{12-}$ tetrahedral cages with the closely related *hexakis*-hydroxyl CTC (figure 1.9, right).[89, 90] Both tetrahedral assemblies are structurally similar, with the cavitand bowl behaving as cornerpieces in the tetrahedron and the six metal centres reside on the edges. The Cu(II) centres possess square-planar geometry, whilst vanadyl unit is square pyramidal, with the oxo-ligand pointing outwards of the capsule, perpendicular to the CTC ligands.

CTV-derived ligands have proven capable of assembling with metal centres to yield platonic solids, and also topologically complex architectures. A key example is a $[Pd_4L_4]^{8+}$ Solomon cube.[91] The assembly comprises of two $[M_2L_2]$ metallacycles which form a Solomon-like link – two interwoven rings with four crossing points, but the two interlocked metallacycles are linked by Pd(II) centres.

The assembly also contains eight vertices, each of which is triple-connecting, rendering it a cube. A CTV-type ligand has also assembled with Cu(II) to yield [Cu_6L_6] metallacycles, which form an infinite Borromean network, with each ring forming a network with six nearest neighbours.[92] Borromean rings are Brunnian links containing (at least) three overlapping, but non-interlocking rings. Removal of one ring from the architecture leads to the collapse of the structure.
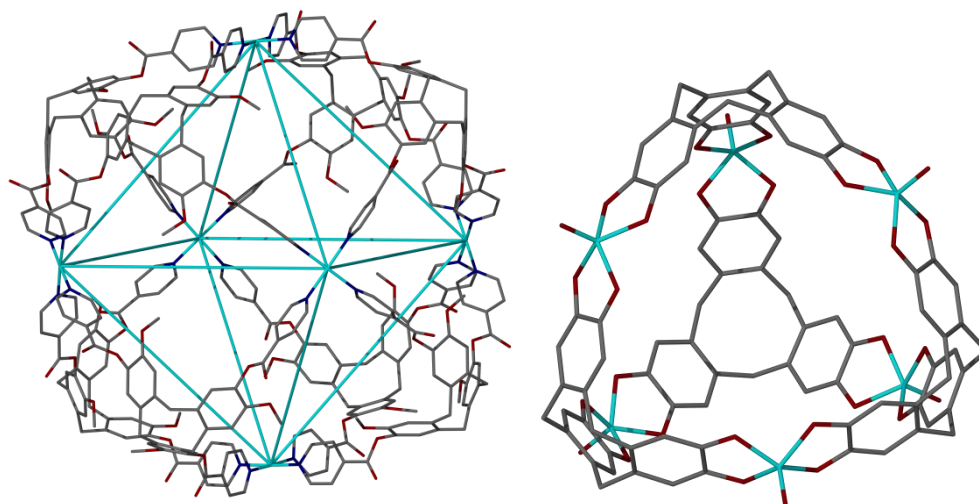
Figure 1.9 Left: Hardie's [Pd_6L_8]$^{12+}$ stellated octahedron. Right: Robson's [($VO)_6(CTC)_4$] tetrahedron.[82, 90]

1.1.4 Metallo-supramolecular assemblies in catalysis

Utilising supramolecular systems in catalytic transformations, as catalysts themselves or reaction vessels to either initiate or accelerate a reaction is an emerging and significant field. Many examples stem from confining a substrate within a cage, facilitating a reaction and then releasing the cargo, in a similar method to enzymatic transformations within biological systems. Catalysis within a cage is antithetical to the inhibition of P_4 oxidation observed by Nitschke and co-workers,[22] but the principles and reasoning behind the transformations is the same.

An early example of a supramolecular system influencing reactivity was reported by Breslow in 1971 when investigating the chlorination of anisole.[93] Upon reaction of anisole with hypochlorous acid, *o*- and *p*-chlorination is observed. Breslow added α-cyclodextrin to the reaction mixture, which formed a 1:1 complex with anisole, protecting the *o*- and *m*-positions of anisole within the cyclodextrin cavity, and therefore rendering them inaccessible to reactivity. Only a slight increase

in rate was observed, but Breslow's findings gave early insight into how supramolecular complexation can affect regioselectivity and reactivity.

The Diels-Alder reaction has been well-studied within supramolecular hosts. A study by Sanders and co-workers in 1993 first demonstrating this when carrying out a [4 + 2] cycloaddition between pyridine-containing diene and dienophiles within a Zn-porphyrin trimer.[94] A 200-fold increase in rate was observed upon addition of the molecular host, alongside selective *exo*-cyclisation. The authors proposed a Zn-templated transition-state through coordination of the pyridyl diene to explain the regioselectivity. Rebek and co-workers have employed a deep vase-like cavitand as a catalyst for the Diels-Alder cycloaddition of 9-(hydroxymethyl)anthracene and adamantyl maleimide. The interior of the cavitand is hydrophobic, whilst the upper-rim contains hydrogen-bonding units, giving the maleimide dienophile a strong binding affinity for the cavitand. The confined dienophile readily partook in the expected 9-10 Diels-Alder cycloaddition.[95] Fujita and co-workers employed the $[M_6L_4]$ octahedron shown in figure 1.3 as a reaction vessel to catalyse the same reaction.[31] In this case, the unusual 1,4-Diels Alder product was observed, with the authors proposing π-π interactions between the central anthracene ring and maleimide were too restricted within the cage, leading to selective 1,4-cyclisation. (scheme 1.1). Fujita also prepared a $[Pd_6L_4]$ open bowl, which selectively catalysed the conventional 9,10-cycloaddition. Introducing chirality into the *cis*-protecting tecton of the octahedron, Fujita has since carried out asymmetric [2 + 2] and [2 + 4] Diels-Alder cyclisations with ee (enantiomeric excess) reaching 50%.[96] The octahedron itself does not contain chiral centres, but the walls of the cage distort slightly.
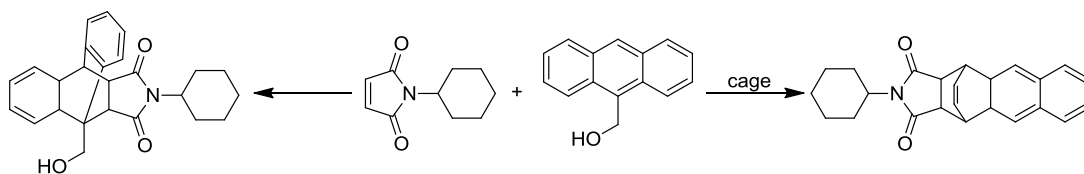
Scheme 1.1 Right: Fujita's 1,4-cycloaddition mediated within a cage. Left: The commonly observed 9,10-cycloaddition product isolated in the absence of a cage catalyst.[31]

Nitschke and co-workers have employed a tetrahedral cage as a catalyst for the hydrolysis of the insecticide dichlorovos, which is chemically similar to chemical warfare agents, by accelerating its decomposition.[97] The recognition may be mediated by hydroxyl groups *exo*- to the cages rather than within the cavity. Ward and co-workers have more recently prepared a $[Co_8L_{12}]^{16+}$ capable of catalysing the

Kemp elimination of benzisoxazole to 2-cyanophenolate within the cubic cavity, in aqueous media (scheme 1.2, top).[98] A 2×10^5-fold increase in rate was observed, and was proposed to occur within the cavity, whilst assisted by hydrogen bonding interactions with hydroxyl groups on the cube edges.

Raymond's anionic $[Ga_4L_6]^{11-}$ tetrahedral cages have proven to be excellent catalysts across a range of reactions, displaying >800-fold rate accelerations in a number of cases. The clusters have a high affinity for cationic species, and can efficiently catalyse the Aza-Cope rearrangements of enammonium cations within the cavity, forcing the reactive groups in close proximity of one another. After cyclisation, $[NMe_4]^+$ displays a greater affinity for the cage, outcompeting the rearrangement product, which becomes hydrolysed, neutral and hence non-competitive with the $[NMe_4]^+$ guest.[99-101] In addition to the aza-Cope rearrangement, the same class of cages can catalyse the Nazarov cyclisation of pentamethylpentadienol, yielding pentamethylcyclopentadiene (Cp*H) with a rate acceleration of 2.1×10^6 (k_{cat}/k_{uncat}).[102]

As an extension to confining a guest within the anionic cages, Raymond has encapsulated cationic (pre)catalysts such as $[Ir(Cp^*)(PMe_3)(CH_3)(C_2H_4)]^+$ and $[Rh(COD)(PMe_3)_2]^+$ species within tetrahedral cages, which display size- and shape-selectivities in the C-H activation of ketones and ethers, and isomerisation of allylic alcohols respectively.[103, 104]

Reek and co-workers have prepared a number of cage molecules encapsulating organometallic catalysts and delivering an increase in rate. An early key example was a Rh(I) organometallic complex bearing a *tris*-4-pyridylphosphine ligand. The nitrogen atoms of the pyridines coordinated to a Zn porphyrin leading to a twofold increase in activity for the hydroformylation of 1-octene compared to in the absence of porphyrins.[105] By taking advantage of the pyridyl-Zn interaction within a porphyrin-containing scaffold, Reek and co-workers have encapsulated a Rh(I) complex bearing a pyridine-grafted BINAP (2,2'bisdiphenylphosphino-1,1'-binaphthyl) ligand within a Zn-porphyrinic cage, and witnessed a marked increase in rate, alongside ee of 79% in the enantioselective hydroformylation of styrene.[106]

Resorcinarenes often form hydrogen-bonded hexameric cages in solution.[107] Reek has encapsulated the Au(I)-NHC catalyst [Au(IPr)(OTf)] within the cage,

leading to remarkably different reactivity with 4-phenylbutyne in water-saturated benzene (scheme 1.2, bottom).[108] The free catalyst hydrates the triple bond, leading to the ketone being formed as the Markovnikov product, with quantitative conversions observed after 30 mins. The encapsulated complex displays much lower selectivity, and was a less active catalyst (28% conversion after 400 min). The Markovnikov product was observed in a 12% conversion, the anti-Markovnikov aldehyde (4%) and unusually, an intramolecular-cyclised product (12%), which only exists in the absence of water, and the authors stated was present due to the incapability of water to penetrate the cage.
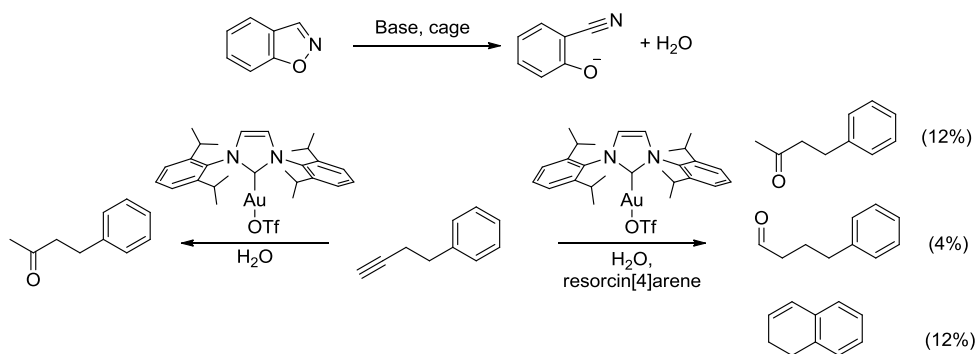
Scheme 1.2 Top: Ward's Kemp elimination of 2-cyanophenolate within a cubic cage.[98] Bottom: Reek's alkyne hydration and cyclisation catalysed by an Au(I)-NHC complex encapsulated within the resorcin[4]arene hexamer.[108]

A class of supramolecular cage regularly employed in catalysis within the CTV family is the hemicryptophane. In contrast to cryptophanes which possess two CTV units linked together in a head-to-head fashion, hemicryptophanes are heterotopic, possessing one CTV-terminus and a different C_3-symmetric capping unit, such as *tris*(2-aminoethyl)amine (tren).[109] Despite requiring extensive, multi-step syntheses, the capping group and linkers of hemicryptophanes can be relatively easily tuned for a range of applications, including primary ammonium encapsulation, with the NH_3 moiety forming hydrogen-bond interactions with an aza-crown capping unit, and the hydrophobic CTV bowl encasing an alkyl chain, as elegantly demonstrated by Lehn and co-workers in 1982.[8] Hemicryptophane complexes have more recently been trialled as tuneable catalysts. The south capping unit can often be a group such as tren, which strongly bind to metals. The first example was reported by Dutasta in 2009, who endohedrally coordinated a $\{VO\}^{3+}$ moiety within a trialkanolamine capped hemicryptophane in a trigonal bipyramidal geometry (figure 1.10). The encaged vanadium complex proved to be an excellent catalyst for the oxidation of

sulfides to sulfoxides, outcompeting a bowl-shaped catalyst.[110, 111] By incorporating BINOL (1,1'-bi-2-naphthol) groups into the walls of the hemicryptophane, Martinez and co-workers increased the hydrophobicity of the cage, which accelerated catalysis to give turnover numbers of up to 10000 per catalyst.[112] The tren-capped hemicryptophanes have proven a versatile host to endohedrally coordinated metals. Makita and co-workers coordinated Zn(II) within the south capping unit of a hemicryptophane, which led to a twofold rate increase compared to a Zn-tren catalyst.[113, 114] Makita also demonstrated a RuCl₂ hemicryptophane was capable of oxidising primary alcohols, selectively trapping the aldehyde, whereas a free Ru-tren catalyst displayed little discrimination between the aldehyde and carboxylic acid.[115] Cu(II)-hemicryptophanes developed by Dutasta and Martinez have proven capable of oxidising cycloalkanes, whilst partly discriminating between cyclohexane, cyclooctane and adamantane, suggesting catalysis was occurring within the cavity.[116] C-H activation of alkanes remains a highly challenging reaction.
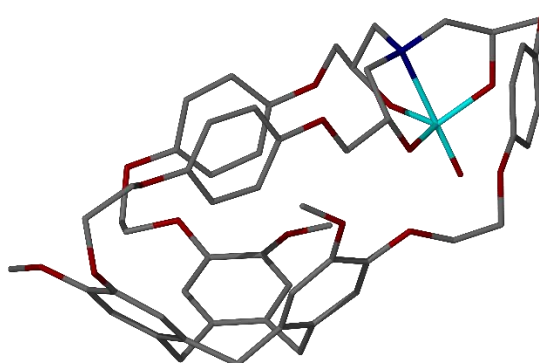
Figure 1.10 Dutasta's hemicryptophane possessing an endohedrally coordinated vanadium moiety.[110, 112]

1.2 Carbene ligands

1.2.1 Introduction to carbenes

Carbene ligands are two-electron donor ligands in organometallic chemistry, and bear six valence electrons and no formal charge.[117] Carbenes can be referred to as singlet or triplet, depending on the electronic nature of the centre. In singlet carbenes, the bonding orbital obtains some s character, stabilising the orbital by lowering its energy in its free form, whereas the p_z orbital remains unchanged. The pairing energy of electrons is also lower than the band gap between sp^2 and p_z

orbitals. In the bent triplet state, the energy gap between sp^2 and p orbitals is less than the electron pairing energy. Triplet carbenes can also be considered to be diradicals, hence can be observed using EPR spectroscopy. In an extreme case, triplet carbenes can be considered as sp^3 hybridised, with singly occupied molecular orbitals being degenerate.
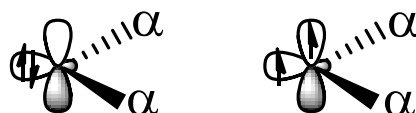
Figure 1.11 Frontier orbital diagrams of left: bent singlet and right: bent triplet carbenes of sp²
multiplicity.

Carbenes were first reported as organometallic ligands in the mid-20th century, with Fischer carbenes the primary carbenes to emerge.[118] Fischer carbenes have singlet multiplicity prior to metal coordination and are both strong σ-donor ligands and π-acceptors, hence primarily are found coordinating to low oxidation state, electron rich metal centres. In 1974, Schrock carbenes emerged.[119] Contrary to Fischer carbenes, the Schrock variety are triplet in nature, in the free state, are dianionic and prefer metals in higher oxidation states.

Electronic effects of the α-substituent strongly dictate the multiplicity of the carbene. Strongly Strongly π-donating groups, such as -NR$_2$ donate electron density into the p$_z$ orbital, destabilising it and in turn increasing the sp^2 – p energy difference (figure 1.12, left). On the other hand, triplet carbenes can be promoted by π-withdrawing groups stabilising the p$_z$ orbital, leading to a smaller sp^2 – p energy difference. Strong σ-donating α-substituents can also destabilise the sp^2 energy level, decreasing the sp^2 – p energy difference (figure 1.12, right).
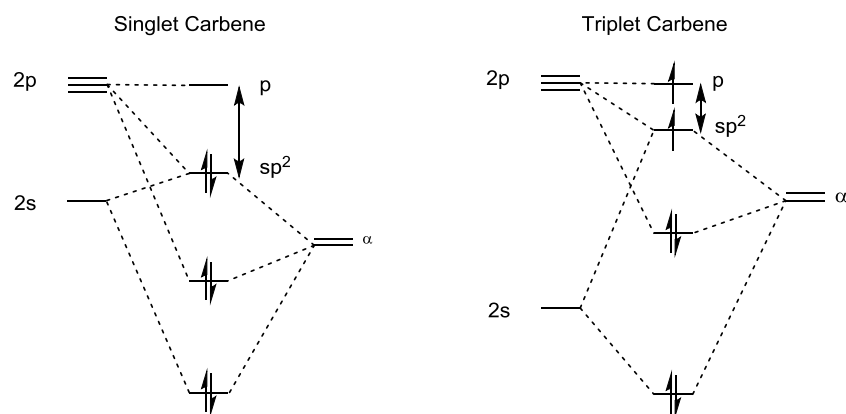
Figure 1.12 Relative orbital energies for left: singlet and right: bent sp² hybridised carbenes.

1.2.2 N-Heterocyclic carbenes

A third class of carbene is the N-heterocyclic carbene (NHC). NHCs are constrained in a five-membered ring system, which in addition to mesomeric effects caused by π-donation from α-nitrogen atoms into the empty p_z orbital, as well as σ-induction from the divalent carbon towards the more electronegative α-nitrogen atoms renders NHCs as bent, singlet carbenes. Cyclic NHCs are also 6π systems obeying Hückel's rules of aromaticity. Whilst this affords a secondary stabilisation factor, this is not as prominent as anticipated.[120] NHCs share similarities with Fischer carbenes, but the extent of π-donation from α-nitrogen atoms to the empty p_z orbital negates backbonding from taking place (figure 1.13). M-C bonds are noticeably longer when employing NHC ligands compared to Fischer carbenes because of the lack of back-donation from the metal centre into the p_π orbital of the carbene. Unlike Fischer and Schrock carbenes, NHC ligands can coordinate to metal cations in both high and low oxidation states because the absence of back-donation from the metal centre does not hamper metal coordination. However, when considering hard soft acid and base (HSAB) theory, NHCs are soft donors, therefore coordination to lower oxidation state metals is more straightforward. The NHC motif is often seen as analogous to phosphines by virtue of being strong σ-donors. The key difference between phosphines and NHCs involve back-bonding metrics, where it is much more pronounced between metal and phosphine. Phosphines are considerably more labile, whereas NHCs are persistent ligands.

A major advantage of NHC ligands is that the parent imidazolium salts are indefinitely stable, whereas phosphines slowly oxidise over time, which could easily see NHC-ligated complexes replace phosphines in a number of industrial catalytic transformations.[121]
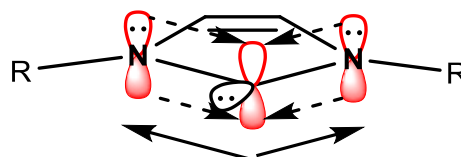
Figure 1.13 Frontier orbital diagram of an N-heterocyclic carbene.

NHCs were first hypothesised as early as 1957 by Breslow as an intermediate in the catalytic cycle of the thiazolium containing vitamin B1 when rapid H-D exchange of the NCHS proton of the thiazolium ring was observed in NMR studies.[122] In 1962,

Wanzlick tried to prepare a free carbene by elimination of chloroform from 2-(trichloromethyl)-1,3-(diphenyl)imidazolinium salts, but instead observed dimerisation of two carbene equivalents.[123]

The first metal-NHC complexes reported were by Wanzlick and Öfele in 1968 (scheme 1.3).[124, 125] Wanzlick employed the basic metal precursor, mercury(II) acetate to simultaneously deprotonate and coordinate to Hg(II) in a concerted, one-step mechanism. On the other hand, Öfele reported the rearrangement of an imidazolium pentacarbonylhydridochromium salt at elevated temperatures to yield a Cr(0)-NHC complex.
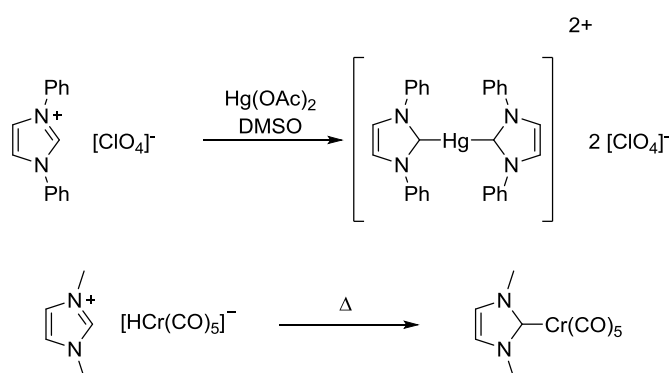
Scheme 1.3 Top: Wanzlick's synthesis of a Hg(II) NHC complex[124]. Bottom: Öfele's Cr(0) NHC preparation *via* a redistribution pathway.[125]

Few examples of N-heterocyclic carbene complexes were reported for over two decades, before Arduengo reported the isolation of the first stable free carbene in 1991 (scheme 1.4).[126] The field has rapidly expanded since Arduengo's discovery, and NHC chemistry has developed remarkably over a short space of time, where they are now considered a ligand at the frontier of organometallic chemistry.
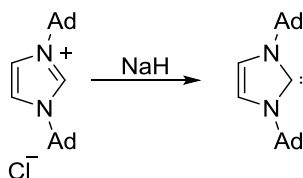
Scheme 1.4 Arduengo's isolation of a free carbene.[126]

1.2.3 Synthesis of metal-NHC complexes

1.2.3.1 The free carbene method

A commonly employed method in the synthesis of metal-NHC complexes follows on from Arduengo's pioneering work, and employs a strong base such as ^{n}BuLi or NaH to deprotonate the imidazolium salt, liberating a highly reactive free carbene, which can be isolated and characterised. Introduction of the free carbene to a metal precursor leads to metal-ligand interaction and preparation of a (typically) stable complex. The groups of Grubbs and Nolan have both reacted 1,3-bis(2,4,6-trimethylphenyl)imidazole-2-ylidene (IMes) with Grubbs' 1st generation catalyst and one phosphine ligand was displaced by the NHC, leading to the isolation of the more active 2nd generation catalyst (scheme 1.5).[127, 128] The same group have also prepared Au(I)-NHC complexes via addition of the free carbene to a metal precursor, albeit more effective methodologies to prepare this class of complex have since been reported.[129]
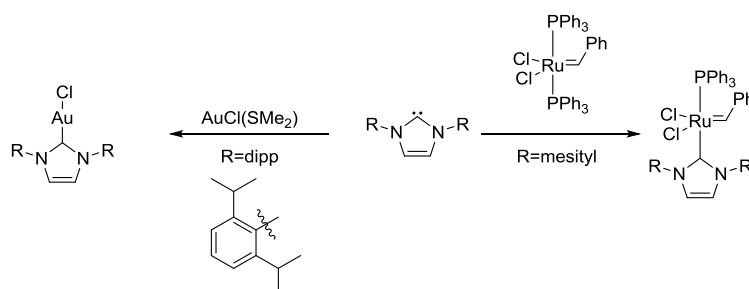
Scheme 1.5 Nolan's synthesis of Au(I) and Ru(II)-NHC complexes *via* a free carbene.[127, 129]

The free carbene route towards preparing metal-NHC complexes is commonly used, with little prerequisite regarding the metal precursors employed, but there are a number of disadvantages to this methodology. Isolation of highly air- and moisture-sensitive free carbenes is necessary, which is highly challenging. Additionally, the substrate scope for free carbene generation is somewhat limited. The use of strong bases prevents any imidazolium salt bearing base-sensitive *N*-substituents, including, but not limited to picolyl, carboxylate and a number of methylene-bearing precursors.[130] A wide range of synthetic protocols have been documented, which bypass the need to liberate free carbenes.

1.2.3.2 *In situ* deprotonation and metallation, basic metal precursors and transmetallation routes
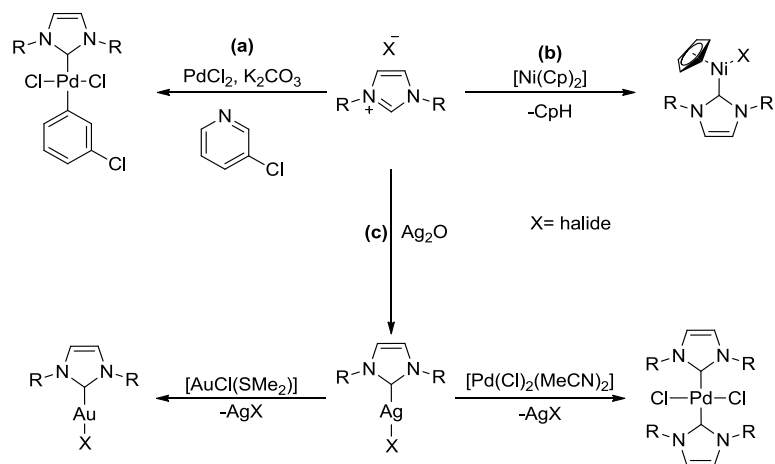
Scheme 1.6 Metal-NHC coordination *via* (a) *in situ* deprotonation and metallation,[131] (b) addition of a basic metal precursor,[132] (c) Ag(I)-NHC generation and transmetallation pathways.[133]

The *in situ* deprotonation of an imidazolium salt bypasses the need to isolate the reactive carbenic species, and is compatible with a variety of transition metal precursors (scheme 1.6). The need for strong bases is also diminished, and a number of reported examples employ weaker bases, such as potassium carbonate.

A commonly encountered class of complex whose synthesis employs this strategy are the PEPPSI™ complexes pioneered by Organ and co-workers (scheme 1.6(a)).[131] PEPPSI stands for **p**yridine **e**nhanced **p**recatalyst **p**reparation **s**tabilisation and **i**nitiation. Complexes are straightforward to prepare, giving near-quantitative yields under aerobic conditions. PEPPSI™ complexes are known for catalysing a range of transformations, including both C-C[134-139] and C-heteroatom[140-143] coupling with a vast substrate scope. This class of complex have proven to catalyse cross-coupling reactions regioselectively,[144] and when incorporating chiral groups into the NHC scaffold, Kündig and co-workers have demonstrated PEPPSI™ complexes can mediate asymmetric Suzuki-Miyaura reactions.[145]

An alternative to addition of both a base and metal precursor is to employ a basic metal precursor, such as an acetate, oxide or amide. Synergic pathways often dominate, where simultaneous deprotonation and metallation occur in a single transition step. Wanzlick's Hg(II)-NHC complex (scheme 1.3) was the first example of a metal-NHC complex prepared *via* this route.[124] Palladium(II) acetate is a

popular precursor in the preparation of Pd(II)-NHC complexes, where the acetate ligand mediates both deprotonation and coordination in a concerted single step.[146, 147] Ni(II) complexes derived from nickelocene are also well-established, and can be prepared following a similar mechanism (scheme 1.6(b)).[131, 148-150] Nickelocene is a 20-electron complex and is also highly basic. It is one of the few reported complexes which readily loses a cyclopentadienyl ligand upon reaction with an imidazolium halide.[131] A subsequent concerted deprotonation and metallation occurs, liberating the volatile protonated cyclopentadiene, and coordination of both the carbene and halide, with the formation of an 18-electron complex an additional driving force.

A somewhat popular approach to metal-NHC complexes is *via* Ag(I)-NHC transfer (scheme 1.6(c)). Ag(I) carbenes are straightforward to prepare using the basic metal precursor Ag$_2$O. In 1993, Arduengo reported the first example of an Ag(I)-NHC complex,[151] but their transmetallation capabilities were not realised until 1998 upon discovery by Lin and co-workers,[152] who upon deprotonating an imidazolium salt with Ag$_2$O in the presence of Pd(II) or Au(I) precursors, reported the Ag(I) carbene transfer in high yields, with significant AgCl precipitation as a by-product. In the absence of Pd(II) or Au(I), Ag(I)-NHC complexes can be isolated, whereas the reaction does not proceed in the absence of Ag$_2$O. Transmetallation primarily occurs because of the high lattice enthalpy associated with silver halide formation.[153] The low Ag-C bond strength also contributes but is a secondary force compared to the formation of AgX. Similar to the first three methods introduced, poor tolerance of basic groups on the carbene wingtips is a potential pitfall.[130]

1.2.4 NHC ligands in supramolecular chemistry

The implementation of multimetallic NHC complexes is an emerging topic in organometallic and supramolecular chemistry. Systems can have disadvantages commonly encountered when discussing the synthesis of metal-NHC complexes, for example, many cavitands bear base-sensitive groups, which significantly limit the methodologies that can be employed. Additionally incorporating multiple imidazolium moieties onto an often aromatic scaffold can lead to solubility problems, which can further restrict the synthetic strategies that can be employed. Despite these disadvantages, the strong metal-NHC interactions allow for more

facile postsynthetic modification, which can be challenging on a number of metallo-supramolecular assemblies, due to the labile nature of M-N bonds in many complexes.

Hahn has led the field of poly-NHC ligands in metallo-supramolecular chemistry.[154] This work stemmed from the assembly of a molecular rectangle in 2008 by reaction of a dinuclear Ni(II)-NHC with 4,4-bipyridine in the presence of AgBF$_4$[155] (figure 1.14). Peris has recently prepared slightly larger Ni$_4$L$_4$ rectangles as receptors for polyaromatic hydrocarbons.[156] The employment of the piano stool motif as cornerpieces in polyhedra has been utilised on multiple occasions (mainly Rh or Ir-Cp* derived), but architectures directed by Werner-type ligands have dominated the field.[157] Carbon coordination has generally been through C-H activation-directed assembly rather than carbene coordination.[158] Hahn and co-workers coordinated the same *bis*-carbene ligand to Au(I), and upon ligand exchange with dppe in the presence of AgBF$_4$ yielded a much narrower [Au$_4$(dppe)$_2$(NHC)$_2$] with carbene units undergoing π-π stacking arrangements with one another.[159]
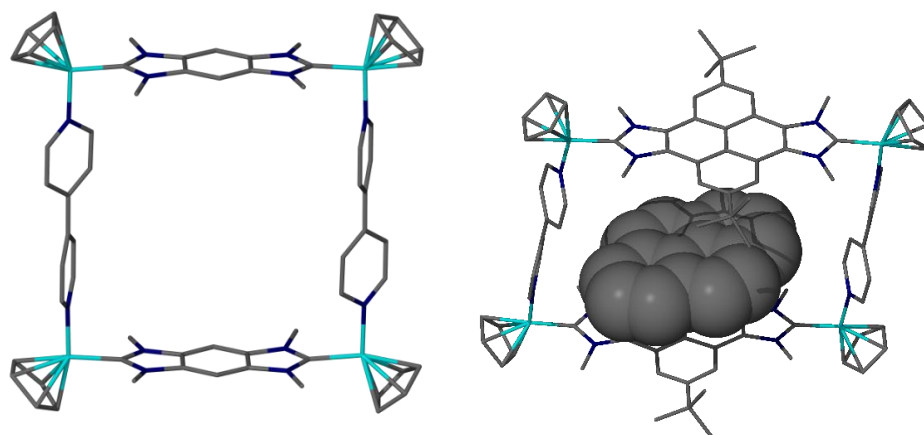
Figure 1.14 Left: Hahn's molecular rectangle. Right: Peris's rectangle encapsulating one pyrene guest. Only the first carbon of the *N*-butyl chains is shown for clarity.[155, 156]

Since this discovery, Hahn and co-workers have prepared purely organometallic squares and rectangles, initially through stepwise syntheses by preforming the architecture bearing ditopic *o*-siloxyisocyanate ligands, before a subsequent acid-mediated deprotection and carbene generation, liberating protic NHC complexes (scheme 1.7). This has been demonstrated in a homoleptic fashion, by generating a Ir(III) square linked by isocyanate ligands,[160] or heteroleptic, by

preforming a dinuclear Pt(II)-NHC complex and interacting with the same isocyanate ligand.[161]
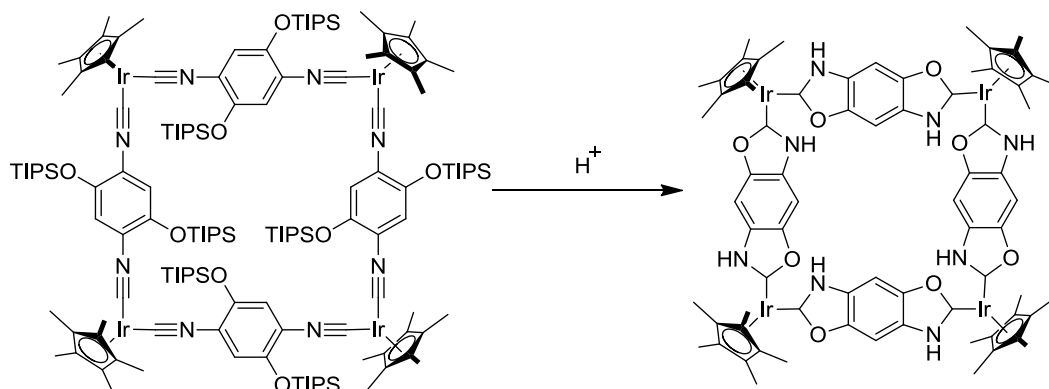
Scheme 1.7 Hahn's synthesis of a homoleptic molecular square.[160]

More recently, the same group have reported the one-step synthesis of homoleptic $[M_4L_4]^{n+}(PF_6)_n$ molecular squares with Pd^{II}-allyl or Ir^I-COD cornerpieces,[162] in a straightforward manner similar to Fujita's pioneering work in 1990.[15] The realisation that simple 2D shapes can be assembled through metal-carbene interactions under facile conditions may lead to the one-pot assembly of 3D polyhedra which have previously been thought of as inaccessible.

In addition to $[M_4L_4]^{n+}$ molecular squares and rectangles, Hahn and co-workers have also extensively investigated *bis*- and *poly*-NHC complexes of coinage metals (Cu, Ag, Au) for the preparation $[M_2L_2]^{2+}$ rectangles and 3D containers, preparing carbene ligands on a *tris*-1,3,5-imidazolylbenzene scaffold, similar to those reported by Kaim in the early 2000s.[163, 164] Divergent *bis*-imidazolium salts are well documented for their propensity to form dinuclear $[AgNHC_2]_2^+$ complexes when employed as a salt of a non-coordinating anion.[153, 165-167] Hahn and co-workers prepared a series of $[M_2L_2]^{2+}$ complexes incorporating functionality into the NHC scaffold, with reactive handles for postsynthetic modifications. A *bis*-imidazolium salt incorporating a *trans*-stilbene moiety was coordinated to Ag(I), yielding a $[M_2L_2]^{2+}$ $2PF_6^-$ rectangle, which upon irradiation at $\lambda = 365$ nm, a [2 + 2] cycloaddition occurred, yielding a cyclobutane (scheme 1.8). By constraining the two alkene groups so they are parallel to one another, this facilitates the [2 + 2] cycloaddition which would not occur should the two olefin units not be aligned in this manner. Treatment of the Ag(I)-NHC complexes with NH_4Cl reprotonated the carbene.[168] Instead of an internal stilbene-derived ligand, the same group prepared a *bis*-imidazolium salt with pendant coumarin groups, which

was coordinated to Ag(I), Au(I) and Cu(I).[169] Upon radiation with UV light at $\lambda = 365$ nm, a [2 + 2] cycloaddition of coumarin groups was initiated. The authors state that photodimerisation of coumarin typically yields four isomers, the *syn*-HH, *anti*-HH, *syn*-HT and *anti*-HT (H = head, T = tail). In the case of the molecular rectangles, only the *syn*-HH isomer was observed. Furthermore, irradiation of the photodimerised Au(I) complex at $\lambda = 365$ nm led to the reversible photocleavage of the cyclobutane groups, and regeneration of the coumarin-terminated rectangle. Recently, Hahn and co-workers have extended photocyclisation to $[M_3L_2]^{3+}$ molecular containers for the templation of 3D *hexakis*-imidazolium cages.[170] Huynh and co-workers have also utilised the $[Au_2L_2]$ rectangle motif using a more flexible ligand scaffold, bearing a pincer in the centre of the ligand scaffolds and behaves as a host to the BF4 anion.[171] Upon the addition of $CoCl_2 \cdot 6H_2O$, the flexible interior of the complex folds, leading to the formation of a heterobimetallic helicate.

λ = 365 nm

M= Ag, Au
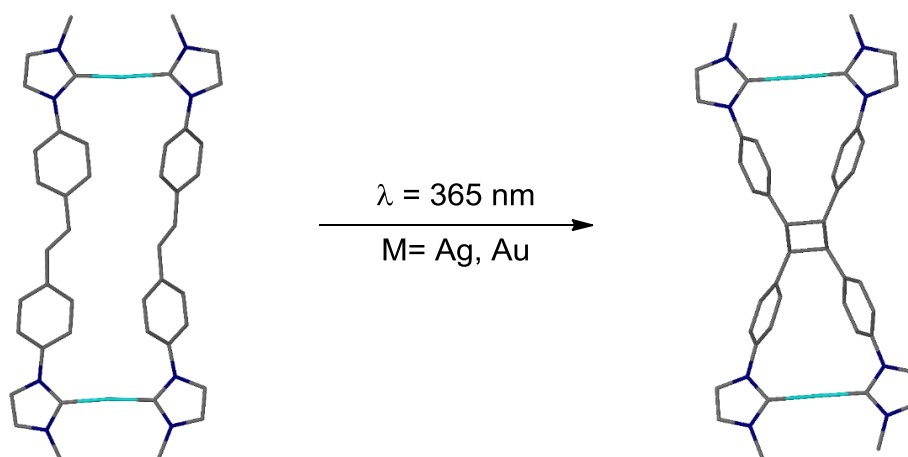
Scheme 1.8 Hahn's [2+2] cycloaddition of stilbene within a dinuclear metal-NHC complex.[168]

In 2002, Meyer and co-workers prepared the *tris*-imidazolium precursor 1,1,1-[tris-3-(methylimidazolium-1-yl)methyl]ethane tribromide, which upon coordination to Ag(I) after salt metathesis to the hexafluorophosphate salt, yielded a $[Ag_3L_2](PF_6)_3$ complex, seen as the first three-dimensional carbene complex.[172] By preparing imidazolium derivatives of similar systems to Kaim's disc shaped ligands,[163, 164] the preparation of organometallic cylinder-shaped assemblies has become possible by reaction of 1,3,5-tris-imidazolium-1-ylbenzene and 1,2,4,5-tetrakis-imidazolium-1-ylbenzene salts with Ag_2O. The first M_3L_2 and M_4L_2 hexacarbene and octacarbene cylinders were prepared by Hahn and co-workers in 2010, and their transmetallation onto Au(I) and Cu(I) investigated, whilst retaining

the cage topology (figure 1.15, left).[173, 174] In addition to cage synthesis by reaction of the imidazolium hexafluorophosphate with $Hg(OAc)_2$ or $[PdCl(allyl)]_2$ under basic conditions.[175, 176] A sterically crowded $[Ag_6L_2]$ cylinder was prepared with six imidazolium units bonded to a benzene core, and its transmetallation onto Au(I) was successful.[170] The aromatic core of *tris*-imidazolium salts can be further extended and coordination to Ag(I) remains successful, yielding nanometre-sized cylinders.[177] Transmetallation onto Au(I) or Cu(I) was again successful, with Au···Au separations of 1.1-1.4 nm. Peris and co-workers extended investigations by preparing a mesionic carbene-coordinated $[Ag_3L_2]^{3+}$ cylinder.[178] A 1:1 mixture of both Peris and Hahn's cylinders was dissolved in methanol, with the expectation of a statistical mixture of homoleptic and heteroleptic cages to be observed, but only the mixed ligand system was detected. Albrecht and co-workers also reported similar redistribution of ligands in Au(I)-mesionic carbene complexes in a similar fashion to that observed by Peris and co-workers in the presence of $AgBF_4$ during an Au(I) catalysed aldol condensation, caused by an Ag(I) carbene transfer and Au(I) dissociation.[179] These NHC and MIC ligands have since been coordinated to Ni(II), Ir(I), Rh(I), Pd(II) and Ir(III) as a flat disk-type complexes, and in the case of Pd(II) and Ir(III), were generally slightly better catalysts than monometallic analogues, as reported by Sarkar and co-workers (figure 1.15, right).[180-182]
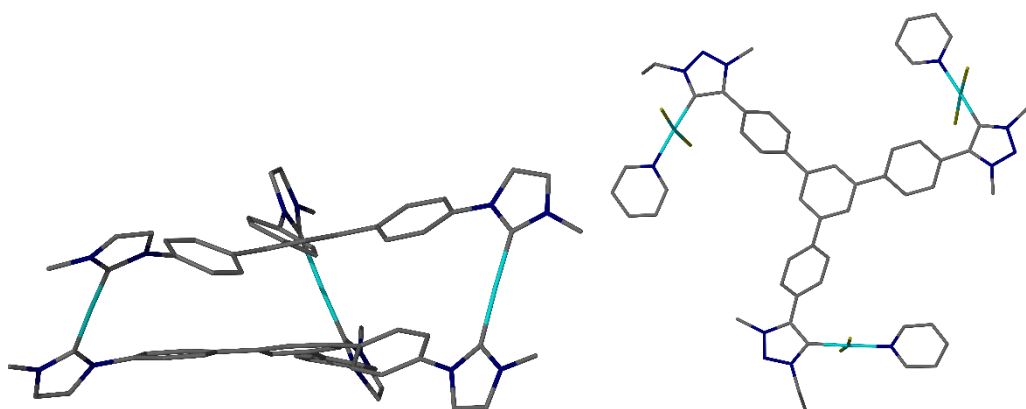
Figure 1.15 Left: Hahn's $[Ag_3L_2]^{3+}$ molecular container.[173] Right: Sarkar's Pd(II)-abnormal NHC complex bearing a C_3-symmetric disk-shaped ligand.[182]

A recent study by Hahn and co-workers contrasts the results published by Peris *et al.*, Ag_2O was added to a 1:1:1 ratio of three imidazolium salts with identical coordination modes, but different size arene spacers between them, and only homoleptic Ag_3L_2 cylinders were observed by HRMS and ^1H NMR spectroscopy.[183]

Furthermore, the transmetallation of the homoleptic cages onto Au(I) was carried with retention of architectures.

Narcissistic self-sorting was also observed in a similar reaction between Ag_2O and a 1:1 ratio of similarly sized *tris-* and *tetrakis-*imidazolium salts, and again only homoleptic complexes were obtained with high fidelity. Narcissistic self-sorting is a phenomenon in supramolecular chemistry that has primarily been observed for Werner-type systems, such as Lehn's helicates,[10] which are able to self-correct if the thermodynamic product does not form initially. Narcissistic self-sorting of M-C bonds had not previously been studied, mainly because the vast majority of organometallic interactions are non-reversible and therefore unable to correct. Labile Ag-NHC interactions are an exception to this and have led to their implementation as supramolecular building blocks, elegantly combining organometallic chemistry and self-assembly.

One method to access poly-NHC complexes is to employ flat, polyaromatic imidazolium salts as ligands. Peris and co-workers have used triphenylene-functionalised imidazolium salts to prepare C_3-symmetric Pd(II) and Au(I) complexes, which have proven to be highly active in catalytic reactions, and more so than monometallic analogs.[184] However, electrochemical and DFT calculations on Rh(I) complexes using the same ligand set suggested electronic communication between metals is negligible, and stereoelectronic properties are comparable to a monometallic benzimidazol-2-ylidene complex.[185] Catalytic enhancement may instead be through metal centres being closer in proximity due to extensive π-π stacking interactions between complexes.[186] More recent developments have been in the extension of the π system, both through increased conjugation and the incorporation of nitrogen atoms in a hexaazatriphenylene system.[187]

In addition to C_{3v}-symmetric flat carbene complexes, Peris and co-workers have also studied Pd(II) and Au(I) complexes of a D_{3h}-symmetric triptycene-fused *tris*-carbene, which was crystallographically elucidated by Bielawski and co-workers in 2010.[184, 188] In collaboration with Kuck, Peris prepared a tribenzotriquinacene-fused (TBTQ) carbene complex of Rh(I) (the crystal structure or the imidazolium salt is displayed in figure 1.16).[189] TBTQ is a fused C_3-symmetric cavitand closely related to cyclotriveratrylene. The authors stated that

due to high steric repulsion, different Rh(I) local environments existed and free rotation about the Rh(I) centre was unlikely. This was backed up by $^{13}C\{^{1}H\}$ NMR spectroscopy.
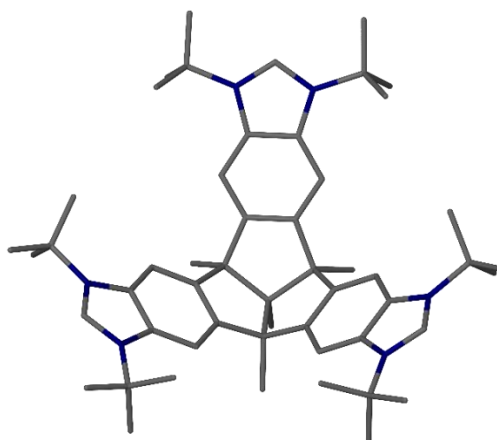
Figure 1.16 Kuck's TBTQ-annulated imidazolium salt.[189]

Employing calixarenes and resorcinarenes as a wingtip for NHC ligands has extensively been studied throughout the past ten years, with most examples involving Pd(II). First investigating phosphine derivatives, Matt and Brenner prepared a calix[4]arene monophosphine, which behaved as a ligand towards Pd(II) as a precatalyst. This phosphine complex could catalyse the Suzuki-Miyaura reaction with TOF values often >200,000 in a number of screens.[190] Later studies focused on extending the family from phosphines to NHC ligands. A family of calix[4]arenylimidazolium salts were prepared, and their coordination to Pd(II) investigated. Mono-NHC complexes with similar coordination modes to the PEPPSI family and [Pd(NHC)$_2$(Br)$_2$] complexes have also been investigated as catalysts.[191] Complexes were still highly active at catalysing the Suzuki-Miyaura reaction, with quantitative results at 0.1 mol% loading. Bis-NHC complexes bridging across the upper-rim of the same cavitand were also targeted and still displayed 'breathing' of the calixarene backbone, but were poorly active, presumably because of a reduced disposition to reductively eliminate substrates during catalysis when the two NHC ligands coordinated *trans* with respect to one another. The phosphine complexes did display supramolecular enhancement to catalysis, with much higher activities displayed than small phosphines, whereas the NHC complexes in this case displayed similar activities to much smaller analogues, suggesting the calixarene was not behaving as a receptor, and simply performing as a bulky ligand.
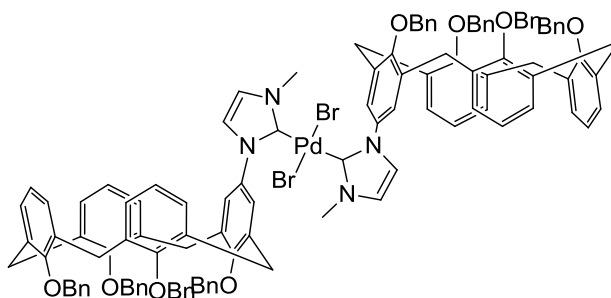
Figure 1.17 Matt and Toupet's calix[4]arene-NHC complex.[191]

Willans and co-workers have also investigated Pd(II)-NHC complexes incorporating calix[4]arene groups, on this occasion focusing on tetranuclear complexes.[192] Decreasing the catalyst loading led to increased turnover numbers (TON) in the Suzuki-Miyaura reaction of 4-bromotoluene and phenylboronic acid. This behaviour has been coined as homeopathic by de Vries and co-workers.[193] As well as calixarenes, Pd(II), Ni(II) and Cu(I) resorcin[4]arene derivatives, both tethered with phosphines[194] and imidazolium species,[195-199] have also been studied in a range of catalytic reactions with similar results. Chianese has prepared an Ir(I)-NHC complex, with the NHC wingtip being dendritic side groups which form a bowl-shaped assembly.[200] The Ir(I)-NHC complex displayed shape-selectivity when carrying out the hydrosilylation on a mixture of ketones.

The fusion of NHC ligands and rigid cavitands in the CTV family are limited to Kuck and Peris' Rh(I) complex fused onto the TBTQ scaffold,[189] and Hardie's metallo-cryptophanes decorated with *bis*-NHC ligands (figure 1.8). Employment of alternative *cis*-protecting units such as ethylenediamines led to rearrangement of the M_3L_2 metallo-cryptophane to M_6L_8 stellated octahedral assemblies (figure 1.9).[78]

NHCs have also been incorporated into rotaxane systems. Huynh and co-workers have studied the reactivity of bridged Pd(II)-NHC dimers, in particular their reactivity towards nucleophiles, and in catalysis.[201] Upon reaction with ditopic *bis*-pyridines, the Pd(II) dimer can be split, leading to the formation of a dinuclear complex terminated by a Pd(II)-NHC. The same bis-pyridine chain can behave as an axle in [2]-pseudorotaxane formation, and upon reaction with the Pd(II) dimer, cap the pyridyl termini and construct a [2]-rotaxane.[202]

In 2015, Pöthig and co-workers reported the synthesis of the macrocycle calix[4]imidazolium[2]pyrazole, bearing four imidazolium units and two pyrazoles linked by methylene spacers, along with its coordination to Ni(II), yielding a

dinuclear saddle-shaped complex.[203] Upon addition of a halide source, the Ni(II) complex encapsulates one halide ion, forming a capsoplex by encompassing one guest within two saddle-shaped molecules which assemble in a tennis-ball motif.[204] Upon reaction of the macrocycle with Ag_2O, an $[Ag_8L_2]^{8+}$ complex assembles, coined as a pillarplex, bearing eight Ag-NHC interactions and eight Ag-pyrazole links.[205] Pillarplexes are highly functional materials and upon anion exchange can be tuned to exhibit aqueous or organic solubility. In addition, the octanuclear carbene complex was successfully transmetallated onto Au(I), with the Au(I)-pillarplex being luminescent.[205] This class of cavitand behaves as a host towards linear guests such as 1,8-diaminooctane in aqueous media. A more recent study into the Ag(I) pillarplex involved the preparation of an organometallic [2]-rotaxane in excellent yield by threading a longer alkyl chain and capping.[206] Upon altering the pH of the system, it is possible to cycle between an organometallic [2]-rotaxane and organic [3]-rotaxane by repeatedly regenerating the imidazolium salt and subsequent deprotonations (scheme 1.9).
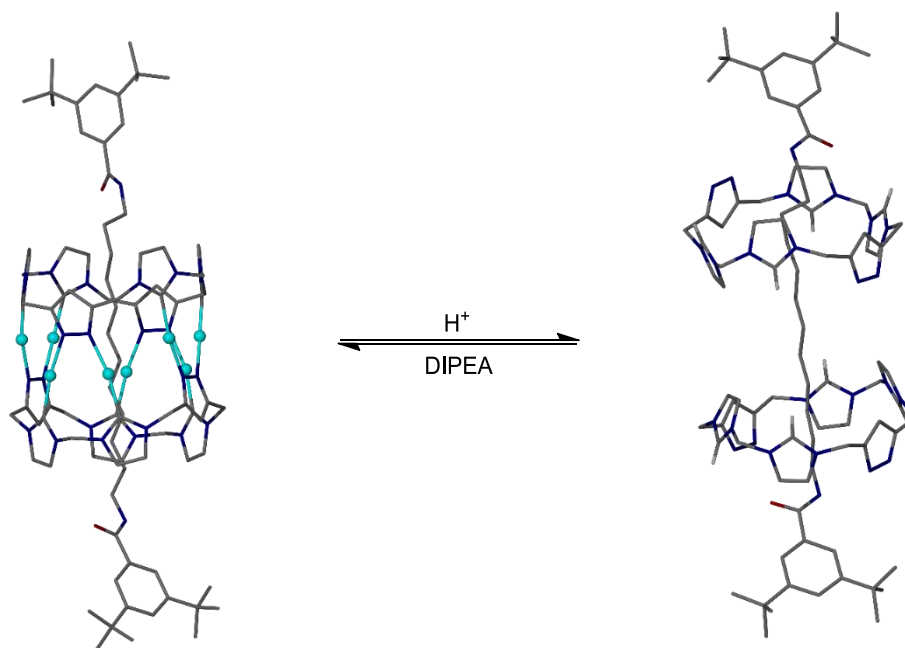
Scheme 1.9 Pothig's organometallic [2]-rotaxane (left) and organic [3]-rotaxane (right) after treatment with acid.[206]

1.3 Project outline

This project deals with preparing new azole-functionalised cyclotriveratrylenes. The vast majority of literature precedent involving metallo-supramolecular architectures built upon CTV scaffolds deal with pyridyl donor systems, and save Ag(I) assemblies, the rationale behind their assembly with well-defined metal centres and prediction of topology is becoming better understood. Five-membered ring systems offer the potential to coordinate to metals at different angles to their pyridyl counterparts, with respect to the CTV bowl, which in turn could allow accessibility towards larger metallo-supramolecular cages currently not attainable using the pyridyl ligands.

Furthermore, azoles are precursors to NHC ligands. The use of hybrid carbene-cavitand systems has, in a number of cases, led to extremely active complexes in catalytic transformations, namely Pd(II) or Ni(II) catalysed cross-coupling reactions.[191, 194-199] The flexible calix[4]arene and resorcin[4]arene scaffolds have dominated this field, whereas use of the rigid CTV cavitand has not been previously reported beyond a C_1 imidazolium salt used as an organocatalyst in Michael additions.[207] A number of multimetallic complexes using disk-shaped ligands have been reported, and their behaviour as catalysts compared to monometallic analogues, but comparative studies investigating cavitand complexes are limited to conformationally flexible hosts. Therefore, it would be of interest to investigate whether CTV-functionalised carbene complexes are superior catalysts to monometallic analogues, and if so, rationalise reasoning behind this and whether supramolecular factors regarding either (a) the cavitand or (b) communication between metal centres can enhance catalysis in such cases.

1.4 References

1.   K.-T. Tang, J. P. Toennies, *Angew. Chem. Int. Ed.*, 2010, **49**, 9574-9579.

2.   H. Kunz, *Angew. Chem. Int. Ed.*, 2002, **41**, 4439-4451.

3.   The Nobel Prize in Chemistry, **1987**,
        https://www.nobelprize.org/nobel_prizes/chemistry/laureates/1987/

4.   J. D. Watson, F. H. C. Crick, *Cold Spring Harbor Symposia on Quantitative Biology*, 1953, **18**, 123-131.

5.   C. Mao, W. Sun, Z. Shen, N. C. Seeman, *Nature*, 1999, **397**, 144.

6.   C. J. Pedersen, *J. Am. Chem. Soc.*, 1967, **89**, 2495-2496.

7.   C. Pedersen, *J. Inclusion Phenom.*, 1988, **6**, 337-350.

8.   J. Canceill, A. Collet, J. Gabard, F. Kotzyba-Hibert, J. M. Lehn, *Helv. Chim. Acta*, 1982, **65**, 1894-1897.

9.   L. Echegoyen, E. Perez-Cordero, J. B. Regnouf de Vains, C. Roth, J. M. Lehn, *Inorg. Chem.*, 1993, **32**, 572-577.

10. J. M. Lehn, A. Rigault, J. Siegel, J. Harrowfield, B. Chevrier, D. Moras, *Proc. Nat. Acad. Sci.*, 1987, **84**, 2565-2569.

11. R. Kramer, J. M. Lehn, A. Marquis-Rigault, *Proc. Nat. Acad. Sci.*, 1993, **90**, 5394.

12. B. Hasenknopf, J.-M. Lehn, B. O. Kneisel, G. Baum, D. Fenske, *Angew. Chem. Int. Ed.*, 1996, **35**, 1838-1840.

13. J.-F. Ayme, J. E. Beves, D. A. Leigh, R. T. McBurney, K. Rissanen, D. Schultz, *Nat. Chem*, 2012, **4**, 15-20.

14. R. Chakrabarty, P. S. Mukherjee, P. J. Stang, *Chem. Rev.*, 2011, **111**, 6810-6918.

15. M. Fujita, J. Yazaki, K. Ogura, *J. Am. Chem. Soc.*, 1990, **112**, 5645-5647.

16. H. V. R. Dias, H. V. K. Diyabalanage, M. A. Rawashdeh-Omary, M. A. Franzman, M. A. Omary, *J. Am. Chem. Soc.*, 2003, **125**, 12072-12073.

17. P. J. Stang, N. E. Persky, J. Manna, *J. Am. Chem. Soc.*, 1997, **119**, 4777-4778.

18. D. L. Caulder, R. E. Powers, T. N. Parac, K. N. Raymond, *Angew. Chem., Int. Ed.*, 1998, **37**, 1840-1843.

19. M. Ziegler, J. L. Brumaghim, K. N. Raymond, *Angew. Chem. Int. Ed.*, 2000, **39**, 4119-4121.

20. P. Mal, D. Schultz, K. Beyeh, K. Rissanen, J. R. Nitschke, *Angew. Chem. Int. Ed.*, 2008, **47**, 8297-8301.

21. J. R. Nitschke, *Acc. Chem. Res.*, 2007, **40**, 103-112.

22. P. Mal, B. Breiner, K. Rissanen, J. R. Nitschke, *Science*, 2009, **324**, 1697-1699.

23. D. Yang, J. Zhao, L. Yu, X. Lin, W. Zhang, H. Ma, A. Gogoll, Z. Zhang, Y. Wang, X.-J. Yang, B. Wu, *J. Am. Chem. Soc.*, 2017, **139**, 5946-5951.

24. S. Roche, C. Haslam, S. L. Heath, J. A. Thomas, *Chem. Commun.*, 1998, 1681-1682.

25. W. J. Ramsay, F. T. Szczypiński, H. Weissman, T. K. Ronson, M. M. J. Smulders, B. Rybtchinski, J. R. Nitschke, *Angew. Chem. Int. Ed.*, 2015, **54**, 5636-5640.

26. M. M. J. Smulders, A. Jiménez, J. R. Nitschke, *Angew. Chem. Int. Ed.*, 2012, **51**, 6681-6685.

27. M. Fujita, K. Umemoto, M. Yoshizawa, N. Fujita, T. Kusukawa, K. Biradha, *Chem. Commun.*, 2001, 509-518.

28. M. Fujita, D. Oguro, M. Miyazawa, H. Oka, K. Yamaguchi, K. Ogura, *Nature*, 1995, **378**, 469-471.

29. T. Kusukawa, M. Fujita, *J. Am. Chem. Soc.*, 2002, **124**, 13576-13582.

30. T. Kusukawa, M. Fujita, *J. Am. Chem. Soc.*, 1999, **121**, 1397-1398.

31. M. Yoshizawa, M. Tamura, M. Fujita, *Science*, 2006, **312**, 251-254.

32. M. Tominaga, K. Suzuki, M. Kawano, T. Kusukawa, T. Ozeki, S. Sakamoto, K. Yamaguchi, M. Fujita, *Angew. Chem. Int. Ed.*, 2004, **43**, 5621-5625.

33. Q.-F. Sun, J. Iwasa, D. Ogawa, Y. Ishido, S. Sato, T. Ozeki, Y. Sei, K. Yamaguchi, M. Fujita, *Science*, 2010, **328**, 1144-1147.

34. D. Fujita, Y. Ueda, S. Sato, H. Yokoyama, N. Mizuno, T. Kumasaka, M. Fujita, *Chem*, 2016, **1**, 91-101.

35. D. Fujita, Y. Ueda, S. Sato, N. Mizuno, T. Kumasaka, M. Fujita, *Nature*, 2016, **540**, 563.

36. B. Olenyuk, J. A. Whiteford, A. Fechtenkötter, P. J. Stang, *Nature*, 1999, **398**, 796.

37. T. Z. Xie, K. Guo, Z. Guo, W. Y. Gao, L. Wojtas, G. H. Ning, M. Huang, X. Lu, J. Y. Li, S. Y. Liao, Y. S. Chen, C. N. Moorefield, M. J. Saunders, S. Z. D. Cheng, C. Wesdemiotis, G. R. Newkome, *Angew. Chem. Int. Ed.*, 2015, **54**, 9224-9229.

38. Y. Liu, C. Hu, A. Comotti, M. D. Ward, *Science*, 2011, **333**, 436-440.

39. D. J. Cram, *Science*, 1983, **219**, 1177-1183.

40. C. D. Gutsche, R. Muthukrishnan, *J. Org. Chem.*, 1978, **43**, 4905-4906.

41. C. D. Gutsche, J. A. Levine, *J. Am. Chem. Soc.*, 1982, **104**, 2652-2653.

42. C. D. Gutsche, M. Iqbal, D. Stewart, *J. Org. Chem.*, 1986, **51**, 742-745.

43. C. D. Gutsche, L. J. Bauer, *J. Am. Chem. Soc.*, 1985, **107**, 6052-6059.

44. M. Coletta, R. McLellan, S. Sanz, K. J. Gagnon, S. J. Teat, E. K. Brechin, S. J. Dalgarno, *Chem. Eur. J.*, 2017, **23**, 14073-14079.

45. M. Coletta, S. Sanz, L. J. McCormick, S. J. Teat, E. K. Brechin, S. J. Dalgarno, *Dalton Trans.*, 2017, **46**, 16807

46. M. Yamanaka, Y. Yamada, Y. Sei, K. Yamaguchi, K. Kobayashi, *J. Am. Chem. Soc*, 2006, **128**, 1531-1539.

47. T. Haino, M. Kobayashi, M. Chikaraishi, Y. Fukazawa, *Chem. Commun.*, 2005, 2321-2323.

48. S. Pasquale, S. Sattin, E. C. Escudero-Adán, M. Martínez-Belmonte, J. de Mendoza, *Nat. Commun.*, 2012, **3**, 785.

49. J. W. Steed, P. C. Junk, J. L. Atwood, M. J. Barnes, C. L. Raston, R. S. Burkhalter, *J. Am. Chem. Soc*, 1994, **116**, 10346-10347.

50. M. J. Hardie, C. L. Raston, *Chem. Commun.*, 1999, 1153-1163.

51. A. S. Lindsey, *J. Chem. Soc.*, 1965, 1685-1692.

52. G. M. Robinson, *J. Chem. Soc., Trans.*, 1915, **107**, 267-276.

53. B. F. Abrahams, N. J. FitzGerald, T. A. Hudson, R. Robson, T. Waters, *Angew. Chem. Int. Ed.*, 2009, **48**, 3129-3132.

54. J. J. Loughrey, N. J. Patmore, A. Baldansuren, A. J. Fielding, E. J. L. McInnes, M. J. Hardie, S. Sproules, M. A. Halcrow, *Chem. Sci.*, 2015, **6**, 6935-6948.

55. N. B. McKeown, B. Gahnem, K. J. Msayib, P. M. Budd, C. E. Tattershall, K. Mahmood, S. Tan, D. Book, H. W. Langmi, A. Walton, *Angew. Chem. Int. Ed.*, **45**, 1804-1807.

56. J. J. Henkelis, M. J. Hardie, *Chem. Commun.*, 2015, **51**, 11929-11943.

57. Nuriman, B. Kuswandi, W. Verboom, *Anal. Chim. Acta*, 2009, **655**, 75-79.

58. O. Lafon, P. Lesot, H. Zimmermann, R. Poupko, Z. Luz, *J. Phys. Chem. B*, 2007, **111**, 9453-9467.

59.   J. Canceill, A. Collet, J. Gabard, G. Gottarelli, G. P. Spada, *J. Am. Chem. Soc*, 1985, **107**, 1299-1308.

60.   S. Kai, T. Kojima, F. Thorp-Greenwood, M. Hardie, S. Hiraoka, *Chem. Sci.*, 2018, DOI: 10.1039/C8SC01062E

61.   J. Gabard, A. Collet, *J. Chem. Soc., Chem. Commun.*, 1981, 1137-1139.

62.   T. Brotin, J.-P. Dutasta, *Chem. Rev.*, 2009, **109**, 88-130.

63.   A. Collet, *Tetrahedron*, 1987, **43**, 5725-5759.

64.   S. T. Mough, J. C. Goeltz, K. T. Holman, *Angew. Chem. Int. Ed.*, 2004, **43**, 5631-5635.

65.   J. Canceill, L. Lacombe, A. Collet, *J. Am. Chem. Soc.*, 1985, **107**, 6993-6996.

66.   M. A. Little, J. Donkin, J. Fisher, M. A. Halcrow, J. Loder, M. J. Hardie, *Angew. Chem. Int. Ed.*, 2012, **51**, 764-766.

67.   L. Garel, H. Vezin, J.-P. Dutasta, A. Collet, *Chem. Commun.*, 1996, 719-720.

68.   C. Garcia, D. Humiliere, N. Riva, A. Collet, J.-P. Dutasta, *Org. Biomol. Chem.*, 2003, **1**, 2207-2216.

69.   K. Bartik, M. Luhmer, J.-P. Dutasta, A. Collet, J. Reisse, *J. Am. Chem. Soc.*, 1998, **120**, 784-791.

70.   A. I. Joseph, G. El-Ayle, C. Boutin, E. Leonce, P. Berthault, K. T. Holman, *Chem. Commun.*, 2014, **50**, 15905-15908.

71.   R. M. Fairchild, K. T. Holman, *J. Am. Chem. Soc.*, 2005, **127**, 16364-16365.

72.   K. Travis Holman, G. William Orr, J. L. Atwood, J. W. Steed, *Chem. Commun.*, 1998, 2109-2110.

73.   K. T. Holman, J. L. Atwood, J. W. Steed, *Angew. Chem. Int. Ed.*, 1997, **36**, 1736-1738.

74.   K. T. Holman, M. M. Halihan, S. S. Jurisson, J. L. Atwood, R. S. Burkhalter, A. R. Mitchell, J. W. Steed, *J. Am. Chem. Soc.*, 1996, **118**, 9567-9576.

75.   Z. Zhong, A. Ikeda, S. Shinkai, S. Sakamoto, K. Yamaguchi, *Org. Lett.*, 2001, **3**, 1085-1087.

76.   A. Schaly, Y. Rousselin, J. C. Chambron, E. Aubert, E. Espinosa, *Eur. J. Inorg. Chem.*, 2016, 832-843.

77.   V. E. Pritchard, D. R. Martir, S. Oldknow, S. Kai, S. Hiraoka, N. J. Cookson, E. Zysman-Colman, M. J. Hardie, *Chem. Eur. J.*, 2017, **23**, 6290-6294.

78.   J. J. Henkelis, C. J. Carruthers, S. E. Chambers, R. Clowes, A. I. Cooper, J. Fisher, M. J. Hardie, *J. Am. Chem. Soc.*, 2014, **136**, 14393-14396.

79.   J. J. Henkelis, T. K. Ronson, L. P. Harding, M. J. Hardie, *Chem. Commun.*, 2011, **47**, 6560-6562.

80.   S. T. Mough, K. T. Holman, *Chem. Commun.*, 2008, 1407-1409.

81.   R. M. Fairchild, A. I. Joseph, K. T. Holman, H. A. Fogarty, T. Brotin, J.-P. Dutasta, C. Boutin, G. Huber, P. Berthault, *J. Am. Chem. Soc.*, 2010, **132**, 15505-15507.

82.   T. K. Ronson, J. Fisher, L. P. Harding, M. J. Hardie, *Angew. Chem. Int. Ed.*, 2007, **46**, 9086-9088.

83. N. J. Cookson, J. J. Henkelis, R. J. Ansell, C. W. G. Fishwick, M. J. Hardie, J. Fisher, *Dalton Trans.*, 2014, **43**, 5657-5661.

84. J. J. Henkelis, J. Fisher, S. L. Warriner, M. J. Hardie, *Chem. Eur. J.*, 2014, **20**, 4117-4125.

85. C. J. Sumby, M. J. Hardie, *Angew. Chem. Int. Ed.*, 2005, **44**, 6395-6399.

86. C. J. Sumby, J. Fisher, T. J. Prior, M. J. Hardie, *Chem. Eur. J.*, 2006, **12**, 2945-2959.

87. C. J. Sumby, M. J. Carr, A. Franken, J. D. Kennedy, C. A. Kilner, M. J. Hardie, *New J. Chem.*, 2006, **30**, 1390-1396.

88. C. Carruthers, T. K. Ronson, C. J. Sumby, A. Westcott, L. P. Harding, T. J. Prior, P. Rizkallah, M. J. Hardie, *Chem. Eur. J.*, 2008, **14**, 10286-10296.

89. B. F. Abrahams, N. J. FitzGerald, R. Robson, *Angew. Chem. Int. Ed.*, 2010, **49**, 2896-2899.

90. B. F. Abrahams, B. A. Boughton, N. J. FitzGerald, J. L. Holmes, R. Robson, *Chem. Commun.*, 2011, **47**, 7404-7406.

91. T. K. Ronson, J. Fisher, L. P. Harding, P. J. Rizkallah, J. E. Warren, M. J. Hardie, *Nat. Chem*, 2009, **1**, 212-216.

92. F. L. Thorp-Greenwood, A. N. Kulak, M. J. Hardie, *Nat. Chem*, 2015, **7**, 526-531.

93. R. Breslow, P. Campbell, *Bioorg. Chem.*, 1971, **1**, 140-156.

94. C. J. Walter, H. L. Anderson, J. K. M. Sanders, *J. Chem. Soc., Chem. Commun.*, 1993, 458-460.

95. R. J. Hooley, J. Rebek Jr, *Org. Biomol. Chem.*, 2007, **5**, 3631-3636.

96. T. Murase, S. Peschard, S. Horiuchi, Y. Nishioka, M. Fujita, *Supramol. Chem.*, 2011, **23**, 199-208.

97. J. L. Bolliger, A. M. Belenguer, J. R. Nitschke, *Angew. Chem. Int. Ed.*, 2013, **52**, 7958-7962.

98. W. Cullen, M. C. Misuraca, C. A. Hunter, N. H. Williams, M. D. Ward, *Nat. Chem*, 2016, **8**, 231-236.

99. D. Fiedler, R. G. Bergman, K. N. Raymond, *Angew. Chem. Int. Ed.*, 2004, **43**, 6748-6751.

100. D. Fiedler, H. van Halbeek, R. G. Bergman, K. N. Raymond, *J. Am. Chem. Soc.*, 2006, **128**, 10240-10252.

101. D. M. Dalton, S. R. Ellis, E. M. Nichols, R. A. Mathies, F. D. Toste, R. G. Bergman, K. N. Raymond, *J. Am. Chem. Soc.*, 2015, **137**, 10128-10131

102. C. J. Hastings, M. D. Pluth, R. G. Bergman, K. N. Raymond, *J. Am. Chem. Soc.*, 2010, **132**, 6938-6940.

103. D. H. Leung, R. G. Bergman, K. N. Raymond, *J. Am. Chem. Soc.*, 2006, **128**, 9781-9797.

104. D. H. Leung, R. G. Bergman, K. N. Raymond, *J. Am. Chem. Soc.*, 2007, **129**, 2746-2747.

105. V. F. Slagt, J. N. H. Reek, P. C. J. Kamer, P. W. N. M. v. Leeuwen, *Angew. Chem. Int. Ed.*, 2001, **40**, 4271-4274.

106. C. García-Simón, R. Gramage-Doria, S. Raoufmoghaddam, T. Parella, M. Costas, X. Ribas, J. N. H. Reek, *J. Am. Chem. Soc.*, 2015, **137**, 2680-2687.

107. T. Evan-Salem, I. Baruch, L. Avram, Y. Cohen, L. C. Palmer, J. Rebek, *Proc. Nat. Acad. Sci.*, 2006, **103**, 12296-12300.

108. A. Cavarzan, A. Scarso, P. Sgarbossa, G. Strukul, J. N. H. Reek, *J. Am. Chem. Soc.*, 2011, **133**, 2848-2851.

109. D. Zhang, A. Martinez and J. P. Dutasta, *Chem. Rev*, 2017, **117**, 4900-4942.

110. A. Martinez, J.-P. Dutasta, *J. Catal.*, 2009, **267**, 188-192.

111. A. Martinez, V. Robert, H. Gornitzka, J. P. Dutasta, *Chem. Eur. J.*, 2010, **16**, 520-527.

112. D. Zhang, K. Jamieson, L. Guy, G. Gao, J.-P. Dutasta, A. Martinez, *Chem. Sci.*, 2017, **8**, 789-794.

113. Y. Makita, K. Sugimoto, K. Furuyoshi, K. Ikeda, S.-i. Fujiwara, T. Shin-ike, A. Ogawa, *Inorg. Chem.*, 2010, **49**, 7220-7222.

114. Y. Makita, K. Ikeda, K. Sugimoto, T. Fujita, T. Danno, K. Bobuatong, M. Ehara, S.-i. Fujiwara, A. Ogawa, *J. Organomet. Chem.*, 2012, **706-707**, 26-29.

115. Y. Makita, T. Fujita, T. Danno, M. Inoue, M. Ueshima, S.-i. Fujiwara, A. Ogawa, in *Supramol. Cat.*, 2013, **1**, 9-11

116. O. Perraud, A. B. Sorokin, J.-P. Dutasta, A. Martinez, *Chem. Commun.*, 2013, **49**, 1288-1290.

117. D. Bourissou, O. Guerret, F. P. Gabbai, G. Bertrand, *Chem. Rev.*, 2000, **1**, 39-92

118. E. O. Fischer, A. Maasböl, *Angew. Chem. Int. Ed.*, 1964, **3**, 580-581.

119. R. R. Schrock, *J. Am. Chem. Soc.*, 1974, **96**, 6796-6797.

120. C. Boehme, G. Frenking, *J. Am. Chem. Soc.*, 1996, **118**, 2039-2046.

121. A. R. Cochrane, C. Idziak, W. J. Kerr, B. Mondal, L. C. Paterson, T. Tuttle, S. Andersson, G. N. Nilsson, *Org. Biomol. Chem.*, 2014, **22**, 3598-3603.

122. R. Breslow, *J. Am. Chem. Soc.*, 1957, **79**, 1762-1763.

123. H. W. Wanzlick, *Angew. Chem. Int. Ed.*, 1962, **1**, 75-80.

124. H. W. Wanzlick, H. J. Schönherr, *Angew. Chem. Int. Ed.*, 1968, **7**, 141-142.

125. K. Öfele, *J. Organomet. Chem.*, 1968, **12**, P42-P43.

126. A. J. Arduengo, *J. Am. Chem. Soc.*, 1991, 113, 361-363

127. J. Huang, E. D. Stevens, S. P. Nolan, J. L. Petersen, *J. Am. Chem. Soc.*, 1999, **121**, 2674-2678.

128. M. Scholl, T. M. Trnka, J. P. Morgan, R. H. Grubbs, *Tetrahedron Lett.*, 1999, **40**, 2247-2250.

129. P. de Frémont, N. M. Scott, E. D. Stevens, S. P. Nolan, *Organometallics*, 2005, **24**, 2411-2418.

130. D. J. Nelson, *Eur. J. Inorg. Chem.*, 2015, **12**, 2012-2027.

131. C. J. O'Brien, E. A. B. Kantchev, C. Valente, N. Hadei, G. A. Chass, A. Lough, A. C. Hopkinson, M. G. Organ, *Chem. Lett.*, 2006, **12**, 4743-4748.

132. C. D. Abernethy, H. Alan, Cowley, R. A. Jones, *J. Organomet. Chem.*, 2000, **596**, 3-5.

133. H. M. J. Wang, I. J. B. Lin, *Organometallics*, 1998, **17**, 972-975.

134. S. Calimsiz, M. G. Organ, *Chem. Commun.*, 2011, **47**, 5181-5183.

135. S. Calimsiz, M. Sayah, D. Mallik, M. G. Organ, *Angew. Chem., Int. Ed.*, 2010, **49**, 2014-2017

136. M. G. Organ, S. Calimsiz, M. Sayah, K. H. Hoi, A. J. Lough, *Angew. Chem. Int. Ed.*, 2009, **48**, 2383-2387.

137. M. Pompeo, R. D. J. Froese, N. Hadei, M. G. Organ, *Angew. Chem. Int. Ed.*, 2012, **51**, 11354-11357.

138. G. A. Price, A. R. Bogdan, A. L. Aguirre, T. Iwai, S. W. Djuric, M. G. Organ, *Catal. Sci. Technol.*, 2016, **6**, 4733-4742.

139. C. Valente, S. Calimsiz, K. H. Hoi, D. Mallik, M. Sayah, M. G. Organ, *Angew. Chem. Int. Ed.*, 2012, **51**, 3314-3332.

140. C. Lombardi, J. Day, N. Chandrasoma, D. Mitchell, M. J. Rodriguez, J. L. Farmer, M. G. Organ, *Organometallics*, 2017, **36**, 251-254.

141. C. Lombardi, D. Mitchell, M. J. Rodriguez, M. G. Organ, *Eur. J. Org. Chem.*, 2017, **2017**, 1510-1513.

142. M. G. Organ, M. Abdel-Hadi, S. Avola, I. Dubovyk, N. Hadei, E. A. B. Kantchev, C. J. O'Brien, M. Sayah, C. Valente, *Chem. Eur. J.*, 2008, **14**, 2443-2452.

143. C. Valente, M. Pompeo, M. Sayah, M. G. Organ, *Org. Process Res. Dev.*, 2014, **18**, 180-190.

144. J. L. Farmer, H. N. Hunter, M. G. Organ, *J. Am. Chem. Soc.*, 2012, **134**, 17470-17473.

145. L. Benhamou, C. Besnard, E. P. Kündig, *Organometallics*, 2014, **33**, 260-266.

146. J. Wencel-Delord, T. Droge, F. Liu, F. Glorius, *Chem. Soc. Rev.*, 2011, **40**, 4740-4761.

147. M. Anand, R. B. Sunoj, H. F. Schaefer, *J. Am. Chem. Soc.*, 2014, **136**, 5535-5538.

148. H. M. Sun, Q. Shao, D. M. Hu, W. F. Li, Q. Shen, Y. Zhang, *Organometallics*, 2005, **24**, 331-334.

149. L.-Z. Xie, H.-M. Sun, D.-M. Hu, Z.-H. Liu, Q. Shen, Y. Zhang, *Polyhedron*, 2009, **28**, 2585-2590.

150. V. Ritleng, A. M. Oertel, M. J. Chetcuti, *Dalton Trans.*, 2010, **39**, 8153-8160.

151. A. J. Arduengo, III, H. V. R. Dias, J. C. Calabrese, F. Davidson, *Organometallics*, 1993, **12**, 3405-3409.

152. H. M. J. Wang, I. J. B. Lin, *Organometallics*, 1998, **17**, 972-975.

153. J. C. Y. Lin, R. T. W. Huang, C. S. Lee, A. Bhattacharyya, W. S. Hwang, I. J. B. Lin, *Chem. Rev.*, 2009, **109**, 3561-3598.

154. N. Sinha, F. E. Hahn, *Acc. Chem. Res.*, 2017, **50**, 2167-2184.

155. F. E. Hahn, C. Radloff, T. Pape, A. Hepp, *Organometallics*, 2008, **27**, 6408-6410.

156. V. Martínez-Agramunt, S. Ruiz-Botella, E. Peris, *Chem. Eur. J.*, 2017, **23**, 6675-6681.

157. Y.-F. Han, G.-X. Jin, *Acc. Chem. Res.*, 2014, **47**, 3571-3579.

158. Y.-F. Han, H. Li, L.-H. Weng, G.-X. Jin, *Chem. Commun.*, 2010, **46**, 3556-3558.

159. C. Radloff, J. J. Weigand, F. E. Hahn, *Dalton Trans.*, 2009, 9392-9394.

160. F. M. Conrady, R. Fröhlich, C. Schulte to Brinke, T. Pape, F. E. Hahn, *J. Am. Chem. Soc.*, 2011, **133**, 11496-11499.

161. M. Schmidtendorf, T. Pape, F. E. Hahn, *Angew. Chem. Int. Ed.*, 2012, **51**, 2195-2198.

162. N. Sinha, F. Roelfes, A. Hepp, F. E. Hahn, *Chem. Eur. J.*, 2017, **23**, 5939-5942.

163. C.-Y. Su, Y.-P. Cai, C.-L. Chen, F. Lissner, B.-S. Kang, W. Kaim, *Angew. Chem., Int. Ed.*, 2002, **41**, 3371-3375.

164. C.-Y. Su, Y.-P. Cai, C.-L. Chen, M. D. Smith, W. Kaim, H.-C. Zur Loye, *J. Am. Chem. Soc.*, 2003, **125**, 8595-8613.

165. X.-J. Wan, F.-B. Xu, Q.-S. Li, H.-B. Song, Z.-Z. Zhang, *Organometallics*, 2005, **24**, 6066-6068.

166. C. A. Quezada, J. C. Garrison, M. J. Panzner, C. A. Tessier, W. J. Youngs, *Organometallics*, 2004, **23**, 4846-4848.

167. J. C. Garrison, W. J. Youngs, *Chem. Rev.*, 2005, **105**, 3978-4008.

168. Y.-F. Han, G.-X. Jin, F. E. Hahn, *J. Am. Chem. Soc.*, 2013, **135**, 9263-9266.

169. Y.-F. Han, G.-X. Jin, C. G. Daniliuc, F. E. Hahn, *Angew. Chem. Int. Ed.*, 2015, **54**, 4958-4962.

170. C. Segarra, G. Guisado-Barrios, F. E. Hahn, E. Peris, *Organometallics*, 2014, **33**, 5077-5080.

171. Q. Teng, H. V. Huynh, *Chem. Commun.*, 2015, **51**, 1248-1251.

172. X. Hu, Y. Tang, P. Gantzel, K. Meyer, *Organometallics*, 2003, **22**, 612-614.

173. A. Rit, T. Pape, F. E. Hahn, *J. Am. Chem. Soc.*, 2010, **132**, 4572-4573.

174. A. Rit, T. Pape, A. Hepp, F. E. Hahn, *Organometallics*, 2011, **30**, 334-347.

175. A. Rit, T. Pape, F. E. Hahn, *Organometallics*, 2011, **30**, 6393-6401.

176. R. Maity, A. Rit, C. Schulte to Brinke, C. G. Daniliuc, F. E. Hahn, *Chem. Commun.*, 2013, **49**, 1011-1013.

177. N. Sinha, F. Roelfes, A. Hepp, C. Mejuto, E. Peris, F. E. Hahn, *Organometallics*, 2014, **33**, 6898-6904.

178. C. Mejuto, G. Guisado-Barrios, D. Gusev, E. Peris, *Chem. Commun.*, 2015, **51**, 13914-13917.

179. D. Canseco-Gonzalez, A. Petronilho, H. Mueller-Bunz, K. Ohmatsu, T. Ooi, M. Albrecht, *J. Am. Chem. Soc.*, 2013, **135**, 13193-13203.

180. Carmen Mejuto, Beatriz Royo, Gregorio Guisado-Barrios, E. Peris, *Beilstein J. Org. Chem.*, 2015, **11**, 2584-2590.

181. C. Mejuto, G. Guisado-Barrios, E. Peris, *Organometallics*, 2014, **33**, 3205-3211.

182. R. Maity, A. Mekic, M. van der Meer, A. Verma, B. Sarkar, *Chem. Commun.*, 2015, **51**, 15106-15109.

183. N. Sinha, T. T. Y. Tan, E. Peris, F. E. Hahn, *Angew. Chem., Int. Ed.*, 2017, **56**, 7393-7397.

184. S. Gonell, M. Poyatos, E. Peris, *Angew. Chem. Int. Ed.*, 2013, **52**, 7009-7013.

185. S. Gonell, R. G. Alabau, M. Poyatos, E. Peris, *Chem. Commun.*, 2013, **49**, 7126-7128.

186. E. Peris, *Chem. Commun.*, 2016, **52**, 5777-5787.

187. S. Ibanez-Maella, M. Poyatos, E. Peris, *Chem. Commun.*, 2017, **53**, 3733-3736

188. K. A. Williams, C. W. Bielawski, *Chem. Commun.*, 2010, **46**, 5166-5168.

189. C. Segarra, J. Linke, E. Mas-Marza, D. Kuck, E. Peris, *Chem. Commun.*, 2013, **49**, 10572-10574.

190. L. Monnereau, D. Sémeril, D. Matt, L. Toupet, *Chem. Eur. J.*, 2010, **16**, 9237-9247.

191. E. Brenner, D. Matt, M. Henrion, M. Teci, L. Toupet, *Dalton Trans.*, 2011, **40**, 9889-9898.

192. E. K. Bullough, M. A. Little, C. E. Willans, *Organometallics*, 2013, **32**, 570-577.

193. A. H. M. de Vries, J. M. C. A. Mulders, J. H. M. Mommers, H. J. W. Henderickx, J. G. de Vries, *Org. Lett.*, 2003, **5**, 3285-3288.

194. L. Monnereau, H. El Moll, D. Sémeril, D. Matt, L. Toupet, *Eur. J. Inorg. Chem.*, 2014, **8**, 1364-1372.

195. N. Şahin, D. Sémeril, E. Brenner, D. Matt, İ. Özdemir, C. Kaya, L. Toupet, *Eur. J. Org. Chem.*, 2013, **20**, 4443-4449.

196. H. El Moll, D. Semeril, D. Matt, L. Toupet, J.-J. Harrowfield, *Org. Biomol. Chem.*, 2012, **10**, 372-382.

197. L. Ngodwana, S. Bose, V. J. Smith, W. A. L. van Otterlo, G. E. Arnott, *Eur. J. Inorg. Chem.*, 2017, **13**, 1923-1929.

198. N. Natarajan, T. Chavagnan, D. Sémeril, E. Brenner, D. Matt, R. Ramesh, L. Toupet, *Eur. J. Inorg. Chem.*, 2018, **7**, 890-896.

199. M. Kaloğlu, N. Şahin, D. Sémeril, E. Brenner, D. Matt, İ. Özdemir, C. Kaya, L. Toupet, *Eur. J. Org. Chem.*, 2015, **33**, 7310-7316.

200. A. R. Chianese, A. Mo, D. Datta, *Organometallics*, 2009, **28**, 465-472.

201. D. Yuan, H. V. Huynh, *Organometallics*, 2010, **29**, 6020-6027.

202. H. V. Huynh, W. Sim, C. F. Chin, *Dalton Trans.*, 2011, **40**, 11690-11692.

203. P. J. Altmann, C. Jandl, A. Pothig, *Dalton Trans.*, 2015, **44**, 11278-11281.

204. P. J. Altmann, A. Pothig, *Chem. Commun.*, 2016, **52**, 9089-9092.

205. P. J. Altmann, A. Pöthig, *J. Am. Chem. Soc.*, 2016, **138**, 13171-13174.

206. P. J. Altmann, A. Pothig, *Angew. Chem. Int. Ed.*, 2017, **56**, 15733-15736.

207. J.-R. Song, Z.-T. Huang, Q.-Y. Zheng, *Tetrahedron*, 2013, **69**, 7308-7313.

Chapter 2

**Synthesis, characterisation and self-assembly of tripodal
benzimidazole and oxazole ligands**

*This chapter highlights the preparation of benzimidazole and oxazole-appended
cyclotriveratrylene ligands, and their metal-mediated assembly yielding
metallo-cryptophanes and coordination polymers respectively. A number of novel
cyclotriveratrylenes were also reported, but their coordination to defined metal
centres proved unsuccessful.*

2.1 Introduction

Imidazole is a five-membered ring containing nitrogen atoms in the 1- and
3-positions. Five membered diazoles are aromatic systems, obeying Hückel's 4n+2
rule, and the nitrogen atom displaying protic character donates two electrons into the
π-system. The second nitrogen atom has a basic lone pair associated, and can be
compared to that in pyridine as it also contributes just one electron to the π-cloud
(figure 2.1).
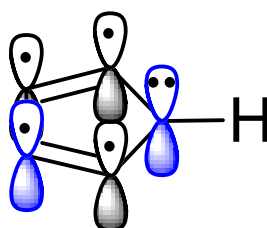
Figure 2.1 Frontier orbital diagram of imidazole. Blue orbitals represent the nitrogen atoms.

Imidazole is thus amphoteric, displaying both acid and base character. The protic
nitrogen (N1) displays acidic character, whilst N3 is more basic than pyridine, and
behaves in the same manner. Nucleophilic aromatic substitution can occur at C2,
which is electron deficient as this site is between by two electronegative nitrogen
atoms.

Imidazoles are widespread throughout nature, and found in a diverse range of
biologically significant molecules, including vitamin B-12 whose structure was
realised crystallographically by Hodgkin,[1] and the purine nucleotides comprised
within the scaffold of DNA and RNA.[2] Imidazole-containing compounds have a rich

coordination chemistry, spanning diverse materials such as complexes bearing *N*-coordination similar to pyridyl complexes,[3] zeolitic imidazolate frameworks (ZIFs)[4] and N-heterocyclic carbene complexes.[5, 6] In 2002, Kaim and co-workers prepared a number of M_3L_2 cages incorporating *tris*-1,3,5-(1-methylbenzimidazoyl)mesitylene, by taking advantage of the linear binding mode of the group ten metals silver and copper. In the case of Ag(I), a BF_4^- anion is encapsulated within the cage, whereas the Cu(I) system with CuI starting material interestingly encapsulated a $[CuI_3]^{2-}$ anion.[7]

The same group also prepared ditopic *bis*-benzimidazolyl ligands on a 4,6-dimethylbenzene scaffold, and upon altering stoichiometries of Ag(I):ligand, M_2L_2 rectangles were accessible, whereby benzimidazole moieties π-π stack with one another (figure 2.2).[8] By simply introducing an additional methyl group to the arene spacer, a different M_2L_2 rectangle assembles. In this case, the arene groups sit flat at the top and bottom of the rectangle, and anionic guests reside within the cavity. Such small rectangular targets are rarer than 3D trigonal-bipyramidal or tetrahedral cages.[9] Upon altering the position, and/or number of benzimidazolyl substituents on the arene, the number of and position of methyl groups, and also the metal used, a library of C_2, C_3 and C_4 symmetric cages could be targeted using a simple ligand system.
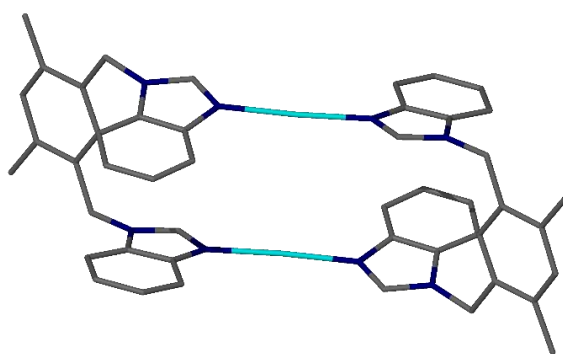
Figure 2.2 An Ag₂L₂ rectangle reported by Kaim and co-workers.[8]

2.2 Imidazolyl ligand syntheses

Cyclotriguaiacylene (CTG) **2.3** was prepared in a three-step synthesis according to previous methodologies (scheme 2.1).[10, 11] The phenolic allyl-protection of 4-hydroxy-3-methoxybenzyl alcohol was achieved quantitatively to yield **2.1**, followed by an acid-catalysed trimerisation as a dry melt, precipitating **2.2** in a 62%

yield. Reactions can be limited by stirrer capability, caused by reaction solidification due to precipitation of **2.2**. A Pd-catalysed reductive deallylation of **2.2** afforded **2.3** in a 69% yield (scheme 2.1). The ^{1}H NMR spectrum of CTG contains the two characteristic doublets at 4.71 and 3.50 ppm, corresponding to the *endo-* and *exo-* protons of the CTG methylene bridge. The *endo-* proton resonance appears further downfield because it undergoes steric compression with neighbouring *endo-* protons associated with the tribenzo[*a,d,g*]cyclononatriene core, as a consequence of being within *ca.* 2 Å, of one another.[12]
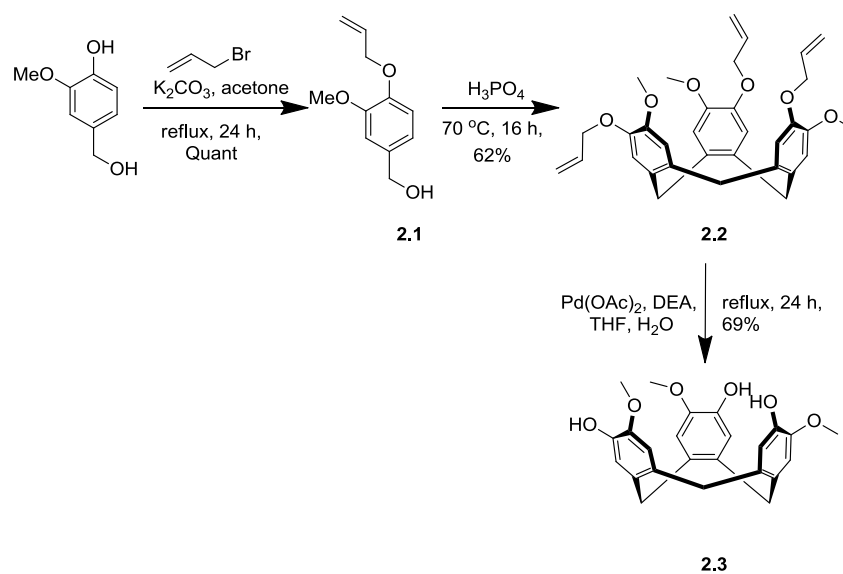
Scheme 2.1 Synthesis of CTG 2.3.
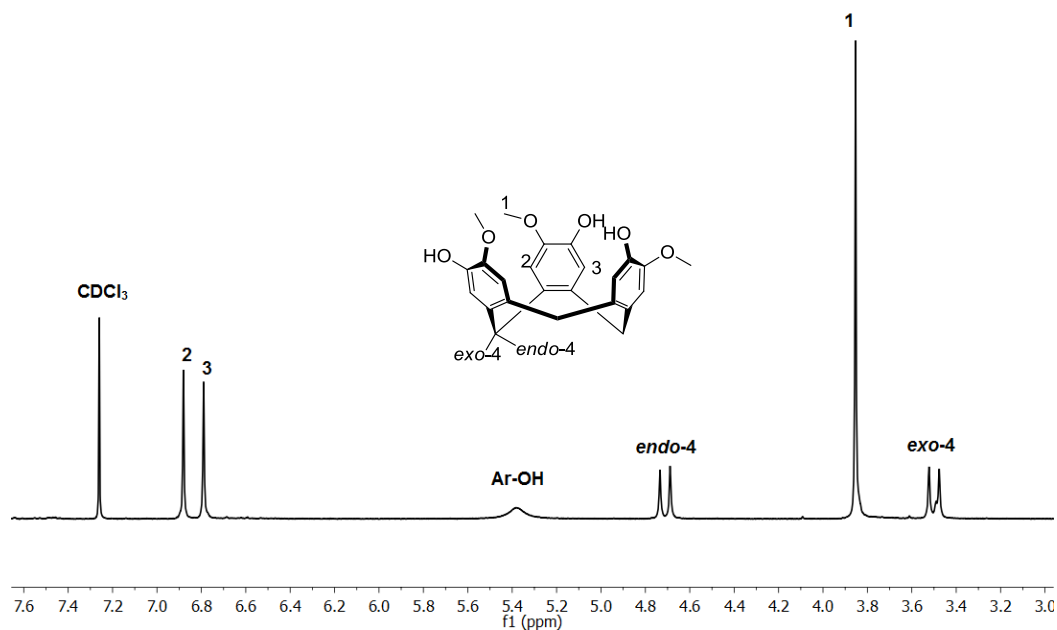
Figure 2.3 ^{1}H NMR spectrum (293 K, 300 MHz, CDCl$_3$) of CTG 2.3. Inset: Molecular structure of 2.3.

A racemic mixture of CTG **2.3** was employed for all manipulations. As introduced in Chapter 1, CTG displays helical chirality about the upper rim, and there is a route for interconversion between enantiomers *via* the saddle confirmation. Whilst separation of enantiomers is possible using chiral HPLC methods, such a method is highly challenging and racemisation occurs over time.[13]
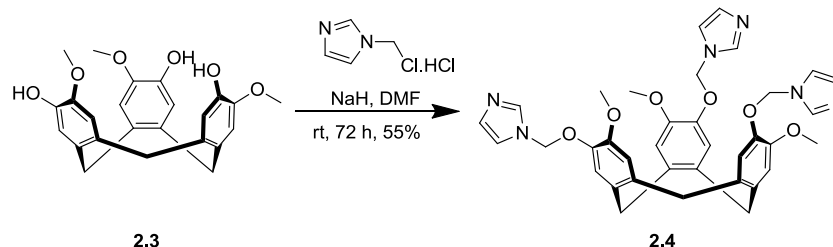
Scheme 2.2 Synthesis of imidazole 2.4.

Imidazole **2.4** was prepared according to previous methodology by reaction of CTG with 1-(chloromethyl)imidazole hydrochloride under basic conditions, displayed in scheme 2.2.[14] The synthesis proved unreliable due to the instability of precursor 1-(chloromethyl)imidazole hydrochloride (**2.6**, whose synthesis is shown in scheme 2.3), and repeatability was low. The electron-withdrawing nature of both the imidazole moiety and chloride lead to an activated methylene group, which was highly susceptible to nucleophilic attack and self-condensation reactions owing to the nucleophilicity of imidazole. Reactions to prepare ligand **2.4** were carried out on a small scale in anhydrous, anoxic DMF, a polar aprotic solvent, using NaH as base, but this was not always successful. Utilisation of weaker bases led to increased reaction times, and significantly more polymer formation. In addition to high reactivity in solution, precursor **2.6** proved extremely hygroscopic and deliquescent, turning from a white solid, to a thick gel, to an aqueous solution within seconds of exposure to air. When **2.6** was worked up using Schlenk techniques and stored in a glove box, the deliquescence could be suppressed, although upon dissolution for installation onto CTG, polymerisation in solution occurred and outcompeted the desired reaction.
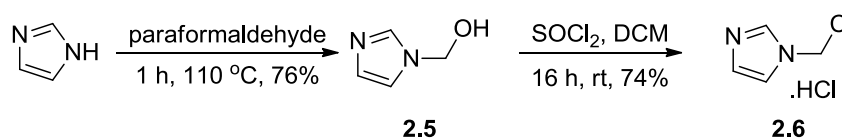
Scheme 2.3 Synthesis of imidazole precursor 2.6.

The ^{1}H NMR spectrum of **2.4** contains the diagnostic *endo-* and *exo-* protons at 4.59 and 3.39 ppm respectively, and the presence of only two doublets diagnostic for a C_3-symmetric CTV derivative. *N*-functionalised imidazoles typically contain three resonances, the furthest downfield being the proton residing between nitrogen atoms, and the two backbone protons upshifted by *ca.* 0.5 ppm. H^4 has split into a *pseudo*-quartet due to the diastereotopicity at this site, and appears somewhat downfield compared to methylene spacers on other ether-linked CTG ligands, owing to the neighbouring electronegative atoms.[14, 15]
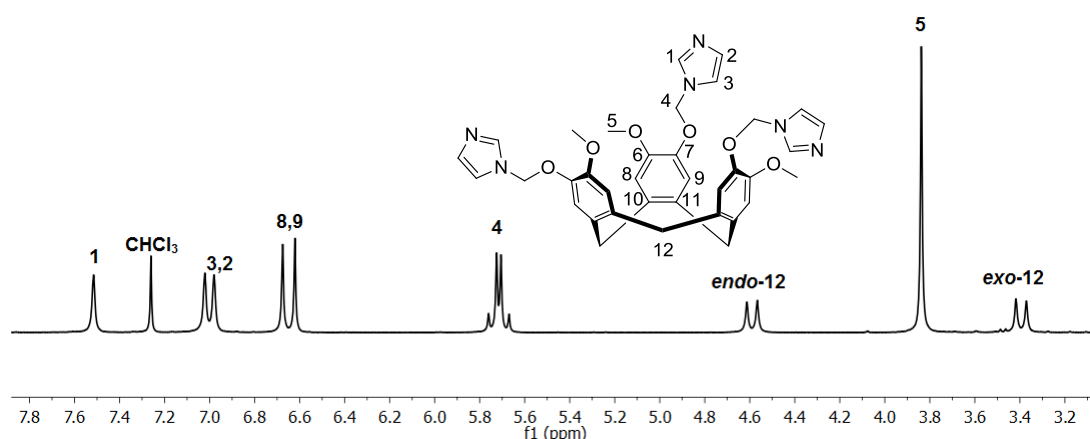
Figure 2.4 ^{1}H NMR spectrum (293 K, 300 MHz, CDCl$_3$) of ligand 2.4. Inset: Molecular structure of 2.4.

The problematic 1-(chloromethyl)imidazole·HCl caused inconsistencies in the preparation of ligand **2.4**. When the ligand was successfully prepared, previous results in the Hardie group showed the assembly of **2.4** with AgReO$_4$ led to the growth of 1D coordination polymer crystals, displaying the dimeric handshake motif, where a reciprocal host-guest relationship between CTV bowl and neighbouring ligand arm was observed.[14]
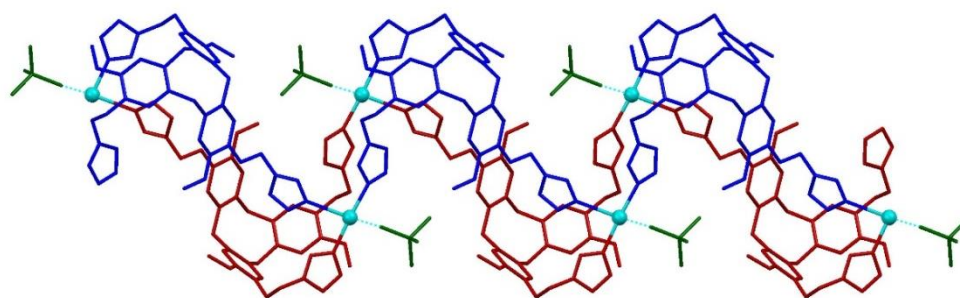
Figure 2.5 An Ag(I) imidazolyl coordination polymer reported by Hardie and co-workers.[14]

The unreliable synthesis of **2.4** led to alternative ligand sets being desired, despite the obvious appeal of an imidazolyl ligand.

2.2.1 Ethyl-tethered imidazole ligand

Extending the alkyl spacer between CTG and imidazole was a route considered, in order to give a more stable ligand without the issues of a highly active electrophilic centre. The nucleophilic substitution of 1-(chloromethyl)imidazole could proceed *via* S_N1 or S_N2 pathways due to resonance stabilisation of the generated carbocation upon loss of chloride. Utilising an ethyl spacer would prevent such a pathway from occurring, thus promoting the direct S_N2 reaction with trianionic CTG. Haloethylimidazoles would likely be more straightforward to prepare than the challenging (bromoethyl)CTV.

The commercially available 2-(hydroxyethyl)imidazole was chlorinated using thionyl chloride, affording 2-(chloroethyl)imidazole hydrochloride as a non-hygroscopic solid. Unfortunately, no reaction ensued when added to a DMF solution of CTG over NaH, so a better leaving group was required. By using thionyl bromide instead, bromo-derivative **2.7** could be prepared, as shown in scheme 2.4.[16]
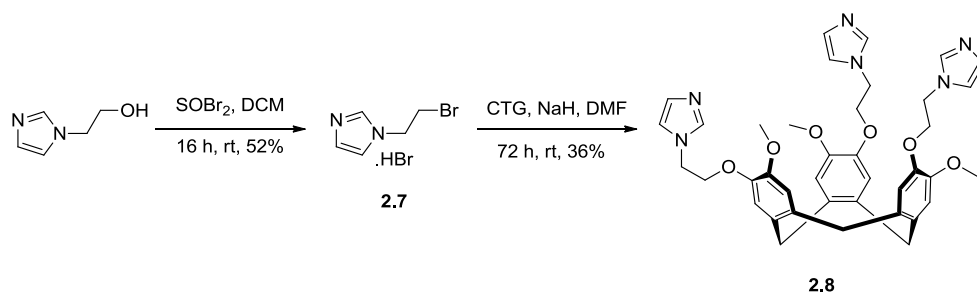
Scheme 2.4 Synthesis of imidazole 2.8.

Imidazole **2.7** only proved hygroscopic when isolated as a powder. When allowed to crystallise by standing at -20 ºC for 48 h in a 1:1 methanol: diethyl ether solution, orange crystals were isolated, which were stable and easy to handle under ambient conditions. Upon scale-up, difficulties were encountered with oligomerisation. Reactions were only possible on a small scale. The preparation of derived CTG **2.8** was low yielding and again reproducibility was erratic. The ^{1}H NMR spectrum of ligand **2.8** (figure 2.6) displayed the characteristic *endo-* and *exo-* doublets associated with the CTV-methylene bridge at 4.66 and 3.47 ppm. Two CH_2 groups assigned using HMQC and DEPT-135 spectroscopy were reported as multiplets at 4.28 and 4.17 ppm. HRMS comprised of peaks {M+H}$^+$ and {M+H$_2$}$^{2+}$ with *m/z*

299.1395 (2+) and 596.2718 (1+) attributed to *bis*-functionalised CTG and 346.1668 (2+) and 691.3257 (1+) corroborating with the *tris*-substituted compound, but the presence of one set of doublets attributed to H^{12} suggests ionisation of one ligand arm was responsible for this.
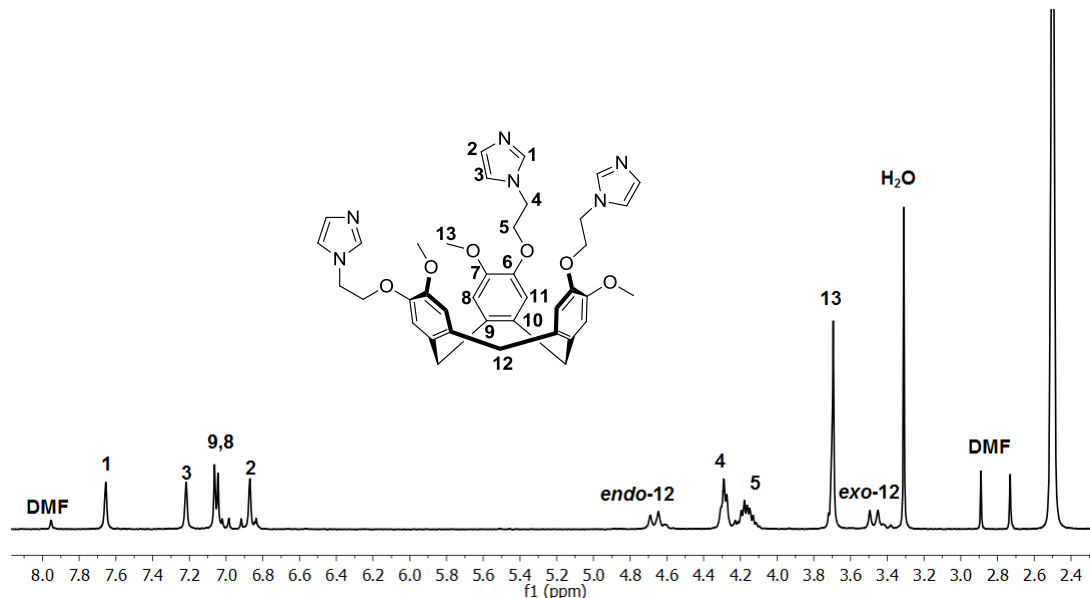
Figure 2.6 ^{1}H NMR spectrum (293 K, 300 MHz, DMSO-d_6) of 2.8. Inset: Molecular structure of 2.8.

Crystals of ligand **2.8** suitable for diffraction using synchrotron radiation were grown from the diffusion of diethyl ether and acetone vapours into a DMSO solution of **2.8**. Compound **2.8** crystallised in the trigonal $P\bar{3}$ space group. The asymmetric unit comprised of one third of **2.8**, with the whole ligand possessing strict C_3 symmetry. The imidazole ring is disordered over two positions.
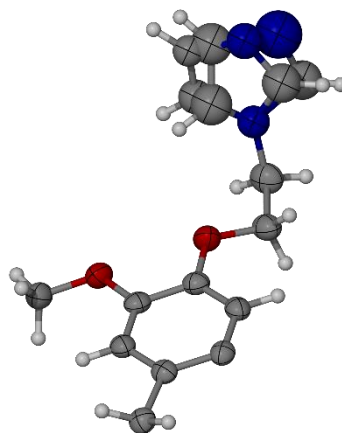
Figure 2.7 Asymmetric unit of 2.8, ellipsoids are shown at the 50% probability.

Crystals of **2.8** were racemic, with bowl-in-bowl stacks comprising of the same enantiomer (figure 2.8) and with centroid-centroid separations of *ca.* 4.68 Å, and therefore not interacting through π-π stacking arrangements. Bowl-in-bowl stacking arrangements are a well-known packing motif in CTV chemistry.[15] Stacks constituting opposite enantiomers were antiparallel with respect to one another. In both cases, the imidazole arms align perfectly. Methoxy groups of neighbouring cavitands are relatively close in proximity, with $C_{Me}\cdots O$ separations of *ca.* 3.29 Å.
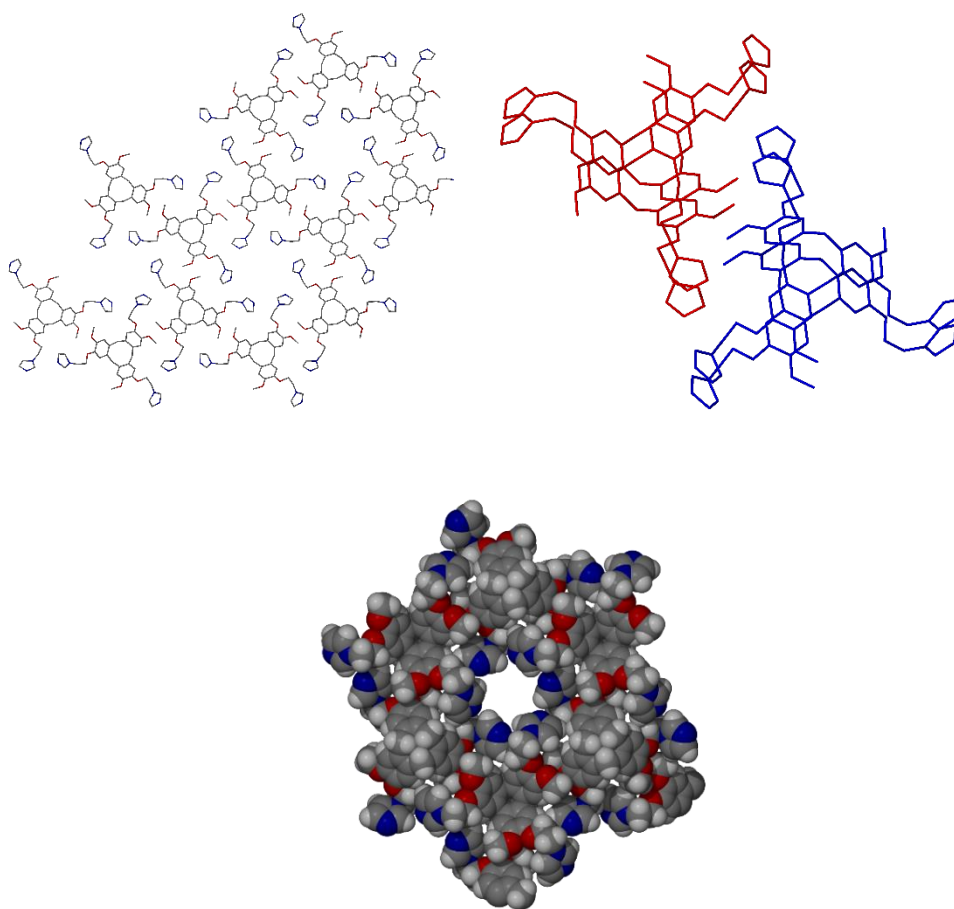
Figure 2.8 Left: Packing diagram of 2.8. Right: enantiomeric bowl-in-bowls. Bottom: space-filling model of packing motif. One imidazole position has been omitted for clarity.

The low yields, small scales and requirement of further steps associated with the ethyl-tethered ligand, **2.8**, mean alternative imidazole targets were sought. One route considered would be to use a backbone-functionalised azole. Rather than *N*-haloalkylimidazoles, derivatising the backbone could yield a more stable precursor that is less prone to oligomerisation, and this approach could lead to better yields. This strategy would however be limited to azoles with only one nitrogen atom present, such as oxazole. The protic nature of imidazole is anticipated to be

troublesome, an average proton population of 50:50 at both nitrogens. A 1:1 ratio of tautomers exists, which are inseparable, and relevant when using unsymmetrical imidazoles. Additional steps would be required with the need to protect and deprotect a nitrogen atom. Furthermore, multiple isomers would be anticipated because of the potential for both tautomers of the imidazole to be present on a CTV scaffold. The tautomers are displayed in figure 2.9. Alterations to the imidazole scaffold were therefore required.
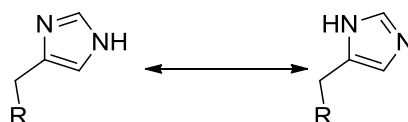
Figure 2.9 Tautomers of a backbone-functionalised imidazole.

2.3 Benzimidazole-functionalised CTG

One selected method to improve yields and increase precursor stability would be to prepare a 1-(methyl)benzimidazolyl ligand. The presence of a hydrophobic benzo-backbone should lower the affinity of such a system towards water, reducing hygroscopicity and deliquescent behaviour. Benzimidazole is slightly less basic than imidazole because of further conjugation into the arene system. Incorporating the aryl backbone of benzimidazoles could also afford the potential for π-π stacking interactions with another benzimidazole group, or the CTG arene faces, which could promote crystallisation of ligands and complexes.

Kaim and co-workers employed planar, tripodal benzimidazolyl ligands as ligands for metallo-supramolecular cages[7, 8] The benzimidazole motif has also found use in rotaxane synthesis, both as an effective receptor for the axle[17] and as a stopper group.[18]

Benzimidazole, **2.11** was a previously unpublished, but known problematic compound in the Hardie group.[19] The formerly-used synthetic route employed 8 eq. of 1-(chloromethyl)benzimidazole hydrochloride, **2.10** as the electrophile, which dimerised to form 1,1'-methylenebisimidazole as a by-product. Such dimerisation had previously been reported by Mokhtari and co-workers when reacting 1-(chloromethyl)benzimidazole·HCl with guaiacol (2-methoxyphenol) under similar conditions.[20] The by-product also proved difficult to remove using chromatographic methods, and displayed a higher affinity for DCM than water during extractions. To

circumvent dimerisation of **2.10**, the number of equivalents of **2.10** was lowered from 8 to 3.4 in the preparation of **2.11**. This both suppresses the dimerisation of **2.10**, and also reduces reaction times by over half. The extraction step was also modified. Most alkyl halides used in the preparation of CTV-type ligands are water soluble, and can easily be removed by simple extraction methods. Neutralised salt **2.10** (and any dimerised by-product if prepared in trace quantities) have inherently poorer aqueous solubility. By simultaneously quenching sodium hydride and precipitating **2.11** upon addition of water to the reaction, and filtering the precipitate, the by-products can be removed *via* much simpler means. The by-product and starting electrophile remained in solution at this stage, and could easily be discarded rather than carrying out a chromatographic separation.
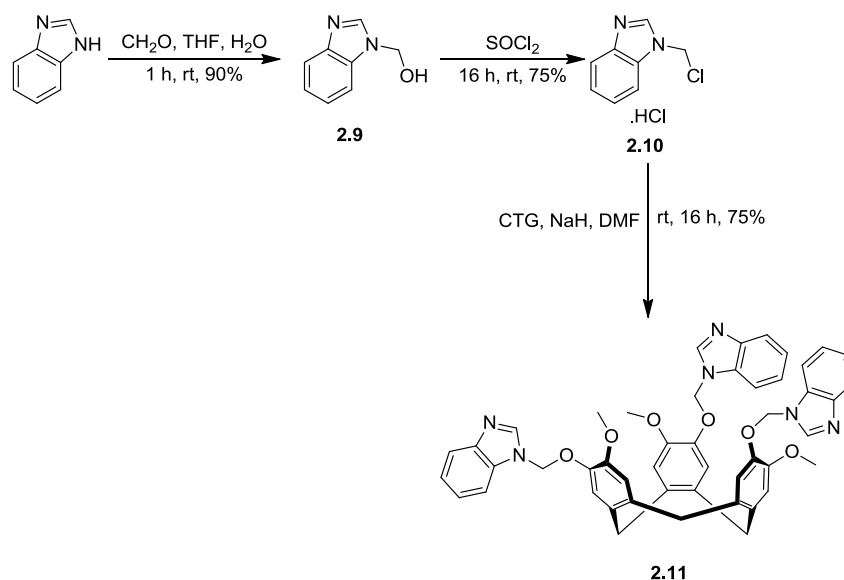
Scheme 2.5 Synthesis of benzimidazole 2.11.

Compound **2.9** was prepared by formaldehyde-mediated hydroxymethylation of benzimidazole. An aqueous formaldehyde solution was selected rather than the dry melt method using paraformaldehyde described in the synthesis of precursor **2.5** due to the much higher melting point of benzimidazole (170 °C compared to 88 °C for imidazole). The chlorination of **2.9** was carried out in neat thionyl chloride due to its insolubility in chlorinated solvents. Salt **2.10** was prepared as a non-hygroscopic solid, which is also indefinitely stable under ambient conditions. Ligand **2.11** was prepared in good yields overnight, and fully characterised using 2D NMR methods alongside mass spectrometry, microanalysis and infrared spectroscopy. NMR spectra were assigned in DMSO-d_6, despite the high solubility of **2.11** in chloroform, because this would give direct comparisons to benzimidazolium salts

discussed in Chapter 4. Additionally, the ^{1}H NMR spectrum in CDCl$_3$ contained a triplet at 7.27 ppm, which overlapped with the residual chloroform peak.

As expected, H^1 was the furthest downfield proton at 8.34 ppm. The characteristic doublets of the tribenzo[*a,d,g*]cyclononatriene core appeared at 4.69 and 3.47 ppm. The H^8 resonances at 6.16 ppm are diastereotopic, and thus display subtle splitting. The HRMS spectrum contained a single peak at 821.3065 corresponding to {M+Na}$^+$ (calculated 821.3059).
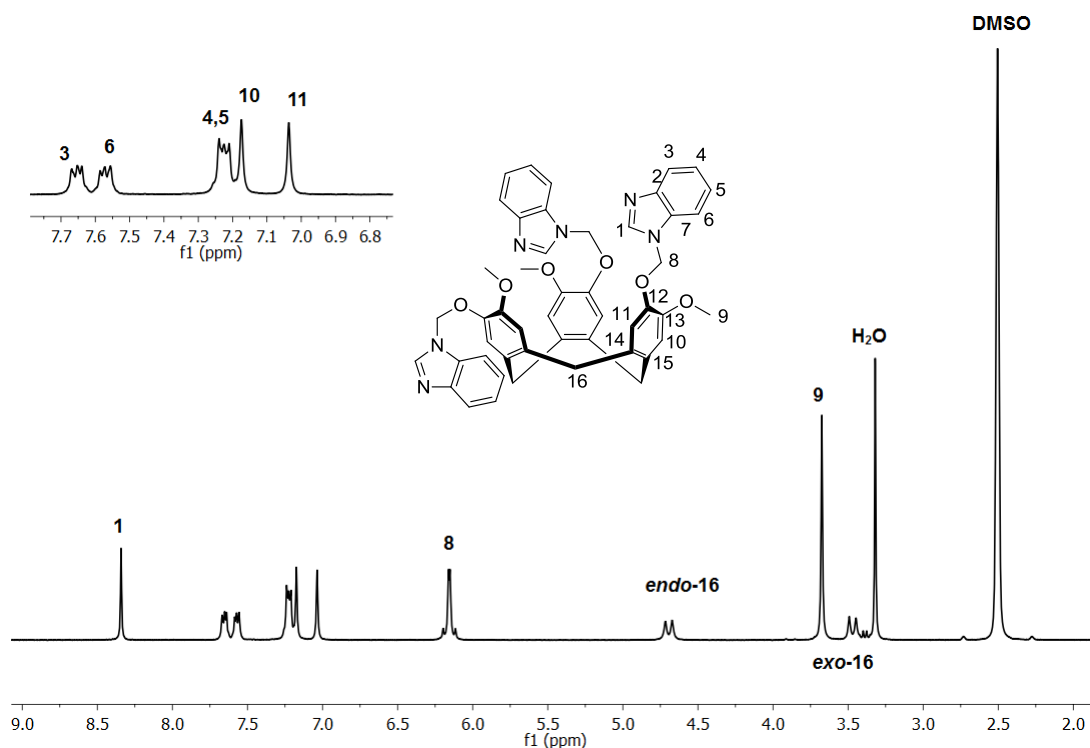
Figure 2.10 ^{1}H NMR spectrum (293 K, 300 MHz, DMSO-*d*$_6$) of benzimidazole 2.11. Inset: Molecular structure of 2.11 and 7.7-6.8 ppm.

Crystals of **2.11** were grown from the slow evaporation of an acetone solution. The ligand crystallised in the triclinic $P\bar{1}$ space group. The asymmetric unit comprises of one molecule of **2.11** (figure 2.11). The three benzimidazole groups are oriented towards the centre of the CTG cavitand, with each arm being of different orientation C$_{Arene}$-O-C-N$_{benzimidazole}$ torsion angles were measured as 70.0, 85.1 and 63.6°. This motif effectively blocks the bowl from behaving as a molecular host.
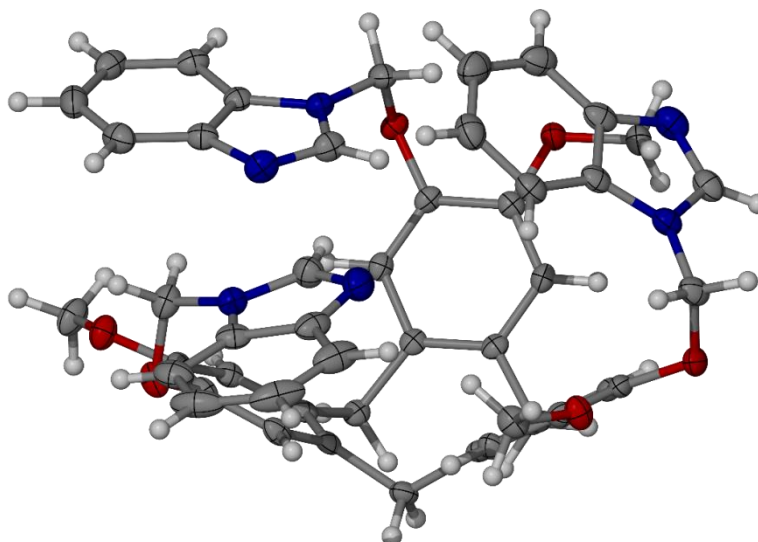
Figure 2.11 Asymmetric unit of 2.11, ellipsoids are shown at the 50% probability.

Weak intramolecular C-H⋯N interactions exist between the benzimidazolyl groups of **2.11**, the closest having a C⋯N separation of *ca.* 3.51 Å. Of the three inward-folded benzimidazole groups, two of the imidazole moieties point towards the centre of the bowl, whereas one points outwards, and partakes in a weak C-H⋯O interaction with a neighbouring methoxy group at C⋯O separation of *ca.* 3.25 Å. The *ab* plane comprises of primitive layers of **2.11**, whilst in the *c* direction, enantiomeric layers stack in inverted orientations.
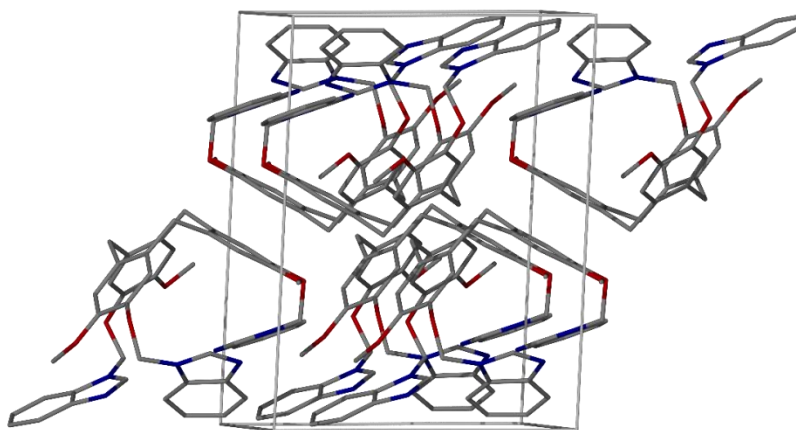
Figure 2.12 Unit cell of 2.11, as shown in the crystallographic *a* axis.

Co-crystals of **2.11**·CTG were also grown from the slow evaporation of an acetone solution. A small crop of crystals were initially grown by David Martin (MChem student) when attempting to crystallise **2.11** which was contaminated by trace quantities of **2.3** (CTG), but it has since been proven that the same crystals grow

from an acetone solution of **2.11** and **2.3** in a 1:1 ratio. Co-crystals crystallised in the trigonal *P*3c1 space group, and the asymmetric unit comprised of one third of both components (figure 2.13).
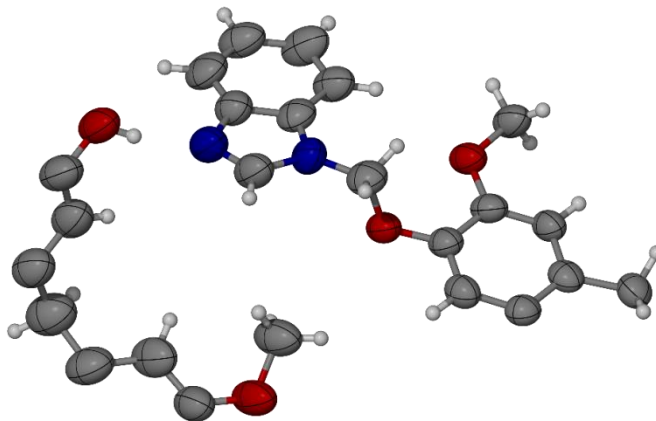
Figure 2.13 Asymmetric unit of 2.11·CTG. Ellipsoids are drawn at the 50% probability.

The co-crystals assembled into a 2D hydrogen-bonding network with O-H···N interactions between hydroxyl group of CTG and benzimidazole nitrogen atoms at O···N separation of *ca.* 2.79 Å (figure 2.14). Each CTG molecule hydrogen bonds to three neighbouring benzimidazole units in a 6^3 topology. The CTG and **2.11** molecules in one network are of opposite enantiomers. Both components of the co-crystal engage in bowl-in-bowl stacking interactions with the opposite enantiomer, rendering hydrogen-bonded layers as homochiral, whilst the crystal itself is racemic. Bowl-in-bowl stacking is well documented for cyclotriveratrylene,[21, 22] but less commonly encountered for ligand derivatives.[23-26]
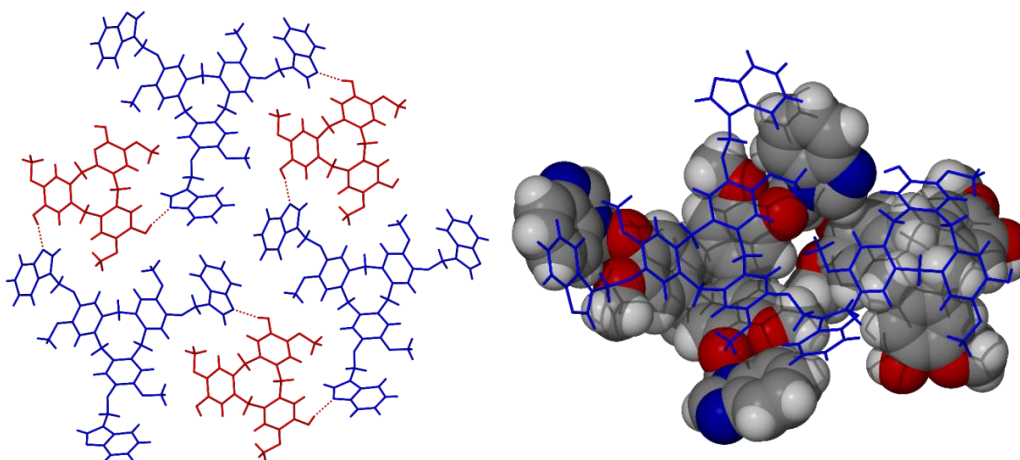
Figure 2.14 Left: Hydrogen bonded network, H-bond shown in red. Right: bowl-in-bowl stacking exhibited in 2.11·CTG.

A powder pattern of the bulk material is a good match to the simulated spectrum derived from the crystal, with a number of overlapping peaks implying the crystalline material is phase pure (figure 2.15).
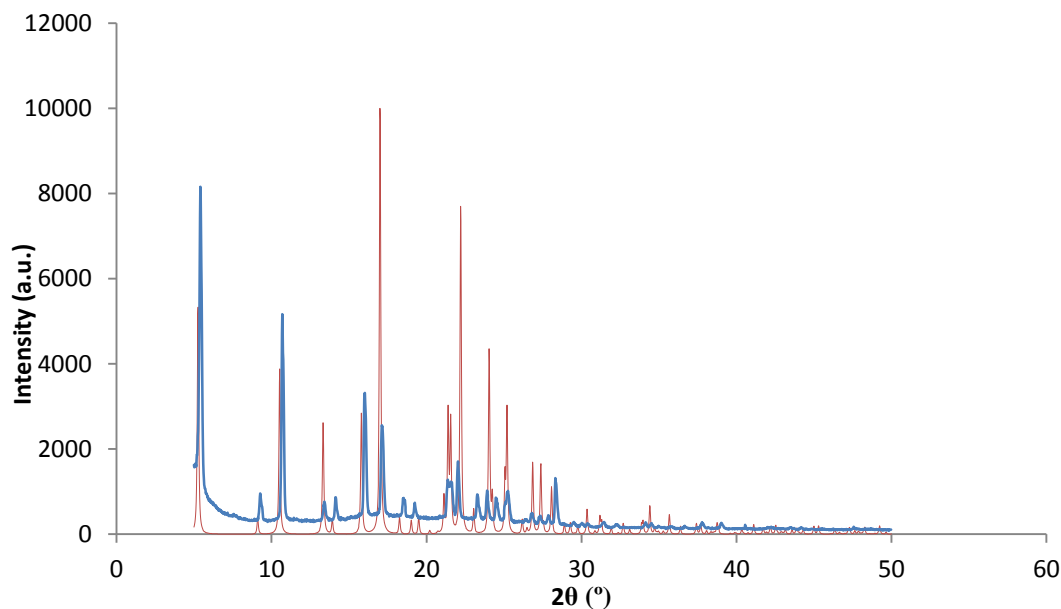
Figure 2.15 Powder X-Ray diffraction pattern of 2.11·CTG. Simulated (red trace) (100 K) and observed data (blue trace) (293 K).

2.4 Assembly of a neutral metallo-cryptophane

The assembly of ligand **2.11** with a range of metals (M = Co(II), Ni(II), Cu(I), Cu(II), Zn(II), Pd(II), Ag(I)) with counterions including halides, nitrates and non-coordinating anions such as BF_4^- and PF_6^- was investigated, but in most cases proved unsuccessful. After stirring a DMF solution of **2.11** with 1.5 eq. [Pd(Cl)$_2$(MeCN)$_2$] for 24 h, as shown in scheme 2.6, before diffusing diethyl ether vapours into the vial, a pale yellow powder initially precipitated after 7 days, which proved highly insoluble once formed. After three months, a small crop of pale yellow crystals grew, the single crystal data confirmed the structure of **2.12** as [Pd$_3$Cl$_6$(**2.11**)$_3$·(H$_2$O)]·1.5H$_2$O·3DMF. Crystals proved insoluble when isolated Capsule **2.12** is a rare example of a *trans*-linked metallo-cryptophane, a motif previously only observed with d^{10} Ag(I) and Cu(II).[26] *trans*-Coordination of Pd(II) is known in calix[4]arene chemistry; Tsuji and co-workers reported the assembly of a neutral [Pd$_2$L$_2$Cl$_4$] capsule.[27] In order to prepare a metallo-cryptophane using a square-planar metal such as Pd(II), a strong σ-donating, *cis*-protecting ligand such as

a *bis*-phosphine or *bis*-NHC typically has to be adopted, forcing the two incoming donors to coordinate *cis*- with respect to one another.[26, 28-32]
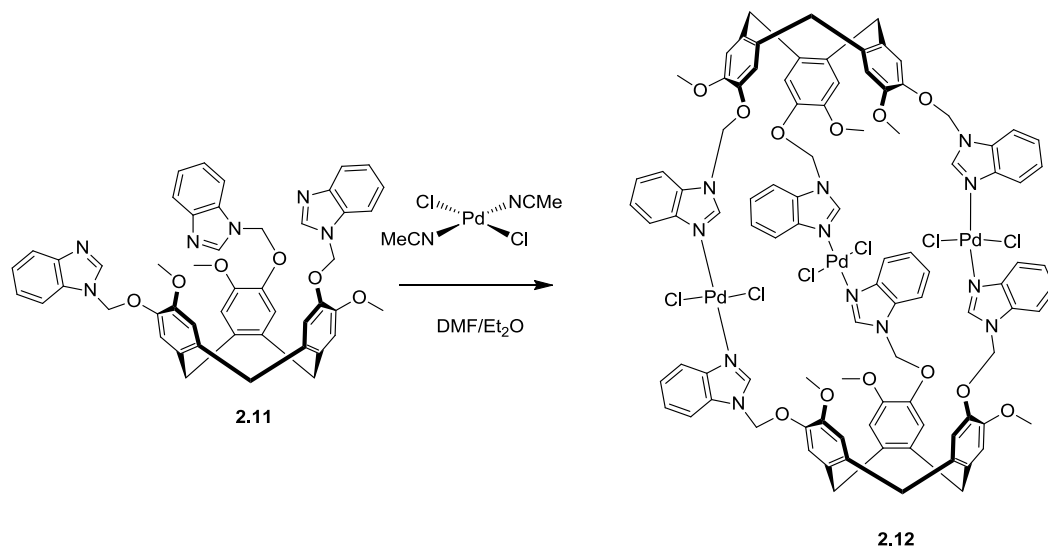
Scheme 2.6 Synthesis of metallo-cryptophane 2.12.

Metallo-cryptophane **2.12** crystallised in the cubic $Pa\overline{3}$ space group. The asymmetric unit comprises of two one-third components of the CTV-type ligand, one Pd(II) centre, one DMF and two water molecules, of which one is of half occupancy and shown in figure 2.16. The two chloride ligands coordinate *trans* with respect to one another with Pd-Cl bond lengths of 2.2747(15) and 2.2944(15) Å with a Cl-Pd-Cl angle of 177.77°. The Pd-N benzimidazole distances are 2.012(4) and 2.013(5) Å with a N-Pd-N angle of 179.01°, with the Pd centre displaying near-square planar geometry. Both benzimidazole groups are crystallographically inequivalent and not coplanar with respect to the palladium centre, and a torsion angle of 53° between the planes. The Pd(II) centres are buried within the core of the assembly, with Pd···Pd separations *ca.* 5.74 Å forming a trigonal node at a much closer distance than in cis-protected Pd(II) cryptophanes, which were reported as 16.29 Å in bis-NHC protected cryptophanes.[29] The benzo-backbones of benzimidazoles reside *exo*-to the cage, with imidazole NCHN pointing towards the centre of the capsule. The azole groups π-π stack with one another at separation of *ca.* 3.47 Å, stabilising the strained C_{arene}-O-C-N_{imid} torsion angles of 66.3 and 73.4°. The space-filling diagram shows the pinched nature of Pd(II) nodes limit any guest encapsulation in the cryptophane by covering the windows of the architecture (figure 2.17). One water guest molecule is trapped within the core of the cryptophane, which was likely present in the DMF solvent during reaction. The

water molecule has a nearest contact to an imidazole NCHN moiety, at O···C separation of *ca.* 2.57 Å. DMF molecules reside above the external enclosed windows of the cryptophane.
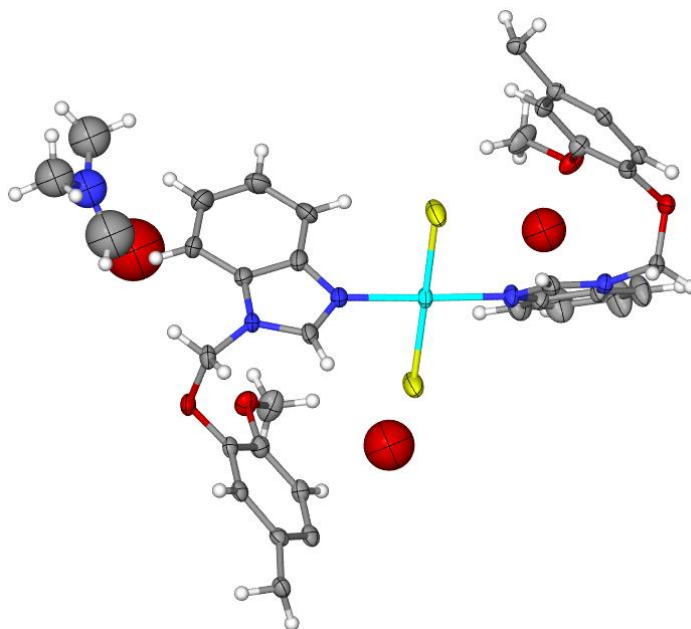
Figure 2.16 Asymmetric unit of [Pd$_3$(2.11)$_2$Cl$_6$]. Ellipsoids are drawn at the 50% probability.
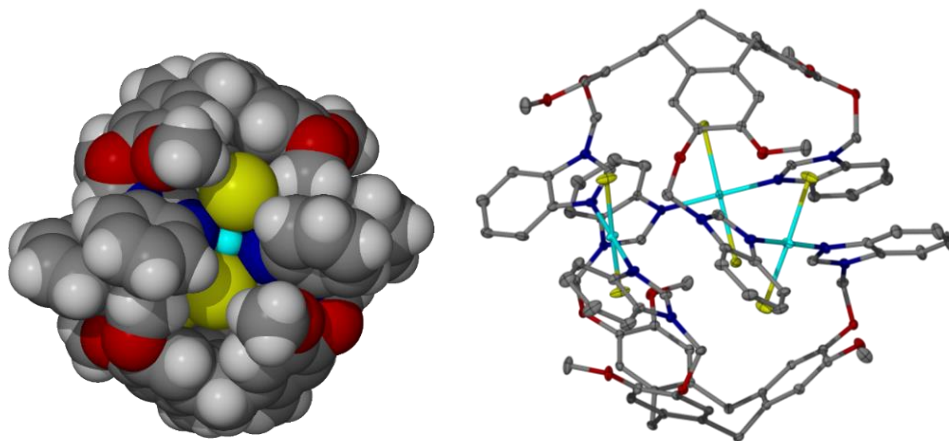
Figure 2.17 Left: space filling diagram of [Pd$_3$(2.11)$_2$Cl$_6$]. Right ellipsoid diagram of cryptophane [Pd$_3$(2.11)$_2$Cl$_6$].

Both **2.11** ligands in cryptophane **2.12** are of the same enantiomer, rendering this an *anti*-metallo-cryptophane. The crystals however, are racemic, with opposite enantiomers of cryptophane packing in a checkerboard-like conformation (figure 2.18, left). The unit cell comprises of eight cryptophanes in a 2 x 2 x 2 cube motif within the cell and displayed in figure 2.18, right.
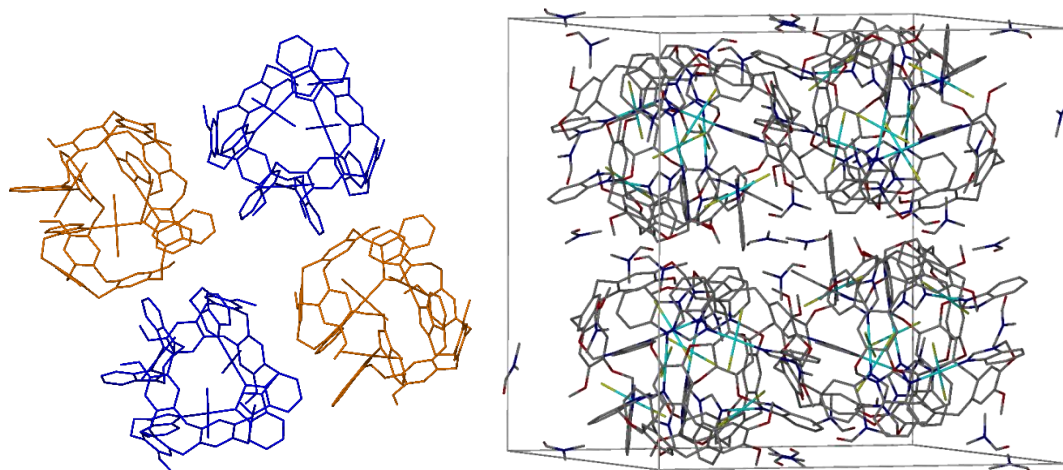
Figure 2.18 Left: checkerboard motif of cryptophane enantiomers. Right: unit cell diagram looking down the crystallographic *a* axis.

Solution studies performed in conjunction with David Martin confirms the presence of cryptophane in DMF and DMSO, but a number of components were also detected, indicating assembly took place over a long period of time, backed up by the duration of crystallisation. The HRMS spectrum (figure 2.19) was dominated by {Pd(**2.11**)Cl}$^+$ at *m/z* 941.1833, with a small product peak of {Pd$_3$(**2.11**)$_2$Cl$_5$(MeCN)}$^+$ present at *m/z* 2134.2070, which was an excellent match to the simulated isotopic pattern. The small peak *m/z* at 1916.3352 matched the cryptophane less one Pd(II) centre.
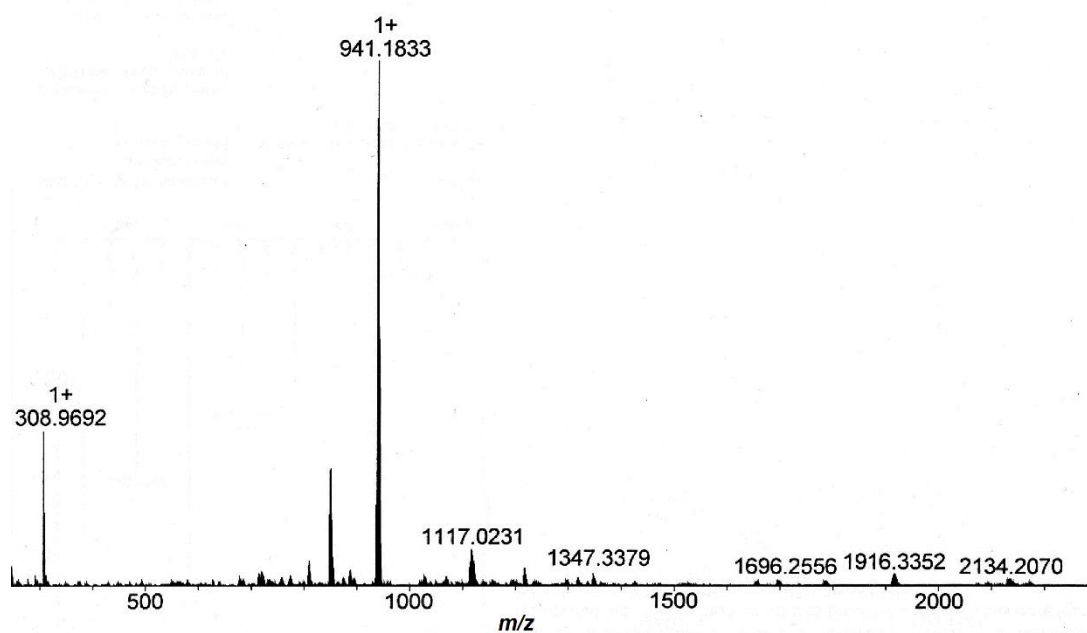
Figure 2.19 HRMS of 2.12.
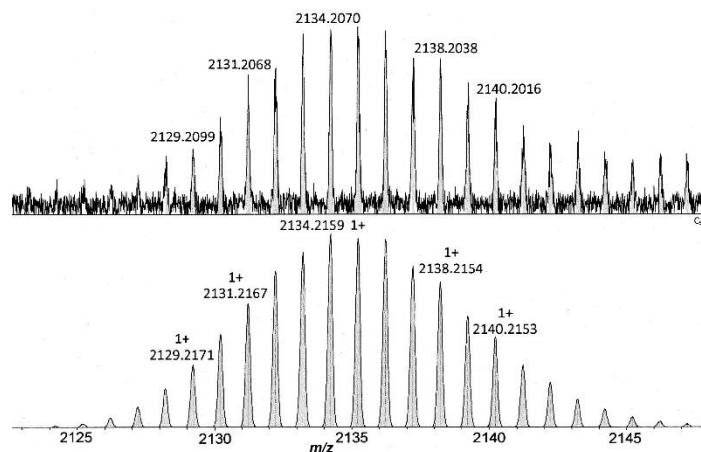
Figure 2.20 Observed (top) vs simulated (bottom) isotope pattern for [Pd₃(2.11)₂(Cl)₅(MeCN)]⁺ (m/z = 2134.2070).

¹H NMR spectroscopy also backed up the notion that more than one species was present in solution. HRMS obtained in DMSO also contained **2.12** as a trace peak, so studies in DMSO-*d*₆ (figure 2.21) and DMF-*d*₇ (figure 2.22) were carried out. In both cases, very weak spectra with numerous peaks were present, suggesting multiple species in solution. Both spectra contained significant liberated free MeCN (denoted by *), suggesting this was being displaced by benzimidazolyl ligands.
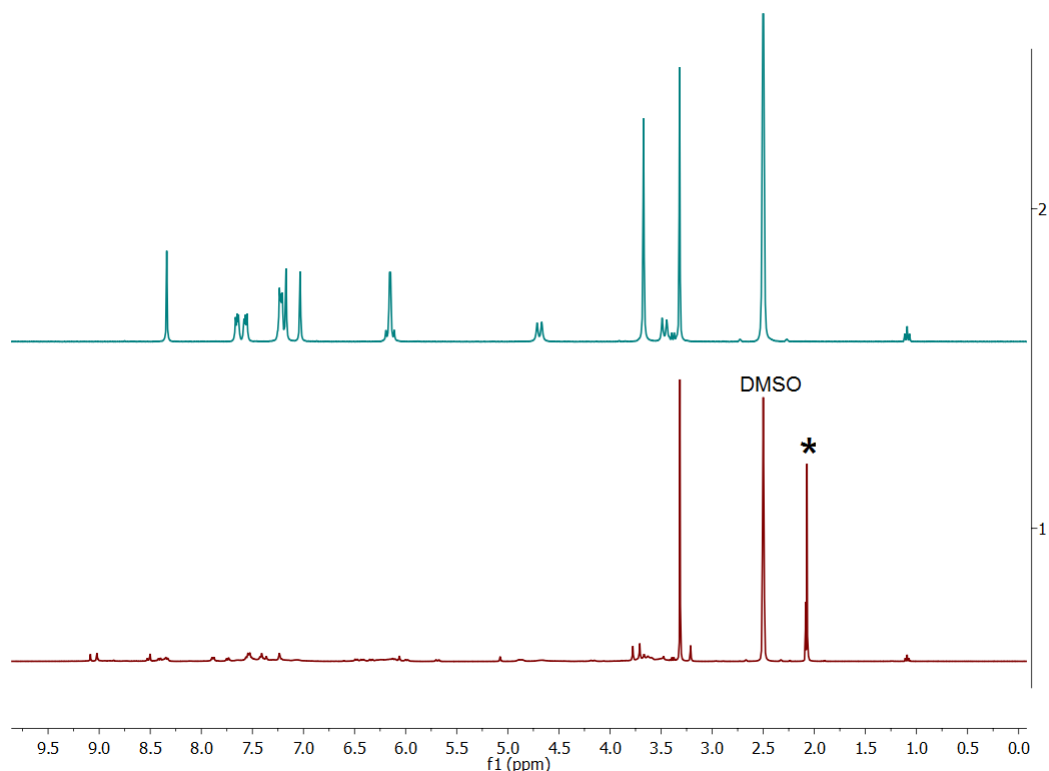
Figure 2.21 ¹H NMR spectrum (293 K, 300 MHz, DMSO-*d*₆) of 2.11 (top), 2.11 + [Pd(Cl)₂(MeCN)₂] after 24 h (bottom). Liberated acetonitrile denoted by *.

The ^{1}H NMR spectrum was also obtained in DMF-d_7, and once again significant free acetonitrile was liberated indicating coordination of benzimidazole groups to Pd(II), but similarly, the sheer number of peaks indicates numerous species in solution.
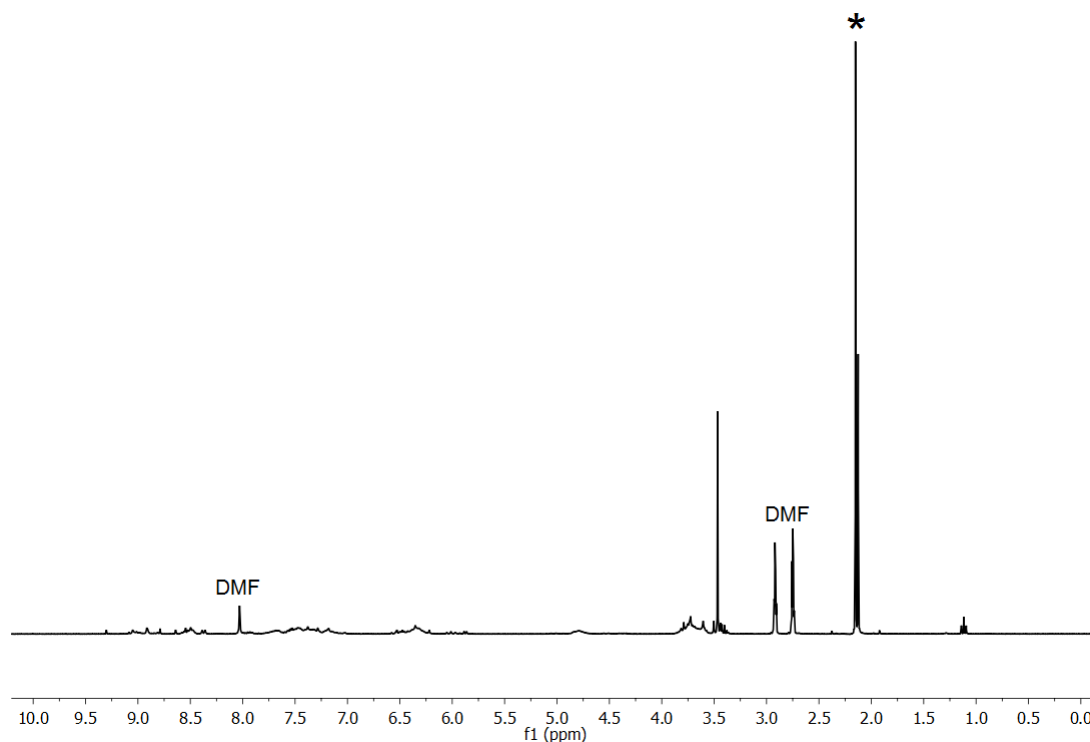
Figure 2.22 ^{1}H NMR spectrum (293 K, 300 MHz, DMF-d$_7$) of 2.11 + [Pd(Cl)$_2$(MeCN)$_2$] after 24 h. Liberated MeCN denoted by *.

Powder X-ray diffraction was carried out on the pale yellow solid, but it was evident the powder was amorphous in nature. An insufficient quantity of crystals was grown to yield a powder pattern of sufficient quality.

The precipitation of a pale yellow powder was observed in all cases during the attempted crystallisation of **2.11** with a range of other Pd(II) salts including [Pd(MeCN)$_4$](BF4)$_2$, [Pd(dppe)$_2$(Cl)$_2$], Pd(OTf)$_2$, and Pd(NO$_3$)$_2$, but crystals only grew when using [Pd(Cl)$_2$(MeCN)$_2$].

2.5 A benzotriazole substituted CTV

Another class of azole considered were 1,2,3-triazole-based compounds. 1,2,3-triazoles can readily be prepared in a Cu-catalysed click reaction between organic azides and alkynes.[33, 34] Benzotriazole is commercially available, but can be

prepared by the monodiazotisation of *o*-phenylenediamine, followed by spontaneous cyclisation. The employment of benzotriazoles avoids the use of potentially explosive azides, and can also give rise to a rich coordination chemistry. The main limitation of benzotriazole compared to benzimidazole within the scope of this project is that it cannot be used to prepare NHC complexes.
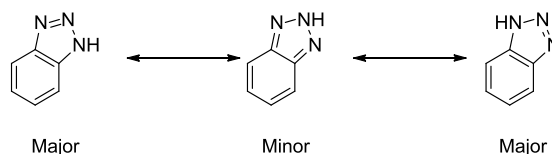
Figure 2.23 Resonance forms of benzotriazole.

Regarding metal coordination and functionalisation, N3 is the most Lewis-basic, so most commonly partakes in reactivity, but consideration for N2 (central nitrogen) competing must be taken, and reactions at this centre are known, albeit rarer and historically challenging to control.[35] Similarly to benzimidazoles, the protic nitrogen (N1 in major isomers) donates two electrons into the π-cloud, hence is typically much less basic and can only be functionalised upon deprotonation. Breit and co-workers have designed different Rh(I) catalysts which can be used to functionalise either N1 or N2 with high selectivities.[36]
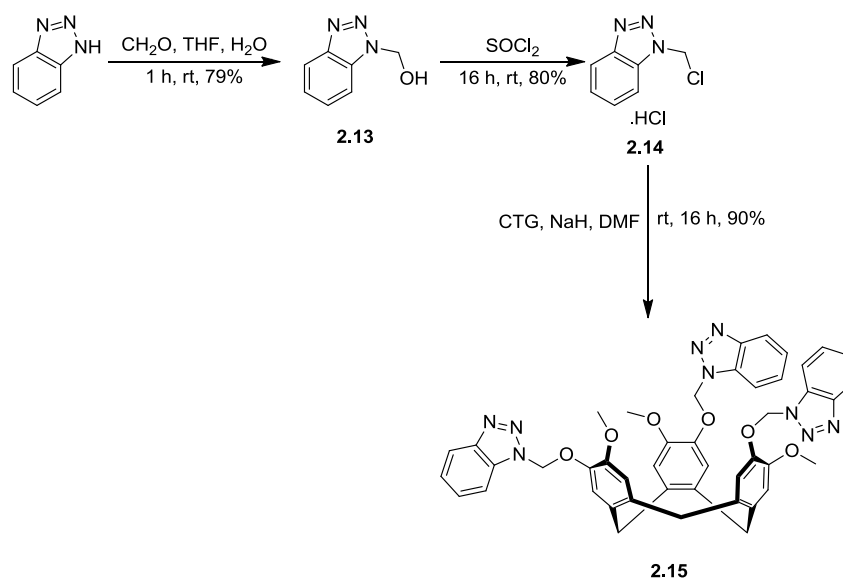
Scheme 2.7 Synthesis of benzotriazole 2.15.

The synthesis of the novel benzotriazole **2.15** mirrored that selected to prepare benzimidazole **2.11** and is shown in scheme 2.7. Compound **2.13** was prepared according to previous methodologies.[37] The ¹H NMR spectrum gave no evidence to suggest N2 functionalisation under the above conditions. Similarly to

1-(hydroxymethyl)benzimidazole, benzotriazole derivative **2.13** proved insoluble in chlorinated solvents, so neat thionyl chloride was employed when preparing **2.14**. Compound **2.15** was prepared employing the same conditions as **2.11**, and consideration for potential dimerisation of **2.14** in a manner similar to benzimidazole **2.10** led to only a slight excess of electrophile being added. Benzotriazole **2.15** was prepared in good yields overnight and fully characterised using NMR and mass spectrometry. The HRMS spectrum (figure 2.24) comprised of a single peak at 824.2933 (calculated 824.2916) corresponding to {M+Na}$^+$.
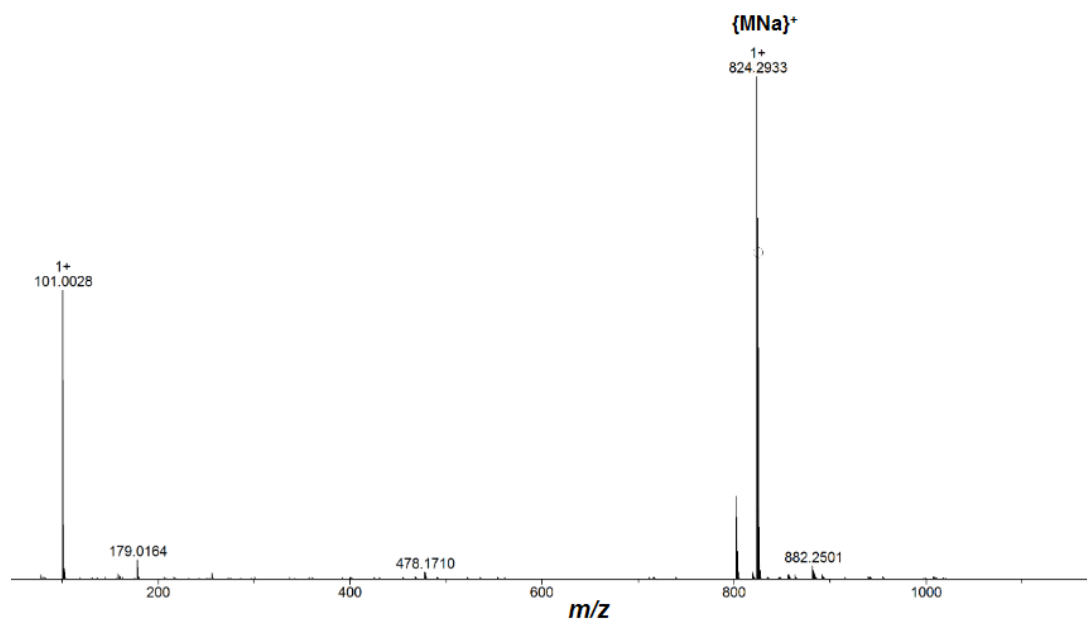
Figure 2.24 HRMS of 2.15.

The ^{1}H NMR spectrum contained the characteristic doublets corresponding to the CTG *endo*- and *exo*-protons (H^{15}). The presence of two doublets confirming the preparation of a single C_3-symmetric product. H^7 splits into two doublets due to diastereotopicity at this site. No protons reside on the azole ring, therefore no peaks further downfield than those associated with the benzo-backbone were detected in the ^{1}H NMR spectrum (figure 2.25).
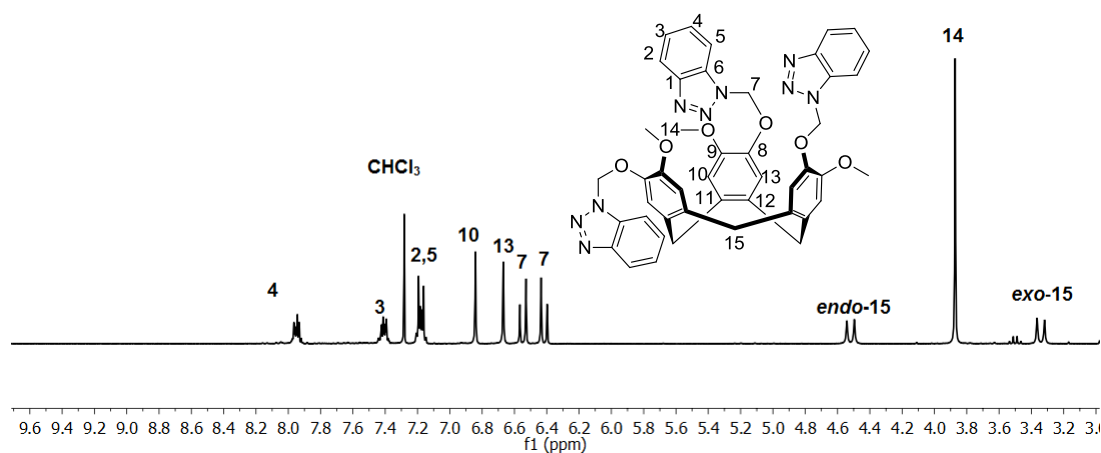
Figure 2.25 ^{1}H NMR spectrum (293 K, 300 MHz, CDCl$_3$) of 2.15. Inset: Molecular structure of 2.15.

The coordination chemistry of **2.15** was investigated, but crystals could not be grown from a range of solvent systems, and no concrete evidence of metal coordination could be ascertained. Similarly to benzimidazole **2.11**, assemblies with Pd(II) precursors led to the precipitation of an insoluble pale-yellow solid after *ca.* one week, but in this case, no crystals grew after a prolonged period of time.

2.6 Oxazole-furnished CTG ligand

A concept explored in **2.2.1** was to incorporate an aprotic azole moiety as a ligand group. Oxazoles were selected for this purpose. Ethyl oxazole-5-carboxylate is a commercially available starting material, whereby the ester group is connected to the backbone carbon adjacent to the oxygen atom of the oxazole ring.
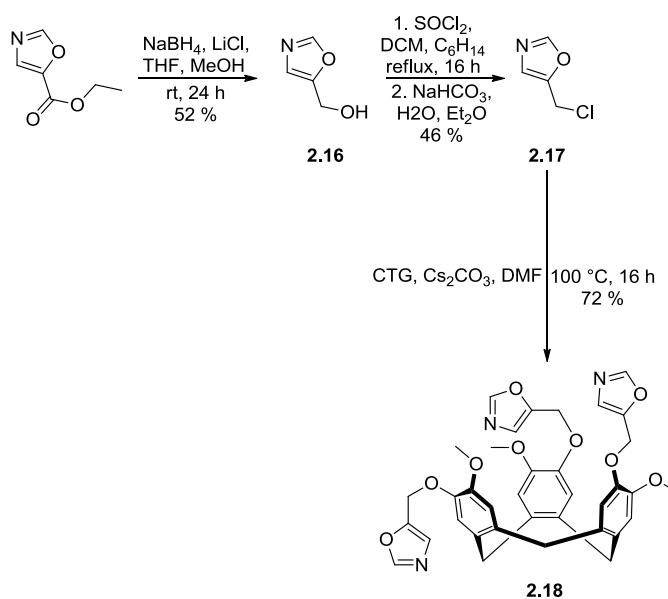
Scheme 2.8 Synthesis of oxazole 2.18.

The preparation of alcohol **2.16** proved to be low yielding, but gave sufficient material to carry forward (scheme 2.8). Ester reductions typically require lithium aluminium hydride as a reducing agent due to the weaker Al-H bond than that in a borohydride counterpart. The reduction carried out to prepare **2.16** involved the *in-situ* preparation of $LiBH_4$, which is a stronger reducing agent than its sodium counterpart. Borohydride-mediated reductions are generally carried out in protic solvent, but by using a mixture of THF and methanol, the scope of reducible carbonyl compounds is increased and includes esters. This system allows for reduction of more challenging substrates, whilst avoiding the handling issues associated with $LiAlH_4$ and stronger reducing agents. A number of theories for this have been postulated, including the *in situ* generation of the highly reducing trimethoxyborohydride anion.[38, 39] The THF solvent could also form a Lewis adduct with neutral group 13 species by coordinating into the unoccupied p-orbital of the boron atom, in the same manner that $BH_3 \cdot THF$ can reduce esters to the corresponding alcohol.[40] A simple thionyl chloride-mediated chlorination to prepare **2.17** as the hydrochloride salt was then carried out. Reaction of 5-(chloromethyl)oxazole·HCl with CTG under basic conditions was unsuccessful, presumably due to deprotonation of the oxazole hydrochloride outcompeting deprotonation of CTG. Oxazoles are weakly basic azoles, with inductive effects associated with the electronegative oxygen atom stabilising the protic oxazolium form.[41] It was therefore necessary to neutralise **2.17** in aqueous sodium hydrogen carbonate, extract into DCM and add the neutral electrophile to a DMF solution of CTG and Cs_2CO_3. **2.18** was isolated as a sandy-brown solid in good yield.

The ^1H NMR spectrum contains the characteristic *endo-* and *exo-* doublets at 4.73 and 3.53 ppm (figure 2.26). The methylene bridge, H^4 displays subtle splitting due to diastereotopicity at this site. These protons are further upfield by *ca.* 1.4 ppm compared to that observed in the nitrogen-appended ligands such as **2.15** because of lower inductive effects at this position. The most acidic proton, H^1, was located at 7.87 ppm.
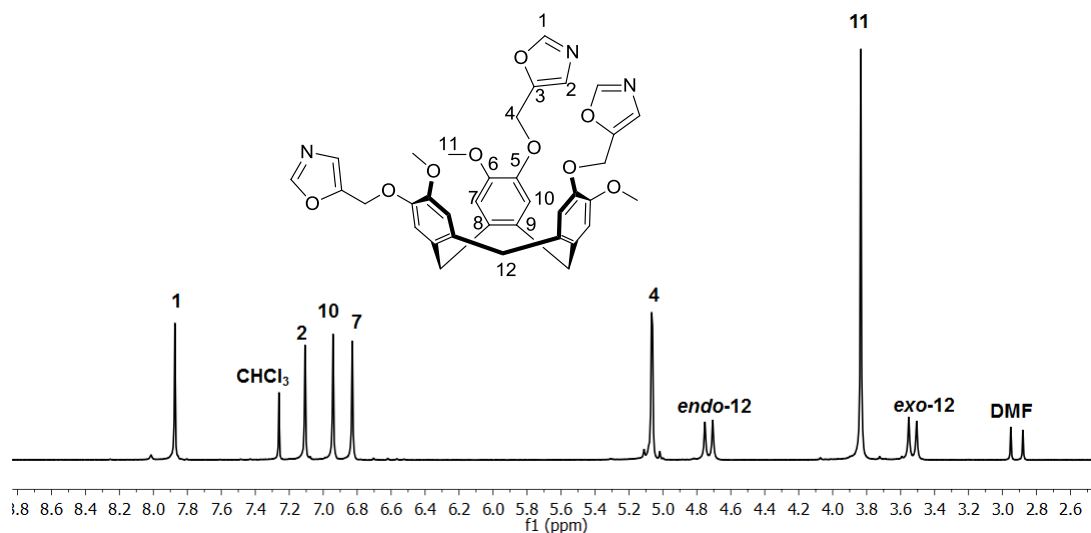
Figure 2.26 ^{1}H NMR spectrum (293 K, 300 MHz, CDCl$_3$) of 2.18. Inset: Molecular structure of 2.18.

The ^{13}C{^{1}H} NMR spectrum (figure 2.27) contained comparatively fewer peaks than benzimidazole **2.11** due to four less benzo-backbone resonances. As seen for other azole ligands prepared, C^6, the aromatic carbon adjacent to methoxy group is the furthest downfield carbon centre. DEPT-135, HMQC and HMBC spectra aided full assignment of all carbon atoms (see Appendix).
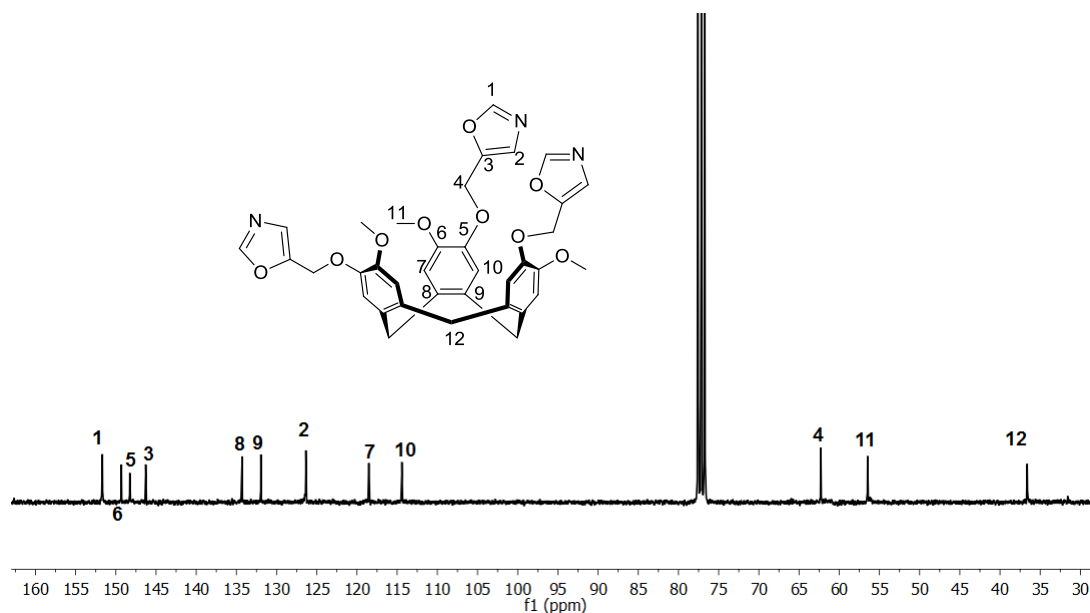
Figure 2.27 ^{13}C{^{1}H} NMR spectrum (293 K, 75 MHz, CDCl$_3$) of 2.18. Inset: Molecular structure of 2.18.

The mass spectrum (figure 2.28) contained two dominant molecular ion peaks {M+H}$^+$ (calculated 652.2290) and {M+Cs}$^+$ (calculated 784.1266). The lack of

mono- or *bis*-oxazolyl peaks confirmed the *tris*-substituted ligand as the desired product.
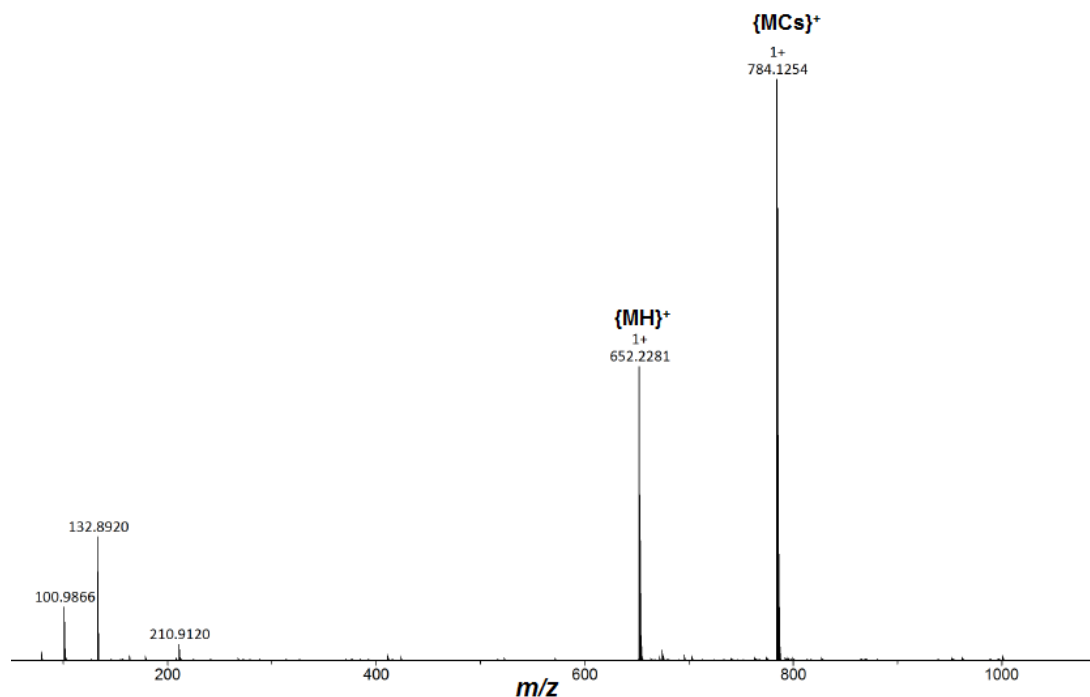
Figure 2.28 HRMS of 2.18.

Single crystals suitable for X-ray diffraction could be isolated by diffusing diethyl ether vapours into a DMF solution of **2.18**. **(2.18)**$_4$·H_2O crystallised in the hexagonal *P*6$_3$ space group. The asymmetric unit comprises of one and a third ligands (figure 2.29). Both crystallographically independent **2.18** molecules were of the same enantiomer and note *P*6$_3$ is a chiral space group. Hence, each crystal contains only one enantiomer of ligand. A material comprising of a single enantiomer is known as a conglomerate. The three oxazole groups of the full CTV ligand in the asymmetric units are of different orientations, with one oxazole oxygen atoms pointing towards the centre of the bowl, one almost in-line with the CTV-arene faces, and one pointing outwards. Bowl-in-bowl stacks were observed, but rather than the commonly found α-stacking motif, where tribenzo[*a,d,g*]cyclononatriene bowls are parallel to neighbours in that column, β-stacks instead formed.[42] One methylene group of tribenzo[*a,d,g*]cyclononatriene cores points into the centre of the below bowl, giving rise to every other molecule being of like-orientation. Stacks are also antiparallel, with alternating columns running in the opposite orientation. A partially occupied water molecule resides within the asymmetric unit. Isomorphic nitromethane-solvate crystals could also be grown, but data were of poor quality.
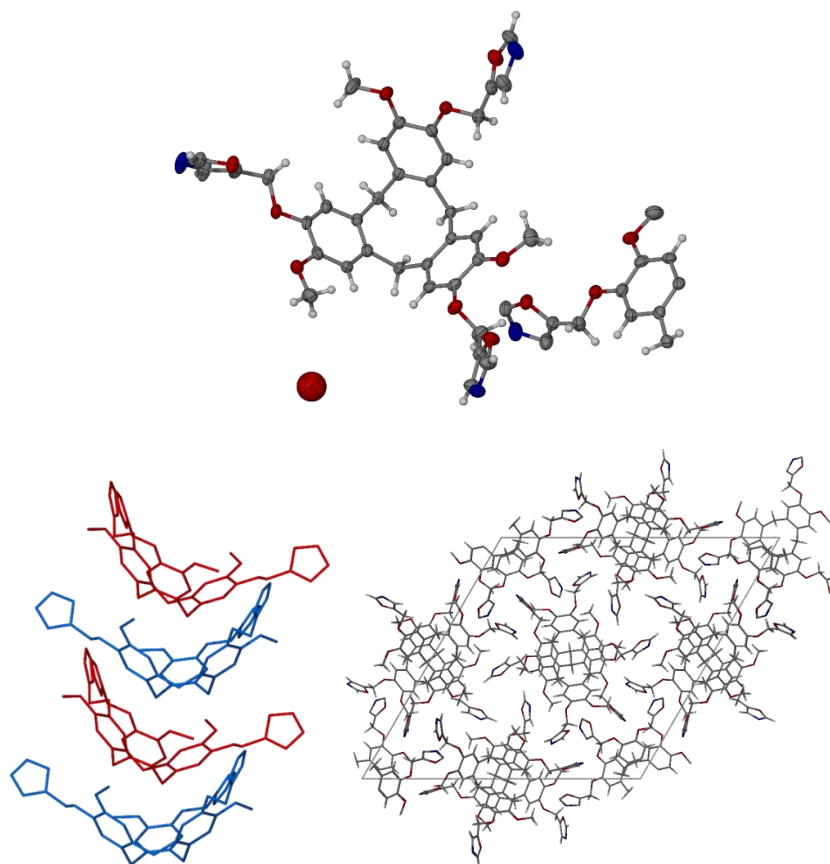
Figure 2.29 Top: Asymmetric unit of (2.18)₄·H₂O, ellipsoids are drawn at the 50% probability. Bottom left: β-bowl-in-bowl stacking. Bottom right: unit cell as shown down the crystallographic *c*-axis.

2.7 Assembly of Co(II) coordination polymers

The coordinative properties of oxazole **2.18** were trialled with a range of transition metal precursors covering Co(II) to Zn(II), Pd(II), and Ag(I) halides and non-coordinating anions. It was envisaged that a similar metallo-cryptophane to **2.12** could assemble, minus the π-π stacking interactions of the benzimidazole backbones, but crystals could not be grown, and only intractable yellow solid isolated. No evidence of crystalline material, or coordination could be attained in most reactions.

Diffusion of diethyl ether vapours into a DMF solution of **2.18** and $CoCl_2·6H_2O$ in 1:1 proportions gave a mixture of two crystalline products $[Co(Cl)_2(2.18)_2]_n$, **2.19a** and $[Co(Cl)_2(2.18)]_n$, **2.19b**.

Polymer **2.19a** crystallised in the $P\overline{1}$ space group. Each octahedral Co(II) centre coordinates axially to two chloride ligands at distances of 2.4608(12) Å, and four

equatorial oxazolyl moieties with Co-N bond lengths of 2.146(3) and 2.151(3) Å. The asymmetric unit comprised of one whole ligand unit, one Co atom of half occupancy on the unit cell vertex, one Cl atom, three DMF molecules, one disordered over two positions and three water molecules (figure 2.30).
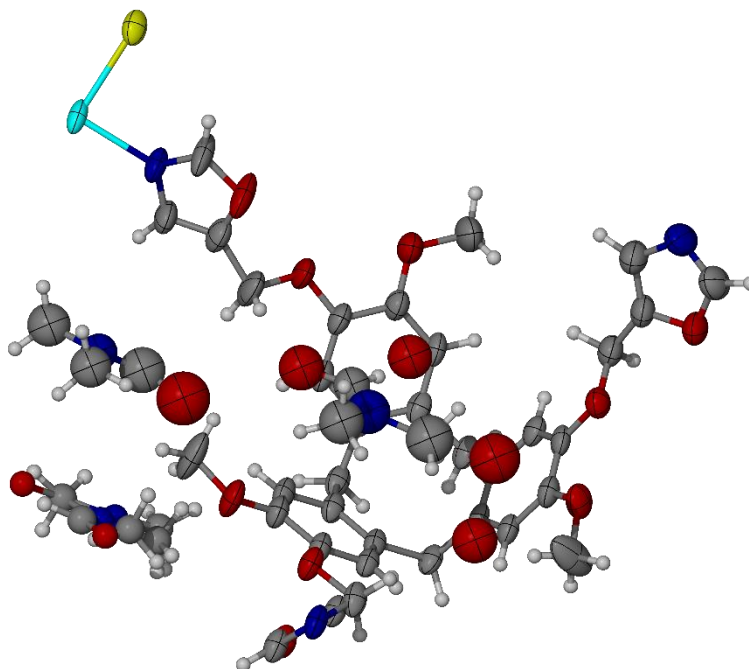
Figure 2.30 Asymmetric unit of 2.19a. Ellipsoids are drawn at the 50% probability

Crystals could only be grown at low-ambient temperatures (*ca.* 6 ℃). Attempts to regrow crystals above and below this temperature were ultimately unsuccessful and oils were obtained. Crystallisations in the fridge also failed, likely caused by too cold an environment, and/or increased humidity.

Near-diamond-shaped channels arise throughout the polymer chains with a Co-CTV$_{centroid}$-Co angle of *ca.* 85.5º. One oxazolyl moiety per cavitand is non-coordinating, and interdigitates with a neighbouring polymer chain, facilitated by π-π stacking of one non-coordinating and one ligated oxazole at separation of *ca.* 3.49 Å (figure 2.31), effectively filling the channels of the doubly bridged chest structure.
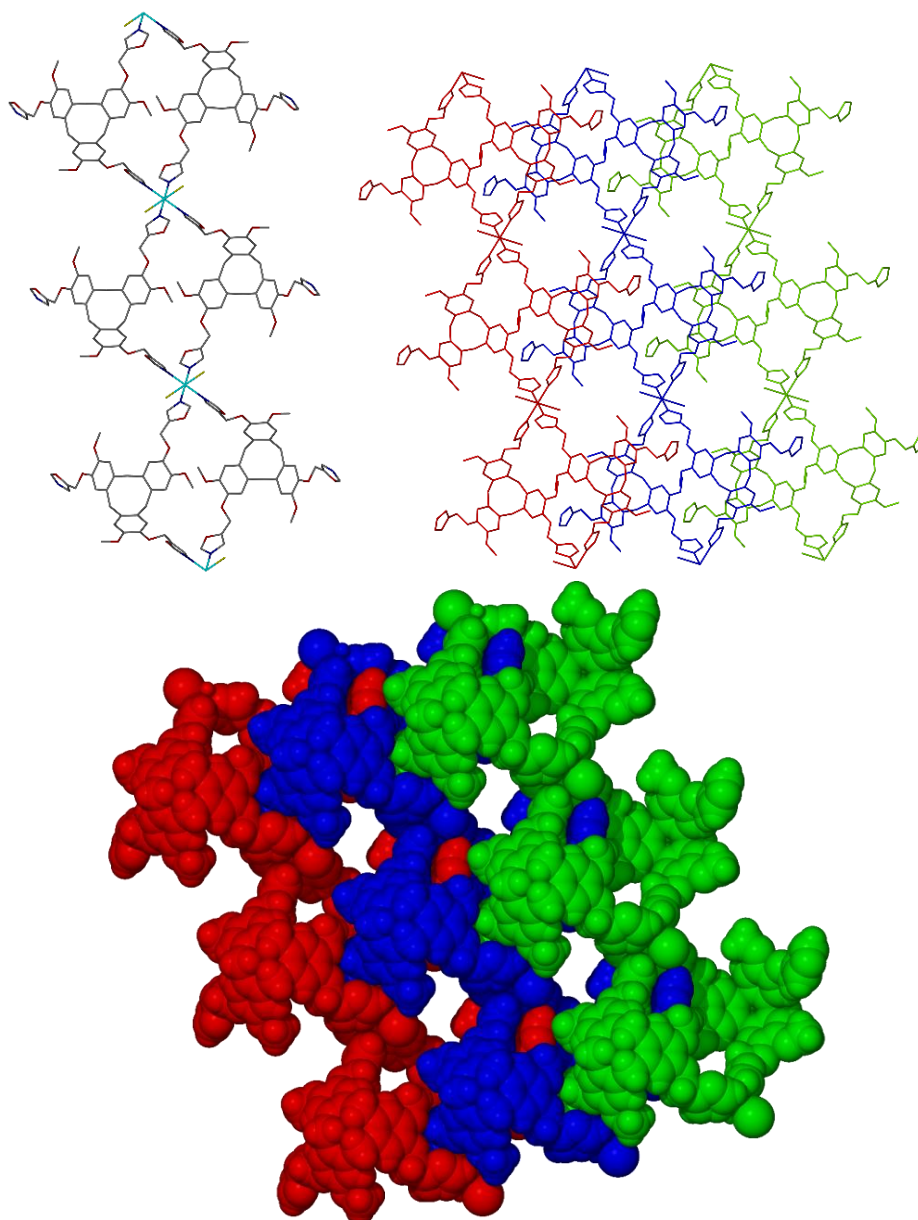
Figure 2.31 Top left: 1D chain of 2.19a. Top right: three interwoven polymer chains. Bottom: space filling model of chains.

A second composite of polymer (**2.19b**) of composition $[Co(Cl)_2(\textbf{2.18})]_n \cdot 3H_2O$ was also grown from the same batch and the structure obtained using synchrotron radiation. The asymmetric unit comprised of one $[Co(Cl)_2(\textbf{2.18})]$ unit and three water solvent molecules (figure 2.32).
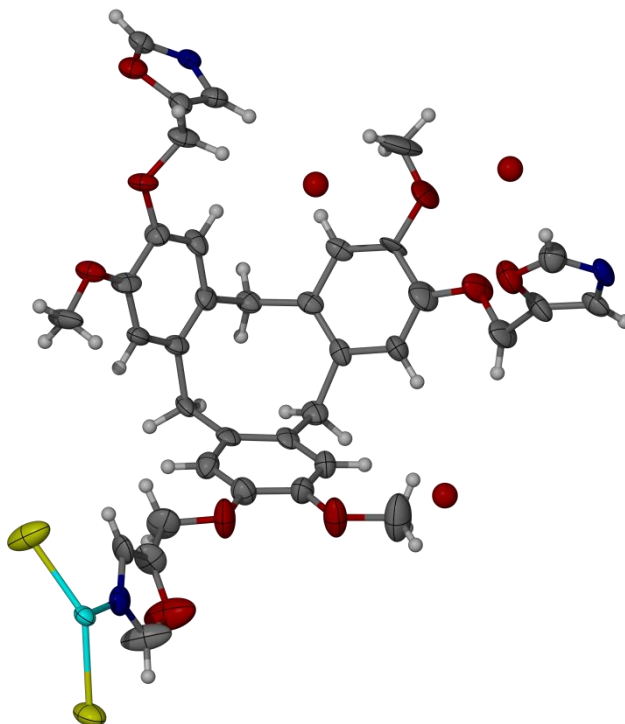
Figure 2.32 Asymmetric unit of 2.19b. Ellipsoids are drawn at the 50% probability.

Crystal data were of poor redundancy. Polymer 2.19b assembled as a ladder-like polymorph with rungs running between two parallel chains of ligand. The Co(II) centres here were contorted-trigonal bipyramidal, with oxazole ligands occupying the two axial sites and one equatorial position. The two chloride ligands were also equatorial. The two $Co\text{-}N_{ax}$ bond lengths were 1.994(9) and 2.016(7) Å, and a $Co\text{-}N_{equatorial}$ bond length of 2.211(9) Å. The Co-Cl bond lengths were 2.270(3) and 2.316(2) Å. The $N_{ax}\text{-}Co\text{-}N_{ax}$ bond angle was near-linear at 178.6(3)°, with significant distortion around the equator, with a Cl-Co-Cl angle of 145.01(15)° and $Cl\text{-}Co\text{-}N_{eq}$ angles of 108.4(2)° and 106.5(2)°. In contrast to **2.19a**, interdigitation between polymers was not observed in the case of **2.19b**. Instead, π-π stacking interactions between arene faces of the CTV core were observed, at a distance of *ca.* 3.62 Å measured between arene centroids (figure 2.33). There are well-defined pores within each polymer chain, however, the orientation of neighbouring chains does block them from passing through the whole structure.
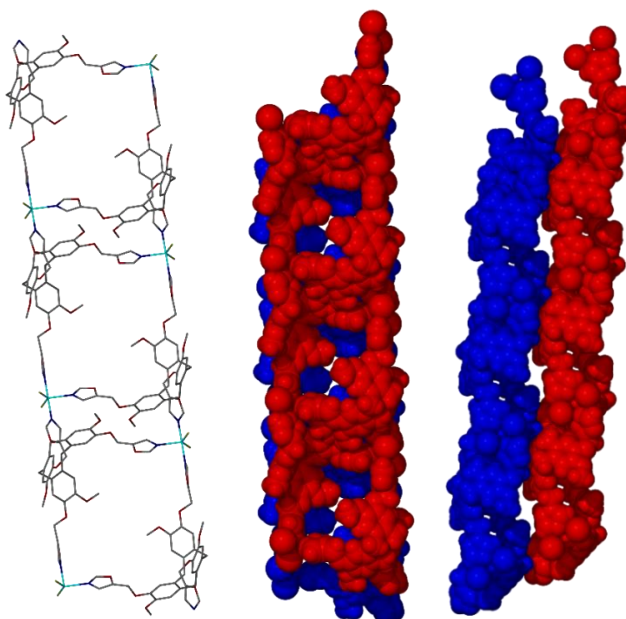
Figure 2.33 Left: Stick model of 2.19b. Centre: Space filling of two front-on chains. Right: two side-on chains.

Crystals were also grown from a vial containing $Co(NO_3)_2$ and ligand **2.18** from the diffusion of diethyl ether into an N-methylpyrrolidone (NMP) solution. SCXRD analysis using synchrotron radiation proved a polymer with composition $[Co(NO_3)_2(\textbf{2.18})_2]_n$, complex **2.20**. The unit cell parameters of **2.19a** and **2.20** were similar, with the major differences in **2.20** being with two NMP molecules in the asymmetric unit rather than DMF, and *trans*-nitrate anions as opposed to chlorides (figure 2.34).
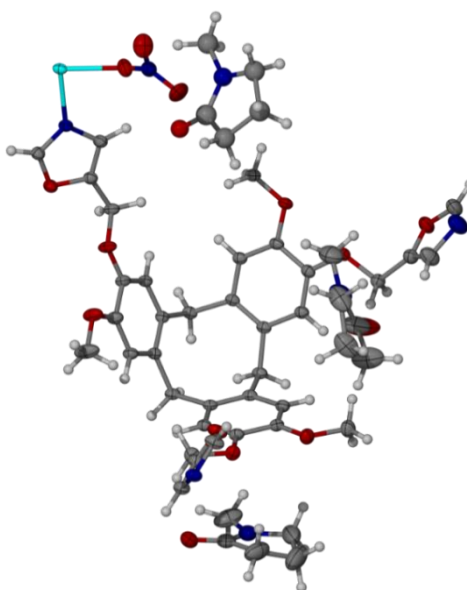
Figure 2.34 Asymmetric unit of 2.20. Ellipsoids are drawn at the 50% probability.

All four oxazole groups are equatorial about the octahedral Co(II) centre with Co-N bond lengths of 2.1256(12) and 2.1507(13) Å. The Co-O bond length was measured at 2.1254(13) Å, shorter than that noted for the chloride ligand by 0.2 Å. The same oxazole-oxazole π-π stacking between overlapping chains is also observed at centroid-centroid separation of *ca.* 3.67 Å.
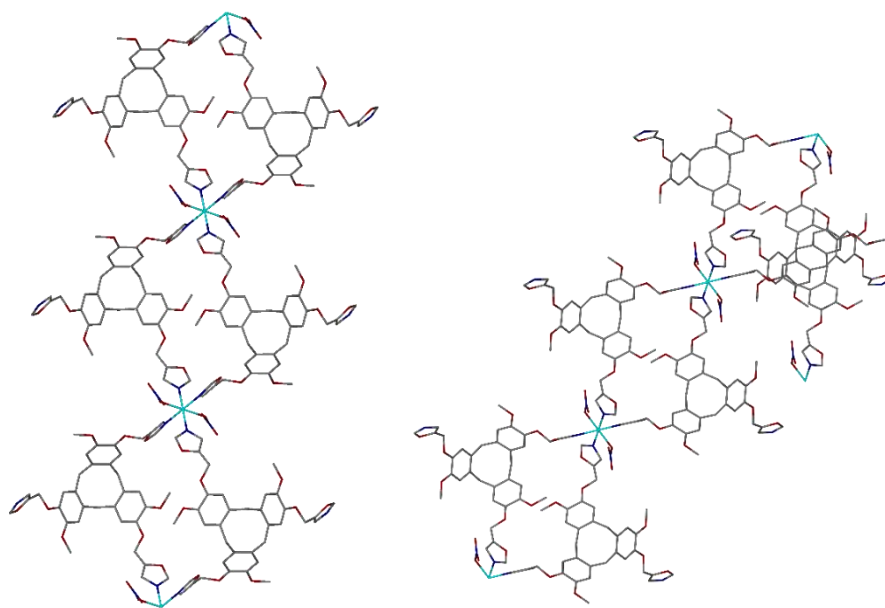
Figure 2.35 Left: three repeating units of 2.20. Right: exert showing capsular aggregation.

The observed powder pattern for bulk material related to **2.19a** and **2.19b** is indicative of a mixture of components (figures 2.36 and 2.37). Whilst there is peak overlap with the simulated X-ray spectra for **2.19a** and **2.19b**, it is not clear whether crystals of other composites were present in the bulk material. A number of crystals were screened, however only crystals with the same unit cell as **2.19** were found. Multiple composites of polymers are not uncommon because of the low thermodynamic driving force to induce polymerisation. Coordination polymer **2.20** displayed similar results, with peak overlap between the bulk material and simulated pattern for the single crystal studied, but it is unclear whether multiple composites were present in the bulk material. Crystals with the same unit cell parameters as **2.20** could only be found during screening.

It is worth noting that the experimental powder pattern was obtained at room temperature, whereas the simulated pattern was derived from data collected at

100-120 K, therefore peak intensities and also slight variations in angles are likely to occur.
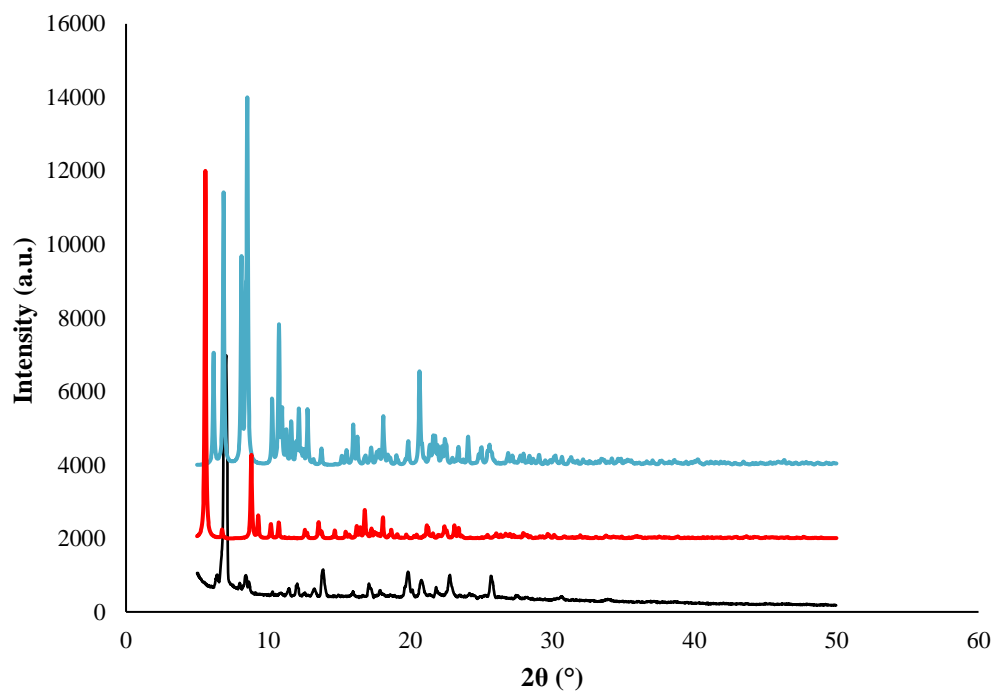
Figure 2.36 Powder pattern for 2.19a and 2.19b. Simulated data from crystal structures (100 K) of polymer 2.19a (blue trace) and 2.19b (red trace). Observed data from bulk material (rt) (black trace).
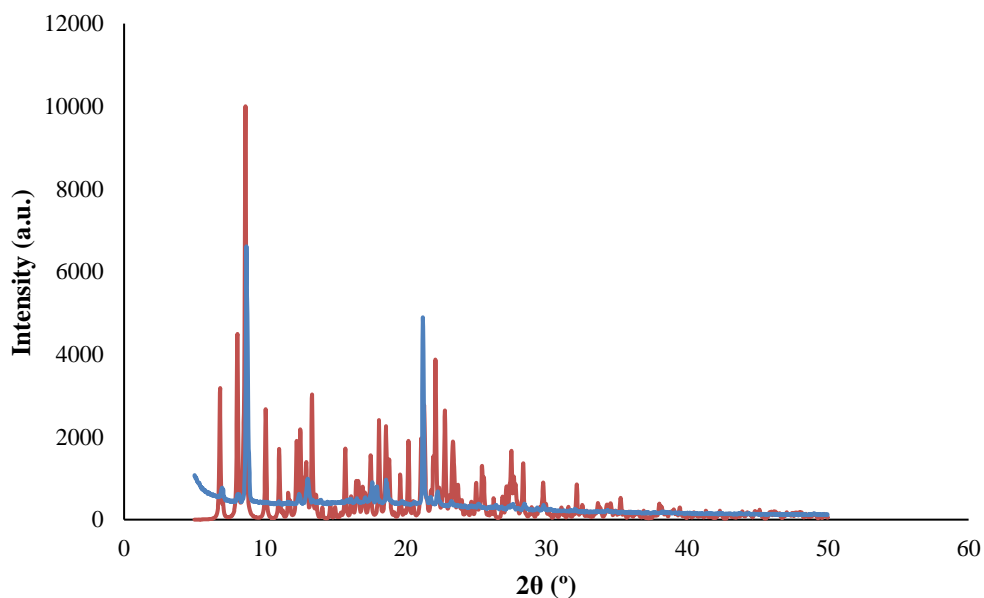
Figure 2.37 Powder pattern for 2.20. Simulated spectrum from crystal structure (100 K) (red trace). Observed data from bulk material (rt) (blue trace).

2.8 Conclusions and future work

Two imidazole-functionalised cyclotriguaiacylene ligands were prepared, but scale up and reproducibility were challenging because of the instability of precursors. Therefore, benzimidazole **2.11** was prepared and fully characterised and upon optimisation of synthetic protocol, overcame problems associated with the imidazole counterparts. Ligand **2.11** assembled with [Pd(Cl)$_2$(MeCN)$_2$] to yield *anti*-metallo-cryptophane **2.12**, and crystals of composition [Pd$_3$Cl$_6$(**2.11**)$_3$·(H$_2$O)]·1.5H$_2$O·3DMF. Both ligands in cryptophane **2.12** were of the same enantiomer, with crystals being racemic overall. Complex **2.12** was a rare example of a *trans*-linked metallo-cryptophane. Most examples of metallo-cryptophanes incorporating Pd(II) require *cis*-protecting groups such as a *bis*-NHC, forcing incoming cavitand ligands to coordinate *cis*- with respect to one another. These cryptophanes are typically also charged species.

Benzotriazolyl ligand **2.15** was also prepared in good yield, but its assembly with a range of metal precursors was unsuccessful. One azole not furnished on a CTV scaffold during this project was the 1,2,3-triazole derivative. 1,2,3-triazoles are straightforward to prepare using click chemistry, and have been appended onto CTV in a three-step synthesis to prepare dendrimer-functionalised cyclotriveratrylenes,[43] but coordination chemistry of this group tethered onto CTV remains untrialled.

A 5-oxazolyl ligand was also synthesised, and assembled with two Co(II) salts to yield 1D coordination polymers. Single-crystal and powder X-ray diffraction revealed the presence of (at least) two composites. Total yields were low, and crystals could only be grown at low ambient temperatures.

Future work could involve investigating the assembly of ligands **2.11**, **2.15** and **2.18** with the *cis*-protecting Pd(II)-*bis*-NHC tectons. It would be anticipated that they could assemble into *anti*-metallo-cryptophanes, with the bite angle of donor atoms relative to CTV reasonably similar to the pyridyl donors previously employed.

2.9 Experimental section

Unless stated in the experimental section, chemicals were bought from commercial suppliers (Sigma Aldrich, Fisher Scientific, Alfa Aesar, Fluorochem) and used without further purification. Reactions performed under an atmosphere of dry

nitrogen were carried out using standard Schlenk and glovebox procedures. Nitrogen gas was dried by passing through a twin column of 4 Å molecular sieves and P_2O_5. Anhydrous solvents (THF, DCM, CHCl₃, MeCN) were dried by passing through a column of activated alumina, degassed *via* the freeze-pump-thaw method prior to use and stored over 4 Å molecular sieves. Anhydrous DMF was bought from commercial suppliers, and both further dried and stored over 4 Å molecular sieves, and subsequently degassed *via* the freeze-pump-thaw method prior to use.

^{1}H, ^{13}C{^{1}H}, ^{19}F and ^{31}P NMR spectra were obtained using either a Bruker DPX 300 MHz spectrometer, Bruker Avance III HD-400 400 MHz spectrometer, or a Bruker Avance 500 MHz spectrometer. Full characterisation of novel compounds by ^{1}H and ^{13}C{^{1}H} NMR spectroscopy was aided by ^{1}H-^{1}H COSY, DEPT-135, HMBC and HMQC experiments. Electrospray mass spectra were obtained using a Bruker microTOF-Q spectrometer. FT-IR spectra were obtained using a Perkin-Elmer Spectrum One spectrophotometer. Elemental analyses were performed by Mrs. Tanya Marinko-Covell of the University of Leeds analytical service, or Mr. Stephen Boyer of the London Metropolitan University. Crystal structures were obtained using either synchrotron radiation from beamline I19 at the Diamond light source, or an Agilent SuperNova single crystal X-ray diffractometer.

Synthesis of 3-methoxy-4-(propenyloxy)benzyl alcohol, 2.1

4-Hydroxy-3-methoxybenzyl alcohol (30.74 g, 195.0 mmol), potassium carbonate (27.26 g, 197.0 mmol) and allyl bromide (19.10 mL, 216.0 mmol) were added to acetone and the solution heated to reflux under Ar for 24 h. The solvent was removed *in vacuo* and residue washed with DCM and water, the layers were separated and the organic layer dried with MgSO₄, DCM was removed *in vacuo*, affording **2.1** as a white solid. Yield 37.62 g, 193.7 mmol, 99%. ^{1}H NMR (300 MHz, CDCl₃) δ (ppm) 6.94 (s, 1H, H^{7}), 6.86 (s, 2H, H^{8}, H^{6}), 6.09 (m, 1H, H^{3}), 5.40 (dq, 1H, $J = 17.2$, 1.5 Hz, *trans*-H^{2}), 5.28 (dd, 1H, $J = 10.6$, 1.3 Hz, *cis*-H^{2}), 4.61 (m, 4H, H^{9}, H^{4}), 3.29 (s, 3H, H^{1}) ^{13}C{^{1}H} NMR (75 MHz, CDCl₃) δ (ppm) 150.0 (C5), 148.0 (C11), 134.4 (C^{3}), 133.7 (C^{11}), 119.7 (C^{2}), 118.4 (C^{7}), 113.8 (C^{8}), 111.3 (C^{6}), 70.4 (C^{4}), 65.7 (C^{9}), 56.3 (C^{1}). All data are consistent with those reported in the literature.[11]
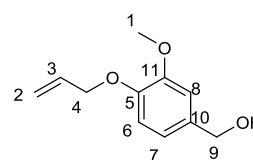
Synthesis of (±)-2,7,12-trimethoxy-3,8,13-*tris*-(propenyloxy)-10,15-dihydro-5*H*-tribenzo[*a,d,g*]-cyclononene, 2.2

3-Methoxy-4-(propenyloxy)benzyl alcohol (37.16 g, 193.1 mmol) was melted at 70 ºC and phosphoric acid (spatula tip) added. The reaction was stirred for 24 h until it solidified. The resulting solid was triturated in methanol (400 mL) before being filtered and dried *in vacuo*, affording **2.2** as a white solid. Yield 21.34 g, 40.0 mmol, 63%. ^{1}H NMR (300 MHz, CDCl$_3$) δ (ppm) 6.86 (s, 3H, H^5), 6.81 (s, 3H, H^4), 6.07 (m, 3H, H^2), 5.38 (dd, 3H, J = 17.3, 1.4 Hz, *trans*-H^1), 5.26 (dd, 3H, J = 10.5, 1.2 Hz, *cis*-H^1), 4.75 (d, 3H, J = 13.79 Hz, *endo*-H^6), 4.60 (m, 6H, H^3), 3.84 (s, 9H, H^7), 3.53 (d, 3H, J = 14.2 Hz, *exo*-H^6); ^{13}C{^{1}H} NMR (75 MHz, CDCl$_3$) δ (ppm) 148.2, (C^{11}) 146.1 (C^{10}), 133.7 (C^2), 132.4 (C^8), 131.7 (C^9), 117.5 (C^1), 115.6 (C^5), 113.6 (C^4), 70.2 (C^3), 56.1 (C^7), 36.5 (C^6). All data are consistent with those reported in the literature.[10]
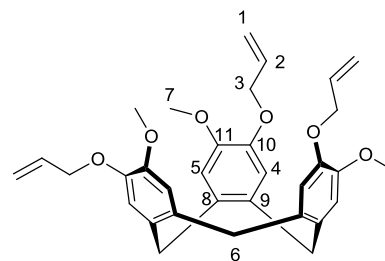
Synthesis of (±)-2,7,12-trimethoxy-3,8,13-*tris*-(hydroxy)-10,15-dihydro-5*H*-tribenzo[*a,d,g*]-cyclononene (CTG), 2.3

(±)-2,7,12-Trimethoxy-3,8,13-*tris*-(propenyloxy)-10,15-dihydro-5*H*-tribenzo[*a,d,g*]-cyclononene (10.30 g, 19.4 mmol) was added to a mixture of anhydrous THF (250 mL), diethylamine (91 mL) and water (90 mL), the reaction mixture degassed and backfilled with N$_2$, and heated to 80 ºC under Ar for 3 h. Palladium acetate (0.32 g, 1.4 mmol) and triphenylphosphine (0.95 g, 3.6 mmol) were added and the black solution held at reflux overnight. The mixture was filtered through celite, giving an orange solution. The solvents were removed *in vacuo* and the residue triturated in methanol, affording **2.3** as an off-white solid. Yield: 5.50 g, 13.5 mmol, 69%; ^{1}H NMR (300 MHz, CDCl$_3$) δ (ppm) 6.89 (s, 3H, H^2), 6.80 (s, 3H, H^3), 4.72 (d, 3H, J = 13.6 Hz, *endo*-H^4), 3.86 (s, 9H, H^1), 3.51 (d, 3H, J = 13.8 Hz, CTG *exo*-H^4); ^{13}C NMR (75 MHz, DMSO-d_6) δ (ppm) 145.96, 144.87, 132.57, 130.42, 116.78, 113.97, 55.97, 35.02. All data are consistent with those reported in the literature.[11]
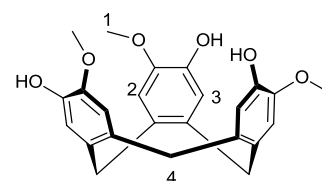
Synthesis of 1,1',1''-(((3,8,13-trimethoxy-10,15-dihydro-5H-tribenzo[*a,d,g*][9]annulene-2,7,12-triyl)tris(oxy))tris(methylene))tris(1H-imidazole), 2.4

CTG (200 mg, 0.5 mmol) was added to a suspension of sodium hydride (118 mg, 4.9 mmol) in anhydrous, degassed DMF (10 mL) and stirred for 30 mins. 1-(chloromethyl)imidazole·HCl (0.48 g, 3.2 mmol) was added and the mixture stirred at room temperature under N_2 for 72 h. The mixture was extracted with water (500 mL) and dichloromethane (3 x 300 mL). The organic layers were washed with water, (100 mL) and dried with $MgSO_4$, DCM was removed *in vacuo* and the product extracted from residual DMF with Et_2O, affording the title compound as a white solid. Yield 176 mg, 0.3 mmol, 55%. LC-MS (ESI)$^+$ m/z 649.3, Calcd. for $C_{36}H_{37}N_6O_6$ 649.2775; ^{1}H NMR (300 MHz, CDCl$_3$) δ (ppm) 7.52 (s, 3H, H^1), 7.02 (s, 3H, H^3), 6.98 (s, 3H, H^2), 6.68 (s, 3H, H^8), 6.62 (s, 3H, H^9), 5.73 (m, 6H, H^4), 4.59 (d, 3H, *J* = 13.9 Hz, *endo*-H^{12}), 3.84 (s, 9H, H^5), 3.39 (d, *J* = 13.8 Hz, *exo*-H^{12}); ^{13}C {^{1}H} NMR (75 MHz, CDCl$_3$) δ 150.18, 143.39, 137.78, 136.59, 131.68, 129.88, 123.25, 119.32, 114.10, 76.66, 56.20, 36.37. All data are consistent with those reported in the literature.[14]
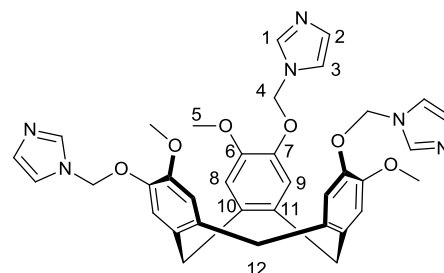
Synthesis of 1-(hydroxymethyl)imidazole, 2.5

Imidazole (10.00 g, 147.1 mmol) and paraformaldehyde (4.30 g, 143.1 mmol) were heated in a dry melt at 110 ºC for 1 h and the liquid solidified upon cooling. The solid residue was triturated in ethyl acetate, affording the title compound as a free-flowing white solid. Yield 10.49 g, 106.9 mmol, 76%. HRMS (ESI)$^+$ m/z 99.0552 Calcd. for {$C_4H_7N_2O$}$^+$ 99.0558; ^{1}H NMR (300 MHz, CDCl$_3$) δ (ppm) 7.30 (s, 1H, H^1), 7.10 (s, 1H, H^3), 6.98 (s, 1H, H^2), 5.41 (s, 2H, H^4); m.p. 37-39 ºC (lit. 36-38 ºC); ^{13}C{^{1}H} NMR (75 MHz, CDCl$_3$) δ (ppm) 136.29 (C1), 128.60 (C2), 118.88 (C3), 70.41 (C4) All data are consistent with those reported in the literature.[44]
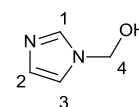
Synthesis of 1-(chloromethyl)imidazole hydrochloride, 2.6

1-(Hydroxymethyl)imidazole (1.0 g, 10 mmol) was dissolved in dry dichloromethane (30 mL) at 0 °C and thionyl chloride (3 mL) added. The mixture was warmed to room temperature and stirred under argon overnight. Solvent and excess thionyl chloride were removed *in vacuo* and the residue washed with acetonitrile, affording the title compound as a hygroscopic white solid. Yield 0.87 g, 7.5 mmol, 73.5%. ^{1}H NMR (300 MHz, D$_2$O) δ (ppm) 9.09 (s, 1H, H[1]), 7.77 (s, 1H, H[3]), 7.57 (s, 1H, H[2]), 6.09 (s, 2H, H[4]); ^{13}C {^{1}H} NMR (75 MHz, DMSO-d_6) δ (ppm) 138.11 (C[1]), 129.20 (C[2]), 119.91 (C[3]), 68.14 (C[4]). All data are consistent with those reported in the literature.[37]
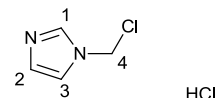
Synthesis of 1-(2-bromoethyl)imidazole hydrobromide, 2.7

Thionyl bromide (2.21 mL, 28.6 mmol) was added dropwise to a Schlenk flask containing 1-(2-hydroxyethyl)imidazole (1.07 g, 9.5 mmol) in anhydrous DCM (40 mL) at 0 °C. The solution held at 0 °C for 20 mins before warming to rt and stirred overnight. Solvent and excess thionyl bromide were removed *in vacuo*, affording a red oil which was dissolved in water and neutralised with saturated sodium carbonate. The product was extracted in chloroform and solvent removed *in vacuo*, affording the title compound as an orange solid. Yield 1.10 g, 6.6 mmol, 71%. ^{1}H NMR (300 MHz, CDCl$_3$) δ (ppm) 7.63 (s, 1H, H[1]), 7.11 (s, 1H, H[3]), 6.99 (s. 1H, H[2]), 4.37 (t. 2H, *J* = 6.4 Hz, H[4]), 3.60 (t, 2H, *J* = 6.4 Hz, H[5]); ^{13}C{^{1}H} NMR (75 MHz, CDCl$_3$) δ (ppm) 137.41, 129.93, 118.85, 48.54, 30.46. All data are consistent with those reported in the literature.[17]
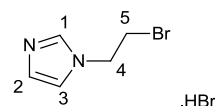
Synthesis of 1,1',1''-(((3,8,13-trimethoxy-10,15-dihydro-5H-tribenzo[*a,d,g*][9]annulene-2,7,12-triyl)tris(oxy))tris(ethane-2,1-diyl))tris(1H-imidazole), 2.8

CTG (200 mg, 0.49 mmol) was added to a suspension of sodium hydride (118 mg, 4.9 mmol) in anhydrous, degassed DMF (10 mL) at room temperature and stirred for 30 mins. 1-(bromoethyl)imidazole·HCl (0.8 g, 3.2 mmol) was added in portions and the reaction mixture stirred for 96 h under N$_2$. The solution was extracted with water (500 mL) and
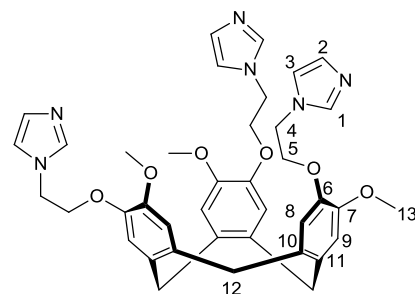
dichloromethane (3 x 300 mL). The organic layers were combined, washed with water (200 mL) and dried with $MgSO_4$. DCM was removed *in vacuo* and the product extracted from residual DMF with Et_2O, affording the title compound as a white solid. Yield 123 mg, 0.2 mmol, 36%. HRMS (ESI[+]) m/z 299.1395 $\{C_{34}C_{38}N_4O_6\}^{2+}$, 346.1668 $\{C_{39}H_{44}N_6O_6\}^{2+}$ 597.2718 $\{C_{34}H_{37}N_4O_6\}^+$ 691.3257 $\{C_{39}H_{43}N_6O_6\}^+$, Calcd. for 299.1390, 346.1656, 597.2708, 691.3239 respectively; ^{1}H NMR (300 MHz, DMSO-d_6) δ (ppm) 7.65 (s, 3H, H[1]), 7.21 (s, 3H, H[3]), 7.06 (s, 3H, H[9]), 7.04 (s, 3H, H[8]), 6.86 (s, 3H, H[2]), 4.66 (d, 3H, J = 13.3 Hz, *endo*-H[12]), 4.28, (m, 6H, H[4]), 4.17 (m, 6H, H[5]), 3.69 (s, 9H, H[13]), 3.47 (d, 3H, J = 13.3 Hz, *exo*-H[12]); ^{13}C {^{1}H} NMR (75 MHz, DMSO-d_6) δ (ppm) 147.70 (C[7]), 145.92 (C[8]), 137.58 (C[1]), 132.94 (C[10]), 132.05 (C[9]), 128.20 (C[2]), 119.67 (C[3]), 115.66 (C[9]), 114.19 (C[8]), 68.56 (C[5]), 56.06 (C[13]), 45.64 (C[4]), 34.93 (C[12]); FTIR ν (cm^{-1}) 2917, 2846, 1669, 1607, 1509, 1260.

Synthesis of 1-(hydroxymethyl)benzimidazole, 2.9

Benzimidazole (1.57 g, 13 mmol) was dissolved in THF (40 mL) and formaldehyde (1 mL, 13 mmol, 37% in H_2O) was added slowly. The pale yellow solution was stirred for 1 h under ambient conditions. Solvents were removed *in vacuo*, affording a white solid as the title compound with no need to purify. Yield 1.78 g, 12.2 mmol, 90%. HRMS (ESI[+]) 149.0705, Calcd. for $C_8H_9N_2O$ 149.0709; ^{1}H NMR (501 MHz, DMSO-d_6) δ (ppm) 8.25 (s, 1H, H[1]), 7.65 (d, 2H, J = 8.9 Hz, H[3], H[6]), 7.27 (t, 1H, J = 8.0 Hz, H[4]), 7.22 (t, 1H, J = 8.0 Hz, H[5]), 6. (t, 1H, J = 7.0 Hz, H[9]), 5.60 (d, 2H, J = 6.8 Hz, H[8]); ^{13}C{^{1}H} NMR (126 MHz, DMSO-d_6) δ (ppm) 143.44, 141.51, 133.14, 122.06, 121.40, 119.10, 110.54, 67.21. All other data are consistent with those reported in the literature.[37]
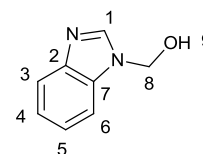
Synthesis of 1-(chloromethyl)benzimidazole hydrochloride, 2.10

1-(Hydroxymethyl)benzimidazole (2.32 g, 15.7 mmol) was stirred in thionyl chloride (15 mL, 200.0 mmol) at room temperature under argon overnight. Thionyl chloride was removed *in vacuo* and the residue recrystallised from MeOH and Et_2O, affording a white solid as the title compound. Yield 2.37 g, 11.7 mmol, 75%. HRMS (ESI[+]) 167.0368, Calcd. for $\{C_8H_8ClN_2\}^+$ 167.0371; ^{1}H NMR (300 MHz, CD_3OD) δ (ppm) 9.74 (s,
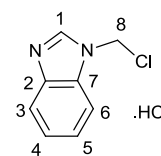
1H, H^1), 8.11-8.05 (m, 1H, H^3), 7.96-7.89 (m, 1H, H^6), 7.81-7.71 (m, 2H, H^4, H^5), 6.50 (s, 2H, H^8); ^{13}C{^{1}H} NMR (75 MHz, CD$_3$OD) δ 143.28, 132.46, 131.42, 128.85, 128.59, 116.24, 114.34, 53.66. All data are consistent with those reported in the literature.[45]

(±)-2,7,12-Trimethoxy-3,8,13-*tris*(methylbenzimidazol-1-yl)-10,15-dihydro-5*H*-tribenzo[a,d,g]cyclononene, 2.11

CTG (400 mg, 1.0 mmol) was added to a suspension of NaH (60% dispersion in mineral oil) (0.84 g, 20.8 mmol) in anhydrous, degassed DMF (10 mL) under an N$_2$ atmosphere at room temperature, and stirred for 30 mins. 1-(Chloromethyl)benzimidazole hydrochloride (694 mg, 3.4 mmol) was added in portions and the mixture stirred for 16 h. Water (100 mL) was added and the resulting grey precipitate filtered. The grey residue was re-dissolved in dichloromethane (60 mL), dried over MgSO$_4$, and solvents removed *in vacuo*. The residue was sonicated in diethyl ether (50 mL), affording the title compound as a white solid. Yield 0.58 g, 0.73 mmol, 75%; HRMS (ESI$^+$) 821.3065 {MNa}$^+$, calculated for {C$_{48}$H$_{42}$N$_6$NaO$_6$}$^+$ 821.3059; ^{1}H NMR (300 MHz, DMSO-*d$_6$*) δ (ppm) 8.35 (s, 3H, H^1), 7.65 (dd, 3H, *J* = 6.1, 2.9 Hz, H^6), 7.59-7.55 (m, 3H, H^3), 7.25-7.20 (m, 6H, H^4, H^5), 7.18 (s, 3H, H^{10}), 7.04 (s, 3H, H^{11}), 6.20-6.10 (m, 6H, H^8), 4.69 (d, 3H, *J* = 13.5 Hz, *endo*-H^{16}), 3.67 (s, 9H, H^9), 3.47 (d, 3H, *J* = 13.6 Hz, *exo*-H^{16}); ^{13}C{^{1}H} NMR (75 MHz, DMSO-*d$_6$*) δ (ppm) 148.76 (C^{13}), 144.34 (C^1), 143.50 (C^2), 143.46 (C^7), 134.88 (C^{15}), 133.47 (C^{12}), 131.79 (C^{14}), 122.90 (C^5), 122.21 (C^4), 119.51 (C^6), 119.01 (C^{10}), 114.34 (C^{11}), 110.76 (C^3), 73.03 (C^8), 55.93 (C^9), 35.06 (C^{16}); Elemental analysis for C$_{48}$H$_{42}$N$_6$O$_6$·1.5(H$_2$O) Calcd. C 69.79, H 5.50, N 10.18; Found: C 69.82, H 5.01, N 10.32; FT-IR (cm^{-1}) 3092, 2958, 2926, 1611, 1452, 1273, 1198, 970, 745.
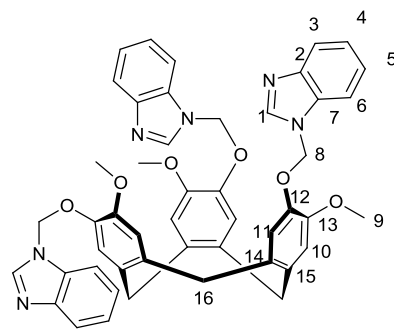
[Pd$_3$Cl$_6$(L2)$_2$] metallo-cryptophane, 2.12

A solution of L2 (7 mg, 8 μmol) and [PdCl$_2$(MeCN)$_2$] (3.4 mg, 13 μmol) in DMF (1 mL) was stirred for 24 h. Two drops were taken for HRMS characterisation, and the rest set up as a vapour diffusion with diethyl ether anti-solvent. A pale yellow solid precipitated after one week, and small number of pale yellow blocks grew after three

months. HRMS (ESI$^+$) m/z 941.1833 for species $\{PdCl(L2)\}^+$, 2134.21 $\{Pd_6Cl_5L_2(MeCN)\}^+$; FT-IR (cm^{-1}) 1611, 1508, 1264, 1182, 1141, 1066, 1025, 742. Satisfactory microanalysis was not obtained from powdered material which is likely a mixture of cage and PdCl$_2$: Found C 47.39 H 3.41 N 7.73 % Calcd. for $[Pd_3Cl_6(L2)_2]$ C 54.12, H 3.98, N 7.89; for $[Pd_3Cl_6(L2)_2].PdCl_2$ C 49.96, H 3.67, N 7.29.

Synthesis of 1-(hydroxymethyl)benzotriazole, 2.13

Benzotriazole (5 g, 41.9 mmol) was dissolved in THF (60 mL) and formaldehyde (37% in H$_2$O) (3.4 mL, 41.9 mmol) added. The colourless solution was stirred for 1 h, solvent removed *in vacuo* and the residue washed with methanol, affording the title compound as a white solid. Yield (4.92 g, 33.0 mmol, 79%). ^{1}H NMR (300 MHz, DMSO-d_6) δ (ppm) 8.06 (d, J = 8.4 Hz, H^2), 7.91 (d, 1H, J = 9.1 Hz, H^5), 7.64-7.52 (m, 1H, H^4), 7.43 (m, 1H, H^3), 7.19 (t, 1H, J = 7.7 Hz, H^8), 6.02 (d, 2H, J = 7.6 Hz, H^7) ^{13}C{^{1}H} NMR (75 MHz, DMSO-d_6) δ (ppm) 146.38 (C^1), 133.14 (C^6) 127.34 (C^4), 124.08 (C^3), 119.04 (C^2), 110.92 (C^5), 70.20 (C^7). All data are consistent with those reported in the literature.[46]
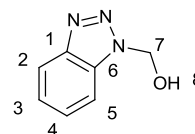
Synthesis of 1-(chloromethyl)benzotriazole·HCl, 2.14

1-(Hydroxymethyl)benzotriazole (2.0 g, 13.4 mmol) was stirred in thionyl chloride (10 mL) at room temperature under a N$_2$ atmosphere overnight. Solvents were removed in vacuo, and the residue recrystallised from MeOH/Et$_2$O in the freezer, affording the title compound as a colourless crystalline solid (2.2 g, 10.8 mmol, 80%). HRMS (ESI+) 168.0321, Calcd. for $\{MH: C_7H_7ClN_3\}^+$ 168.0323; ^{1}H NMR (300 MHz, CDCl$_3$) δ (ppm) 8.14-8.09 (m, 1H, H^2), 7.68 (dt, 1H, J = 8.3, 1.0 Hz, H^5), 7.64-7.57 (m, 1H, H^4), 7.46 (ddd, 1H, J = 8.1, 6.9, 1.1 Hz, H^3), 6.41 (s, 2H, H^7); ^{13}C{^{1}H} NMR (75 MHz, CDCl$_3$) δ (ppm) 142.67 (C^1), 133.08 (C^6), 128.77 (C^4), 125.06 (C^3), 120.75 (C^2), 109.69 (C^5), 53.58 (C^7). All data are consistent with those reported in the literature.[47]
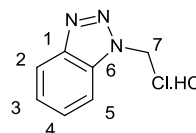
Synthesis of (±)-1,1',1''-(((3,8,13-trimethoxy-10,15-dihydro-5H-tribenzo[a,d,g][9]annulene-2,7,12-triyl)tris(oxy))tris(methylene))tris(1H-benzo[d][1,2,3]triazole), 2.15

CTG (100 mg, 0.2 mmol) and NaH (60% dispersion) (220 mg, 5.5 mmol) were dissolved in anhydrous, degassed DMF (5 mL) and stirred for 30 mins at rt under an atmosphere of N_2. 1-(chloromethyl)benzotriazole·HCl (226 mg, 1.1 mmol) was added and the reaction stirred at rt overnight. Water (20 mL) was added to the burgundy solution and a pale pink solid precipitated. The solid was filtered under reduced pressure, and washed with water (5 mL), MeOH (5 mL) and diethyl ether (5 mL), affording **2.15** as a pale pink solid. Yield 180 mg, 0.2 mmol, 94%. HRMS (ESI$^+$) 824.2933, Calcd. for {MNa: $C_{45}H_{39}N_9NaO_6$}$^+$ 824.2916; ^{1}H NMR (300 MHz, CDCl$_3$) δ (ppm) 7.98-7.89 (m, 3H, H^4), 7.44-7.35 (m, 3H, H^3), 7.20-7.12 (m, 6H, H^2, H^5), 6.82 (s, 3H, H^{10}), 6.65 (s, 3H, H^{13}), 6.52 (d, 3H, J = 11.3 Hz, H^7), 6.39 (d, 3H, J = 11.3 Hz, H^7), 4.50 (d, 3H, J = 13.7 Hz, *endo*-H^{15}), 3.85 (s, 9H, H^{14}), 3.32 (d, 3H, J = 13.9 Hz, *exo*-H^{15}); ^{13}C{^{1}H} NMR (75 MHz, CDCl$_3$) δ (ppm) 149.45 (C^9), 146.20 (C^1), 144.20 (C^8), 135.84 (C^{11}), 133.18 (C^6), 131.56 (C^{12}), 128.03 (C^5), 124.42 (C^2), 120.54 (C^{10}), 119.81 (C^4), 113.81 (C^{13}), 109.97 (C^3), 76.66 (C^7), 56.32 (C^{14}), 36.28 (C^{15}). Elemental analysis for $C_{45}H_{39}N_9O_6$ Calcd. C 67.40, H 4.90, N 15.72; Found: C 67.28, H 5.09, N 15.57.
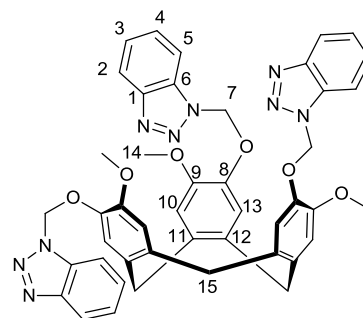
Synthesis of 5-hydroxymethyloxazole, 2.16

Ethyl oxazole-5-carboxylate (3 mL, 25.0 mmol) and lithium chloride (6.37 g, 150.0 mmol) were dissolved in anhydrous THF (50 mL) and methanol (100 mL) under a N_2 atmosphere and cooled to 0 °C. Sodium borohydride (5.67 g, 150.0 mmol) was added in small portions over a 30 min period, warmed to rt and stirred for 24 h. Water (100 mL) was added and the product extracted into ethyl acetate (3 x 150 mL) and DCM (3 x 50 mL). The organic layers were combined, dried over MgSO$_4$, filtered and solvents removed *in vacuo*, affording the title compound as an orange oil. Yield 1.40 g, 14.1 mmol, 56%. ^{1}H NMR (300 MHz, CDCl$_3$) δ (ppm) 7.85 (s, 1H, H^1), 7.01 (s, 1H, H^2), 4.69 (s, 2H, H^3), 2.61 (s, 1H, H^4); ^{13}C {^{1}H} NMR (75 MHz, DMSO-d_6) δ (ppm) 151.74, 151.56, 123.98, 55.34. All data were consistent with those reported in the literature.[48]
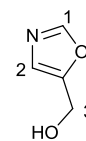
Synthesis of 5-Chloromethyloxazole, 2.17

2.16 (1.4 g, 14.1 mmol) was dissolved in anhydrous DCM (5 mL) and anhydrous hexane (5 mL) under a N_2 atmosphere and cooled to 0 ℃. Thionyl chloride (5 mL) was added and the reaction mixture gradually heated to reflux over a 1 h period and stirred for 16 h. The reaction was cooled and quenched with H_2O (15 mL), sat. $NaHCO_3$ (20 mL) and extracted into Et_2O (3 x 30 mL). The organic layers were combined, dried over $MgSO_4$, filtered and solvents removed in vacuo, affording the title compound as a pale yellow oil. Yield 0.71 g, 6.0 mmol, 43%. ^1H NMR (300 MHz, $CDCl_3$) δ (ppm) 7.89 (s, 1H, H^1), 7.10 (s, 1H, H^2), 4.62 (s, 2H, H^3) ^{13}C {^1H} NMR (75 MHz, DMSO-d_6) δ (ppm) 153.31, 148.22, 128.23, 42.26. All data were consistent with those reported in the literature.[48]
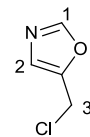
Synthesis of 5,5',5''-(((3,8,13-trimethoxy-10,15-dihydro-5H-tribenzo[*a*,*d*,*g*][9]annulene-2,7,12-triyl)tris(oxy))tris(methylene))tris(oxazole), 2.18

CTG (100 mg, 0.2 mmol) and caesium carbonate (797 mg, 2.4 mmol) were dissolved in DMF (5 mL) and heated to 100 ℃ for 1 h. 5-(Chloromethyl)oxazole (200 mg, 1.7 mmol) was added and the reaction stirred at 100 ℃ for 16 h, during which the reaction mixture turned brown. Water was added and the brown residue was filtered, washed with water (5 mL), methanol (5 mL) and diethyl ether (10 mL), affording the title compound as a tan solid. Yield (113 mg, 17.3 mmol, 72%). HRMS (ESI+) 784.1275, Calcd. for {M+Cs: $C_{36}H_{33}N_3O_9$}$^+$ 784.1266; ^1H NMR (300 MHz, $CDCl_3$) δ (ppm) 7.87 (s, 3H, H^1), 7.11 (s, 3H, H^2), 6.94 (s, 3H H^7), 6.83 (s, 3H, H^{10}), 5.06 (s, 6H, H^4), 4.73 (d, 3H, *J* = 13.0 Hz, endo-H^{12}), 3.83 (s, 9H, H^{11}), 3.53 (d, 3H, *J* = 13.7 Hz, exo-H^{12}); ^{13}C{^1H} NMR (75 MHz, $CDCl_3$) δ (ppm) 151.67 (C^1), 149.31 (C^6), 148.27 (C^3), 146.29 (C^5), 134.28 (C^8), 131.95 (C^9), 126.35 (C^2), 118.52 (C^7), 114.40 (C^{10}), 62.28 (C^4), 56.47 (C^{11}), 36.62 (C^{12}). Elemental analysis for $C_{36}H_{33}N_2O_9$·(H_2O) Calcd. C 64.57, H 5.27, N 6.45; Found: C 64.43, H 5.52, N 6.26.
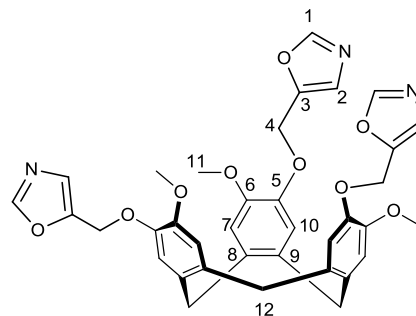
Synthesis of polymers 2.19a and 2.19b

2.18 (5.0 mg, 0.007 mmol), $CoCl_2 \cdot 6H_2O$ (1.8 mg, 0.007 mmol) and DMF (1 mL) were added to a vial and stirred for 5 min. Diethyl ether vapours were diffused into the vial and pale blue blocks grew after *ca.* 3 weeks. Total yield 2.1 mg, 31%.

Insufficient material led to only single crystal and powder X-ray diffraction analysis being attainable. Crystal growth was very sensitive towards ambient temperature, and could only be grown between *ca.* 5-8 ºC.

Synthesis of polymer 2.20

2.18 (5.0 mg, 0.007 mmol), $Co(NO_3)_2 \cdot 6H_2O$ (2.2 mg, 0.007 mmol) and NMP (1 mL) were added to a vial and stirred for 5 min. Diethyl ether vapours were diffused into the vial and pale pink blocks grew after *ca.* 3 weeks. Yield 1.8 mg, 0.002 mmol, 25%.

Insufficient material led to only single crystal and powder X-ray diffraction analysis being attainable. Crystal growth was very sensitive towards ambient temperature, and could only be grown between *ca.* 5-8 ºC.

2.10 Supplementary crystallography information

Crystals were mounted under inert oil on a MiTeGen tip and flash frozen using an OxfordCryosystems low temperature device. X-ray diffraction data were collected using CuKα radiation ($\lambda = 1.54184$ Å) or MoKα ($\lambda = 0.71073$ Å) using an Agilent Supernova dual-source diffractometer with Atlas S2 CCD detector and fine-focus sealed tube generator, or using synchrotron radiation ($\lambda = 0.6889$ Å) at Beamline I19 at the Diamond light source. Data were corrected for Lorenztian and polarization effects and absorption corrections were applied using multi-scan methods. The structures were solved by direct methods using SHELXS-97 and refined by full-matrix on F^2 using SHELXL-97.[49] Unless otherwise specified, all non-hydrogen atoms were refined as anisotropic, and hydrogen positions were included at geometrically estimated positions.

2.10.1 Additional crystallographic details

2.8

The imidazole ring was disordered over two positions, each with 50% occupancy.

(2.11)·(2.3)

The crystal data were of poor quality with poor internal consistency, and did not diffract to high angles, even when using synchrotron radiation.

[2.12·(H₂O)]·1.5H₂O·3DMF

Water and DMF molecules were refined isotropically, one guest water molecule displayed threefold site-symmetry, and another was at 50% occupancy. Hydrogen positions for water molecules were not included.

(2.18)₄·H₂O

The water molecule was refined as isotropic and the hydrogen positions not included.

2.19a

All DMF solvent molecules were refined as isotropic, one was disordered over two positions with a 1:1 distribution of electron-density between the sites. C41 was split between both positions, behaving as both the carbonyl carbon and a N-methyl carbon in separate symmetry partners. Water molecules were refined as isotropic and hydrogen positions not included.

2.19b

Data were of low redundancy due to the small size of the dataset. Attempts to find this crystal composite in further grown batches was unsuccessful for better quality data collection were unsuccessful. Three water molecules observed in the asymmetric unit were refined as isotropic and hydrogen positions not included.

2.20

One NMP solvent molecule was disordered over two positions and of 0.5 occupancy. The NMP solvent molecule displaying site-symmetry was refined as isotropic.

Table 2.1 data. a = CuKα radiation, b = synchrotron radiation

Compound	2.8[b]	2.11[a]	(2.11)·(2.3)[b]	[2.12·(H$_2$O)]·1.5H$_2$O·3DMF[a]	(2.18)$_4$·H$_2$O[a]
Formula	C$_{39}$H$_{42}$N$_6$O$_6$	C$_{48}$H$_{42}$N$_6$O$_6$	C$_{72}$H$_{66}$N$_6$O$_{12}$	C$_{105}$H$_{110}$Cl$_6$N$_{15}$O$_{17.5}$Pd$_3$	C$_{144}$H$_{119}$N$_{12}$O$_{37}$
Mr	690.79	798.88	1207.31	2393.98	2609.50
Crystal size	0.15 x 0.08x0.08	0.31 x 0.05 x 0.05	0.05 x 0.02 x 0.02	0.07 x 0.06 x 0.05	0.05 x 0.09 x 0.18
Crystal system	Trigonal (hexagonal axes)	Triclinic	Trigonal	Cubic	Hexagonal
Space group	$P\bar{3}$	$P\bar{1}$	$Pc31$	$Pa\bar{3}$	$P6_3$
a (Å)	20.9167(6)	10.7347(5)	19.4199(10)	27.7884(3)	27.8461(4)
b (Å)	20.9167(6)	12.6277(4)	19.4119(10)	27.7884(3)	27.8461(4)
c (Å)	4.6836(2)	14.8026(6)	9.0953(8)	27.7884(3)	9.89520(10)
α (^{0})	90	83.722(3)	90	90	90
β (^{0})	90	86.985(4)	90	90	90
γ (^{0})	120	79.149(3)	120	90	120
V (Å^3)	1774.58(13)	1957.81(14)	2968.1(4)	21458.1(4)	6644.8(2)
Z	2	2	2	8	2
ρ_{calc} (g.cm^{-3})	1.293	1.355	1.351	1.482	1.304
θ range (^{0})	1.329- 33.041	3.58-73.75	2.10-20.81	3.18-73.79	3.174- 74.345
No. data collected	17698	15677	23054	19190	44555
No. unique data	2683	7391	2079	7084	8533
R_{int}	0.0750	0.0281	0.1652	0.0430	0.0606
No. obs. Data ($I > 2\sigma(I)$)	1793	6235	1967	5598	7363
No. parameters	155	544	274	414	582
No. restraints	0	0	1	0	1
R_1 (obs data)	0.0939	0.0375	0.0762	0.0675	0.0572
wR_2 (all data)	0.3210	0.0927	0.1936	0.1994	0.1673
S	1.099	1.022	1.124	1.040	1.089
Max. shift/esd	0.001	0.001	0.000	0.001	0.000
Largest difference peak and hole/ (e Å^3)	1.431, -0.379	0.205, -0.219	0.248, -0.215	2.155, -1.143	1.257, -0.563

Table 2.2 Crystallographic data. a = CuKα radiation, b = synchrotron radiation

Compound	2.19a[a]	2.19b[b]	2.20[b]
Formula	$C_{87}H_{107}Cl_2CoN_{11}O_{26}$	$C_{36}H_{32}Cl_2CoN_3O_{12}$	$C_{97}H_{102}CoN_{12}O_{29}$
Mr	1852.67	828.47	1958.83
Crystal size	0.17 x 0.21 x 0.33	0.08 x 0.10 x 0.11	0.11 x 0.12 x 0.14
Crystal system	Triclinic	Triclinic	Triclinic
Space group	$P\bar{1}$	$P\bar{1}$	$P\bar{1}$
a (Å)	11.8619(5)	10.68120(10)	11.97940(10)
b (Å)	15.3330(5)	16.5920(2)	14.98320(10)
c (Å)	16.0976(7)	17.0517(2)	15.91110(10)
α (^{0})	110.509(3)	102.1580(10)	115.25
β (^{0})	100.788(3)	105.3480(10)	98.9990(10)
γ (^{0})	105.274(3)	99.0730(10)	105.5150(10)
V (Å^3)	2515.64(17)	2774.83(6)	2365.97(3)
Z	1	2	1
ρ_{calc} (g.cm^{-3})	1.223	0.992	1.375
θ range (^{0})	3.08- 73.85	1.977- 25.068	1.522- 29.477
No. data collected	21162	5923	40329
No. unique data	9487	4633	14188
R_{int}	0.0277	0.0191	0.0422
No. obs. Data ($I > 2\sigma(I)$)	7839	4379	12279
No. parameters	547	475	634
No. restraints	4	0	1
R_1 (obs data)	0.1113	0.1456	0.0582
wR_2 (all data)	0.3398	0.4529	0.1798
S	1.444	2.423	1.070
Max. shift/esd	0.001	0.001	0.000
Largest difference peak and hole/ (e Å^3)	1.714, -0.665	1.964, -0.753	1.352, -0.536

2.11 References

1. D. C. Hodgkin, J. Pickworth, J. H. Robertson, K. N. Trueblood, R. J. Prosen, J. G. White, *Nature*, 1955, **176**, 325.

2. J. D. Watson, F. H. C. Crick, *Cold Spring Harbor Symposia on Quantitative Biology*, 1953, **18**, 123-131.

3. S. Sinnecker, N. Svensen, E. W. Barr, S. Ye, J. M. Bollinger, F. Neese, C. Krebs, *J. Am. Chem. Soc.*, 2007, **129**, 6168-6179.

4. K. S. Park, Z. Ni, A. P. Côté, J. Y. Choi, R. Huang, F. J. Uribe-Romo, H. K. Chae, M. O'Keeffe, O. M. Yaghi, *Proc. Nat. Acad. Sci.*, 2006, **103**, 10186-10191.

5. H. W. Wanzlick, *Angew. Chem. Int. Ed.*, 1962, **1**, 75-80.

6. H. W. Wanzlick, H. J. Schönherr, *Angew. Chem. Int. Ed.*, 1968, **7**, 141-142.

7. C.-Y. Su, Y.-P. Cai, C.-L. Chen, F. Lissner, B.-S. Kang, W. Kaim, *Angew. Chem., Int. Ed.*, 2002, **41**, 3371-3375.

8. C.-Y. Su, Y.-P. Cai, C.-L. Chen, M. D. Smith, W. Kaim, H.-C. Zur Loye, *J. Am. Chem. Soc.*, 2003, **125**, 8595-8613.

9. R. Chakrabarty, P. S. Mukherjee, P. J. Stang, *Chem. Rev.*, 2011, **11**, 6810-6918

10. J. L. Scott, D. R. MacFarlane, C. L. Raston, C. M. Teoh, *Green Chem.*, 2000, **2**, 123-126.

11. T. Brotin, T. Devic, A. Lesage, L. Emsley, A. Collet, *Chem. Eur. J.*, 2001, **7**, 1561-1573.

12. A. Collet, *Tetrahedron*, 1987, **43**, 5725-5759.

13. J. Canceill, A. Collet, G. Gottarelli, P. Palmieri, *J. Am. Chem. Soc.*, 1987, **109**, 6454-6464.

14. C. Carruthers, T. K. Ronson, C. J. Sumby, A. Westcott, L. P. Harding, T. J. Prior, P. Rizkallah, M. J. Hardie, *Chem. Eur. J.*, 2008, **14**, 10286-10296.

15. F. L. Thorp-Greenwood, V. E. Pritchard, M. P. Coogan, M. J. Hardie, *Organometallics*, 2016, **35**, 1632-1642.

16. M. Yamaguchi, K. Kamei, T. Koga, M. Akima, T. Kuroki, N. Ohi, *J. Med. Chem.*, 1993, **36**, 4052-4060.

17. M. J. Langton, P. D. Beer, *Acc. Chem. Res.*, 2014, **47**, 1935-1949.

18. K. Zhu, G. Baggi, V. N. Vukotic, S. J. Loeb, *Chem. Sci.*, 2017, **8**, 3898-3904.

19. T.K. Ronson, M. J. Hardie, *Unpublished Results*.

20. A. Khalafi-Nezhad, M. N. Soltani Rad, G. H. Hakimelahi, B. Mokhtari, *Tetrahedron*, 2002, **58**, 10341-10344.

21. R. M. Payne, C. L. Oliver, *CrystEngComm*, 2016, **18**, 7965-7971.

22. J. W. Steed, H. Zhang, J. L. Atwood, *Supramol. Chem.*, 1996, **7**, 37-45.

23. J. M. Fowler, F. L. Thorp-Greenwood, S. L. Warriner, C. E. Willans, M. J. Hardie, *Chem. Commun.*, 2016, **52**, 8699-8702.

24. T. K. Ronson, J. Fisher, L. P. Harding, M. J. Hardie, *Angew. Chem. Int. Ed.*, 2007, **46**, 9086-9088.

25. J. J. Henkelis, J. Fisher, S. L. Warriner, M. J. Hardie, *Chem. Eur. J.*, 2014, **20**, 4117-4125.

26. J. J. Henkelis, T. K. Ronson, L. P. Harding, M. J. Hardie, *Chem. Commun.*, 2011, **47**, 6560-6562.

27. K. Takenaka, Y. Obora, L. H. Jiang, Y. Tsuji, *Organometallics*, 2002, **21**, 1158-1166.

28. M. J. Hardie, C. L. Raston, *Chem. Commun.*, 1999, 1153-1163.

29. J. J. Henkelis, C. J. Carruthers, S. E. Chambers, R. Clowes, A. I. Cooper, J. Fisher, M. J. Hardie, *J. Am. Chem. Soc.*, 2014, **136**, 14393-14396.

30. A. Schaly, Y. Rousselin, J. C. Chambron, E. Aubert, E. Espinosa, *Eur. J. Inorg. Chem.*, 2016, **6**, 832-843.

31. N. J. Cookson, J. M. Fowler, D. P. Martin, J. Fisher, J. J. Henkelis, T. K. Ronson, F. L. Thorp-Greenwood, C. E. Willans, M. J. Hardie, *Supramol. Chem.*, 2018, **4**, 255-266.

32. Z. Zhong, A. Ikeda, S. Shinkai, S. Sakamoto, K. Yamaguchi, *Org. Lett.*, 2001, **3**, 1085-1087.

33. J. Liu, M. Liu, Y. Yue, M. Yao, K. Zhuo, *Chin. J. Chem.*, 2012, **30**, 644-650.

34. A. Gorbunov, D. Cheshkov, V. Kovalev, I. Vatsouro, *Chem. Eur. J.,* 2015, **21**, 9528-9534.

35. P. I. P. Elliott, in *Organometallic Chemistry*, ed. I.J.S. Fairlamb, J.M. Lynam, The Royal Society of Chemistry, 2014, vol. 39, 1-25.

36. K. Xu, N. Thieme, B. Breit, *Angew. Chem. Int. Ed.*, 2014, **53**, 7268-7271.

37. Sebastian Juliá, Carlos Martínez-Martorell, J. Elguero, *Heterocycles*, 1986, **24**, 2233-2237.

38. M. V. Nora de Souza, T. R. Alves Vasconcelos, *Appl. Organomet. Chem.*, 2006, **20**, 798-810.

39. J. V. B. Kanth, M. Periasamy, *J. Org. Chem.*, 1991, **56**, 5964-5965.

40. H. C. Brown, T. P. Stocky, *J. Am. Chem. Soc.*, 1977, **25**, 8218-8226

41. P. Haake, W. B. Miller, *J. Am. Chem. Soc.*, 1963, **85**, 4044-4045.

42. M. A. Little, J. Donkin, J. Fisher, M. A. Halcrow, J. Loder, M. J. Hardie, *Angew. Chem. Int. Ed.*, 2012, **51**, 764-766.

43. G. E. Mulder, H. C. Quarles van Ufford, J. van Ameijde, A. J. Brouwer, J. A. W. Kruijtzer, R. M. J. Liskamp, *Org. Biomol. Chem.*, 2013, **11**, 2676-2684.

44. S. Majumdar, M. M. Spaeth, S. Sivendran, J. Juntunen, J. D. Thomas, K. B. Sloan, *Tetrahedron Lett.*, 2007, **48**, 4609-4611.

45. M. Schnopp, G. Haberhauer, *Eur. J. Org. Chem.*, 2009, **2009**, 4458-4467.

46. A. R. Katritzky, S. Perumal, G. P. Savage, *J. Chem. Soc., Perkin Trans. 2*, 1990, 921-924.

47. S.-D. Cho, J. Hwang, H.-K. Kim, H.-S. Yim, J.-J. Kim, S.-G. Lee, Y.-J. Yoon, *J. Heterocycl. Chem.*, 2007, **44**, 951-960.

48. J. A. Bull, E. P. Balskus, R. A. J. Horan, M. Langner, S. V. Ley, *Chem. Eur. J.*, 2007, **13**, 5515-5538.

49. G. Sheldrick, *Acta Crystallogr. Sect. A*, 2008, **64**, 112-122.

Chapter 3
Synthesis and structural variation of Ag(I) thiazolyl metallo-supramolecular assemblies

This chapter focuses on the preparation of a novel tripodal thiazolyl ligand and its assembly with Ag(I) salts, giving rise to a range of assemblies, including the first cyclotriveratrylene-based coordination cubes, and a diverse array of coordination polymers of complex connectivity.

3.1 Introduction

3.1.1 The thiazole motif in metallo-supramolecular chemistry

Thiazoles are somewhat chemically similar to oxazoles, simply possessing a different chalcogen atom in sulfur rather than oxygen. Thiazoles are slightly stronger bases than oxazoles, and the mesomeric effects observed with oxazole systems are effectively suppressed because of the lower electronegativity of sulfur compared to oxygen.[1] In contrast to oxazoles, which are not particularly abundant in biological systems, thiazoles are more commonly observed, with key biologically-relevant thiazole containing compounds including thiamine (vitamin B$_1$)[2] and the bioluminescent firefly luciferin.[3]

Coordination complexes incorporating thiazole ligands have been extensively studied, with thiazoles being integrated into both monodentate and multidentate systems. The nitrogen-coordinating motif is ubiquitous in thiazole coordination chemistry. A key example includes Andersson's Ir(I) complexes, which were capable of quantitatively catalysing asymmetric hydrogenations of trisubstituted alkenes, favouring the *S* enantiomer in >99% ee when using a cycloheptene-fused thiazole ligand (figure 3.1).[4] The authors stated olefin-coordination at Ir(I) was only possible on the re face of the alkene, which exposed the si face, allowing asymmetric hydrogenation to take place.
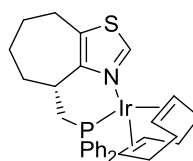
Figure 3.1 Andersson's Ir(I)-thiazolyl cationic complex.[3] The [BArF]⁻ anion is omitted.

The thiazole motif has found use in metallo-supramolecular chemistry. Early work by Rice and co-workers incorporated pyridylthiazoles as ligand systems in double and triple Cu(II) helicates.[5] Through assembly of two disk-shaped thiazolyl ligands at Ag(I), Shionoya and co-workers assembled $[Ag_3L_2]^{3+}$ complexes which assembled in a helical manner. The *M* and *P* enantiomers were observed at 298 K in a 1:1 ratio and crystals grown were of the racemate.[6] Heating solutions of helicates to 328 K led to coalescence of signals, which upon taking advantage of the labile Ag-N interactions led to flipping between the *P* and *M* enantiomers at elevated temperatures (figure 3.2, left). A further study by the same group investigated a heteroleptic analogue possessing a hexathiazolylbenzene ligand.[7] The $[M_3L^1L^2]^{3+}$ complex assembled quantitatively through heterotopic recognition. VT NMR spectroscopy revealed that molecular motion was being exhibited by association and dissociation of the thiazole groups on the hexathiazolyl disk. A more recent example by Leigh and co-workers incorporated a thiazolo[5,4-d]thiazole unit into a ligand scaffold to prepare an interwoven 2 x 2 molecular grid (figure 3.2, right). After closing the grid using alkene metathesis chemistry, an interwoven Solomon link was isolated.[8]
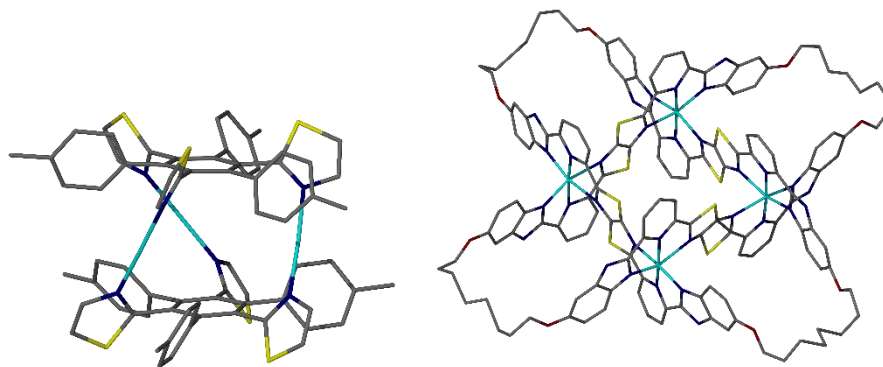
Figure 3.2 Left: Shiyonoya's molecular gear, solvents and anions are omitted for clarity. Right: Leigh's molecular grid. Isopentyl groups and anions are omitted for clarity.

Assemblies of coordination polymers from thiazolyl ligands are somewhat scarcer than discrete complexes, and only a handful have been reported.[9] A Cu(II)-MOF reported by zur Loye and co-workers incorporated a 2-(4-pyridyl)thiazole-4-carboxylate scaffold, and assembled into a moganite topology.[10] The authors remarked that the moganite topology is rarely seen, but is similar to the quartz topology. Aside from zur Loye's MOF, examples are limited to coordination polymers incorporating non-coordinating thiazole spacers,[11] or grown

solvothermally from a thiazole solution with metals bearing coordinating solvent molecules.[12]

3.1.2 Ag(I) assemblies of CTV ligands

Metal ions with predictable geometries due to crystal field effects can assemble with CTV ligands to yield well-defined architectures. For example, when furnished with *cis*-protecting ligands, the square-planar Pd(II) ion assembles with CTV-ligands to yield metallo-cryptophanes.[13-16] If *cis*-protecting ligands are not employed, or the bidentate ligand is not a sufficiently strong σ-donor, the predicted stella octangula assembles with high fidelity.[17, 18] In a contrasting manner, Ag(I) cations predominantly adopt linear and tetrahedral coordination modes, but trigonal planar and T-shaped geometries can also be observed. The lack of crystal field effects associated with Ag(I) means predicting the coordination mode and conformation of assemblies, and also the network topology of polymeric material is much more challenging, especially when ligands have a degree of flexibility associated. An incredibly diverse library of Ag(I) assemblies with CTV-ligands have been published, including mechanically interlocked cryptophanes[19] (figure 3.3, left), tetrahedra (figure 3.3, right),[20, 21] and a number of 1D,[22, 23] 2D[23-27] and 3D coordination polymers.[24, 25, 28] The applications of Ag(I) assemblies can be limited by their stability, owing to the high lability of Ag(I) complexes, which can dissociate when dissolved in coordinating solvent, in addition to photosensitivity.
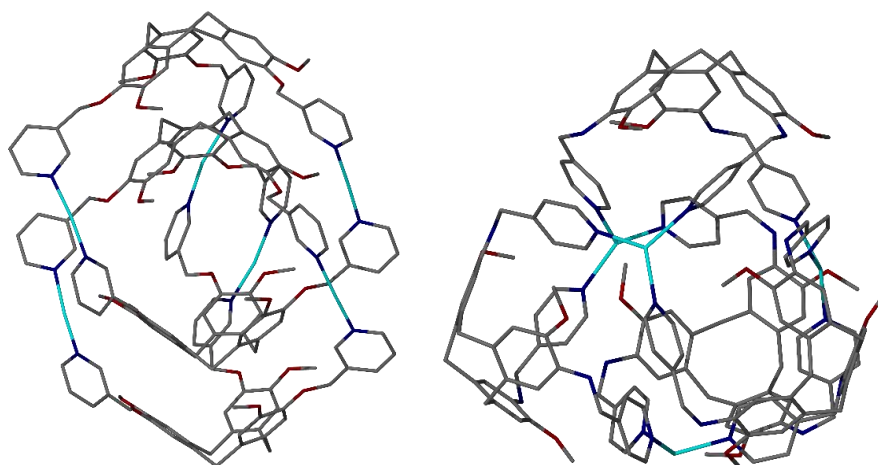
Figure 3.3 Left: Hardie's catenated metallo-cryptophane. Right: Hardie's Ag_4L_4 tetrahedron. Solvent molecules and anions are omitted for clarity.

3.2 Synthesis of a thiazole-appended CTV ligand

In a similar fashion to oxazole ligand **2.18**, a thiazole ligand group was desired because of the poor stability of the imidazole precursor and problems encountered upon scale-up (Chapter 2). As ligands, thiazoles display a somewhat similar binding motif to imidazoles, where the nitrogen atom is Lewis basic, and the sulfur seldom partakes in coordination chemistry in the same way the protic nitrogen atom of imidazole does not. C-S bonds are the longest on the diazole due to a poorer orbital overlap between carbon and sulfur atoms, and the C-S-C portion of the ring becomes puckered as a result. Thiazolium salts can also be targeted, and M-NHC complexes bearing thiazolium-derived ligands have been previously reported, including a thiazolium derivative of Grubbs' second generation catalyst as a key example.[29] The major disadvantage of thiazol-2-ylidene ligands is that they afford complexes of lower stability than imidazolyl counterparts because the sulfur atom cannot be functionalised, leading to no steric protection of the metal from one side of the carbene, in addition to poorer π-overlap of sulfur p-orbitals with the carbenic p_z orbital, and diminished σ-withdrawal compared to imidazol-2-ylidene systems.

CTG **2.3** was furnished with thiazolyl groups upon reaction with the commercially available 4-(chloromethyl)thiazole hydrochloride, affording ($\pm$)-4,4',4"-(((3,8,13-trimethoxy-10,15-dihydro-5H-tribenzo[a,d,g][9]annulene-2,7,12-triyl)*tris*(oxy))tris(methylene))trithiazole, **3.1** in good yields when employing caesium carbonate as the base, as shown in scheme 3.1. Upon the slow addition of water to the reaction mixture, **3.1** precipitated as a spectroscopically pure compound. Microanalysis suggested **3.1** was isolated as a hydrochloride salt, displaying a good match to **3.1**·(HCl)·0.5(H_2O).

The ^{1}H NMR spectrum of **3.1** (figure 3.4) suggested the successful synthesis of a C_3-symmetric CTV ligand, with *endo-* and *exo-* doublets of H^{12} sited at 4.71 and 3.49 ppm. The methylene bridge between azole and CTV was observed at 5.30 ppm, considerably further upfield than the *N*-substituted benzimidazole (**2.11**) due to the decreased acidity of the methylene bridge located from 6.20-6.10 ppm. The two azolyl resonances, H^1 and H^2 were assigned at 8.81 and 7.38 ppm, considerably downfield compared to oxazole ligand **2.18**, whose azolyl resonances were sited at 7.87 and 7.11 ppm, presumably due to the more polarised H^1 compared to the analogous proton in **2.18**. Ligand **3.1**·HCl can easily be neutralised by washing a

DCM solution of ligand with aqueous NaHCO$_3$, before passing the organic phase through a silica plug.
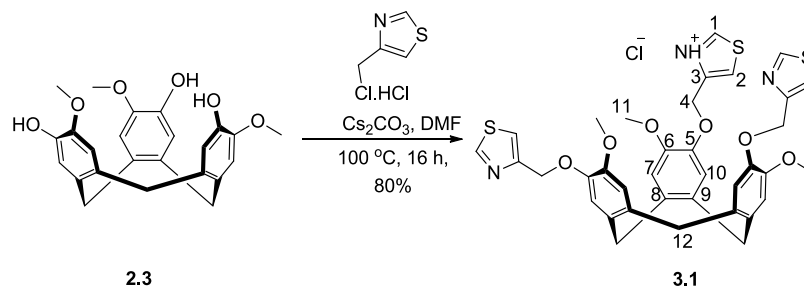
Scheme 3.1 Synthesis of thiazole ligand 3.1.
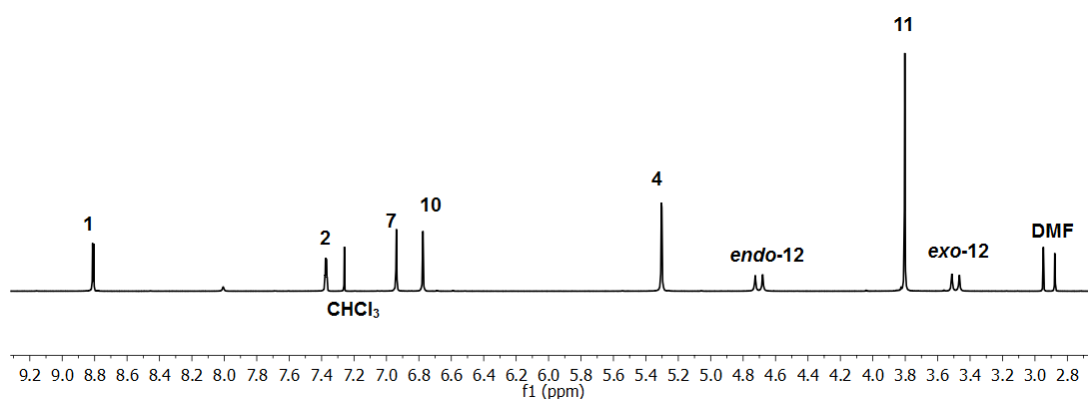
Figure 3.4 ^{1}H NMR spectrum (300 MHz, 293 K, CDCl$_3$) of 3.1.

Assignment of the ^{13}C{^{1}H} NMR spectrum was aided by HMQC and HMBC experiments. The two CH$_2$ groups, C^4 and C^{12} assigned as 67.82 and 36.62 ppm respectively, with the HMQC NMR spectrum displaying ^1J coupling between the two *endo-* and *exo-* protons of the CTV bowl and the carbon environment at 36.62 ppm. ^{13}C{^{1}H} NMR and DEPT-135 spectra are displayed in figure 3.5.

The HRMS spectrum (figure 3.6) was also diagnostic, containing three molecular ion fragments assigned as {M+H}$^+$ (*m/z* 700.1623), {M+Na}$^+$ (*m/z* 722.1414) and {M$_2$+H}$^+$ (*m/z* 1399.3143) peaks (calculated at *m/z* 700.1605, 722.1424 and 1399.3136 respectively). When monitoring reactions, the {MCs}$^+$ fragment dominates.
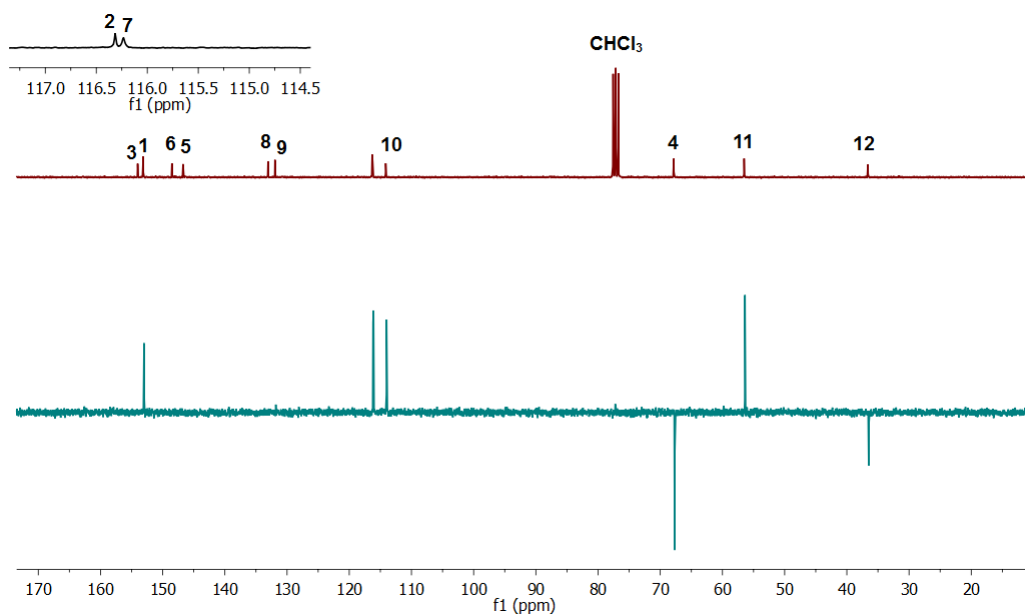
Figure 3.5 $^{13}C\{^1H\}$ **NMR spectrum (75 MHz, 293 K, CDCl₃) of 3.1 (top, black trace) with 117.0-114.5 inset. DEPT-135 spectrum (bottom, blue trace).**

The HRMS spectrum (figure 3.6) was also diagnostic, containing three molecular ion fragments assigned as $\{M+H\}^+$ (*m/z* 700.1623), $\{M+Na\}^+$ (*m/z* 722.1414) and $\{M_2+H\}^+$ (*m/z* 1399.3143) peaks (calculated at *m/z* 700.1605, 722.1424 and 1399.3136 respectively). When monitoring reactions, the $\{MCs\}^+$ fragment dominates.
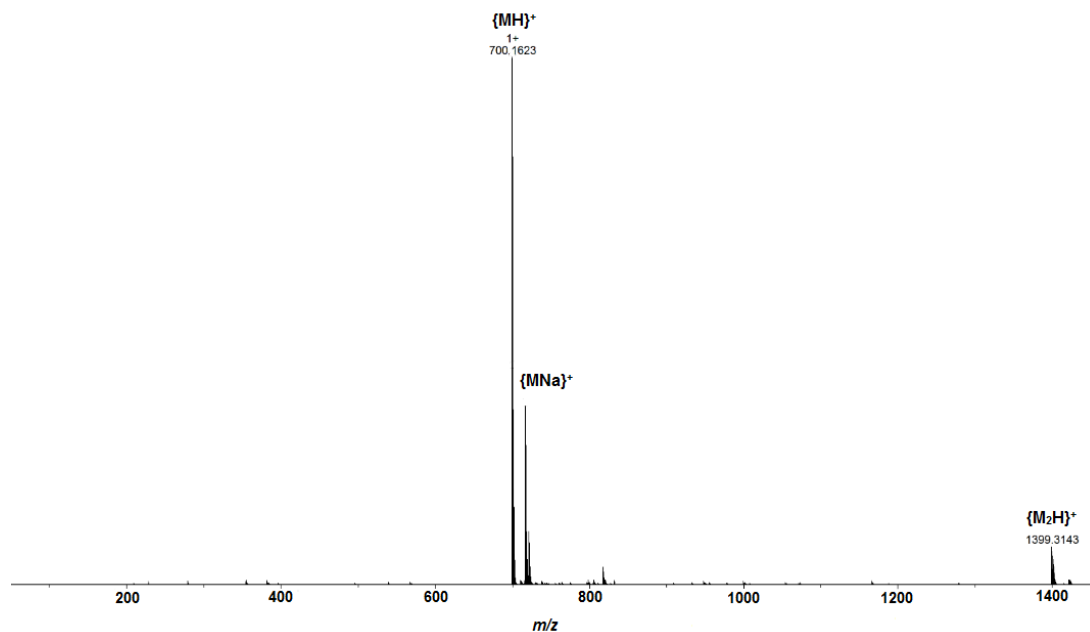
Figure 3.6 HRMS (ESI⁺) of 3.1.

Crystals of **3.1**·4(H$_2$O) were grown by Dr. Flora Thorp-Greenwood, by standing **3.1** in a mixture of DMF and H$_2$O. Clathrate **3.1**·4(H$_2$O) crystallised in the chiral, hexagonal $P6_3$ space group. The asymmetric unit comprises of one third of a CTG bowl and two crystallographically distinct water molecules (figure 3.7, left). Spontaneous resolution upon crystallisation occurred, with a single enantiomer of ligand observed in a particular crystal. Conglomerate **3.1**·4(H$_2$O) exhibits bowl-in-bowl stacking, with a CTG centroid separations of 5.135 Å, which is a considerably longer distance than a number of previous example ligands.[30] The ligands do not quite sit flush, with each bowl rotated about 60º throughout the stack in an ABAB arrangement (figure 3.7, right). The ligand arms are extended outwards, and align in the plane of the arene groups of the CTG bowl. The C$_{thiazole}$-C-O-C$_{arene}$ torsion angle is near-linear at -179.3º, with the thiazole sulfur atom sitting furthest away from the CTG bowl, and the nitrogen atom aligned towards the methoxy group.
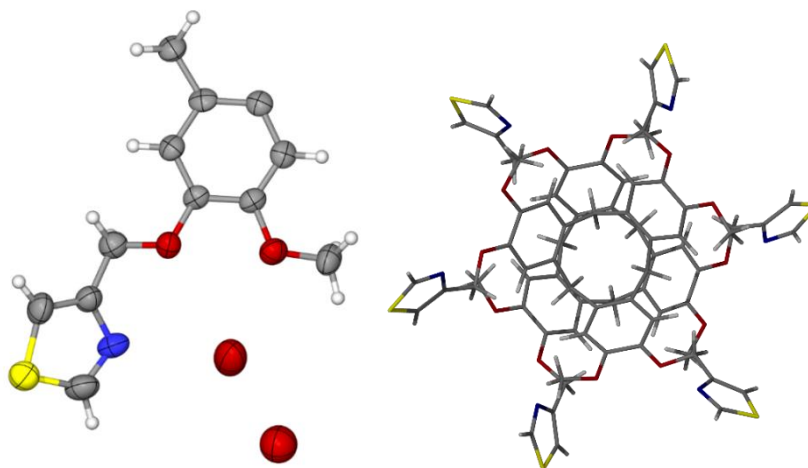
Figure 3.7 Left: Asymmetric unit of 3.1·4H$_2$O. Ellipsoids are drawn at the 50% probability. Right: Bowl-in-bowl stacks of 3.1 ligands.

Four waters of crystallisation reside within the pores of the crystal lattice and form a 2D hydrogen-bonding network with thiazole nitrogen atoms at a N···O separation of 2.895 Å (figure 3.8, top). The crystallographically distinct water within the tetramer is separated from neighbouring oxygen atoms by O···O distances of 2.915 Å. The hydrogen bonding network forms a 6^3 network topology with a honeycomb structure, as shown in figure 3.8.
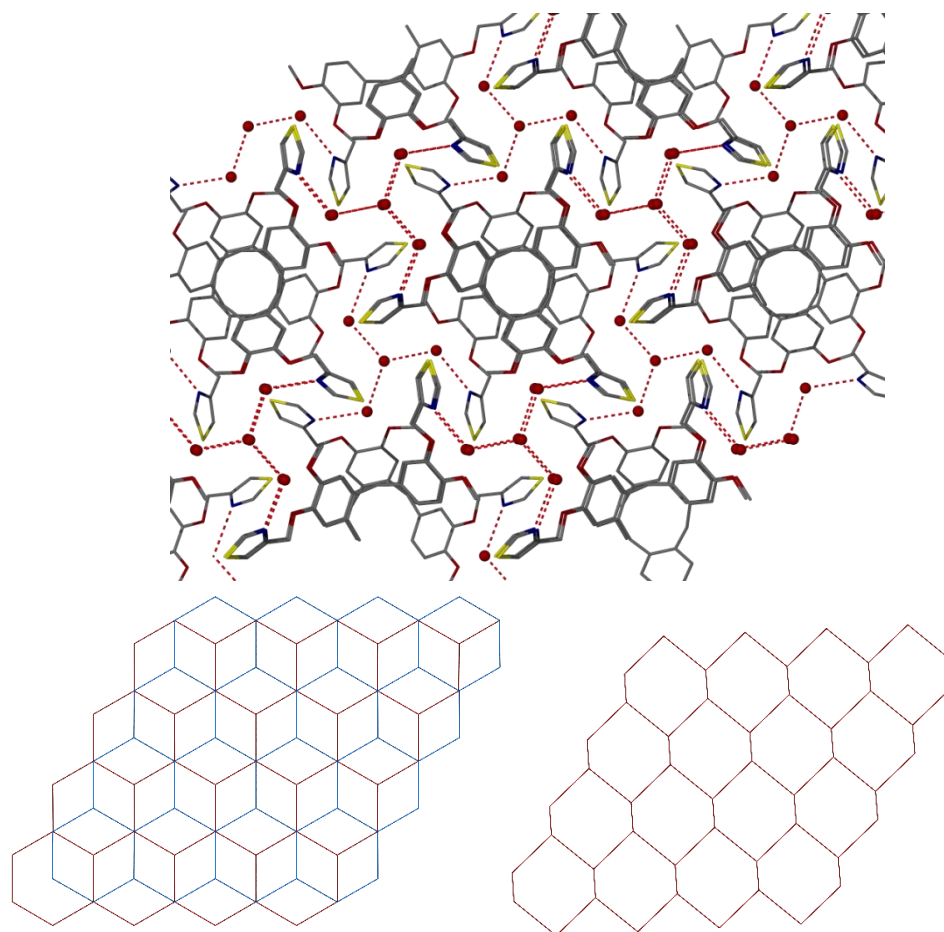
Figure 3.8 Top: 6^3 topological 2D-hydrogen bonding network, Bottom left: 6^3 topology of 2D sheets in ABAB array with individual sheets shown in red and blue. Bottom right: A single hexagonal layer.

A second conglomerate of thiazole ligand crystals, in the form of **3.1**·3(MeNO$_2$) were grown by diffusing diethyl ether vapours into a solution of **3.1** in nitromethane. Clathrate **3.1**·3(MeNO$_2$) crystallised in the hexagonal $R\bar{3}$ space group, with the asymmetric unit comprising of one third of **3.1** and a fully occupied nitromethane solvate molecule (Figure 3.9). Similarly to **3.1**·4(H$_2$O), nitromethane clathrate **3.1** displayed chiral self-sorting, A C$_{thiazole}$-C-O-C$_{arene}$ torsion angle of 178.9º was noted, which once again is near-linear, but the thiazole groups in both structures have distinct rotations. In the **3.1**·3(MeNO$_2$) case, the thiazole nitrogen atom is pointing away from the methoxy group as opposed to being of opposite orientation in **3.1**·4(H$_2$O).
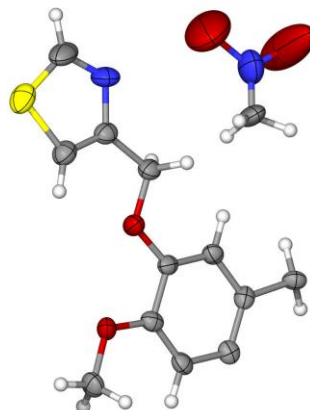
Figure 3.9 Asymmetric unit of 3.1·3MeNO₂. Ellipsoids are drawn at the 50% probability.

Both **3.1**·4(H₂O) and **3.1**·3(MeNO₂) display bowl-in-bowl stacking, in the nitromethane clathrate case, at a separation of 4.4 Å, a considerably shorter distance than the hydrogen-bonding network. Channels run down the crystallographic c axis of **3.1**·3(MeNO₂), containing three crystallographically identical MeNO₂ molecules, as shown in figure 3.10. The stacks are also perfectly aligned in **3.1**·3(MeNO₂). The thiazole nitrogen atoms are directed towards the nitromethane-filled pores, the methyl groups of MeNO₂ align themselves within the hydrophobic pocket of the CTV outer-rim at a $C_{MeNO2}\cdots C_{OMe}$ separation of 3.645 Å. $N_{thiazole}\cdots N_{MeNO2}$ and O···O distances between nitromethane guests of 3.645 Å and 3.818 Å respectively exist in the clathrate.
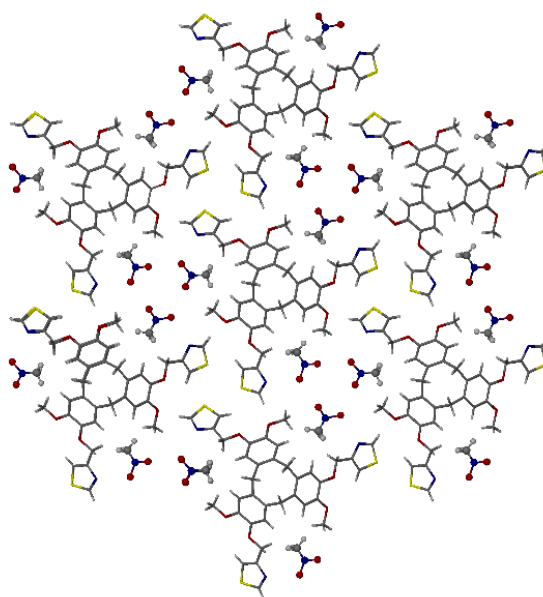
Figure 3.10 Packing diagram of 3.1·3MeNO₂ looking down the crystallographic c axis.

Both enantiomers of ligand crystallised. Fortuitously, the studied crystal of **3.1**·4(H_2O) was of the *P*-enantiomer of ligand, whereas **3.1**·3($MeNO_2$) comprised of the *M*-enantiomer.

3.3 Metallo-cube assembly

Drawing inspiration from cryptophane **2.12**, linear *trans*-coordinating metals were desired, and initially, coordination studies with Pd(II) sources including [Pd(Cl)$_2$($MeCN$)$_2$] which offer this geometry were targeted. Within *ca.* 7 days, a pale yellow solid precipitated, and HRMS of the mother liquor revealed no evidence of Pd(II) coordination. The common linear 2-coordinate geometry exhibited by Ag(I) would allow for **3.1** to use the same binding mode. Attempts to assemble ligand **3.1** with Co(II), Ni(II), Cu(I), Cu(II), Zn(II) and Pd(II) were unsuccessful, with no solution-state evidence implying complexes had assembled. It was intriguing that only Ag(I) salts yielded crystalline coordination complexes with ligand **3.1**.
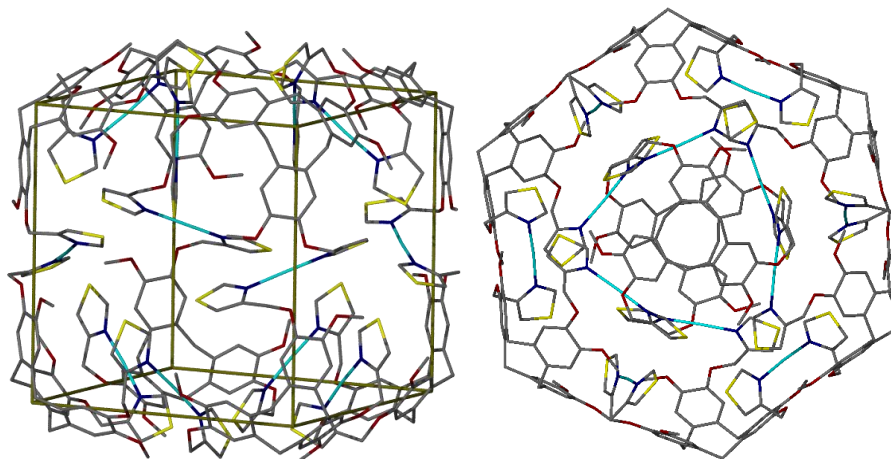
Figure 3.11 Crystal structure images of 3.2.

Diffusion of diethyl ether vapours into mixtures of 1.5 eq. of $AgBF_4$ or $AgReO_4$, and **3.1**·**HCl** in DMF, which were kept in the dark led to the assembly of isostructural [$Ag_{12}L_8$]12X^- metallo-cubes (X = ReO_4^- = **3.2**, X = BF_4^- = **3.3**), which crystallised as pale orange cube-shaped crystals within a week (figure 3.11). A powdered contaminant also appeared in the vial, assumed to be AgCl. Crystals initially grew on the base of the vial where AgCl resided, behaving as a nucleation bed. Cube crystals did still grow after neutralisation of ligand, but crystal growth required much longer durations, was much lower yielding and side-reactivity occurred (see

Section 3.4). Cube crystals grown after neutralising the ligand were also orange, although much paler in colour. The unit cell parameters were identical in all cases.

Crystals of **3.2** and **3.3** also be grown from DMAC and NMP solutions, which bore the same unit cell parameters as their counterparts grown in DMF. Studies in this chapter only involved complex grown from DMF. EDX (energy-dispersive X-ray spectroscopy) analysis of cube crystals grown confirmed the only heavy elements present were Ag, S, and Re for **3.2** and Ag, S, and F for **3.3**. No chlorine was detected, so it is unlikely AgCl templated assembly of metallo-cubes.

The asymmetric unit of **3.2**, $[Ag_{12}(\textbf{3.1})_8]12(ReO_4)\cdot n(DMF)$ comprises of a third of a ligand, one silver ion, and fragments of two perrhenate anions, one of which is external to the cubic core, and an internal perrhenate anion of low occupancy, which resides on a four-fold symmetry axis and is therefore subjected to symmetry-induced disorder (figure 3.12, left). Metallo-cubes **3.2** and **3.3**, $[Ag_{12}(\textbf{3.1})_8]12(BF_4)\cdot n(DMF)$, both crystallised in the chiral, cubic *F*432 space group and are isostructural. The asymmetric unit of **3.3** comprises of a third of a ligand and one Ag(I) ion (figure 3.12, right). Neither anions nor solvent in the structure of complex **3.3** could be located within the difference map, therefore the SQUEEZE function of PLATON was employed on this structure.[31]
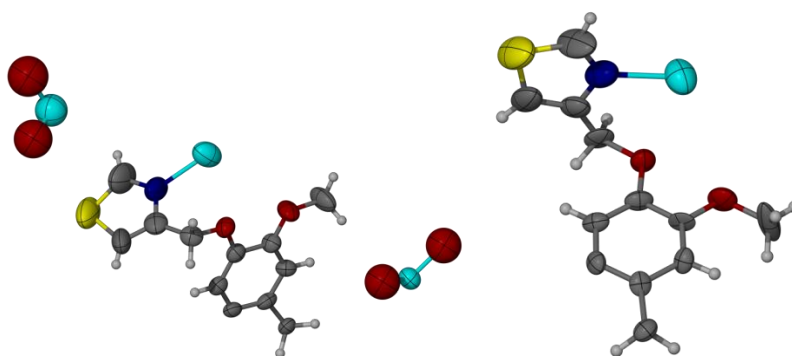
Figure 3.12 Left: Asymmetric unit of 3.2. Right: Asymmetric unit of 3.3. Ellipsoids are drawn at the 50% probability.

Only nitrogen atoms coordinated to Ag(I) cations in **3.2**, with a Ag-N bond length of 2.151(15) Å. Near-linear coordination of thiazoles was exhibited, with N-Ag-N bond angles 175.9(8)°. The thiazolyl ligands were askew from a plane, with a C-N-N-C torsion angle of -31.9°. A weak H-bonding interaction between the NC*H*S

thiazolyl proton and partially occupied internal perrhenate anion was measured, with a C···O separation of 3.30 Å.

The ligands in **3.2** and **3.3** adopt threefold symmetry. Each CTV ligand behaves as a cornerpiece, and is connected to three nearest neighbours through coordination to Ag(I), which in turn connect two ligands in an $M_{12}L_8$ fashion. Rather than the anticipated scenario of Ag(I) cations residing on the cube edges, the thiazolyl group adopts a $C_{thiazole}$-C-O-C_{arene} torsion angle of -83.6º and fold inwards above the bowl, as opposed to residing in the plane of the cavitand benzo-groups. This folding motif buries the Ag(I) cations within the interior of the cube, preventing *exo*-coordination (figure 4.14, bottom), and they also cannot be observed in the space-filling model (figure 3.13, right)). The thiazole sulfur atom is orientated on the external face of the cube, with the coordinating nitrogen internally.
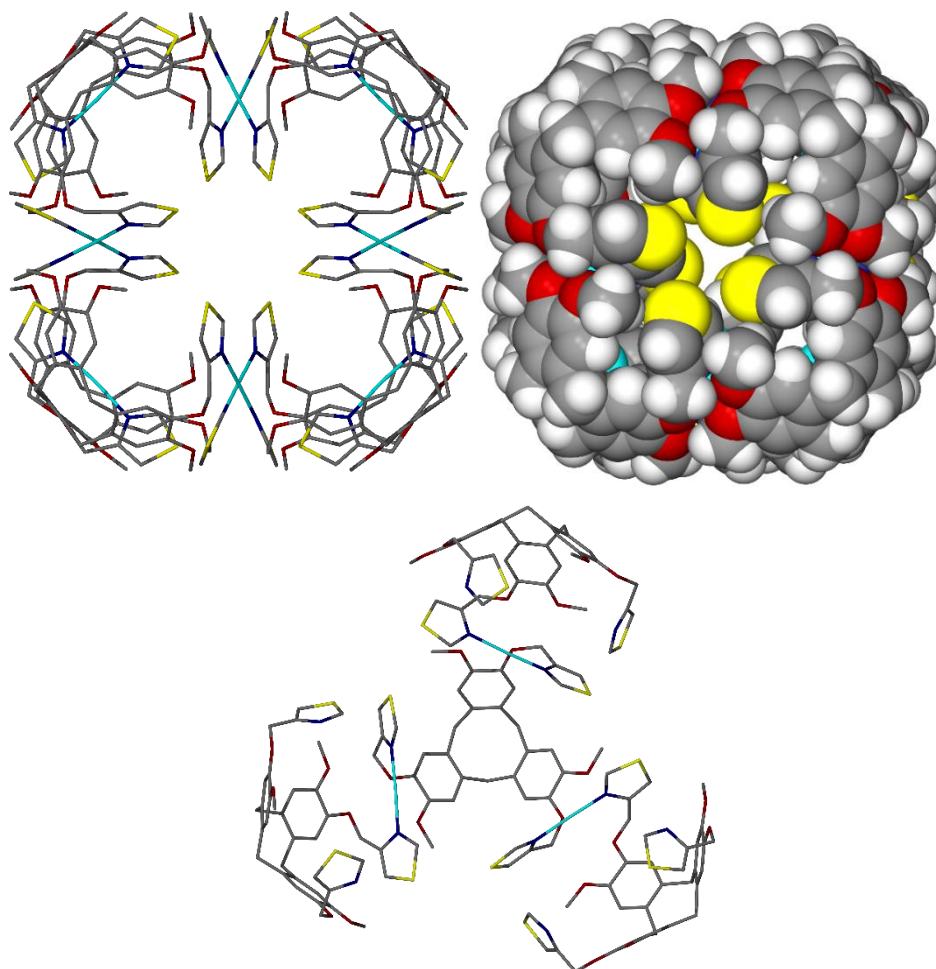
Figure 3.13 Top left: Metallo-cube 3.2 looking down a face one vertex. Top right: Space-filling diagram displaying sulfur-edged windows. Bottom: Ag(I)-connectivity between 3.1 ligands.

Small windows exist on each face of the cube (figure 3.12), at S···S diameters of 6.00 Å, and the overall diameter of the cube measured from the centroids of tribenzo[a,d,g]-cyclononatriene ligand core was 14.7 Å, and 25.4 Å across the diagonal body. Separations of 8.71 Å were measured between Ag(I) cations, and the internal volume of $M_{12}L_8$ cubes was measured as *ca.* 5000 Å^3 excluding anions when using a 1.2 Å probe.

Extensive π-π stacking interactions were observed at the vertices, between arene faces of tribenzo[a,d,g]-cyclononatriene cores at separation of 3.81 Å. **3.2** and **3.3** both engage in cubic close packing arrays. One cube complex interacts with twelve neighbouring cubes in a close cubic packing array, with π-stacking occurring on the cube edges (figure 3.14).
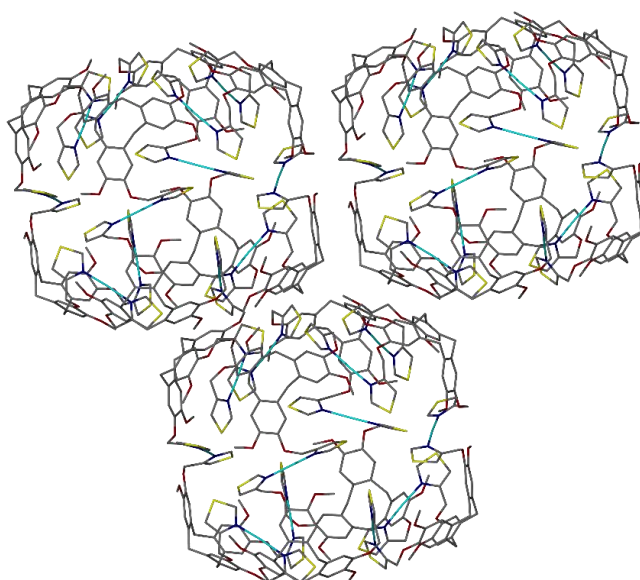
Figure 3.14 Edge-directed π-π stacking of metallo-cubes.

Homochiral recognition is also observed in **3.2** and **3.3** crystals, and all eight ligands in a single cube complex are the same enantiomer. Examples of racemic ligands undergoing homochiral self-sorting upon metal-directed assembly are known,[32, 33] including cages[34-38] and a number of CTV-systems.[15, 17, 39, 40] Complexes **3.2** and **3.3** both display a further level of homochirality, with spontaneous resolution occurring and crystallisation as conglomerates; only one ligand enantiomer is seen in a single crystal of **3.2** or **3.3**. Spontaneous resolution of both cages and the bulk mixture is known, but a much rarer phenomenon than just the former. Examples include a cage reported by Rissanen and co-workers,[41] and CTV derivatives including a hemicryptophane[42] and organic cryptophanes.[43, 44] For a timely review on chiral

metallo-supramolecular assemblies, see Shiyonoya *et al*.[45] The bulk sample contained both enantiomers of cube complexes, and fortuitously, the crystals of **3.2** and **3.3** studied in single crystal X-ray diffraction were of opposite handedness. The unit cell of both **3.2** and **3.3** reveal face-centred cubic packing, as shown in figure 3.14.
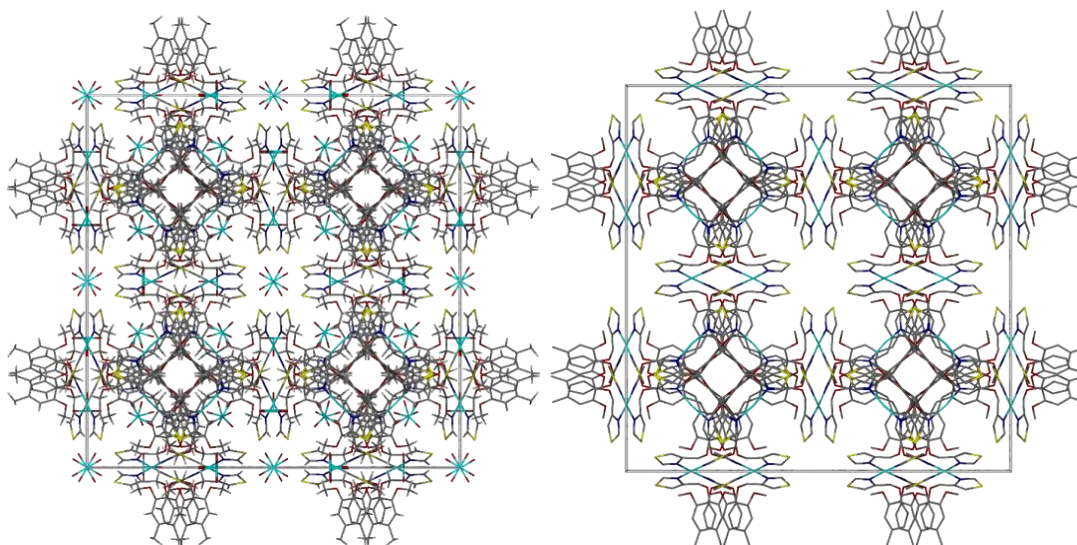
Figure 3.15 Left: Unit cell diagram of 3.2. Right: Unit cell of 3.3, both display the FCC motif.

Very high symmetry is associated with **3.2**, with a Russian Doll arrangement of components observed, as shown in figure 3.16. The six internal perrhenate anions sited behind each S_4 window on each face of a cube formed an octahedron, which were surrounded by a cuboctahedron of Ag(I) cations, encompassed within the cube of ligand centroids, which were all inside a rhombicuboctahedron comprising of the external perrhenate anions.
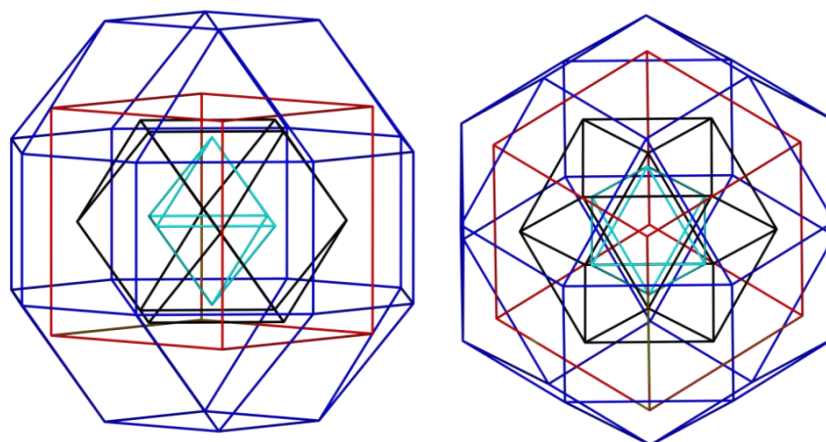
Figure 3.16 Matryoshka diagrams of 3.2. Internal anion connectivity shown in light blue, Ag(I) connectivity in black, CTV centroids in red and external anions in blue.

FTIR spectra of **3.2** and **3.3** both contain the relevant B-F and Re-O stretches at 1046 and 903 cm^{-1} respectively. PXRD patterns for both **3.2** (figure 3.17) and **3.3** (figure 3.18) are a good match to the simulated spectra obtained from the .res files associated with studied crystals, suggesting the bulk crystalline material is phase-pure.
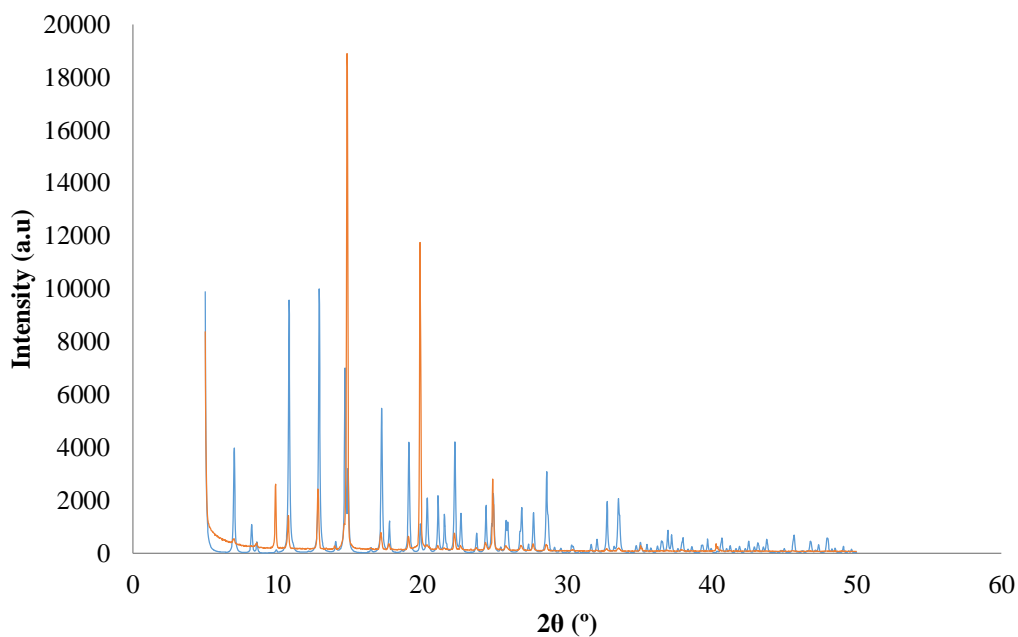
Figure 3.17 PXRD spectrum of 3.2. Simulated data from crystal structure (100 K, blue), Observed data from bulk material (rt, red).
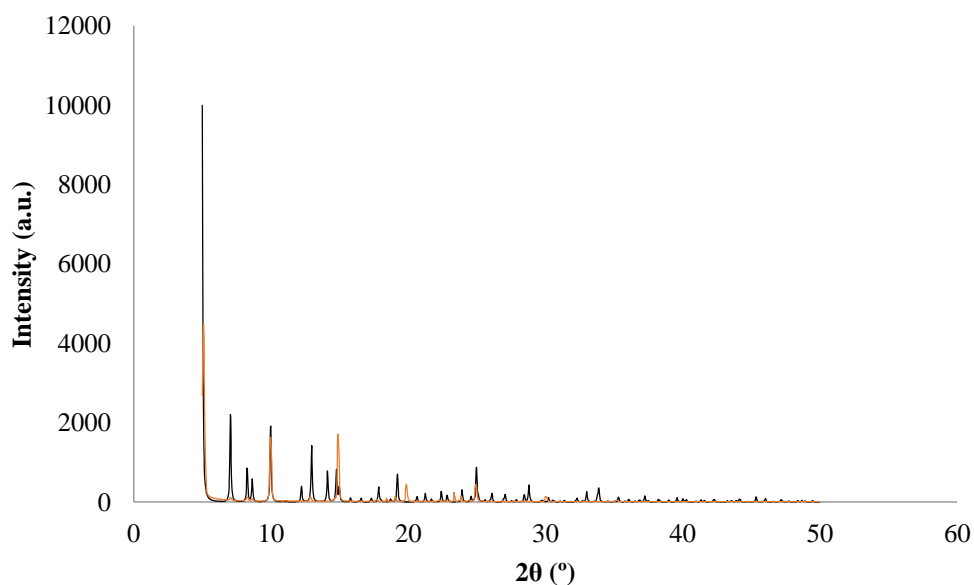
Figure 3.18 PXRD spectrum of 3.3. Simulated data from crystal structure (100 K, black), observed data from bulk material (rt, red).

Cube-shaped crystals grew within *ca.* 7 days of initial reaction. Naturally, the longer the crystals were untouched, the larger growth, and it was not uncommon to observe crystals >400 μm in diameter if vials were stored in the dark for 3-4 weeks. SEM and optical microscopy imaging revealed cube crystals to have a regular truncated cube shape (SEM figure 3.18 top left, and optical microscopy figure 3.19 bottom). Defects did begin to appear when drying crystals *in vacuo*, and surface cracks were evident (figure 3.19 top right). Whilst samples were always stored in darkness when not studied as a precaution to the known photosensitivity of silver, a crop of **3.2** deliberately exposed to light for 24 h showed no obvious signs of decomposition. SEM and optical microscopy experiments were performed by Dr. Alex Kulak.
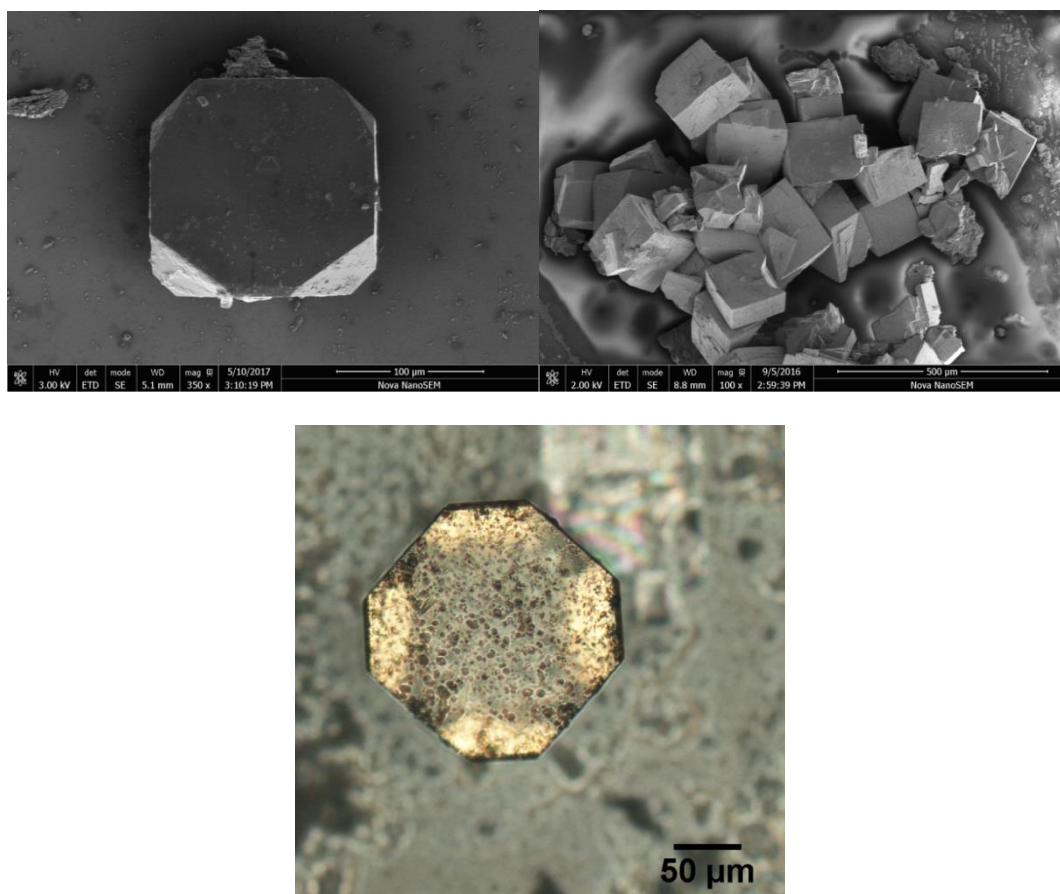
Figure 3.19 SEM image of a single cube crystal of 3.3 (top left) and a crop of 3.3 crystals (top right). Bottom: Optical microscopy image of a crystal of 3.3.

3.2 and **3.3** are rare examples of metallo-cubes bearing ligand-residing vertices of $M_{12}L_8$ stoichiometry. Robson and co-workers reported the first example of a $Cu_{12}L_8$ metallo-cube of such nature in 1999, whilst Li and co-workers have prepared rigid tritopic terpyridyl ligands which behaved as cornerpieces in the edge-directed assembly of platonic cubes.[46, 47] Metallo-cubes are more commonly the inverse, with

the metal residing on the corner in an edge-directed M_8L_{12} assembly[48] or a face-directed M_8L_6 fashion.[49]

CTV offers itself as an ideal cornerpiece for a cube, with all three hydroxyl groups roughly orthogonal to one another with respect to the centroid of the cyclononatriene core, assembly of coordination cubes were previously elusive. Organic derivatives were however known; Warmuth and co-workers reported an organic cube assembling through edge-directed dynamic covalent chemistry, by reacting an aldehyde-functionalised CTV with p-phenylenediamine.[50] Kuck,[51] Beuerle[52] more recently Mastalerz[53] have reported organic supramolecular cubes assembling through similar means using vertices based on the closely related tribenzotriquinacene (TBTQ) motif.

Despite the organic precedent, edge-directed metallo-supramolecular cubes bearing CTV-derived ligands had previously not been reported. Instead, an assortment of 3D assemblies, with the thermodynamically favourable cryptophanes being most dominant.[13, 19] Stellated octahedra[17, 18, 40] and a Pd_4L_4 topologically complex Solomon cube[40] were the closest examples to $M_{12}L_8$ cubes, prior to their discovery.

3.3.1 Solution state studies of 3.2 and 3.3

Crystals could be redissolved in polar aprotic solvents such as DMF and DMSO, but evidence suggested dissociation of the labile Ag-N bonds in solution was occurring, and that both **3.2** and **3.3** were not remaining intact upon dissolution. The ^{1}H NMR spectrum of a mixture of **3.1** and AgBF$_4$ in DMF-d_7 after 24 h was very broad (figure 3.20), whilst the HRMS of **3.2** dissolved in DMF contained peaks corroborating [AgL]$^+$ (808.0561) and [AgL$_2$]$^+$ (1507.2125), calculated 808.0574 and 1507.2015 respectively, as shown in figure 3.21. Metal coordination is occurring in solution, although the labile Ag-N bonds in **3.2** and **3.3** are appearing to dissociate, therefore solution state data is unlikely to be reflective of $[M_{12}L_8]^{12+}$ metallo-cubes. The high resolution mass spectrum of **3.2** was obtained by Dr. Stuart Warriner using direct injection techniques.
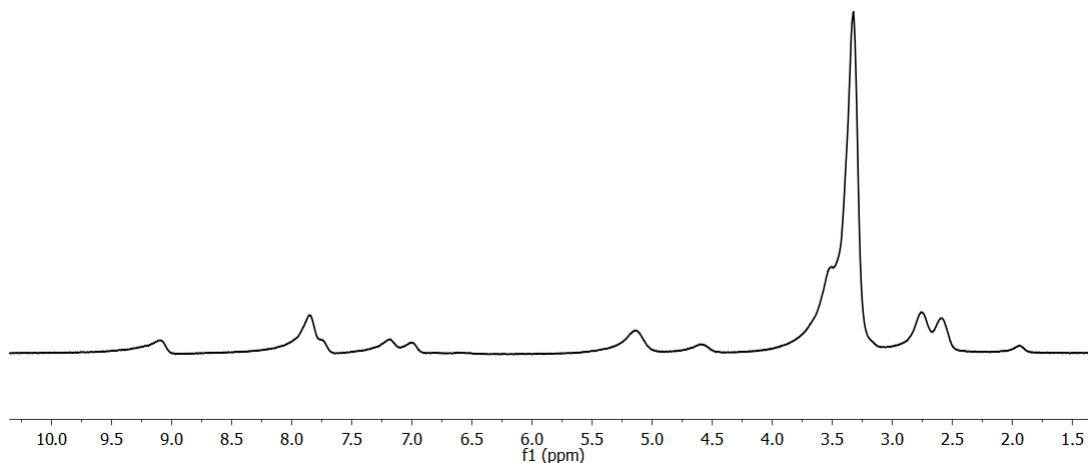
Figure 3.20 ^{1}H NMR spectrum (300 MHz, 293 K, DMF-d_7) of AgBF$_4$ and 3.1 after 24 h.
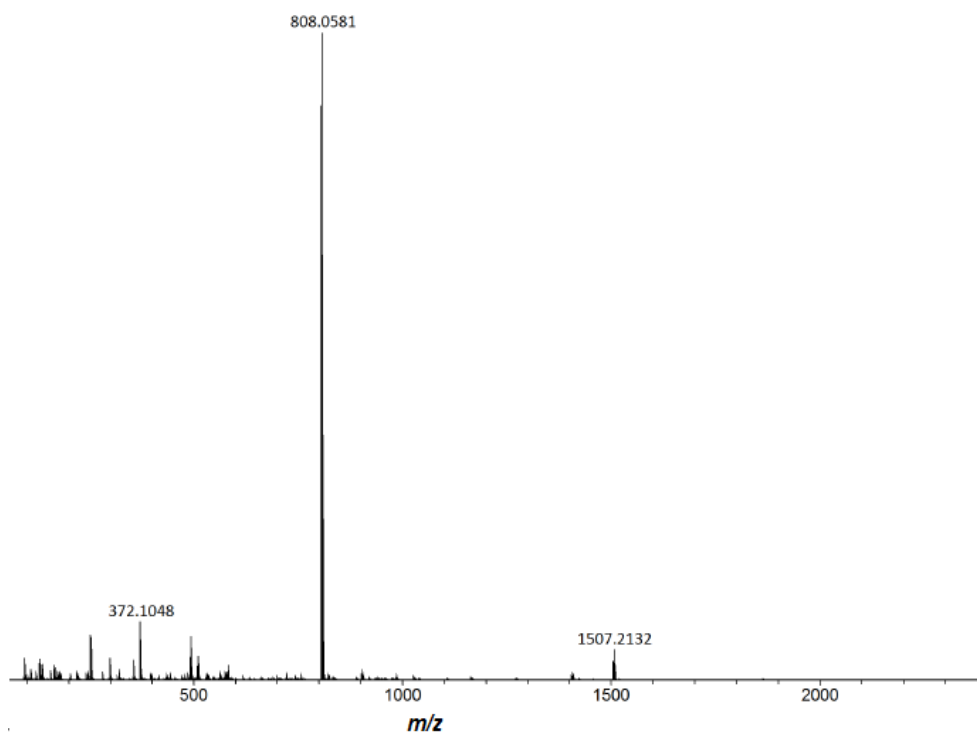
Figure 3.21 HRMS of complex 3.2.

3.3.2 Investigations into applications of metallo-cubes

A number of studies on **3.2** and **3.3** were carried out, with guest-binding and post-synthetic modification the primary targets. Assessment of their material properties was then carried out. Powder XRD suggested the **3.2** and **3.3** were phase-pure (figures 3.17 and 3.18). Crystals of **3.2** and **3.3** were then activated by soaking in DCM for 48 h before vacuum filtration and drying. The diffraction pattern obtained for DCM-soaked crystals of **3.3** is less distinct (figure 3.22), possibly indicating a deterioration of crystallinity in the sample.
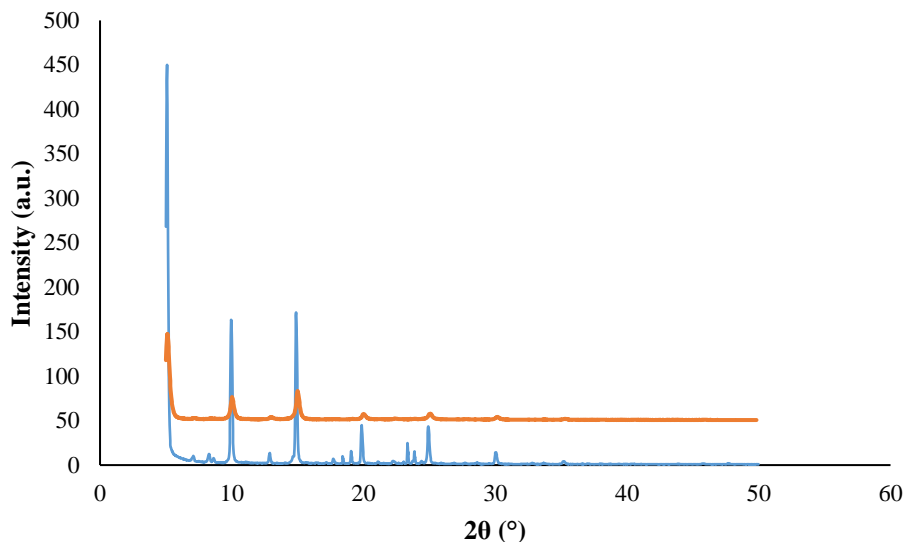
Figure 3.22 PXRD spectrum of 3.3·nDMF (blue trace) and 3.3 after soaking in DCM and drying in vacuo (red trace).

A number of strategies for post-synthetic modifications were carried out, many revolved around the notion of imparting reactivity at the Ag(I) centres, and/or transmetallating onto other substrates. Iodine uptake was attempted, both through diffusion of vapours into a vial of crystals, and soaking crystals in an ethereal solution of iodine, but was unsuccessful. A white powder appeared instead, and it may be possible that redox activity ensued. Ag(I) reactions with elemental iodine is a primary method to prepare the I^+ cation. No evidence of transmetallation onto I^+ yielding a halogen-bonded adduct was observed. Taking this on board, transmetallation onto other linear, d^{10} metals was also attempted, including reactions with solutions of $[Cu(MeCN)_4]BF_4$, $[Au(nbe)_3]BF_4$ (nbe = norbornene), and $Zn(BF_4) \cdot XH_2O$, but were to no avail.

The only access to the internal cavity is through the small 6 Å windows of the cube faces, therefore any potential guest species must be able to thread through the small openings of the assembly. Linear dinitriles were targeted as they may be able to permeate the windows of the cube, in addition to internally coordinating to Ag(I), skewing the coordination geometry of the metal, and potentially altering the size and shape of the architecture. A range of chain lengths were trialled, ranging from malononitrile ($NC(CH_2)CN$) to sebaconitrile ($NC(CH_2)_8CN$). FTIR would provide a strong handle for encapsulation studies, with the target $[3.3 \subset (NC(CH_2)CN)_n]$ expected to display a strong vibrational mode at *ca.* 2000

cm^{-1}. There was however no evidence of coordination or uptake of dinitriles into the cubic lattice. Hardie and co-workers have previously coordinated dintriles to linear Ag(I) salts, leading to the assembly of coordination polymers assembled about tetrahedral Ag(I).[54]

A BET isotherm was obtained on a 50 mg sample of **3.3**, to determine the ability of metallo-cubes adsorbing N_2 onto the internal and external surface of metallo-cubes. An extremely low BET surface area was, however, calculated of 3.3769 ± 0.6444 m^{2}g^{-1}, so further studies into gas sorption were not carried out. The isotherm gave a linear positive gradient, perhaps suggesting a non-porous material. A calixarene coordination cage has a calculated surface area of 558 m^{2}g^{-1} displaying hysteresis in the BET isotherm,[55] which is considerably less than Farha's MOF, possessing a calculated surface area of *ca.* 7560 m^{2}g^{-1}.[56]

3.4 Assembly of complexes after neutralising ligand 3.1

Examples of slight contaminants such as HCl encouraging crystallisations have been documented in the Hardie group, so it was of interest to investigate both coordination when using **3.1·HCl**, and neutral **3.1** obtained by washing a DCM solution with aq. NaHCO$_3$, and passing the DCM (5% MeOH) solution through a silica plug (scheme 3.2). When assembling **3.1** with AgBF$_4$, the powdered contaminant presumed to be AgCl was absent, and crystal growth took considerably longer than the week reported previously. A smaller crop of cube crystals grew after one month. Additionally, a small number of colourless rods (*ca.* 10% of the bulk) also grew in the vial. Separation of rods and cubes was difficult because rod and cube crystals grew within close proximity of one another. Single crystal XRD on the rod-shaped crystals confirmed the structure as a 3D coordination polymer of complex topology.
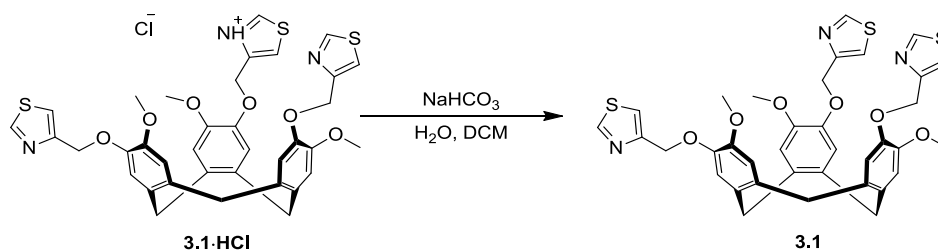
Scheme 3.2 Neutralisation of ligand 3.1.

Crystals of ($[Ag_8\mathbf{3.1}_6](BF_4)_8)_n$, **3.4**, were obtained as a minor impurity from cube assembly from the diffusion of diethyl ether vapours into a DMF solution of $AgBF_4$ and **3.1**. Coordination polymer **3.4** crystallised in the hexagonal *R*3 space group with an asymmetric unit comprising of eight Ag(I) ions and six **3.1** ligands (figure 3.23). The unit cell size was extremely large and measured as 76.13(12) x 76.13(12) x 16.27(3) Å, with a cell volume of 81,651(3) Å^3. Attempts to solve the structure after indexing to a smaller unit cell were unsuccessful. The polymer was of high symmetry, with the smallest repeating unit being $[Ag_8L_6]$. A full complement of anions and solvent molecules could not be located within the difference map, therefore the SQUEEZE routine of PLATON was employed.[31] The six inequivalent ligands have been labelled **a**-**f** to allow for more straightforward rationalisation.
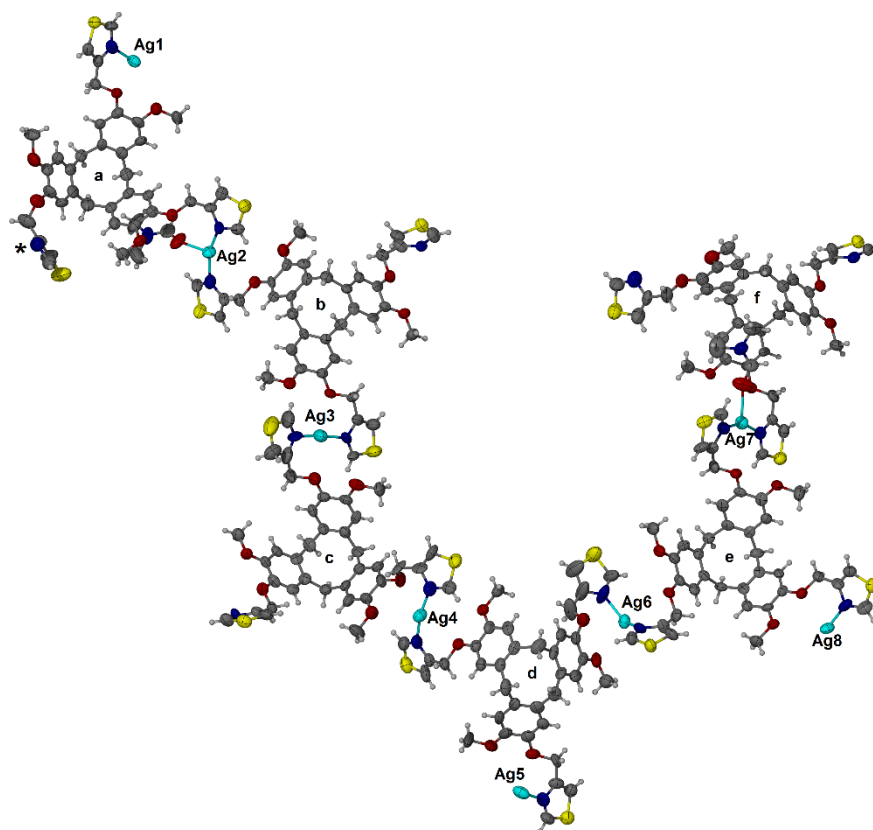
Figure 3.23 Asymmetric unit of $[Ag_8(3.1)_6](BF_4)_8]_n$. Ellipsoids are drawn at the 50% probability. The thiazolyl unit on ligand a denoted by * coordinates to Ag6 rendering 3.4 3D in nature.

Unlike **3.2** and **3.3**, both enantiomers of ligand were observed in the asymmetric unit in a 50:50 ratio. The two-coordinate Ag(I) cations were linked by one *M*- and one *P*-enantiomer of **3.1**. The varying coordination modes of Ag(I) centres gave coordination polymer **3.4** high complexity. Of the eight Ag(I) cations, five (**Ag1**,

Ag3, **Ag4**, **Ag5** and **Ag8**) were 2-coordinate, with Ag-N bond lengths ranging between 2.056(16) Å (Ag3-N7) and 2.212(17) Å (Ag6-N13) and all 2-coordinate N-Ag-N bond angles near-linear from 178.3(6)° (Ag8) to 167.4(6)°. The three remaining Ag(I) centres in the asymmetric unit were 3-coordinate, displaying considerably different coordination modes to one another. **Ag2** and **Ag7** are coordinated to two thiazolyl units and a DMF solvent molecule, with Ag-N bonds of 2.090(13) Å and 2.167(16) Å (Ag2), and 2.153(14) Å and 2.171(14) Å (Ag7), and longer Ag-O lengths of 2.502(17) Å (Ag2) and 2.464(17) Å (Ag7). The N-Ag-N angle about **Ag2** was 159.1(6)° and N-Ag-O angles measured at 85.7(6)° and 114.3(6)°. For **Ag7**, the analogous bond angles were 154.2(6), 84.3(6) and 120.6(6)° respectively. The bond angles of these centres give rise to distorted T-shape geometries. **Ag6** was also 3-coordinate, displaying a coordination mode more typical of an offset trigonal planar Ag(I) centre and coordinates to three thiazolyl moieties, with N-Ag-N bond angles of 106.7(6), 119.1(7) and 130.9(6)°. Two thiazolyl units are in the ASU, with Ag-N bond lengths measured as 2.194(15) and 2.212(17) Å, whilst the third Ag-N bond length was elongated at 2.330(18) Å, and was identified as belonging to ligand **a**. The C_{arene}-O-C-$C_{thiazole}$ torsion angle of this thiazolyl group is markedly different to the rest in the structure, and was measured as 103(2)°. This third thiazolyl moiety links layers of the polymer, and forms helical chains through the *c*-direction. The handedness of the polymeric helicate renders the crystals chiral. The CTV-bowl donating this thiazolyl group to Ag(I) exhibits bowl-in-bowl stacking with a ligand of the same handedness at a centroid-centroid separation of 4.819 Å. Save the aforementioned C_{arene}-O-C-$C_{thiazole}$ torsion angle, the rest of the comparable angles in **3.4** remain within 20° of plane of the CTV arene face, typically with values between -169 -179°, and 162-174°. One thiazolyl unit of the eighteen in the asymmetric unit is non-coordinating, and leads to the hexagonal metallacycles not all being fully connected (figure 3.24).
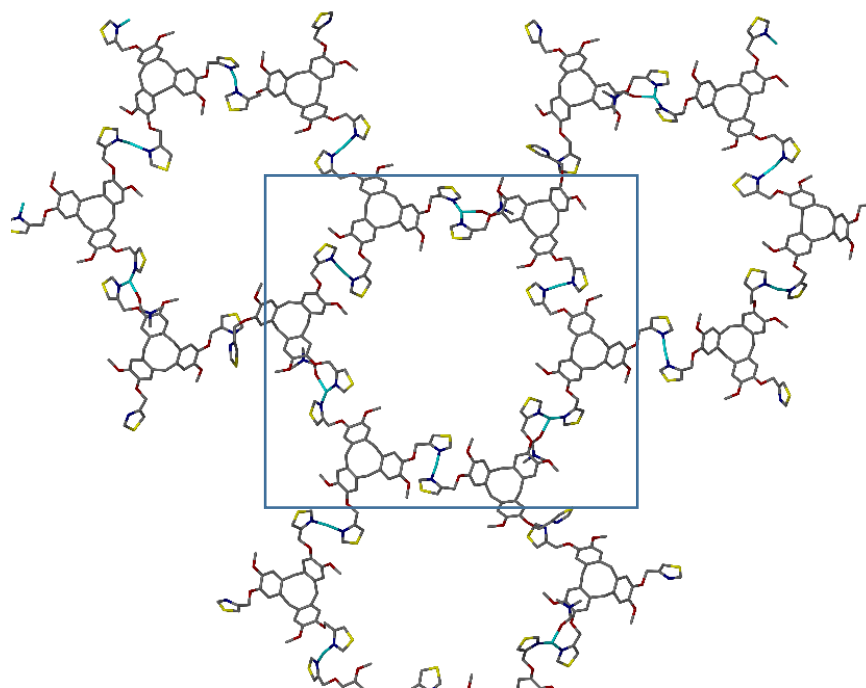
Figure 3.24 An M₆L₆ metallacycle (highlighted in blue box) surrounded by three hexagonal helical arrays in 3.4.

As expected for a material of high complexity, a number of inter-layer interactions were observed, including bowl-in-bowl stacking at centroid-centroid separations between 4.63 and 4.93 Å. CTV bowls in these stacks align near-perfectly. Bowl-in-bowl stacking between two offset cavitands at 6.82 Å were also measured. The non-coordinating thiazole of ligand **f** resides 3.58 Å above Ag3, but the thiazole π-cloud is perpendicular to the Ag(I) cation. A thiazolyl sulfur of ligand **b** resides 3.297 Å above Ag4, undertaking a weak cation-π interaction.

Expanding **3.4** along the crystallographic *c* axis revealed a topologically complex polymer, displaying much more intricate connectivity than the space filling diagram in figure 3.25 suggests. By joining 3-coordinate sites in the network as shown in figure 3.26 (ligand bowl centroids dark blue, Ag6 light blue), a highly complicated helicated array was observed, with both *M* and *P* helices observed within the crystal structure. Each helix comprised of five ligand centroids and one Ag6 equivalent, and did not form a six-membered ring. Furthermore, fully connected hexagons of six ligand centroids were observed on each layer furthest away from Ag6 equivalents. Significant channels were observed in the structure of **3.4** (figure 3.26), with a volume measured at *ca.* 28,000 Å^3 using a 1.2 Å probe.[31]
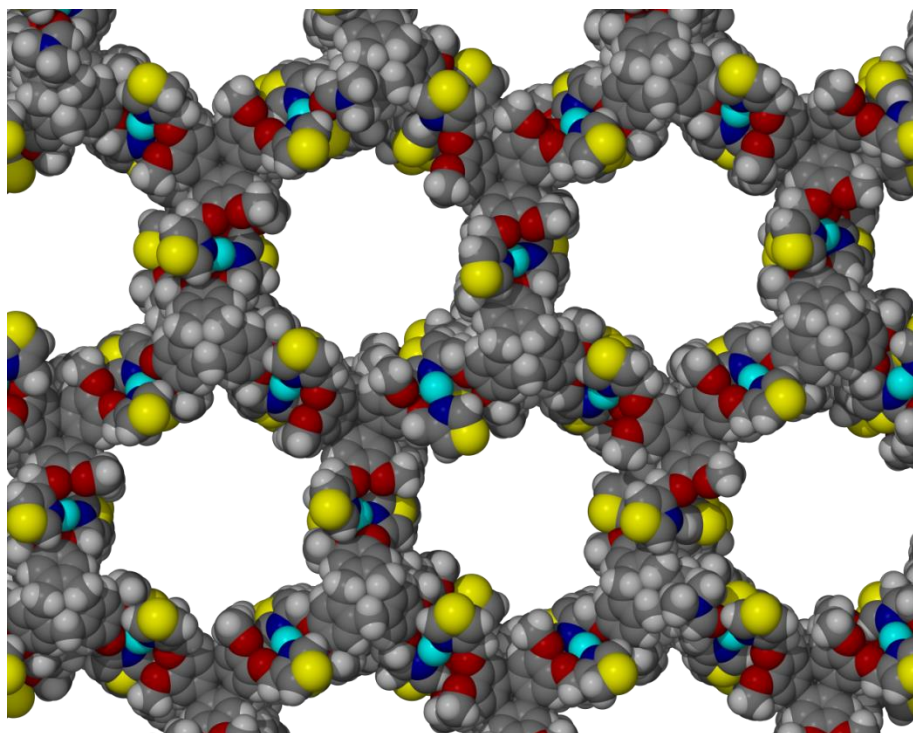
Figure 3.25 Space filling diagram of polymer 3.4 observed down the crystallographic *c* axis.
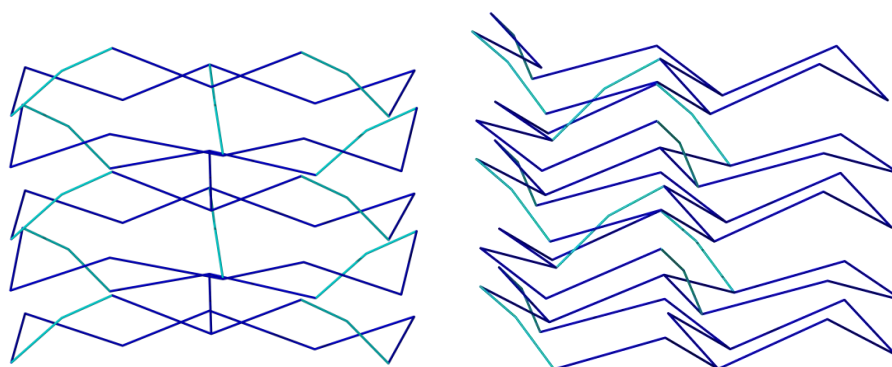
Figure 3.26 Left: 3-fold connectivity of polymer 3.4, displaying helical behaviour. Right: hexagonal L$_6$ channels (right). Connectivity between CTV centroids shown in dark blue and connectivity to Ag6 shown in light blue.

Attempts to increase the ratio of polymer crystals relative to cubes were carried out including decreasing the assembly temperature to -20 ℃, but this inhibited crystallisation. Difficulties separating the small quantity of polymer crystals, and increasing ratios of polymer grown meant further analysis beyond screening a number of crystals was too problematic.

3.4.1 Ag(I)-thiazolyl assemblies of non-tetrahedral anions

When using **3.1·HCl**, cube crystals formed with tetrahedral anions (BF$_4^-$, ReO$_4^-$) subject to symmetry-induced disorder. Crystallisations of the reaction of **3.1·HCl**

- 111 -

with AgPF$_6$ were set up, but crystalline material was not obtained. Post-neutralisation gave different results altogether. Colourless cube-shaped crystals of **3.5** with composition [Ag$_{12}$L$_8$]12(PF$_6$)·5(H$_2$O) with the same cube motif as **3.2** and **3.3** could be grown over a 4-6 week period, with unit cell parameters near identical to those of **3.2** and **3.3**, table **3.2**. Crystals were also obtained in lower yields, consistent with the assembly of **3.2** and **3.3** when using neutral **3.1** as a precursor. The structure of complex **3.5** was solved in the *F*432 space group with the asymmetric unit comprising of one third of a CTV unit, two anions, one internal to the cube of low occupancy and two water molecules, one of full occupancy *exo* to the cube, and one guest of low occupancy residing above the cavitand within the interior of the cube (figure 3.27). The Ag-N bond length was measured as 2.14(2) Å, near-identical to those in **3.2** and **3.3**.
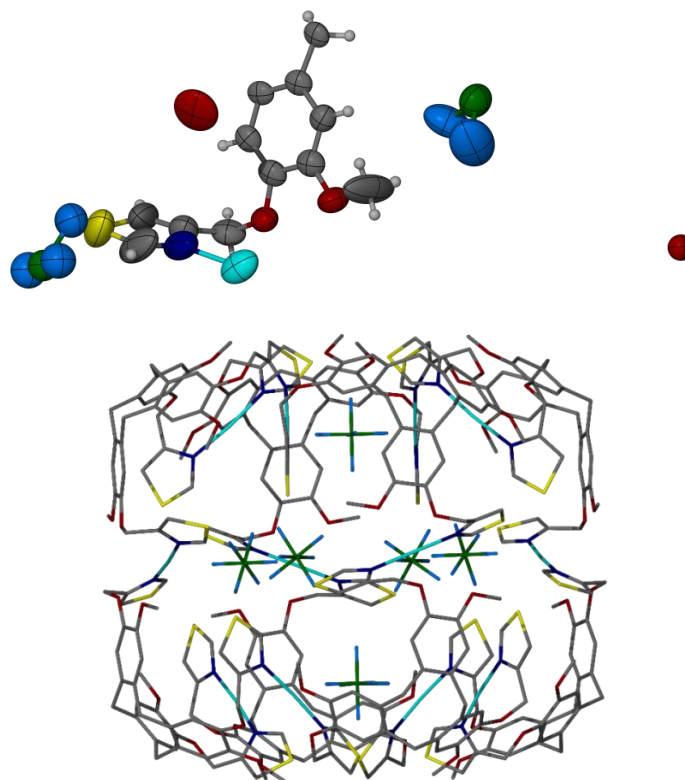
Figure 3.27 Top: Asymmetric unit of [Ag$_{12}$(3.1)$_8$](PF$_6$)$_{12}$·3.66H$_2$O, 3.5. Ellipsoids are drawn at the 50% probability. Bottom: Fully grown complex of 3.5. External anions and water molecules are omitted for clarity.

In addition to cube crystals, a very small crop of colourless rods were grown in the same vial with hexagonal unit cell parameters of *a* = *b* = 76.868(4) Å, *c* = 16.1769(7) Å, the same dimensions as **3.4**. Crystals were of too poor resolution to obtain a full dataset. In addition to AgPF$_6$, a propensity to grow colourless

cube-crystals when employing AgOTf was also exhibited. The unit cell parameters measured in this case during crystal screening were cubic $a = b = c = 35.6991(3)$ Å, consistent with the formation of the $Ag_{12}L_8$ cube. No rod-shaped crystals were visible in this reaction vessel.

One silver salt previously employed in the Hardie group is silver cobalticarborane $Ag[CoCb_2]$, a *bis*-carbollide species containing a Co(III) cation sandwiched between two *nido*-carborane units. **3.1·HCl** and 1.5 eq. $AgCoCb_2$ were dissolved in DMF and diethyl ether vapours diffused into the vial. Hexagonal-shaped plates were grown with unit cell parameters of $a = 47.561(2)$ $b = 27.0856(13)$ $c = 35.7374(14)$, $\alpha = \gamma = 90^{\circ}$ $\beta = 105.639(4)^{\circ}$. Crystals were extremely thin in one plane, which led to poor resolution and no diffraction beyond 1.7 Å. However, after neutralising **3.1**, diffusing diethyl ether into a DMF solution of **3.1** and 1 eq. $AgCoCb_2$, a small crop of pale yellow blocks grew after *ca.* one month which were different to the plates obtained when using **3.1·HCl**. SCXRD revealed the 2D coordination polymer, $[Ag_3\mathbf{3.1}_3](CoCb_2)_3(C_3H_7NO)_5)_n$, complex **3.6**. Crystals were solved in the $P\bar{1}$ space group, with the asymmetric unit comprising of three ligand molecules, three Ag(I) cations, three cobalt bis-carbollide anions and five DMF solvent molecules (figure 3.28).
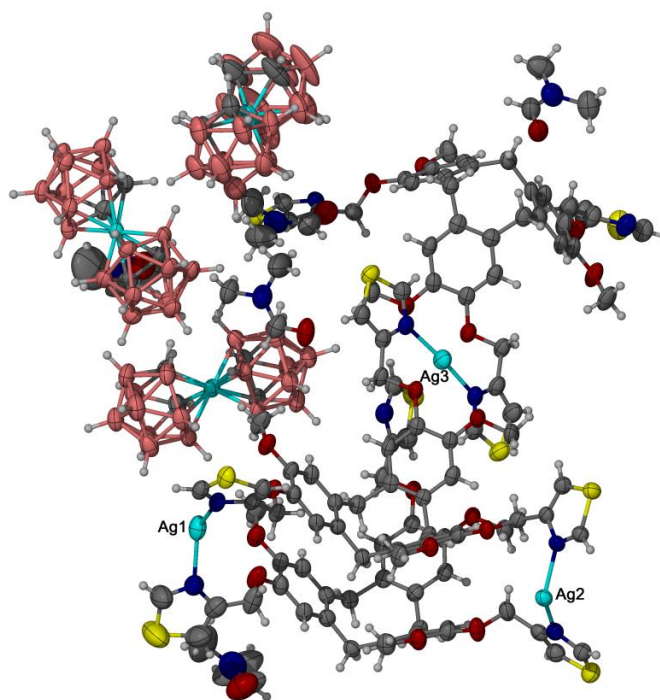
Figure 3.28 Asymmetric unit of $[Ag_3(3.1)_3][Co(C_2B_9H_{11})_2]_3$·5DMF, 3.6. Ellipsoids are drawn at the 50% probability.

The two *P*-enantiomers of ligand **3.1** partake in bowl-in-bowl stacking at a centroid-centroid separation of 4.394 Å, significantly shorter than the bowl-in-bowl stacks observed in polymer **3.4**. Two thiazolyl moieties from both ligands in the stack interact with 3-coordinate Ag(I) centres. The third Ag(I) ion displays near-linear 2-coordinate geometry. The Ag-N bond lengths around 3-coordinate centres range between 2.210(5) (Ag2-N1) and 2.403(7) Å (Ag1-N4), with the longest Ag-N bond being longer than the similar 3-coordinate Ag(I) centre in **3.4**. N-Ag-N bond angles about Ag1 were measured as 85.0(2), 135.3(2) and 139.1(2)º, and 90.72(19), 132.65(18) and 136.04(19)º about Ag2, being heavily distorted from both trigonal planar and T-shaped geometries. The near-linear Ag(I) centre featured an N-Ag-N of 175.0(2)º, almost identical to the angles featured in cube **3.2**. Bond lengths of 2.128(5) Å and 2.136(5) Å were also much shorter than measured about the 3-coordinate Ag(I) centres in **3.6**. C_{arene}-O-C-$C_{thiazole}$ torsion angles displayed on thiazoles bridged by 2-coordinate Ag(I) centres were both near *anti*-periplanar, measured as -179.178 and 167.092º. The *M*-enantiomer of ligand displayed dihedral angles associated with the same group of 163.860 and 177.329º, both of which coordinated to 3-coordinate Ag(I). Torsion angles associated with the same group on uppermost *P*-enantiomer in the stack were in plane with the CTV-arene faces, measured as -179.4 and 178.0º. More strain was exhibited on the torsion angles on the bottom *P*-enantiomer in the stack, whose torsion angles towards 3-coordinate Ag(I) centres, were measured as -132.867 and -132.254º, ca. 30º less than the strained group coordinating to a similar Ag(I) centre in polymer **3.4**. In a manner comparable to polymer **3.4**, one thiazolyl unit remains non-coordinated and is located on the lowest *P*-enantiomer in the stack. The nitrogen atom of this unit was measured as 3.39 Å from the nearest Ag(I) ion, but is both perpendicular and considerably offset from the metal centre.

Extending the structure reveals hexagonal channels are distributed throughout the polymer, but are filled with cobalticarborane anions and DMF solvent molecules, rendering the polymer non-porous and potentially templating polymer assembly (figure 3.29). Extensive bowl-in-bowl stacking was exhibited by **3.6**, with stacks comprising of only one enantiomer. Bowl-in-bowl stacking between polymer sheets were measured at 4.854 Å, slightly longer than between the two stacking in the same polymer unit. Crystals overall were racemic, with alternating sheets comprising of a 2:1 ratio with opposite enantiomers forming the majority. Each

sheet displays a 6^3 topology, with hexagonal channels arising and each CTV ligand connecting to three neighbouring units (figure 3.30). Homochiral recognition was observed in **3.6**, with a 2:1 ratio of *P*:*M* enantiomers of ligand observed in the asymmetric unit, which was consistent throughout that 2D sheet, alongside homochiral bowl-in-bowl stacks. Overall, *T* symmetry renders the crystals racemic, with alternating 2D sheets comprising of ligand ratios P_2M and M_2P.
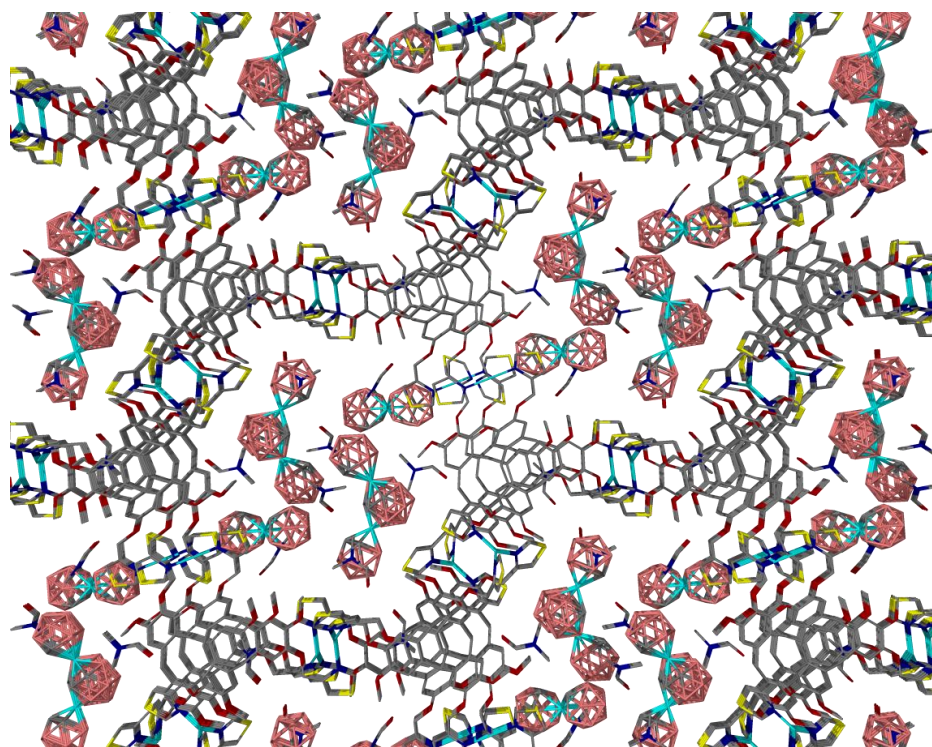
Figure 3.29 Packing diagram of 3.6 looking down the crystallographic *c* axis.
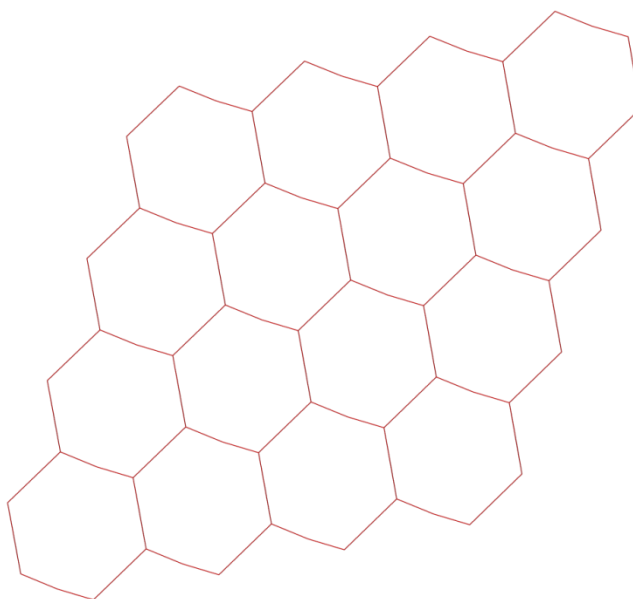
Figure 3.30 6^3 Network topology exhibited by polymer 3.6.

A PXRD spectrum (figure 3.31) was obtained for the bulk material isolated for **3.6**. Key low-angle peaks do overlap. Very few peaks were observed at $2\theta > 20°$, and it is unclear whether the bulk material is phase pure.
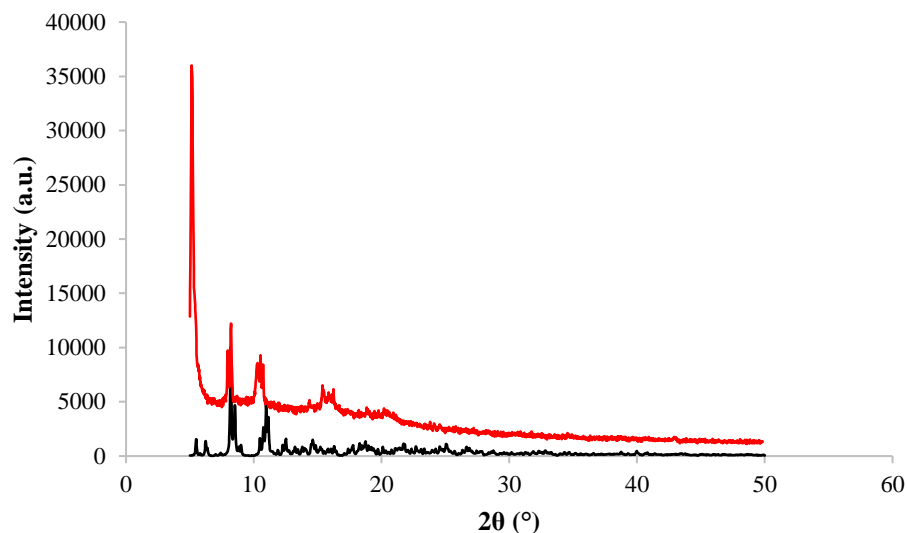
Figure 3.31 PXRD spectrum of polymer 3.6. Simulated pattern (black, 100 K), experimental data (red, rt).

3.5 Synthesis of an ester-linked thiazole ligand

The two major methods used to functionalise CTG **2.3** are through the S_N2 reaction with an alkyl halide, *cf.* **2.4**, **2.11**, **2.18**, **3.1**. The other method not explored yet is through reaction of CTG with an acid chloride. Ester-linked ligands are much more rigid, which can aid crystallisation of metallo-supramolecular assemblies. The archetypal isonicotinoyl ligand has been used to generate a diverse array of materials, including Borromean chainmail[57] and metallo-cryptophanes.[14, 17] Ester-linked analogues of *N*-functionalised benzimidazole **2.11** were avoided because of the arising carbamate group, which would likely hydrolyse under basic conditions, but remain an option for backbone-functionalised azole ligands. The major disadvantage of ester groups on a ligand scaffold is their base-sensitive nature. This would make them unviable materials for the synthesis of metal-NHC complexes desired in this project, so therefore were only used for assembly purposes.

(±)-3,8,13-Trimethoxy-10,15-dihydro-5H-tribenzo[a,d,g][9]annulene-2,7,12-triyl *tris*(thiazole-4-carboxylate), **3.7** was prepared via typical reaction of an acyl

chloride and CTG under weakly basic conditions (scheme 3.3). The reactive nature of acyl chlorides *via* hydrolytic means led to the treatment of thiazole-4-carbonyl chloride as a reaction intermediate. Thiazole-4-carbonyl chloride prepared by heating a solution of carboxylic acid in neat SOCl$_2$ at reflux. SOCl$_2$ was removed *in vacuo* and replaced with THF. The acyl chloride solution subsequently was added to a basic CTG solution in THF.
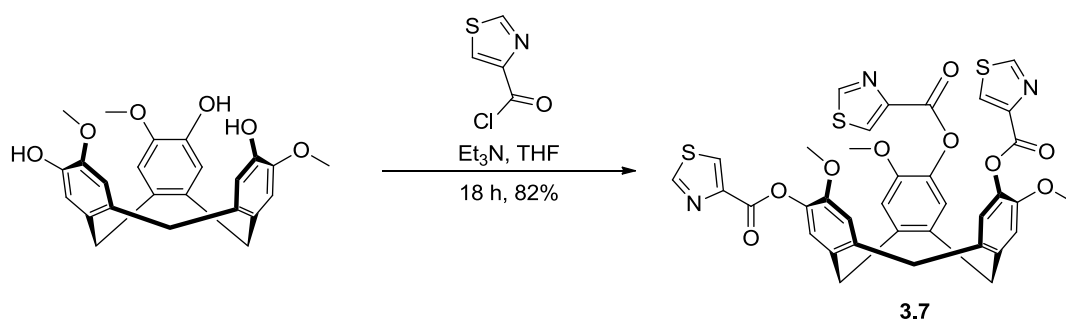
Scheme 3.3 Synthesis of ester-linked ligand 3.7.

Ligand **3.7** displayed poorer solubility than the ether-linked **3.1**, which is a common observation in CTV chemistry because of fewer degrees of rotational freedom associated with the ester group. The ^{1}H NMR spectrum of **3.7** (figure 3.32) was diagnostic for an ester-linked CTV ligand. The two thiazole resonances were significantly further downfield than CTV aromatics at 9.25 and 8.83 ppm. No ethereal CH$_2$ group was present, therefore no resonances were observed in the 2.5 ppm window between the CTV-*endo* protons and the arene groups. The doublet associated with the *endo*-H^{12} proton at 4.89 ppm is diagnostic for a C_3-symmetric CTV ligand. COSY and HMQC NMR spectroscopy confirmed the *exo*-resonance was hidden under the methoxy group.
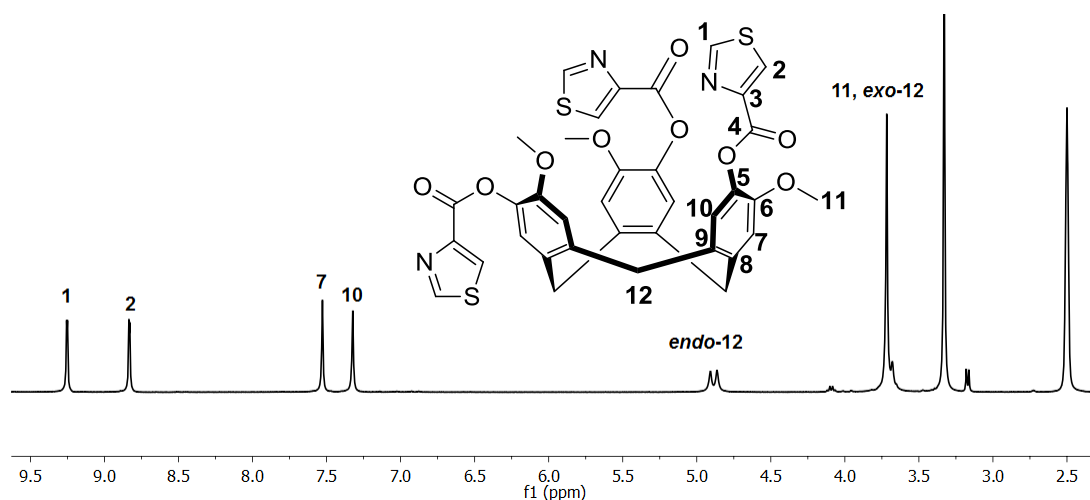
Figure 3.32 ^{1}H NMR spectrum (300 MHz, 298 K, DMSO-d_6) of 3.7.

The $^{13}C\{^{1}H\}$ NMR spectrum (figure 3.33) also displayed a good match to **3.7**. The furthest downfield carbon was assigned as the carbonyl carbon, C^4 at 158.77 ppm, and no HMBC couples were observed at this site. C^{12} appeared at 34.97 ppm, comparable to benzimidazole **2.11**, whose analogous carbon resonance appeared at 37.07 in the same NMR solvent.
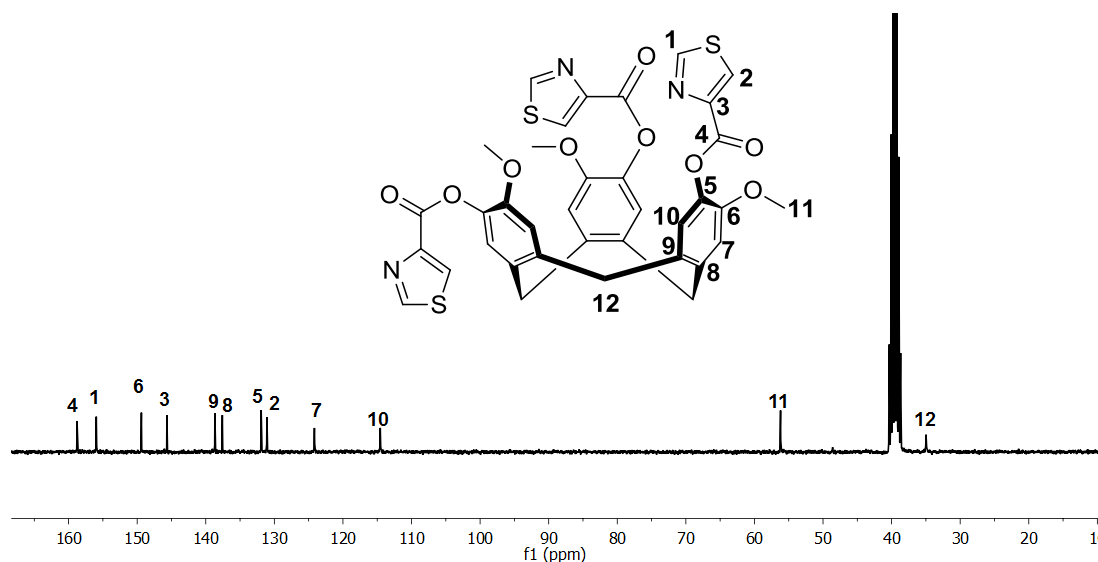
Figure 3.33 $^{13}C\{^{1}H\}$ NMR spectrum (75 MHz, 298 K, DMSO-d_6) of 3.7.

The high-resolution mass spectrum of **3.7** (figure 3.34) displayed an excellent match to the desired product, with the $\{M+H\}^+$ peak dominating the spectrum with $m/z = 742.0979$ (calculated 742.0982). An FTIR spectrum was also obtained, with a strong absorption observed at 1737.41 cm^{-1}, diagnostic for the C=O stretching frequency in a ester group.
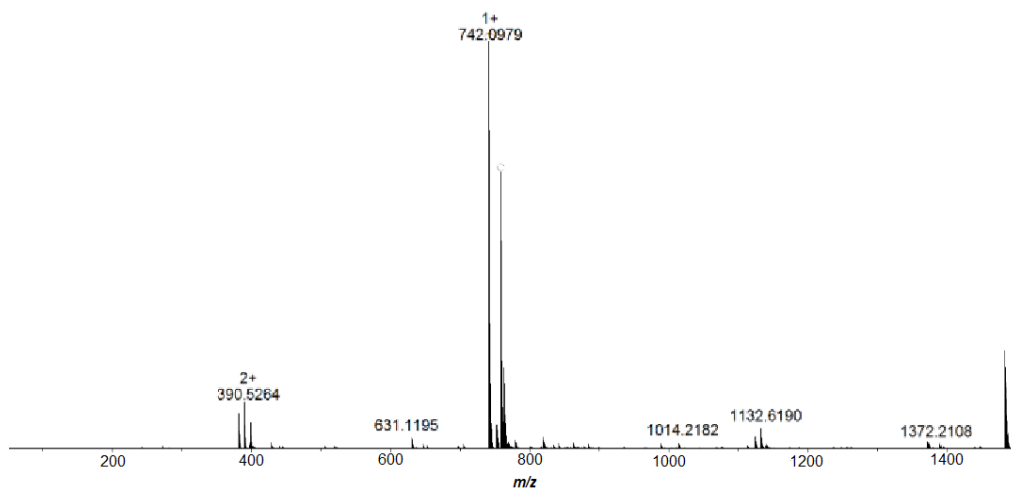
Figure 3.34 HRMS of ligand 3.7.

Single crystals of composition $3.7 \cdot C_4H_{10}O \cdot H_2O$ suitable for diffraction were grown from the diffusion of diethyl ether into an acetonitrile solution of ligand. The structure was solved in the hexagonal $P\bar{3}$ space group, and the asymmetric unit comprised of one third of **3.7**, a partially-occupied diethyl ether molecule and two half-occupied water molecules, as displayed in figure 3.35. The ligand equivalent possesses strict C_3 symmetry. A C_{arene}-O-C-$C_{thiazole}$ torsion angle of -167.789° is slightly out of plane compared to the aqueous and nitromethane solvates of **3.1**, which are much closer to 180°. The azole group is also of a unique rotation, and is orthogonal to the CTV bowl, rather than near parallel to the CTV-arene rim as observed in the structures of **3.1**.
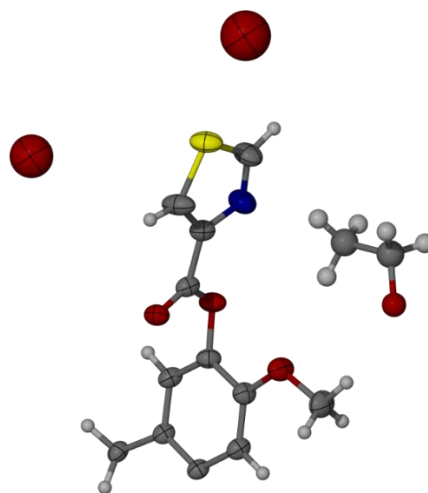
Figure 3.35 Asymmetric unit of 3.7·(C₄H₁₀O)·1.5(H₂O).

Unlike both structures of **3.1**, $3.7 \cdot C_4H_{10}O \cdot 1.5(H_2O)$ crystals are racemic. Enantiomers are close in proximity to one another, and weak hydrogen bonding interactions between ester carbonyl and thiazolyl H5 proton, at C···O separation of 3.216 Å were measured. Ligand stacking was exhibited (figure 3.36), however CTV units were measured as 8.7 Å apart between cyclononatriene centroids, rather than the much more commonly encountered *ca.* 4.6 Å. A diethyl ether molecule residing on a 3-fold symmetry axis was trapped between cavitands at separation of 3.21 Å and could not be refined anisotropically.
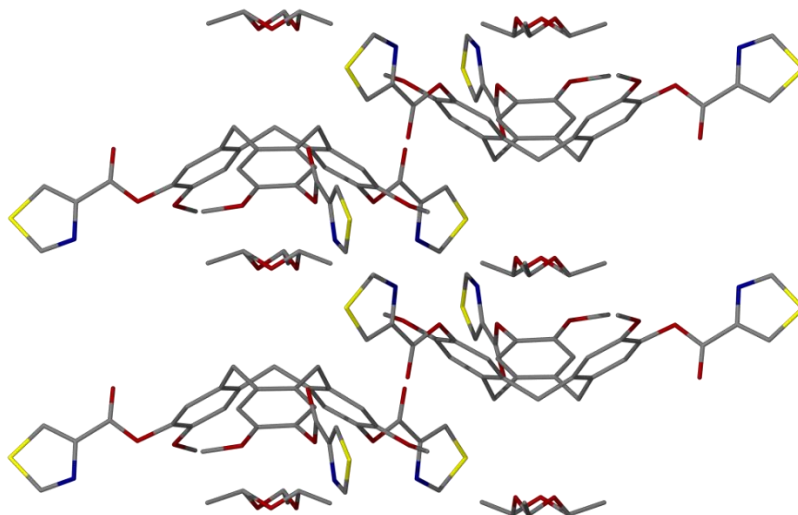
Figure 3.36 Stacking of 3.7 with a three-fold symmetry disordered diethyl ether trapped between cavitands.

3.5.1 Reactivity of ligand 3.7 with metal precursors

In the same fashion as with ligand **3.1**, diffusion of diethyl ether vapours into DMF, DMSO, NMP or MeNO$_2$ solutions of **3.7** with varying stoichiometries of metal precursors was performed. Metals employed included Co-Zn(II), Cu(I), Pd(II) and Ag(I), bearing Cl$^-$, Br$^-$, NO$_2^-$, OTf$^-$, BF$_4^-$ and PF$_6^-$ anions. In all cases where Ag(I) was employed, a black precipitate was observed at the bottom of vials, and Pd(II) saw pale yellow precipitates form over a week, but no crystals were observed in all cases. A vial containing 1.5 eq. CuCl$_2$·2H$_2$O and **3.7** did yield a crop of blue crystals, which SCXRD revealed as the decomposition product [Cu(Cl)(DMF)(H$_2$O)(4-thiazolecarboxylate)], **3.8**. The driving force in this reaction was the formation of a 5-membered metallacycle. HRMS of the mother liquor did not reveal the fate of the remaining portion of CTV.

The asymmetric unit was comprised of one unit of [Cu(Cl)(DMF)(H$_2$O)(4-thiazolecarboxylate)] (figure 3.37). The Cu(II) centre revealed a square pyramidal geometry with the water ligand (O3) at the apex. The N2-Cu1-O1 angle was measured as 170.32(9)°, whereas O2-Cu1-O3, O2-Cu1-Cl1 and O3-Cu1-Cl1 angles measured as 98.73(8), 104.67(6) and 156.52(6)° respectively. Decarboxylation of ester-linked CTV ligands has previously been observed but not published in the Hardie group, and reported in the thesis of Christopher Carruthers when *o*-linked pyridyl ligands were introduced to Cu(II) or Zn(II).[58]
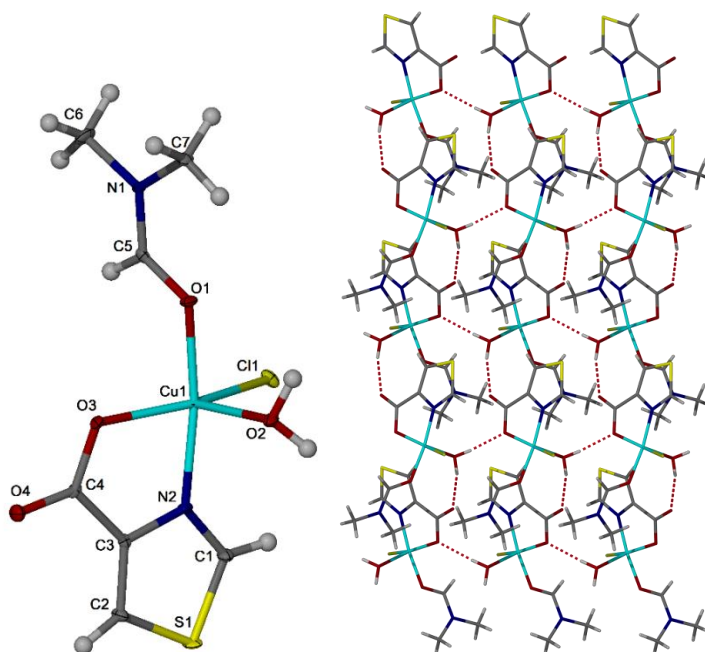
Figure 3.37 Left: Asymmetric unit of 3.8. Ellipsoids are drawn at the 50% probability. Right: 2D sheet of 3.8 displaying hydrogen bonding interactions.

Table 3.1 Selected bond lengths (Å) and angles (º) for 3.8

Cu1-N2	1.962(2)	N2-Cu1-Cl1	94.23(7)
Cu1-O1	1.9428(19)	O1-Cu1-O2	85.68(8)
Cu1-O2	2.232(2)	O1-Cu1-O3	88.70(8)
Cu1-O3	2.027(2)	O2-Cu1-O3	98.73(8)
Cu1-Cl1	2.2764(7)	O1-Cu1-Cl1	94.93(6)
N2-Cu1-O1	170.32(9)	O2-Cu1-Cl1	104.67(6)
N2-Cu1-O2	95.02(9)	O3-Cu1-Cl1	156.52(6)
N2-Cu1-O3	81.65(9)		

The extended structure of [Cu(Cl)(DMF)(H$_2$O)(4-thiazolecarboxylate)] revealed a 2D hydrogen bonded network focused about the water ligand, as shown in figure 3.37. Both water hydrogen atoms donated to neighbouring carboxylate groups, with both the coordinating and non-coordinating oxygen atoms of the carboxylate taking part at O···O separations of 2.841 and 2.832 Å respectively.

3.6 Conclusions and future work

A novel 4-thiazolyl ligand, **3.1·HCl** was prepared and fully characterised. Its assembly with a range of metals investigated. Crude **3.1** displayed a high affinity towards Ag(I), yielding the first examples of coordination cubes derived from a CTV ligand, **3.2** and **3.3**. Cube crystals displayed dual chiral resolution, with all cubes within a single crystal being of a single enantiomer of ligand. The reactivity of metallo-cubes and also their viability as molecular hosts was probed, however these proved to be unsuccessful.

Furthermore, after neutralising **3.1**, cube crystals of **3.3** grew after *ca.* one month rather than one week. In addition, minor side-products were observed in the form of a 3D coordination polymer, **3.4**, which bore considerable pores throughout its structure. Attempts to increase the ratio of polymer:cube crystals were unsuccessful.

Ligand **3.1** also assembled with silver cobalticarborane, which yielded a 2D coordination polymer of 6^3 topology. The hydrochloride salt of **3.1** led to crystal growth of a different morphology, although crystals were too poorly diffracting to obtain meaningful data.

An ester-linked 4-thiazoloyl ligand was also successfully prepared. No evidence of coordination to Ag(I) could be attained. Coordination at Cu(II) led to decarboxylation of **3.6**, and crystals of [Cu(Cl)(H$_2$O)(DMF)(thiazole-4-carboxylate)] grew as a 2D hydrogen-bonded network.

Future work involving **3.2** and **3.3** could involve trying to incorporate donor groups within the sulfur-edged windows of cubes. Whilst seldom coordinating, the positioning of these groups around the windows could facilitate a soft d^8 transition metal such as Rh(I) or Ir(I) to coordinate, which could be a method of trapping metal ions that are air-sensitive in the absence of chelating olefin ligands. Weak hydrogen-bonding interactions could also be targeted at this position, for example, targeting substrates such as H$_2$S.

Additionally, investigating the assembly of metallo-cubes with Ag(I) salts of large anions, such as [BAr$^F_4$] could yield interesting results. If Ag[BAr$^F_4$] could yield cubes, the bulky, internal anions would be within close proximity of one

another and undergo unwanted reactivity caused by confinement. Conversely, an altogether new assembly could be achieved, in the same manner as cobalticarborane.

The tetrafluoroborate and hexafluorophosphate 3D coordination polymers could be viable materials to accommodate large guest species. A reproducible method of preparing these polymers in a good ratio would however be paramount to this application.

3.7 Experimental section

Unless stated in the experimental section, chemicals were bought from commercial suppliers and used without further purification. Unless stated, all reactions were carried out under aerobic conditions. Reactions performed under an atmosphere of dry nitrogen were carried out using standard Schlenk and Glovebox procedures, with solvents dried and degassed using the same methodology described in Section **2.9**. All analytical techniques are also consistent with those described in Section **2.9**.

Synthesis of (±)-4,4',4''-(((3,8,13-trimethoxy-10,15-dihydro-5H-tribenzo[a,d,g][9]annulene-2,7,12-triyl)*tris*(oxy))tris(methylene))trithiazole, 3.1

(±)-Cyclotriguaiacylene (100 mg, 0.24 mmol) and Cs_2CO_3 (800 mg, 2.35 mmol) were dissolved in DMF (5 mL) and stirred at rt for 30 mins. 4-(Chloromethyl)thiazole·HCl (134 mg 1.60 mmol) was added and the brown solution stirred at 100 ℃ overnight. The dark brown mixture was cooled, water (10 mL) was added and the
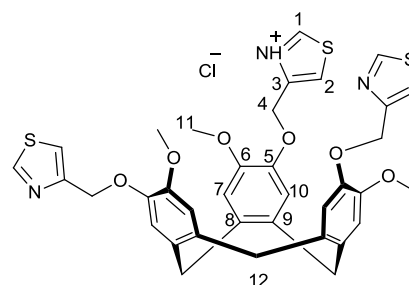
resultant grey precipitate filtered and washed with Et_2O, affording the title compound as a cream solid. Yield 135 mg, 0.19 mmol, 80%. HRMS (ESI$^+$) 700.1621 {M+H: $C_{36}H_{34}N_3O_6S_3$}$^+$, 1399.3143 {M$_2$+H: $C_{72}H_{67}N_6O_{12}S_6$}$^+$ Calcd. for 700.1605 and 1399.3136 respectively; ^{1}H NMR (300 MHz, CDCl$_3$) δ (ppm) 8.81 (d, 3H, J = 2.1 Hz , H^1), 7.38 (s, 3H, H^2), 6.94 (s, 3H, H^7), 6.77 (s, 3H, H^{10}), 5.30 (s, 6H, H^4), 4.71 (d, 3H, J = 13.6 Hz, endo-H^{12}), 3.81 (s, 9H, H^{11}), 3.49 (d, 3H J = 13.5 Hz, exo-H^{12}); ^{13}C{^{1}H} NMR (75 MHz, CDCl$_3$) 154.02 (C^3), 153.12 (C^1), 148.52 (C^6), 146.73 (C^5), 133.05 (C^8), 131.94 (C^9), 116.31 (C^2), 116.23 (C^7), 114.14 (C^{10}), 67.82 (C^4), 56.51 (C^{11}), 36.62 (C^{12}); IR ν (cm^{-1}) 3500, 3404 (broad), 3087, 2920, 1659 (sharp), 1512 (sharp), 1262 (sharp); Elemental analysis Calcd. for

3.1.(HCl).0.5(H$_2$O) C 58.01, H 4.73, N 5.64 Found C 58.30, H 4.50, N 5.50; Elemental analysis Calcd. for **3.1**: C 61.78, H 4.75, N 6.00 Found: C 61.69, H 4.51, N 6.14. X-ray quality crystals were obtained from a saturated DMF:water solution, and the diffusion of diethyl ether vapours into a nitromethane solution of **3.1**.

Ligand **3.1** was isolated as a monohydrochloride salt. Dissolving **3.1**·HCl in DCM and washing with aq. NaHCO$_3$ prior to filtering through silica led to neutralisation of the ligand.

Synthesis of [Ag$_{12}$(3.1)$_8$](ReO$_4$)$_{12}$, 3.2

Crude **3.1·HCl** (7 mg, 0.01 mmol) and AgReO$_4$ (4.6 mg, 0.015 mmol) were dissolved in DMF (1 mL), kept in the dark, and diethyl ether vapours were diffused into the reaction vial, affording cubic crystals of **3.1**, [Ag$_{12}$L$_8$]·(ReO$_4$)$_{12}$·(DMF)$_{10}$, along with a small amount of powdered contaminant likely to be AgCl. Yield 6.1 mg, 49%. FTIR ν (cm^{-1}) 3090, 1653 (DMF C=O), 1508 (sharp), 1260 (sharp), 1086 (sharp), 903 (Re-O). Satisfactory elemental analysis could not be obtained due to high levels of solvation and the presence of minor inorganic impurities. pXRD indicates the crystalline material is phase pure. [Ag$_{12}$L$_8$](ReO$_4$)$_{12}$·10(DMF) calcd. C 35.94, H 3.17, N 4.48, found C 32.74, H 2.26, N 3.59%. HRMS (ESI+) 808.0561 {AgL}$^+$, 1507.2125 {AgL$_2$}$^+$, calcd. 808.0574 and 1507.2106 respectively.

Synthesis of [Ag$_{12}$(3.1)$_8$](BF$_4$)$_{12}$, 3.3

Crude **3.1·HCl** (7 mg, 0.01 mmol) and AgBF$_4$ (2.9 mg, 0.015 mmol) were dissolved in DMF (1 mL), kept in the dark, and diethyl ether vapours were diffused into the reaction vial, affording cubic crystals of complex **3.3**, [Ag$_{12}$L$_8$]·(BF$_4$)12·(DMF)$_{12}$, along with a small amount of powdered contaminant likely to be AgCl. Yield 7.5 mg, 76%. FTIR ν (cm-1) 3098, 1656 (DMF C=O), 1510 (sharp), 1256 (sharp), 1149 (sharp), 1046 (B-F). Satisfactory elemental analysis could not be obtained due to high levels of solvation and the presence of minor inorganic impurities. pXRD indicates the crystalline material is phase pure. [Ag$_{12}$L$_8$](BF$_4$)$_{12}$·12(DMF) calcd. C 44.16, H 3.98, N 5.72, found C 43.20, H 4.58, N 6.46%.

Synthesis of ([Ag$_8$(3.1)$_6$]8(BF$_4$))$_n$, 3.4

Neutralised **3.1** (7 mg, 0.01 mmol) and AgBF$_4$ (2.9 mg, 0.015 mmol) were dissolved in DMF (1 mL), kept in the dark, and diethyl ether vapours were diffused into the reaction vial. A small crop of crystals (2.2 mg) was isolated which were mostly pale orange blocks, alongside a small quantity of colourless needles. Did not grow phase pure so microanalysis was not undertaken.

Synthesis of [Ag$_{12}$(3.1)$_8$](PF$_6$)$_{12}$.3.66H$_2$O, 3.5

Neutralised, **3.1** (7 mg, 0.01 mmol) and AgPF$_6$ (3.4 mg, 0.015 mmol) were dissolved in DMF (1 mL), kept in the dark, and diethyl ether vapours were diffused into the reaction vial. A small crop of colourless crystals (2.8 mg) was isolated. Did not grow phase pure so microanalysis was not undertaken.

Synthesis of ([Ag$_3$(3.1)$_3$][CoCb$_2$]$_3$·5(DMF)$_n$ 3.6

Neutral (±)-*tris*-(4-methylthiazolyl)cyclotriguaiacylene, **3.1** (7 mg, 0.01 mmol) and Ag[CoCb$_2$] (5.5 mg, 0.01 mmol) were dissolved in DMF (1 mL), kept in the dark, and diethyl ether vapours were diffused into the reaction vial. A small crop of pale yellow crystals (3.1 mg) was isolated by filtration and washing with DCM (2 mL). FTIR ν (cm^{-1}) 2927, 2859, 2531 (B-H), 1650, 1258, 1085. Satisfactory elemental analysis could not be obtained due to high levels of solvent. Calculated for [Ag$_3$(3.1)$_3$]$_n$[CoCb$_2$]$_3$·10(C$_3$H$_7$NO)·7(CH$_2$Cl$_2$) C 39.95, H 5.32, N 5.64; Found C 39.72, H 5.33, N 5.64. PXRD indicated the crystalline material was phase pure.

Synthesis of (±)-3,8,13-trimethoxy-10,15-dihydro-5H-tribenzo[a,d,g][9]annulene-2,7,12-triyl *tris*(thiazole-4-carboxylate), 3.7

4-Thiazolecarboxylic acid (0.31 g, 2.40 mmol) was dissolved in thionyl chloride (5 mL) and heated to reflux for 16 h under a N$_2$ atmosphere. Thionyl chloride was removed *in vacuo*, affording 4-thiazolecarbonyl chloride, which was not characterised and treated as an intermediate and assumed to have been prepared quantitatively.
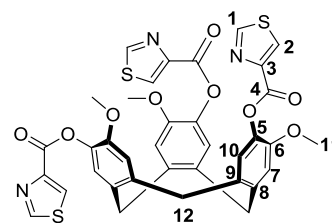
CTG (200 mg, 0.49 mmol) was dissolved in anhydrous THF (15 mL) under a N_2 atmosphere and cooled to 0 ºC. Triethylamine (1.03 mL, 7.35 mmol) was added and the reaction mixture stirred for 30 mins. A solution of 4-thiazolecarbonyl chloride (5 eq.) in THF (15 mL) was added *via* cannula transfer and the reaction mixture stirred at 0 ºC for 120 mins, before warming to rt and stirring for 24 h. Volatiles were removed *in vacuo* and the orange residue triturated in EtOH (50 mL). A cream solid was isolated, washed with MeOH (3 x 20 mL) and Et_2O (3 x 10 mL), affording **3.7** as a cream coloured solid (298 mg, 0.40 mmol, 82%). HRMS (ESI⁺) 360.5264 742.0979 (calculated 742.0982); ¹H NMR (300 MHz, DMSO-d_6) δ (ppm) 9.25 (s, 3H, H¹), 8.83 (s, 3H, H²), 7.53 (s, 3H, H⁷), 7.32 (s, 3H, H¹⁰), 4.88 (d, 3H, *J* = 14.0 Hz, *endo*-H¹²), 3.72 (s, 4H, H¹¹, *exo*-H¹²); ¹³C{¹H} NMR (75 MHz, DMSO-d_6) δ (ppm) 158.77 (C4), 155.96 (C1), 149.38 (C6), 145.67 (C3), 138.67 (C9), 137.58 (C8), 131.92 (C5), 131.08 (C2), 124.15 (C7), 114.55 (C19), 56.19 (C11), 34.97 (C12); IR ν (cm⁻¹) 3088, 1737 (C=O), 1543, 1249, 1165; Elemental analysis for **3.7**·3.5(HCl) Calcd.: C 49.73, H 3.54, N 4.83; Found: C 50.10, H 2.99, N 5.03

3.8 Supplementary crystallographic information

Crystals were mounted under inert oil on a MiTeGen tip and flash frozen using an OxfordCryosystems low temperature device. X-ray diffraction data were collected using CuKα radiation (λ = 1.54184 Å) or MoKα (λ = 0.71073 Å) using an Agilent Supernova dual-source diffractometer with Atlas S2 CCD detector and fine-focus sealed tube generator, or using synchrotron radiation (λ = 0.6889 Å) at Beamline I19 at the Diamond light source. Data were corrected for Lorenztian and polarization effects and absorption corrections were applied using multi-scan methods. The structures were solved by direct methods using SHELXS-97 and refined by full-matrix on F^2 using SHELXL-97. Unless otherwise specified, all non-hydrogen atoms were refined as anisotropic, and hydrogen positions were included at geometrically estimated positions.

3.8.1 Additional crystallographic details

3.2

Oxygen atoms of perrhenate anions were refined as isotropic and Re-O bond lengths restrained to be chemically reasonable. One anion was refined with group *Uiso* for the O sites. One ReO_4 was sited on a 4-fold axis, displaying symmetry-induced

disorder. This ReO_4 was of low occupancy for charge balance. The highest residual peak was a Fourier ripple measured 0.24 Å from Re1.

3.3

The SQUEEZE routine of PLATON was employed[30] because anions could not be located in the difference map, and a void space of *ca.* 45% of the unit cell volume was calculated. Residual electron density could not be meaningfully refined as anions or solvents. Global restraints were placed on the anisotropic displacement parameters.

3.4

Anions could not be located in the difference map, therefore, the SQUEEZE routine of PLATON was employed[30], which calculated a void space of *ca.* 48% of the unit cell volume.

3.6

The highest residual peak was a Fourier ripple measured 1.07 Å from Ag1.

3.7

The diethyl ether molecule was sited on 3-fold symmetry axis, displaying symmetry-induced disorder. The C-O bond in diethyl ether was restrained to be chemically reasonable. The diethyl ether molecule was refined as isotropic.

Table 3.2 Crystallographic data. a = CuKα radiation, b = synchrotron radiation

Compound	**3.1·4(H$_2$O)**[a]	**3.1·3(MeNO$_2$)**[a]	**3.2**[a]	**3.3**[a]
Formula	C$_{36}$H$_{41}$N$_3$O$_{10}$S$_3$	C$_{39}$H$_{42}$N$_6$O$_{12}$S$_3$	C$_{288}$H$_{264}$Ag$_{12}$N$_{24}$O$_{96}$Re$_{12}$S$_{24}$	C$_{288}$H$_{264}$Ag$_{12}$B$_{12}$F$_{48}$N$_{24}$O$_{48}$S$_{24}$
Mr	771.9	882.97	9895.52	7934.84
Crystal colour and shape	Yellow, needle	Colourless, rod	Pale orange, block	Pale orange, block
Crystal size (mm)	0.15 x 0.05 x 0.02	0.20 x 0.03 x 0.02	0.15 x 0.10 x 0.10	0.15 x 0.12 x 0.07
Crystal system	Hexagonal	Trigonal (hexagonal axes)	Cubic	Cubic
Space group	$P6_3$	$R3$	$F432$	$F432$
a (Å)	14.5223(19)	28.138(3)	35.7237(4)	35.4548(7)
b (Å)	14.5223(19)	28.138(3)	35.7237(4)	35.4548(7)
c (Å)	10.2701(12)	4.4445(5)	35.7237(4)	35.4548(7)
α (^{0})	90	90	90	90
β (^{0})	90	90	90	90
γ (^{0})	120	120	90	90
V (Å^3)	1875.8(4)	3047.4(5)	45590.0(9)	44568.2(15)
Z	2	3	4	4
T/K	110(1)	120(1)	120(1)	120(1)
ρ_{calc} (g.cm^{-3})	1.367	1.443	1.442	1.183
θ range (^{0})	3.51 – 73.42	5.45 – 73.82	3.50-73.74	3.53–73.63
No. data collected	4447	4449	9948	4858
No. unique data	2239	2150	3794	2572
R_{int}	0.0604	0.0786	0.0341	0.0286
No. obs. Data ($I > 2\sigma(I)$)	1394	1635	2667	1639
No. parameters	158	183	168	152
No. restraints	1	1	4	42
R_1 (obs data)	0.0886	0.0719	0.0847	0.0718
wR_2 (all data)	0.2598	0.1873	0.2886	0.2256
Flack parameter	-0.07(7)	0.08(5)	0.03(4)	0.15(3)
S	0.996	1.052	1.036	1.042
Max. shift/esd	0.000	0.000	0.001	0.001
Largest difference peak and hole/ (e Å^3)	1.332, -0.326	0.399, -0.315	2.000, -2.126	0.778, -0.479

Table 3.3 Crystallographic data. a = CuKα radiation, b = synchrotron radiation

Compound	3.4[a]	3.5·3.66(H₂O)[a]	3.6·5(C₃H₇NO)[b]	3.7[a]	3.8[a]
Formula	$C_{222}H_{213}Ag_8B_8F_{24}N_{20}O_{38}S_{18}$	$C_{288}H_{264}Ag_{12}F_{84}N_{24}O_{51.67}P_{12}S_{24}$	$C_{267}H_{393}Ag_6B_{108}Co_6N_{27}O_{45}S_{18}$	$C_{40}H_{37}N_3O_{10.75}S_3$	$C_{28}H_{44}Cl_4CuN_8O_{16}S_4$
Mr	15627.45	8981.36	7446.42	829.42	1272.91
Crystal colour and shape	Colourless, needle	Colourless, block	Pale orange, block	Colourless, block	Blue, block
Crystal size (mm)	0.023 x 0.044 x 0.179	0.088 x 0.101 x 0.144	0.061 x 0.08 x 0.093	0.17 x 0.12 x 0.10	0.31 x 0.28 x 0.26
Crystal system	Trigonal (hexagonal axes)	Cubic	Triclinic	Trigonal (hexagonal axes)	Orthorhombic
Space group	$R3$	$F432$	$P\bar{1}$	$P\bar{3}$	$P2_12_12_1$
a (Å)	76.1229(12)	35.7386(3)	16.9206(2)	16.7381(6)	5.51030(10)
b (Å)	76.1229(12)	35.7386(3)	25.1781(2)	16.7381(6)	11.4557(2)
c (Å)	16.2705(3)	35.7386(3)	25.2520(2)	8.7148(4)	18.1230(2)
α (⁰)	90	90	119.2780(10)	90.00	90
β (⁰)	90	90	104.8890(10)	90.00	90
γ (⁰)	120	90	91.4090(10)	120.00	90
V (Å³)	81651(3)	45647.0(13)	8923.53(17)	2114.46(14)	1144.00(3)
Z	9	4	1	2	4
T/K	120(1)	120(2)	120	100(2)	120.01(10)
ρ_{calc} (g.cm⁻³)	0.953	1.307	1.386	1.303	1.848
θ range (⁰)	3.07-44.49	4.103-73.660	1.114-26.237	5.08-73.76	4.566- 73.368
No. data collected	61017	11161	87282	5308	2850
No. unique data	26341	3775	21797	2772	1989
R_{int}	0.0504	0.0366	0.0878	0.0358	0.0163
No. obs. Data ($I > 2\sigma(I)$)	22117	2531	18825	2179	1980
No. parameters	2777	194	2179	171	148
No. restraints	1	0	0	1	0
R_1 (obs data)	0.0504	0.1226	0.0767	0.0701	0.0214
wR_2 (all data)	0.1320	0.3702	0.2398	0.2186	0.0546
Flack parameter	0.276(7)	-0.225 (0.028)			0.039(12)
S	1.017	1.339	1.055	1.095	1.120
Max. shift/esd	0.082	0.001	0.017	0.002	0.001
Largest difference peak and hole/ (e Å³)	0.863, -0.477	1.508, -1.451	4.123, -1.528	1.444, -0.433	0.229, -0.410

3.9 References

1.   P. Haake, W. B. Miller, *J. Am. Chem. Soc.*, 1963, **85**, 4044-4045.

2.   R. Breslow, *J. Am. Chem. Soc.*, 1957, **79**, 1762-1763.

3.   E. H. White, F. McCapra, G. F. Field, *J. Am. Chem. Soc.*, 1963, **85**, 337-343.

4.   C. Hedberg, K. Källström, P. Brandt, L. K. Hansen, P. G. Andersson, *J. Am. Chem. Soc.*, 2006, **128**, 2995-3001.

5.   C. R. Rice, S. Worl, J. C. Jeffery, R. L. Paul, M. D. Ward, *Chem. Commun.*, 2000, 1529-1530.

6.   S. Hiraoka, K. Harano, T. Tanaka, M. Shiro, M. Shionoya, *Angew. Chem. Int. Ed.*, 2003, **42**, 5182-5185.

7.   S. Hiraoka, M. Shiro, M. Shionoya, *J. Am. Chem.Soc.*, 2004, **126**, 1214-1218.

8.   J. E. Beves, J. J. Danon, D. A. Leigh, J.-F. Lemonnier, I. J. Vitorica-Yrezabal, *Angew. Chem. Int. Ed.*, 2015, **54**, 7555-7559.

9.   N. Meundaeng, A. Rujiwatra, T. J. Prior, *J. Solid State Chem.*, 2017, **245**, 138-145.

10.   C.-Y. Su, M. D. Smith, A. M. Goforth, H.-C. zur Loye, *Inorg. Chem.*, 2004, **43**, 6881-6883.

11.   X.-D. Chen, H.-F. Wu, X.-H. Zhao, X.-J. Zhao, M. Du, *Cryst. Growth Des.*, 2007, **7**, 124-131.

12.   N. Dannenbauer, P. R. Matthes, T. P. Scheller, J. Nitsch, S. H. Zottnick, M. S. Gernert, A. Steffen, C. Lambert, K. Müller-Buschbaum, *Inorg. Chem.*, 2016, **55**, 7396-7406.

13.   Z. Zhong, A. Ikeda, S. Shinkai, S. Sakamoto, K. Yamaguchi, *Org. Lett.*, 2001, **3**, 1085-1087.

14.   J. J. Henkelis, C. J. Carruthers, S. E. Chambers, R. Clowes, A. I. Cooper, J. Fisher, M. J. Hardie, *J. Am. Chem. Soc.*, 2014, **136**, 14393-14396.

15.   A. Schaly, Y. Rousselin, J. C. Chambron, E. Aubert, E. Espinosa, *Eur. J. Inorg. Chem.*, 2016, 832-843.

16.   N. J. Cookson, J. M. Fowler, D. P. Martin, J. Fisher, J. J. Henkelis, T. K. Ronson, F. L. Thorp-Greenwood, C. E. Willans, M. J. Hardie, *Supramol. Chem.*, 2018, **30**, 255-266.

17.   T. K. Ronson, J. Fisher, L. P. Harding, M. J. Hardie, *Angew. Chem. Int. Ed.*, 2007, **46**, 9086-9088.

18.   T. K. Ronson, C. Carruthers, J. Fisher, T. Brotin, L. P. Harding, P. J. Rizkallah, M. J. Hardie, *Inorg. Chem.*, 2010, **49**, 675-685.

19.   J. J. Henkelis, T. K. Ronson, L. P. Harding, M. J. Hardie, *Chem. Commun.*, 2011, **47**, 6560-6562.

20.   C. J. Sumby, M. J. Carr, A. Franken, J. D. Kennedy, C. A. Kilner, M. J. Hardie, *New J. Chem.*, 2006, **30**, 1390-1396.

21.   C. J. Sumby, M. J. Hardie, *Angew. Chem. Int. Ed.*, 2005, **44**, 6395-6399.

22.   C. Carruthers, T. K. Ronson, C. J. Sumby, A. Westcott, L. P. Harding, T. J. Prior, P. Rizkallah, M. J. Hardie, *Chem. Eur. J.*, 2008, **14**, 10286-10296.

23.   J. J. Henkelis, M. J. Hardie, *CrystEngComm.*, 2014, **16**, 8138-8146.

24. J. J. Henkelis, S. A. Barnett, L. P. Harding, M. J. Hardie, *Inorg. Chem.*, 2012, **51**, 10657-10674.

25. M. A. Little, M. A. Halcrow, L. P. Harding, M. J. Hardie, *Inorg. Chem.*, 2010, **49**, 9486-9496.

26. T. K. Ronson, M. J. Hardie, *CrystEngComm.*, 2008, **10**, 1731-1734.

27. M. J. Hardie, C. J. Sumby, *Inorg. Chem.*, 2004, **43**, 6872-6874.

28. C. J. Sumby, M. J. Hardie, *Cryst. Growth Des.*, 2005, **5**, 1321-1324.

29. G. C. Vougioukalakis, R. H. Grubbs, *J. Am. Chem. Soc.*, 2008, **130**, 2234-2245.

30. F. L. Thorp-Greenwood, V. E. Pritchard, M. P. Coogan, M. J. Hardie, *Organometallics*, 2016, **35**, 1632-1642.

31. A. Spek, *Acta Crystallogr. Sect. A*, 1990, **46**, c34.

32. O. Gidron, M. Jirásek, N. Trapp, M.-O. Ebert, X. Zhang, F. Diederich, *J. Am. Chem. Soc.*, 2015, **137**, 12502-12505.

33. L. J. Childs, N. W. Alcock, M. J. Hannon, *Angew. Chem. Int. Ed.*, 2002, **41**, 4244-4247.

34. S. A. Boer, D. R. Turner, *Chem. Commun.*, 2015, **51**, 17375-17378.

35. L.-L. Yan, C.-H. Tan, G.-L. Zhang, L.-P. Zhou, J.-C. Bünzli, Q.-F. Sun, *J. Am. Chem. Soc.*, 2015, **137**, 8550-8555.

36. C. Gütz, R. Hovorka, G. Schnakenburg, A. Lützen, *Chem. Eur. J.*, 2013, **19**, 10890-10894.

37. C. Gütz, R. Hovorka, C. Klein, Q.-Q. Jiang, C. Bannwarth, M. Engeser, C. Schmuck, W. Assenmacher, W. Mader, F. Topić, K. Rissanen, S. Grimme, A. Lützen, *Angew. Chem. Int. Ed.*, 2014, **53**, 1693-1698.

38. M. Hardy, N. Struch, F. Topić, G. Schnakenburg, K. Rissanen, A. Lützen, *Inorg. Chem.*, 2017, **57**, 3507-3515.

39. J.-T. Yu, Y.-Y. Shi, J. Sun, J. Lin, Z.-T. Huang, Q.-Y. Zheng, *Sci. Rep.*, 2013, **3**, 2947.

40. T. K. Ronson, J. Fisher, L. P. Harding, P. J. Rizkallah, J. E. Warren, M. J. Hardie, *Nat. Chem*, 2009, **1**, 212-216.

41. P. Bonakdarzadeh, F. Pan, E. Kalenius, O. Jurček, K. Rissanen, *Angew. Chem. Int. Ed.*, 2015, **54**, 14890-14893.

42. Y. Makita, K. Sugimoto, K. Furuyoshi, K. Ikeda, T. Fujita, S.-I. Fujiwara, A. Ogawa, *Supramol. Chem.*, 2011, **23**, 269-272.

43. M. A. Little, J. Donkin, J. Fisher, M. A. Halcrow, J. Loder, M. J. Hardie, *Angew. Chem. Int. Ed.*, 2012, **51**, 764-766.

44. C. Givelet, J. Sun, D. Xu, T. J. Emge, A. Dhokte, R. Warmuth, *Chem. Commun.*, 2011, **47**, 4511-4513.

45. L.-J. Chen, H.-B. Yang, M. Shionoya, *Chem. Soc. Rev.*, 2017, **46**, 2555-2576.

46. B. F. Abrahams, S. J. Egan, R. Robson, *J. Am. Chem. Soc.*, 1999, **121**, 3535-3536.

47. C. Wang, X.-Q. Hao, M. Wang, C. Guo, B. Xu, E. N. Tan, Y.-Y. Zhang, Y. Yu, Z.-Y. Li, H.-B. Yang, M.-P. Song, X. Li, *Chem. Sci.*, 2014, **5**, 1221-1226.

48. S. Roche, C. Haslam, S. L. Heath, J. A. Thomas, *Chem. Commun.*, 1998, 1681-1682.

49. W. J. Ramsay, F. J. Rizzuto, T. K. Ronson, K. Caprice, J. R. Nitschke, *J. Am. Chem. Soc.*, 2016, **138**, 7264-7267.

50.   D. Xu, R. Warmuth, *J. Am. Chem. Soc.*, 2008, **130**, 7520-7521.

51.   J. Strübe, B. Neumann, H.-G. Stammler, D. Kuck, *Chem. Eur. J.*, 2009, **15**, 2256-2260.

52.   S. Klotzbach, F. Beuerle, *Angew. Chem. Int. Ed.*, 2015, **54**, 10356-10360.

53.   D. Beaudoin, F. Rominger, M. Mastalerz, *Angew. Chem. Int. Ed.*, 2016, **55**, 15599-15603.

54.   A. Westcott, N. Whitford, M. J. Hardie, *Inorg. Chem.*, 2004, **43**, 3663-3672.

55.   S. Du, T-Q. Yu, W. Liao, C. Hu, *Dalton Trans.* 2015, **44**, 14394-14402.

56.   O. K. Farha, I. Eryazici, N. C. Jeong, B. G. Hauser, C. E. Wilmer, A. A. Sarjeant, R. Q. Snurr, S. T. Nguyen, A. Özgür Yazaydin, J. T. Hupp, *J. Am. Chem. Soc.*, 2012, **134**, 15016-15021.

57.   F. L. Thorp-Greenwood, A. N. Kulak, M. J. Hardie, *Nat. Chem*, 2015, **7**, 526-531.

58.   C. Carruthers, M. J. Hardie, *Unpublished Results*. The Zn(II) and Cu(II)-mediated ester cleavage of ester-linked CTV ligands.

Chapter 4
Synthesis and characterisation of benzimidazolium salts, and targeted group 11 carbene complexes

This chapter focuses on the preparation and characterisation of novel, tripodal imidazolium salts, and investigations into their coordination to d^{10} metals. A new class of guaiacol-derived mono-benzimidazolium salts were also prepared which are comparable to one-third of the CTV bowl. This ligand-class can potentially both enhance species elucidation, and arise as a pathway to compare activities of monodentate and tridentate systems in catalysis.

4.1 Introduction

Many NHC ligands in organometallic chemistry are derived from *N*-arylated imidazolium salts. These are generally prepared in the Debus-Radziszewski reaction by condensation of glyoxal, an aniline and formaldehyde in acidic media (scheme 4.1). Reactions are facile, but side-reactions such as reverse-aldol condensations also arise, whereby one carbonyl of the glyoxal can be regenerated, leading to often protracted workups.[1] A key example is 1,3-*bis*-mesitylimidazolium chloride (IMes·HCl), (mesityl = 2,4,6-trimethylphenyl), formed when using 2,4,6-trimethylaniline as the amine source in the synthesis. Additionally, the bulkier the aniline, the more challenging (and often unsuccessful) the condensation. Arduengo and co-workers developed a modified procedure of the Debus_Radziszewski reaction to overcome these issues, whereby a diimine could be prepared, before reaction with chloromethyl ethyl ether rather than an aldehyde.[2] This route remains popular for the bulkiest of NHC ligands, including IPr·HCl (1,3-*bis*-(2,6-diisopropylphenyl)imidazolium chloride) and the isopentyl derivative, IPent·HCl. In spite of the drawbacks, the Debus-Radziszewski reaction is extensively used and a highly popular route to prepare imidazolium salts (or substituted imidazoles when ammonia and a secondary amine are used), and is a highly scalable reaction.
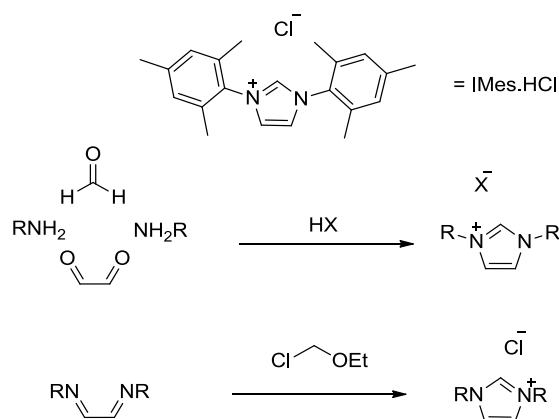
Scheme 4.1 Synthesis of imidazolium salts *via* the Debus-Radziszewski reaction[1, 2]

The *tris*-imidazolium nature of CTV-type ligands would lead to the Debus-Radziszewski route being unviable using suitable cavitands, as the by-product issues would be amplified, with the possibility of mixed-arm by-products offering a number of additional problems. It was therefore decided that the straightforward nucleophilic substitution of an *N*-derivatised imidazole, such as ligand **2.4**, with a pertinent electrophile would be the method of choice (scheme 4.2). The electrophile has to be susceptible to S_N2 reactions, otherwise the E1-elimination reaction often observed with the *tert*-butyl cation may well dominate proceedings. Whilst an amino CTG precursor is known, and reactivity in the Debus-Radziszewski reaction may be possible, the number of potential by-products and likely separative problems would be magnified. Furthermore, Brenner and co-workers have recently prepared *bis*-resorcinarenylimidazolium salts to overcome cavitand scission reactions when preparing Ni(II) complexes.[3-5] This ligand was prepared using the Debus-Radziszewski reaction, and gave only a 13% conversion. It is worth noting the ligand in question here is monocationic rather than the tricationic targets in this project.

4.2 Imidazolium salts on a CTG scaffold

Imidazole **2.4**, which was reported in section **2.2**, could be efficiently alkylated by its reaction with methyl iodide. All reactions involving methyl iodide were carried out in a sealed J. Youngs ampoule because its high volatility and low boiling point led to it evaporating despite the use of condenser tubes (scheme 4.2).
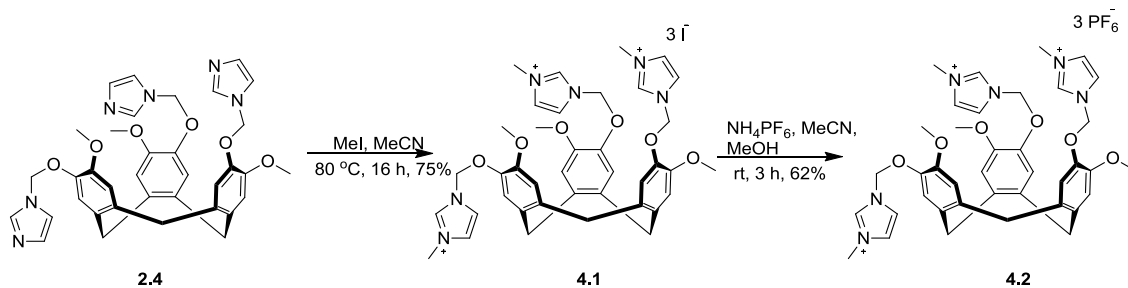
Scheme 4.2 Synthesis of imidazolium salts 4.1 and 4.2.

The ^{1}H NMR spectrum of *tris*-imidazolium iodide, **4.1** (figure 4.1) was diagnostic, with the characteristic downfield shift of imidazolium proton H^1 to 9.32 ppm from 7-8 ppm in imidazoles due to the increased acidity at this site. C_3-symmetry was retained, evidenced by the two doublets attributed to *endo*- and *exo*-H^{12}.
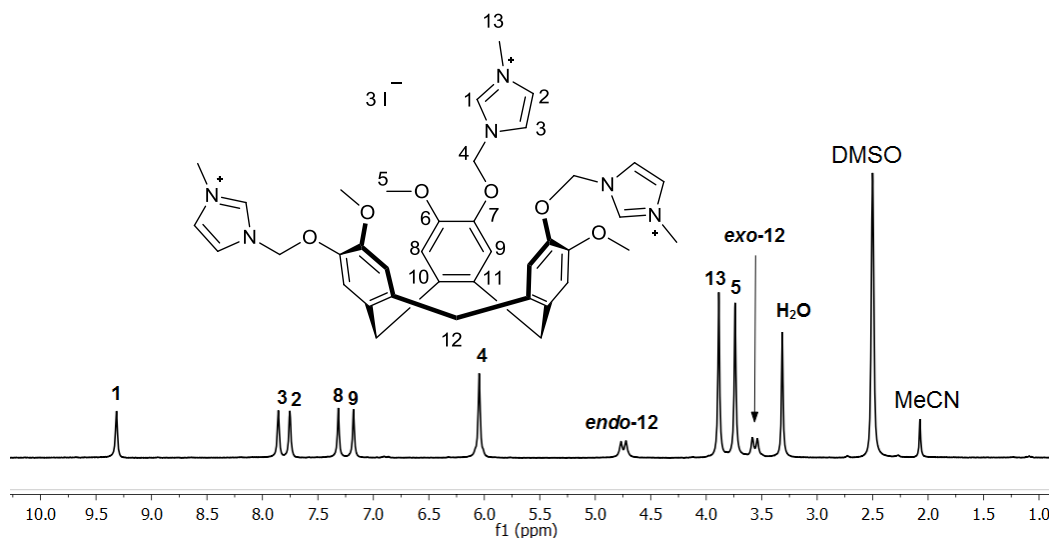
Figure 4.1 ^{1}H NMR spectrum (293 K, 300 MHz, DMSO-d_6) of ligand 4.1.

The mass spectrum of ligand **4.1** (figure 4.2) contains major peaks at *m/z* 410.1258, 947.1506 and 1092.0957 attributed to imidazolium less two and one iodide anions, and also a {M+H}$^+$ species respectively.
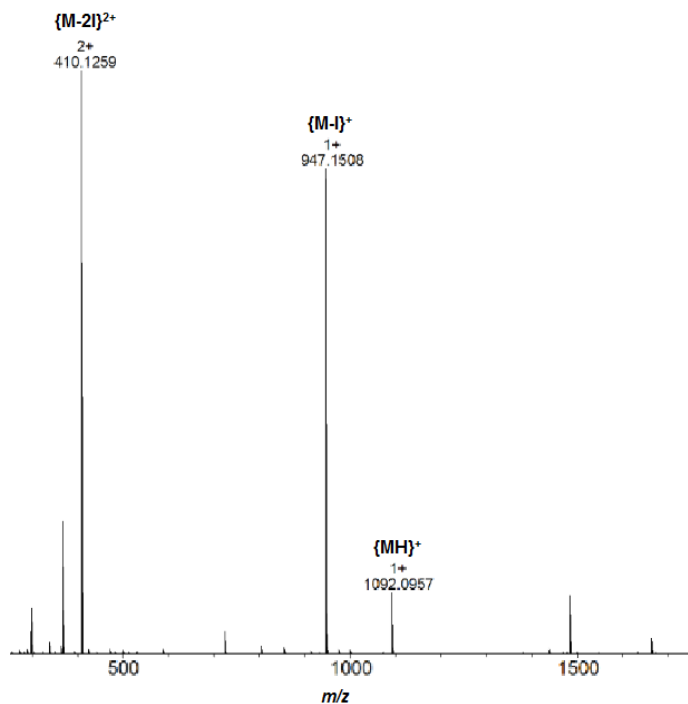
Figure 4.2 HRMS of imidazolium salt 4.1.

Salt-metathesis of **4.1** with NH₄PF₆ yielding hexafluorophosphate **4.2** was facile. ^{1}H NMR spectra of imidazolium halides and hexafluorophosphates often differ slightly. The imidazolium N*H*CN proton in an imidazolium halide is shifted slightly further downfield due to being more acidic than when bearing a non-coordinating anion. This increase in acidity is caused by a weak hydrogen-bonding interaction between the hydrogen atom in question and the halide anion, which can facilitate deprotonation. In the case of **4.1** and **4.2**, both ^{1}H NMR spectra were identical. ^{19}F{^{1}H} NMR spectroscopy, along with HRMS confirmed the successful salt metathesis of **4.1**. The ^{19}F{^{1}H} NMR spectrum contained the characteristic PF₆$^-$ doublet residing at -71.42 ppm ($J_{\text{F-P}}$ = 711.54 Hz) (figure 4.3). The HRMS spectrum contained peaks less varying numbers of hexafluorophosphate anions. HRMS showed no evidence of peaks attributed to iodide-containing fragments, with the hexafluorophosphate salt appearing dominant, as shown in figure 4.4. Major peaks could be assigned as the +3, +2 and +1 peaks for ligand less the relevant number of anions.
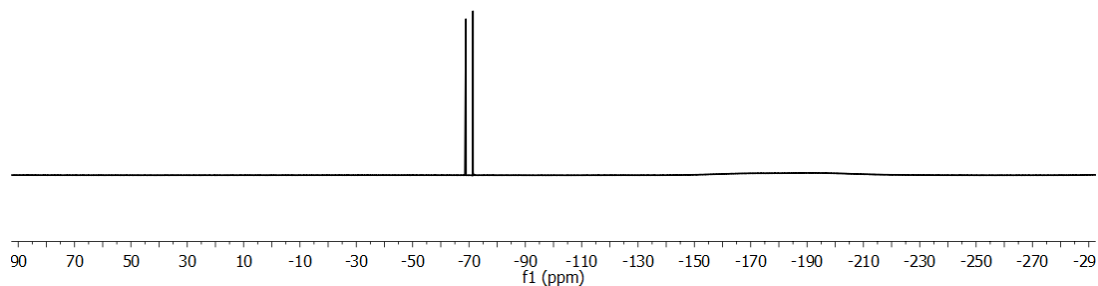
Figure 4.3 ^{19}F{^{1}H} NMR spectrum (293 K, 282 MHz, DMSO-d_6) of 4.2.
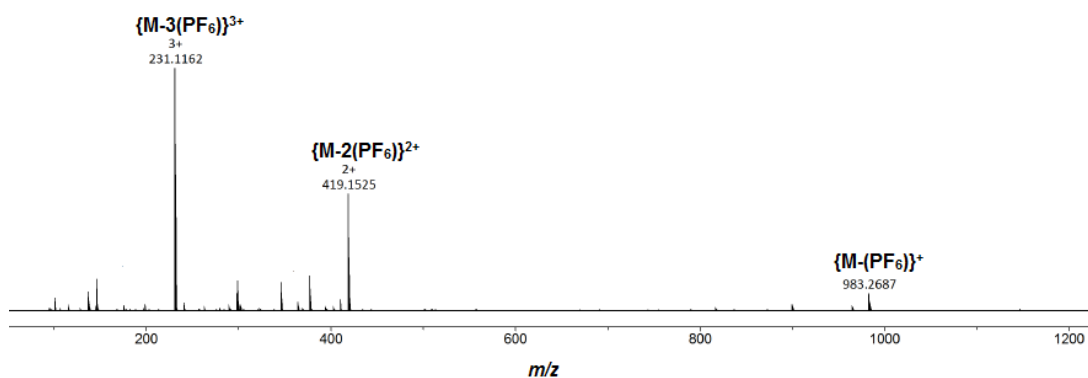
Figure 4.4 HRMS of 4.2.

Crystals suitable for X-ray diffraction were grown from the diffusion of diethyl ether vapours into an acetonitrile solution of **4.2**. The asymmetric unit comprises one third of the ligand, two anions (which are of half occupancy) and a partially occupied acetonitrile molecule (figure 4.5).
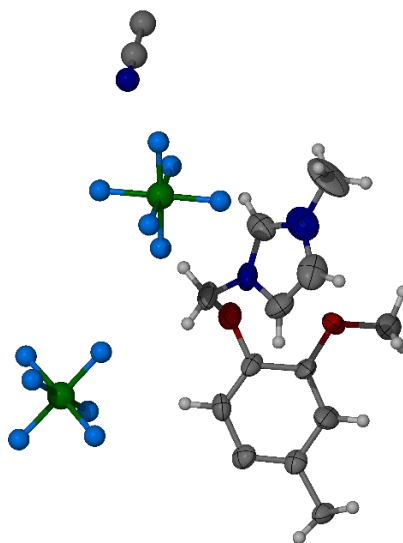
Figure 4.5 Asymmetric unit of 4.2·3(MeCN). Ellipsoids are drawn at the 50% probability, with hexafluorophosphate anions and acetonitrile refined as isotropic. Each hexafluorophosphate anion is of 0.5 occupancy.

The ligand has threefold crystallographic symmetry, and the imidazolium arms were strained with a C_{arene}-O-C-N_{imid} torsion angle measured as 77.2º. Salt **4.2**·3(MeCN) crystallised in the chiral, hexagonal *P6* space group as a conglomerate – only one enantiomer of the ligand crystallised in each crystal. A number of azole ligands crystallised as conglomerates, including solvates of the 4-thiazolyl (**3.1**) and 5-oxazolylcyclotriguaiacylene (**2.18**). Bowl-in-bowl stacking of the single-enantiomer is also exhibited (figure 4.7), with a distance of 4.57 Å between centroids of cyclononatriene bowls, which is marginally less than 4-(pyridyl)methylcyclotriguaiacylene (4.68 Å) and a bipyridyl analogue (4.67 Å).[6, 7] Two ligand molecules reside in the unit cell, with twelve hexafluorophosphate anions of half-occupancy balancing the charge. Acetonitrile molecules reside on the unit cell vertices (figure 4.6). A H···F hydrogen bond is present, with a C-F separation of 3.06 Å between N-methyl carbon and the nearest fluorine of a PF_6^- anion.
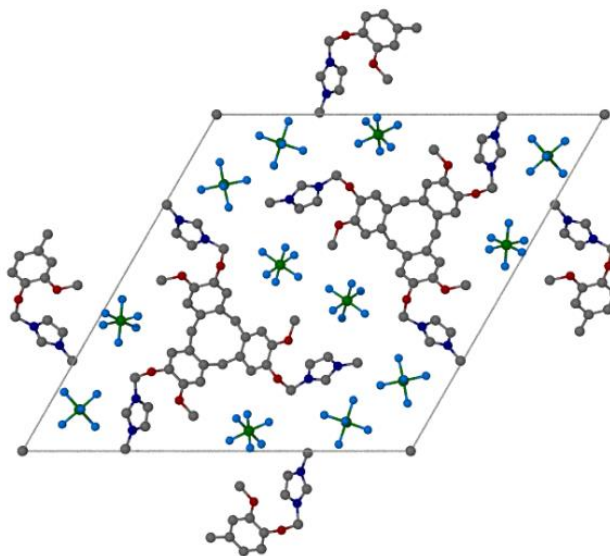
Figure 4.6 Unit cell diagram of 4.2·3(MeCN).
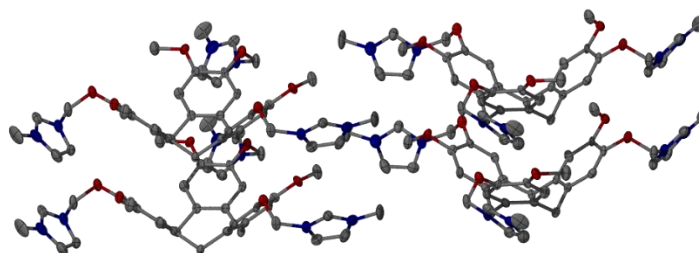
Figure 4.7 Bowl-in-bowl stacking exhibited by conglomerate crystals of 4.2·3(MeCN).

Whilst the synthesis of **4.1** and **4.2** were highly successful, reliability issues posed in the synthesis of **2.4** mean imidazolium salts **4.1** and **4.2** were prepared to prove synthetic methodology, and NHC complexes were not targeted with this system.

4.3 Synthesis and characterisation of a tricationic benzimidazolium salt

Benzimidazole **2.11** can be furnished with a number of alkyl halides. The most straightforward of reactions is that with methyl iodide to afford 1,1',1"-(((3,8,13-trimethoxy-10,15-dihydro-5H-tribenzo[a,d,g][9]annulene-2,7,12-triyl)tris(oxy))tris(methylene))tris(3-methyl-1H-benzimidazolium) iodide, **4.3** (scheme 4.3).
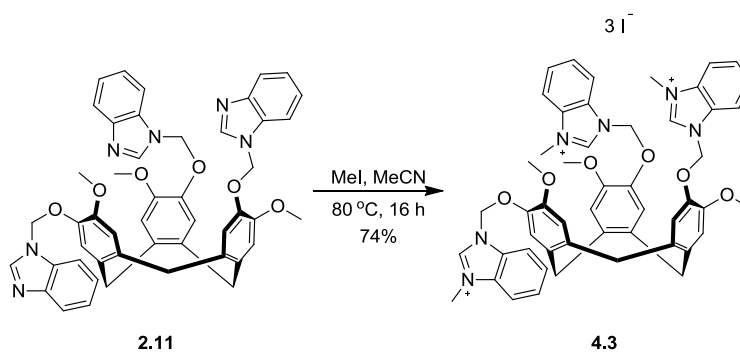
Scheme 4.3 Synthesis of benzimidazolium salt 4.3

The above salt was prepared in good yield and fully authenticated by ^{1}H (figure 4.8) and ^{13}C{^{1}H} NMR spectroscopy (figure 4.9), and mass spectrometry. Peaks in the ^{13}C{^{1}H} NMR spectrum of **4.3** were assigned using HMQC and HMBC spectra. The ^{1}H NMR spectrum displays the downfield shift of H^1 to 9.89 ppm from 8.35 ppm in 2.11, which is diagnostic for the formation of a benzimidazolium salt. The H^{16} *exo*-proton peak appears underneath H^9 at 3.56 ppm. The integral of this peak matched that for the methoxy resonance plus the aforementioned exo-proton. COSY and HMQC spectra confirmed this was the case. The COSY NMR spectrum (figure 4.10) showed the endo-proton coupling to this resonance, and for the HMQC spectrum (figure 4.10) coupling to two carbon environments for the proton peak at 3.58 ppm was observed, which were both confirmed to be C^9 and C^{16}. These two peaks can both be distinguished in the DEPT-135 NMR spectrum. Asymmetric imidazolium species contain three proton resonances, with the two backbone resonances found between 7 and 8 ppm. For benzimidazolium systems, the

benzo-backbone resonances appear in the aromatic region of the NMR spectrum, often occurring as two triplets and two doublets as observed in figure 4.8, although these signals overlapping is not uncommon.
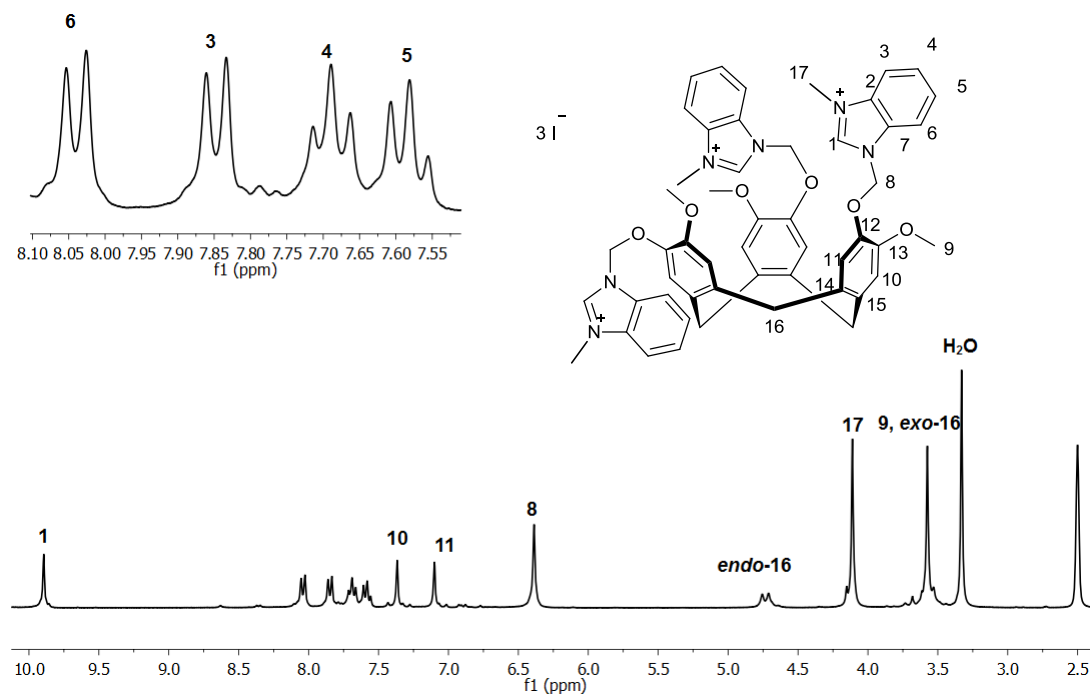
Figure 4.8 ^{1}H NMR spectrum (293 K, 300 MHz, DMSO-d_6) of benzimidazolium salt 4.3.
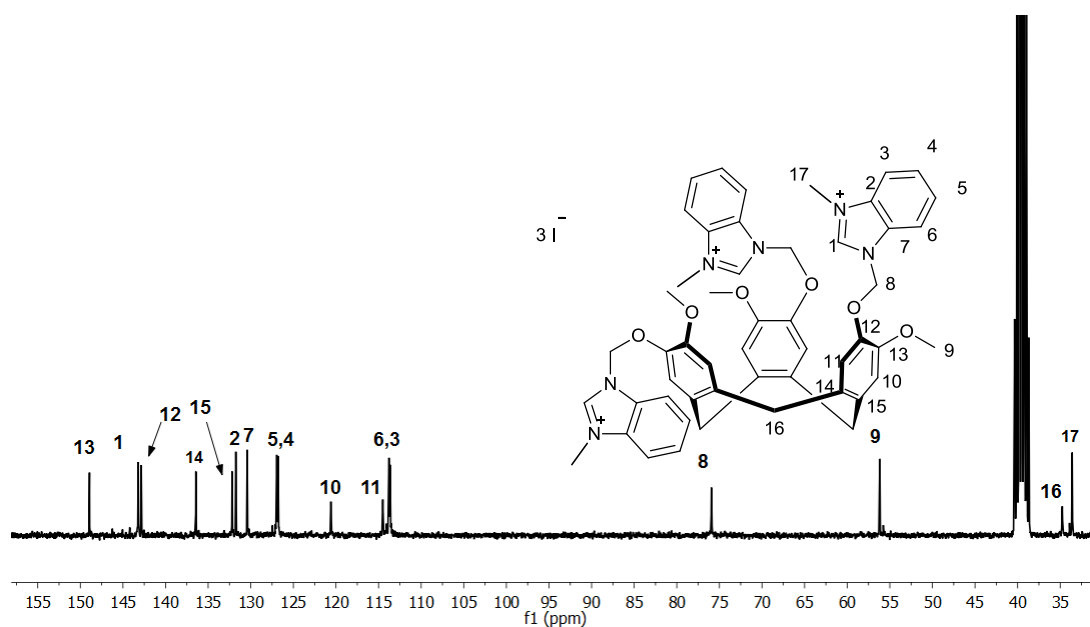
Figure 4.9 ^{13}C{^{1}H} NMR spectrum (293 K, 75 MHz, DMSO-d_6) of benzimidazolium salt 4.3.
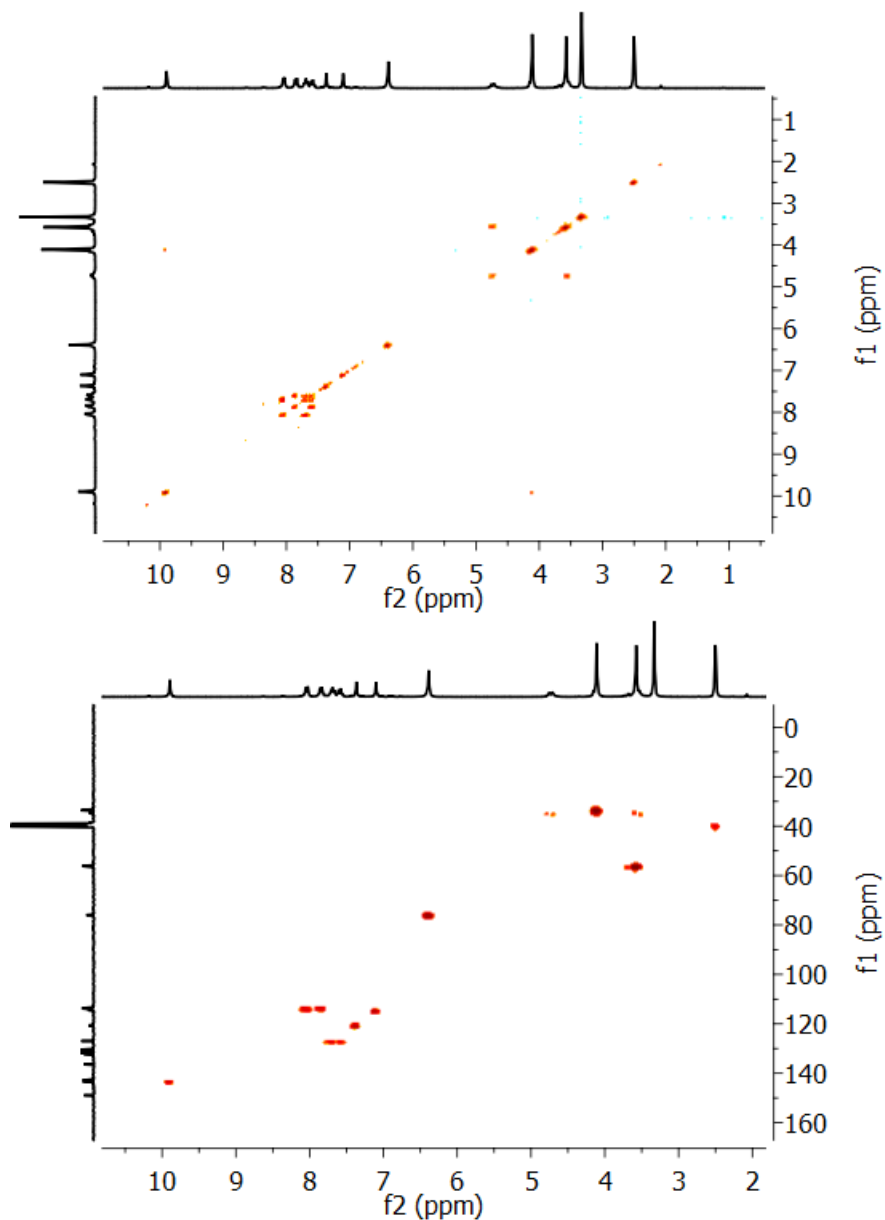
Figure 4.10 Top: COSY and bottom: HMQC spectra of 4.3 (293 K, 300 MHz, DMSO-d_6).

The tricationic nature of the benzimidazolium salt leads to a number of product peaks in the HRMS spectrum (Figure 4.11), namely $\{M-3I\}^{3+}$ (m/z = 281.1484), $\{M-2I\}^{2+}$ (m/z = 485.1465), $\{M-I\}^+$ (m/z = 1097.1959) and $\{M+NH_4\}^+$ (m/z = 1242.1336). The two peaks at 349.1559 and 825.2148 correspond to one imidazolium arm being cleaved in the mass spectrometer. This is a common observation with all the imidazolium salts prepared in this project, with the NMR data and obvious C_3-symmetry suggesting that this is not a contaminant in the product.
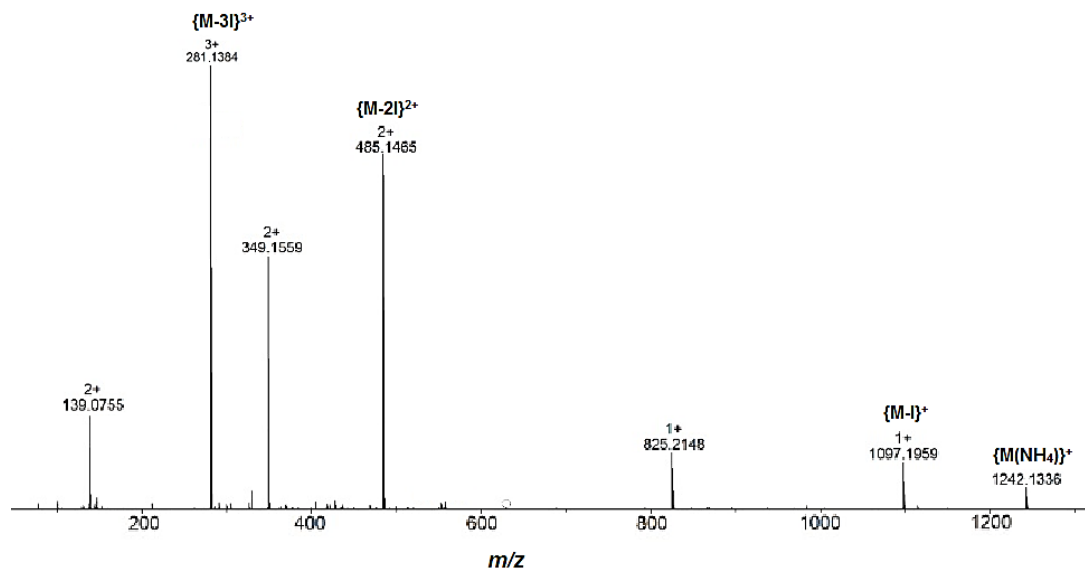
Figure 4.11 HRMS (ESI⁺) of ligand 4.3.

Salt metathesis reactions of **4.3** with ammonium hexafluorophosphate and hexafluroantimonate sources were carried out with the intention of obtaining crystals suitable for structure determination using X-ray diffraction. ^{19}F$\{^{1}$H$\}$ and ^{31}P$\{^{1}$H$\}$ NMR spectroscopy and HRMS indicated successful anion exchange. ^{1}H NMR spectroscopy of imidazolium hexafluorophosphate **4.4** revealed a near-identical spectrum, with negligible upfield shift of the imidazolium proton by 0.05 ppm. The FTIR spectrum also gave good indication that a successful salt metathesis reaction had taken place, with a sharp peak appearing at 834 cm^{-1}, strongly suggesting a P-F stretch. Colourless needles of **4.4** suitable for X-ray diffraction were grown from the diffusion of diethyl ether vapours into an acetonitrile solution of imidazolium salt. The X-ray data were collected by Edward Britton using synchrotron radiation. The signal-to-noise parameter was low due to crystals being extremely thin in two dimensions.

The crystal structure was solved in the triclinic $P\bar{1}$ space group and the asymmetric unit comprised of a whole *tris*-benzimidazolium salt and three hexafluorophosphate anions (figure 4.12).
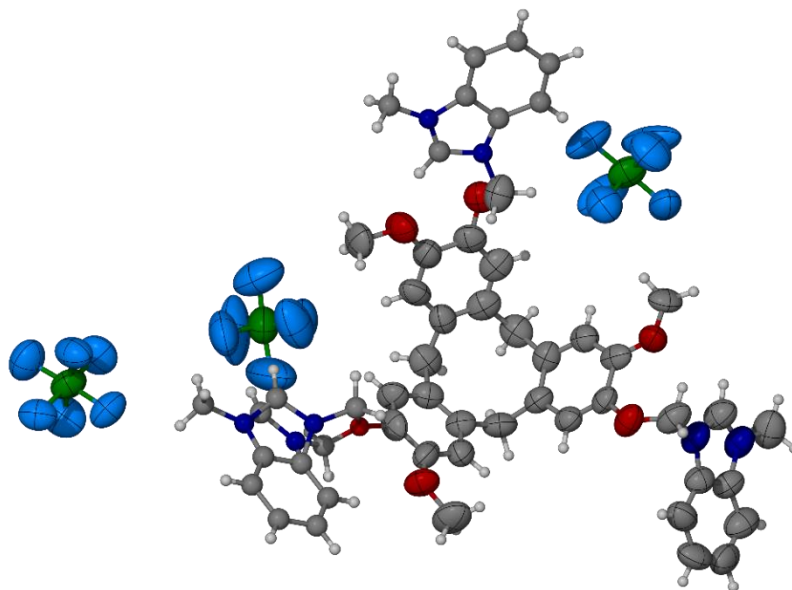
Figure 4.12 Asymmetric unit of 4.4. Ellipsoids are drawn at the 50% probability.

Two benzimidazolium arms were refined as isotropic due to high levels of disorder, and one azole moiety was disordered over two positions. A H$\cdots$F hydrogen bonding interaction between an imidazolium proton was observed at C$\cdots$F separation of 2.901 Å, supporting the minimal upfield shift in ^{1}H NMR spectrum of **4.4** relative to the iodide analogue. A wide variation of C_{arene}-O-C-N_{imid} torsion angles were measured, with the disordered benzimidazole group which intercalates between CTV bowls exhibiting near-antiperiplanar angles of -173.2 and 176.4º. Another dihedral angle was measured as -143.2º and a third highly strained angle of -64.9º, with a H-bonding interaction between the nearest methoxy group and the ether link observed with C$\cdots$O separation of 2.79 Å. The strained benzimidazolium group participates in π-π stacking with an equivalent neighbour belonging to a ligand of opposite enantiomer, at centroid separation of ca. 3.72 Å.

Homochiral stacks are formed which are considerably offset, with the centroid of the cyclononatriene core of one ligand residing above the methoxy group of a neighbouring cavitand of the same handedness, at a distance of *ca.* 3.7 Å. Intercalation of a benzimidazolium group of a neighbouring cavitand of opposite handedness between two ligands was exhibited, with the benzo-backbone of the benzimidazolium salt engaging in π-π stacking interactions with an internal face of the below CTV bowl and exterior of the above cavitand at separation of 3.72 and 3.99 Å respectively (figure 4.13). Intercalation of an arm in this fashion has been observed previously in CTV chemistry, most recently within the crystal structure of

a tripodal Re(I) complex, but bowl-in-bowl stacks involving this case were perfectly aligned.[7]
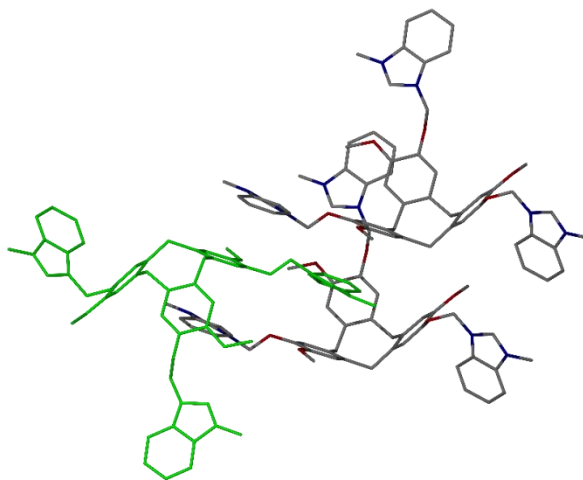
Figure 4.13 Intercalation of *M*-enantiomer of 4.4 between stacks of *P*-enantiomers.

4.4 Synthesis and characterisation of an *N*-benzyl substituted tripodal benzimidazolium salt
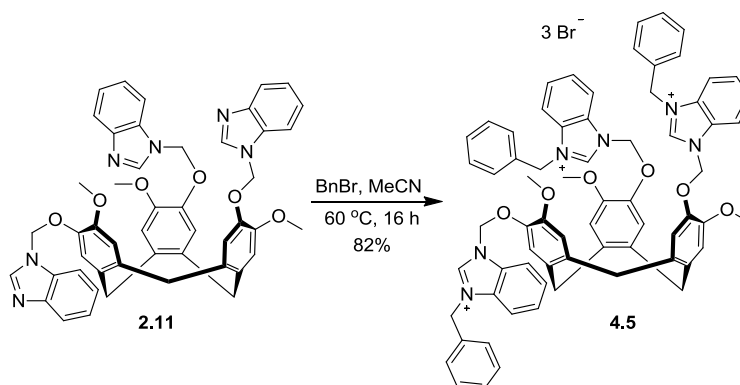
Scheme 4.4 Synthesis of benzimidazolium salt 4.5.

Ligand **4.3** displayed good solubility in DMSO and DMF, and required heat to redissolve in acetonitrile, but once dissolved, remained in solution. Whilst a reliable ligand preparation, the methyl substituent also provides very little steric bulk on one side of the imidazolium salt, and flexible, but also bulkier alternatives were sought.

Another benzimidazolium salt class considered were those bearing a benzyl moiety. Benzyl-tethered carbenes had previously been prepared in the Hardie group for stabilisation of metallo-cryptophanes in order to prevent rearrangement into larger assemblies.[8] *N*-benzyl ligand **4.5** was prepared overnight in good yield (scheme 4.4). The reaction conditions were milder than those used in the preparation

of **4.3**, with heating to 60 ºC and no need to seal reaction vessels. The *tris*-cationic product precipitated from acetonitrile overnight. The benzyl group can provide steric bulk when hinged towards the metal centre, which when part of metal-NHC complexes could stabilise low oxidation state metals during catalytic cycles, whilst also being capable of folding away from the metal centre, thus not hindering substitution reactions about the metal during catalytic cycles. The disadvantage of this ligand is solubility; **4.5** is insoluble in DCM and MeCN, two of the more feasible solvents for NHC complex synthesis *via* basic metal precursors or transmetallation reactions, preferring solvents such as DMF and DMSO. Whilst carbene complexes can be prepared in DMF and DMSO, they are less tolerant of strong bases, limiting the methodologies that can be utilised.[9] The common Ag(I) transmetallation route does not proceed in high yields when using highly polar aprotic solvents, presumably due to solubilisation of Ag(I) halide by-products in such reaction media, reducing the lattice enthalpy associated with AgX formation.

The ^{1}H NMR spectrum of **4.5** confirmed the preparation of a C_3-symmetric imidazolium salt, with the peak for imidazolium H^1 residing at 10.18 ppm, as shown in figure 4.14. The *endo-* and *exo-* protons of the tribenzo[a,d,g]-cyclononatriene core (H^{21}) were located at 4.74 and 3.54 ppm. NCH_2O protons of methylene bridge (H^{13}) split into a pseudo-quartet due to diastereotopicity at this site. The sheer number of aromatic protons (associated with benzimidazole, N-benzyl and cyclotriveratrylene core) was anticipated to give highly complex NMR spectra with large numbers of peaks between 8 and 7 ppm. However, the three N-benzylic resonances, and one CTV environment appeared as one broad overlapped peak at 7.41 ppm.

The aromatic carbon adjacent to the methoxy group of CTV was once again the furthest downfield in the ^{13}C{^{1}H} NMR spectrum (149.17 ppm), as confirmed by HMBC NMR spectroscopy. C^1 was slightly further upfield in benzimidazole **2.12** than in benzimidazolium salt **4.5** at 142.98 ppm (figure 4.15). Three CH_2 environments were noted in the DEPT-135 NMR spectrum; C^{13} at 76.24 ppm, characteristic of NCH_2O groups on all CTV-furnished benzimidazoles. The two protons of the methylene bridge on CTV coupled to one carbon environment at 34.78 ppm in the HMQC spectrum (figure 4.16).
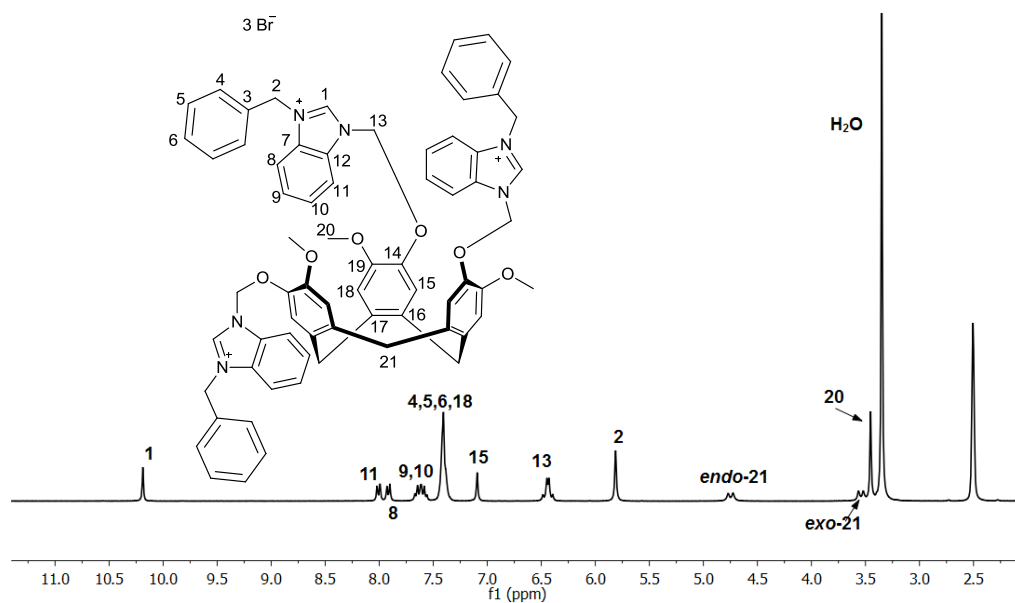
Figure 4.14 ^{1}H NMR spectrum (293 K, 300 MHz, DMSO-d_6) of 4.5.
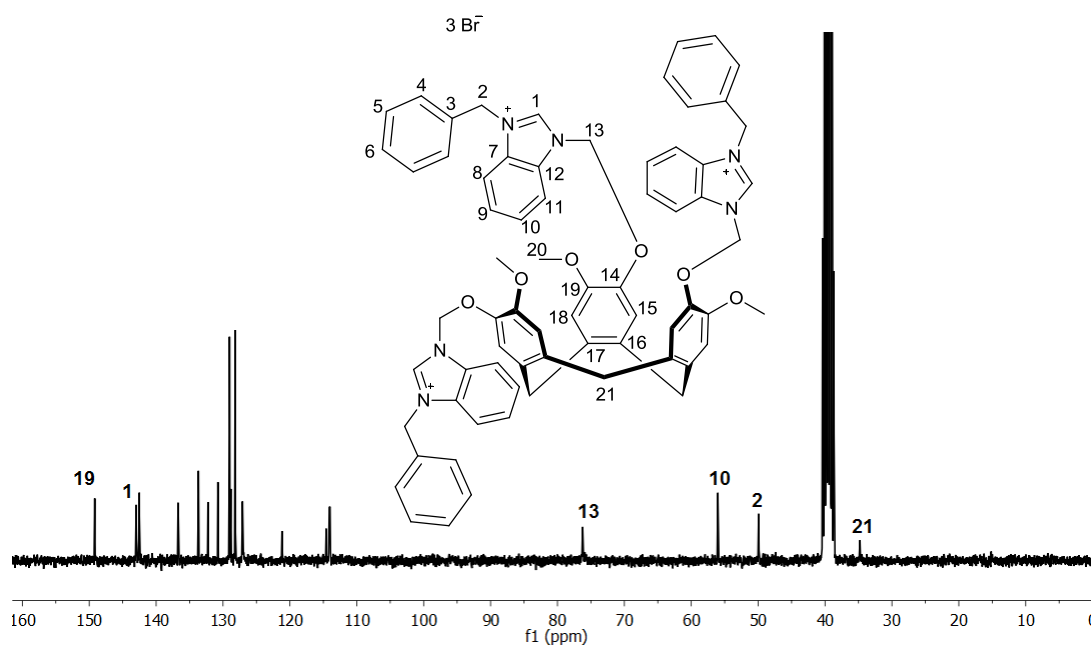
Figure 4.15 ^{13}C{^{1}H} NMR spectrum (293 K, 75 MHz, DMSO-d_6) of 4.5.
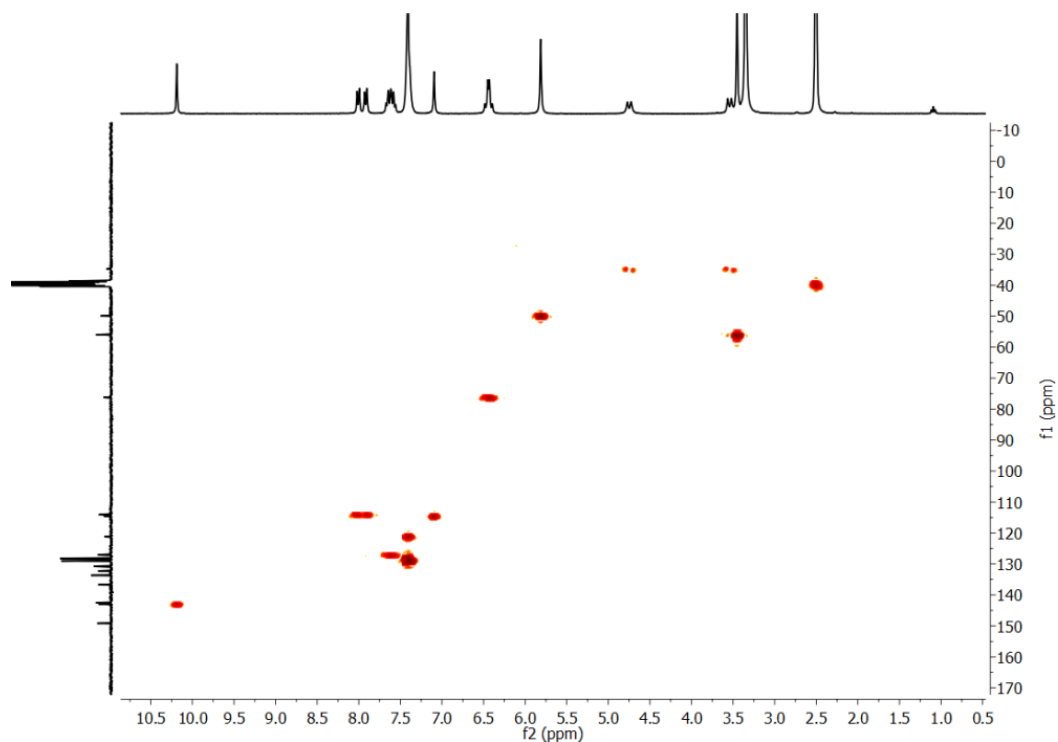
Figure 4.16 HMQC spectrum of 4.5.

The HRMS (figure 4.17) contained the major ion peak as at *m/z* 357.1624 (calculated 357.1698), corresponding to the 3+ peak of **4.5**, less three bromide ions. The peak at *m/z* 490.2127 (calculated 490.2125) is a good match to a *bis*-benzylated imidazolium salt. The ^{1}H NMR spectrum displays obvious C_3-symmetry with a single set of CTV *endo-* and *exo-* peaks being present, so this was thought to be an ionisation event, rather than unwanted partial reactivity.
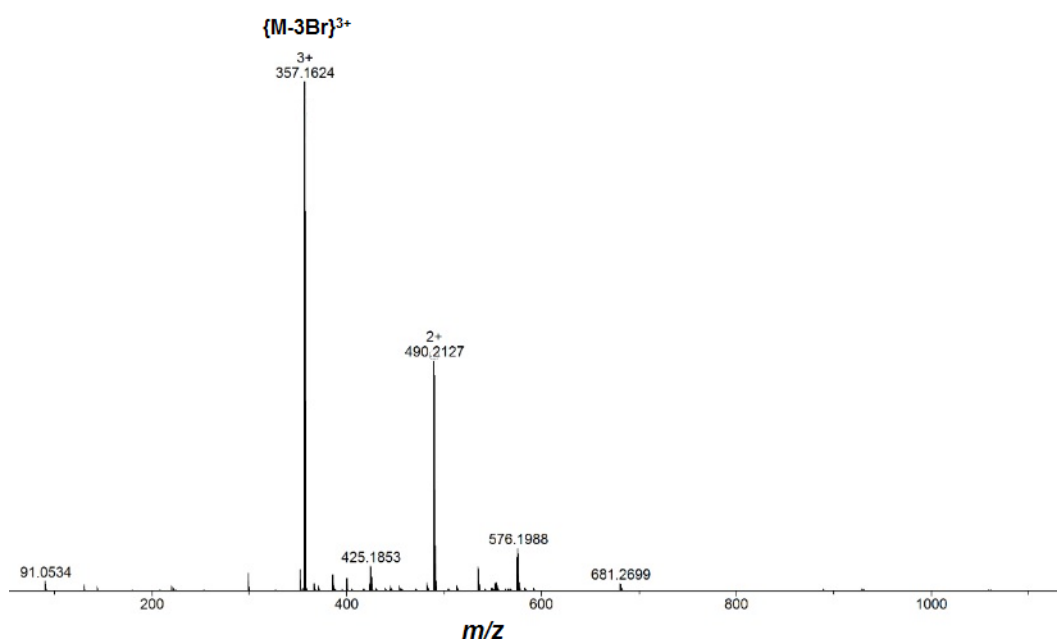
Figure 4.17 HRMS (ESI⁺) of 4.5.

4.5 Investigations into the preparation of more soluble benzimidazolium salts

Solubility was a major consideration when selecting potential *N*-substituents for imidazolium salts on a CTV scaffold. Both **4.3** and **4.5** displayed limited solubility in solvents that are desirable for metal-NHC coordination, such as DCM.

Longer alkyl chains such as ^{n}propyl were considered, but this synthetic route required much harsher reaction conditions (100 $^{\circ}$C in MeCN in a J. Youngs ampoule) over a longer period of time. Reproducibility was inconsistent, and prolonged reaction times (> 5 days as opposed to 16-18 h for **4.3** and **4.5**) meant more viable syntheses should be pursued. Picolyl (2-methylpyridyl) moieties were also targeted. 2-(Bromomethyl)pyridine hydrobromide is commercially available and, upon neutralisation, did slowly react with benzimidazole **2.4** over an extended period of time, but the reaction could not effectively be pushed towards completion.

Allyl substituents both enhance solubility and could potentially stabilise low oxidation state metals by means of π-donation. Allyl ligand **4.6·Br** was prepared in good yield as an oily solid, and displayed high solubility in methanol, a solvent medium CTV-based compounds seldom dissolve in. The methanolic solubility of this ligand allowed for facile salt metatheses with ammonium or sodium salts of non-coordinating anions, facilitating a more straightforward isolation of the imidazolium salts.
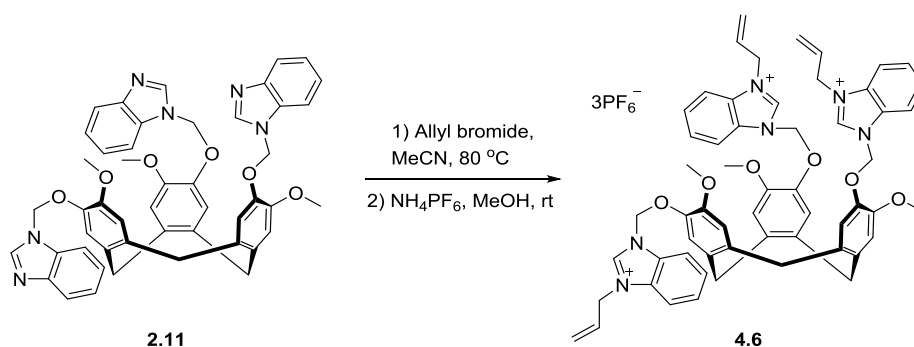
Scheme 4.5 Synthesis of allylic ligand 4.6.
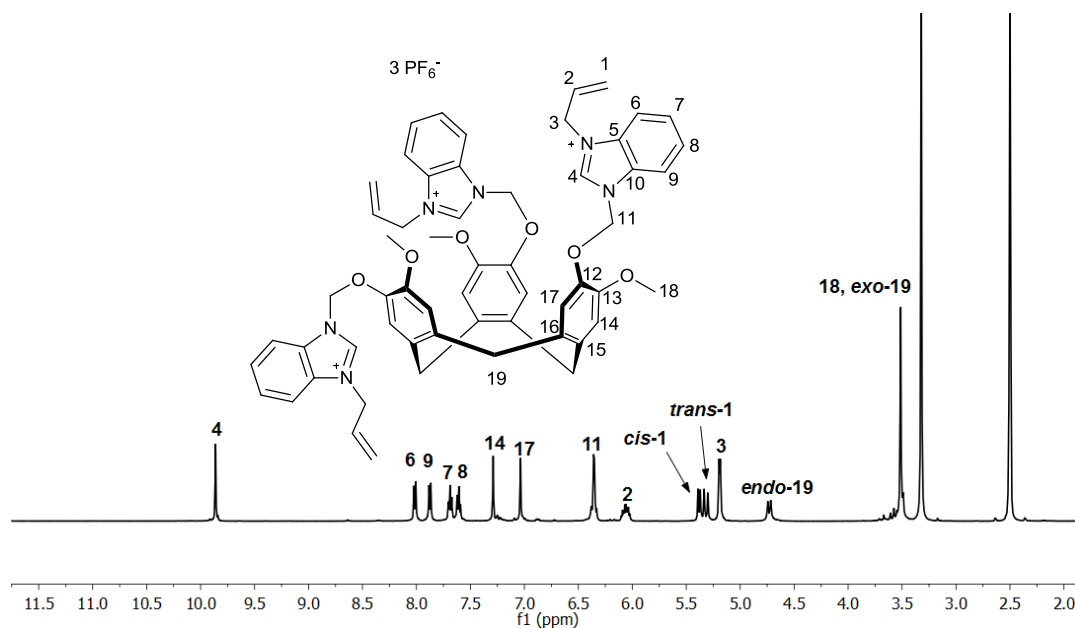
Figure 4.18 ^{1}H NMR spectrum (293 K, 300 MHz, DMSO-d_6) of **4.6.**

HRMS contained a number of peaks confirming the successful preparation of **4.6**, with key peaks of m/z 307.1468, 533.2010 and 1211.3621 excellently matching $\{M-3(PF_6)\}^{3+}$, $\{M-2(PF_6)\}^{2+}$ and $\{M-PF_6\}^+$ fragments (calculated 307.1441, 533.1985 and 1211.3618 respectively. Fragments observed with $m/z = 375.1682$ and 440.1951 correspond to species losing a benzimidazolium arm from the CTV scaffold and a *bis*-allylated product (calculated $m/z = 375.1703$ and 440.1969 respectively), however these are artefacts of ionisation, as confirmed by the C_3 symmetry retained in the ^{1}H NMR spectrum.
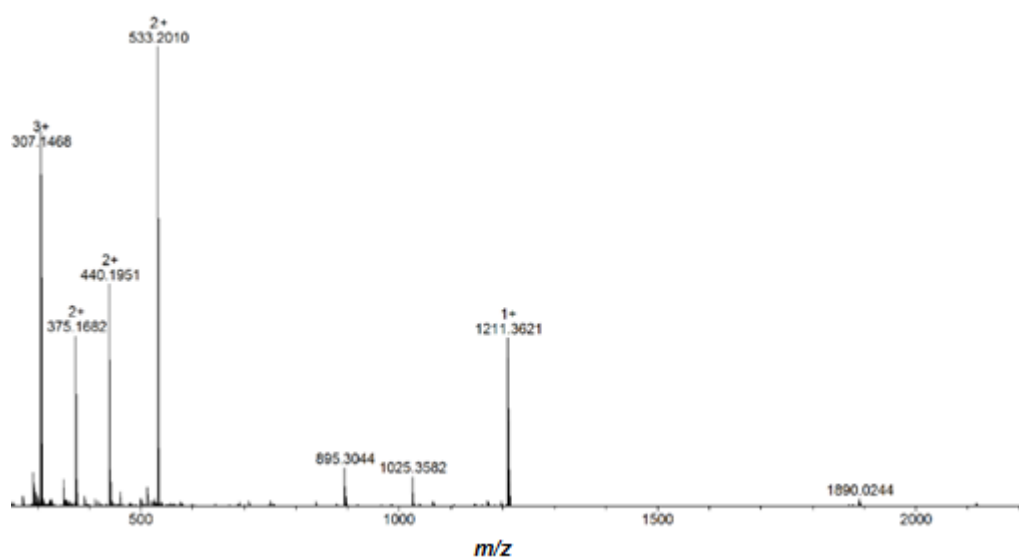
Figure 4.19 HRMS (ESI$^+$) of 4.6.

Previous work in the Hardie group involved using allylic cavitand **2.2** as a coordination ligand to Ag(I), and a range of discrete architectures and organometallic coordination polymers were isolated bearing Ag-alkene interactions.[10] Salt metathesis reactions of the bromide with BF_4^-, PF_6^- and SbF_6^- sources were carried out, and their assembly with the relevant Ag(I) salt trialled, but crystalline material could not be grown in any case.

Despite the initial promise shown by allyl ligand **4.6**, there was also a major disadvantage, as unexpected side-reactivity often occurred which proved difficult to control. A second species was observed in the ^1H NMR spectrum which bore a new imidazolium NC*H*N peak, the ratio of desired product:impurity did vary from reaction to reaction. Whilst still a minor by-product, it would pose problems when preparing metal complexes, and could not be controlled. A peak in the HRMS spectrum at *m/z* 460.2125 (calculated 460.2125) was an excellent match to the proposed cyclisation product (figure 4.20). Both by-product and **4.6** could not be separated using chromatographic techniques or through recrystallization. Similarly to ligand **4.3**, cleavage of a ligand arm was observed in the HRMS (figure 4.21). When the allylic analogue was prepared cleanly, the fragment associated with proposed by-product was not observed. The proposed by-product would have a 2^+ charge, consistent with the HRMS data, and lose HBr with respect to the desired product.
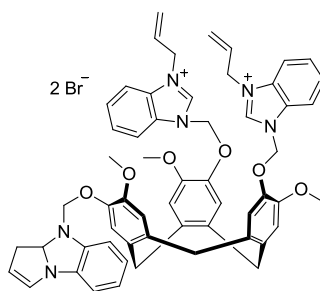
Figure 4.20 Proposed by-product formed in preparation of imidazolium salt 4.6·Br.
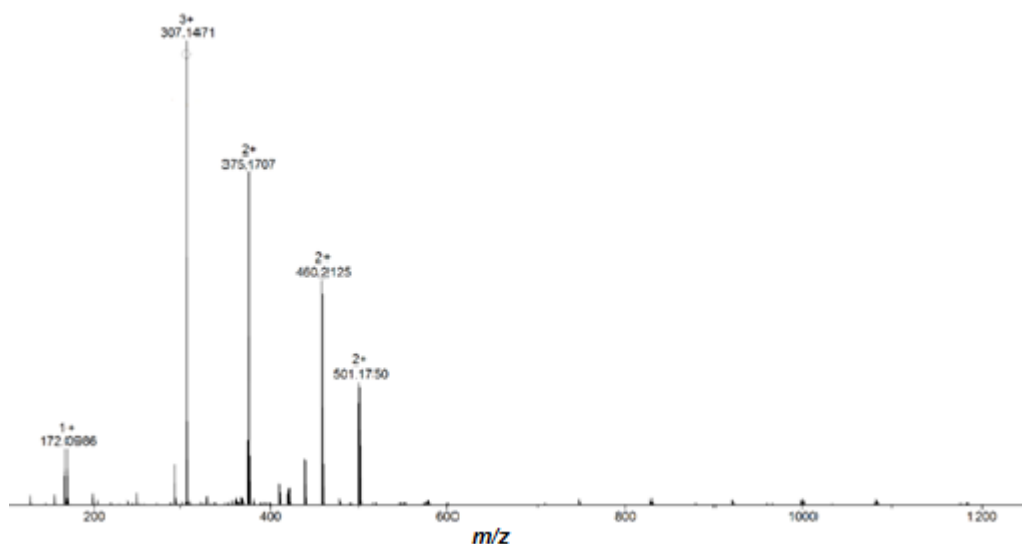
Figure 4.21 HRMS (ESI⁺) of 4.5 showing side-reactivity at m/z = 460.2125.
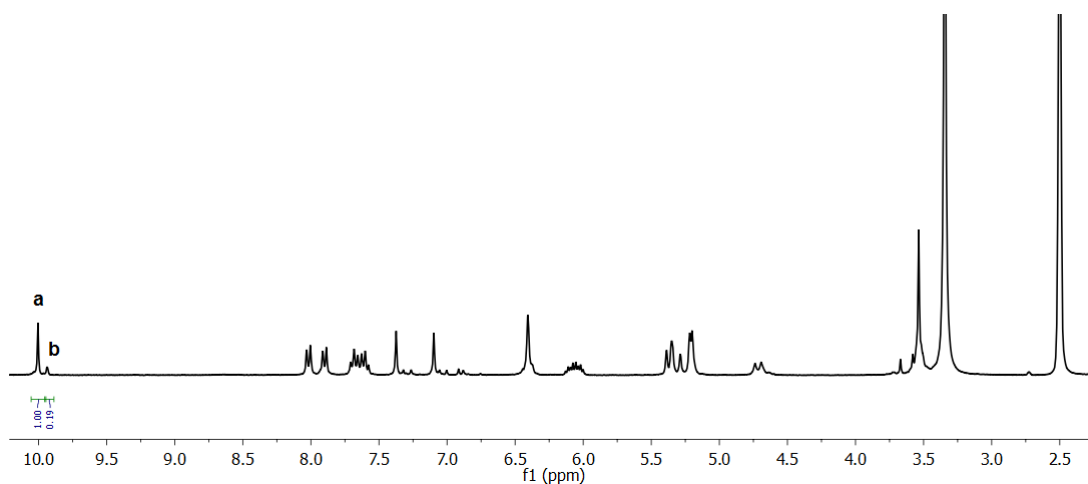
Figure 4.22 ¹H NMR spectrum (293 K, 300 MHz, DMSO-d_6) of by-product-containing imidazolium salt 4.6·Br. Peak a denotes imidazolium proton of desired product, b denotes imidazolium proton of impurity.

It would be expected for such a cyclisation to be metal-mediated. No transition metals were used in the preparation of allyl **4.6** or **2.4**. A Pd(II) catalysed deallylation of **2.2** led to the isolation of CTG **2.3**, so leaching of Pd may have occurred, despite every effort to prevent this by filtration through multiple celite pads. Allyl groups are known to participate in rearrangements and cyclisations, with well-known examples including the Cope, and Claisen rearrangements.[11, 12] Difficulties controlling the side-reactivity of this ligand led to **4.3** and **4.5** becoming the primary ligands employed in this project.

4.6 Synthesis of one-third synthons of tripodal benzimidazolium salts

In order to compare trimetallic complexes to smaller, discrete analogues, similar ligands with a guaiacol (2-methoxyphenylmethyl-) arm on one side of the benzimidazole, as opposed to a cavitand, were prepared. Guaiacol was selected as a precursor as it is readily available (extracted from wood creosote and a common flavourant in coffee and whiskey), and has the same local environment as the benzo-backbone to CTG, minus the methylene bridges of the lower rim.

Imidazole **4.7** was prepared using a modified procedure to that reported in the literature, to suppress the competing dimerisation of 1-(chloromethyl)benzimidazole·HCl observed by both Mokhtari and co-workers, and the Hardie group when initially preparing ligand **2.11** (scheme 4.6).[13] Imidazolium salts were fully characterised using HRMS and multinuclear NMR spectroscopy. NMR spectra in general for guaiacol-derived ligands were more complex than the cavitand counterparts, mainly due to the guaiacol group comprising of four aromatic protons with often more complicated splitting patterns. For **4.3** and **4.5**, the C_3-symmetry and methylene bridges meant only two proton environments are located on the CTG ligands, both of which are *para-* with respect to one another, and appear as singlets.
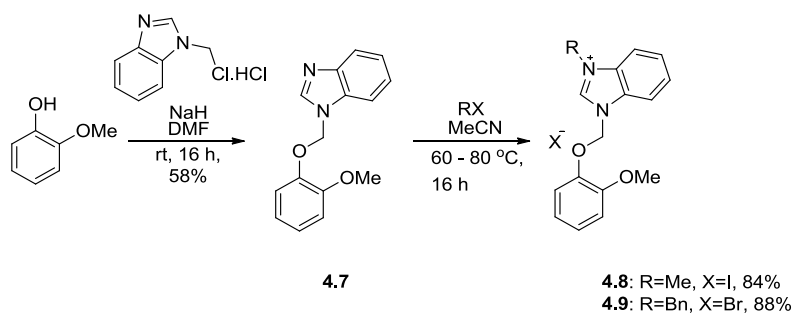
Scheme 4.6 Syntheses of the monopods 4.7-4.9.

The ^{1}H NMR spectrum (figure 4.23) of imidazolium iodide **4.8** was clean, and the acidic NC*H*N proton characteristically had a chemical shift of 9.87 ppm. There were two aromatic resonances attributed with the guaiacol group with integrals of 3:1 relative to one another. The multiplet at 7.16-7.00 ppm could be assigned as H^{12}, H^{13} and H^{15} because the ddd at 6.88 ppm did not couple to C^{11}, and weakly coupled to C^{10} in the HMBC spectrum HRMS contained a single, dominant peak at *m/z*

269.1246 (Calcd. 269.1285), an excellent match to the cation portion of the imidazolium salt.
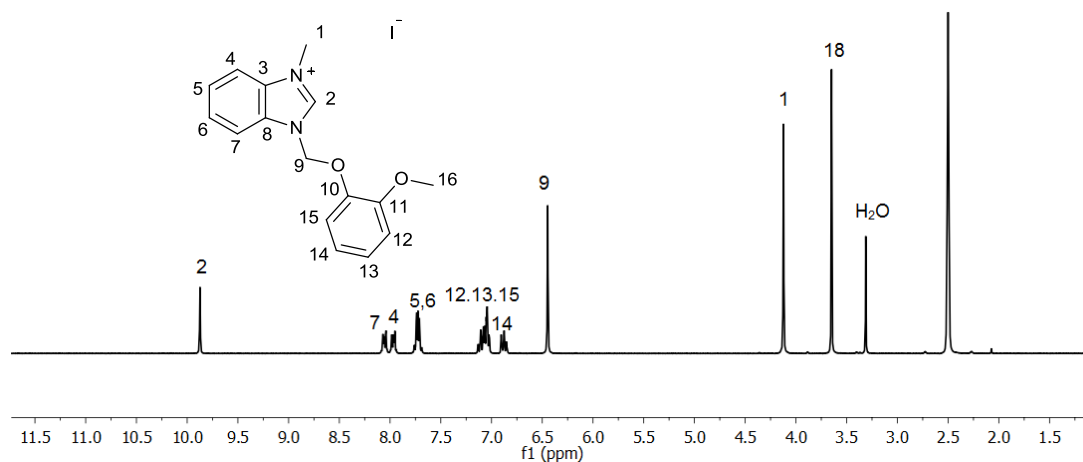
Figure 4.23 ^{1}H NMR spectrum (293 K, 300 MHz, DMSO-d_6) of ligand 4.8.

Crystals of imidazolium salt **4.8** (figure 4.24) grew from the diffusion of diethyl ether vapours into an acetonitrile solution of ligand, and the structure was obtained using synchrotron radiation at the Diamond Light Source.
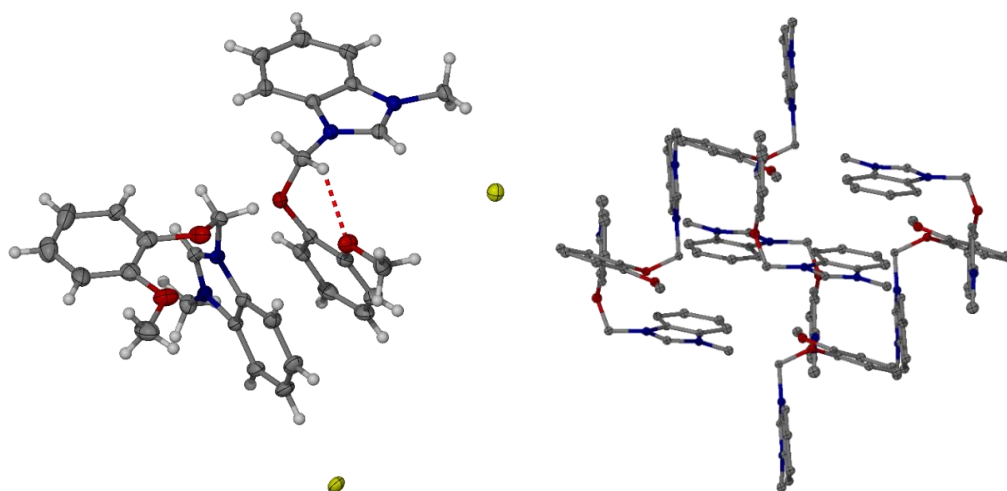
Figure 4.24 Left: Asymmetric unit of 4.8, ellipsoids are drawn at the 50% probability. Right: Packing diagram of 4.8.

Benzimidazolium salt **4.8** crystallised in the $P\overline{1}$ space group with two molecules residing in the asymmetric unit (figure 4.24). There are π-π stacking interactions between benzimidazole backbones, at centroid separation of 3.93 Å. The guaiacol arene unit and benzimidazolium group within the asymmetric unit are not parallel and slightly offset, leading to centroid separations slightly greater than 4 Å, and

therefore not π-π stacking. Both benzimidazolium salts in the asymmetric unit have differing torsion N-C-O-N torsion angles of -73.4 and 63.3°.

The 3-benzyl-1-((2-methoxyphenoxy)methyl)-1H-benzimidazolium bromide, **4.9** could be prepared following a matching procedure to that outlined for ligand **4.5**. The HRMS spectrum was once again diagnostic, with a single peak at *m/z* 345.1611 (calculated 345.1598) displaying an excellent match to the imidazolium cation.

The imidazolium proton H[1] of **4.9** diagnostically resided at 10.04 ppm in the ^{1}H NMR spectrum (figure 4.25). The benzylic CH_2 group resided in a similar position to that observed in CTG ligand **4.5** (5.81 vs 5.80 ppm). Interestingly, the NCH_2O methylene bridge (H[13]) was shifted upfield in the monomer **4.9** by ca. 0.5 ppm relative to the cavitand complex, indicating the CTV bowl has a deshielding effect on the protons at this site. The ^{13}C{^{1}H} NMR spectrum bore similarities to that of **4.5**, with a number of aromatic carbons present, and the two methylene bridges were authenticated by DEPT-135 and HMQC NMR spectroscopy.
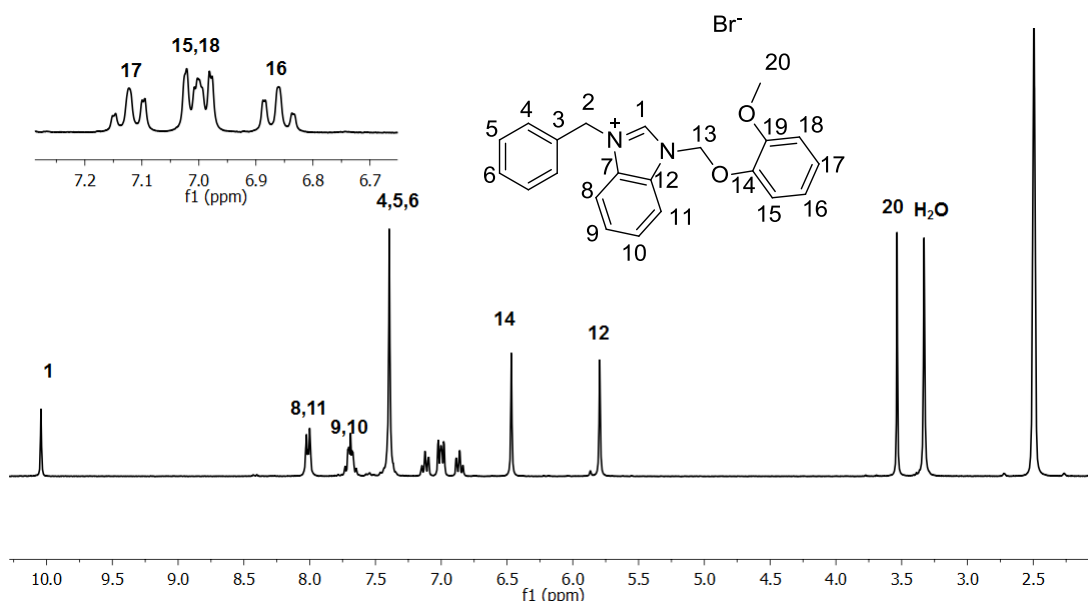
Figure 4.25 ^{1}H NMR spectrum (293 K, 300 MHz, DMSO-*d₆*) of ligand 4.9.

4.7 Investigation towards the synthesis of group 11 carbene complexes

4.7.1 Strategies towards the isolation of a trimetallic Ag(I)-NHC complex

Group 11, d[10] NHC complexes are well established, both as precursors and also catalysts.[14, 15] A common starting point in NHC chemistry is coordination to Ag(I), primarily using Ag_2O as a reagent. A route first reported in 1998 by Lin and

co-workers, these reactions often occur in DCM solvent, and have a strong driving force, forming water as a by-product.[16] In addition to being used as transmetallating agents, Ag(I) carbenes have been trialled as anti-cancer drugs, owing to the anti-microbial properties and low-toxicity of silver compounds.[17, 18]

The preparation of Ag(I)-NHC complexes from Ag_2O (or Cu_2O for the Cu(I) analogues) are well defined (scheme 4.7). In some cases when using the imidazolium halide, ligand scrambling can occur and a cationic *bis*-NHC complex can be isolated, with an $[AgX_2]^-$ anion.[16, 19, 20] The groups of Hahn and Peris have demonstrated the ability of Ag(I)-NHC complexes to be used as supramolecular building blocks, successfully preparing M_3L_2 containers which can both be transmetallated onto other transition metals, and also undergo post-synthetic modification.[21-25]
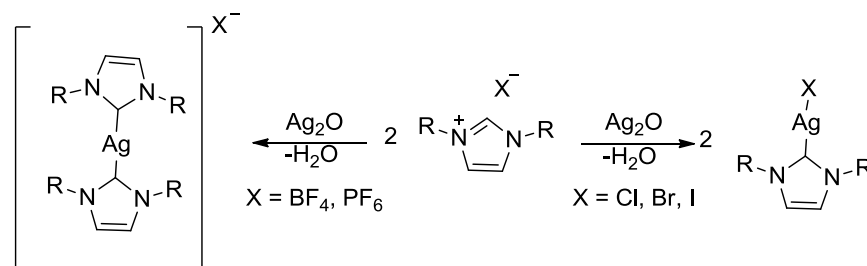
Scheme 4.7 Strategies towards Ag(I)-NHC complexes using Ag_2O.

Ligand **4.3** and silver oxide were heated to 80 ºC in acetonitrile, under a nitrogen atmosphere in the dark. After 24 h, the attempted isolation of tripodal NHC complexes in this case was unsuccessful, with negligible evidence suggesting coordination to Ag(I). The desired product from the reaction of imidazolium salt **4.3** with Ag_2O would be expected to give a sharp ^1H NMR spectrum. The fingerprint of such a reaction would be the loss of an imidazolium proton upon coordination to Ag(I). After 24 h, an imidazolium peak at 9.51 ppm remained, with the *endo*- and *exo*- doublets of the CTV bowl indicating the C_3-symmetric starting material constituted the bulk of the reaction mixture. A number of minor peaks were also present, notably upfield of the imidazolium proton, which could be either C_1-symmetric by-products, or decomposition species (figure 4.26). The high resolution mass spectrum was inconclusive, and showed no obvious signs that an Ag(I) complex was in solution.
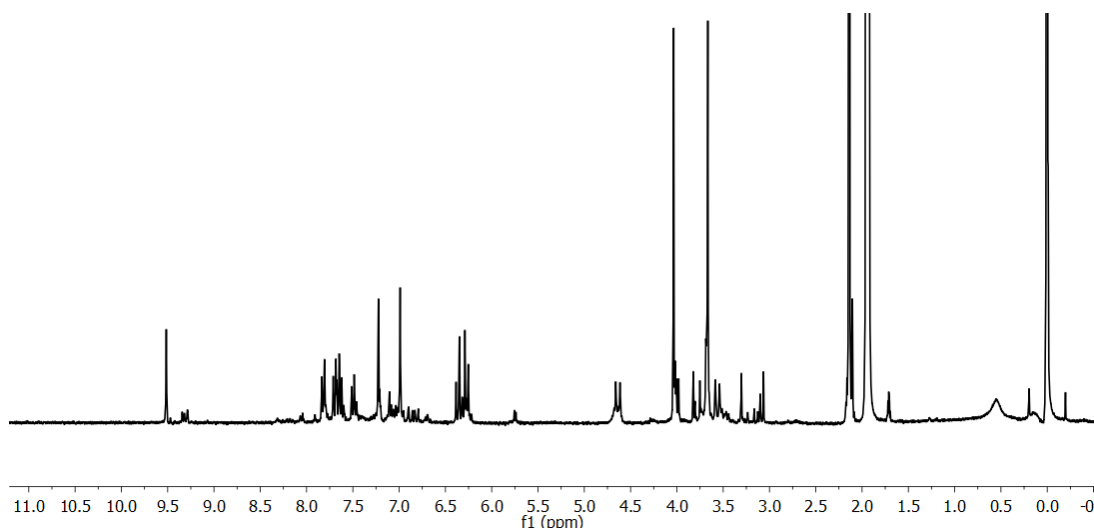
Figure 4.26 ^{1}H NMR spectrum (293 K, 300 MHz, MeCN-d_3) from reaction of 4.3 and Ag$_2$O.

Despite the attempted isolation of Ag(I) NHC complexes being unsuccessful, *in situ* generation of Ag(I) carbenes as reaction intermediates may be possible. The typical driving force for preparing Ag(I)-NHC complexes using Ag$_2$O as the precursor is water liberation. For the tripodal imidazolium salts, this may be an insufficient driving force, and one-pot syntheses where the *in situ* generation of an Ag(I)-NHC complex before transmetallation onto a defined metal precursor, such as a noble metal dimer, are well established.[14, 20, 26] This augments the driving force to prepare a new metal-NHC complex, and the lattice enthalpy associated with silver halide formation drives the reaction.

One reliable method to prepare metal NHC complexes is *via* free carbene generation. Free NHCs are strong Lewis bases. The main disadvantage of this route is the high air- and moisture-sensitivity of free, divalent carbenes. Whilst deprotonation of the imidazolium portion of **4.3**, **4.5**, **4.8** and **4.9** could be attainable, the NCH$_2$O methylene bridge would likely be base-sensitive, and competitive reactions would be probable. Additionally, a solvent mismatch would prevent this route from being viable; free carbenes are typically generated in THF or toluene, which **4.3** and **4.5** proved insoluble in.

4.7.2 Investigations into the synthesis of Au(I)-NHC complexes

Au(I)-NHC complexes display rich chemistry, with applications in catalysis and luminescence.[27-29] Typically, Au(I) NHC complexes are linear, 2-coordinate, so it was postulated that the *trans*-labilisation behaviour displayed by the carbene, in the presence of a ditopic ligand, or a second cavitand, could give rise to

metallosupramolecular architectures (Scheme 4.8). Halide abstraction from Au(I) and replacement with a range of new ligands is well documented; Fairlamb and co-workers have exchanged the halide for phthalimide ligands, yielding complexes that are active cycloisomerisation catalysts.[30] The Au(I)-NHC motif has been utilised in metallo-supramolecular chemistry of late, with Nitschke preparing a tetrahedron with internally gilded Au(I) NHC moieties.[31] Alongside Hahn's $[Au_nL_2]^{n+}$ cylinders,[22, 24, 32, 33] Pöthig and co-workers have reported an Au(I)-pillarplex, a pillar-shaped complex bearing eight equatorial Au(I) ions, all of which coordinate to an NHC.[34] The pillarplexes have a defined cavity, which can encapsulate dibromoalkanes, or when the Ag(I) derivative was prepared, cycle between an organometallic [2]-rotaxane or an organic [3]-rotaxane upon alteration of pH.[35] Simple anion exchange and variation of the imidazolium wingtip has enhanced solubility in all the above cases.

A number of metallo-cryptophanes previously prepared by Hardie and co-workers do suffer from solubility issues.[36-39]. Incorporation of organometallic subcomponents has previously addressed these issues; Holman and co-workers have decorated each arene face of an organic cryptophane with Ru(II) moieties bearing a second η^6-arene group, where each face of the CTV bowls is additionally a sandwich complex.[40] Hardie and co-workers prepared $[Pd_3L_2]^{6+}$ metallo-cryptophanes with *bis*-NHC tectons at Pd(II), but work to directly affix a carbenic centre onto the CTV cavitand has not been previously reported. The *N*-substituent (shown as methyl in scheme 4.8) can easily be tailored, with solubility and also additional functionality in mind.

Au is extremely electronegative for a d-block metal, with an χ_P value 2.54, almost identical to carbon.[41] Au is termed as carbophilic, forming very strong bonds with carbon, essentially covalent in character, and notoriously stable organometallic complexes.

Imidazolium salts **4.3** and **4.5** proved insoluble in DCM; which is often the solvent of choice for group 11 carbene coordination. The tripodal Au(I) NHC complex derived from **4.3** proved extremely difficult to prepare, and a number of procedures were carried out in acetonitrile, and MeCN:DCM mixtures, both with heating and at ambient temperatures. Potassium carbonate and *tert*-butoxide bases were both employed, as well as the *in-situ* transmetallation using Ag$_2$O, but most

reactions gave no trace of complex and turned purple in colour, characteristic of AuNP formation.
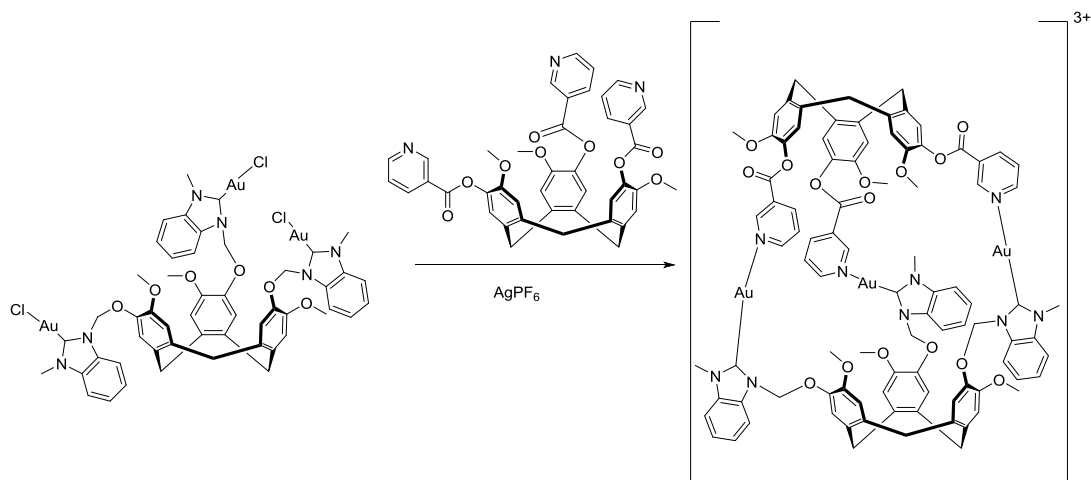
Scheme 4.8 Targeted Au(I)-NHC complex and strategy towards heteroleptic cages.

The reaction of [Au(Cl)(SMe$_2$)] with **4.3** and K$_2$CO$_3$, in MeCN at rt gave a promising ^{1}H NMR spectrum (figure 4.27), with no imidazolium proton present, but by-product formation was also evident.
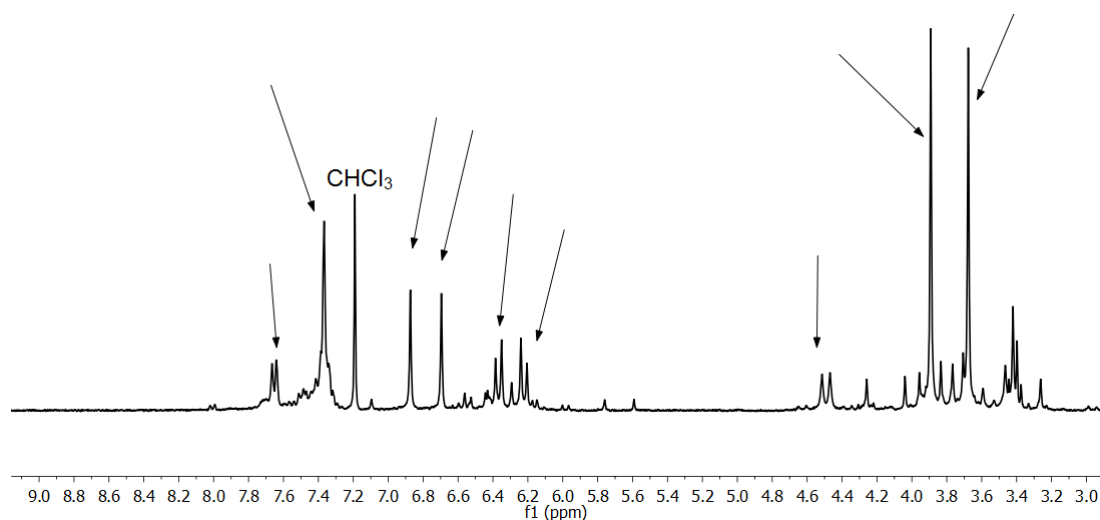
Figure 4.27 Crude ^{1}H NMR spectrum (293 K, 300 MHz, CDCl$_3$) of Au(I) NHC reaction mixture. Arrows denote desired product peaks.

The ^{1}H NMR spectrum of crude Au(I) NHC contained a number of diagnostic peaks, such as the doublet at 4.5 ppm characteristic of the *endo*-methylene bridge of the CTV bowl. Two doublets between 6.0 and 6.5 ppm are characteristic of the diastereotopic N-CH$_2$-O methylene bridge, and two singlets at 6.70 and 6.85 are a good match to the CTV arene-faces. Another promising sign is the lack of NC*H*N imidazolium proton, suggestive that an Au(I)-NHC complex is present. There are a

number of peaks corresponding to by-products, and also hexane upfield. The HRMS (figure 4.28) comprised a number of partial product peaks, and also suspected decomposition products (figure 4.29). The *in situ* salt metathesis to iodo-species was anticipated because of the soft nature of both Au(I) and I⁻. Whilst it is promising that an Au(I)-NHC complex can be prepared, the consistent poor yields (<10%), and potential for more than one complex to be present led to complexes of other metals being sought.
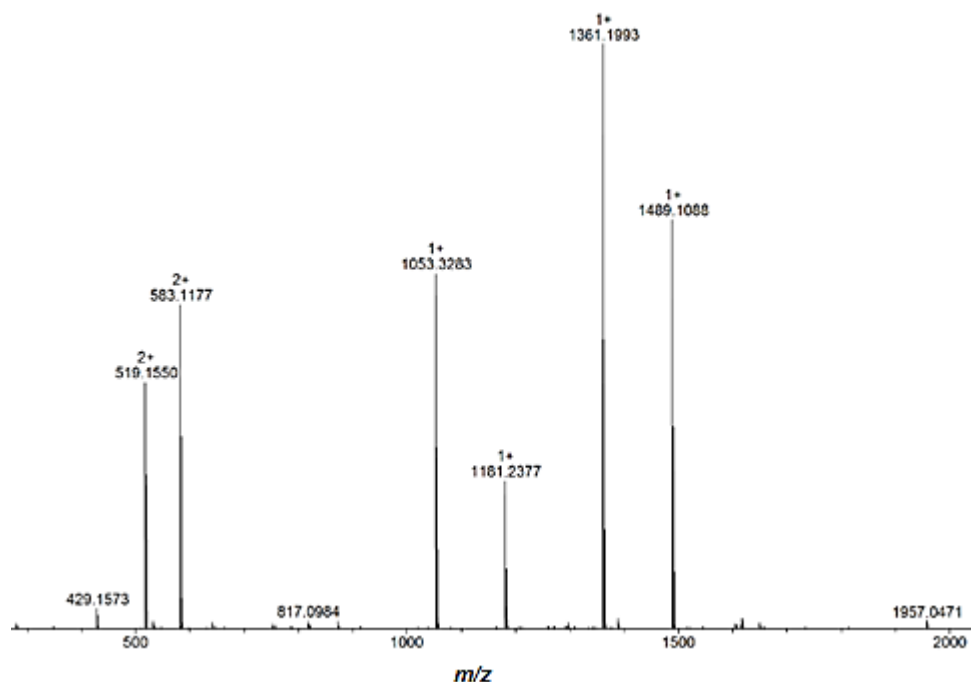
Figure 4.28 HRMS spectrum of Au(I) reaction.
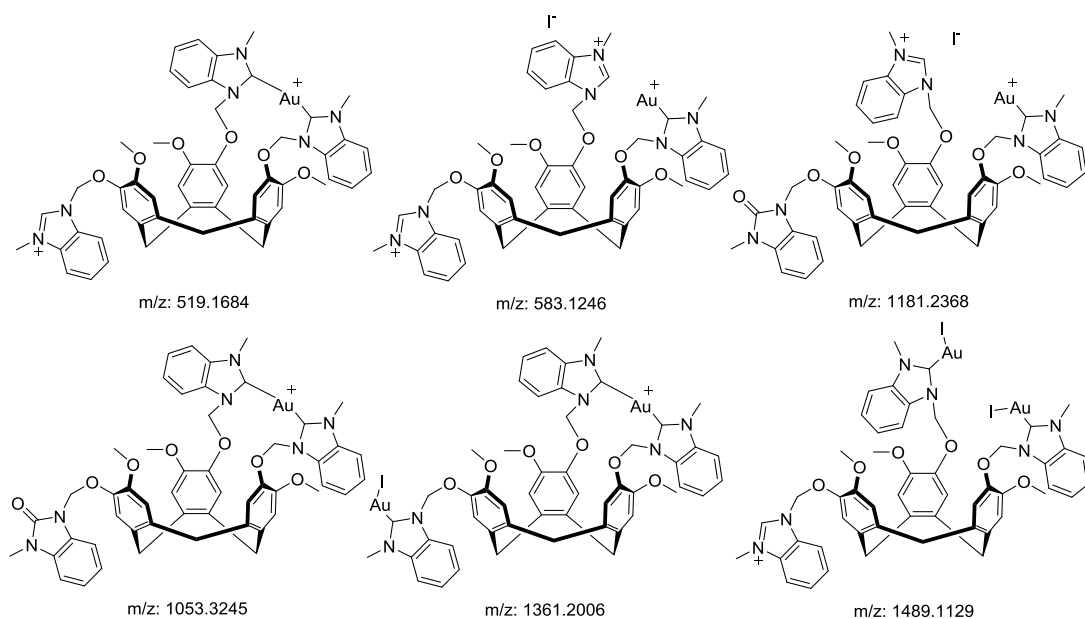
Figure 4.29 By-products in the HRMS spectrum during Au(I)-NHC synthesis.

4.7.3 Investigations towards Cu(I)-NHC complexes

Cu(I) complexes of NHCs are amongst the most well defined of all the 1st row transition metals, with complexes such as Cu-IMes becoming key players in a wide scope of catalytic transformations.[42-44] Cu(I)-NHC complexes are often air-sensitive, although when using sterically encumbering ligands, can be rendered stable to oxygen and moisture. In the same vein as Ag(I) NHC complexes, the reaction of **4.3** with Cu$_2$O was attempted, but no evidence of coordination was obtained. Furthermore, the reaction of **4.3** with CuI in the presence of base was also unsuccessful.

The procedures outlined so far in this chapter that have been tested for metal-NHC formation have vast literature precedent, so it was somewhat surprising that all attempts using this ligand system were unsuccessful. One possible reason for this could be the methylene spacer between benzimidazolium and the cavitand as it resides between a nitrogen and an oxygen atom. Inductive effects at this site caused by the two electronegative atoms may render the hydrogen atoms of this group sensitive to strong bases. The preparation of alternative ligands not possessing a methylene spacer between imidazolium moiety and CTV may allow such complexes to be accessible, but would require multiple highly challenging steps.

One way to avoid further steps would be the electrochemical procedure introduced by Chen, Willans and co-workers.[46, 47] Electrochemical syntheses are typically more functional-group tolerant, and the free carbene liberation at the cathode is dictated by reduction potential of the imidazolium group, as opposed to the pKa. Electrodes of the required metal are inserted into the solution and a voltage applied. Oxidation of the metal occurs at the anode, liberating M^{n+} in solution. The metal cations and carbene combine in solution, yielding a clean metal-NHC complex, and the sole by-product is hydrogen gas (scheme 4.9). Willans and co-workers have previously demonstrated the successful preparation of a *tetrakis*-Cu(I) complex on a calix[4]arene scaffold.[48]
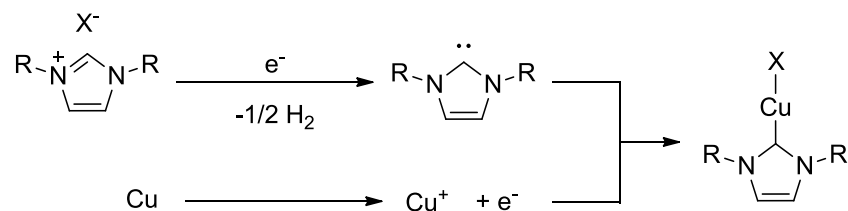
Scheme 4.9 Electrochemical synthesis of Cu(I)-NHC complexes.

A major limiting factor associated with **4.3** was its poor conductivity, leading to very slow reaction. It is unlikely that all three imidazolium groups would be simultaneously reduced at the cathode, therefore multiple products are possible. Simple *mono*-imidazolium salts allow for the charge to be dispersed throughout solution, so conduct electricity much more effectively.

Allyl ligand **4.6** was trialled in the electrochemical reaction with Cu metal, and when used as the hexafluorophosphate salt, was slightly more conducting (although still poor overall). Interestingly, HRMS (figure 4.30) indicated that the ligand had been digested after 24 h, with a number of product peaks/intermediates present (figure 4.31).
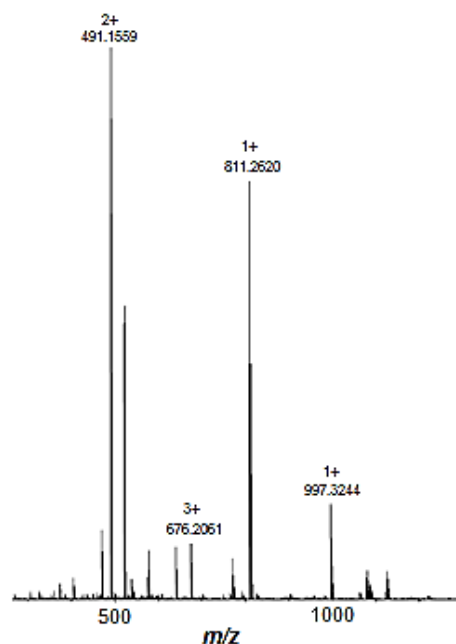
Figure 4.30 HRMS of electrochemical reaction mixture of ligand 4.6 with Cu (rt, 50 mA, 24 h).

m/z: 491.1734

m/z: 811.2552

m/z: 997.3345

m/z: 1127.3116

m/z: 676.2032
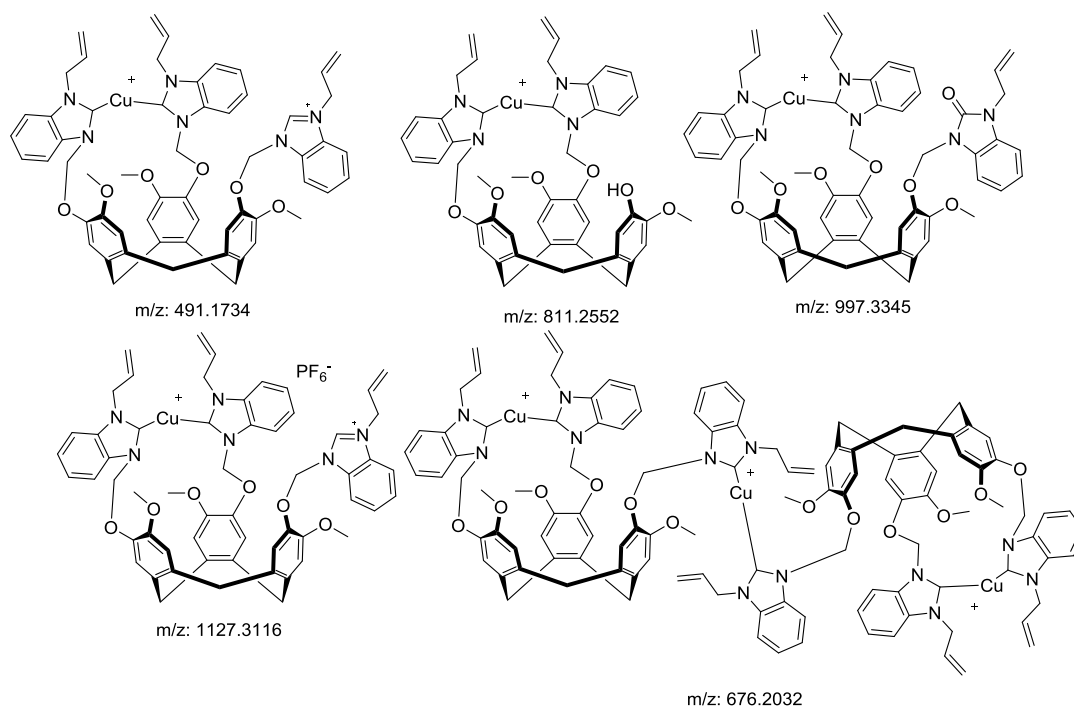
Figure 4.31 Species observed in the HRMS during the electrochemical reaction of 4.3 and Cu metal.

Similarly to when using ligand **4.3**, the same reaction with **4.6** could not be pushed to completion. Five key peaks were observed in the HRMS, most interestingly, the 3+ peak at *m/z* 676.2061. The S-shaped complex would most likely be the final product because of other peaks showing a good match to a *bis*-NHC at Cu(I), and preference for imidazolium hexafluorophosphates to prepare [M(NHC)$_2$]PF$_6^-$ species when coordinating to group 10 metals. An S-shaped complex would likely be the kinetic product in this reaction. The major peak corresponding to *m/z* 811.2620 matches a monometallic complex with one imidazolium arm cleaved (figure 4.32). It is unclear whether this was an ionization event, or occurring during reaction. Cleavage of an azolium arm was commonly encountered during a number of ligand syntheses. The imidazolinone at *m/z* 997.3345 was taken as indication the reaction was still active, as this functional group is the product of reaction between a free carbene and oxygen. Despite the promise of being able to observe product peaks when carrying out electrochemical procedures, the poor conductivity of tripodal imidazolium salts led to extremely slow reactivity that even when left for 24 h, did not reach completion. An overpotential was applied to the electrochemical system which may have led to decomposition of MeCN solvent. Poor conductivity and reactivity towards Cu(I), Ag(I) and Au(I) led to alternative methodologies for the preparation of metal-NHC complexes being pursued.

4.8 Conclusions

A number of benzimidazolium salts were prepared, of which **4.3** and benzyl **4.5** were selected as the key ligands to carry forward due to their facile syntheses when compared to alternative targets such as **4.6** and *N*-propyl variants.

A number of methodologies to prepare group 11 NHC complexes were also attempted, but limited success was achieved, with intractable product obtained in most cases.

Future work would involve expanding the library of benzimidazolium salts, and investigating those which bear additional ligand groups such as pyridyl or picolyl donors. The bidentate nature of these complexes may promote coordination to metal ions such as Ni^{2+} or Fe^{2+}, which have more accessible binding sites than the d^{10} metals. For a bidentate pyridylimidazolium salt, it may be necessary to add an electron-withdrawing group to the pyridyl group, rendering the 2-halopyridine more electron deficient and allowing for a nucleophilic aromatic substitution reaction to proceed.

Routes towards CTV-NHC complexes without the activated methylene bridge would also be viable targets despite the potentially pyrrhic syntheses, this could be *via* coupling measures such as Ullmann or Suzuki reactions. This could however, open up avenues such as free carbene generation, which are unfeasible using the 1st generation of CTV-imidazolium ligands, and therefore allow a much wider scope of metal targets, and new methodologies.

The electrochemical syntheses of metal NHC complexes Willans and co-workers pioneered has very much focused on systems where monometallic complexes have been prepared. It would be thought-provoking to prepare multimetallic supramolecular complexes electrochemically. Whilst ligands prepared in this project displayed their limitations, the fact a tetrakis-Cu(I) calixarene complex could be isolated from an electrochemical procedure suggests there is scope for the preparation of hybrid organometallic-supramolecular complexes using electrochemical procedures. Possible ligand classes could be those based on a 1,3,5-tris(1-methylimidazolyl)benzene scaffold, or the divergent azolium salts prepared by Hahn and co-workers when preparing molecular rectangles. Solubility poses much less of an issue with those systems as opposed to the cyclotriveratrylene family.

Additionally, the guaiacol-derived ligands were untested in the electrochemical synthesis of NHC complexes. The fact complex peaks were observed in the HRMS for CTV complexes is promising, therefore from an organometallic aspect, it would be interesting to trial this ligand class in electrochemical procedures. It would be expected that the poor conductivity issues would not arise for the smaller, more charge dense ligands such as **4.8** and **4.9** with a better dispersed charge throughout solutions.

4.9 Experimental section

Unless stated in the experimental section, chemicals were bought from commercial suppliers and used without further purification. Unless stated, all reactions were carried out under aerobic conditions. Reactions performed under an atmosphere of dry nitrogen were carried out using standard Schlenk and Glovebox procedures, with solvents dried and degassed using the same methodology described in section **2.9**. All analytical techniques are also consistent with those described in section **2.9**.

Synthesis of 1,1',1''-(((3,8,13-trimethoxy-10,15-dihydro-5H-tribenzo[a,d,g][9]annulene-2,7,12-triyl)tris(oxy))tris(methylene))tris(3-methyl-1H-imidazolium) iodide, 4.1

2.4 (119 mg, 0.18 mmol), methyl iodide (0.10 mL, 1.40 mmol) and acetonitrile (5 mL) were added to a sealed ampoule and heated at 80 °C for 16 h. The reaction mixture was cooled and diethyl ether added. A yellow solid precipitated from solution. Yield 148 mg, 0.14 mmol, 75%; HRMS (ESI)$^+$ 410.1259 $\{C_{39}H_{45}IN_6O_6\}^{2+}$ 947.1508$\{C_{39}H_{45}I_2N_6O_6\}^+$, 1092.0957 $\{C_{39}H_{49}I_3N_7O_6\}^+$, Calcd. for 410.1217, 947.1485, 1092.0873 respectively; ^{1}H NMR (300 MHz, DMSO-d_6) δ (ppm) 9.32 (s, 3H, H^1), 7.86 (s, 3H, H^3), 7.75 (s, 3H, H^2), 7.32 (s, 3H, H^8), 7.18 (s, 3H, H^9), 6.05 (s, 6H, H^4), 4.75 (d, 3H, J = 14.1 Hz, *endo*-H^{12}), 3.89 (s, 9H, H^{13}), 3.74 (s, 9H, H^5), 3.56 (d, 3H, J = 13.3 Hz, *exo*-H^{12}); ^{13}C {^{1}H} NMR (75 MHz, DMSO-d_6) δ (ppm) 148.70 (C^6), 142.82 (C^7), 137.28 (C^1), 136.14 (C^{11}), 132.05 (C^{10}), 123.86 (C^2), 122.28 (C^3), 119.89 (C^8), 114.65 (C^9), 77.10 (C^4), 56.31 (C^5), 36.06 (C^{13}), 34.81 (C^{12}); Elemental Analysis for $C_{39}H_{45}I_3N_6O_6$.(3.5 H_2O) Calcd: C 41.18, H 4.61, N 7.39; Found: C 41.10, H 4.40, N: 7.70.
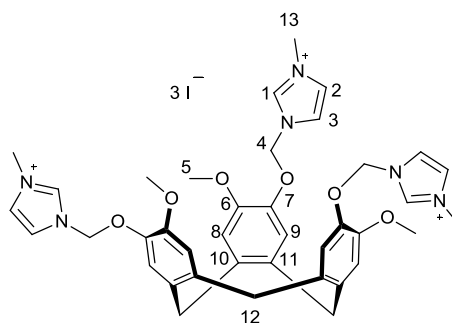
Synthesis of of 1,1',1''-(((3,8,13-trimethoxy-10,15-dihydro-5H-tribenzo[a,d,g][9]annulene-2,7,12-triyl)tris(oxy))tris(methylene))tris(3-methyl-1H-imidazolium) hexafluorophosphate 4.2

4.1 (48 mg, 0.04 mmol) and ammonium hexafluorophosphate (80 mg, 0.49 mmol) were dissolved in acetonitrile (5 mL) and methanol (5 mL), and stirred for 3 h. Diethyl ether (30 mL) was added and the title compound precipitated from solution as a white solid. Yield 28 mg, 0.025 mmol, 62%; HRMS (ESI⁺) 231.1162 $\{C_{39}H_{45}N_6O_6\}^{3+}$, 419.1525 $\{C_{39}H_{45}F_6N_6O_6P\}^{2+}$, 983.2687 $\{C_{39}H_{45}F_{12}N_6O_6P_2\}^+$, 1146.2665 $\{C_{39}H_{49}F_{18}N_7O_6P_7\}^+$; ^1H NMR (501 MHz, DMSO-d_6) δ (ppm) 9.28 (s, 3H, H^1), 7.84 (s, 3H, H^3), 7.74 (s, 3H, H^2), 7.27 (s, 3H, H^9), 7.14 (s, 3H, H^8), 6.02 (s, 6H, H^4), 4.74 (d, 3H, J = 13.3 Hz, endo-H^{12}), 3.88 (s, 9H, H^{13}), 3.73 (s, 9H, H^5), 3.53 (d, 3H, J = 13.6 Hz, exo-H^{12}); $^{13}C\{^1H\}$ NMR (126 MHz, DMSO-d_6) δ (ppm) 148.73 (C^7), 142.90 (C^6), 137.30 (C^1), 136.10 (C^{10}), 132.03 (C^{11}), 123.87 (C^2), 122.29 (C^3), 119.87 (C^9), 114.60 (C^8), 77.11 (C^4), 56.16 (C^5), 36.00 (C^{13}), 34.87 (C^{12}); ^{19}F NMR (282 MHz, DMSO-d_6) δ (ppm) -70.16 (d, J_{F-P} = 711.5 Hz), -71.42 (PF$_6$); Elemental analysis for $C_{39}H_{45}F_{18}N_6O_6P_3 \cdot (2H_2O)$ Calcd. C 40.22, H 4.24, N 7.22 Found: C 40.40, H 4.00, N 7.22.
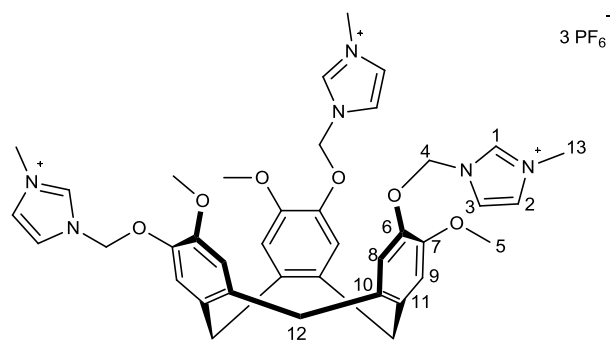
Synthesis of 1,1',1''-(((3,8,13-trimethoxy-10,15-dihydro-5H-tribenzo[a,d,g][9]annulene-2,7,12-triyl)tris(oxy))tris(methylene))tris(3-methyl-1H-benzimidazolium) iodide, 4.3

2.11 (102 mg, 0.13 mmol) was dissolved in MeCN (5 mL) in a J. Youngs ampoule and methyl iodide (0.10 mL, 1.70 mmol) added. The ampoule was sealed and heated to 80 ºC for 18 h and the solution turned orange. Diethyl ether (40 mL) was added dropwise and the title compound precipitated from solution as a cream solid. Yield 117 mg, 0.09 mmol, 74%. HRMS (ESI⁺) 485.1450 $\{C_{51}H_{51}IN_6O_6\}^{2+}$ 1097.1956
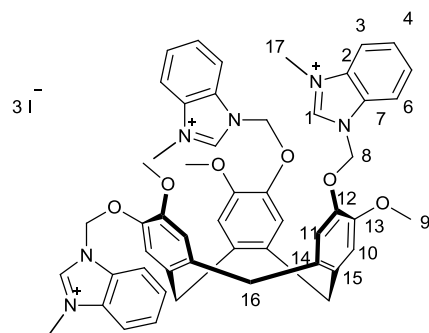
$\{C_{51}H_{51}I_2N_6O_6\}^+$, 1242.1345 $\{C_{51}H_{55}I_3N_7O_6\}^+$ Calcd. for 485.1452, 1097.1954, 1242.1342 respectively; ^{1}H NMR (300 MHz, DMSO-d_6) δ (ppm) 9.86 (s, 3H, H^1), 8.04 (d, 3H, J = 8.3 Hz, H^6), 7.84 (d, 3H, J = 8.3 Hz, H^3), 7.69 (t, 3H, J = 7.4 Hz, H^4), 7.58 (t, 3H, J = 7.5 Hz, H^5), 7.33 (s, 3H, H^{10}), 7.08 (s, 3H, H^{11}), 6.37 (s, 6H, H^8), 4.73 (d, 3H, J = 13.5 Hz, *endo*-H^{16}), 4.10 (s, 9H, H^{17}), 3.56 (s, 9H, H^9), 3.55 (d, 3H, J = 23.1 Hz, *exo*-H^{16}); ^{13}C{^{1}H} (75 MHz, DMSO-d_6) δ (ppm) 148.95 (C^{13}), 143.24 (C^1), 142.90 (C^{12}), 136.43 (C^{14}), 132.19 (C^{15}), 131.78 (C^2), 130.43 (C^7), 126.96 (C^5), 126.81 (C^4), 120.59 (C^{10}), 114.49 (C^{11}), 113.79 (C^6), 113.64 (C^3), 75.92 (C^8), 56.10 (C^9), 34.79 (C^{16}), 33.56 (C^{17}); FTIR ν (cm^{-1}) 2026, 1968, 1509, 1269, 756; m.p 192-194 ºC (dec.); Elemental analysis for $C_{51}H_{51}I_3N_6O_6$·2(H_2O) Calcd.: C 48.59, H 4.40, N 6.67; Found C 48.11, H 4.05, N 7.07.

Synthesis of 1,1',1''-(((3,8,13-trimethoxy-10,15-dihydro-5H-tribenzo[a,d,g][9]annulene-2,7,12-triyl)tris(oxy))tris(methylene))tris(3-methyl-1H-benzimidazolium) hexafluorophosphate 4.4

4.3 (50 mg, 0.04 mmol) and ammonium hexafluorophosphate (20 mg, 0.12 mmol) were dissolved in MeCN (1 mL) and MeOH (5 mL). The pale yellow solution was stirred for 1 h, during which a white solid precipitated, was collected via vacuum filtration, washed with methanol (5 mL) and
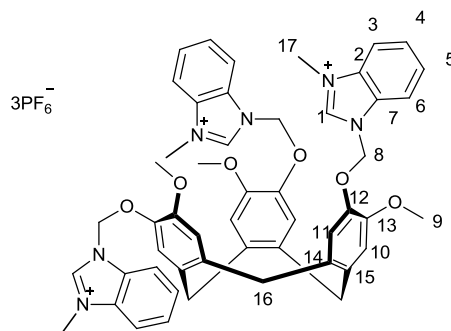
diethyl ether (3 x 5 mL), affording the title compound as a white solid. Yield 43 mg, 0.033 mmol, 83%. HRMS (ESI$^+$) 281.1282 $\{C_{51}H_{51}N_6O_6\}^{3+}$, 349.1499 $\{C_{42}H_{42}N_4O_6\}^{2+}$, 494.2698 $\{C_{51}H_{51}F_6N_6O_6P\}^{2+}$, 1133.3018 $\{C_{51}H_{51}F_{12}N_6O_6P_2\}^+$ Calcd. 281.1285, 349.1547, 494.1751, 1133.3149 respectively; ^{1}H NMR (300 MHz, DMSO-d_6) δ (ppm) 9.86 (s, 3H, H^1), 8.04 (d, 3H, J = 8.3 Hz, H^6), 7.84 (d, 3H, J = 8.3 Hz, H^3), 7.69 (t, 3H, J = 7.4 Hz, H^4), 7.58 (t, 3H, J = 7.5 Hz, H^5), 7.33 (s, 3H, H^{10}), 7.08 (s, 3H, H^{11}), 6.37 (s, 6H, H^8), 4.73 (d, 3H, J = 13.5 Hz, *endo*-H^{16}), 4.10 (s, 9H, H^{17}), 3.56 (s, 9H, H^9), 3.55 (d, 3H, J = 13.1 Hz, *exo*-H^{16}); ^{13}C{^{1}H} (101 MHz, DMSO-d_6) δ (ppm) 149.00 (C^{13}), 143.28 (C^1), 142.97 (C^{12}), 136.43 (C^{14}), 132.18 (C^{15}), 131.80 (C^2), 130.45 (C^7), 126.96 (C^5), 126.82 (C^4), 120.62 (C^{10}), 114.45 (C^{11}), 113.76 (C^6), 113.62(C^3), 75.91 (C^8), 55.96 (C^9), 34.86 (C^{16}), 33.47 (C^{17}); ^{19}F{^{1}H} NMR (376 MHz, DMSO-d_6) δ (ppm) -70.15 (d, J_{F-P} = 711.8 Hz). ^{31}P{^{1}H} NMR

(162 MHz, DMSO-d_6) δ (ppm) -144.19 (hept, J_{P-F} = 711.5 Hz); FTIR ν (cm^{-1}) 834 (P-F bend), 557; Elemental analysis for $C_{51}H_{51}F_{18}N_6O_6P_3$ Calcd.: C 47.90, H 4.02, N 6.57; Found: C 47.77, H 3.93, N 6.64.

Synthesis of 1,1',1''-(((3,8,13-trimethoxy-10,15-dihydro-5H-tribenzo[a,d,g][9]annulene-2,7,12-triyl)tris(oxy))tris(methylene))tris(3-benzyl-1H-benzimidazolium) bromide, 4.5

2.11 (100 mg, 0.12 mmol) was dissolved in acetonitrile (5 mL) and benzyl bromide (0.06 mL, 0.54 mmol) was added. The colourless solution was heated to 60 ℃ for 18 h, during which time a white solid precipitated from solution. The solid was filtered, washed with diethyl ether (20 mL) and dried in air, affording **4.5** as a white solid. Yield 129 mg, 0.22 mmol, 82%. HRMS (ESI+) 357.1624 {$C_{69}H_{63}N_6O_6$}$^{3+}$, 490.2127 {$C_{62}H_{56}N_6O_6$}$^{2+}$; calculated 357.1598,
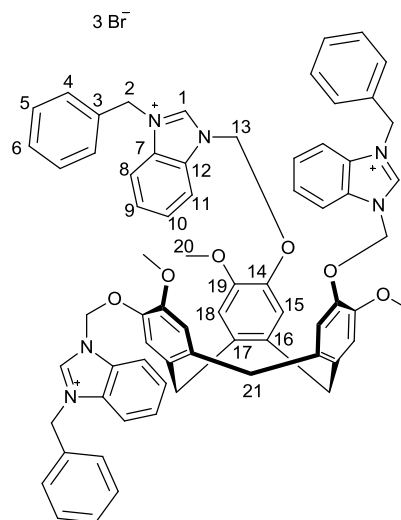
490.2125; ^{1}H NMR (300 MHz, DMSO-d_6) δ (ppm) 10.18 (s, 3H, H^1), 8.00 (d, 3H, J = 8.1 Hz, H^{11}), 7.91 (d, 3H, J = 8.1 Hz, H^8), 7.61 (m, 6H, H^9, H^{10}), 7.40 (bs, 6H, H^4, H^5, H^6, H^{18}), 7.09 (s, 3H, H^{15}), 6.43 (m, 6H, H^{13}), 5.81 (s, 6H, H^2), 4.74 (d, 3H, J = 13.6 Hz, *endo*-H^{21}), 3.54 (d, 3H, J = 13.4 Hz, *exo*-H^{21}), 3.45 (s, 9H, H^{20}); ^{13}C{^{1}H} NMR (75 MHz, DMSO-d_6) δ (ppm) 149.17 (C^{19}), 142.98 (C^1), 142.51 (C^{14}), 136.71 (C^{17}), 133.68 (C^3), 132.25 (C^{16}), 130.76 (C^{12}), 130.72 (C^7), 129.03 (C^5), 128.83 (C^6), 128.17 (C^4), 127.09 (C^{10}), 127.02 (C^9), 121.18 (C^{18}), 114.57 (C^{15}), 114.11 (C^8), 114.00 (C^{11}), 76.24 (C^{13}), 56.02 (C^{20}), 49.92 (C^2), 34.80 (C^{21}); FTIR ν (cm^{-1}) 3432, 2936, 1511, 1269, 766; Elemental analysis for $C_{69}H_{63}Br_3N_6O_6$(HBr) Calcd.: C 59.89, H 4.05, N 6.07; Found: C 59.50, H 4.38, N 6.25.

Synthesis of 1,1',1''-(((3,8,13-trimethoxy-10,15-dihydro-5H-tribenzo[a,d,g][9]annulene-2,7,12-triyl)tris(oxy))tris(methylene))tris(3-allyl-1H-benzimidazolium) bromide, 4.6

2.11 (50 mg, 0.063 mmol), allyl bromide (0.12 mL, 1.3 mmol) and acetonitrile (3 mL) were stirred at 80 ℃ in a sealed J. Youngs ampoule for 16 h. Methanol (5 mL)

was added to dissolve the red oil formed, and solvents removed *in vacuo*, affording a hygroscopic cream coloured solid. The solid was dissolved in methanol (5 mL), NH4PF6 (50 mg) added and stirred for 30 mins. A white solid precipitated, was filtered, and washed with methanol (5 mL) and diethyl ether (5 mL). The title compound was isolated as a white solid. Yield 81 mg, 0.06 mmol, 95%; HRMS (ESI$^+$) 307.1468 $\{C_{57}H_{57}N_6O_6\}^{3+}$, 375.1682 $\{C_{46}H_{46}N_4O_6\}^{2+}$, 440.1951 $\{C_{54}H_{52}N_6O_6\}^{2+}$, 553.2010 $\{C_{57}H_{57}F_6N_6O_6P\}^{2+}$, 895.3044 $\{C_{46}H_{46}F_6N_4O_6P\}^{+}$, 1025.3582 $\{C_{54}H_{52}F_6N_6O_6P\}^{+}$, 1211.3621 $\{C_{57}H_{57}F_{12}N_6O_6P_2\}^{+}$, Calcd. for 307.1441, 375.1703, 440.1969, 533.1985, 895.3054, 1025.3585, 1211.3618 respectively; ^{1}H NMR (500 MHz, DMSO-d_6) δ (ppm) 9.86 (s, 3H, H^4), 8.01 (d, 3H, J = 8.3 Hz, H^6), 7.88 (d, 3H, J = 8.3 Hz, H^9), 7.69 (t, 3H. J = 7.8 Hz, H^7), 7.61 (t, 3H, J = 7.8 Hz, H^8), 7.29 (s, 3H, H^{14}), 7.04 (s, 3H, H^{17}), 6.40 – 6.30 (m, 6H, H^{11}), 6.06 (ddt, 3H, J = 16.2, 10.7, 5.8 Hz, H^2), 5.38 (d, 3H, J = 10.2 Hz, *cis*-H^1), 5.32 (d, 3H, J = 17.2 Hz, *trans*-H^1), 5.19 (d, 6H, J = 5.5 Hz, H^3), 4.73 (d, 3H, J = 13.3 Hz, *endo*-H^{19}), 3.51 (s, 12H, H^{18}, *exo*-H^{19}); ^{13}C$\{^1$H$\}$ NMR (100 MHz, DMSO-d_6) δ (ppm) 149.16 (C^{13}), 142.98 (C^3), 142.84 (C^{12}), 136.66 (C^{15}), 132.21 (C^{16}), 130.93 (C^5, C^{10}), 130.72 (C^2), 127.08 (C^8), 126.97 (C^7), 121.13 (C^{14}), 120.58 (C^1), 114.41 (C^{17}), 113.99 (C^6), 113.93 (C^9), 76.28 (C^{11}), 55.93 (C^{18}), 48.94 (C^3), 34.85 (C19); ^{19}F NMR (376 MHz, DMSO-d_6) δ (ppm) -70.15 (d, J_{F-P} = 711.4 Hz, PF_6); ^{31}P NMR (162 MHz, DMSO-d_6) δ (ppm) -144.18 (hept, J_{P-F} = 711.2 Hz, PF6); Elemental analysis for $C_{57}H_{57}F_{18}N_6O_6P_3$ Calcd.: C 50.45, H 4.23, N 6.19; Found: C 50.36, H 4.34, N 6.24.
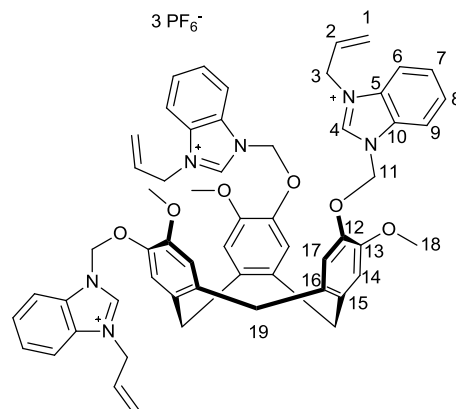
Synthesis of 1-(2-methoxyphenyoxy)methylbenzimidazole, 4.7

Sodium hydride (60% dispersion, 800 mg, 19.48 mmol) was added to anhydrous, degassed DMF (5 mL) under an N2 atmosphere. Guaiacol (400 mg, 0.36 mL, 3.20 mmol) was added dropwise over a period of
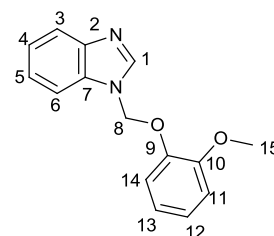
20 mins. The effervescing solution was stirred at rt for 1 h. 1-(chloromethyl)benzimidazole hydrochloride (786 mg, 3.2 mmol) was added and the solution stirred at rt for 16 h. The reaction was quenched with water and the product extracted into dichloromethane (3 x 200 mL). The organic layers were combined, washed with brine, and dried over MgSO$_4$. Solvents were removed in vacuo, and the residue triturated in petroleum ether (60-80), affording the title compound as a white solid Yield 441 mg, 1.90 mmol, 58%. HRMS (ESI+) 255.1136 {C$_{15}$H$_{15}$N$_2$O$_2$}, 277.0949 {C$_{15}$H$_{14}$N$_2$NaO$_2$}$^+$ Calcd. for 255.1129 and 277.0948 respectively; ^{1}H NMR (300 MHz, CDCl$_3$) δ (ppm) 7.81 (s, 1H, H^1), 7.78 (dd, 1H, J = 3.3, 1.2 Hz, H^3), 7.52 – 7.47 (m, 1H, H^5), 7.35 – 7.27 (m, 2H, H^4, H^6), 7.10 – 7.02 (m, 1H, H^{13}), 6.90 (dd, 1H, J = 8.1, 1.5 Hz, H^{14}), 6.75 (td, 1H, J = 7.6, 1.5 Hz, H^{12}), 6.68 (dd, 1H, J = 7.9, 1.8 Hz, H^{11}), 6.03 (s, 2H, H^8), 3.79 (s, 3H, H^{15}); ^{13}C{^{1}H} NMR (101 MHz, CDCl$_3$) δ (ppm) 151.74 (C^{10}), 144.63 (C^2), 144.05 (C^9), 143.34 (C^1), 133.69 (C^7), 125.59 (C^{13}), 123.70 (C^4), 122.91 (C^6), 121.73 (C^{11}), 121.27 (C^{12}), 120.52 (C^3), 112.58 (C^{14}), 110.33 (C^5), 74.91 (C^8), 55.81 (C^{15}). All data were consistent with those reported in the literature.[12]

Synthesis of 1-(2-methoxyphenyoxy)methyl-3-methylbenzimidazolium iodide, 4.8

4.7 (50 mg, 0.19 mmol) and acetonitrile (2 mL) were added to a J. Youngs ampoule. Methyl iodide (0.12 mL, 1.90 mmol) was added, and the ampoule sealed and the pale yellow solution heated to 80 °C for 16 h. Diethyl ether (20 mL) was added and a white solid precipitated from solution. The powder was filtered and washed with diethyl ether (5 mL). The title compound was isolated as a white powder. Yield 60 mg, 0.15 mmol, 84%. HRMS (ESI+) 269.1246 {C$_{16}$H$_{17}$N$_2$O$_2$}$^+$ Calculated 269.1285; ^{1}H NMR (300 MHz, DMSO-d_6) δ (ppm) 9.87 (s, 1H, H^2), 8.11 – 8.01 (m, 1H, H^7), 8.00 – 7.92 (m, 1H, H^4), 7.77 – 7.67 (m, 2H, H^5, H^6), 7.16 – 7.00 (m, 3H, H^{12}, H^{13}, H^{15}), 6.88 (ddd, 1H, J = 8.3, 7.2, 1.7 Hz, H^{14}), 6.45 (s, 2H, H^9), 4.12 (s, 3H, H^1), 3.65 (s, 3H, H^{16}); ^{13}C{^{1}H} NMR (75 MHz, DMSO-d_6) δ (ppm) 150.60 (C^{11}), 144.13 (C^{10}), 143.36 (C^2), 131.82 (C^3), 130.48 (C^8), 127.10 (C^6), 126.83 (C^5), 125.17 (C^{12}), 120.84 (C^{14}), 119.36 (C^{15}), 113.82 (C^7), 113.72 (C^4), 112.98 (C^{13}), 75.66 (C^9), 55.53 (C^{16}), 33.57 (C^1); FTIR ν (cm^{-1}) 1491, 1253, 1124, 1054, 1015, 745; m.p. 145-147 °C; Elemental
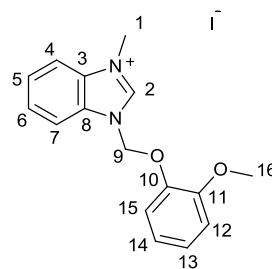
analysis for $C_{16}H_{17}IN_2O_2$ Calcd.: C 48.50, H 4.30, N 7.07; Found C 48.59, H 4.26, N 7.14.

Synthesis of 1-(2-methoxyphenyoxy)benzyl-3-methylbenzimidazolium bromide, 4.9

2-(Methoxyphenoxymethyl)benzimidazole (200 mg, 0.78 mmol) was dissolved in acetonitrile (10 mL) and benzyl bromide (0.92 mL, 7.8 mmol) added. The colourless solution was heated to 60 °C overnight, during which a white solid precipitated. The precipitate was filtered, washed with diethyl ether (20 mL) and dried, affording **4.9** as a white solid. Yield 293 mg, 0.68 mmol, 88%. HRMS (ESI+) 345.1611 $\{C_{22}H_{21}N_2O_2\}^+$ Calculated 345.1598; ^{1}H NMR (300 MHz, DMSO-d_6) δ (ppm) 10.04 (s, 1H, H^1) , 8.06-7.95 (m, 2H. H^8, H^{11}), 7.77 – 7.60 (m, 2H, H^9, H^{10}), 7.39 (s, 5H, H^4, H^5, H^6), 7.12 (t, 1H, J = 7.0 Hz, H^{17}), 7.06 – 6.94 (m, 2H, H^{15}, H^{18}), 6.86 (t, 1H, J = 7.0 Hz, H^{16}), 6.47 (s, 2H, H^{14}), 5.80 (s, 2H, H^2), 3.54 (s, 3H, H^{20}); ^{13}C{^{1}H} NMR (101 MHz, DMSO-d_6) δ (ppm) 150.84 (C^{19}), 143.67 (C^{14}), 143.08 (C^1), 133.66 (C^3), 130.77 (C^7, C^{12}), 129.02 (C^5), 128.80 (C^6), 128.17 (C^4), 127.25 (C^{10}), 127.06 (C^9), 125.47 (C^{17}), 120.89 (C^{16}), 120.02 (C^{18}), 114.14 (C^8), 114.04 (C^{11}), 113.06 (C^{15}), 76.06 (C^{13}), 55.42 (C^{20}), 49.95 (C^2); FTIR ν (cm^{-1}) 2900, 1505, 1252, 1206, 745; Elemental analysis for $C_{22}H_{21}BrN_2O_2$ Calcd.: C 62.13, H, 4.98, N, 6.59; Found C 61.96, H 4.88, N 6.67
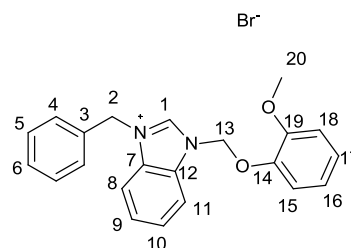
4.10 Supplementary crystallographic information

Crystals were mounted under inert oil on a MiTeGen tip and flash frozen using an OxfordCryosystems low temperature device. X-ray diffraction data were collected using CuKα radiation (λ = 1.54184 Å) or MoKα (λ = 0.71073 Å) using an Agilent Supernova dual-source diffractometer with Atlas S2 CCD detector and fine-focus sealed tube generator, or using synchrotron radiation (λ = 0.6889 Å) at Beamline I19 at the Diamond light source. Data were corrected for Lorenztian and polarization effects and absorption corrections were applied using multi-scan methods. The structures were solved by direct methods using SHELXS-97 and refined by full-matrix on F^2 using SHELXL-97. Unless otherwise specified, all non-hydrogen

atoms were refined as anisotropic, and hydrogen positions were included at geometrically estimated positions.

4.10.1 Additional crystallographic details

(4.2)$_2$.3(MeCN)

Hexafluorophosphate anions were disordered over two positions at 0.5 occupancy and refined as isotropic. Bond lengths and angles restrained to be chemically reasonable. The acetonitrile molecule was refined as isotropic, bond lengths restrained to be chemically reasonable and hydrogen positions not included. Data overall were of poor quality and did not diffract to high angles.

4.4

Two benzimidazolium groups were highly disordered and therefore refined as isotropic. Bond lengths of both benzo-backbones in question were restrained to be chemically reasonable using the AFIX command of SHELX. A portion of one benzimidazole group was disordered over two positions, each of 0.5 occupancy.

Table 4.1 Crystallographic data. a = Cuka radiation, b = synchrotron radiation

Compound	(4.2)$_2$.3(MeCN)[a]	4.4[b]	4.8[b]
Formula	$C_{79}H_{90}F_{36}N_{12.5}O_{12}P_6$	$C_{102}H_{102}F_{36}N_{12}O_{12}P_6$	$C_{32}H_{34}I_2N_4O_4$
Mr	2276.45	2557.78	792.43

Crystal size	0.03 x 0.06 x 0.10	0.03 x 0.01 x 0.01	0.12 x 0.12 x 0.15
Crystal system	Hexagonal	Triclinic	Triclinic
Space group	$P6$	$P\bar{1}$	$P\bar{1}$
a (Å)	26.355(7)	7.4847(9)	9.81010(10)
b (Å)	26.355(7)	16.4088(17)	11.69940(10)
c (Å)	4.5656(18)	22.788(3)	14.63640(10)
α (^{0})	90	75.410(11)	83.3170(10)
β (^{0})	90	80.946(12)	83.0190(10)
γ (^{0})	120	78.773(10)	74.0510(10)
V (Å^3)	2746.3(18)	2639.3(6)	1597.15(3)
Z	2	2	2
ρ_{calc} (g.cm^{-3})	1.376	1.609	1.648
θ range (^{0})	3.354-59.971	1.708- 20.148	1.761-25.502
No. data collected	5103	8730	21318
No. unique data	2277	5085	6465
R_{int}	0.0957	0.0620	0.0317
No. obs. Data ($I > 2\sigma(I)$)	1428	1834	6025
No. parameters	218	641	383
No. restraints	39	4	0
R_1 (obs data)	0.1754	0.1137	0.0318
wR_2 (all data)	0.4525	0.3374	0.1231
S	1.523	0.945	1.051
Max. shift/esd	0.000	0.001	0.001
Largest difference peak and hole/ (e Å^3)	1.454, -0.523	0.830, -0.356	1.830,-0.850

4.11 References

1. B. Radziszewski, *Ber. Dtsch. Chem. Ges.,* 1882, **15**, 2706-2708.

2. A. J. Arduengo, III, R. Krafczyk, R. Schmutzler, H. A. Craig, J. R. Goerlich, W. J. Marshall, M. Unverzagt, *Tetrahedron*, 1999, **55**, 14523-14534.

3. T. Chavagnan, D. Sémeril, D. Matt, J. Harrowfield, L. Toupet, *Chem. Eur. J.*, 2015, **21**, 6678-6681.

4. T. Chavagnan, D. Sémeril, D. Matt, L. Toupet, J. Harrowfield, R. Welter, *Eur. J. Inorg. Chem.*, 2016, **2016**, 497-502.

5. D. Sechet, Z. Kaya, T. A. Phan, M. Jouffroy, E. Bentouhami, D. Armspach, D. Matt, L. Toupet, *Chem.Commun.*, 2017.

6. T. K. Ronson, C. Carruthers, J. Fisher, T. Brotin, L. P. Harding, P. J. Rizkallah, M. J. Hardie, *Inorg. Chem.*, 2010, **49**, 675-685.

7. F. L. Thorp-Greenwood, V. E. Pritchard, M. P. Coogan, M. J. Hardie, *Organometallics*, 2016, **35**, 1632-1642.

8. J. J. Henkelis, C. J. Carruthers, S. E. Chambers, R. Clowes, A. I. Cooper, J. Fisher, M. J. Hardie, *J. Am. Chem. Soc.*, 2014, **136**, 14393-14396.

9. F. E. Hahn, C. Radloff, T. Pape, A. Hepp, *Organometallics*, 2008, **27**, 6408-6410.

10. M. A. Little, M. A. Halcrow, L. P. Harding, M. J. Hardie, *Inorg. Chem.*, 2010, **49**, 9486-9496.

11. A. C. Cope, E. M. Hardy, *J. Am. Chem. Soc.*, 1940, **62**, 441-444.

12. L. Claisen, *Ber. Dtsch. Chem. Ges.*, 1912, **45**, 3157-3166.

13. A. Khalafi-Nezhad, M. N. Soltani Rad, G. H. Hakimelahi, B. Mokhtari, *Tetrahedron*, 2002, **58**, 10341-10344.

14. X. Wang, S. Liu, L.-H. Weng, G.-X. Jin, *Organometallics*, 2006, **25**, 3565-3569.

15. R. Visbal, A. Laguna, M. C. Gimeno, *Chem. Commun.*, 2013, **49**, 5642-5644.

16. H. M. J. Wang, I. J. B. Lin, *Organometallics*, 1998, **17**, 972-975.

17. H. A. Mohamed, C. E. Willans, in *Organometallic Chemistry*, ed. I.J.S. Fairlamb, J,M. Lynam, 2014, vol. 39, 26-50.

18. H. A. Mohamed, B. R. M. Lake, T. Laing, R. M. Phillips, C. E. Willans, *Dalton Trans.*, 2015, **44**, 7563-7569.

19. D. J. Nelson, *Eur. J. Inorg. Chem.*, 2015, **12**, 2012-2027.

20. J. C. Garrison, W. J. Youngs, *Chem. Rev.*, 2005, **105**, 3978-4008.

21. N. Sinha, F. Roelfes, A. Hepp, C. Mejuto, E. Peris, F. E. Hahn, *Organometallics*, 2014, **33**, 6898-6904.

22. C. Segarra, G. Guisado-Barrios, F. E. Hahn ,E. Peris, *Organometallics*, 2014, **33**, 5077-5080.

23. N. Sinha, F. E. Hahn, *Acc. Chem. Res.*, 2017, **50**, 2167-2184.

24. N. Sinha, T. T. Y. Tan, E. Peris, F. E. Hahn, *Angew. Chem., Int. Ed.*, 2017, **56**, 7393-7397.

25. C. Mejuto, G. Guisado-Barrios, D. Gusev, E. Peris, *Chem. Commun.*, 2015, **51**, 13914-13917.

26. A. R. Chianese, X. Li, M. C. Janzen, J. W. Faller, R. H. Crabtree, *Organometallics*, 2003, **22**, 1663-1667.

27. A. J. Arduengo, III, H. V. R. Dias, J. C. Calabrese, F. Davidson, *Organometallics*, 1993, **12**, 3405-3409.

28. T. N. Hooper, C. P. Butts, M. Green, M. F. Haddow, J. E. McGrady, C. A. Russell, *Chem. Eur. J.*, 2009, **15**, 12196-12200.

29. J. Dinda, S. D. Adhikary, S. K. Seth, A. Mahapatra, *New J. Chem.*, 2013, **37**, 431-438.

30. J. P. Reeds, A. C. Whitwood, M. P. Healy, I. J. S. Fairlamb, *Organometallics*, 2013, **32**, 3108-3120.

31. J. Nitschke, W. J. Ramsay, J. A. Foster, K. L. Moore, T. Ronson, R. J. Mirgalet, D. A. Jefferson, *Chem. Sci.*, 2015, **12**, 7326-7331

32. C. Radloff, J. J. Weigand, F. E. Hahn, *Dalton Trans.*, 2009, 9392-9394.

33. A. Rit, T. Pape, F. E. Hahn, *J. Am. Chem. Soc.*, 2010, **132**, 4572-4573.

34. P. J. Altmann, A. Pöthig, *J. Am. Chem. Soc.*, 2016, **138**, 13171-13174.

35. P. J. Altmann, A. Pothig, *Angew. Chem. Int. Ed.*, 2017, **56**, 15733-15736.

36. A. Collet, *Tetrahedron*, 1987, **43**, 5725-5759.

37. K. T. Holman, J. L. Atwood, J. W. Steed, *Angew. Chem. Int. Ed.*, 1997, **36**, 1736-1738.

38. J. J. Henkelis, T. K. Ronson, L. P. Harding, M. J. Hardie, *Chem. Commun.*, 2011, **47**, 6560-6562.

39. N. J. Cookson, J. M. Fowler, D. P. Martin, J. Fisher, J. J. Henkelis, T. K. Ronson, F. L. Thorp-Greenwood, C. E. Willans, M. J. Hardie, *Supramol. Chem.*, 2017, 1-12.

40. K. T. Holman, M. M. Halihan, S. S. Jurisson, J. L. Atwood, R. S. Burkhalter, A. R. Mitchell, J. W. Steed, *J. Am. Chem. Soc.*, 1996, **118**, 9567-9576.

41. L. Pauling, *J. Am. Chem. Soc.*, 1932, **9**, 3570-3582.

40. J. F. Normant, *Synthesis*, 1972, **1972**, 63-80.

41. T. Cohen, I. Cristea, *J. Am. Chem. Soc.*, 1976, **98**, 748-753.

42. C.-T. Yang, Z.-Q. Zhang, Y.-C. Liu, L. Liu, *Angew. Chem. Int. Ed.*, 2011, **50**, 3904-3907.

43. B. R. M. Lake, C. E. Willans, *Chem. Eur.J.*, 2013, **19**, 16780-16790.

44. A. Gorbunov, D. Cheshkov, V. Kovalev, I. Vatsouro, *Chem. Eur. J.*, 2015, **21**, 9528-9534

45. B. Liu, Y. Zhang, D. Xu, W. Chen, *Chem. Commun.*, 2011, **47**, 2883-2885.

46. B. R. M. Lake, E. K. Bullough, T. J. Williams, A. C. Whitwood, M. A. Little, C. E. Willans, *Chem. Commun.*, 2012, **48**, 4887-4889.

47. E. K. Bullough, M. A. Little, C. E. Willans, *Organometallics*, 2013, **32**, 570-577.

Chapter 5
Synthesis and characterisation of Ir, Rh and Ru NHC complexes, and catalytic evaluation in the transfer hydrogenation of acetophenone

This chapter focuses on the preparation of trimetallic Ir(III), Ir(I), Rh(I) and Ru(II)-NHC complexes via the Ag(I) transmetallation route. Appropriate complexes were investigated as catalysts for the transfer hydrogenation of acetophenone.

5.1 Introduction

A number of major discoveries in organometallic chemistry have revolved around complexes of noble metals, with Ir, Rh and Ru being at the forefront of breakthroughs since the mid-20th century. In 1961, Vaska's complex, [Ir(Cl)(CO)(PPh$_3$)$_2$] was reported, which can reversibly bind molecular oxygen.[1] In the 1970s, Wilkinson and Crabtree reported Rh(I) and Ir(I) complexes which could catalyse the hydrogenation of alkenes.[2, 3] Grubbs has demonstrated that Ru(IV)-phosphine and NHC complexes are capable of catalysing alkene metathesis reactions, which has become an invaluable tool in the synthesis of molecular knots.[4] Ir, Rh and Ru complexes are often derived from dimeric μ^2-chlorido species bearing multihaptic or chelating ligands. The dimeric precursors are readily available, and split upon reaction with an incoming ligand.

Many key advancements in organometallic chemistry have been in the field of catalysis. Ir, Rh and Ru complexes and precursors are very expensive, but their cost is offset by low catalyst loading requirements. The transition-metal catalysed transfer hydrogenation (TH) of ketones and aldehydes to yield alcohols is a powerful tool to replace traditional reductions using reducing agents such as sodium borohydride, or carrying out hydrogenations under pressurised H$_2$ environments.[5] TH reactions take place in protic solvents, commonly isopropanol, and the sole by-product is a ketone such as acetone. Clean reactivity is afforded, with a much smaller environmental impact, and there is no need to use the high pressures required for a direct hydrogenation. Furthermore, if a prochiral precursor were to be employed, such as acetophenone, asymmetric TH reactions are possible when using chiral catalysts.[6, 7] The first key breakthrough in TH chemistry was in 1925 with the

discovery of the Meerwein-Pondorf-Verley reaction, an aluminium alkoxide-mediated TH process.[8] Disadvantages included stoichiometric addition of Al and side-reactions occurring. A number of examples of transition metal catalysed TH reactions had been reported up until the mid-1990s, but most catalysts lacked enantioselectivity, or were poorly active.[9-11] In 1997, Noyori made a significant breakthrough, preparing chiral Ru(II) complexes which were capable of catalysing TH reactions in isopropanol solvent, with excellent ee's, high conversions and at low catalyst loadings (figure 5.1, left).[6] NHC complexes have since become valuable tools in TH catalysis. A key example being Nolan's NHC analogues of Crabtree's catalyst (figure 5.2, right).[12] A number of Rh[13-17], Ir[13, 16, 18, 19] and Ru-NHC[20-25] complexes have since been reported to catalyse the TH reaction. Recent efforts have gone into employing complexes of cheaper metals in TH catalysis, with a focus on Fe. Morris and co-workers have prepared an Fe(II) complex comparably active to Noyori's ground-breaking catalyst, but the benefits are offset by a more challenging synthetic protocol.[26]
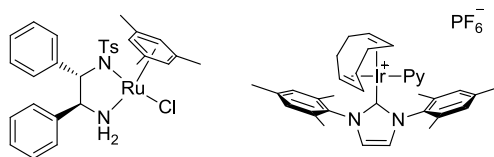
Figure 5.1 Left: Noyori's Ru(II) TH catalyst and right: Nolan's Ir(I)-NHC complex.[5, 6, 12]

The mechanism for TH reactions can be complex, with the pathway being dependent on a number of factors including the metal cation, and also the ligand framework. Mechanisms can be classed as inner- or outer-sphere mediated. The inner-sphere TH (scheme 5.1, bottom left) involves coordination of the deprotonated alcoholic solvent before subsequent 'oxidation' of the alkoxide mediated by the migration of the β-hydride. Ligand exchange then occurs prior to migratory insertion of the hydride ligand, reducing the carbonyl to an alcohol, which is then released from the metal upon coordination of solvent. The outer-sphere mechanism (scheme 5.1, bottom right) dominates when the ligand bears a Brønsted basic group, such as an amine. A pericyclic intermediate is formed through interaction of the alcohol and C-H with metal and ligand, oxidising the alcohol and yielding a hydrido complex. A second transition-state arises through interaction of the ketone with the hydride ligand, and the reduced alcohol is then eliminated.[27] This reactivity was pioneered by Noyori, whose catalysts often followed this pathway in asymmetric TH

reactions.[5, 6] Morris has, however, prepared Ru(II)-NHC complexes bearing a coordinating aniline pendant, and discovered that an inner-sphere mechanism was more favourable in this case.[28] Hintermair and Crabtree have observed Cp* loss as a pathway when employing [Ir(Cp*)(NHC)$_2$(Cl)]$^+$ catalysts, but this is mediated by an unusual scenario of Cp* being the weakest-bound ligand on intermediates when employing their catalysts.[29]

Inner-sphere TH
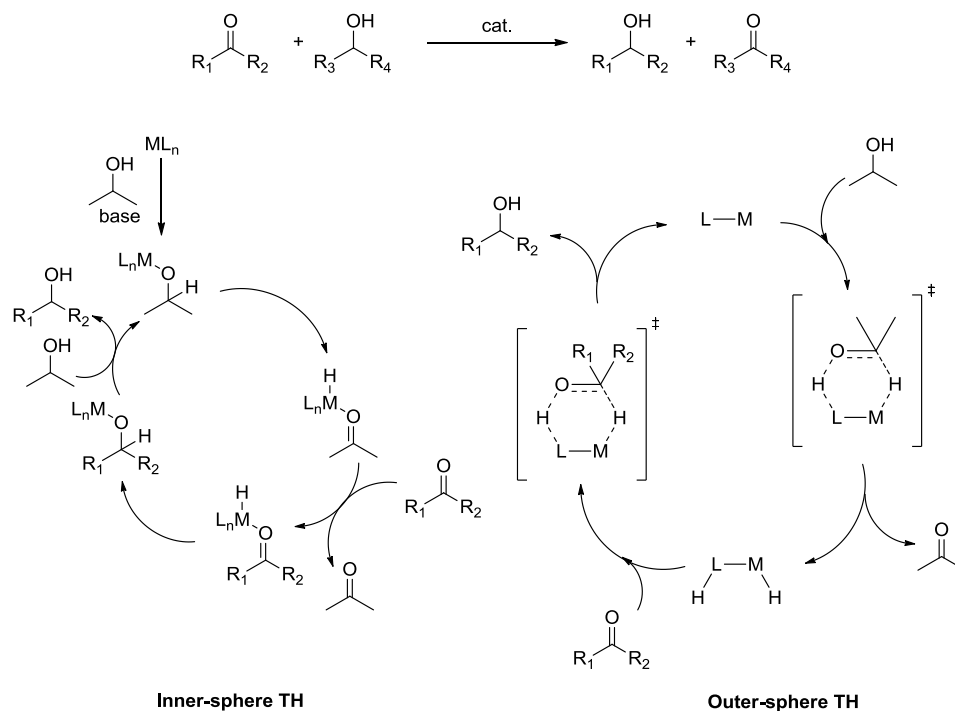
Outer-sphere TH

Scheme 5.1 TopL TH reaction. Bottom left: generally accepted inner-sphere and bottom right: outer-sphere mechanisms.

Kück and Peris have previously reported a trimetallic Rh(I)-NHC complex annulated onto the TBTQ scaffold, which is structurally similar to CTG. The complex possesses *pseudo-C$_3$*-symmetry with two NHC environments in the $^{13}C\{^1H\}$ NMR spectrum, suggesting there is no rotation about Rh-C bonds in [Rh(COD)(NHC)(Cl)] complexes.[30] Crabtree has previously demonstrated this is general for Rh(I) and Ir(I)-NHC complexes bearing COD ligands, and this remained the case on the NMR timescale at 105 °C.[31] Carbonylating the complexes led to fluxionality and coalescence of the diastereotopic peaks, suggesting the COD ligand conformationally locks the complex. It would be reasonable to predict conformational locking is common in most NHC complexes bearing multihaptic ligands, such as Cp*.

5.2 Preparation of Ir(III) NHC complexes

The selected route for the preparation of trimetallic NHC complexes tethered to the CTV scaffold was the transmetallation from a Ag(I)-NHC transfer agent. It was discussed in Chapter 4 how the isolation of Ag(I)-NHC complexes of ligand **4.3** proved unsuccessful, but widespread literature precedent for transmetallation onto noble metals exists, in particular when using dimeric precursors. The additional enthalpic driving force of Ag(I) halide precipitation further enhances the yield of coordination of carbene to metal. Examples of Ir(III)-NHC synthesis have been reported which employ weak alkali metal bases instead of Ag_2O, but it was decided that the strong driving force associated with AgX precipitation would afford the best chance of preparing desired complexes. Typically, the preparation of Ir(III) complexes *via* this methodology is carried out in DCM, with acetonitrile also previously being used.[32] Tripodal imidazolium salts **4.3** and **4.5** were insoluble in chlorinated solvents, therefore reactions were carried out in MeCN. Ligand **4.3** exhibited solubility in acetonitrile, whereas **4.5** did not, hence ligand **4.3** was selected for this investigation. The precursor $[Ir(Cp*)(Cl)_2]_2$ is readily available and reacts with nucleophiles to yield two equivalents of a piano-stool complex. The methyl groups of the Cp* ligand increase the π-donating capabilities of the multihaptic ligand, in addition to improving solubility of complexes.
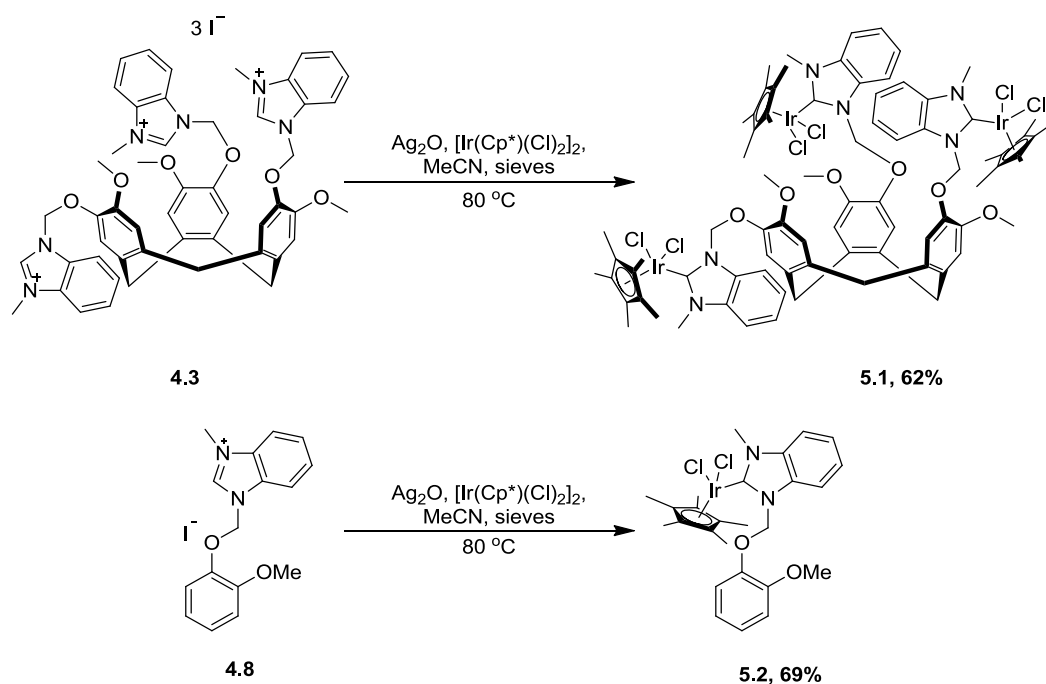
Scheme 5.2 Synthesis of Ir(III)-NHC complexes 5.1 and 5.2.

Trimetallic Ir(III) complex **5.1** was successfully prepared following the methodology described in scheme 5.2. The orange solid obtained was indefinitely stable to air and moisture. Careful stoichiometric control was necessary to prevent residual [Ir(Cp*)(Cl)$_2$]$_2$ from remaining, whilst an excess of **4.3** would give incomplete reactivity, with *mono-* or *bis*-metallated complex present, proving difficult to separate. HRMS suggested reactions reached completeness after 18 h, and a pale yellow solid precipitated from solution, consistent with AgI formation. Ag$_2$O was not observed in the Schlenk flask. Consideration for the photosensitivity of Ag(I) species, along with potential air- and moisture sensitivity was paramount, so 4 Å molecular sieves were added to reactions and manipulations carried out in the dark under an atmosphere of dry nitrogen gas. Reactions were filtered through multiple Celite™ pads in an attempt to remove Ag(I) impurities, however, in some cases AgI was observed in the product even after multiple filtrations. In order to circumvent Ag by-product formation, the synthesis of **5.1** employing Cs$_2$CO$_3$ as base was attempted, but gave low yields (<15%). Complex **5.2** could be prepared following the same methodology applied to **5.1** by employing ligand **4.8**, in addition to reducing the stoichiometries of Ag$_2$O and [Ir(Cp*)(Cl)$_2$]$_2$ to 0.5 by virtue of each complex molecule only bearing one metal centre.

HRMS was an excellent tool for characterising complexes derived from noble metal dimers, and diagnostic isotope patterns were observed for complexes prepared. The obtained spectrum of **5.1** (figure 5.2) contained a major peak at *m/z* 643.1692 {M-3Cl}$^{3+}$ (calculated 643.1665). Additional peaks with a +4 and +2 charge for similar species minus relevant number of halide ions were also detected at *m/z* 473.6436 and 982.2344 respectively (calculated as 473.6236 and 982.2345 respectively).

Complex **5.2**, η^5-1,2,3,4,5-pentamethylcyclopentadienyl dichloro (1-methyl-3-((2-methoxyphenoxy)methyl)benzimidazol-2-ylidene)iridium(III) followed a similar trend, and the major peak observed in the HRMS was {M–Cl}$^+$ with *m/z* = 631.1700 (calculated 631.1698) displaying a good match to the simulated isotope pattern (figure 5.3).
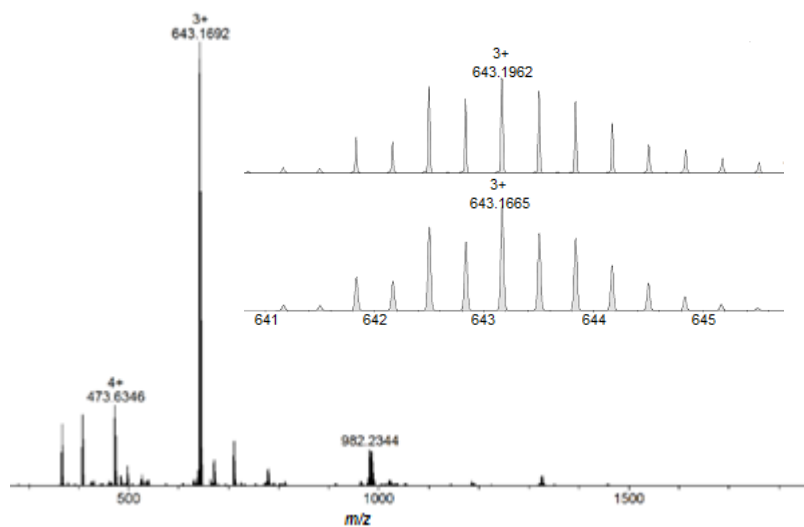
Figure 5.2 HRMS of complex 5.1. Inset: observed (top) vs simulated (bottom) isotope pattern for m/z = 643.1692, {M-3Cl}$^{3+}$.
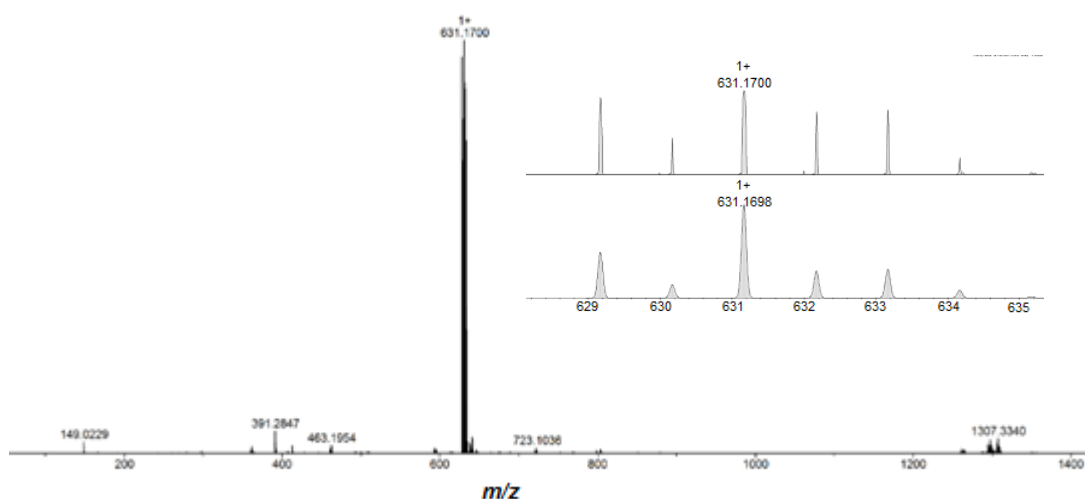
Figure 5.3 HRMS of complex 5.2. Inset: Observed (top) vs simulated (bottom) isotope pattern for m/z 631.1700, {M-Cl}$^{+}$.

^{1}H NMR spectroscopy was a less useful tool when interpreting spectra of trimetallic complexes. The extremely rigid trimetallic complexes gave highly broadened spectra, which often precluded their full assignment. VT NMR spectroscopy was carried out in CDCl$_3$ and MeCN-d_3 between 223 and 323 K, but no changes to spectra were observed. No peaks were observed in the ^{13}C{^{1}H} spectrum of **5.1**, even after further concentrating the sample. Nonetheless, key peaks including the methylene bridge and both CH$_3$ groups could be determined using 2D NMR spectroscopy. Heteronuclear 2D experiments were also carried out to ratify the relative position of carbon atoms, which proved invaluable in determining the

carbenic nature of the complexes. Monometallic complexes afforded a valuable NMR tool for understanding the behaviour of CTV-derived complexes in solution, with key peaks in mono- and trimetallic complexes appearing at similar chemical shifts.

For complex **5.1**, the Cp* methyl resonances surprisingly split into two peaks at 1.71 and 1.57 ppm, both of which were observed coupling to a single carbon in the HMQC spectrum. The peak at 1.51 ppm does overlap with the chemical shift of water in CDCl$_3$, but 2D analysis suggests this peak is related to the bulk complex. Significantly, both of these Cp* resonances couple to the carbenic carbon in the HMBC spectrum, suggesting they are associated with the sole C_3-symmetric NHC complex. A single peak at 1.69 ppm in the ^{1}H NMR spectrum was observed of **5.2** corresponding to the Cp* methyl protons. The protons of the methylene bridge H^{11} in **5.2** split into two environments at 5.88 and 7.42-7.27 ppm. This was confirmed using COSY and HMQC experiments. Similar coupling was observed in the COSY and HMQC spectra of **5.1**, with the most upfield peak appearing at *ca.* 5.3 ppm, suggesting shielding of this proton from the magnetic field. Preagostic interactions may well offer an explanation for the large splitting between seemingly similar protons.[33] The deshielded proton interacts with the Ir(III) centre in solution, and such splitting is typical for this particular phenomenon.[27] For **5.2**, the *N*-methyl and methoxy resonances were sited at 4.22 and 3.79 ppm respectively, and significant peaks were observed at similar chemical shifts in complex **5.1**. A broad doublet at 4.81 ppm coupled to a second broad peak at 3.59 ppm in the COSY experiment for **5.1**, which are suggestive of the *endo-* and *exo-* protons of the CTV lower rim. The observation of a doublet, in addition to no further Cp* resonances or no imidazolium resonances at >9 ppm, implies that in the case of complex **5.1**, a single trimetallic complex was prepared. SEM-EDX analysis was also carried out, which eliminated the possibility of halide mixing as a consequence of employing the imidazolium iodide alongside an iridium chloride precursor.
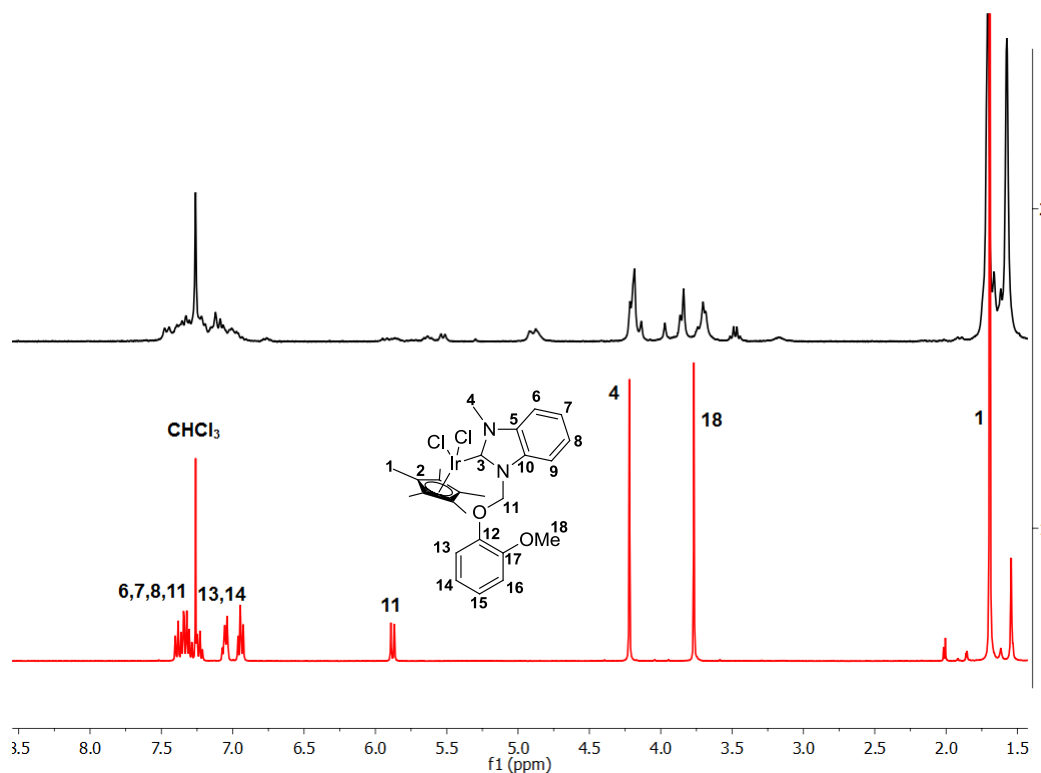
Figure 5.4 ^{1}H NMR spectra (300 MHz, 293 K, CDCl$_3$) of 5.1 (top, black trace) and 5.2 (bottom, red trace).

A ^{13}C{^{1}H} NMR spectrum could not be obtained for complex **5.1**, even when adding 30-40 mg of sample to 0.5 mL of CDCl$_3$. A weak DEPT-135 spectrum was obtained (shown as the vertical axis in figure 5.6), which revealed two CH$_2$ resonances at 77.93 and 34.47 ppm, consistent with the fully formed complex and comparable to the NCH$_2$O and CTV lower rim resonances on a number of CTV-type complexes. 2D NMR spectroscopy, in particular HMQC and HMBC experiments, could be used to suggest relative positions of carbon resonances for comparison with **5.2**. Importantly, coupling between peaks at 4.12 ppm (^{1}H) and 171.37 ppm (^{13}C) in the HMBC spectrum was observed, diagnostic for the *N*-methyl group coupling with the divalent carbon of the NHC ligand. The Cp* protons were also observed weakly coupling to the carbenic centre. The ^{13}C{^{1}H} NMR spectrum of **5.2** (figure 5.5) contained a carbenic resonance (C^3) in **5.2** at 173.05 ppm, comparable to that observed in the HMBC spectrum of **5.1**. A single CH$_2$ resonance at 77.71 ppm was observed in the DEPT-135 experiment. The Cp* methyl protons of **5.2** coupled to a carbon at 90.31 ppm in the HMBC spectrum, confirmed as the cyclopentadienyl carbons (C^2).
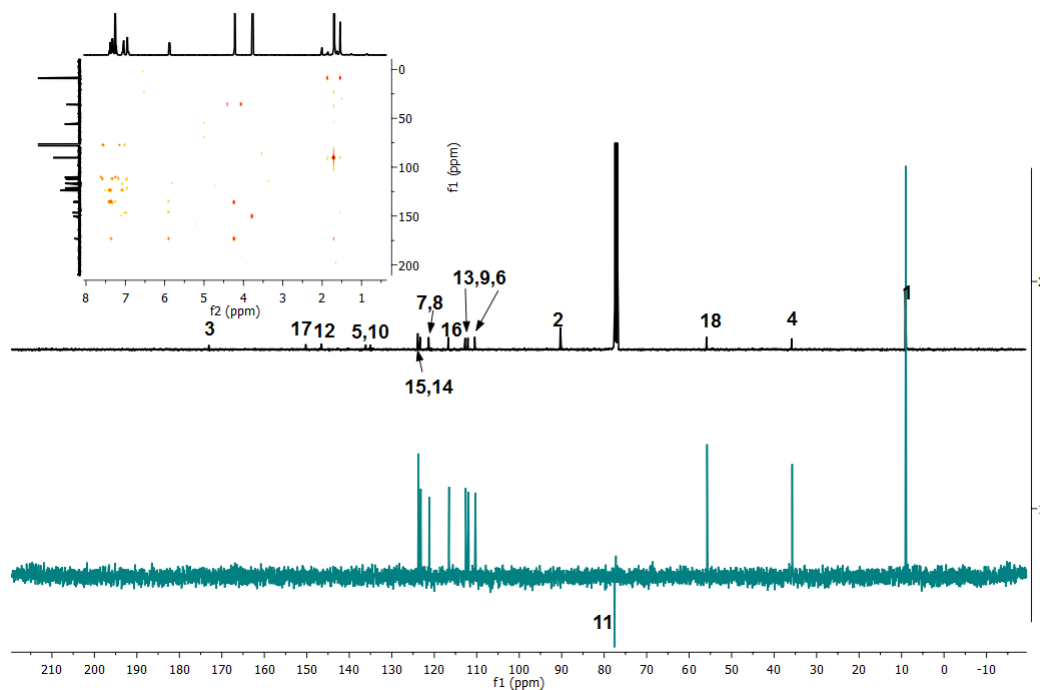
Figure 5.5 ^{13}C{^{1}H} NMR spectrum of 5.2 (top) with DEPT-135 spectrum (bottom). Inset: HMBC spectrum.
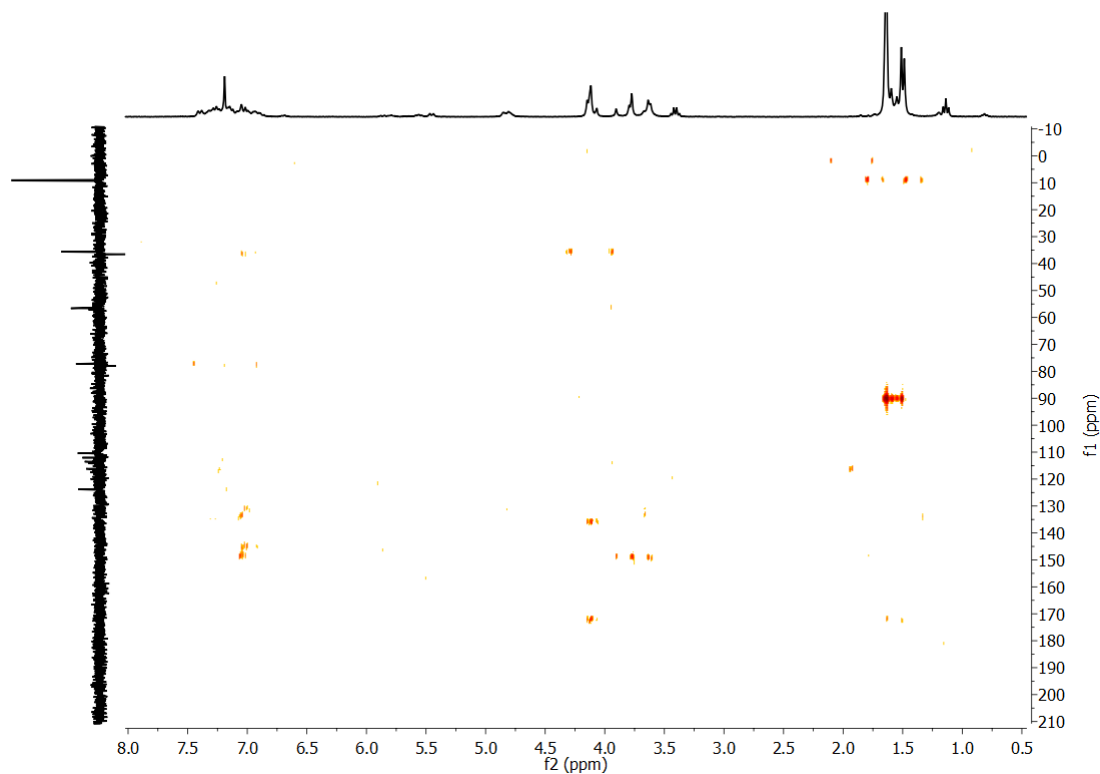
Figure 5.6 HMBC spectrum of 5.1 with DEPT-135 NMR spectrum shown on vertical axis.

^{1}H-^{1}H NOESY NMR spectroscopy was a valuable tool for confirming the highly restricted rotation associated with complex **5.1**. The Cp* protons weakly interacted with the *N*-methyl group of the carbene and more weakly with the furthest

downfield NCH$_2$O proton (figure 5.7). This was compared to the ^{1}H-^{1}H NOESY spectrum of **5.2** (figure 5.8), which revealed through-space interactions between the Cp* and *N*-methyl protons, in addition to the Cp* protons interacting with both NCH$_2$O resonances, the methoxy group and also one of the guaiacol protons. The above data suggest that **5.1** is rotationally locked, whereas **5.2** displays many more degrees of rotational freedom, which perhaps explains the broad nature of NMR spectra for the trimetallic complex.
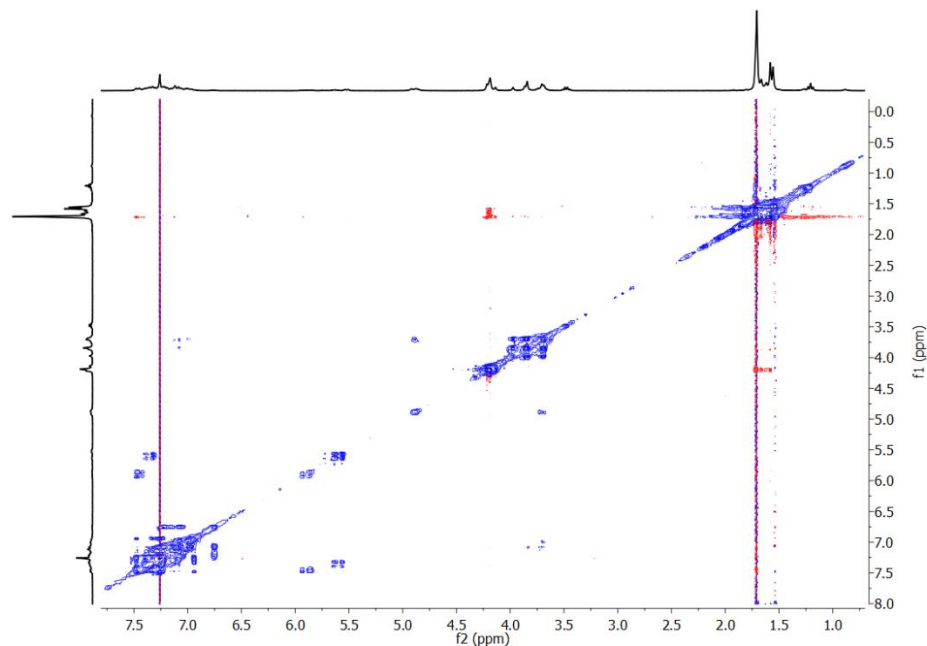
Figure 5.7 NOESY spectrum of 5.1. Through space coupling shown in red.
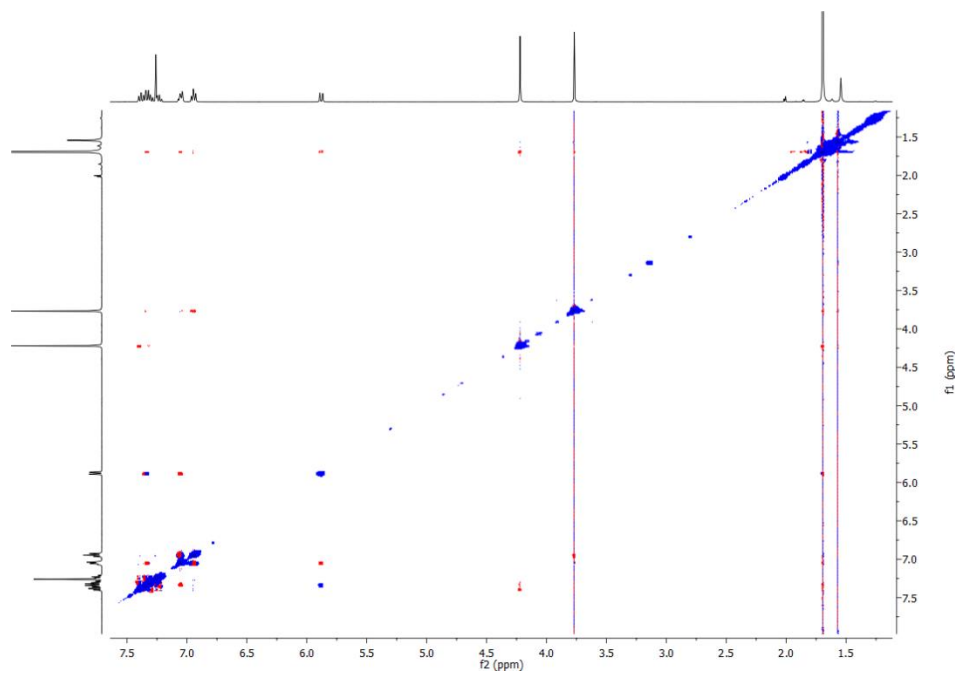
Figure 5.8 NOESY spectrum of 5.2. Through-space interactions shown in red.

Pale yellow rhombohedral crystals of complex **5.1** suitable for diffraction were grown from the diffusion of diethyl ether vapours into an acetonitrile solution of the complex after *ca.* one week. Complex **5.1** crystallised in the hexagonal $R\overline{3}c$ space group. The asymmetric unit (figure 5.9) comprised of one-third of the complex, with **5.1** possessing strict crystallographic C_3 symmetry. A crystal structure could be obtained when collecting data using CuKα radiation, which revealed poorly resolved acetonitrile solvent molecules in the asymmetric unit, but the data was of poor quality due to strongly absorbing heavy atoms. Collecting data using MoKα radiation did resolve the absorption problems caused by the Ir atoms when using CuKα radiation, but the acetonitrile molecules could not be located within the difference map due to poor high angle diffraction, therefore the SQUEEZE routine using PLATON was applied.[34]
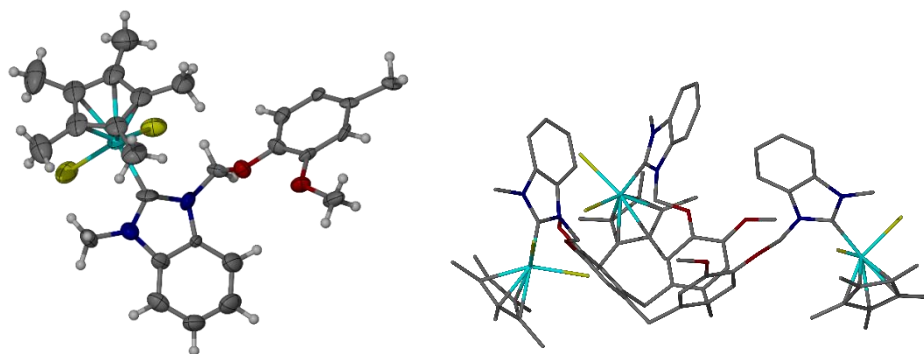
Figure 5.9 Left: Asymmetric unit of 5.1. Ellipsoids are drawn at the 50% probability. Right: Stick model of trimetallic 5.1.

The Ir-C_{NHC} bond length was measured as 2.073(11) Å, comparable to previously reported Ir(III)-NHC complexes.[32] Ir-Cl bond lengths were 2.421(3) and 2.422(3) Å, and an Ir-Cp* centroid distance of 1.810 Å calculated. A C_{arene}-O-C-N_{NHC} torsion angle of 168.9° was measured, with the NHC nitrogen atom lying close to the plane of the CTV arene faces. The Ir(III) centre is pointed away from the CTV bowl, in the direction of the lower rim. The outer rim of the cavitand shields one face of the Ir(III) centre, exerting significant bulk on the system. Only part of the benz-backbone of the NHC lies in the plane of the CTV arenes. Hydrogen bonding interactions between chloride ligands and hydrogen atoms from the *N*-methyl group and a hydrogen atom from the NCH_2O methylene bridge may have arisen, with C⋯Cl separations of 3.318 Å and 3.191 Å respectively. Preagostic interactions between a calculated methylene bridge proton and Ir(III) centres may be present, at a

calculated Ir···H separation of 2.886 Å, with a C-H-Ir angle of 117.53º, obeying the rules proposed by Ellman.[33] Neutron diffraction would confirm preagostic interactions by locating the hydrogen atoms, as opposed to using calculated positions.

Complex **5.1** crystallised as a head-to-head dimer (figure 5.10, left), with π-π stacking interactions between benzo-backbones of the NHC at centroid separation of 3.69 Å. The dimers comprised of a single enantiomer of **5.1**, whilst crystals overall were racemic. The three Ir(III) centres are peripheral to the CTV bowl at Ir···Ir separation of 14.171 Å, *ca.* 3 Å less than that reported for an emissive metallo-cryptophane, although the coordination mode about the Ir(III) centre and the ligand groups on the CTV bowl in both cases are considerably different because the Ir(III) centres were sited on equatorial positions of the capsule.[35] The space filling diagram (figure 5.10, right) also shows the ligand buttressing encases Ir(III) centres (light blue) with high efficiency, and are only slightly exposed above the two chloride ligands. This may have implications from a catalytic point of view, however, it is worth noting that the halides are displaced in catalytic transformations involving Ir(III), and some flexibility will exist in this system, so may not suppress the catalytic viability of **5.1**.
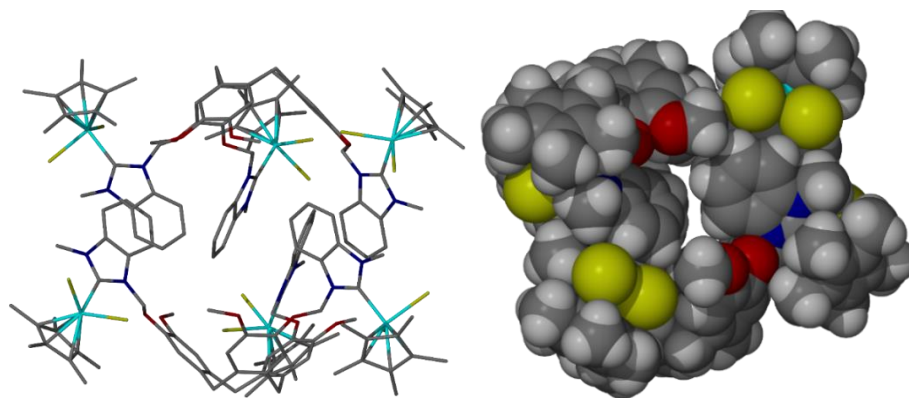
Figure 5.10 Left: dimeric aggregation of 5.1. Right: space-filling model of dimer.

Complementary close packing of Cp* ligands with a neighbouring CTV-arene face were observed, with closest contacts of 3.632 Å, but the groups are too far offset to be engaging in π-π stacking interactions. The dimer does contain three small windows intersecting the equator of the capsular assembly, potentially allowing the incorporation of guest species within the pore (figure 5.10). The internal and external void space was calculated as *ca.* 9700 Å^3 using a 1.2 Å probe.[34] Attempts to

encapsulate the small, flexible guest DME (dimethoxyethane) by taking advantage of H-atoms held in place on the benzimidazole backbone as potential hydrogen bonding sites were unsuccessful, and no evidence of DME encapsulation crystallographically, or in solution (^{1}H NMR spectroscopy) was attained. Solution-state encapsulation of *o*-carborane and ferrocene was attempted but no evidence to suggest guest binding was obtained.

The unit cell of **5.1** was extremely large ($a = b = 23.5277(12)$, $c = 77.681(4)$ Å), containing twelve discrete complexes. Attempts to solve the structure after indexing to a smaller unit cell were unsuccessful. Dimeric aggregates of **5.1** zig-zag along the crystallographic *c*-axis through complementary close-packing of Cp* and arene face units, leaving significant solvent-filled voids throughout the structure.
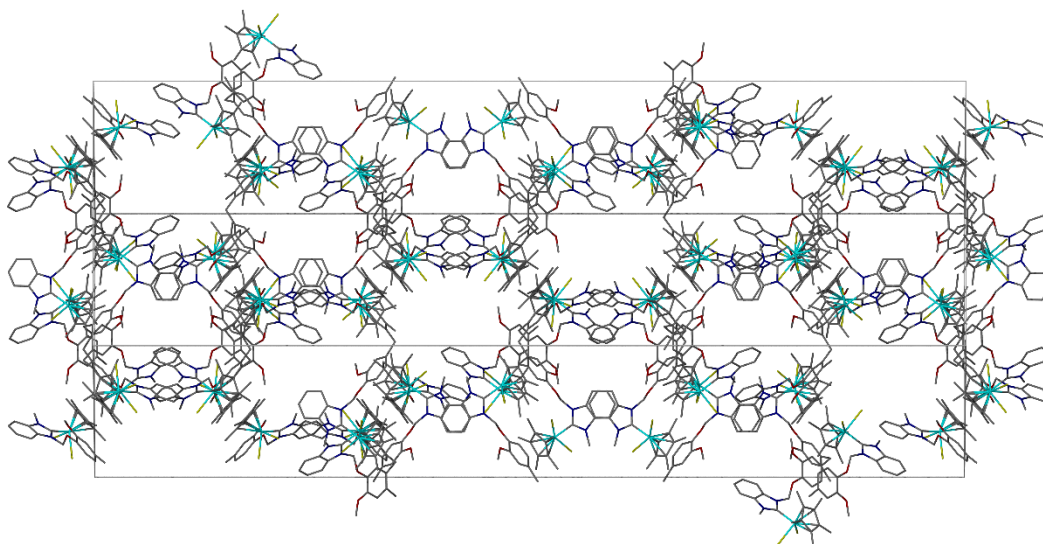
Figure 5.11 Unit cell of 5.1.

Crystals were brittle, and when attempting to obtain SCXRD data, a number did break upon contact with the MiTeGen loop. Optical microscopy images of the crystals showed their rhombohedral shape, whilst the SEM images displayed lots of defects and cracks, attributed to exposure to the vacuum chamber prior to imaging (figure 5.12).
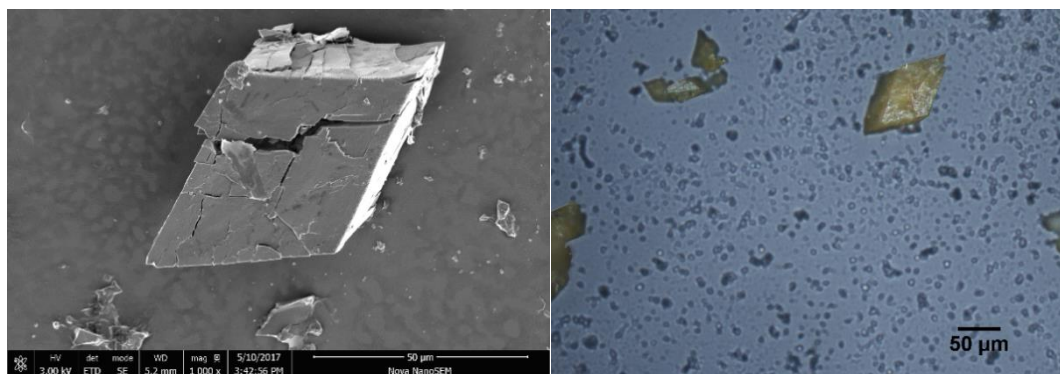
Figure 5.12 SEM (left) and optical microscopy (right) images of 5.1 crystals.

Crystals of **5.2** suitable for diffraction analysis could be grown from the diffusion of pentane vapours into a dichloromethane solution of the complex. The structure was solved in the orthorhombic *Pbca* space group. And the asymmetric unit comprised a full complex molecule. The guaiacol group is of opposite orientation in the crystal structure of **5.2** compared to that of **5.1**, and the methoxy group is aligned away from the Ir(III) centre (figure 5.13). The space filling model of **5.2** shows the ancillary ligands afford excellent steric protection of the metal centre.
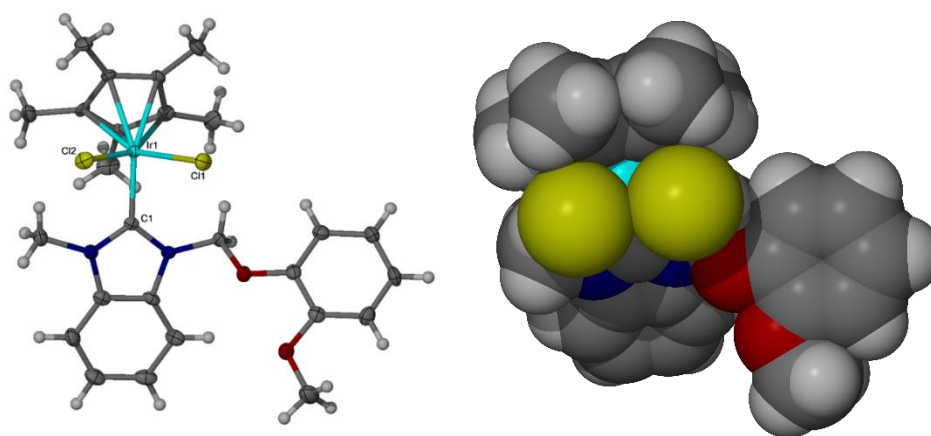
Figure 5.13 Left: asymmetric unit of 5.2. Ellipsoids are drawn at the 50% probability. Right: space-filling diagram of 5.2.

Bond lengths and angles about the Ir(III) centre of **5.2** bore stark similarities to those in **5.1**, with bond lengths being almost identical, and angles through Ir(III) varying by 2° at most (table 5.1). The C_{arene}-O-C-N_{NHC} torsion angles were also comparable, with that in **5.1** being slightly less than in **5.2**. The methoxy group of the guiacol NHC wingtip in **5.2** is aligned away from the Ir(III) centre, as opposed to **5.1**, where it aligns towards the metal centre. Complex **5.2** exhibited weak CH···π interactions

between a Cp* methyl group and the π-cloud of a neighbouring Cp* ligand at a C_{Me}-Cp* centroid separation of 3.4 Å.

Table 5.1 Selected bond lengths (Å) and angles (°) for 5.1 and 5.2

	5.1	5.2
Ir-C$_{NHC}$	2.073(11)	2.027(4)
Ir-Cl1	2.421(3)	2.4155(11)
Ir-Cl2	2.422(3)	2.4084(11)
Ir-Cp* centroid	1.810 (measured)	1.811
Cl1-Ir-Cl2	85.92(12)	86.33(4)
C$_{NHC}$-Ir-Cl1	90.7(3)	92.44(13)
C$_{NHC}$-Ir-Cl2	91.2(3)	93.09(12)
Cl1-Ir-Cp* centroid	125.07	124.14
Cl2-Ir-Cp* centroid	122.65	122.53
C$_{NHC}$-Ir-Cp* centroid	129.13	127.31
C$_{arene}$-O-C-N$_{NHC}$	168.9	174.1

5.2.1 Catalytic evaluation of 5.1 and 5.2

Complexes **5.1** and **5.2** were examined as catalysts in the TH of acetophenone, and their activity compared to the Ir(III) precursor, [Ir(Cp*)(Cl)$_2$]$_2$. Catalyst loading was measured by mol% Ir, because **5.2** contains one metal centre, the precursor two, and **5.1** three. The reactions were also carried out in the absence of metal catalyst because the base-catalysed[36] TH and disproportionation[37] of ketones and alcohols are known pathways following a similar mechanism to the Meerwein-Pondorf-Verley reaction, where the alkali metal cation templates the reaction. A fourfold increase in conversions was noted when employing Ir(III) catalysts, suggesting the Ir(III) complexes are catalytically active in the TH of acetophenone..
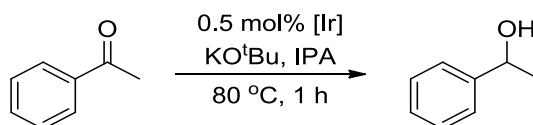
Scheme 5.3 Transfer hydrogenation of acetophenone using Ir(III) complexes as catalysts.

Table 5.2 Conversions for the transfer hydrogenation of acetophenone using 5.1-2 as catalysts, and control reactions.

Complex	Conversion (%)
Transition metal and base-free	0(±0)
Transition metal-free	4(±2)
[Ir(Cp*)(Cl)$_2$]$_2$	27(±4)
5.1	18(±3)
5.2	18(±5)

Conversions are the average of 2 runs and were obtained using ^{1}H NMR spectroscopy by comparing the methyl resonance of 1-phenylethanol and 1,4-dimethoxybenzene as an internal standard.

Conversions overall were low, with all three Ir(III) complexes displaying somewhat similar activities. **5.1** and **5.2** were expected to have lower conversions than the Ir(III) dimer, which is capable of splitting upon nucleophilic attack, affording an extra active site. Ir(III) is a kinetically inert metal, and complexes often display pronounced stability. **5.1** and **5.2** bear four strongly bound ligands in Cp*, an NHC and two chloride ligands, which are likely to exchange slowly in solution. Complexes **5.1** and **5.2** were similarly active, indicating that the three Ir(III) centres of **5.1** are behaving independently of one another. A typical inner-sphere mechanism is likely occurring for **5.1** and **5.2**, with the methoxy group being a poor hydrogen acceptor. Kühn and co-workers have previously demonstrated that weaker NHC donors and increased bulk enhance TH catalysis, so such similar conversions observed between **5.1** and **5.2** were unexpected.[18] Sarkar and co-workers have prepared a triply metallated disk-shaped ligand, which displayed enhanced activities compared to a monometallic analogue through π-π stacking interactions between NHC backbones.[38]

A strategy employed to target more active catalysts was to abstract the halide ions and replace with more labile solvent molecules, which are easily displaced in catalytic transformations, affording an active site on the catalyst. This reaction was carried out in acetonitrile in the presence of Ag(I) salts (scheme 5.4). Such manipulations are widely used in Ir(III) chemistry, both with NHC ligands and also phenylpyridine derivatives for luminescent applications.[39] Halide abstractions

involving **5.1** were unsuccessful, both when employing $AgPF_6$ and the $[BAr^F]^-$ anion (BAr^F = tetrakis-[3,5-bis(trifluoromethyl)phenyl]borate, in order to enhance solubility in less polar solvents. An insoluble white solid precipitated after 24 h, and HRMS of the reaction mixture indicated no Ir was present. Crystals did grow from solution when employing $AgPF_6$, but these proved to be $[Ag(MeCN)_4]PF_6$. This suggests that the halide abstraction may have partially occurred, but as the overall charge and degree of metathesis increases, the solubility of the system decreases. After the unsuccessful halide abstraction, altering the oxidation state of the Ir precursor could be an approach to catalyst optimisation. Ir(I) complexes are often stabilised by alkene ligands, which form labile interactions with metal ions, affording two active sites on the metal centre. Additionally, the oxidative addition of ligands at Ir(I) is facile, yielding Ir(III) complexes and facilitating a number of mechanistic processes for the same reaction. Ir(I)-NHC complexes are viable targets by applying similar methodology to the preparation of **5.1** and **5.2**.
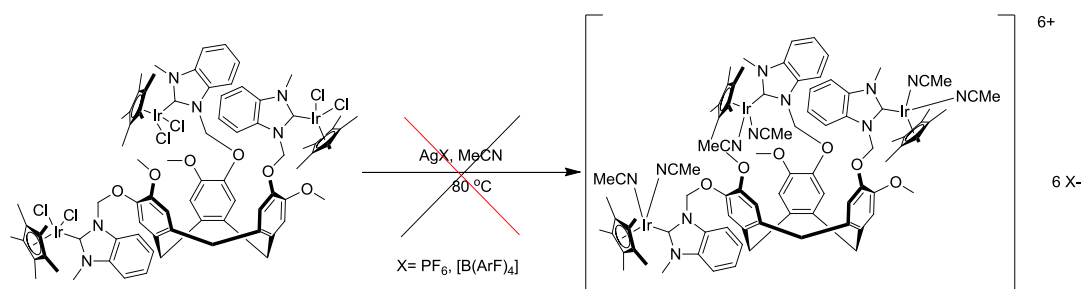
Scheme 5.4 Attempted halide abstraction of 5.1.

5.2.2 Cell-line studies of 5.1 and 5.2

Previous work by McGowan and Sadler have shown Ir(III), Rh(III) and Ru(II) half-sandwich complexes to be effective anti-cancer agents *in vitro*.[40-42] Liu and co-workers have recently demonstrated half-sandwich Ir(III)-NHC complexes as promising anti-cancer drugs, with IC_{50} values as low as 2.9 μM against a cervical cancer cell-line.[43] In collaboration with Pablo Carames-Mendez of the McGowan group, complexes **5.1** and **5.2** were investigated *in vitro* against the pancreatic carcinoma Mia PaCa-2 using MTT-based assays. An IC_{50} value of < 20 μM is classed as highly active, 20-50 μM as moderately active, 50-100 μM as poorly active and > 100 μM inactive. **5.2** proved to be inactive against the pancreatic cancer cell-line, whilst **5.1** gave an IC_{50} value of 97.57 ± 4.20 μM, suggesting poor activity and overlapping with inactive drug molecules. Compounds **5.1** and **5.2** were also examined against healthy cells where a high IC_{50} value is desired, and both gave

values of > 100 μM, suggesting they are non-toxic. Hydrolysis of M-Cl bonds to form aqua species is a possible *in vivo* pathway for the activation of metallo-drugs, but Ir(III) complexes **5.1** and **5.2** may be too kinetically inert to be hydrolysed in hydrous media.[44] The high barriers to activation may also explain the low catalytic activities observed for **5.1** and **5.2**.

5.3 Synthesis and characterisation of Ir(I) and Rh(I) complexes

5.3.1 Preparation of Ir(I) complexes

One pathway to potentially prepare more active catalysts would be the introduction of a more labile ligand, such as an alkene. In addition, decreasing oxidation state from Ir(III) to Ir(I) may allow for more favourable energetics in the oxidative addition steps during catalytic transformations. Alkene ligands are often used to stabilise low-valent transition metals. Their propensity as π-acids gives them excellent back-bonding properties, facilitating stabilisation of complexes of electron-rich metals such as Ir(I). *Bis*-ethene and *bis*-cyclooctene complexes derived from dimeric olefin-bearing precursors are known, but in many instances are not isolable, or are highly unstable.[45-47] The chelate effect offered by 1,5-cyclooctadiene (COD) overcomes this, yielding often air-stable complexes. Iridium-COD complexes have a rich history in catalytic transformations, with Crabtree's catalyst, $[Ir(COD)(py)(PCy_3)]PF_6$ being a much-documented hydrogenation catalyst.[3]

Ir(I) complex **5.3**, could be prepared following similar methodology to that for **5.1** and **5.2**, with an alteration to solvents used (scheme 5.5). Ligand **4.3** was soluble in MeCN, whereas **5.3** had a high affinity for chlorinated solvents, and was barely soluble in MeCN, therefore a 1:1 mixture of MeCN and $CHCl_3$ was applied. EDX analysis was also carried out on a sample of **5.3**, which confirmed the absence of iodine, thus eliminating the possibility of halide mixing at Ir(I) as a competing reaction. The monometallic complex 1,5-cyclooctadiene chloro (1-methyl-3-((2-methoxyphenoxy)methyl)benzimidazol-2-ylidene)iridium(I), **5.4** was also prepared.
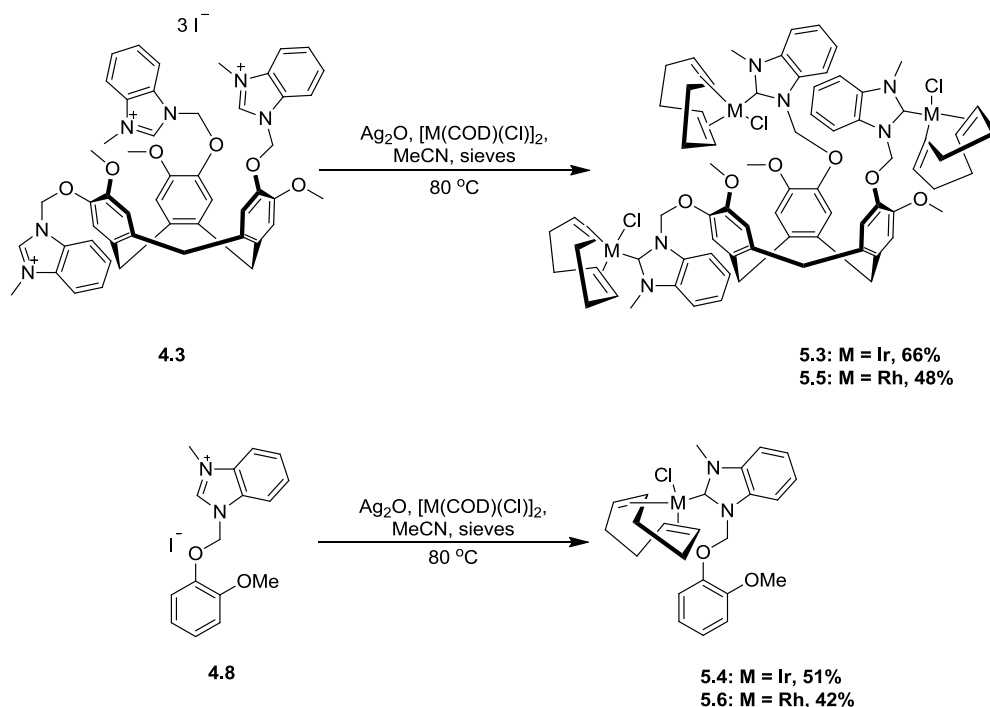
Scheme 5.5 Synthesis of Ir(I) and Rh(I)-NHC complexes 5.3-5.6

HRMS once again proved the most effective tool for characterising complex **5.3**, although there were discrepancies (Figure 5.14). The major peak observed was $\{M-3Cl\}^{3+}$ with m/z = 580.5009 (calculated = 580.5100). Two other dominant peaks were noted, but were poor matches to the calculated m/z peaks despite bearing the same isotope pattern to that expected. A $\{M-Cl\}^+$ was observed with m/z = 1812.5251 (calculated 1812.4722) and m/z = 883.7722, five units from the calculated m/z of 888.2497 for the $\{M-2Cl\}^{2+}$ fragment. A sister peak with m/z = 888.2411 was adjacent to the dominant peak, and both displayed the characteristic isotope pattern simulated for these fragments. An imidazolium iodide ligand was employed alongside an iridium chloride precursor. If AgI was solubilised, halide exchange upon ionisation may offer an explanation to the poorer HRMS matches, although changes to isotope patterns would also occur.

Three peaks were observed in the HRMS of **5.4**, with the dominant peak at m/z = 569.1786 (calculated 569.1775) matching the $\{M-Cl\}$ peak (figure 5.15). A peak at m/z = 1162.3563 best matches $\{M_2-COD+MeCN+Na\}^+$ (calculated 1162.2133). A third peak was also present with m/z = 837.2985 (calculated 837.2986) which matched the rearrangement product $\{Ir(COD)(NHC)_2\}^+$. Relative ^{1}H NMR integrals between NHC and COD eliminated this from being a side-

product in the reaction. Herrmann and co-workers previously reported the transfer of NHC ligands between Rh(I) centres, which would be plausible for Ir(I) analogues.[48] Such rearrangement must be considered for Rh(I)-NHC complexes prepared.
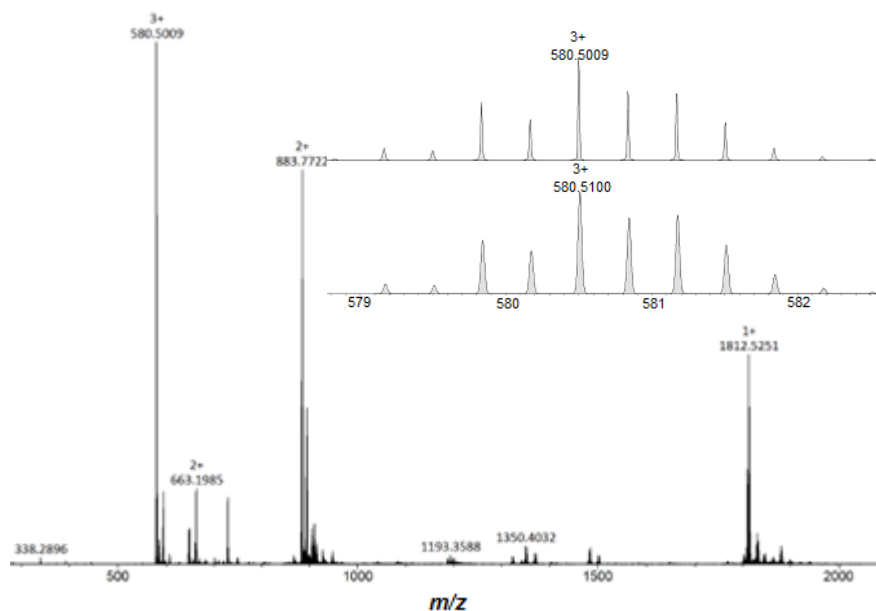
Figure 5.14 HRMS of 5.3. Inset: observed (top) vs simulated (bottom) isotope pattern for *m/z* **580.5009, {M-3Cl}³⁺.**
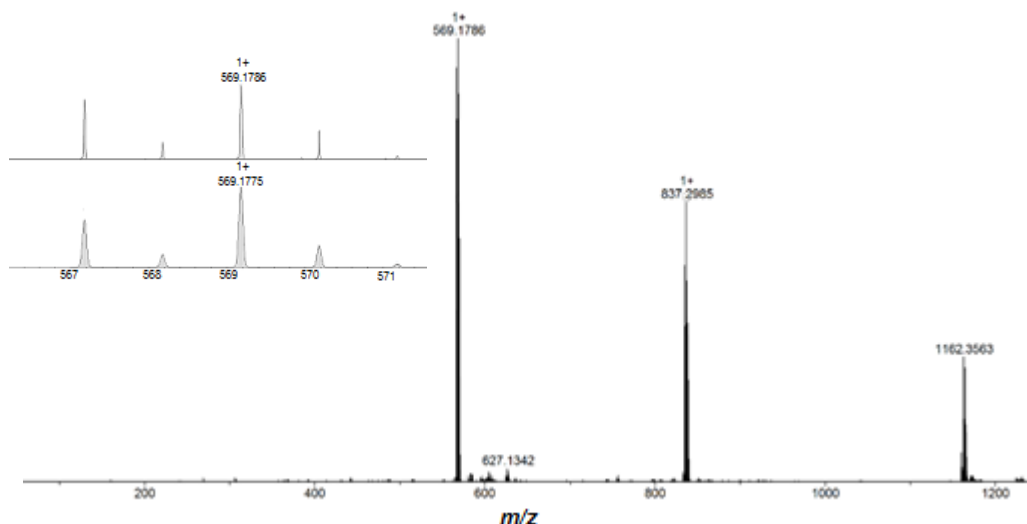
Figure 5.15 HRMS of 5.4. Inset: observed (top) vs simulated (bottom) isotope pattern for *m/z* **569.1786, {M-Cl}⁺.**

As anticipated, the ¹H NMR spectrum of **5.3** was broad, but peaks did overlap with monometallic derivative **5.4** (figure 5.16). Furthermore, no imidazolium peaks were present downfield of 8 ppm, indicating the deprotonation of all imidazolium

groups. The ^{1}H NMR spectrum of **5.4** revealed NCH$_2$O methylene bridge separated by *ca.* 1 ppm which, whilst less than complex **5.3**, is significant. The most upfield of these protons in both **5.3** and **5.4** displayed similar chemical shifts, indicating no further shielding of this group by the cavitand. Two broad peaks at 4.74 and 3.55 ppm coupled with one another in the COSY NMR spectrum, consistent with the *endo-* and *exo-* protons of the CTV lower rim. The peak at 4.75 ppm appears at the same chemical shift as a COD resonance in monomer **5.4**, which could explain the higher integral of this peak. A number of broad peaks in the ^{1}H NMR spectra of both **5.3** and **5.4** between 1.6 and 3 ppm coupled with one another, and were therefore assigned as COD protons. The *N*-methyl and methoxy resonances in **5.4** were observed at 4.19 and 3.89 ppm respectively, and peaks were observed at similar chemical shifts in **5.3**. Surprisingly however, the methoxy resonance in **5.3** appeared to split into two peaks, with a second sharp peak at 3.65 ppm coupling to the same carbon atom. Neither of these peaks couple to one another in the COSY NMR spectrum (appendix), but they are both associated with the same carbon resonance in the HMQC spectrum (appendix), and ^3J coupling from both peaks to the *ipso*-carbon of the CTV rim was observed in the HMBC spectrum. The reasoning behind such splitting remains unclear, but the absence of ^2J coupling between these peaks may imply a break in C_3-symmetry.
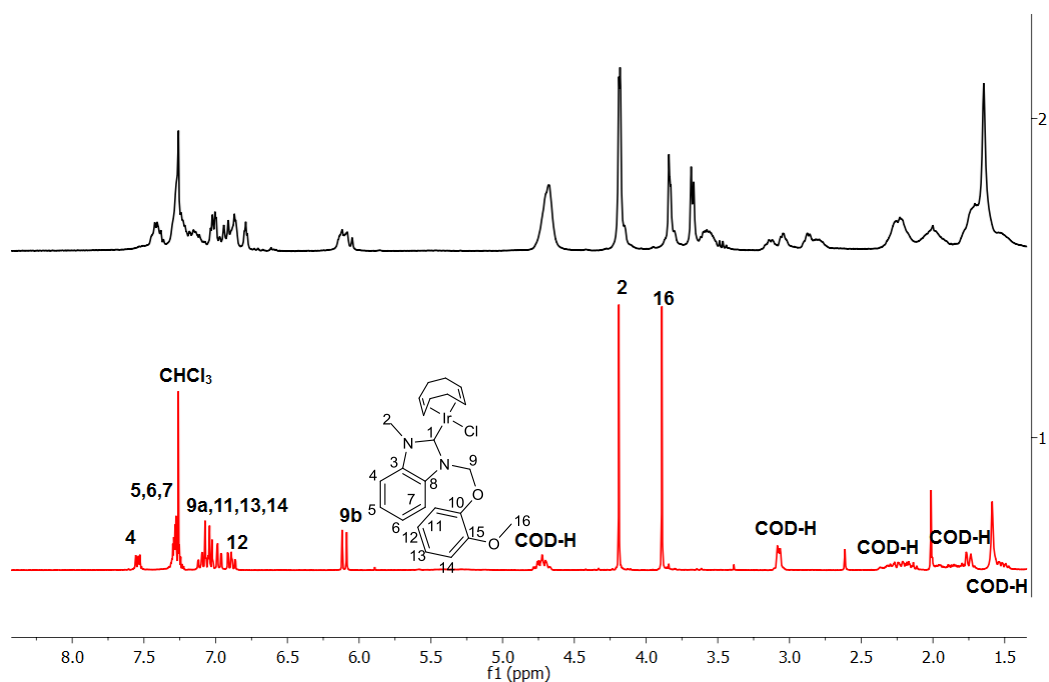
Figure 5.16 ^{1}H NMR spectra (300 MHz, 293 K, CDCl$_3$) of 5.3 (top, black trace) and 5.4 (bottom, red trace).

A $^{13}C\{^1H\}$ NMR spectrum could not be obtained for **5.3**, therefore HMQC and HMBC spectroscopy were once again important tools (figure 5.17). Significantly, the *N*-methyl resonance (^1H, 4.2 ppm) coupled with a single observed ^{13}C peak at *ca.* 200 ppm in the HMBC spectrum, implying a single C_3-symmetric NHC complex. The NHC carbene resonance is sensitive towards the Lewis acidity of a metal centre, which is dependent upon both the metal ion itself and the donor strength of co-ligands, shifting downfield when greater electron density is associated with the Lewis acidic metal.[49, 50] Hence, it was unsurprising to see a near 30 ppm difference between carbenic chemical shifts in **5.1** and **5.3**.
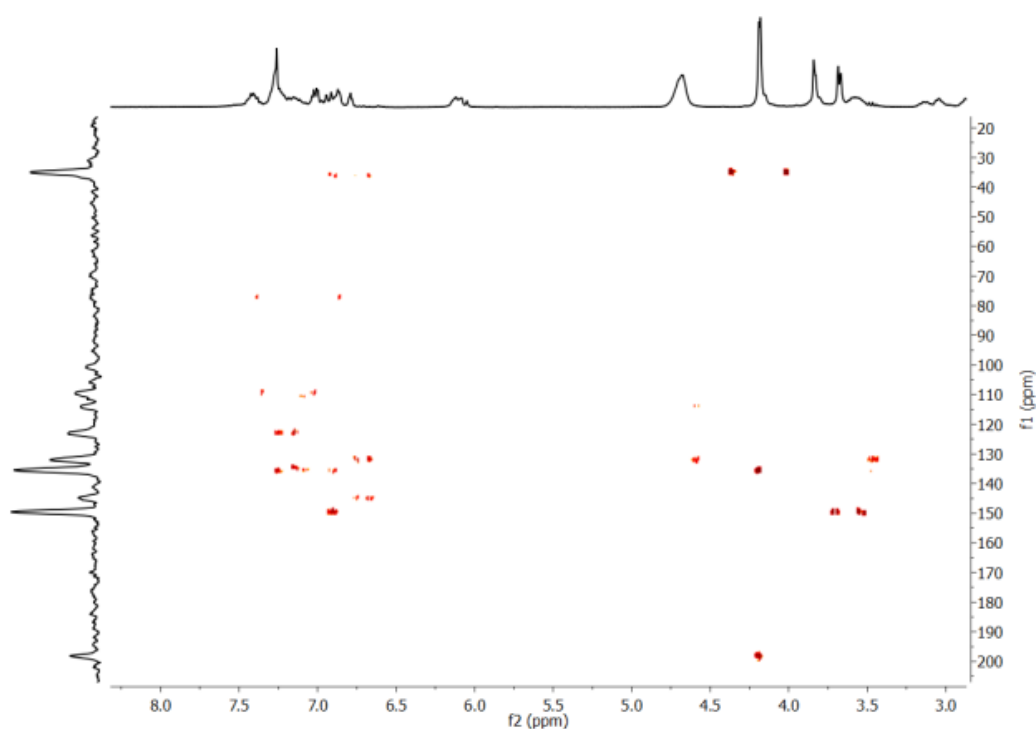
Figure 5.17 HMBC NMR spectrum of 5.3.

A $^{13}C\{^1H\}$ NMR spectrum was attainable for **5.4** (figure 5.18). Significantly, the carbenic carbon was located at 193.28 ppm, comparable to the position in the trimetallic complex **5.3**, and once again was corroborated by HMBC analysis, where long range C-H coupling was observed between the carbenic carbon and both the NHC R-groups. The NCH_2O methylene bridge was sited at 78.89 ppm and one of five CH_2 groups present in **5.4** as confirmed by DEPT-135 NMR spectroscopy, which also included four $COD-CH_2$ resonances.
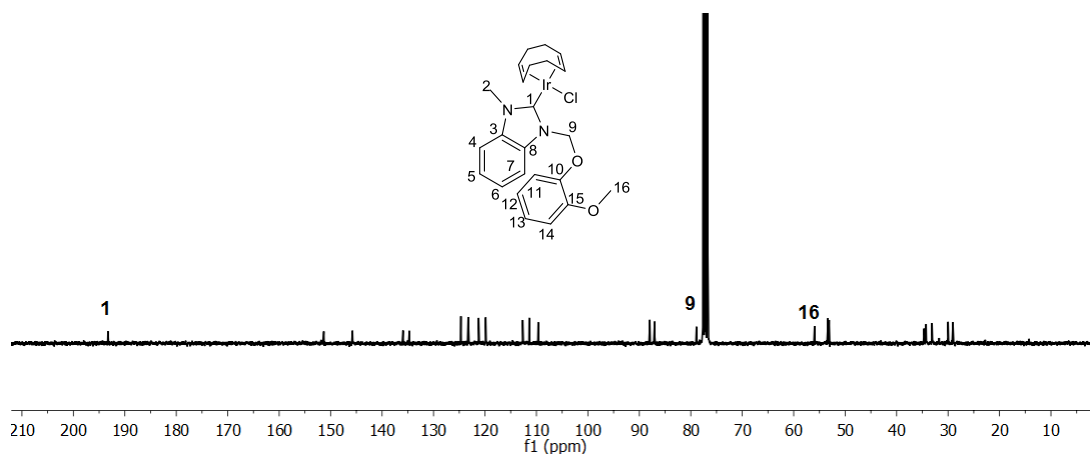
Figure 5.18 ^{13}C{^{1}H} NMR spectrum (75 MHz, 293 K, CDCl$_3$) of 5.4.

Complex **5.3** could not be crystallised despite repeated attempts from a range of vapour diffusion and slow-evaporations containing the limited number of solvents **5.3** would dissolve in (DCM, CHCl$_3$, DMF, DMSO). However, yellow single crystals of **5.4** suitable for diffraction could be grown from the diffusion of pentane into a dichloromethane solution. The structure was solved in the triclinic $P\bar{1}$ space group, and the asymmetric unit comprised of two crystallographically distinct molecules of **5.4** (figure 5.19).
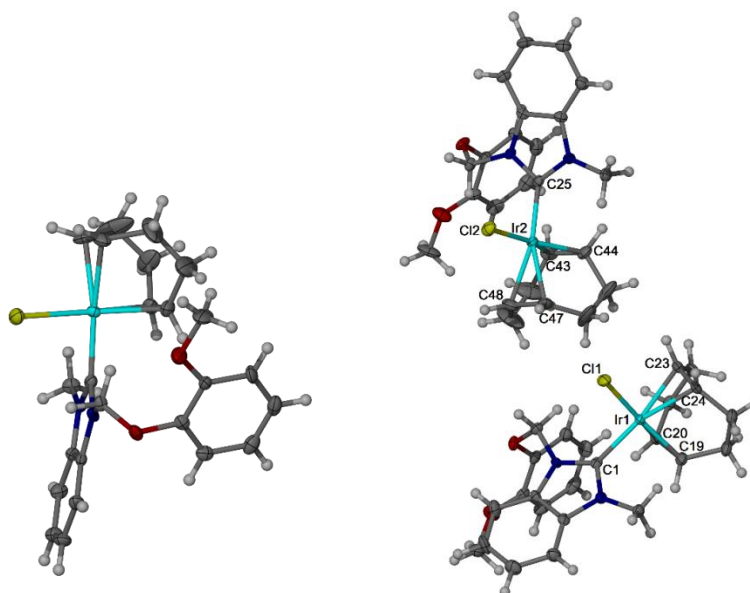
Figure 5.19 Molecular structure of 5.4 (left) and asymmetric unit (right). Ellipsoids are drawn at the 50% probability.

Table 5.3 Selected bond lengths (Å) and angles (º) in 5.4.

Ir1-Cl1	2.3519(10)	Ir2-Cl2	2.3632(10)
Ir1-C1	2.018(4)	Ir2-C25	2.004(4)
Ir1-C19	2.122(4)	Ir2-C43	2.102(4)
Ir1-C20	2.090(4)	Ir2-C44	2.096(5)
Ir1-C23	2.201(4)	Ir2-C47	2.193(5)
Ir1-C24	2.165(4)	Ir2-C48	2.184(5)
C1-Ir1-Cl1	87.63(11)	C25-Ir2-Cl2	86.21(12)
C1-Ir1-C19	94.11(16)	C25-Ir2-C43	92.71(17)
C1-Ir1-C23	167.36(16)	C25-Ir2-C44	94.81(18)
C19-Ir1-Cl1	164.65(12)	C25-Ir2-C48	158.14(19)
C19-Ir1-C23	89.83(17)	C44-Ir2-Cl2	158.19(14)
C20-Ir1-Cl1	155.55(12)	C44-Ir2-C48	94.2(2)
C20-Ir1-C23	81.21(17)	C47-Ir2-Cl2	91.60(14)
C23-Ir1-Cl1	91.75(12)	C48-Ir2-Cl2	92.73(15)

Ir(I) centres in both equivalents of **5.5** display a pseudo square-planar geometry. The COD ligands in both equivalents are of slightly different orientations. COD ligand coordinated to Ir1 is slightly staggered when looking down the d_z axis of Ir(I) centres, whereas Ir2 coordinates to a COD ligand which is eclipsed along a mirror plane. The C_{arene}-O-C-N_{NHC} torsion angles in both cases were of similar rotations in opposite orientations, measured at 73.33 and -78.15º. The COD ligands on both equivalents of **5.5** in the asymmetric unit were of slightly different orientations. C=C bond lengths on the COD ligands ranged between 1.395(7)-1.429(7) Å, implying appreciable back donation from the electron-rich Ir(I) centres into the alkene π^* orbitals. Ir-C_{COD} bond lengths *trans* with respect to the NHC ligand were slightly longer than the Ir-C *cis*-COD lengths as a consequence of the strong *trans* influence of the carbene.

5.3.2 Preparation of isostructural Rh(I) complexes

As a consequence of the lanthanide contraction, Rh(I) and Ir(I) complexes are chemically similar, so would be comparable to the parent Ir(I) complexes reported in this chapter. Iridium does not possess spin-active nuclei, whereas ^{103}Rh is NMR active ($I = \frac{1}{2}$) with 100% abundance, affording a potentially powerful spectroscopic handle. Whilst $^{13}C\{^1H\}$ NMR spectra were unlikely to be viable analytical tools for CTV-complexes, the carbenic carbon and four alkenyl COD carbons would appear as doublets in the $^{13}C\{^1H\}$ NMR spectra, and also heteronuclear 2D NMR experiments, due to Rh-C coupling interactions.

Trimetallic Rh(I0 complex **5.5** and monometallic **5.6** were prepared following the same methodology employed for **5.3** and **5.4**, albeit obtained in lower yields by employing [Rh(COD)(Cl)]₂ as the precursor. The ^1H NMR spectrum of complex **5.5** (figure 5.20) was near-identical to **5.3**. No peaks were observed beyond 8 ppm, suggesting a single complex had been isolated, with no evidence of partial reactivity. The methoxy protons appeared at 3.6 and 3.8 ppm again, and COSY NMR spectroscopy revealed the splitting of the NCH₂O methylene bridge to two inequivalent resonances at 6.1 and 7.3 ppm, and the CTV *endo-* and *exo-* protons were attributed to broad peaks at 3.5 and 4.4 ppm. The same splitting for methoxy resonances was observed in **5.5** as in trimetallic complex **5.3**. This was not observed in **5.6**, as was also the case for Ir(I) monomer **5.4**.

The major fingerprint in the NMR assignment of **5.5** came in the HMBC spectrum (figure 5.21). The *N*-methyl protons coupled to two peaks at *ca.* 198 ppm, which were attributed to the carbenic doublet. J_{Rh-C} was measured as *ca.* 80 Hz, which whilst wider than a typical Rh-C coupling constant,[27] is an approximation because collection of $^{13}C\{^1H\}$ NMR data was impeded.
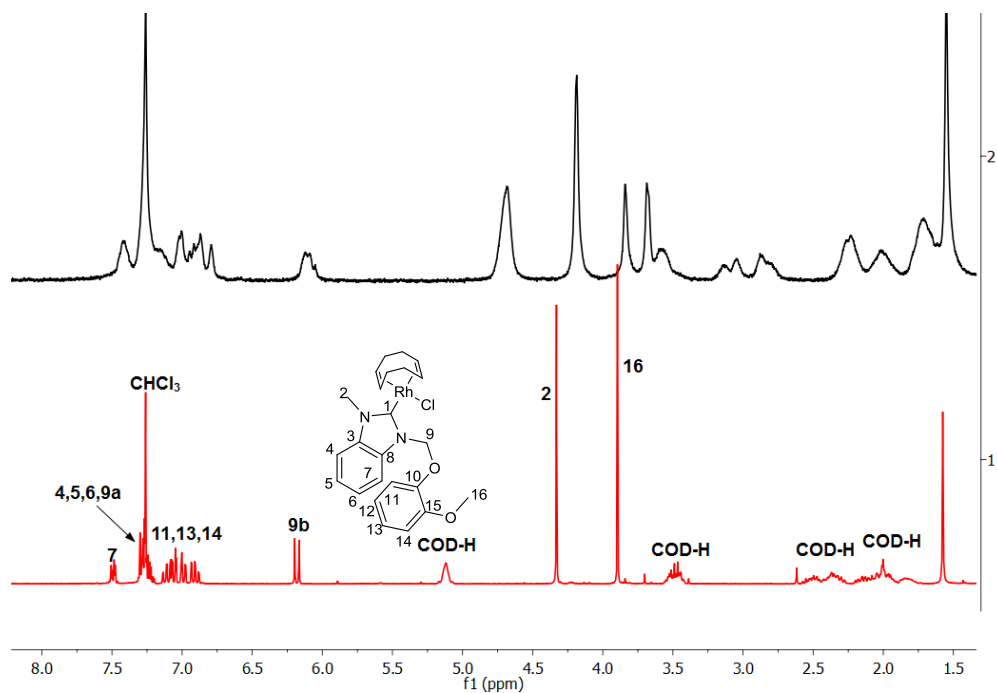
Figure 5.20 ^{1}H NMR spectra (300 MHz, 293 K, CDCl$_3$) of **5.5** (top, black trace) and **5.6** (bottom, red trace).
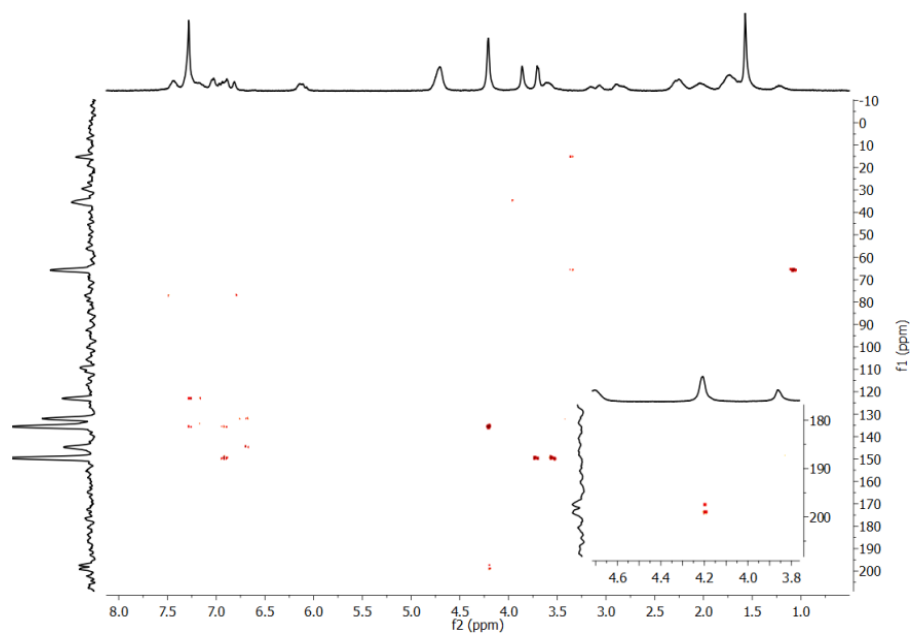
Figure 5.21 HMBC spectrum of **5.5**. Inset: ^3J coupling interaction between N-methyl protons and carbenic carbon.

The ^{13}C{^{1}H} NMR spectrum of **5.6** revealed the carbenic carbon appeared at 198.29 ppm, with a J_{Rh-C} of 51.0 Hz which is typical for a Rh-C coupling constant (figure 5.22).[27] Four further doublets were observed, which were attributed to the COD alkene carbons.
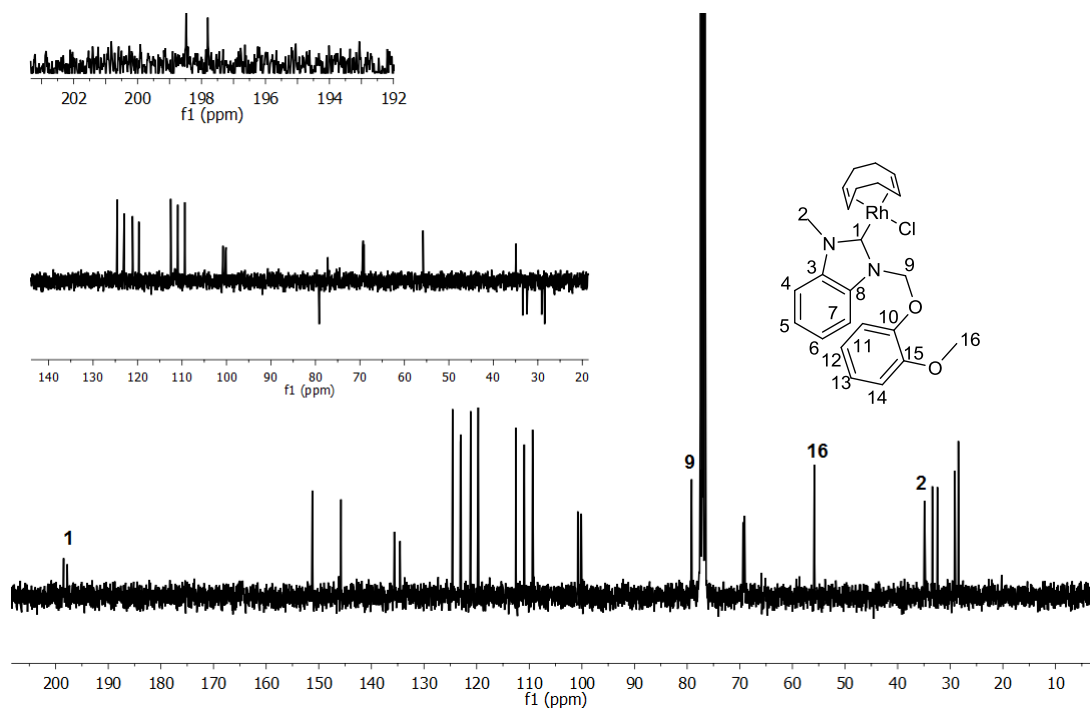
Figure 5.22 ^{13}C{^{1}H} NMR spectrum (75 MHz, 293 K, CDCl$_3$) of 5.6. Top inset: expansion of carbenic resonance. Lower inset: DEPT-135 spectrum.

Kück and Peris reported a trimetallic Rh(I)-NHC complex fused onto the related TBTQ cavitand and observed two sets of carbenic resonances in the ^{13}C{^{1}H} NMR spectrum, with the complex displaying pseudo-C_3v symmetry.[30] This was attributed to the lack of free rotation about the Rh-C bond caused by their steric repulsion from the *tert*-butyl wingtips. A lack of free rotation is evident in **5.5**, but only one carbenic resonance was observed in the HMBC NMR spectrum, suggesting atropisomers about the Rh-C bond may not be significant in this case, and the restricted rotation may be about the NCH$_2$O group.

HRMS in the case of **5.5** bore similarities to Ir(I)-NHC complex **5.3**, with the dominant peak being {M-3Cl}$^{3+}$ with m/z = 491.1194 (calculated = 491.1200) (figure 5.23). A {M-2Cl}$^{2+}$ peak was observed at m/z = 754.1630 (calculated 754.1648). The 2+ peak at m/z = 639.1764 may be a consequence of ligand scrambling, with [{Rh(NHC)$_2$(COD)}{Rh(NHC)(COD)}·H$_2$O]$^{2+}$ bearing a calculated m/z of 640.1859.

The HRMS of **5.6** was diagnostic, and the spectrum comprised of the analogous peaks observed when interpreting **5.4**. The dominant peak was {M-Cl}$^+$ with m/z = 479.1218 (calculated 479.1201), with the simulated isotope pattern displaying an excellent match to the observed data (figure 5.24). Similarly to

complex **5.4**, ligand-scrambling was observed in the HRMS, with $\{Rh(NHC)_2(COD)\}^+$, $m/z = 747.2411$ (calculated 747.2413) and $\{[Rh(NHC)_3(Cl)]+Na+H_2O\}^+$ $m/z = 984.2436$ (calculated $= 984.2410$) detected. ^{1}H NMR spectroscopy suggested the mono-NHC complex had exclusively been prepared, and ligand scrambling was consequence of ionisation.
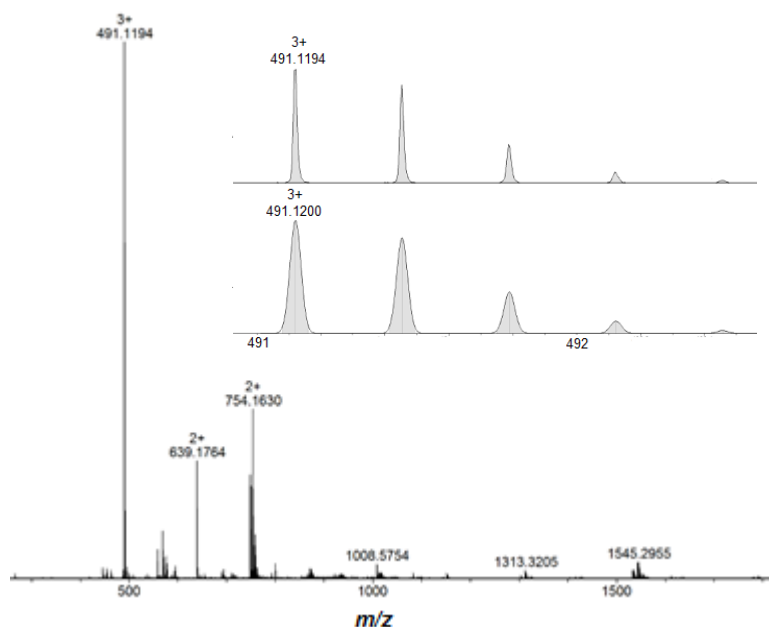
Figure 5.23 HRMS of 5.5. Inset: Observed (top) vs simulated (bottom) isotope pattern of *m/z* 491.1194, {M-3Cl}$^{3+}$.
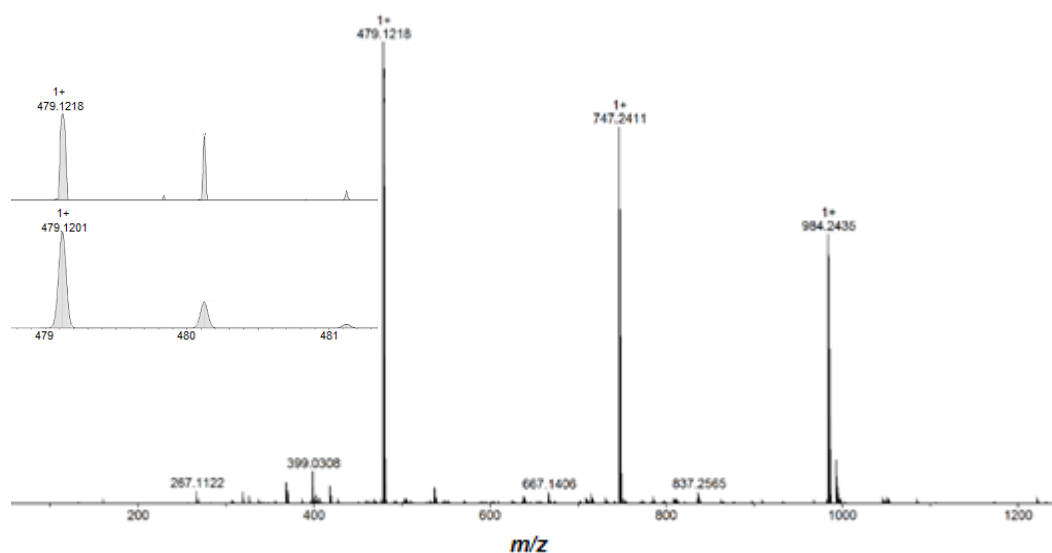
Figure 5.24 HRMS of 5.6. Inset: Observed (top) vs simulated (bottom) isotope pattern for *m/z* 479.1218, {M-Cl}$^+$.

Complex **5.6** could be crystallised from the diffusion of pentane into a dichloromethane solution of complex. The crystal structure was solved in the

triclinic $P\bar{1}$ space group and the asymmetric unit was isostructural to complex **5.4**, comprising of two crystallographically inequivalent complex molecules (figure 5.25). Rh-C_{NHC} bond lengths were measured as 2.004(3) and 2.018(3) Å, identical to the isostructural Ir(I)-complex **5.4**. Complex 2 within the asymmetric unit (bearing Rh2) displayed π-π stacking interactions between guaiacol units of the same equivalency at separation of 3.92 Å and as expected for the d^8 metal cation, both equivalents of complex within the asymmetric unit displayed *pseudo*-square-planar geometry. The *trans*-influence of the NHC ligand is again subtly displayed, with *trans*-Rh-alkene bonds being ca. 0.1 Å longer than the *cis*-Rh-alkene bond with respect to the NHC ligand.
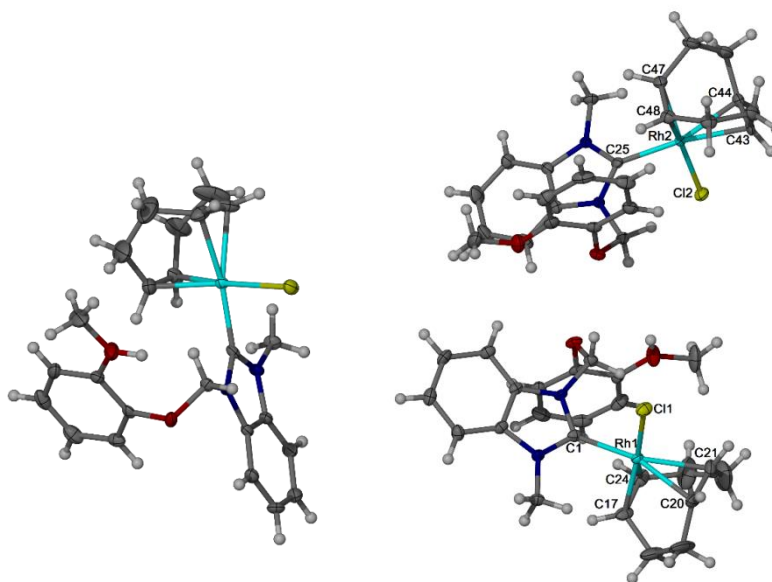
Figure 5.25 Left: Molecular structure of 5.6. Right: asymmetric unit. Ellipsoids are drawn at the 50% probability.

Complexes **5.3** and **5.5** were intended to be investigated as catalysts in TH reactions, but only displayed solubility in solvents unsuitable for catalytic transformations such as DCM and DMSO, which are either base-sensitive, or contain groups which may competitively react with substrates.

5.4 Ru(II)-NHC complex synthesis and characterisation

One investigative line to optimise TH catalysis would be to move to Ru(II). The precursor [Ru(*p*-cymene)(Cl)$_2$]$_2$ is a common entry point to Ru(II) organometallic chemistry, being straightforward to prepare and also commercially available. Reactivity mirrors that of the Ir dimers, whereby addition of Lewis bases yields

monometallic adducts. The *p*-cymene ligand is a poorer π-donor ligand than Cp*
and less strongly bound to Ru(II). In solution, the *p*-cymene ligand can be displaced
much more readily.[51] This may have implications in catalytic transformations.
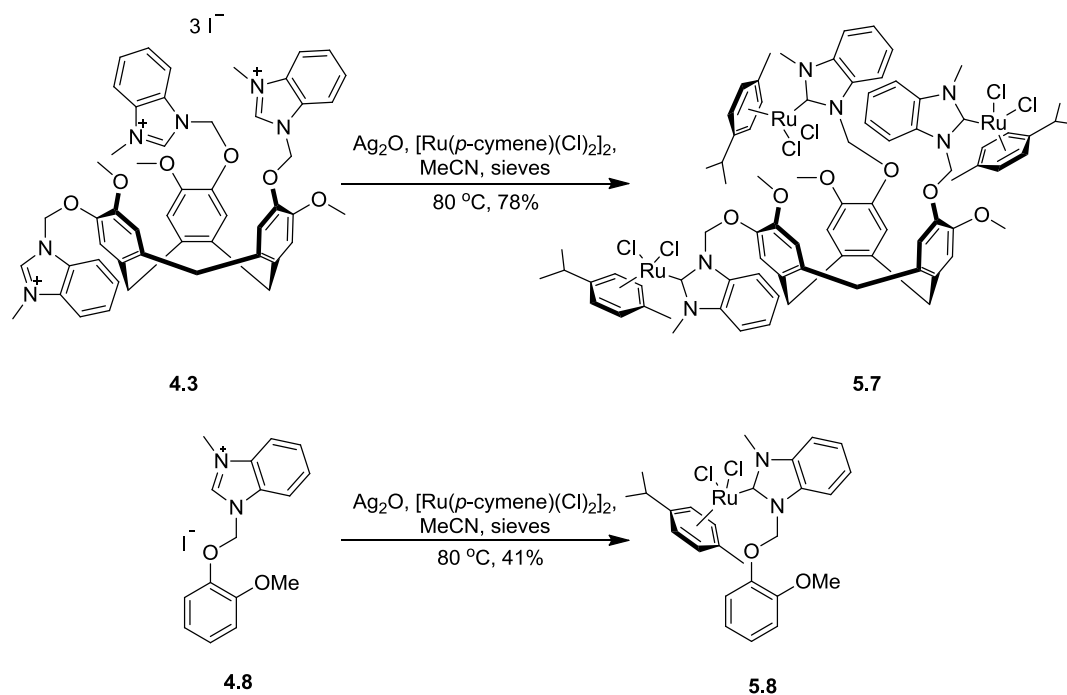
Scheme 5.6 Synthesis of Ru(II)-NHC complexes 5.7 and 5.8.

Trimetallic Ru(II) complex **5.7** was prepared following the same methodology used
throughout this chapter (scheme 5.6). The complex itself proved air-sensitive upon
dissolution in hydrous, oxic solvents, and turned from orange to black within *ca.* 10
mins. Hence, storage and handling in a glovebox was necessary, alongside the use of
anhydrous, degassed solvents. As a solid, **5.7** appeared more stable, and could be
handled as a solid for *ca.* one month before decomposing. The work-up process in
isolating Ru(II) complex **5.7** involved removing MeCN *in vacuo*, before
redissolution in DCM and filtering through two Celite™ plugs before removal of
DCM *in vacuo* and the addition of diethyl ether as antisolvent. Promisingly, **5.7**
displayed much greater solubility than **5.3** and **5.5**, opening up the possibility of
employing the triruthenium complex as a catalyst in TH reactions.

Monomer **5.8** was prepared following the same methodology and employing
ligand **4.8** as a precursor. The monomer displayed greater air- and moisture-
sensitivity than **5.7** and exposure of solutions to air for a matter of seconds led to
decomposition and an insoluble black solid precipitated.

HRMS provided an excellent tool for characterising Ru(II) complexes, and a single $\{M\text{-}3(Cl)\}^{3+}$ molecular ion peak with m/z = 551.1033 was observed, excellently matching the simulated pattern predicted with m/z = 551.1037 (figure 5.26) .
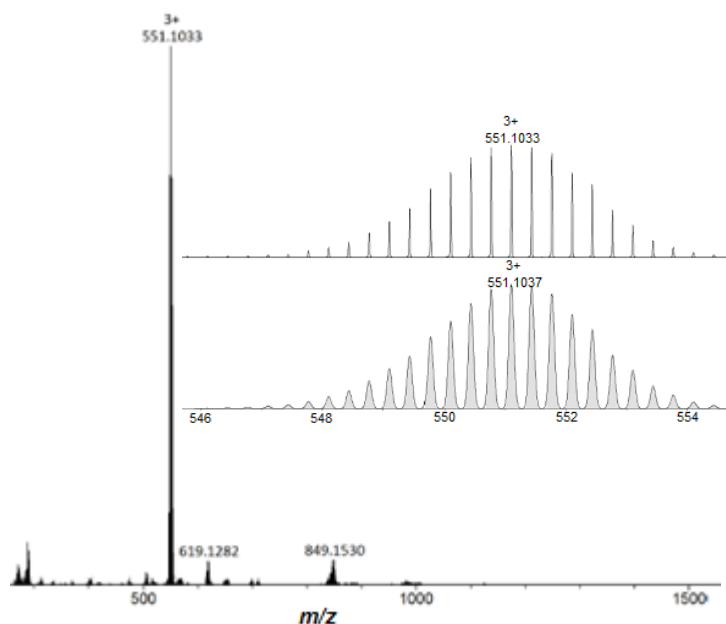
Figure 5.26 HRMS of 5.7. Inset: Observed (top) vs simulated (bottom) isotope pattern for m/z 551.1033, $\{M\text{-}3Cl\}^{3+}$.

Monomer **5.8** behaved similarly in the HRMS spectrum, and the spectrum was dominated by the anticipated $\{M\text{-}Cl\}^+$ fragment, detected at m/z = 539.1048 (figure 5.27). This matched the calculated mass of 539.1039, and the observed data displayed a good isotopic match to the simulated pattern. A second $\{M_2\text{-}Cl\}^+$ fragment at m/z 1114.1769 (calculated 1114.1744) was also detected.
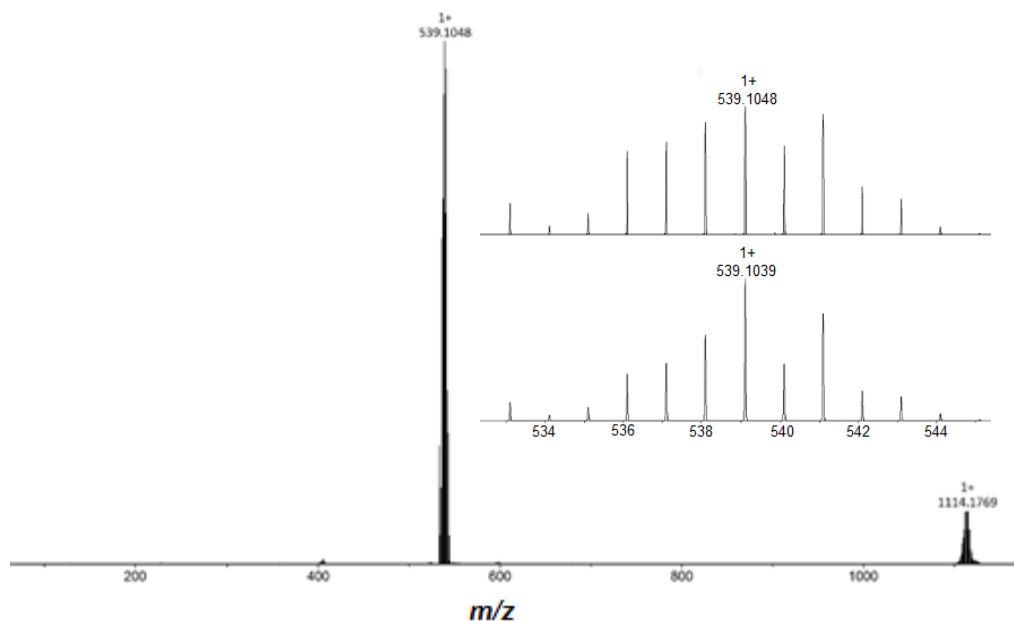
Figure 5.27 HRMS of 5.8. Inset: Observed (top) vs simulated (bottom) isotope pattern of *m/z* 539.1048, {M-Cl}⁺.

The ^{1}H NMR spectrum of **5.7** followed the same pattern as **5.1**, **5.3** and **5.5**, and was extremely broad and difficult to assign (figure 5.28). 2D NMR spectroscopy was once again used as a tool to offer some insight into the behaviour of the complex. The sharper doublet at 4.94 ppm in the spectrum of **5.7** suggests a C_3-symmetric complex, and is typical of the *endo*-proton of the CTV lower-rim. Otherwise, peaks observed in the ^{1}H NMR spectrum of **5.7** overlap excellently with the much sharper resonances of the monomer **5.8**. The *N*-methyl and methoxy resonances afforded NMR handles at 4.26 and 3.78 ppm respectively, overlapping with major peaks in the ^{1}H NMR spectrum of **5.7**.

Arene resonances associated with the η^6-*p*-cymene ring are shielded and appear between 5-6 ppm, characteristic of the upfield shift upon coordination due to withdrawal of electron density from the π-cloud. All four *p*-cymene aromatic protons in **5.8** were inequivalent, with three peaks observed in a 1:2:1 ratio. The two peaks integrating to one proton coupled to one another, whereas no coupling was observed to the larger integrating peak, suggesting these two protons are adjacent to one another and on the opposite side of the arene. The *p*-cymene methyl CH$_3$ group resided at 2.04 ppm. The two methyl groups of the isopropyl moiety became inequivalent, and subtly split by 0.03 ppm, as well as by ca 2 ppm in the ^{13}C{^{1}H} NMR spectrum. This is caused by one pointing towards the metal centre and one pointing away. The C-H of the tertiary isopropyl proton was sited at 3.00 ppm.

Significantly, peaks in the ^{1}H NMR spectrum of **5.7** corresponding to the *p*-cymene ring overlapped with those in **5.8**.

The NCH$_2$O methylene bridge splits into two doublets, with a potential preagostic interaction again arising. COSY and HMQC NMR spectroscopy confirmed the two doublets are sited at 5.92 ppm and 7.35 ppm. Again, the absence of resonances beyond 8 ppm is indicative of the absence of imidazolium hydrogen.
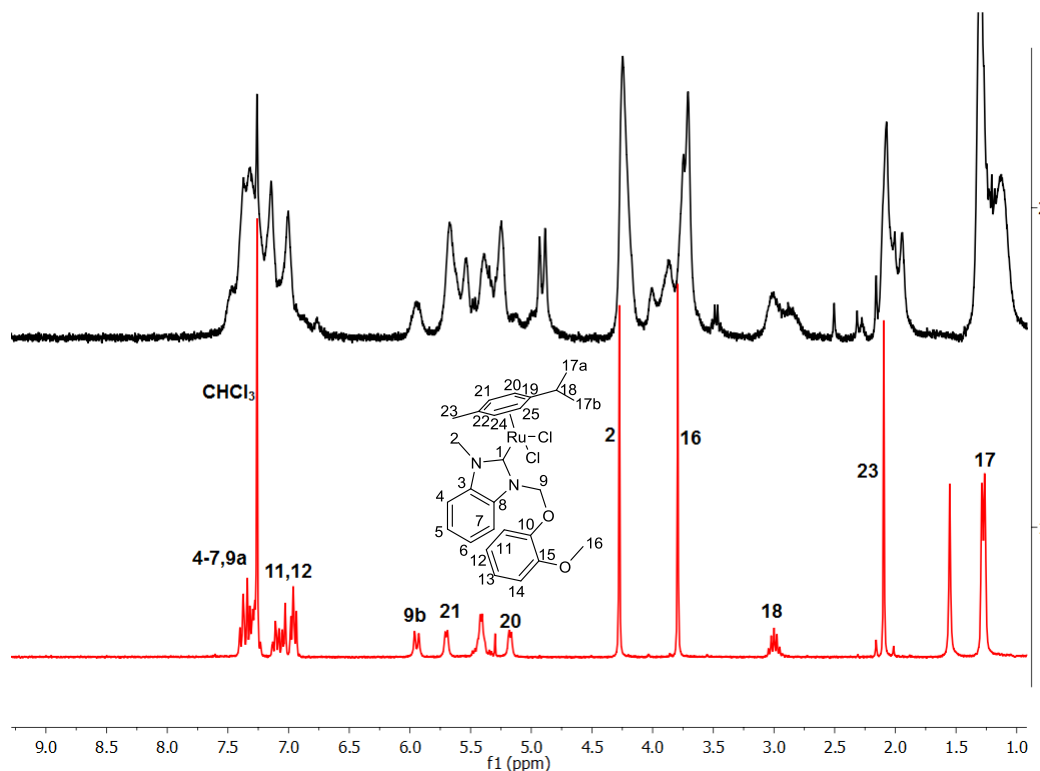
Figure 5.28 ^{1}H NMR spectra (300 MHz, 293 K, CDCl$_3$) of 5.7 (top trace, black) and 5.8 (bottom trace, red).

Similarly to trimetallic Ir(III), Ir(I) and Rh(I)-NHC complexes, a ^{13}C{^{1}H} NMR spectrum of **5.7** could not be obtained, even when running 8000 scans. The ^{13}C{^{1}H} NMR spectrum of **5.8** further suggested NHC coordination at Ru(II), and the carbenic carbon was located at 193.32 ppm (figure 5.29).
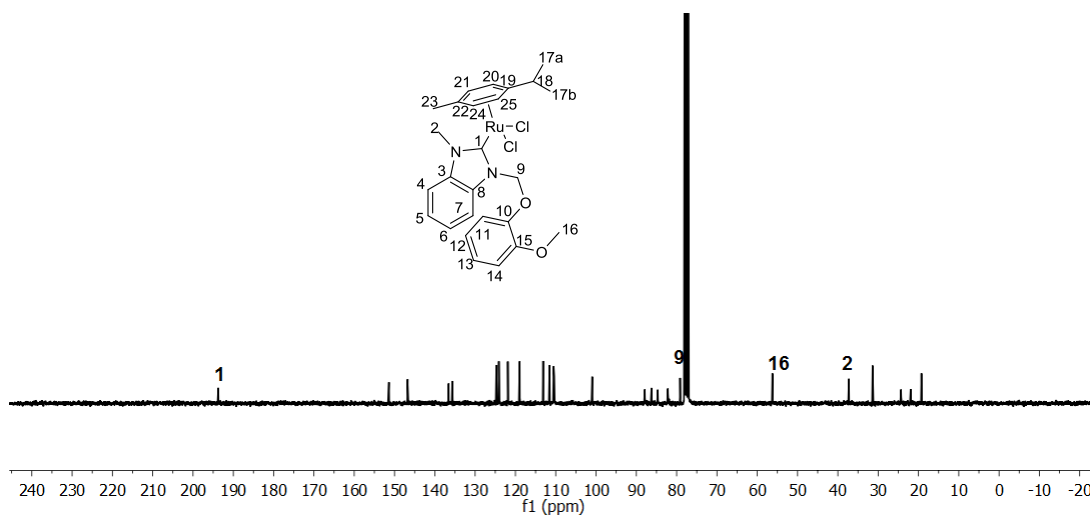
Figure 5.29 ^{13}C{^{1}H} NMR spectrum (75 MHz, 293 K, CDCl$_3$) of 5.8.

2D NMR spectra of **5.7** were weak, even when dissolving ca. 30 mg of sample. The HMBC spectrum did not display all expected coupling, but the anticipated ^3J coupling between *N*-methyl group at *ca.* 4.20 ppm and carbenic carbon at *ca.* 193 ppm was observed (figure 5.30). This is chemically similar to the analogous peaks in complex **5.8**. The HMQC spectrum of **5.7** displayed what appeared to be two doublets at 4.91 and 3.75 ppm coupling to the same carbon atom at ca. 40 ppm in the ^{13}C{^{1}H} NMR spectrum, consistent with the *endo-* and *exo* protons of the CTV lower-rim, implying a C_3-symmetric complex. The upfield doublet overlapped with the methoxy group, which coupled to a carbon atom in the HMQC spectrum at *ca.* 56.4 ppm, which is a good match to the methoxy resonance of **5.8** at 55.81 ppm.
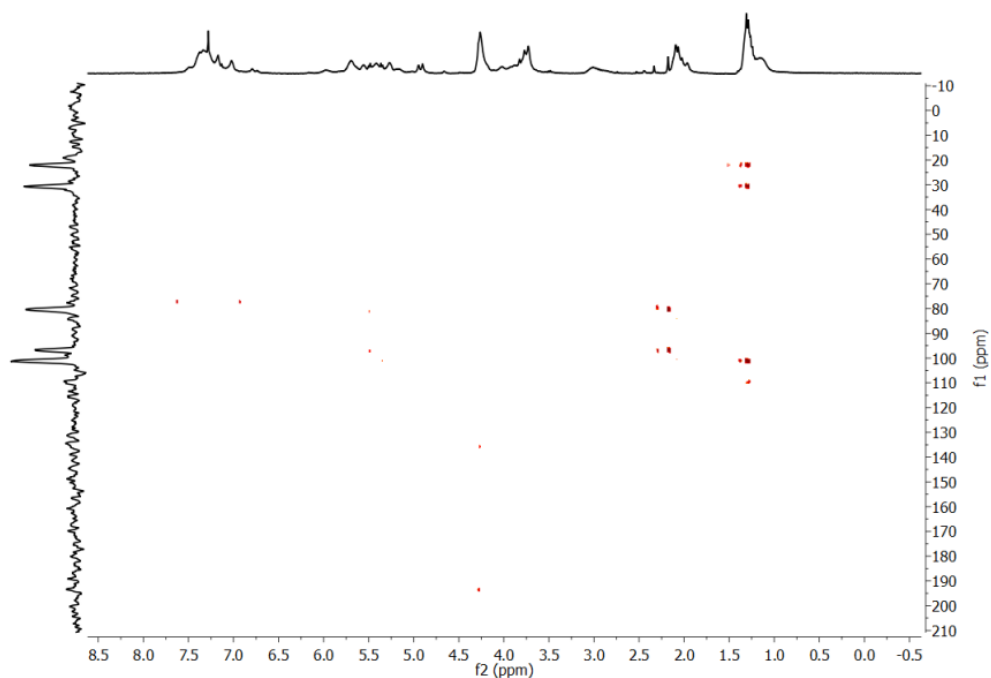
Figure 5.30 HMBC spectrum of 5.7.

5.4.1 Catalytic examination of complexes 5.7 and 5.8

Complexes **5.7** and **5.8** were tested in the TH of acetophenone, and as anticipated, displayed higher activities than the Ir(III) counterparts **5.1** and **5.2** (table 5.4).
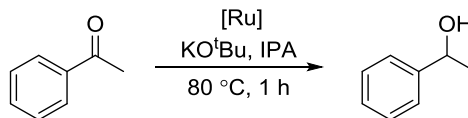
Scheme 5.7 Ru(II) catalysed TH of acetophenone

Table 5.4 Conversions obtained for the TH of acetophenone catalysed by 5.7 and 5.8.

Catalyst	0.5 mol% Ru Conversion (%)	0.25 mol% Ru Conversion (%)
[Ru(*p*-cymene)(Cl)₂]₂	32(±2)	44(±2)
5.7	>99(±1)	56(±2)
5.8	70(±2)	61(±3)

Conversions were the average of two runs, obtained by ¹H NMR spectroscopy by comparing the methyl resonances of 1-phenylethanol and 1,4-dimethoxybenzene as an internal standard.

Complexes were compared to [Ru(*p*-cymene)(Cl)₂]₂ which surprisingly became less active when catalyst loading was increased, possibly indicating an aggregative deactivation pathway during catalysis. Nguyen and co-workers have studied catalyst deactivation of immobilised {IrCp*} catalysts in TH reactions, and discovered anionic [Ir(Cp*)(OR)₃]⁻ species may be the cause of deactivation (R = ⁱPr or ᵗBu).[52] Such species would also be likely when employing [Ru(*p*-cymene)(Cl)₂]₂ as a catalyst. Coordination of a persistent NHC ligand at Ru(II) or Ir(III) would prevent deactivation of a catalyst *via* the formation of an ionic species. At 0.25 mol% Ru, both **5.7** and **5.8** were both similarly active, and displayed higher activities than the dimer. Upon increasing catalyst loading to 0.5 mol% Ru, **5.7** gave near-quantitative conversions after 1 h, whereas a conversion of 70% was observed employing monomer **5.8**. This potentially implies that at low loading, each Ru(II) centre on **5.7** behaves independently, following similar trends to those noted by Matt and Toupet's Pd(II) calixarenyl-NHC complexes.[53] Increased activities at higher loading of **5.7** may be a consequence of intermolecular cooperative effects upon greater

concentrations of catalyst being present in solution. It is unlikely that intramolecular cooperativity plays a major role in this increased activity due to the rigidity of the complex observed using ^{1}H NMR spectroscopy. X-ray crystallography could have given insights into how molecules interact with one another in the solid state, but single crystals suitable for diffraction could not be grown.

The increased conversion of acetophenone to 1-phenylethanol when increasing catalyst loading of **5.7** with respect to **5.8** may be indicative of intermolecular cooperativity. This has previously been reported by Peris and co-workers for planar multimetallated NHC complex through aggregation of catalysts by means of π-π stacking interactions between the polyaromatic backbone to complexes,[54] but this has not been established for cavitand-based systems. One possible mechanism of intermolecular aggregation involving complex **5.7** are bowl-in-bowl stacking which is commonly observed crystallographically for ligands and also some M$_3$L complexes.[55] Secondly, π-π stacking interactions between benzo-backbones of the NHC ligands would allow for metal-metal interactions between molecules of **5.7**. This could be achieved in a similar fashion to that observed crystallographically when studying complex **5.1** in the solid state. Host-guest interactions between the CTV bowl and acetophenone are possible, however the similar conversions observed when employing **5.7** and **5.8** as catalysts at lower loading suggests this is not influential.

A handful of bimetallic and trimetallic Ru(II) have been prepared. Domski and co-workers recently reported a bimetallic Ru(II)-NHC complex which displayed lower activities than the similar monometallic complexes in the TH of acetophenone.[56] Barbasiewicz and co-workers prepared bimetallic Grubbs' catalysts, with Ru(II) centres behaving independently of one another.[57] A small number of bimetallic and trimetallic Ru(II)-phosphine complexes were reported displaying high activities in the TH of acetophenone, but were still lower than some monometallic catalysts.[58, 59]

Whilst the arene exchange of *p*-cymene is a known pathway in organoruthenium chemistry, the substitution of an electron-rich *p*-cymene for an electron-deficient π-donor in acetophenone would be energetically unfavourable. To confirm this, isopropanol and CDCl$_3$ solutions of **5.7** and acetophenone were heated to reflux, with no change in ^{1}H NMR or mass spectra observed. Watanabe and

Nelson have both proposed η^6-η^4 ring-slippage of arenes as plausible inner-sphere pathways when employing Ru(II) piano-stool complexes as catalysts in TH reactions.[60, 61] An inner-sphere mechanism is likely as the methoxy group is a poor hydrogen acceptor, but may be mechanistically significant as a hemilabile ligand to Ru, potentially *via* second-sphere coordination because of the steric effects of the CTV bowl in **5.7**. Jiménez and co-workers have previously observed hemilabile assistance of methoxy groups on ligands at Ir(I) and Rh(I).[62]

5.5 Conclusions and future work

Eight new organometallic complexes were prepared, four affixed onto a CTV cavitand, and four monopodal analogues, which proved effective as catalytic comparatives and also for spectroscopic corroboration. HRMS proved a valuable assignment tool, particularly for the trimetallic complexes, whose full elucidation by NMR spectroscopy was precluded by extremely broad spectra caused by species being conformationally locked. In addition, microanalysis suggested that by-products were present, presumably AgI which proved extremely difficult to remove. Solubility issues arose with monovalent COD-complexes, which could not be investigated in catalytic reactions using chemically reasonable solvents. Ir(III) complexes proved poorly active in the TH of acetophenone, likely caused by the kinetically inert Ir(III) centres and strongly bound ligands yielding highly stable complexes. To overcome this, more reactive Ru(II)-NHC complexes were prepared, which proved excellent catalysts in the TH of acetophenone at low catalyst loading.

Future work would revolve around expanding the substrate scope in the Ru(II)-catalysed TH reaction. Metal-catalysed TH reactions are an attractive alternative to carrying out hydrogenations using H_2 gas at high pressure, but substrate scope can be limited. Quinolines and imines are suitable, but more challenging substrates in the TH reaction for the preparation of secondary amines.[63] Conversions are often lower, with higher catalyst loading and often extended reaction times required. In the case of imine reductions, coordination of the amine product to the metal may deactivate catalysts, therefore protection of the imine is often necessary prior to TH.[64] Complex **5.7** has proven highly effective at catalysing the TH of acetophenone, and the rigid, extremely bulky ligands may inhibit such deactivation pathways from proceeding.

A further direction would be to prepare noble metal complexes that do not bear multihaptic or multidentate ligands. This would be most achievable for Ir(I) and Rh(I), and could be achieved by either removing the π-ligand post-synthetically, for example by treatment with carbon monoxide gas, or employing a new dimeric precursor, such as $[Ir(C_2H_4)_2Cl]_2$, or $[Rh(CO)_2Cl]_2$. Complexes bearing ethene or carbonyl ligands would be anticipated to display more flexibility than the trimetallic complexes introduced in this chapter, allowing for more straightforward assignment, whilst still being sufficiently labile to enhance catalytic activity.

5.6 Experimental section

Unless stated in the experimental section, chemicals were bought from commercial suppliers and used without further purification. All reactions were performed under an atmosphere of dry nitrogen using standard Schlenk and glovebox procedures, with solvents dried and degassed using the same methodology described in section **2.9**. All analytical techniques are also consistent with those described in section **2.9**.

Synthesis of *Tris*(η^5-1,2,3,4,5-pentamethylcyclopentadienyl) hexachloro 3,3',3''-(((3,8,13-trimethoxy-10,15-dihydro-5H-tribenzo[a,d,g][9]annulene-2,7,12-triyl)tris(oxy))tris(methylene))tris(1-benzylbenzimidazol-2-ylidene)triiridium(III), 5.1

Ligand **4.3** (102 mg, 0.08 mmol), [Ir(Cp*)(Cl)$_2$]$_2$ (100 mg, 0.12 mmol), Ag$_2$O (29 mg, 0.12 mmol) and several activated 4 Å molecular sieves were added to a flame dried Schlenk flask. MeCN (5 mL) was added and the orange reaction mixture was heated to 70 ºC for 16 h in the absence of
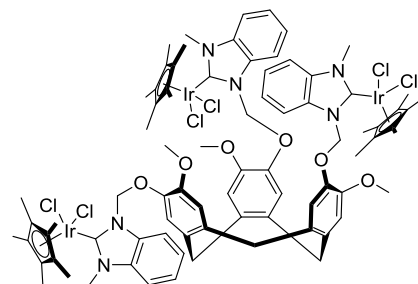
light, during which time Ag$_2$O was digested and a pale yellow precipitate formed. Solvents were removed *in vacuo* and replaced with DCM (10 mL). The yellow-orange solution was filtered through two Celite plugs, DCM reduced in volume to 1 mL in vacuo, and diethyl ether added, precipitating **5.1** as an orange solid. Yield 101 mg, 0.05 mmol, 62%. HRMS (ESI$^+$) 473.6345 {C$_{81}$H$_{93}$Cl$_2$Ir$_3$N$_6$O$_6$}$^{4+}$, 643.1692 {C$_{81}$H$_{93}$Cl$_3$Ir$_3$N$_6$O$_6$}$^{3+}$, 982.2344 {C$_{81}$H$_{93}$Cl$_4$Ir$_3$N$_6$O$_6$}$^{2+}$, calculated 473.6236, 643.1665, 982.2345. Full ^{1}H NMR assignment was precluded by extremely broad spectra. FTIR υ (cm^{-1}) 2916, 1508, 1370, 1264, 1023; Elemental analysis for

$C_{81}H_{92}Cl_6Ir_3N_6O_6 \cdot 0.5(AgI)$ Calcd.: C 45.20, H 4.31, N 3.90 Found: C 45.60, H 4.21, N 4.26.

Synthesis of η⁵-1,2,3,4,5-pentamethylcyclopentadienyl dichloro (1-methyl-3-((2-methoxyphenoxy)methyl)benzimidazol-2-ylidene)iridium(III), 5.2

Ligand **4.8** (25 mg, 0.06 mmol), [Ir(Cp*)(Cl)$_2$]$_2$ (26 mg, 0.03 mmol), Ag$_2$O (8 mg, 0.03 mmol) and several activated 4 Å molecular sieves were added to a flame dried Schlenk flask. MeCN (5 mL) was added and the red reaction mixture was heated to 70 °C for 16 h in the absence of light, during which
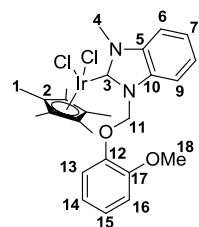
time Ag$_2$O was digested and a pale yellow precipitate formed. Solvents were removed *in vacuo* and replaced with DCM (10 mL). The yellow-orange solution was filtered through two Celite plugs, DCM reduced in volume to 1 mL *in vacuo*, and diethyl ether added, precipitating **5.2** as an orange solid. Yield 29 mg, 0.04 mmol, 69%. HRMS (ESI$^+$) *m/z*= 631.1702 {$C_{26}H_{31}ClIrN_2O_2$}$^+$ Calcd. 631.1698; ^{1}H NMR (400 MHz, CDCl$_3$) δ (ppm) 7.42-7.27 (m, 4H, H^6, H^7, H^8. H^{11a}), 7.23 (m, 1H, H^9), 7.09-7.01 (m, 2H, H^{13}, H^{14}), 6.97-6.93 (m, 2H, H^{15}, H^{16}), 5.88 (d, 1H, *J* = 9.7 Hz, H^{11b}), 4.22 (s, 3H, H^4), 3.77 (s, 3H, H^{18}), 1.69 (s, 15H, H^1) ;^{13}C{^{1}H} NMR (100 MHz, CDCl$_3$) δ (ppm) 173.05 (C^3), 150.23 (C^{17}), 146.52 (C^{12}), 136.12 (C^5), 134.99 (C^{10}), 123.86 (C^{15}), 123.31 (C^{14}), 121.31 (C^{7,8}), 116.66 (C^{16}), 112.73 (C^{13}), 112.07 (C^9), 110.47 (C^6), 90.31 (C^2), 77.71 (C^{11}), 55.93 (C^{18}), 35.88 (C^4), 9.13 (C^1); FTIR υ (cm^{-1}) 2911, 1507, 1253, 1013, 759; Satisfactory elemental analysis could not be obtained, presumably due to solvent and AgI contamination Calculated for $C_{26}H_{31}Cl_2IrN_2O_2 \cdot 0.4(CH_3CN) \cdot 0.2(AgI)$ C 44.09, H 4.45, N, 4.60; Found: C 44.01, H 3.76, N 4.86.

Synthesis of *Tris*(1,5-cyclooctadiene) trichloro 3,3',3''-(((3,8,13-trimethoxy-10,15-dihydro-5H-tribenzo[a,d,g][9]annulene-2,7,12-triyl)tris(oxy))tris(methylene))tris(1-benzylbenzimidazol-2-ylidene)triiridium(I), 5.3

Ligand **4.3** (50 mg, 0.04 mmol), [Ir(COD)(Cl)]$_2$ (41 mg, 0.06 mmol), Ag$_2$O (15 mg 0.06 mmol) and several activated 4 Å molecular sieves were added to a flame dried Schlenk flask. MeCN (2.5 mL) and CHCl$_3$ (2.5 mL) were added and the red reaction mixture was heated to 70 °C for 16 h in the absence of light, during which time

Ag$_2$O was digested and a pale yellow precipitate formed. MeCN was removed *in vacuo* and replaced with DCM (10 mL). The yellow solution was filtered through two Celite plugs, DCM reduced in volume to 1 mL in vacuo, and diethyl ether added,
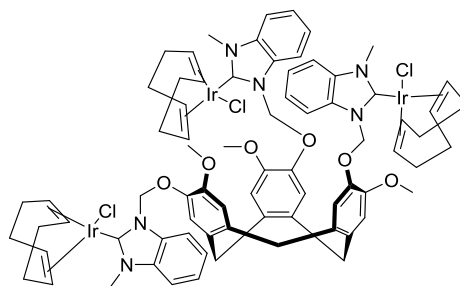
precipitating **5.3** as a yellow solid which was isolated *via* vacuum filtration. Yield 49 mg, 0.026 mmol, 66%. HRMS (ESI$^+$) 580.5009 {C$_{75}$H$_{84}$Ir$_3$N$_6$O$_6$}$^{3+}$, 1812.5251 {C$_{75}$H$_{84}$Cl$_2$Ir$_3$N$_6$O$_6$}$^+$, calculated 580.5100, 1812.4722; Full ^{1}H NMR assignment was precluded by extremely broad spectra. FTIR υ (cm^{-1}) 2933, 1507, 1097, 1025, 742; Elemental analysis for C$_{75}$H$_{84}$Cl$_3$Ir$_3$N$_6$O$_6$·0.83(AgI) Calcd.: C 44.07, H 4.14, N 4.11, Found: C 43.78, H 4.22, N 4.27.

Synthesis of 1,5-cyclooctadiene chloro (1-methyl-3-((2-methoxyphenoxy)methyl)benzimidazol-2-ylidene)iridium(I), 5.4

Ligand **4.8** (50 mg, 0.12 mmol), [Ir(COD)(Cl)]$_2$ (42 mg, 0.06 mmol), Ag$_2$O (15 mg, 0.06 mmol) and several activated 4 Å molecular sieves were added to a flame dried Schlenk flask. MeCN (5 mL) was added and the red reaction mixture was heated
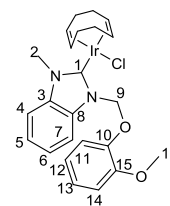
to 70 ℃ for 16 h in the absence of light, during which time Ag$_2$O was digested and a pale yellow precipitate formed. Solvents were removed *in vacuo* and replaced with DCM (10 mL). The yellow-orange solution was filtered through two Celite plugs, DCM reduced in volume to 1 mL in vacuo, and diethyl ether added, precipitating **5.4** as a yellow solid. Yield 37 mg, 0.06 mmol, 51%. HRMS (ESI$^+$) 569.1786 {C$_{24}$H$_{28}$IrN$_2$O$_2$}$^+$, 837.2985 {C$_{40}$H$_{44}$IrN$_4$O$_4$}$^+$, 1162.3563 {C$_{42}$H$_{47}$Cl$_2$Ir$_2$N$_5$NaO$_4$}$^+$, calculated 569.1775, 837.2986, 1162.2133; ^{1}H NMR (300 MHz, CDCl$_3$) δ (ppm) 7.59–7.50 (m, 1H, H^4), 7.34-7.27 (m, 3H, H^5, H^6, H^7), 7.15 – 6.94 (m, H^{9a}, H^{11}, H^{13}, H^{14}), 6.89 (t, *J* = 7.6 Hz, 1H, H^{12}), 6.10 (d, *J* = 9.3 Hz, 1H, H^{9b}), 4.73 (dd, *J* = 11.7, 5.2 Hz, 2H, COD-H), 4.19 (s, 3H, H^2), 3.89 (s, 3H, H^{16}), 3.14 – 3.02 (m, 2H, COD-H), 2.36-2.10 (m, 3H, COD-H), 1.94 – 1.68 (m, 3H, COD-H), 1.52 (m, 2H, COD-H); ^{13}C{^{1}H} NMR (75 MHz, CDCl$_3$) δ 193.28 (C^1), 151.33 (C^{15}), 145.76 (C^{10}), 135.93 (C^3), 134.70 (C^8), 124.68 (C^{17}), 123.36 (C^6), 123.26 (C^5), 121.24 (C^{12}), 119.87 (C^{14}), 112.66 (C^{11}), 111.39 (C^4), 109.64 (C^7), 87.99 (COD-*C*H), 87.03 (COD-*C*H), 78.89 (C^9), 55.94 (C^{16}), 53.36 (COD-*C*H), 53.11 (COD-*C*H), 34.68

(C^2), 34.28 (COD-CH_2), 33.12 (COD-CH_2), 30.00 (COD-CH_2), 29.05 (COD-CH_2); FTIR υ (cm^{-1}) 2975, 2913, 1507, 1373, 1256, 1017; Elemental analysis for $C_{24}H_{28}ClIrN_2O_2 \cdot 0.3(AgI)$ Calcd.: C 42.73, H 4.18, N 4.15; Found: C 42.82, H 4.48, N 4.27.

Synthesis of *Tris*(1,5-cyclooctadiene) trichloro 3,3',3''-(((3,8,13-trimethoxy-10,15-dihydro-5H-tribenzo[a,d,g][9]annulene-2,7,12-triyl)tris(oxy))tris(methylene))tris(1-benzylbenzimidazol-2-ylidene)trirhodium(I), 5.5

Ligand **4.3** (50 mg, 0.04 mmol), [Rh(COD)(Cl)]$_2$ (30 mg, 0.06 mmol), Ag$_2$O (14 mg, 0.06 mmol) and several activated 4 Å molecular sieves were added to a flame dried Schlenk flask. MeCN (2.5 mL) and CHCl$_3$ (2.5 mL) were added and the red
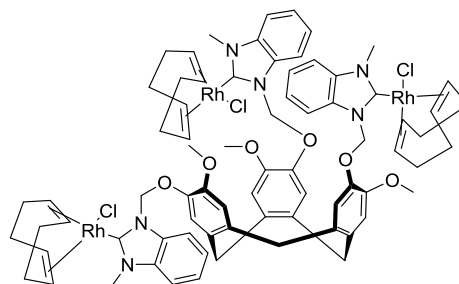
reaction mixture was heated to 70 ºC for 16 h in the absence of light, during which time Ag$_2$O was digested and a pale yellow precipitate formed. MeCN was removed *in vacuo* and replaced with DCM (10 mL). The yellow solution was filtered through two Celite plugs, DCM reduced in volume to 1 mL *in vacuo*, and diethyl ether added, precipitating **5.5** as a pale yellow solid, which was isolated *via* vacuum filtration. Yield 29 mg, 0.018 mmol, 48%. HRMS (ESI+) 491.1194 $\{C_{75}H_{84}N_6O_6Rh_3\}^{3+}$, 754.1630 $\{C_{75}H_{84}N_6O_6Rh_3\}^{3+}$, calculated 491.1200, 754.1648; Full ^{1}H NMR assignment was precluded by extremely broad spectra; FTIR υ (cm^{-1}) 2932, 1507, 1374, 1264, 1086; Elemental analysis for $C_{75}H_{84}Cl_3N_6O_6Rh_3 \cdot 0.5(AgI)$ Calcd.: C 53.05, H 4.99, N 4.95; Found C 52.96, H 4.90, N 5.25.

Synthesis of 1,5-cyclooctadiene chloro (1-methyl-3-((2-methoxyphenoxy)methyl)benzimidazol-2-ylidene)iridium(I), 5.6

Ligand **4.8** (50 mg, 0.12 mmol), [Rh(COD)(Cl)]$_2$ (31 mg, 0.06 mmol), Ag$_2$O (15 mg 0.06 mmol) and several activated 4 Å molecular sieves were added to a flame dried Schlenk flask. MeCN (5 mL) was added and the orange reaction mixture was heated to 70 ºC for 16 h in the absence of light, during which time Ag$_2$O was digested and a pale yellow precipitate formed. Solvents were removed *in*
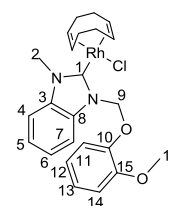
vacuo and replaced with DCM (10 mL). The yellow-orange solution was filtered through two Celite plugs, DCM reduced in volume to 1 mL in vacuo, and diethyl ether added, precipitating **5.6** as a pale yellow solid. Yield 26 mg, 0.05 mmol, 42%. HRMS (ESI+) 479.1219 $\{C_{24}H_{28}RhN_2O_2\}^+$, 747.2411 $\{C_{40}H_{44}RhN_4O_4\}^+$, 984.2436 $\{C_{48}H_{50}ClN_6NaO_7Rh\}^+$, calculated 479.1201, 747.2413, 984.2410; ^1H NMR (300 MHz, CDCl$_3$) δ (ppm) 7.48 (s, 1H, H^7), 7.31 – 7.20 (m, 4H, H^4, H^5, H^6, H^{9a}), 7.14 – 6.96 (m, 3H, H^{11}, H^{13}, H^{14}), 6.91 (td, J = 7.8, 1.5 Hz, 1H, H^{12}), 6.18 (d, J = 9.4 Hz, 1H, H^{9b}), 5.12 (s, 2H, COD-H), 4.33 (s, 3H, H^2), 3.90 (s, 3H, H^{16}), 3.57-3.40 (m, 2H, COD-H), 2.58 – 2.42 (m, 1H, COD-H), 2.42 – 2.22 (m, 2H, COD-H), 2.22 – 1.92 (m, 4H, COD-H), 1.84 (s, 1H, COD-H); $^{13}C\{^1H\}$ NMR (75 MHz, CDCl$_3$) δ (ppm) 198.29 (d, J_{Rh-C} = 51.0 Hz, C^1) , 151.36 (C^{15}), 145.93 (C^{10}), 135.80 (C^3), 134.71 (C^8), 124.71 (C^{13}), 123.21 (C^6), 123.13 (C^5), 121.27 (C^{11}), 119.84 (C^{12}), 112.69 (C^{14}), 111.09 (C^7), 109.51 (C^4), 100.97 (d, J_{Rh-C} = 6.6 Hz, COD-H), 100.30 (d, J_{Rh-C} = 6.7 Hz, COD-H), 79.30 (C^9), 69.46 (d, J_{Rh-C} = 7.6 Hz, COD-H), 69.27 (d, J_{Rh-C} = 7.3 Hz, COD-H), 55.96 (C^{16}), 35.04 (C^2), 33.55 (COD-H$_2$), 32.59 (COD-H$_2$), 29.29 (COD-H$_2$), 28.60 (COD-H$_2$); FTIR υ (cm^{-1}) 2917, 1605, 1507, 1373, 1264, 1085, 1024, 742; Elemental analysis for $C_{24}H_{28}ClN_2O_2Rh·0.17(AgI)$ Calcd.: C 52.03, H, 5.09, N 5.06; Found C 52.24, H 5.03, N 5.43.

Synthesis of *Tris*(η^6-*p*-cymene) hexachloro 3,3',3''-(((3,8,13-trimethoxy-10,15-dihydro-5H-tribenzo[a,d,g][9]annulene-2,7,12-triyl)tris(oxy))tris(methylene))tris(1-benzylbenzimidazol-2-ylidene)triruthenium(II), 5.7

Ligand **4.3** (50 mg, 0.04 mmol), [Ru(*p*-cymene)(Cl)$_2$]$_2$ (36 mg, 0.06 mmol), Ag$_2$O (14 mg 0.06 mmol) and several activated 4 Å molecular sieves were added to a flame dried Schlenk flask. MeCN (5 mL) was added and the red reaction mixture was heated to 70 ºC for 16 h in the absence of light, during which time Ag$_2$O was digested and a pale yellow precipitate formed. Solvents were removed *in vacuo* and anhydrous DCM (10 mL) was added *via* cannula transfer. The orange solution was filtered through two Celite plugs, DCM reduced in volume to 1 mL *in vacuo*, and diethyl ether added, precipitating **5.7** as an orange solid, which
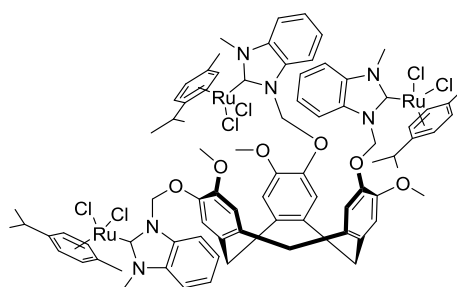
was filtered *via* cannula filtration and dried *in vacuo*. Yield 55 mg, 0.03 mmol, 78%. HRMS (ESI$^+$) 551.1033 $\{C_{81}H_{90}Cl_3N_6O_6Ru_3\}^{3+}$, calculated 551.1037. Full ^{1}H NMR assignment was precluded by extremely broad spectra. FTIR υ (cm^{-1}) 2961, 1508, 1462, 1370, 1264, 1085, 744; Satisfactory elemental analysis could not be obtained presumably due to AgI and solvent contamination, alongside potential decomposition. $C_{81}H_{90}Cl_6N_6O_6Ru_3\cdot1.35(AgI)\cdot(CH_3CN)$ Calcd.: C 47.08, H 4.43, N 4.63; Found C 46.57, H 3.94, N 4.91.

Synthesis of η⁶-*p*-cymene dichloro (1-methyl-3-((2-methoxyphenoxy)methyl)benzimidazol-2-ylidene)ruthenium(II), 5.8

Ligand **4.8** (50 mg, 0.12 mmol), [Ru(*p*-cymene)(Cl)$_2$]$_2$ (39 mg, 0.06 mmol), Ag$_2$O (15 mg 0.06 mmol) and several activated 4 Å molecular sieves were added to a flame dried Schlenk flask. MeCN (5 mL) was added and the orange reaction mixture was heated to 70 ºC for 16 h in the absence of light, during which time Ag$_2$O was digested and a pale yellow precipitate formed. Solvents were removed *in vacuo* and anhydrous DCM (10 mL) was added *via* cannula transfer. The orange solution was filtered through two Celite plugs, DCM reduced in volume to 1 mL *in vacuo*, and diethyl ether added, precipitating **5.8** as an orange solid, which was filtered *via* cannula filtration and dried *in vacuo*. Yield 28 mg, 0.05 mmol, 41%. HRMS (ESI$^+$) 539.1048 $\{C_{26}H_{30}ClN_2O_2Ru\}^+$, 1114.1769 $\{C_{52}H_{60}Cl_3N_4O_4Ru_2\}^+$, calculated 539.1039, 1114.1744; ^{1}H NMR (300 MHz, CDCl$_3$) δ (ppm) 7.42 − 7.27 (m, 5H, H^4, H^5, H^6, H^7, H^{9a}), 7.15 − 7.00 (m, 2H, H^{13}, H^{14}), 6.96 (t, 2H, J = 6.9 Hz, H^{11}, H^{12}), 5.94 (d, 1H, J = 10.4 Hz, H^{9b}), 5.70 (d, 1H, J = 5.7 Hz, H^{21}), 5.41 (d, 2H, J = 4.7 Hz, H^{24}, H^{25}), 5.17 (d, 1H, J = 5.0 Hz H^{20}), 4.27 (s, 3H, H^2), 3.79 (s, 3H, H^{16}), 3.00 (hept J = 7.44, 7.44, 7.89, 7.89, 7.89, 7.89 Hz, ^{1}H, H^{18}), 2.09 (s, 3H, H^{23}), 1.29 (s, 3H, H^{17a}), 1.26 (s, 3H, H^{17b}); ^{13}C$\{^1$H$\}$ NMR (75 MHz, CDCl$_3$) δ (ppm) 193.32 (C^1), 150.96 (C^{15}), 146.32 (C^{10}), 136.15 (C^3), 135.23 (C^8), 123.68 (Benzimidazole *C*H), 123.64 (Benzimidazole *C*H), 121.46 (C^{11}), 118.53 (C^{13}), 112.70 (C^{12}), 111.11 (Benzimidazole *C*H), 110.09 (Benzimidazole *C*H), 109.95 (C^{19}), 100.52 (C^{22}), 87.49 (C^{21}), 85.82 (C^{24}), 84.27 (C^{25}), 81.76 (C^{20}), 78.73 (C^9), 55.81 (C^{16}), 36.85 (C^2), 30.96 (C^{18}), 23.91 (C^{17a}), 21.51 (C^{17b}), 18.83 (C^{23}); FTIR υ (cm^{-1}) 2961, 1507, 1372, 1253, 1119, 969; Elemental analysis for
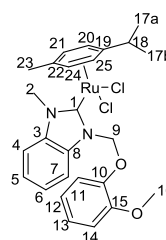
$C_{26}H_{30}Cl_2N_2O_2Ru \cdot 0.2(AgI)$ Calcd.: C 50.25, H, 4.87, N, 4.51; Found: C 50.53, H 4.56, N 4.67.

General catalytic procedure

Potassium *tert*-butoxide (14 mg, 0.1 mmol), catalyst and 1,4-dimethoxybenzene (69.1 mg, 0.5 mmol) were added to a Schlenk flask. Acetophenone (118 μL, 1 mmol) and isopropanol (2.3 mL) were added and the solution heated to 80 ºC for 1 h. An aliquot of the reaction mixture (0.1 mL) was added to $CDCl_3$ (0.4 mL) and the conversion obtained by ^1H NMR spectroscopy.

5.7 Crystallographic remarks

Crystals were mounted under inert oil on a MiTeGen tip and flash frozen using an OxfordCryosystems low temperature device. X-ray diffraction data were collected using CuKα radiation ($\lambda = 1.54184$ Å) or MoKα ($\lambda = 0.71073$ Å) using an Agilent Supernova dual-source diffractometer with Atlas S2 CCD detector and fine-focus sealed tube generator, or using synchrotron radiation ($\lambda = 0.6889$ Å) at Beamline I19 at the Diamond light source. Data were corrected for Lorenztian and polarization effects and absorption corrections were applied using multi-scan methods. The structures were solved by direct methods using SHELXS-97 and refined by full-matrix on F^2 using SHELXL-97. Unless otherwise specified, all non-hydrogen atoms were refined as anisotropic, and hydrogen positions were included at geometrically estimated positions.

5.7.1 Additional crystallographic details

5.1

Crystals did not diffract to high angles using MoKα radiation, and the SQUEEZE routine of PLATON was applied.[34]

5.4

The largest peak was a Fourier ripple 0.75 Å from Ir1.

Table 5.5 Table of crystallographic data. a = CuKa radiation, b = MoKa radiation

Compound	5.1[b]	5.2[a]	5.4[b]	5.6[b]
Formula	$C_{972}H_{1116}Cl_{72}Ir_{36}N_{72}O_{72}$	$C_{208}H_{248}Cl_{16}Ir_8N_{16}O_{16}$	$C_{96}H_{114}Cl_4Ir_4N_8O_8$	$C_{96}H_{114}Cl_4N_8O_8Rh_4$
Mr	24432.26	5333.04	2416.52	2059.36
Crystal colour and shape	Yellow, block	Yellow, block	Yellow, block	Yellow, block
Crystal size (mm)	0.07 x 0.08 x 0.10	0.03 x 0.04 x 0.07	0.07 x 0.08 x 0.11	0.05 x 0.07 x 0.12
Crystal system	Hexagonal (trigonal edges)	Orthorhombic	Triclinic	Triclinic
Space group	$R\bar{3}c$	$Pbca$	$P\bar{1}$	$P\bar{1}$
a (Å)	23.5277(12)	8.53799(19)	8.9535(3)	8.9560(5)
b (Å)	23.5277(12)	20.0779(5)	12.9352(4)	12.8612(7)
c (Å)	77.681(4)	29.0881(7)	20.3565(5)	20.3426(10)
α (^{0})	90	90	91.617(2)	91.712(4)
β (^{0})	90	90	102.372(2)	102.480(4)
γ (^{0})	120	90	109.306(2)	109.169(5)
V ($Å^3$)	37239(4)	4986.4(2)	2160.78(11)	2148.0(2)
Z	12	8	4	4
T/K	120	120	120	120
ρ_{calc} (g.cm^{-3})	1.089	1.776	1.857	1.592
θ range (^{0})	2.898- 20.815	3.038-74.271	2.825-30.7840	2.834-26.022
No. data collected	26406	20650	25022	18664
No. unique data	4338	5056	8751	8166
R_{int}	0.0974	0.0579	0.0274	0.0346
No. obs. Data ($I > 2\sigma(I)$)	3274	3817	7715	6812
No. parameters	314	305	545	545
No. restraints	75	0	0	0
R_1 (obs data)	0.0547	0.0322	0.0269	0.0350
wR_2 (all data)	0.1473	0.0766	0.0972	0.0825
S	1.023	0.996	0.788	1.030
Max. shift/esd	0.005	0.002	0.001	0.001
Largest difference peak and hole/ (e $Å^3$)	1.924, -0.891	1.687, -1.127	1.715, -0.824	0.643, -0.703

5.8 References

1. L. Vaska, J. W. DiLuzio, *J. Am. Chem.Soc.*, 1961, **83**, 2784-2785.

2. J.A. Osborn, G. Wilkinson, J.J. Mrowca, in *Inorganic Syntheses*, ed. E.L. Muetterties, 1967, vol. 10, 67-71

3. R. Crabtree, *Acc. Chem. Res.*, 1979, **12**, 331-337.

4. J.-F. Ayme, J. E. Beves, D. A. Leigh, R. T. McBurney, K. Rissanen, D. Schultz, *Nat. Chem*, 2012, **4**, 15-20.

5. M. Kitamura, M. Tokunaga, R. Noyori, *J. Am. Chem. Soc.*, 1995, **117**, 2931-2932.

6. R. Noyori, S. Hashiguchi, *Acc. Chem. Res.*, 1997, **30**, 97-102.

7. S. Gladiali, E. Alberico, *Chem. Soc. Rev.*, 2006, **35**, 226-236.

8. W. Ponndorf, *Angew. Chem.*, 1926, **39**, 138-143.

9. D. Wang, D. Astruc, *Chem. Rev.*, 2015, **115**, 6621-6686.

10. Y.M.Y. Haddad, H.B. Henbest, J. Husbands, T.R.B. Mitchell, *Proc. Chem. Soc. London*, 1964, 361-365.

11. J. Trocha-Grimshaw, H. B. Henbest, *Chem. Commun.*, 1967, 544-544.

12. A. C. Hillier, H. M. Lee, E. D. Stevens, S. P. Nolan, *Organometallics*, 2001, **20**, 4246-4252.

13. H. Türkmen, T. Pape, F. E. Hahn, B. Çetinkaya, *Eur. J. Inorg. Chem.*, 2008, **2008**, 5418-5423.

14. M. Albrecht, R. H. Crabtree, J. Mata, E. Peris, *Chem. Commun.*, 2002, 32-33.

15. N. B. Jokić, M. Zhang-Presse, S. L. M. Goh, C. S. Straubinger, B. Bechlars, W. A. Herrmann, F. E. Kühn, *J. Organomet.Chem.*, 2011, **696**, 3900-3905.

16. W. B. Cross, C. G. Daly, Y. Boutadla, K. Singh, *Dalton Trans.*, 2011, **40**, 9722-9730.

17. V. Gierz, A. Urbanaite, A. Seyboldt, D. Kunz, *Organometallics*, 2012, **31**, 7532-7538.

18. S. C. Zinner, C. F. Rentzsch, E. Herdtweck, W. A. Herrmann, F. E. Kuhn, *Dalton Trans.*, 2009, 7055-7062.

19. A. Pontes da Costa, M. Viciano, M. Sanaú, S. Merino, J. Tejeda, E. Peris, B. Royo, *Organometallics*, 2008, **27**, 1305-1309.

20. A. Sinha, S. M. Wahidur Rahaman, M. Sarkar, B. Saha, P. Daw, J. K. Bera, *Inorg. Chem.*, 2009, **48**, 11114-11122.

21. S. Enthaler, R. Jackstell, B. Hagemann, K. Junge, G. Erre, M. Beller, *J. Organomet. Chemistry*, 2006, **691**, 4652-4659.

22. M. Poyatos, J. A. Mata, E. Falomir, R. H. Crabtree, E. Peris, *Organometallics*, 2003, **22**, 1110-1114.

23. A. A. Danopoulos, S. Winston, W. B. Motherwell, *Chem. Commun.*, 2002, 1376-1377.

24. M. Poyatos, A. Maisse-François, S. Bellemin-Laponnaz, E. Peris, L. H. Gade, *J. Organomet. Chem.*, 2006, **691**, 2713-2720.

25. F. E. Fernández, M. C. Puerta, P. Valerga, *Organometallics*, 2012, **31**, 6868-6879.

26. W. Zuo, R. H. Morris, *Nat. Protoc.*, 2015, **10**, 241-257.

27. J. Holmes, C. M. Pask, C. E. Willans, *Dalton Trans.*, 2016, **45**, 15818-15827.

28. W. W. N. O, A. J. Lough, R. H. Morris, *Organometallics*, 2011, **30**, 1236-1252.

29. J. Campos, U. Hintermair, T. P. Brewster, M. K. Takase, R. H. Crabtree, *ACS Catal.*, 2014, **4**, 973-985.

30. C. Segarra, J. Linke, E. Mas-Marza, D. Kuck, E. Peris, *Chem Commun.*, 2013, **49**, 10572-10574.

31. A. R. Chianese, X. Li, M. C. Janzen, J. W. Faller, R. H. Crabtree, *Organometallics*, 2003, **22**, 1663-1667.

32. A. Bartoszewicz, R. Marcos, S. Sahoo, A. K. Inge, X. Zou, B. Martín-Matute, *Chem. Eur. J.*, 2012, **18**, 14510-14519.

33. J. C. Lewis, J. Wu, R. G. Bergman, J. A. Ellman, *Organometallics*, 2005, **24**, 5737-5746.

34. A. Spek, *Acta Crystallogr. Sect. A*, 1990, **46**, c34.

35. V. E. Pritchard, D. R. Martir, S. Oldknow, S. Kai, S. Hiraoka, N. J. Cookson, E. Zysman-Colman, M. J. Hardie, *Chem. Eur. J.*, 2017, **23**, 6290-6294.

36. R. Radhakrishnan, D. M. Do, S. Jaenicke, Y. Sasson, G.-K. Chuah, *ACS Catal.*, 2011, **1**, 1631-1636.

37. L. Bagnell, C. R. Strauss, *Chem. Commun.*, 1999, 287-288.

38. R. Maity, A. Mekic, M. van der Meer, A. Verma, B. Sarkar, *Chem. Commun.*, 2015, **51**, 15106-15109.

39. P. Coppo, E. A. Plummer, L. De Cola, *Chem. Commun.*, 2004, 1774-1775.

40. S. J. Lucas, R. M. Lord, R. L. Wilson, R. M. Phillips, V. Sridharan, P. C. McGowan, *Dalton Trans.*, 2012, **41**, 13800-13802.

41. Z. Almodares, S. J. Lucas, B. D. Crossley, A. M. Basri, C. M. Pask, A. J. Hebden, R. M. Phillips, P. C. McGowan, *Inorg. Chem.*, 2014, **53**, 727-736.

42. Z. Liu, L. Salassa, A. Habtemariam, A. M. Pizarro, G. J. Clarkson, P. J. Sadler, *Inorg. Chem.*, 2011, **50**, 5777-5783.

43. C. Wang, J. Liu, Z. Tian, M. Tian, L. Tian, W. Zhao, Z. Liu, *Dalton Trans.*, 2017, **46**, 6870-6883.

44. Z. Liu, A. Habtemariam, A. M. Pizarro, S. A. Fletcher, A. Kisova, O. Vrana, L. Salassa, P. C. A. Bruijnincx, G. J. Clarkson, V. Brabec, P. J. Sadler, *J. Med. Chem.*, 2011, **54**, 3011-3026.

45. O. V. Zenkina, E. C. Keske, R. Wang, C. M. Crudden, *Organometallics*, 2011, **30**, 6423-6432.

46. R. Dorta, E. D. Stevens, S. P. Nolan, *J. Am. Chem. Soc.*, 2004, **126**, 5054-5055.

47. N. M. Scott, R. Dorta, E. D. Stevens, A. Correa, L. Cavallo, S. P. Nolan, *J. Am. Chem. Soc.*, 2005, **127**, 3516-3526.

48. A. Bittermann, E. Herdtweck, P. Härter, W. A. Herrmann, *Organometallics*, 2009, **28**, 6963-6968.

49. W. A. Herrmann, O. Runte, G. Artus, *J. Organomet. Chem.*, 1995, **501**, C1-C4.

50. H. V. Huynh, Y. Han, R. Jothibasu, J. A. Yang, *Organometallics*, 2009, **28**, 5395-5404.

51. H. Tobita, K. Hasegawa, J. J. Gabrillo Minglana, L.-S. Luh, M. Okazaki, H. Ogino, *Organometallics*, 1999, **18**, 2058-2060.

52.   G. J. Sherborne, M. R. Chapman, A. J. Blacker, R. A. Bourne, T. W. Chamberlain, B. D. Crossley, S. J. Lucas, P. C. McGowan, M. A. Newton, T. E. O. Screen, P. Thompson, C. E. Willans, B. N. Nguyen, *J. Am. Chem. Soc.*, 2015, **137**, 4151-4157.

53.   E. Brenner, D. Matt, M. Henrion, M. Teci, L. Toupet, *Dalton Trans.*, 2011, **40**, 9889-9898.

54.   E. Peris, *Chem. Commun.*, 2016, **34**, 5777-5787.

55.   F.L. Thorp-Greenwood, V. E. Pritchard, M. P. Coogan, M. J. Hardie, *Organometallics*, 2016, **11**, 1632-1642.

56.   I. G. Smith, J. C. Zgrabik, A. C. Gutauskas, D. L. Gray, G. J. Domski, *Inorg. Chem. Commun.*, 2017, **81**, 27-32.

57.   K. Grudzień, M. Malinska, M. Barbasiewicz, *Organometallics*, 2012, **31**, 3636-3646.

58.   N. Meriç, F. Durap, M. Aydemir, A. Baysal, *Appl. Organomet. Chem.*, 2014, **28**, 803-808.

59.   N. Raja, R. Ramesh, *Tetrahedron Lett.*, 2012, **53**, 4770-4774.

60.   S. Ogo, T. Abura, Y. Watanabe, *Organometallics*, 2002, **21**, 2964-2969.

61.   K. Y. Ghebreyessus, J. H. Nelson, *J. Organomet. Chem.*, 2003, **669**, 48-56.

62.   M. V. Jiménez, J. Fernández-Tornos, J. J. Pérez-Torrente, F. J. Modrego, S. Winterle, C. Cunchillos, F. J. Lahoz, L. A. Oro, *Organometallics*, 2011, **30**, 5493-5508.

63.   C. Wang, C. Li, X. Wu, A. Pettman, J. Xiao, *Angew. Chem. Int. Ed.*, 2009, **48**, 6524-6528.

64.   D. Guijarro, Ó. Pablo, M. Yus, *J. Org. Chem.*, 2010, **75**, 5265-5270.

Chapter 6
Synthesis and catalytic assessment of trimetallic Pd(II) N-heterocyclic carbene complexes

This chapter focuses on the preparation of four Pd(II) N-heterocyclic carbene complexes, their characterisation and viability as catalysts in Suzuki-Miyaura cross-coupling reactions, with the intention of observing a supramolecular benefit to tethering three metal centres to one scaffold.

6.1 Introduction

Chapter 5 discussed the preparation of NHC complexes containing Ir, Ru and Rh. The four classes of complex prepared contained either a multihaptic π-donor, or bidentate COD ligand for square-planar Ir(I) and Rh(I) complexes, occupying 50% of the available coordination sites of the metal in question. The NHC and π-donating environments both exerted significant bulk on the systems and led to restricted rotation about a number of sites on the complexes, thus complicating NMR analysis. An obvious method to relieve some steric strain would be to prepare complexes not bearing multihaptic or chelating ligands.

Palladium N-heterocyclic carbene complexes are amongst the most established in the literature. A diverse array of NHC ligands have been observed coordinating to Pd(II), including monodentate NHCs,[1] bis-NHCs,[2, 3] chelating pyridyl-NHC ligands[4, 5] amongst others. One particular class of complexes which have become synonymous with organometallic chemistry are the PEPPSI™ complexes pioneered by Organ and co-workers in the early 21st Century.[6]

6.1.1 PEPPSI™ complexes

PEPPSI™ complexes (**P**yridine **E**nhanced **P**recatalyst **P**reparation **S**tabilisation and **I**nitiation) have become one of the most widely encountered classes of NHC bearing species. This is to their ease of synthesis, which in a number of cases can be carried out in air. Reactions are often high yielding, with yields of >90% not uncommon for PEPPSI™-IMes (IMes = *bis*-mesitylimidazol-2-ylidene) or PEPPSI™-IPent (IPent = bis-2,6-diisopentylphenylimidazol-2-ylidene. Organ and co-workers demonstrated scalability when preparing PEPPSI™-IMes, and achieved a 93% yield carrying out its synthesis in a coffee mug, using 10 g of PdCl$_2$.[6]
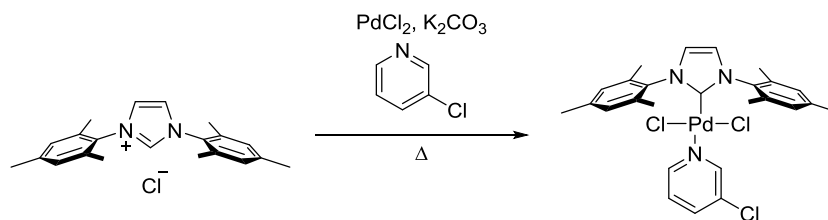
Scheme 6.1 Organ's synthesis of PEPPSI™-IMes[6].

The 3-chloropyridyl ligand behaves as a throwaway ligand, both stabilising the active Pd(0) catalyst, and being easily displaced during catalytic cycles. PEPPSI™ catalysts are remarkably robust (can be heated indefinitely in DMSO to 120 ℃ without decomposition). The complexes have become key catalysts in academic and industrial laboratories, owing to their straightforward and scalable synthesis, functional-group tolerance and ability to catalyse an incredible substrate scope across a variety of C-C[7-13] and C-N[14-17] coupling reactions, including regioselective[18] and enantioselective[19] examples, when employing a chiral NHC ligand. Goldup and Larrosa have reported the highly selective polybutylation of polybromobenzenes when using one eq. butylzinc bromide in PEPPSI™-catalysed Negishi couplings, proposing that a minimum of two distinct Pd(0) species mediate the oxidative addition step.[20] The first reacts under activation control, the typical reactivity observed when employing Pd(0) catalysts. The second arises from the reductive elimination step yielding 'ultra-active' Pd(0) species stabilised within a solvent cage, which exhaustively substitute the polybromobenzene under diffusion control. DFT calculations have suggested a PEPPSI™-IPr mediated reductive elimination product from ethylbenzene and ethylzinc bromide would be a Pd(0)-ZnBr$_2$ adduct,[21] which if stabilised within a solvent cage could lead to exhaustive substitution. The PEPPSI™ complexes display selective polyfunctionalisations in a number of cross-coupling reactions in addition to the Negishi reaction, including the Kumada coupling and also to a lesser extent the Suzuki-Miyaura reaction.[22] This suggests that polyfunctionalisation of polybromoarenes is a general property of PEPPSI™ complexes, rather than by the stabilisation of a Pd(0)-ZnBr$_2$ adduct.

6.2 Synthesis of trimetallic *trans*-3-chloropyridyl complexes

6.2.1 Preparation of trimetallic *N*-methyl Pd(II)-NHC 6.1

By following the methodology introduced by Organ and co-workers in the preparation of PEPPSI™ complexes, imidazolium salt **4.3** could be deprotonated using potassium carbonate as the base and 3-chloropyridine as both solvent and ligand (scheme 6.2). Trimetallic complex **6.1** was isolated in good yield, and unlike the complexes introduced in Chapter 5, sharp, diagnostic NMR spectra were obtained. The preparation of **6.1** could be carried out in hydrous 3-chloropyridine under aerobic conditions, but yields dropped from 84% to 40%, therefore standard Schlenk procedures were applied.
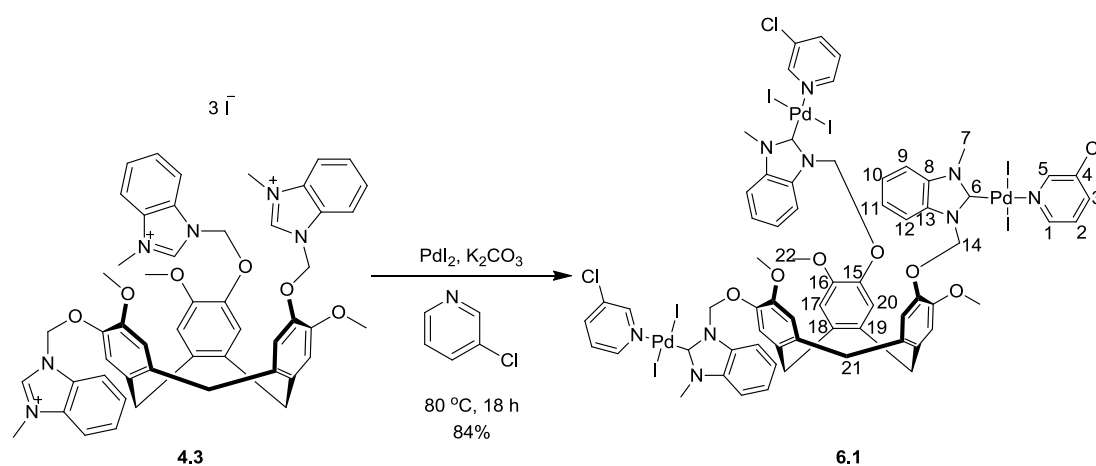
Scheme 6.2 Synthesis of complex 6.1.

The disappearance of the NC*H*N proton in the ^{1}H NMR spectrum associated with the benzimidazolium unit is indicative of a deprotonation taking place, and the formation of a Pd(II)-NHC complex (figure 6.1). The three chemical shifts appearing furthest downfield in the ^{1}H NMR spectrum were all coupling to one another in the ^{1}H-^{1}H COSY NMR spectrum, and are attributed to protons on the 3-chloropyridyl ligand. The two doublets assigned as H[14] correspond to diastereotopic protons on the NCH$_2$O methylene bridge. Both doublets assigned as H[14] also couple to the same carbon environment in the HMQC spectrum. It can be conjectured that solution-state preagostic interactions were not observed in **6.1**, as was seen with **5.1-5.8**. The splitting at H[14] is typical for a diastereotopic site, as opposed to the wider splitting noted in Ir(III) complexes caused by influence of the metal on a proton at this site. The *endo-* and *exo-* doublets associated with the CTV bowl were located at 4.44 and 3.41 ppm, again implying a C_3-symmetric product.
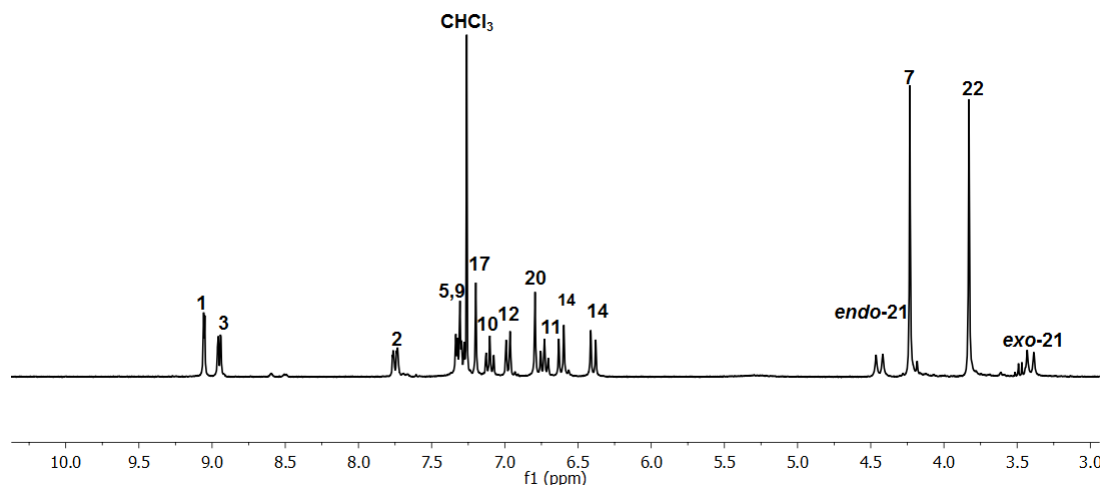
Figure 6.1 ^{1}H NMR spectrum (300 MHz, 293 K, CDCl$_3$) of complex 6.1.

A peak at 161.69 ppm corresponded to the carbenic carbon in the ^{13}C{^{1}H} NMR spectrum (figure 6.2), and coupled to both the N-methyl (H^7) and diastereotopic N-CH$_2$-O (H^{14}) hydrogen atoms in the HMBC spectrum. A carbenic ^{13}C{^{1}H} resonance of *ca.* 160 ppm is typical for a Pd(II)-NHC *trans* to a pyridyl ligand.[23] HMQC spectroscopy confirmed the identities of both C^{14} and C^{21} at 79.20 and 35.76 ppm.
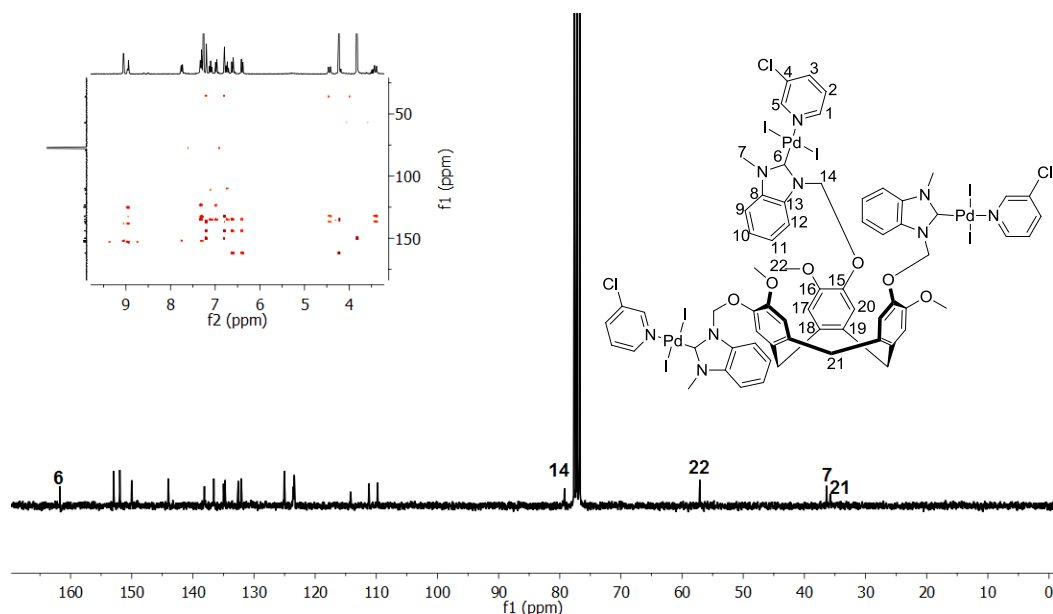
Figure 6.2 ^{13}C{^{1}H} NMR spectrum (75 MHz, 293 K, CDCl$_3$) of complex 6.1. Inset HMBC spectrum.

The HRMS of **6.1** contained a single peak at *m/z* = 1794.5960 corresponding to the complex losing one iodide and three 3-chloropyridine ligands during the ionisation process, and the observed isotope pattern was an excellent match to the simulated

pattern (figure 6.3). The loss of 3-chloropyridine during electrospray ionisation was anticipated due to the strong *trans*-influence of NHC ligands.
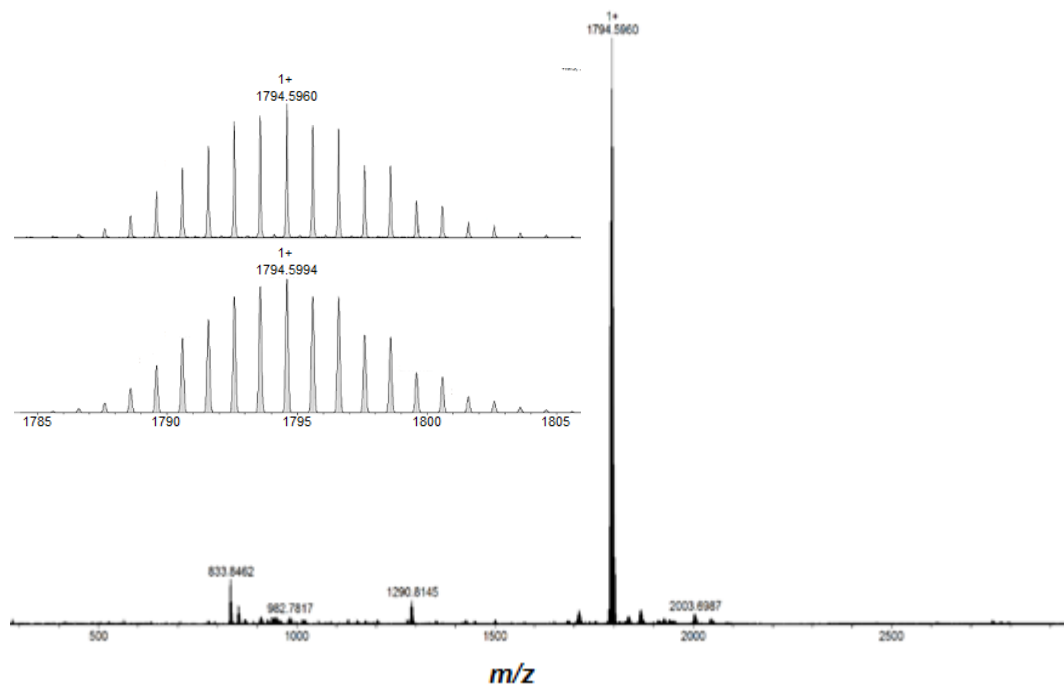
Figure 6.3 HRMS (ESI⁺) of complex 6.1. Inset: observed isotope pattern (top), simulated isotope pattern (bottom).

Single crystals of composition $6.1 \cdot (CH_2Cl_2)_{0.5} \cdot (C_5H_{14})_2 \cdot (H_2O)_2$ were grown from the diffusion of pentane vapours into a dichloromethane solution. The structure was determined by X-ray diffraction. The asymmetric unit comprised a molecule of **6.1**, dichloromethane at half occupancy, water sites and two pentane solvent molecules. The diffuse nature of lattice solvent led to crystals desolvating within seconds of exposure to air, and the crystallographic data are of poor quality. One 3-chloropyridyl ligand was disordered over two positions (figure 6.4), as was one pentane.
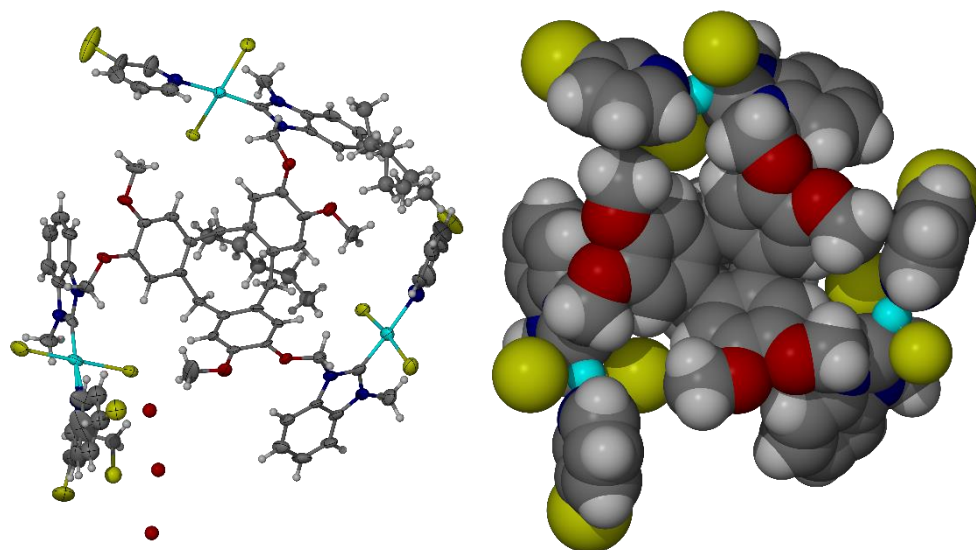
Figure 6.4 Left: Molecular structure of 6.1·(CH₂Cl₂)₀.₅·(C₅H₁₄)₂·(H₂O)₂ (left). Ellipsoids are drawn at the 50% probability. Right: Space filling drawing of 6.1.

The three metallated arms were external to the bowl, directed towards the base of the cavitand, with C_{arene}-O-C-N_{NHC} torsion angles between -66.9 and -67.2°. The Pd-C bond lengths are between 1.931(13) and 1.943(12) Å, comparable with the bond length of 1.969(3) Å reported by Organ *et al.* for PEPPSI™-IPr.[6] All three benzo-backbones of NHC ligands undertake π-π stacking interactions with neighbouring NHCs, at centroid-centroid distances of 3.68-3.72 Å (figure 6.5, left). A dimeric handshake (concept introduced in Section 2.2) was also observed between neighbouring complexes, whereby one 3-chloropyridyl ligand behaves as a guest species to an adjacent cavitand, as shown in figure 6.5 (right). This interaction is reciprocated; in this case, the meta-hydrogen atom of the 3-chloropyridyl ligand is directed towards the hydrophobic cavity, with a C_{py}-centroid separation of 3.944 Å. Crystals grown were racemic, with the dimeric handshake undertaken by *M* and *P* isomers of complex **6.1**. Distances between a calculated H atom of the NCH₂O methylene bridge and Pd centres were between 2.8 and 2.9 Å, but were not aligned in the same manner as Ellman's Rh complexes to suggest preagostic interactions.[24] The space-filling model shows significant exposure of Pd(II) above and below the equatorial plane of the metal cation, potentially enhancing catalytic activity.
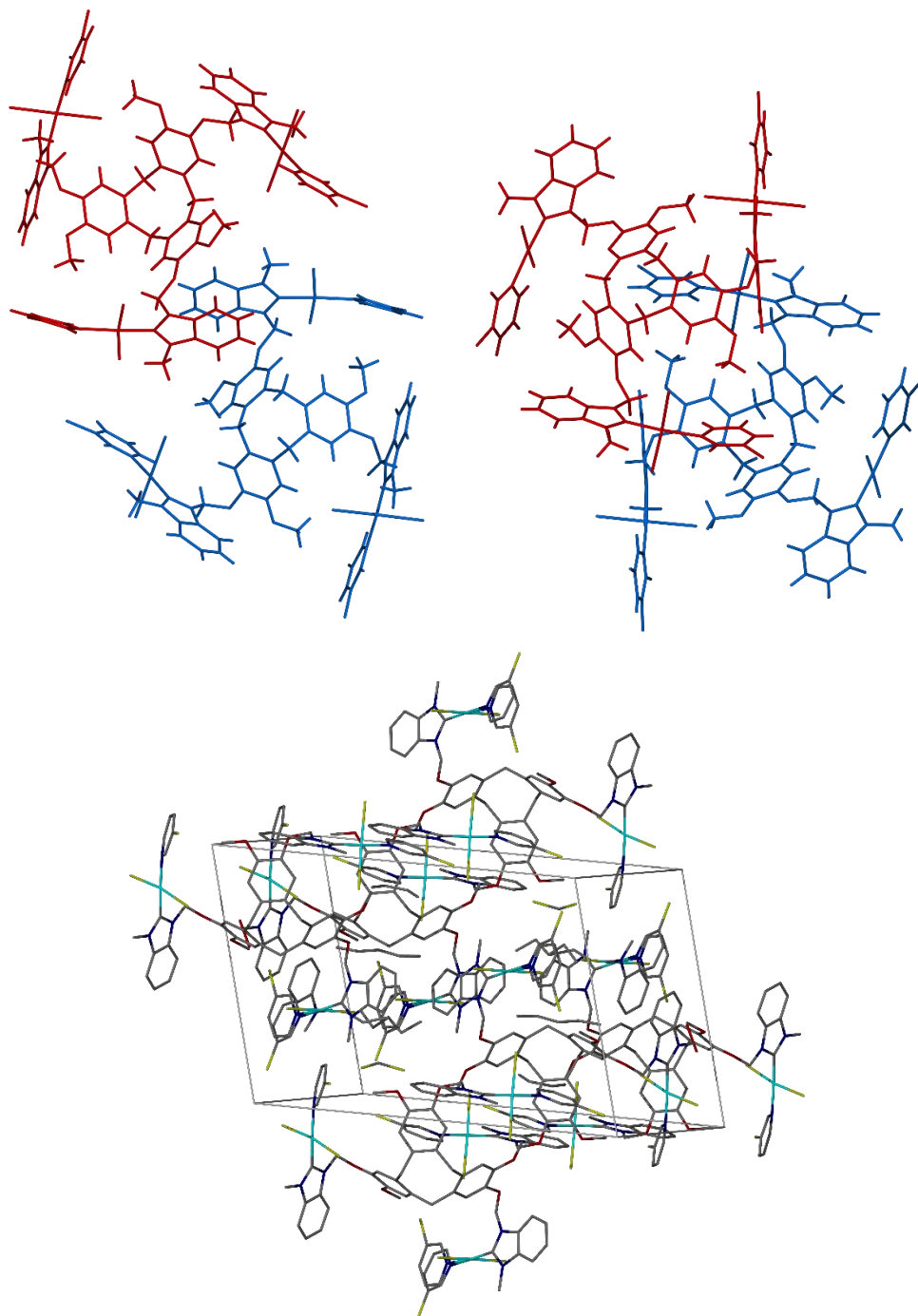
Figure 6.5 Top left: π-π Stacking arrangements between enantiomers of 6. Top right: Dimeric handshake interaction. Opposite enantiomers are shown in red and blue. Bottom: packing diagram of 6.1·(CH₂Cl₂)₀.₅·(C₅H₁₄)₂·(H₂O)₂.

Orange needles of $(6.1)_2 \cdot (C_4H_8O_2)_6$ also grew from the diffusion of diethyl ether vapours into a 1,4-dioxane solution of **6.1**, and the structure was determined by X-ray diffraction. Crystals were of much better quality, and did not readily decompose when removed from the mother liquor. The asymmetric unit comprised of two crystallographically distinct **6.1** complexes and 7.5 dioxane positions, some

refined to 0.5 occupancy to a total of 6 dioxane molecules. As opposed to the pentane solvate, the metallated arms of the complex point upwards, crowning the cavitand (figure 6.6). It was anticipated that the significantly bulky NHC complexes linked to the CTV bowl would undergo steric clashes with one another. However, the metallated arms were observed both above and below the upper rim of the cavitand in two different crystal structures, suggesting there is a barrier to overcome restricted rotation observed heavily in Chapter 5.
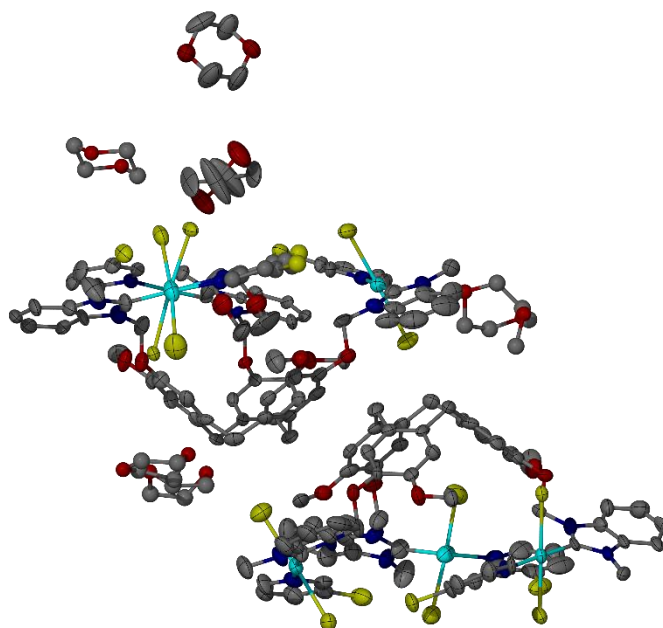
Figure 6.6 Asymmetric unit of (6.1)$_2$· (C$_4$H$_{10}$O$_2$)$_6$. Ellipsoids are drawn at the 50% probability and H atoms omitted for clarity.

The arene faces in the solid-state structure of **6.1** lay flat at the top of the complex, with the 3-chloropyridyl ligands slightly inclined towards the top of the complex. The orientation of metallated arms allows for both the NHC backbone and 3-chloropyridine ligands to engage in π-π stacking interactions with neighbouring complexes. Contrary to **6.1**·(CH$_2$Cl$_2$)$_{0.5}$·(C$_5$H$_{14}$)$_2$·(H$_2$O)$_2$, π-π stacking interactions are between NHC backbone and a 3-chloropyridyl moiety, rather than two NHC groups. Triple deckers of 3-chloropyridyl-NHC backbone-3-chloropyridyl form the buttress to this assembly, at separation of 3.673 and 3.649 Å. Pd-C bond lengths varied between 1.93-1.97 Å, which was comparable to the pentane solvate. The C$_{arene}$-O-C-N$_{NHC}$ torsion angles of both complexes in the asymmetric unit were between -175.4 and -180.0° with near-planar alignment of this group. Three dioxane molecules were ordered and were constrained within a capsule-like assembly,

whereas other solvent molecules were refined at low occupancies, and rigid restraints were applied (figure 6.7, right). Both distinct molecules of **6.1** π-π stack with one another through the CTV bowl at separation of 3.6 Å.
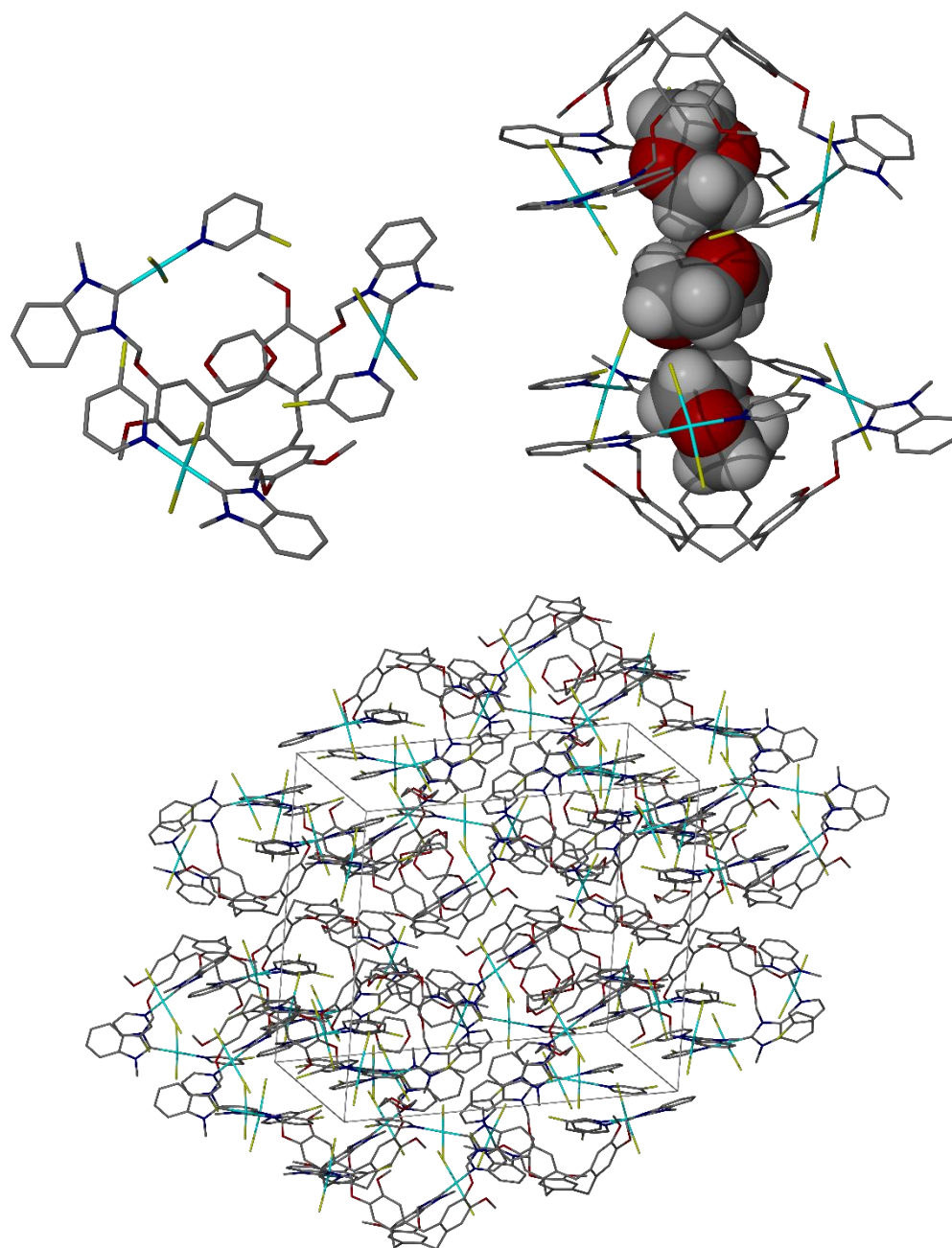
Figure 6.7 Top left:One equivalent of 6.1 with dioxane guest partaking in second-sphere coordination. Top right: and capsule-like assembly of (6.2)₂ encapsulating three dioxane molecules. Bottom: unit cell diagram.

Inclusion of a dioxane guest within the cavity of CTV **6.1** was observed, with one C_2H_4 wall pointing towards the hydrophobic bowl and, potentially encouragingly for catalysis purposes, an interaction between dioxane oxygen and Pd(II) at a

second-sphere coordination distance of 4.5 Å (figure 6.7, left). This could potentially open a gateway towards a supramolecular influence upon site-selective cross-coupling reactions.

6.2.2 Synthesis and characterisation of *N*-benzyl derivative 6.2

Coordination of benzyl ligand **4.5** to Ir, Ru and Rh was not viable because of a considerable solubility mismatch; the ligand only proved soluble in the most coordinating of solvents, such as DMF and DMSO, and insoluble in acetonitrile. Ligand **4.5** was, however, soluble in 3-chloropyridine, which opened the possibility of preparing a Pd(II) NHC complex analogous to **6.1** (scheme 6.3). When aligned towards the metal, the benzylic arm would simultaneously add steric bulk to both sides of the NHC and impart a flexible site on an otherwise rigid system, a feature which has been shown to improve cross-coupling reactions when using Pd-pyridyl-NHC crossover systems as catalysts in the Suzuki-Miyaura reaction.[4] Using similar methodology applied to complex **6.1**, the bulkier Pd(II) *N*-benzyl NHC complex **6.2** could also be prepared. The synthetic methodology was varied slightly to that used when preparing **6.1**, with the necessary addition of potassium iodide to suppress halide mixing due to the benzimidazolium ligand bearing bromide anions rather than iodides.
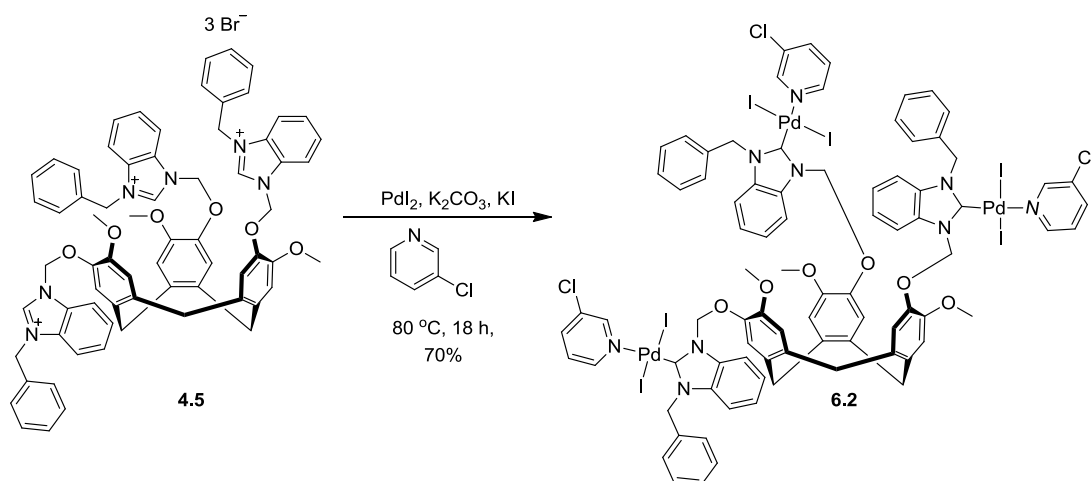
Scheme 6.3 Synthesis of complex 6.2.

HRMS was diagnostic, with the main peak matching complex less one iodide ion and all three 3-chloropyridyl ligands at $m/z = 2022.6935$ (calculated 2022.6951), displaying an excellent match between simulated and observed isotope patterns, as shown in figure 6.8.
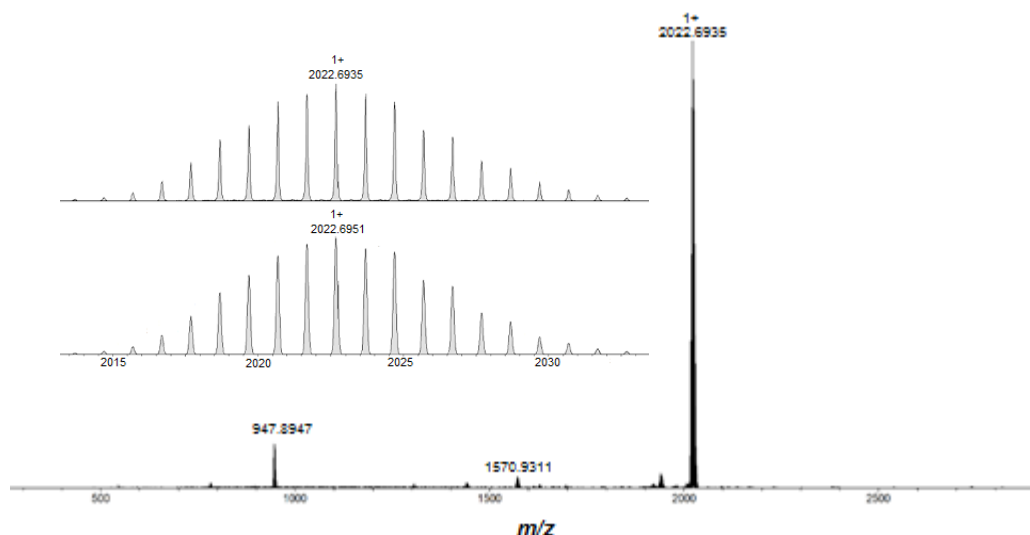
Figure 6.8 HRMS (ESI$^+$) of 6.2. Inset: Observed (top) vs simulated (bottom) isotope pattern

The complex also gave diagnostic ^{1}H NMR data, and the issues associated with trimetallic complexes seen in Chapter 5 did not arise. Ligand **4.5** conveniently contained a single peak encompassing all benzylic aromatic groups (figure 6.9). This was not the case in complex **6.2**, where a sharp spectrum comprising of many resonances was obtained. A number of peaks between 7 and 8 ppm were observed attributed to the N-benzyl aromatics, the CTG arene protons, the NHC benzo-backbone and *meta*-3-chloropyridyl proton. Similarly to complex **6.1**, the loss of imidazolium proton was observed, and *endo-* and *exo-* protons of H^{26} at 4.53 and 3.49 ppm confirmed the presence of a single species in solution. Two methylene bridges proximal to the divalent carbon underwent diastereotopic splitting. H^{18}, associated with the NCH$_2$O methylene bridge appeared further downfield by virtue of deshielding at this site, with doublets assigned as 6.67 and 6.52 ppm. The benzylic CH$_2$ group (H^7) split into two doublets sited at 6.19 and 5.94 ppm.

^{13}C{^{1}H} NMR spectroscopy was also carried out (figure 6.10), with full assignment complemented by DEPT-135, HMQC and HMBC experiments. DEPT-135 NMR spectroscopy allowed for the elucidation of C^7, C^{18} and C^{26}, with recorded chemical shifts of 54.90, 79.64 and 35.97 ppm respectively. The carbenic carbon, C^6, was assigned as 162.69 ppm and confirmed by HMBC spectroscopy, coupling to both *N*-substituents of the NHC.
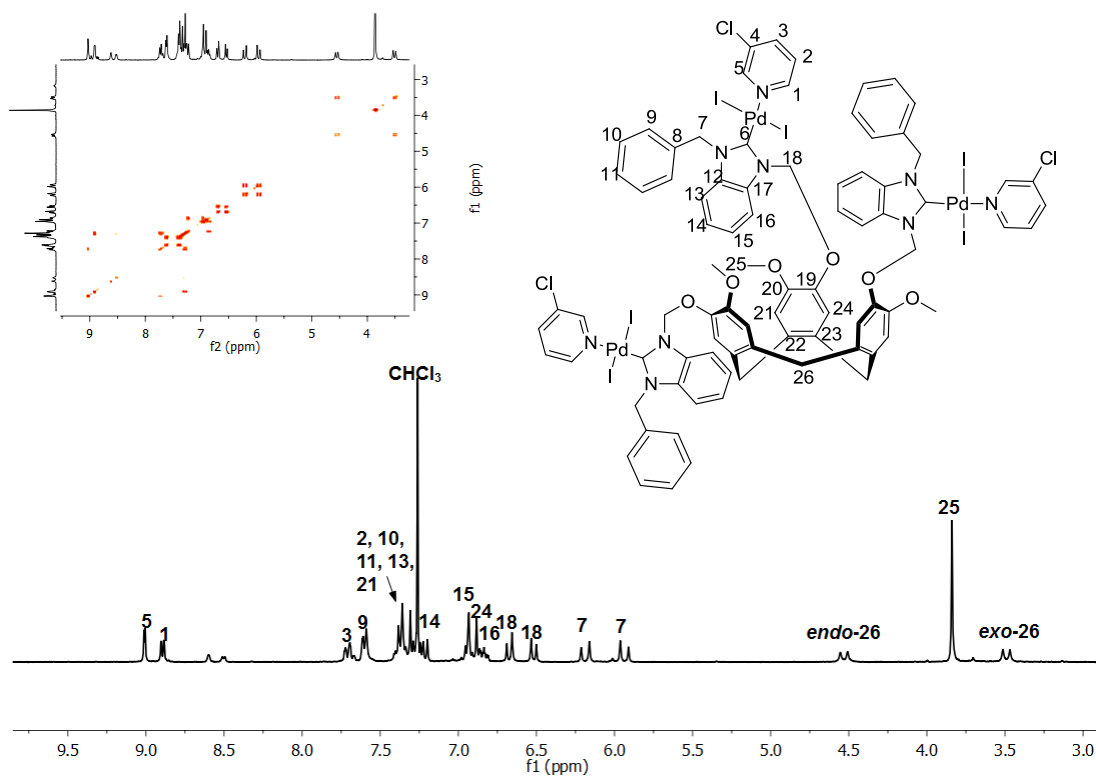
Figure 6.9 ^{1}H NMR spectrum of **6.2** (300 MHz, 293 K, CDCl$_3$). Inset: COSY NMR spectrum.
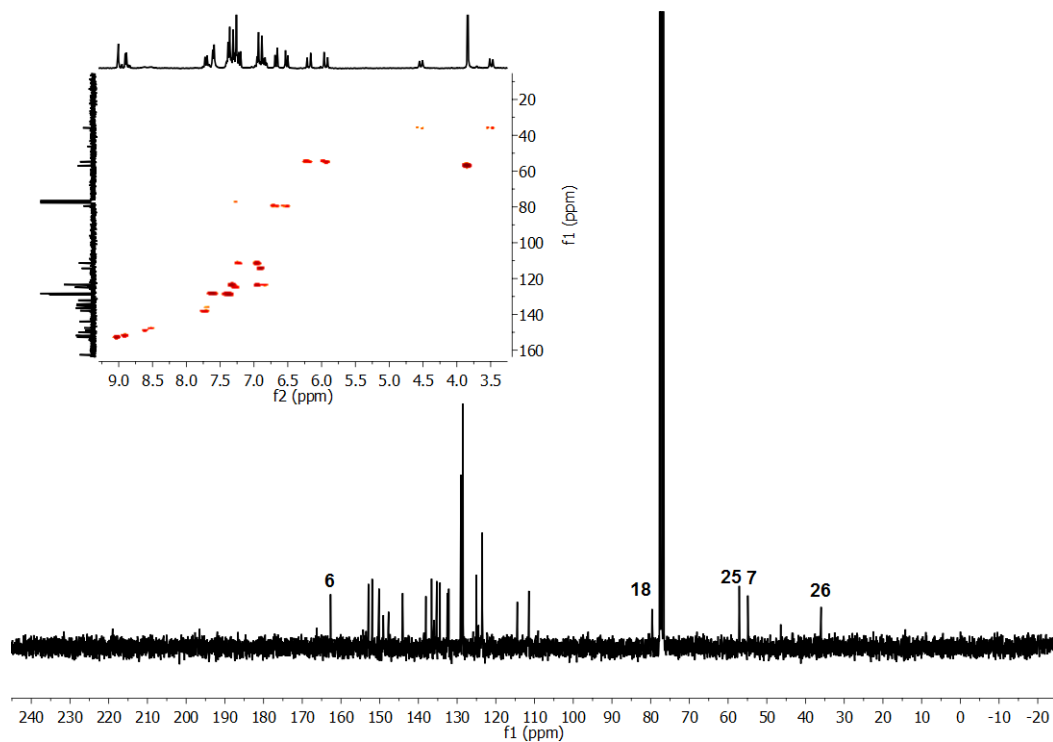
Figure 6.10 ^{13}C{^{1}H} NMR spectrum of **6.2** (75 MHz, 293 K, CDCl$_3$). Inset: HMQC spectrum.

6.3 Guaiacol-derived Pd(II) NHC complexes

6.3.1 Synthesis and characterisation of an *N*-methyl monometallic complex

In a similar vein to Chapter 5, monometallic Pd(II) NHC complexes 3-chloropyridyl diiodo (1-methyl-3-((2-methoxyphenoxy)methyl)benzimidazol-2-ylidene)palladium, **6.3** and 3-chloropyridyl diiodo (1-benzyl-3-((2-methoxyphenoxy)methyl)benzimidazol-2-ylidene)palladium, **6.4** were synthesised to give new catalysts bearing a similar environment to the arene faces of the CTV core, with the intention of comparing monometallic and trimetallic complexes in catalytic transformations.
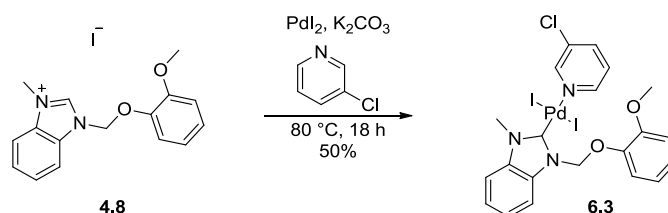
Scheme 6.4 Synthesis of complex 6.3.

The *N*-methyl monopalladium complex **6.3** was prepared in reasonable yield according to the same procedure as **6.1**. The ^{1}H NMR spectrum of **6.3** contained the NMR handle afforded by the *N*- and *O*-methyl resonances assigned as 4.20 and 3.96 ppm. Peaks assigned as H-atoms proximal to the Pd(II) centre in both **6.1** and **6.3** appeared at near-identical chemical shifts. H^{14} was marginally downfield in **6.3** compared to **6.1**, with this site perhaps being slightly deshielded compared to the cavitand complex. Diastereotopic splitting of H^{14} was not observed in the ^{1}H NMR spectrum of **6.3**, suggesting this hinge is flexible, in addition to preagostic interactions being absent. Whilst chemically similar, the main discrepancy in ^{1}H NMR spectra lay with the guaiacol group. **6.1** bears two protons on each CTV face which are *para* with respect to one another, affording two singlets in the ^{1}H NMR spectrum. Conversely, **6.3** contains four aromatic protons on its pendant guaiacol arm, all of which couple to one another, causing some convolution of the aromatic region in its ^{1}H NMR spectrum.
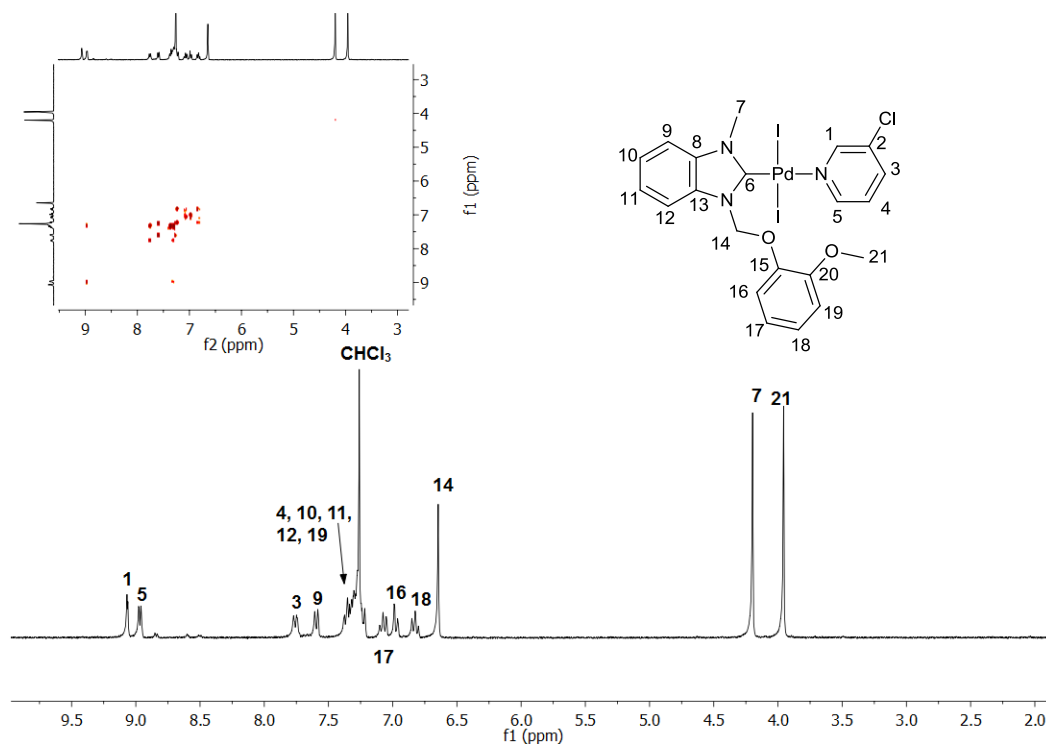
Figure 6.11 ^{1}H NMR spectrum (300 MHz, 293 K, CDCl$_3$) of complex 6.3.

Carbon atoms were fully assigned using HMQC, HMBC and DEPT-135 NMR spectroscopy (see appendix). The ^{13}C{^{1}H} NMR spectrum of **6.3** (figure 6.12) bore similarities to **6.1**, with chemical shifts proximal to Pd(II) being highly comparable. The carbenic carbon, C^6 was sited at 161.36 ppm. The methylene bridge C^{14} was assigned as 79.38 ppm, and N-methyl resonance as 36.21 ppm. Complex **6.1** depicted these relative environments as 161.69, 79.20 and 36.36 ppm respectively.

The anticipated {M-(I)-(3Clpy)}$^+$ fragment dominated the mass spectrum (ESI)$^+$ (figure 6.13) and displayed an excellent isotopic match to the simulated model. The fragment observed at m/z = 1130.7631 was identified as a {**6.3**}$_2$$^+$ fragment, with the loss of one iodide ion and two 3-chloropyridyl donors (calculated m/z = 1130.7626).
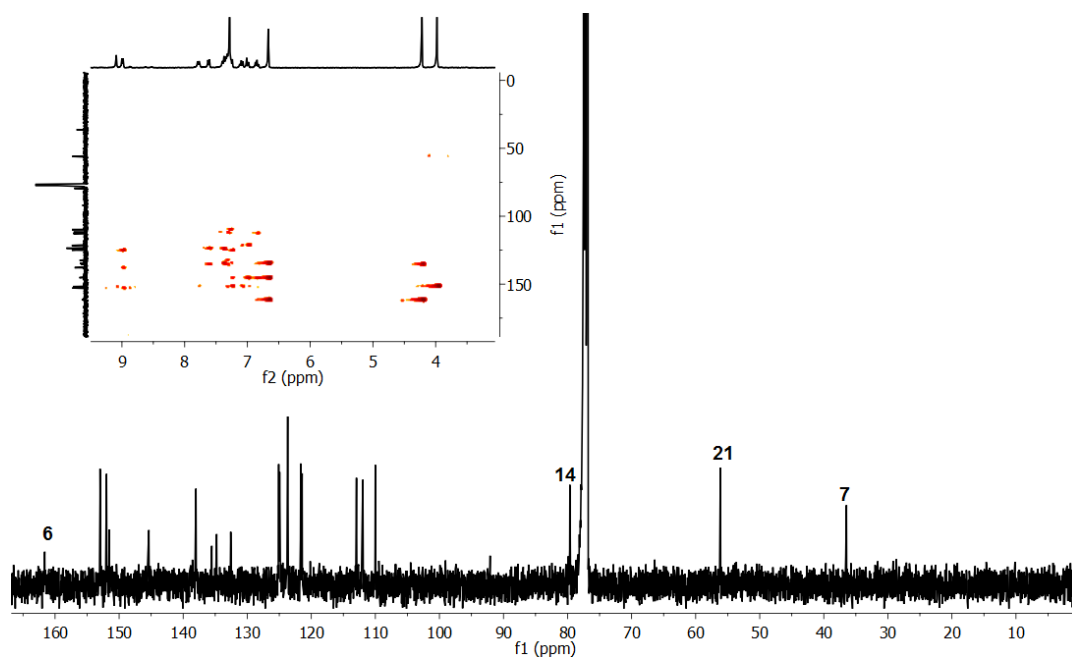
Figure 6.12 ^{13}C{^{1}H} NMR spectrum (75 MHz, 293 K, CDCl$_3$) of complex 6.3. Inset: HMBC spectrum.
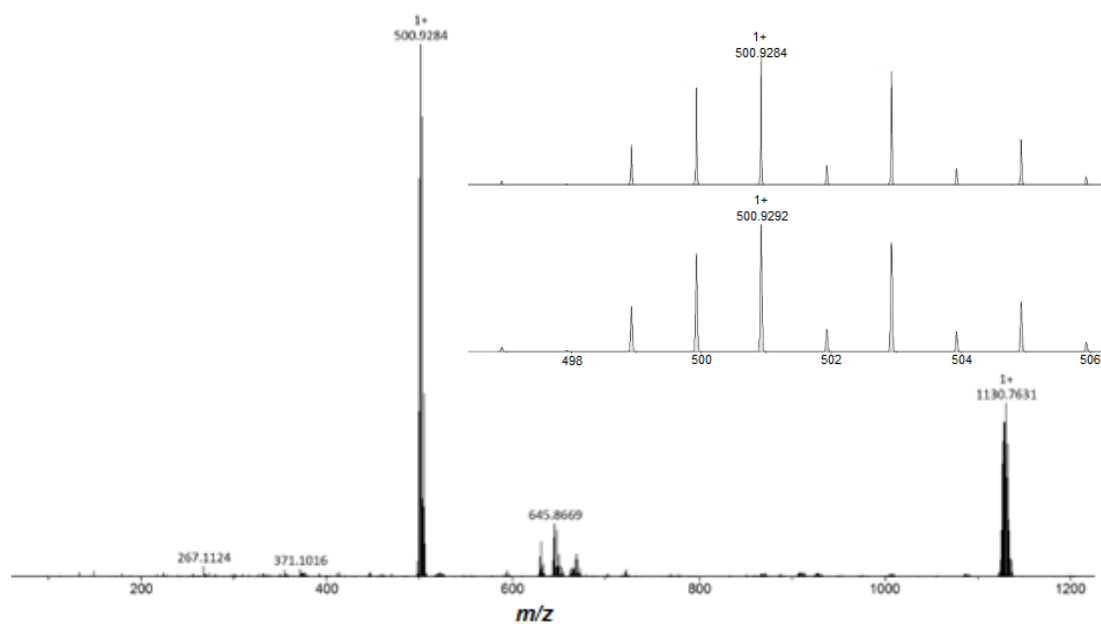
Figure 6.13 HRMS (ESI$^+$) of complex 6.3. Inset: Observed (top) vs simulated (bottom isotope patterns for the main peak

Single crystals suitable for diffraction were grown from the diffusion of pentane into a dichloromethane solution of **6.3**. The structure was solved in the monoclinic $P2_1$/c space group, with the asymmetric unit comprising of one whole unit of **6.3**, as shown in figure 6.14.
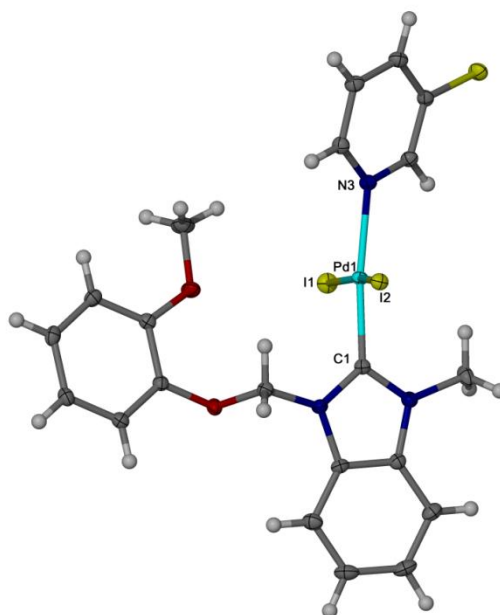
Figure 6.14 Asymmetric unit of 6.3. Ellipsoids are drawn at the 50% probability.

The structure was highly ordered, with no anticipated positional disorder about the 3-chloropyridyl ligand, selected bond lengths and angles are shown in table 6.1.

Table 6.1 List of selected bond lengths (Å) and angles (°) for 6.3.

Pd1-I1	2.61062(14)	I1-Pd1-C1	88.13(4)
Pd1-I2	2.61109(14)	I2-Pd1-N3	92.02(4)
Pd1-N3	2.1117(13)	I2-Pd1-C1	87.73(4)
Pd1 C1	1.9568(15)	C1-Pd1-N3	173.37(6)
I1-Pd1-I2	172.219(6)	C10-O1-C9-N2	-169.837
I1-Pd1-N3	92.85(4)		

Molecules of **6.3** interact with each other through π-π stacking interactions between neighbouring 3-chloropyridine ligands at separation of 3.68 Å. Guaiacol groups and the benzo-backbone of NHC ligands are within 3.5 Å of one another at their closest contacts, but are aligned incorrectly to engage in π-π stacking, and the bulk of both rings are separated by a distance of greater than 4 Å. C-H···π interactions were also noted between the 5-position of 3-chloropyridyl ring and the centroid of guaiacol pendants, at a C···centroid separation of 3.34 Å.

6.3.2 Preparation and characterisation of *N*-benzyl monomer 6.4

The *N*-benzyl monomer, **6.4** was prepared following the same procedure to that of the CTV derivative **6.2** (scheme 6.5) and was isolated as a sticky solid.
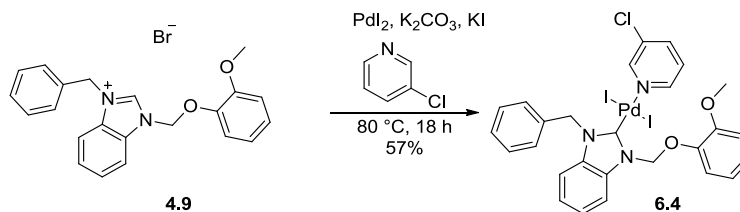
Scheme 6.5 Synthesis of complex 6.4

The propensity of these complexes to ionise and form {M–I-(3Clpy)}$^+$ fragments was again observed (figure 6.15), with a peak of *m/z* = 576.9599 dominating the HRMS. The observed isotope pattern displayed an excellent match to the simulated model. Furthermore, an additional two fragments were detected, firstly at *m/z* = 449.0491, which corroborated with a bidentate Pd(II)-NHC fragment bearing no iodide ligands and a cyclometallated benzylic moiety (calculated *m/z* = 449.0476). ^{1}H NMR spectroscopy disproved the presence of this fragment in the bulk solution as a side-product, and no observed Pd-C peaks arising from cyclometallation in the ^{13}C{^{1}H} NMR spectrum in their characteristic range of 150-160 ppm. Therefore, *m/z* = 449.0476 was attributed as a result of ionisation. The third peak present displayed an excellent match to K[Pd(NHC)I$_2$]$^+$ with *m/z* = 742.8273 (calculated *m/z* = 742.8281).

The ^{1}H NMR spectrum of **6.4** (figure 6.16) contains twelve aromatic resonances within a 1 ppm range. The diastereotopic NCH$_2$O and N-benzyl CH$_2$ protons both appear as singlets at 6.72 and 6.03 ppm, without splitting as was observed in **6.1** and **6.2**. Similarly to **6.1**-**6.3**, the doublet and doublet of doublets at 9.02 and 8.92 ppm were good matches to resonances on the 3-chloropyridyl ligand.
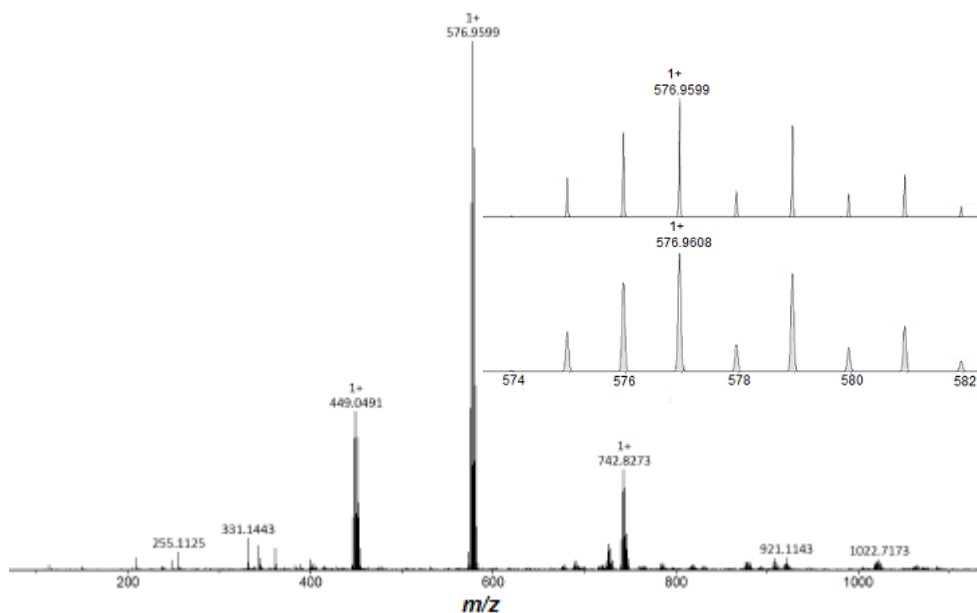
Figure 6.15 HRMS (ESI⁺) of complex 6.4. Inset: Observed (top) vs simulated (bottom) isotope patterns for the major peak in the spectrum
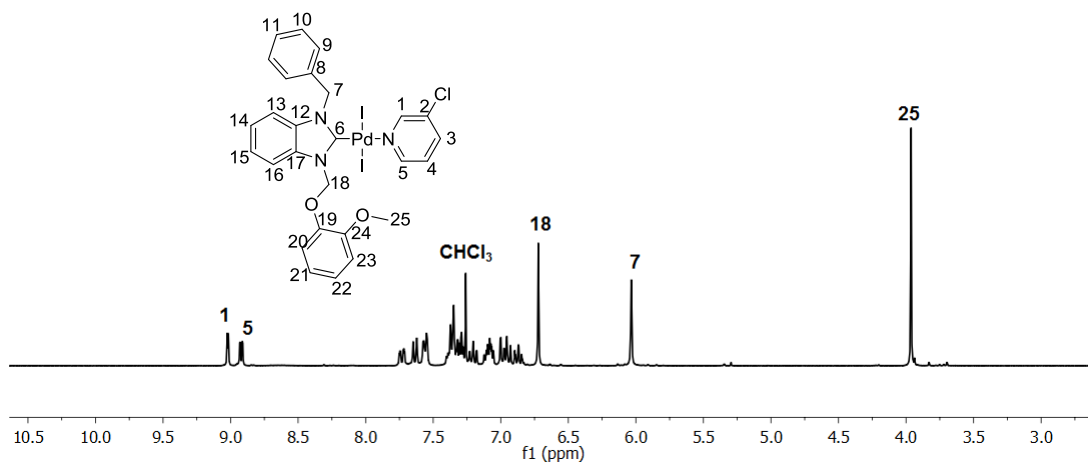
Figure 6.16 ^{1}H NMR spectrum (300 MHz, 293 K, CDCl₃) of 6.4.

The ^{13}C{^{1}H} NMR spectrum of **6.4** (figure 6.17) showed similarities to **6.1**-**6.3**, with the carbenic carbon C^6 resonating at 162.57 ppm. The carbenic carbon was observed within a 1.5 ppm range for complexes **6.1**-**6.4**, suggesting that fusing a Pd(II)-NHC complex with *N*-methyl or *N*-benzyl arms onto a rigid CTV bowl does not have a significant effect on the electronic factor of the NHC ligand. Two CH_2 peaks were observed in the DEPT-135 spectrum, 79.99 and 55.01 ppm, which were assigned as C^{18} and C^7 respectively.
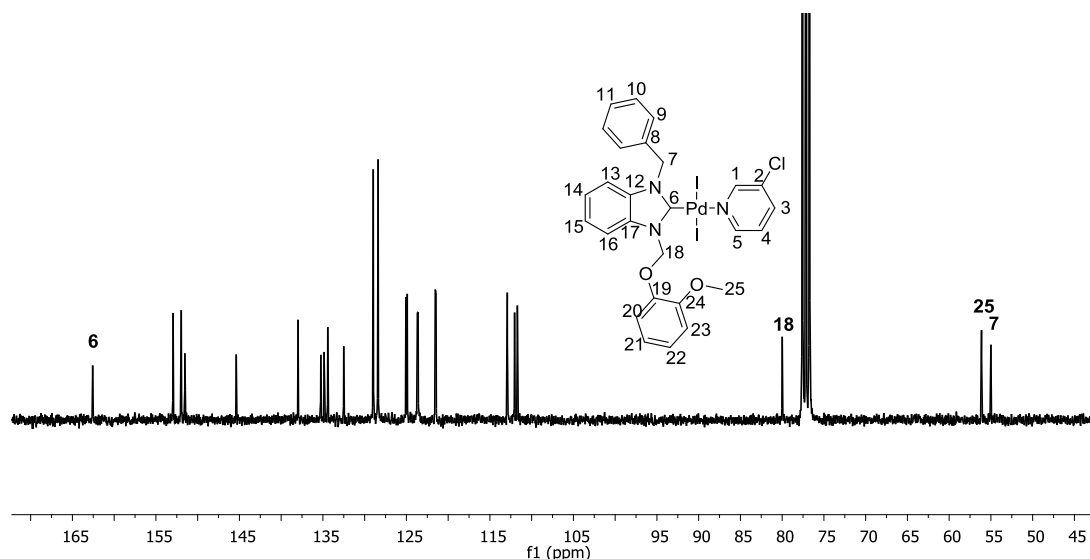
Figure 6.17 ^{13}C{^{1}H} NMR spectrum (75 MHz, 293 K, CDCl$_3$) of 6.4.

Single crystals of **6.4** could be grown from the diffusion of diethyl ether vapours into an acetonitrile solution of the complex. The X-ray data were collected by Edward Britton using synchrotron radiation. The structure was solved in the orthorhombic *P*2$_1$/*n* space group, and the asymmetric unit comprised two crystallographically distinct **6.4** molecules, which interact through π-π stacking arrangements between 3-chloropyridyl ligands and NHC benzo-backbones at a separation of 3.6 Å (figure 6.18). The NHC *N*-substituents of both **6.4** molecules are of different orientations, The NHC wingtips associated with complex 1 (containing Pd1) were both folded towards the same face of the complex, and the second complex contains *N*-substituents bent towards opposite faces of the ligand. The aryl groups on both substituents are aligned away from the Pd centres on both complexes. Chains grow throughout the crystal lattice by means of CH-π interactions between the methoxy group of the N-(2-methoxyphenoxymethyl) component of one complex (Pd1) and the N-benzyl substituent of the second complex, at a C⋯centroid separation of 3.53 Å. Bond lengths and angles about the Pd(II) centres are similar to one another, with differences of no more than 4° in bond angles when comparing the crystallographically distinct complex molecules. Both have considerably dissimilar C$_{arene}$-O-C-N$_{NHC}$ torsion angles, with complex 1 being close to antiperiplanar, whilst complex 2 is much more strained, with a measured torsion angle of -71.943°. The N-benzyl arms were of similar orientations in both complex equivalents, and resided roughly perpendicular to the Pd-C bond. Selected bond lengths and angles are given in table 6.2.
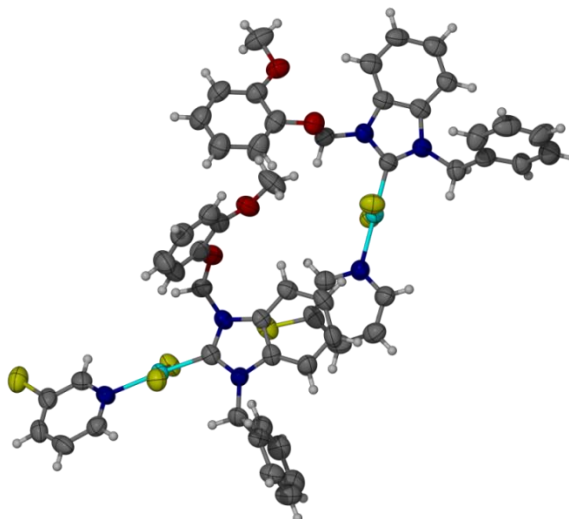
Figure 6.18 Asymmetric unit of (6.4)₂. Ellipsoids are drawn at the 50% probability.

Table 6.2 Selected bond lengths (Å) and angles (°) from the crystal structure of (6.4)₂.

Pd1-I1	2.6099(8)	Pd2-I3	2.6142(8)
Pd1-I2	2.5983(8)	Pd2-I4	2.5882(8)
Pd1-N3	2.086(7)	Pd2-N6	2.131(6)
Pd1-C1	1.957(7)	Pd2-C28	1.969(7)
I1-Pd1-I2	172.32(3)	I3-Pd2-I4	174.45(3)
I1-Pd1-N3	91.36(18)	I3-Pd2-N6	93.06(18)
I1-Pd1-C1	88.4(2)	I3-Pd2-C28	88.3(2)
I2-Pd1-N3	92.52(18)	I4-Pd2-N6	92.19(18)
I2-Pd1-C1	87.8(2)	I4-Pd2-C28	86.4(2)
C1-Pd1-N3	179.6(3)	C28-Pd2-N6	176.7(3)
C16-O1-C15-N1	172.738	C43-O4-C42-N4	-71.943
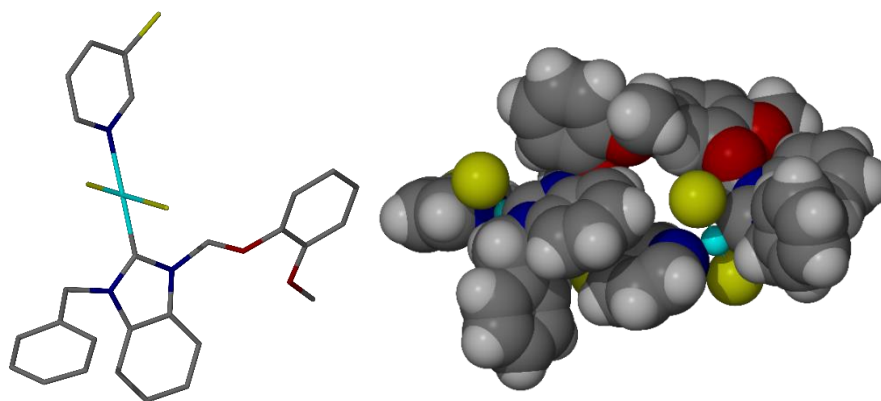
Figure 6.19 Left: One equivalent of 6.4. Right: space-filling diagram of the asymmetric unit.

The main intermolecular interaction driving crystallisation were the π-π stacking interactions between 3-chloropyridine and NHC benzo-backbone. Whilst the two aromatic wingtips did not partake in π-π stacking, the flexible groups aligned themselves into a closely packed structure, with guaiacol groups sandwiched perpendicularly between two 3-chloropyridine units at separations of *ca.* 3.9 and 4.5 Å.

6.4 Catalytic assessment of Pd(II) complexes

6.4.1 Catalytic activity in the Suzuki-Miyaura reaction of phenylboronic acid and 4-bromotoluene

Cross-coupling reactions are widespread, and applicable in many branches of synthetic chemistry as a facile method of C-C bond formation, replacing traditional procedures which used harsh conditions and organolithium reagents. Common coupling reactions involve those between aryl halides and alkenes (Heck),[25] alkyne and aryl halides in the presence of a Cu(I) co-catalyst (Sonogashira),[26] as well as Negishi[27] and Kumada[28, 29] couplings, which use more reactive organozinc or Grignard reagents as coupling substrates. The reactions have been mainstays in synthetic chemistry for almost half a century, and for their work on developing such significant reactions, Suzuki, Heck and Negishi were awarded the 2010 Nobel Prize in Chemistry.[30] The active catalyst in cross-coupling reactions is typically a Pd(0) species, although the facile *in situ* reduction of much more stable Pd(II) complexes by reaction with an excess of boronic acid allows for straightforward reactivity.

The Suzuki-Miyaura reaction was first reported in 1979 for the coupling between alkenyl halides and alkenyl boronic acids.[31] Nowadays, the reaction is the

primary method for biaryl synthesis, and has become a mainstay in synthetic chemistry. Boronic acids are commercially available, or straightforward to prepare by reaction of a Grignard reagent with a trialkyl borate, which is hydrolysed to the boronic acid upon aqueous workup. Extensive development of this reaction has led to an assortment of catalysts being reported, with substrate scope also being extensive. The main components of the Suzuki reaction are an aryl halide or triflate, which can be coupled with a boronic acid, pinacolato boronate ester, or in the most resistant of cases, an aryl bismuth reagent.[32-34] The base (shown as NaOH in scheme 6.6) performs a number of roles, notably reacting with the boronic acid to yield a more nucleophilic boronate salt.[35] The active catalyst is a Pd(0) species, and a battery of ligand classes have been used to stabilise such complexes, including phosphines and NHCs.

The generally accepted mechanism for the Suzuki-Miyaura reaction (scheme 6.6) involves first reducing the Pd(II) complex to Pd(0) where necessary, before the oxidative addition of aryl halide. Halide abstractions can occur when using alkali metal bases, replacing the halide with a more labile ligand. A transmetallation step then proceeds, where the labile ligand is substituted for the aryl of the boronic acid, producing a soluble borate salt as by-product. A *cis-trans* isomerisation reversibly ensues (irrelevant when *cis*-chelating or significantly bulky ligands are used), prior to the reductive elimination of biaryl component and the regeneration of a Pd(0) species. Deactivation pathways known include homocoupling (often involves two equivalents of boronic acid), and also colloidal Pd nanoparticle (also known as palladium black) aggregation which, depending on the nature of the nanoparticles, may or may not be catalytically active.

Complexes **6.1-6.4** were all examined in the Suzuki-Miyaura reaction between 4-bromotoluene and phenylboronic acid (scheme 6.7). The effect of tethering three catalytic sites to a rigid cavitand to see whether supramolecular interactions enhance or hinder catalysis was assessed.
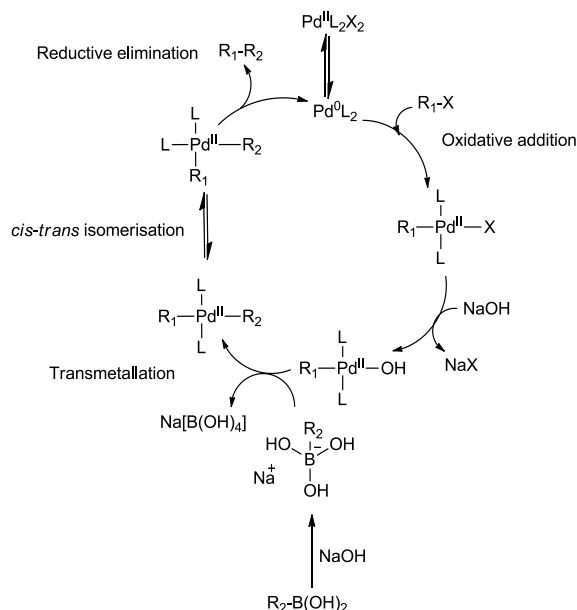
Scheme 6.6 Generally accepted mechanism for the Pd(0)-catalysed Suzuki-Miyaura reaction.
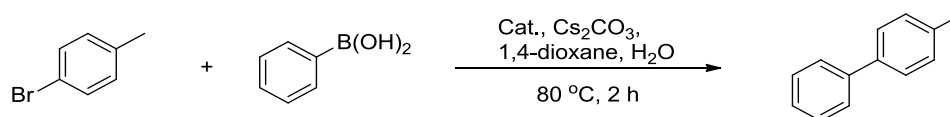
Scheme 6.7 Suzuki-Miyaura reaction between 4-bromotoluene and phenylboronic acid.

Table 6.3 Conversions and TONs for the Suzuki-Miyaura reaction between 4-bromotoluene and phenylboronic acid catalysed by 6.1-6.4.

	0.25 mol% Pd		0.5 mol% Pd		1 mol% Pd	
Catalyst	Conversion (%)	TON (TOF, h^{-1})	Conversion (%)	TON (TOF, h^{-1})	Conversion (%)	TON (TOF, h^{-1})
Pd(OAc)$_2$ + PPh$_3$	-	-	56 ($\pm$1)	110 (55)	-	-
6.1 (CTV)	21 ($\pm$1)	84 (42)	24 ($\pm$1)	48 (24)	20 ($\pm$2)	20 (10)
6.2 (CTV)	37 ($\pm$5)	148 (74)	41 ($\pm$3)	82 (41)	22 ($\pm$1)	22 (11)
6.3	22 ($\pm$6)	88 (44)	23 ($\pm$2)	46 (23)	42 ($\pm$6)	42 (21)
6.4	26 ($\pm$11)	104 (52)	32 ($\pm$2)	64 (32)	55 ($\pm$3)	55 (22.5)

Conversions were obtained using ^{1}H NMR spectroscopy, were the average of two runs and compared to 1,4-dimethoxybenzene as an internal standard. Turnover number defined as moles of product/moles Pd.

Monometallic complexes **6.3** and **6.4** showed increased conversions on increasing the catalyst loading. This is in contrast to the trimetallic complexes **6.1** and **6.2**, which displayed similar conversions at 0.25, 0.5 and 1 mol% Pd loading. Turnover

numbers (TON) revealed a homeopathic effect in all four cases, where a decrease in catalyst loading leads to increased activities.[36] Homeopathic effects in catalysis occur when low catalyst loading leads to higher performing results than when higher concentrations of catalysts are applied. This can be connected to nanoparticle formation at higher catalyst concentrations, where the active site of nanoparticles is poorly defined compared to a homogeneous catalyst. Turnover numbers in this chapter are defined as the moles of product formed per Pd centre. TON were slightly higher for **6.1** and **6.2** at lower catalyst loading compared to **6.3** and **6.4**, although the presence of a *N*-benzyl component appeared to have a greater impact on catalysis rather than guaiacol vs CTV. Pd black was liberated in screens involving all four catalysts. The formation of Pd nanoparticles occurred within minutes when employing **6.3** or **6.4** as catalysts, whereas this was offset for *ca.* 1 h during reactions catalysed by **6.1** and **6.2**, suggesting that whilst the cavitand may not enhance catalysis in this case, it may afford a stabilising effect to complexes. Turnover frequencies (TOF) also decreased significantly as catalyst loading increased, with values ranging from 74 h^{-1} for **6.2** at 0.25 mol% Pd loading to 10 h^{-1} for **6.1** at 1 mol% Pd loading. TOF is defined as the turnover number per hour. CTV catalysts **6.1** and **6.2** were much more active at low loading, but became considerably less active than **6.3** and **6.4** when catalyst loading was increased. This could be due to nanoparticle formation, which may be poorly active or inactive at catalysing the cross-coupling of 4-bromotoluene and phenylboronic acid. TONs associated with **6.3** and **6.4** do not decrease significantly when increasing catalyst loading from 0.5 mol% to 1 mol%. Alongside the observation of rapid palladium black formation, the similar TONs between examinations could suggest the formation of catalytically active nanoparticles. All reactions at 0.5 mol% were compared to the commonly employed $Pd(OAc)_2$ and PPh_3 system, which was more active than all four reported complexes. A palladium-free screen gave no conversion.

The groups of Matt, Toupet and Brenner have studied catalytic efficacy of mononuclear calix[4]arene[37] or resorcin[4]arene[38] tethered Pd-NHC complexes and compared to a Pd(II) arene-wingtipped complex. Their results revealed similar activities between the more conventional complex and their cavitand derivative, suggesting the bowl does not behave as a receptor, and the cavitand is merely behaving as a bulky ligand, contrasting their previous findings when employing

phosphine analogues.[39] This remains relatively consistent with the CTV derivatives, which generally do not enhance nor impede the coupling of 4-bromotoluene and phenylboronic acid. Matt's resorcin[4]arene complexes bearing *mono*, *bis* and *tetrakis* NHC ligands all displayed similar activities, suggesting each Pd(II) centre behaves independently from others on the scaffold.

Contrasting behaviour is seen when comparing disk-shaped multimetallic complexes containing extended polyaromatic systems. Peris and co-workers have reported a number of multimetallic complexes which have a propensity to π-π stack with one another leading to much higher catalytic activities than in monometallic analogues (M= Pd, Au).[40] Doping catalytic reactions with pyrene and hexafluorobenzene led to severely reduced conversions for multimetallic examples, implying that stacking arrangements leading to cooperativity between complexes are responsible for this increase.[41] DFT studies revealed little communication between metals in the extended aromatic multimetallic complexes.[42]

A cross-coupling reaction that PEPPSI™ complexes are known to catalyse is the Buchwald-Hartwig amination reaction, historically between a secondary amine and an aryl halide, yielding a tertiary amine.[43] Coupling a less bulky primary amine, or even ammonia are much more challenging due to the propensity of the amine to bind to the metal, however sterically encumbered catalysts can help remediate this.[44, 45] With this in mind, complex **6.1** was tested in the cross-coupling between aniline and 4-bromotoluene at a reasonably high catalyst loading of 3 mol%. After 24 h, a conversion of 9% was observed by ^{1}H NMR spectroscopy. This conversion is considerably lower than a number of reported examples for what is a reasonably well-documented, but still challenging reaction.[46] Therefore it was decided to remain with the Suzuki-Miyaura reaction and alter the substrates.

6.4.2 Determining the nature of catalysis

A number of Pd-catalysed reactions can be facilitated by nanoparticles, therefore it is critical to determine whether homogeneous or heterogeneous catalysis is occurring. In the Suzuki-Miyaura reaction between 4-bromotoluene and phenylboronic acid catalysed by complexes **6.1**-**6.4**, a significant quantity of Pd black precipitated from reactions; for the trimetallic complexes this occurred from ca. 1 h onwards, whereas for the monometallic complexes it was almost immediate after reaching 80 ℃. As detailed in section **6.5.1**, a homeopathic effect was

observed, where lower catalyst loading led to elevated activity.[36] This can be an indication of inhomogeneity, whereby a higher concentration of catalyst being present induces aggregation, and the formation of inactive nanoparticles. One method of qualitatively determining the nature of the active catalyst is the mercury drop test.[47] The precatalyst is reduced to its Pd(0) form, before the addition of 150-300 eq. elemental Hg. Any colloidal Pd(0) amalgamates with the Hg, leaving only mononuclear (or trinuclear in the case of **6.1** and **6.2**) catalyst in solution. In the case of a positive mercury drop test, biaryl is detected in the reaction which suggests that homogeneous catalysis is occurring as the colloidal Pd(0) is absent. If no product is detected, the reaction is therefore thought to be catalysed in a heterogeneous manner. Palladium nanoparticle formation has been monitored using UV-vis spectroscopy, but monitoring their formation during a reaction under inert conditions may be challenging.[48]

For complexes **6.1**-**6.4** at 0.5 mol% Pd, identical conditions to the previous screens (table 6.3, scheme 6.7) were carried out, with the addition of Hg. ^{1}H NMR spectra after 2 h revealed the presence of 4-phenyltoluene in all four examples, albeit in heavily reduced conversions of *ca.* 10%, suggesting a level of homogeneous catalysis is ongoing. The reduced activities in mercury drop tests can be caused by catalytically active nanoparticles rendered inactive by amalgamation, so only gives a qualitative indication that heterogeneous catalysis is contributory towards the overall reaction. De Vries suggested the formation of Pd nanoparticles via soluble Pd clusters is reversible, so equilibration between states could also be an important factor.[36]

6.4.3 Towards regioselective Suzuki-Miyaura reactions

Second-sphere coordination of a guest 1,4-dioxane to a Pd(II) centre in the crystal structure of **(6.1)$_2$·(C$_4$H$_8$O$_2$)$_6$** was observed. Should this be extended to heteroarenes such as pyridyl substrates bearing more than one halide, regioselectivity mediated by confinement could allow for a different product distribution for reactions catalysed by trimetallic complexes compared to the monometallic counterparts. Reactivity between 4-bromotoluene and phenylboronic acid was sluggish, therefore an electron-rich boronic acid was selected alongside a more electron-deficient pyridyl substrate.

The reaction of 2,5-dibromopyridine and 4-methoxyphenylboronic acid was selected because of the potential for regioselective catalysis. This particular cross-coupling reaction has been examined for regioselectivity in previous studies, with regioselectivity at the 2-position dominating (scheme 6.8). In order to preferentially cross-couple at the 5-position, a more reactive halide has to be employed. Rao has employed 2-bromo-5-iodopyridine and 2-iodo-5-bromopyridine to afford site-selectivity.[33] An established number of regioselective reactions using the 2,5-dibromopyridine substrate have been reported, including Suzuki,[33, 49, 50] Sonogashira[51, 52] and Stille coupling.[53] In all cases, regioselectivity was observed at the anticipated electron-deficient 2-position. Studies by Handy and co-workers led to the monosubstitution at the 2-position in modest yield, however, under some conditions hydrodehalogenation of the 5-bromo substrate dominated proceedings, so could be a potential pathway to further byproducts.[54]
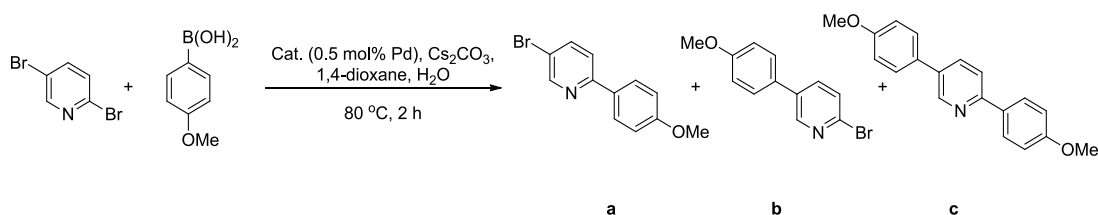
Scheme 6.8 The Suzuki-Miyaura reaction between 2,5-dibromopyridine and 4-methoxybenzeneboronic acid, and potential products.

Using a supramolecular approach to regioselective catalysis in this particular reaction is undocumented, although a number of cases stem from Fujita's pioneering Diels-Alder reactions within an octahedral cage.[55]

Cid and co-workers proposed Pd(II) binuclear complexes as reaction intermediates in the Suzuki-Miyaura reaction, and upon reacting Pd(PPh$_3$)$_4$ with 2,4-dibromopyridine, oxidative addition at the 2-position yielded a dinuclear complex, which equilibrated with a mononuclear species, observing a clear pathway for o-coupling to dominate (figure 6.20).[56] The same intermediates would be anticipated in the cross-coupling of 2,5-dibromopyridine with boronic acids.

Figure 6.20 Cid's bimetallic species isolated from the reaction of 2,4-dibromopyridine and [Pd(PPh$_3$)$_4$][54].

Reactions catalysed by **6.1**-**6.4** were compared to a Pd(OAc)$_2$ and PPh$_3$ catalyst system. The cross-coupling reaction catalysed by Pd(OAc)$_2$ and PPh$_3$ was highly regioselective, with biaryl **a** being the major product (table 6.4). When using **6.1**-**6.4** as preformed catalysts, observed conversions were lower and there was no indication of regioselectivity. Considerable quantities of **b** were observed in the ^{1}H NMR spectra alongside traces of **c**. A palladium-free screen gave no conversion.

Table 6.4 Conversion and ratios of products observed for the Suzuki-Miyaura reaction between 2,5-dibromopyridine and 4-methoxybenzeneboronic acid.

Catalyst	Net Conversion (%)	TON	Ratio **a**:**b**:**c**
Pd(OAc)$_2$, PPh$_3$	83 ($\pm$3)	166	70:5:5
6.1 (CTV)	59 ($\pm$3)	118	31:23:7
6.2 (CTV)	51 ($\pm$2)	102	26:20:5
6.3	56 ($\pm$2)	112	29:18:6
6.4	46 ($\pm$2)	92	24:18:4

Conversions and ratios were interpreted by ^{1}H NMR spectroscopy compared to the OMe resonance of 1,4-dimethoxybenzene internal standard (3.78 ppm) and are the average of two runs. Methoxy groups of a, b and c all overlapped at ca. 3.85 ppm. The 6-pyridyl resonance (a, 8.68 ppm; b, 8.54 ppm; c, 8.87 ppm).[32]

Whilst the four NHC complexes all displayed poor levels of regioselectivity in this particular reaction, **6.1** and **6.2** were slightly more active when compared to **6.3** and **6.4** respectively. Net conversions were also greater than when screening the synthesis of 4-phenyltoluene. In a reverse manner to the previous Suzuki-Miyaura reactions, *N*-methyl complexes were more active than their *N*-benzyl counterparts. The fact that ratios of each product were similar in all four screens suggests encapsulation of a guest substrate is not influential in this example. Much greater activity at the 5-position was observed when compared to the control reaction, which was unexpected considering this position is less favourable. Electronic factors including the presence of directing groups can influence regioselective transformations, however, the bulky NHC wingtips of **6.1**-**6.4** may hinder intermediates similar to Cid's from forming, propagating the less favourable cross-coupling reaction at the 5-position. A similar stoichiometric study was carried

out with complex **6.1** and 2,4-dibromopyridine in the presence of excess Cs_2CO_3, but only the precatalyst and 2,4-dibromopyridine were observed. It is worth noting that Cid used a Pd(0) precursor, whereas **6.1** would require reducing prior to the oxidative addition of 2,4-dibromopyridine. PEPPSI™ complexes are known to be reduced by an excess of boronic acid prior to catalysis, which could initiate a catalytic cycle so was not attempted.[57]

The aryl halide substrate was changed to 2,4-dibromopyridine, which bears two electronically similar bromide substituents. A handful of regioselective transformations of 2,4-dibromopyridine have been documented, with most Pd-catalysed examples favouring *o*-substitution of the pyridyl ring.[52, 33, 50] Very few examples of preferential *p*-coupling when using 2,4-dibromopyridine have been reported. Rao and co-workers reported Suzuki-Miyaura reactions between 2,4-dibromopyridine and triarylbismuth reagents, whereby *p*-substitution was favoured in a 5:1 ratio, with significant *bis*-substituted product also forming.[32] Regioselectivity at the 4-position has otherwise been achieved employing 2-bromo-4-iodopyridine.[49, 58] If **6.1**-**6.4** did display a lower affinity towards *o*-substitution as postulated for the cross-coupling of 2,5-dibromopyridine with 4-methoxyphenylboronic acid, the strongly *ortho-para* directing pyridine may afford an additional driving force for reactivity at the 4-position of 2,4-dibromopyridine, which could well direct regioselectivity at this site.
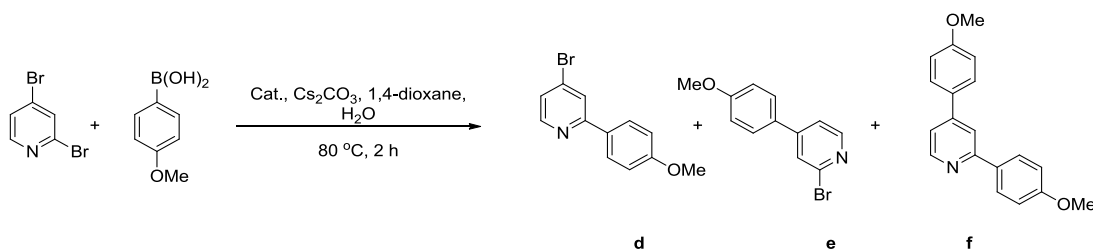
Scheme 6.9 Suzuki-Miyaura reaction between 2,4-dibromopyridine and 4-methoxybenzeneboronic acid and potential products.

Table 6.5 Conversions and product ratios obtained for the Suzuki-Miyaura reaction between 2,4-dibromopyridine and 4-methoxybenzeneboronic acid (1.2 eq.) catalysed by 6.1-6.4

Catalyst	0.25 mol% Pd			0.5 mol% Pd		
	Net conversion (%)	TON	Ratio **d:e:f**	Net conversion (%)	TON	Ratio **d:e:f**
Pd(OAc)₂, PPh₃	N/A		N/A	79 (±4)	158	25:33:21
6.1 (CTV)	44 (±1)	176	2:19:23	68 (±3)	136	3:32:33
6.2 (CTV)	41 (±3)	164	2:17:22	59 (±4)	118	4:27:29
6.3	39 (±1)	156	2:16:21	58 (±2)	116	3:27:28
6.4	46 (±1)	184	3:20:24	53 (±2)	106	4:26:24

Conversions are monitored by ^{1}H NMR spectroscopy relative to 1,4-dimethoxybenzene as an internal standard and are the average of two runs. The 6-pyridyl resonances (d, 8.43 ppm; e, 8.35 ppm; f, 8.67 ppm)[56] were compared to the methoxy resonance of 1,4-dimethoxybenzene.

As predicted, complexes **6.1**-**6.4** all displayed a preference towards **e** and **f** (scheme 6.9 and table 6.5), with trace quantities of 2-(4-methoxyphenyl)pyridine, **d**, being observed. The fact that all four complexes are displaying the preference towards **e** and **f** eliminates cooperative effects between Pd sites on **6.1** and **6.2**. The CTV cavitand is merely behaving as a bulky ligand, which happens to tether three independent catalytically active metal centres to the same scaffold. After reducing the loading to 0.25 mol% Pd, conversions did diminish to 40-50%, and all catalysts were similarly active. The reaction was compared to the control reaction using Pd(OAc)₂ and PPh₃ as precatalyst components, which gave a total conversion higher than complex **6.1**, although no regioselectivity was observed. A Pd-free screen gave no conversion. At lower catalyst loading, a slightly higher quantity of triaryl **c** was observed in all cases, compared to a marginally greater ratio of **e** at 0.5 mol% Pd. In all cases, TONs and hence TOFs were higher at lower catalyst loading, suggesting a homeopathic effect. All reactions remained pale yellow in colour, with no blackening to suggest Pd(0) formation.

Both **e** and **f** were detected in similar quantities, which led to reactions being profiled in order to determine the ordering of cross-coupling reactions. This could be *via* pathways including *o*-substituted **d** being formed first before being digested to yield **f**, or **e** simply dominating, followed by the subsequent *o*-coupling, yielding **f**. Interestingly, catalytic transformations occurred on a very fast timescale, with a screen involving **6.1** already reaching a total 32% conversion after 120 s, with a 1:12:19 ratio of **d**:**e**:**f**. After 20 mins, the conversions reach a level of 95% of the final screen, with ratios of products being similar to those observed after 2 h, suggesting a slow cessation of catalysis. The fast turnovers after 120 s at 80 °C led to the order of coupling being unclear, and whilst a higher ratio of **c** was present at this moment, the trace of **a** observed shed no light on reaction chronology. One method employed was to reduce the temperature to 50 °C to decelerate reactivity, to hopefully shed light on the coupling order (figures 6.21 and 6.22).
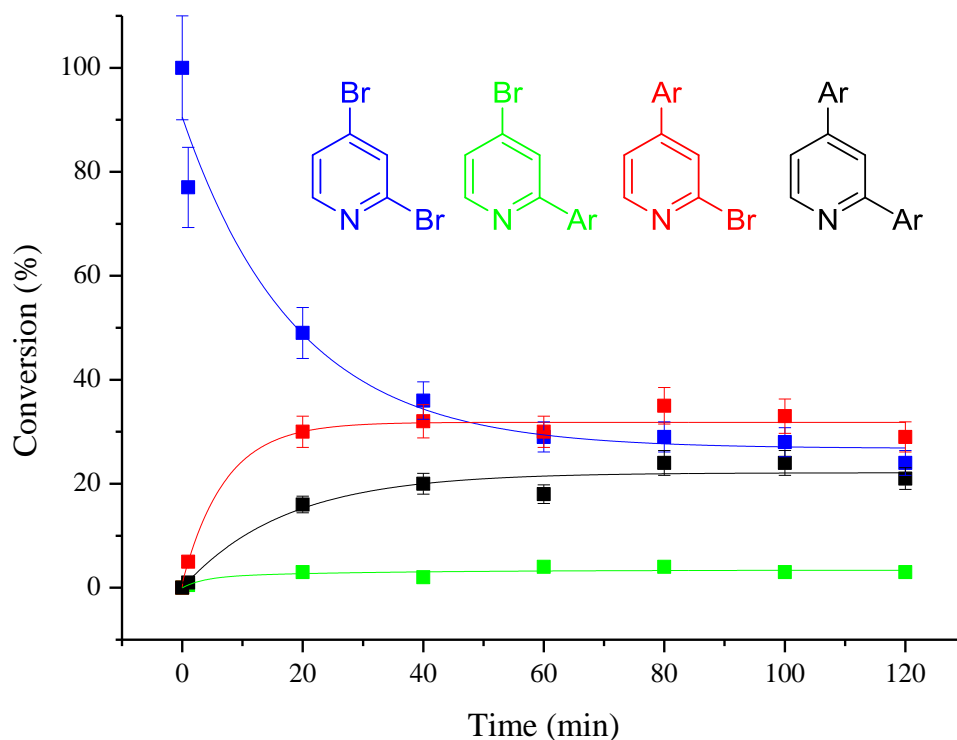
Figure 6.21 Profile of the Suzuki-Miyaura reaction between 2,4-dibromopyridine and 4-methoxyphenylboronic acid catalysed by complex 6.1. 2,4-Dibromopyridine (blue trace), product d, 2-aryl (green), product e, 4-aryl(red), product f, *bis*-aryl (black).
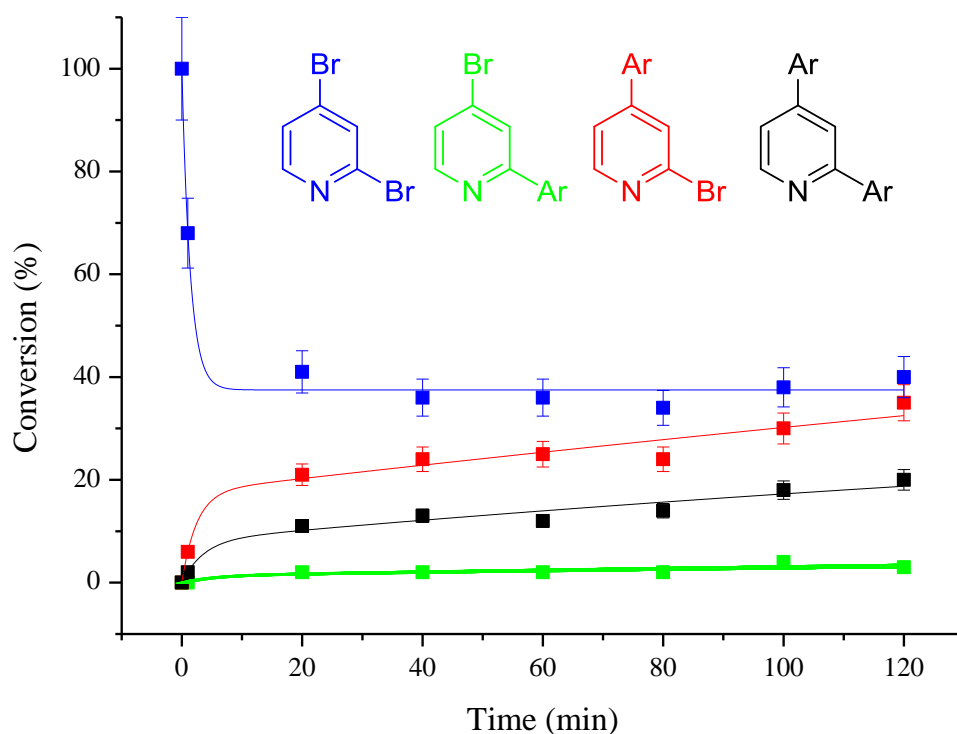
Figure 6.22 Profile of the Suzuki-Miyaura reaction between 2,4-dibromopyridine and 4-methoxyphenylboronic acid catalysed by 6.3. 2,4-Dibromopyridine (blue trace), product d, 2-aryl (green), product e, 4-aryl (red), product f, *bis*-aryl (black).

Complexes **6.1** and **6.3** were selected, with aliquots taken every twenty minutes up to 2 h, and an additional aliquot taken after 60 s. Both **6.1** and **6.3** displayed similar behaviours throughout the 2 h reactions, with **6.1** faring slightly better. An initial spike in catalysis was observed at 50 ºC, albeit considerably lower than after 2 mins at 80 ºC, before a smoothing of gradients. The net conversion after 2 h when employing **6.1** was also ca. 20% lower at 50 ºC than at 80 ºC. Most reactivity in the formation of products **e** (2-bromo-4-(*p*-methoxyphenyl)pyridine) and **f** occurs within the first 20 mins, with a gradual increase until cessation of the reaction. The formation of **e** and **f** appeared at a similar rate (figures 6.21 and 6.22), whereas product **d** was observed at a low, relatively constant level throughout the reaction, indicating the syntheses of **e** and **f** may be of similar favourabilities.

Goldup and Larrosa found that PEPPSI™ complexes catalyse the polyfunctionalisation of polyhaloarenes in the Negishi, Kumada, and to a lesser extent Suzuki-Miyaura coupling reaction with high selectivities.[20] The authors suggested that alongside the 'normal' activation-controlled Pd(0) active catalyst, a

second species of Pd(0) catalyses the polyfunctionalisation of polyhaloarenes exhaustively substituting the polyhaloarene through diffusion controlled oxidative addition within a solvent cage. When monitoring the Suzuki-Miyaura reaction between 2,4-dibromopyridine and 1.2 eq. of 4-methoxybenzeneboronic acid catalysed by **6.1**-**6.4**, concentrations of both **e** and **f** remained relatively constant with respect to one another, which in this case could imply both an 'activation' pathway to prepare **e** and 'diffusion-controlled' pathway forming **f** were occurring at similar rates. The significantly high quantities of **f** detected early in catalytic examinations may also be evidence of exhaustive substitution occurring during this particular reaction.

6.5 Conclusions and future work

Four complexes have been prepared, structurally authenticated and assessed as catalysts in two Suzuki-Miyaura reactions. Lower activities than anticipated were observed for the coupling of 4-bromotoluene and phenylboronic acid, but a positive mercury drop test in all cases indicates that both homogeneous and heterogeneous catalysis are occurring. The CTG complexes fared better than monomers at low loadings, displaying a homeopathic Pd effect. Benzyl-NHC complexes proved superior to the methyl analogues, and in terms of turnover numbers, the trimetallic complexes outperformed the monometallic counterparts. A second Suzuki-Miyaura reaction was carried out between 2,5-dibromopyridine and 4-methoxyphenylboronic acid. Higher turnovers and conversions were observed, but the desired regioselectivity for trimetallic complexes was not observed, with a highly elevated proportion of the less-favoured 5-substituted product being present. Unusual regioselectivity towards 4-substitution in the Suzuki-Miyaura reaction of 2,4-dibromopyridine and 4-methoxyphenylboronic acid was observed, implying the anticipated *o*-substitution on the pyridyl ring was unfavourable. Complexes **6.1**-**6.4** displayed similar activities in all reactions tested, and therefore the behaviours of monometallic vs trimetallic complexes cannot be described as dichotomous. This aligns with Matt's studies using flexible calix[4]arene-NHC complexes, who described a similar effect where the bulk of the cavitand did not influence activity of catalysts in the same manner as the analogous phosphine complexes.[37, 39]

The substrate scope for regioselective transformations could also be expanded to the quinoline family. Furthermore, alternative cross-coupling reactions could be pursued.

Future work in this section could focus on expanding the Pd(II)-NHC complexes on a CTV scaffold by investigating the effect of altering the *trans*-ligand. Complexes in this chapter only focus on the *trans*-3-chloropyridyl series. Altering the ligand could lead to subtle changes in catalytic behaviours, for example, Navarro and co-workers have prepared *trans*-triethylamine Pd(II) complexes which are active catalysts in room-temperature Buchwald-Hartwig aminations.[59, 60] Furthermore, ditopic ligands such as DABCO and pyrazine,[61] in addition to tritopic derivatives,[62] are attracting attention as the transoid ligand of Pd(II) *mono*-NHC complexes. Employment of such ligands in the place of 3-chloropyridine could lead to the assembly of $[M_6L_2]$ or higher-order cages with linkers between metal centres, which could both be catalytically active, and provide an approach to preparing more soluble metallo-supramolecular assemblies based on the CTV scaffold.

6.6 Experimental section

Unless stated in the experimental section, chemicals were bought from commercial suppliers and used without further purification. Unless stated, all reactions were carried out under aerobic conditions. Reactions performed under an atmosphere of dry nitrogen were carried out using standard Schlenk and Glovebox procedures, with solvents dried and degassed using the same methodology described in Section 2.9. All analytical techniques are also consistent with those described in Section 2.9.

Synthesis of *tris*(3-chloropyridyl) hexaiodo 3,3',3''-(((3,8,13-trimethoxy-10,15-dihydro-5H-tribenzo[a,d,g][9]annulene-2,7,12-triyl)tris(oxy))tris(methylene))tris(1-methylbenzimidazol-2-ylidene)tripalladium(II), 6.1

Palladium(II) iodide (100 mg, 0.28 mmol), potassium carbonate (192 mg, 1.40 mmol) and **4.3** (113 mg, 0.09 mmol) were dissolved in 3-chloropyridine (3 mL) and the reaction mixture degassed. The orange suspension was stirred at 80 ºC under an N_2 atmosphere for 24 h. Water (10 mL) and DCM (10 mL) were added. The organic layer was separated, and washed with water (3 x 5 mL) before being dried over

MgSO$_4$. Solvents were removed *in vacuo*, and the residue triturated in pentane (5 mL). The resulting solid was filtered, affording **6.1** as an orange solid. Yield 171 mg, 0.08 mmol, 84%. HRMS (ESI$^+$) 1794.5960 Calcd. for {M-(I)-3(3-Clpy):C$_{51}$H$_{48}$I$_5$N$_6$O$_6$Pd$_3$}$^+$
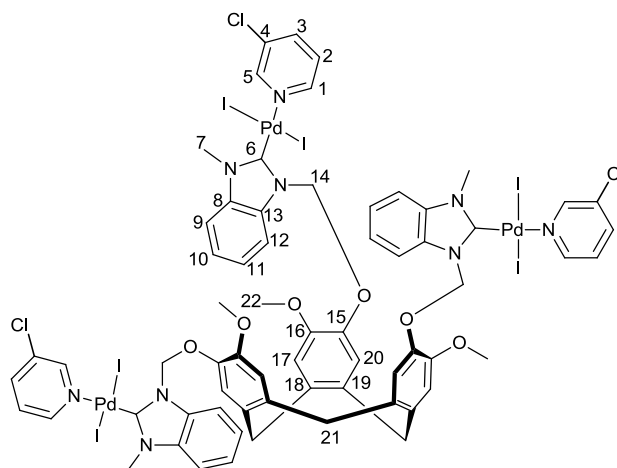
1794.5962; ^{1}H NMR (300 MHz, CDCl$_3$) δ (ppm) 9.05 (d, 3H, *J* = 2.2 Hz, H^1), 8.95 (dd, 3H, *J* = 5.4, 1.1 Hz, H^3), 7.77-7.72 (m, 3H, H^2), 7.34-7.27 (m, 6H, H^5, H^9), 7.20 (s, 3H, H^{17}), 7.10 (t, 3H, *J* = 7.7 Hz, H^{10}), 6.98 (d, 3H, *J* = 8.2 Hz, H^{12}), 6.79 (s, 3H, H^{20}), 6.73 (t, 3H, *J* = 7.8 Hz, H^{11}), 6.61 (d, 3H, *J* = 10.2 Hz, H^{14}), 6.40 (d, 3H, *J* = 10.2 Hz, H^{14}), 4.44 (d, 3H, *J* = 13.8 Hz, *endo*-H^{21}), 4.23 (s, 9H, H^7), 3.83 (s, 9H, H^{22}), 3.41 (d, 3H, *J* = 13.8 Hz, *exo*-H^{21}); ^{13}C{^{1}H} NMR (75 MHz, CDCl$_3$) δ (ppm) 161.69 (C^6), 152.88 (C^1), 151.92 (C^{13}), 149.97 (C^{16}), 143.99 (C^{15}), 138.10 (C^2), 136.55 (C^{18}), 134.96 (C^8), 134.68 (C^{13}), 132.54 (C^4), 132.07 (C^{19}), 125.04 (C^5), 123.54 (C^{10}), 123.41 (C^{11}), 123.36 (C^{17}), 114.19 (C^{20}), 111.15 (C^{12}), 109.78 (C^9), 79.20 (C^{14}), 57.07 (C^{22}), 36.36 (C^7), 35.76 (C^{21}); FTIR ν (cm^{-1}) 1506, 1461, 1264, 743; m.p 165-167 °C (dec.); Elemental analysis for C$_{66}$H$_{60}$Cl$_3$I$_6$N$_9$O$_6$Pd$_3$ Calcd.: C 35.04, H 2.67, N 5.57; Found C 35.15, H 2.80, N 5.30.

Synthesis of tris(3-chloropyridyl) hexaiodo 3,3',3''-(((3,8,13-trimethoxy-10,15-dihydro-5H-tribenzo[a,d,g][9]annulene-2,7,12-triyl)tris(oxy))tris(methylene))tris(1-benzylbenzimidazol-2-ylidene)tripalladium(II), 6.2

Palladium(II) iodide (41 mg, 0.11 mmol), potassium carbonate (79 mg, 0.57 mmol), potassium iodide (95 mg, 0.57 mmol) and **4.5** (50 mg, 0.04 mmol) were dissolved in 3-chloropyridine (3 mL) and the reaction mixture degassed. The orange suspension was stirred at 80 °C under an N$_2$ atmosphere for 24 h. Water (10 mL) and DCM (10 mL) were added. The organic layer was separated, and washed with water (3 x 5 mL) before being dried over MgSO$_4$. Solvents were removed *in vacuo*, and the residue triturated in pentane (5 mL). The resulting solid was filtered, affording **6.2** as

a yellow-orange solid. Yield 70 mg, 0.028 mmol, 70%. HRMS (ESI$^+$) 2022.6935 Calcd. for {M-(I)-3(3-Clpy):$C_{69}H_{60}I_5N_6O_6Pd_3$}$^+$; ^{1}H NMR (300 MHz, CDCl$_3$) δ (ppm) 9.01, (d, 3H, J = 2.3 Hz H^5), 8.89 (dd, 3H, J = 5.5, 1.4 Hz, H^1), 7.70 (tdd, 3H, J = 8.5, 2.4, 1.3 Hz, H^3), 7.63 − 7.57 (m, 6H, H^9), 7.42 − 7.28 (m, 18H, H^2, H^{10}, H^{11}, H^{13}, H^{21}), 7.21 (d, 6H, J = 8.2 Hz, H14), 6.94 (d, 3H, J = 6.3 Hz H^{15}), 6.91 (s, 3H, H^{24}), 6.84 (ddd, 3H, J = 8.3, 6.1, 2.3 Hz, H^{16}), 6.67 (d, 3H, J = 10.0 Hz, H^{18}), 6.52 (d, 3H, J = 9.9 Hz, H^{18}), 6.19 (d, 3H, J = 15.7 Hz, H^7), 5.94 (d, 3H, J = 15.8 Hz, H^7) 4.53 (d, 3H J = 13.8 Hz, endo-H^{26}), 3.84 (s, 9H, H^{25}), 3.49 (d, 3H, J = 13.5 Hz, exo-H^{26}); ^{13}C{^{1}H} NMR (75 MHz, CDCl$_3$) δ (ppm) 162.69 (C^6), 152.90 (C^5), 151.94 (C^1), 150.17 (C^{20}), 144.07 (C^{19}), 138.06 (C^3), 136.60 (C^{22}), 135.24 (C^{17}), 134.47 (C^{12}), 134.41 (C^8), 132.52 (C^4), 132.15 (C^{23}), 129.00 (C^{10}, C^{11}), 128.49 (C^9), 125.01 (C^2), 124.47 (C^{13}), 123.51 (C^{16}, C^{21}), 114.45 (C^{24}), 111.50 (C^{15}), 111.46 (C^{14}), 79.64 (C^{18}), 57.12 (C^{25}), 54.90 (C^7), 35.97 (C^{26}); FTIR ν (cm^{-1}) 1414, 1356, 1266, 1028, 742; Elemental analysis for $C_{84}H_{72}Cl_3I_6N_9O_6Pd_3$ Calcd.: C 40.51, H 2.91, N 5.06; Found C 40.55, H 2.86, N 5.04.
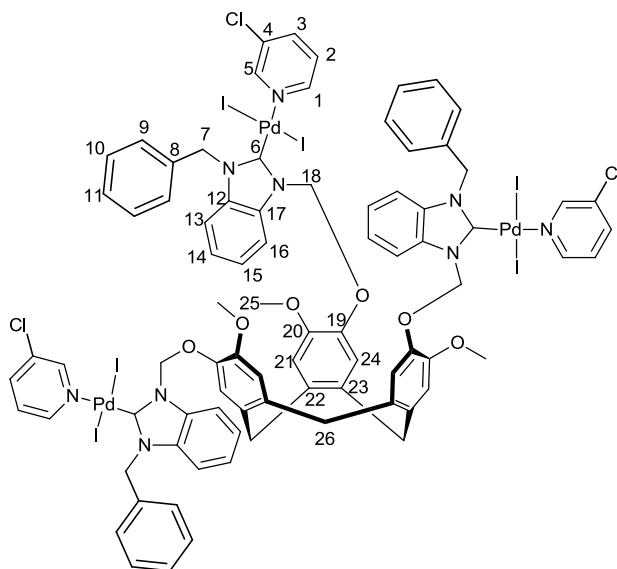
Synthesis of 3-chloropyridyl diiodo (1-methyl-3-((2-methoxyphenoxy)methyl)benzimidazol-2-ylidene)palladium(II), 6.3

Ligand **4.8** (40 mg, 0.12 mmol), palladium(II) iodide (44 mg, 0.12 mmol) and potassium carbonate (85 mg, 0.6 mmol) were dissolved in anhydrous, degassed 3-chloropyridine (2 mL). The reaction mixture was heated to 80 ℃ under an N$_2$ atmosphere for 24 h and turned dark brown. Water (20 mL) was added and the product was extracted into dichloromethane (3 x 20 mL), and the solvents separated. The organic layer was washed with water (3 x 20 mL), and organic solvents dried over MgSO$_4$, and then removed *in vacuo*. The orange residue was triturated in
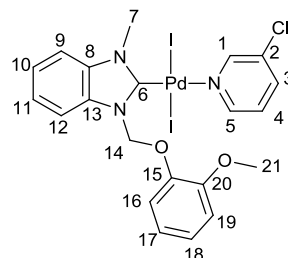
hexane, and the resultant orange solid filtered. The title compound was isolated as an orange solid. Yield 44.3 mg, 0.05 mmol, 50%. HRMS (ESI$^+$) 500.9284, 1130.7631, Calcd. for {M-(I)-(3Clpy): $C_{16}H_{16}IN_2O_2Pd$}$^+$ 500.9286, {2M-(I)-2(3Clpy): $C_{32}H_{32}I_3N_4O_4Pd_2$}$^+$ 1130.7626; ^{1}H NMR (300 MHz, CDCl$_3$) δ (ppm) 9.07 (d, 1H, J = 2.3 Hz, H^1), 8.97 (dd, 1H, J = 5.4, 1.4 Hz, H^5), 7.76 (dt, 1H, J = 8.2, 1.8 Hz, H^3), 7.64-7.54 (m, 1H, H^9), 7.41-7.19 (m, 5H, H^4, H^{10}, H^{11}, H^{12}, H^{19}), 7.07 (td, 1H, J = 7.8, 1.7 Hz, H^{17}), 6.97 (dd, 1H, J = 8.2, 1.6 Hz, H^{16}), 6.82 (td, 1H, J = 7.6, 1.6 Hz, H^{18}), 6.65 (s, 2H, H^{14}), 4.20 (s, 3H, H^7), 3.96 (s, 3H, H^{21}); ^{13}C{^{1}H} NMR (126 MHz, CDCl$_3$) δ (ppm) 161.36 (C^6), 152.72 (C^1), 151.72 (C^5), 151.29 (C^{20}), 145.11 (C^{15}), 137.76 (C^3), 135.28 (C^8), 134.52 (C^{13}), 132.32 (C^2), 124.83 (C^4), 124.77 (C^{17}), 124.69 (C^{11}), 123.43 (C^{10}), 121.40 (C^{19}), 121.18 (C^{18}), 112.69 (C^{16}), 111.70 (C^9), 109.75 (C^{12}), 79.38 (C^{14}), 55.88 (C^{21}), 36.21 (C^7); FTIR ν (cm^{-1}) 2160, 1497, 1413, 1258, 742; m.p. 145ºC (dec.); Elemental analysis for $C_{21}H_{20}ClI_2N_3O_2Pd$ Calcd.: C 33.99, H 2.72, N 5.66; Found C 33.87, H 2.64, N 5.62.

Synthesis of 3-chloropyridyl diiodo (1-methyl-3-((2-methoxyphenoxy)methyl)benzimidazol-2-ylidene)palladium(II), 6.4

Ligand **4.9** (40 mg, 0.09 mmol), palladium(II) iodide (34 mg, 0.09 mmol), potassium iodide (78 mg, 0.47 mmol) and potassium carbonate (65 mg, 0.47 mmol) were dissolved in anhydrous, degassed 3-chloropyridine (2 mL). The reaction mixture was stirred at 80 ºC under an N$_2$ atmosphere for 24 h. Water (20 mL) was added and the product was extracted
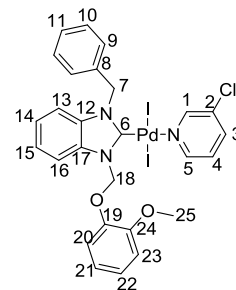
into dichloromethane (3 x 20 mL), and the solvents separated. The organic layer was washed with water (3 x 20 mL), and organic solvents dried over MgSO$_4$, and then removed *in vacuo*. The orange residue was triturated in hexane, and the resultant orange solid filtered. The title compound was isolated as an orange solid. Yield 42 mg, 0.05 mmol, 57%. HRMS (ESI$^+$) 449.0471, 576.9599, 742.8273, Calcd. for {M-2(I)-H-(3Clpy)}: 449.0476, {M-(I)-(3Clpy): $C_{22}H_{20}IN_2O_2Pd$}$^+$ 576.9599 {M+K-(3Clpy): $C_{22}H_{20}I_2KN_2O_2Pd$}$^+$ 742.8281; ^{1}H NMR (300 MHz, CDCl$_3$) δ (ppm) 9.02 (d, 1H, J = 2.3 Hz, H^1), 8.92 (dd, 1H, J = 5.5, 1.3 Hz, H^5), 7.73 (ddd, 1H, J = 8.2, 2.4, 1.3 Hz, H^3), 7.63 (d, 1H, J = 8.1 Hz, H^{13}), 7.56 (dd, 2H J = 7.5, 2.0 Hz, H^{10}), 7.42 – 7.27 (m, 5H, H^4, H^9, H^{11}, H^{23}), 7.20 (td, 1H, J = 8.3, 7.8, 1.2 Hz, H^{15}), 7.14 – 7.04 (m, 2H, H^{14}, H^{22}), 6.99 (dd, 1H, J = 8.2, 1.6 Hz, H^{20}) 6.94 (d, 1H, J = 8.9 Hz,

H^{16}), 6.87 (td, 1H, J = 7.7, 1.6 Hz, H^{21}), 6.72 (s, 2H, H^{18}), 6.03 (s, 2H, H^7), 3.96 (s, 3H, H^{25}); ^{13}C{^{1}H} NMR (75 MHz, CDCl$_3$) δ (ppm) 162.57 (C^6), 152.95 (C^1), 151.96 (C^5), 151.54 (C^{24}), 145.39 (C^{19}), 137.98 (C^3), 135.26 (C^{17}), 134.86 (C^{12}), 134.42 (C^8), 132.51 (C^2), 128.98 (C^9), 128.42 (C^{10}), 128.39 (C^{11}), 125.07 (C^{22}), 124.90 (C^4), 123.69 (C^{14}), 123.60 (C^{15}), 121.55 (C^{23}), 121.46 (C^{21}), 112.92 (C^{20}), 112.05 (C^{13}), 111.72 (C^{16}), 79.99 (C^{18}), 56.13 (C^{25}), 55.01 (C^7); FTIR ν (cm^{-1}) 1504, 1252, 1212, 1026, 745; Elemental analysis for C$_{27}$H$_{24}$ClI$_2$N$_3$O$_2$Pd Calcd. C 39.64, H 2.96, N 5.14; Found C 39.55, H 2.89, N 5.07.

General catalytic procedure

Aryl bromide (1 mmol), boronic acid (1.2 mmol), caesium carbonate (625 mg, 2 mmol), catalyst (0.25-1 mol% Pd)and 1,4-dimethoxybenzene (69.1 mg, 0.5 mmol) were added to a Schlenk flask or carousel tube and dried *in vacuo* for 10 mins. 1,4-Dioxane (2.5 mL) and degassed water (2.5 mL) were added, and the reaction heated to 80 ºC for 2 h. An aliquot of the reaction mixture (0.1 mL) was added to CDCl$_3$ (0.4 mL) and the conversion obtained by ^{1}H NMR spectroscopy.

6.7 Supplementary crystallographic information

Crystals were mounted under inert oil on a MiTeGen tip and flash frozen using an OxfordCryosystems low temperature device. X-ray diffraction data were collected using CuKα radiation (λ = 1.54184 Å) or MoKα (λ = 0.71073 Å) using an Agilent Supernova dual-source diffractometer with Atlas S2 CCD detector and fine-focus sealed tube generator, or using synchrotron radiation (λ = 0.6889 Å) at Beamline I19 at the Diamond light source. Data were corrected for Lorenztian and polarization effects and absorption corrections were applied using multi-scan methods. The structures were solved by direct methods using SHELXS-97 and refined by full-matrix on F^2 using SHELXL-97.[47] Unless otherwise specified, all non-hydrogen atoms were refined as anisotropic, and hydrogen positions were included at geometrically estimated positions.

6.7.1 Additional crystallographic details

6.1·(CH$_2$Cl$_2$)$_{0.5}$·(C$_5$H$_{14}$)$_2$·H$_2$O$_2$

Crystal data were of poor quality because crystals rapidly decomposed upon contact with air. One 3-chloropyridyl group was disordered over two positions of 0.75 and 0.25 occupancies, the lower occupancy position was refined as isotropic. All solvent molecules were refined as isotropic and hydrogen positions of the water molecule omitted. One pentane solvent molecule was disordered over two positions.

(6.1)$_2$·7.5(C$_4$H$_8$O$_2$)

One 3-chloropyridine ligand was disordered over two positions, each of 0.5 occupancy and C-Cl bonds restrained to be chemically reasonable. The AFIX command of SHELX was applied to restrain both disordered pyridine rings. 4.5 dioxane molecules were refined as isotropic, bond lengths and angles were restrained to be chemically reasonable. Rigid restraints were applied to both **6.1** molecules using the RIGU command of SHELX. The largest peak was a Fourier ripple 0.95 Å from I3.

(6.4)$_2$

The largest residual electron density was 0.95 Å from I2 and is likely a Fourier ripple.

Table 6.6 Table of crystallographic data. a = Cuκα radiation, c = synchrotron radiation

Compound	6.1·(CH₂Cl₂)₀.₅·(C₅H₁₄)₂·H₂O₂[a]	(6.1)₂·6(C₄H₈O₂)[a]	6.3[c]	(6.4)₂[c]
Formula	$C_{153}H_{170}Cl_8I_{12}N_{18}O_{17}Pd_6$	$C_{313}H_{334}Cl_{12}I_{24}N_{36}O_{48}Pd_{12}$	$C_{21}H_{20}ClI_2N_3O_2Pd$	$C_{54}H_{48}Cl_2I_4N_6O_4Pd_2$
Mr	4929.86	5006.91	742.05	1636.28
Crystal size	0.06 x 0.08 x 0.11	0.07 x 0.06 x 0.05	0.05 x 0.02 x 0.02	0.09 x 0.01 x 0.01
Crystal system	Triclinic	Triclinic	Monoclinic	Monoclinic
Space group	$P\bar{1}$	$P\bar{1}$	$P2_1/c$	$P2_1/n$
a (Å)	15.6946(6)	18.4409(5)	13.617	11.02430(10)
b (Å)	15.8484(8)	21.9443(8)	10.995	14.5623(2)
c (Å)	21.6110(10)	23.7505(8)	15.82040(10)	35.8034(5)
α (⁰)	104.839(4)	99.360(3)	90	90
β (⁰)	111.072(4)	97.234(3)	93.46	98.4410(10)
γ (⁰)	98.298(3)	103.156(3)	90	90
V (Å³)	4679.2(4)	9100.5(5)	2364.260(15)	5685.58(12)
Z	2	2	4	4
ρ_{calc} (g.cm⁻³)	1.767	1.827	2.085	1.912
θ range (⁰)	3.115-54.242	3.116-74.228	1.452-29.998	1.115- 25.502
No. data collected	16063	71312	40488	74794
No. unique data	9748	34313	7553	11597
R_{int}	0.0356	0.0929	0.0391	0.0869
No. obs. Data ($I > 2\sigma(I)$)	7663	18012	7258	7865
No. parameters	934	1931	273	651
No. restraints	17	57	0	0
R_1 (obs data)	0.0533	0.0804	0.0181	0.0520
wR_2 (all data)	0.1506	0.2329	0.0444	0.1566
S	1.026	1.018	0.912	1.035
Max. shift/esd	0.001	0.001	0.002	0.002
Largest difference peak and hole/ (e Å³)	2.018, -1.120	2.824, -1.459	0.677, -0.481	1.952, -1.269

6.8 References

1.   T. Weskamp, V. P. W. Böhm, W. A. Herrmann, *J. Organomet. Chem.*, 1999, **585**, 348-352.

2.   J. J. Henkelis, C. J. Carruthers, S. E. Chambers, R. Clowes, A. I. Cooper, J. Fisher, M. J. Hardie, *J. Am. Chem. Soc.*, 2014, **136**, 14393-14396.

3.   D. Munz, A. Pöthig, A. Tronnier, T. Strassner, *Dalton Trans.*, 2013, **42**, 7297-7304.

4.   M. R. Chapman, B. R. M. Lake, C. M. Pask, B. N. Nguyen, C. E. Willans, *Dalton Trans.*, 2015, **44**, 15938-15948.

5.   T. Samanta, S. K. Seth, S. K. Chattopadhyay, P. Mitra, V. Kushwah, J. Dinda, *Inorg. Chim. Acta*, 2014, **411**, 165-171.

6.   C. J. O'Brien, E. A. B. Kantchev, C. Valente, N. Hadei, G. A. Chass, A. Lough, A. C. Hopkinson, M. G. Organ, *Chem. Eur. J.*, 2006, **12**, 4743-4748.

7.   M. G. Organ, S. Calimsiz, M. Sayah, K. H. Hoi, A. J. Lough, *Angew. Chem., Int. Ed.*, 2009, **48**, 2383-2387.

8.   S. Calimsiz, M. Sayah, D. Mallik, M. G. Organ, *Angew. Chem., Int. Ed.*, 2010, **49**, 2014-2017

9.   S. Calimsiz, M. G. Organ, *Chem. Commun.*, 2011, **47**, 5181-5183.

10.   E. C. Keske, O. V. Zenkina, R. Wang, C. M. Crudden, *Organometallics*, 2012, **31**, 6215-6221.

11.   M. Pompeo, R. D. J. Froese, N. Hadei, M. G. Organ, *Angew. Chem., Int. Ed.*, 2012, **51**, 11354-11357.

12.   C. Valente, S. Calimsiz, K. H. Hoi, D. Mallik, M. Sayah, M. G. Organ, *Angew. Chem., Int. Ed.*, 2012, **51**, 3314-3332.

13.   G. A. Price, A. R. Bogdan, A. L. Aguirre, T. Iwai, S. W. Djuric, M. G. Organ, *Catal. Sci. Technol.*, 2016, **6**, 4733-4742.

14.   K. H. Hoi, J. A. Coggan, M. G. Organ, *Chem. Eur. J.*, 2013, **19**, 843-845.

15.   C. Valente, M. Pompeo, M. Sayah, M. G. Organ, *Org. Process Res. Dev.*, 2014, **18**, 180-190.

16.   C. Lombardi, D. Mitchell, M. J. Rodriguez, M. G. Organ, *Eur. J. Org. Chem.*, 2017, **2017**, 1510-1513.

17.   C. Lombardi, J. Day, N. Chandrasoma, D. Mitchell, M. J. Rodriguez, J. L. Farmer, M. G. Organ, *Organometallics*, 2017, **36**, 251-254.

18.   J. L. Farmer, H. N. Hunter, M. G. Organ, *J. Am. Chem. Soc.*, 2012, **134**, 17470-17473.

19.   L. Benhamou, C. Besnard, E. P. Kündig, *Organometallics*, 2014, **33**, 260-266.

20.   I. Larrosa, C. Somoza, A. Banquy, S. M. Goldup, *Org. Lett.*, 2011, **13**, 146-149.

21.   G. A. Chass, C. J. O'Brien, N. Hadei, E. A. B. Kantchev, W.-H. Mu, D.-C. Fang, A. C. Hopkinson, I. G. Csizmadia, M. G. Organ, *Chem. Eur. J.*, 2009, **15**, 4281-4288.

22.   B. J. Groombridge, S. M. Goldup, I. Larrosa, *Chem. Commun.*, 2015, **51**, 3832-3834.

23.   H. V. Huynh, Y. Han, R. Jothibasu, J. A. Yang, *Organometallics*, 2009, **28**, 5395-5404.

24.   J. C. Lewis, J. Wu, R. G. Bergman, J. A. Ellman, *Organometallics*, 2005, **24**, 5737-5746.

25.   R. F. Heck, J. P. Nolley, *J. Org. Chem.*, 1972, **37**, 2320-2322.

26.	K. Sonogashira, Y. Tohda, N. Hagihara, *Tetrahedron Lett.*, 1975, **16**, 4467-4470.

27.	S. Baba, E. Negishi, *J. Am. Chem. Soc.*, 1976, **98**, 6729-6731.

28.	K. Tamao, K. Sumitani, M. Kumada, *J. Am. Chem. Soc.*, 1972, **94**, 4374-4376.

29.	R. J. P. Corriu, J. P. Masse, *J. Chem. Soc., Chem. Commun.*, 1972, 144a-144a.

30.	The Nobel Prize in Chemistry **2010**,
	https://www.nobelprize.org/nobel_prizes/chemistry/laureates/2010/.

31.	N. Miyaura, K. Yamada, A. Suzuki, *Tetrahedron Lett.*, 1979, **20**, 3437-3440.

32.	M. L. N. Rao, R. J. Dhanorkar, *Eur. J. Org. Chem.*, 2014, **2014**, 5214-5228.

33.	M. L. N. Rao, R. J. Dhanorkar, *Tetrahedron*, 2015, **71**, 338-349.

34.	M. L. N. Rao, J. B. Talode, *Asian J. Org. Chem.*, 2016, **5**, 98-106.

35.	C. F. R. A. C. Lima, A. S. M. C. Rodrigues, V. L. M. Silva, A. M. S. Silva, L. M. N. B. F. Santos, *ChemCatChem*, 2014, **6**, 1291-1302.

36.	A. H. M. de Vries, J. M. C. A. Mulders, J. H. M. Mommers, H. J. W. Henderickx, J. G. de Vries, *Org. Lett.*, 2003, **5**, 3285-3288.

37.	E. Brenner, D. Matt, M. Henrion, M. Teci, L. Toupet, *Dalton Trans.*, 2011, **40**, 9889-9898.

38.	H. El Moll, D. Semeril, D. Matt, L. Toupet, J.-J. Harrowfield, *Org. Biomol. Chem.*, 2012, **10**, 372-382.

39.	L. Monnereau, D. Sémeril, D. Matt, L. Toupet, *Chem. Eur. J.*, 2010, **16**, 9237-9247.

40.	E. Peris, *Chem. Commun.*, 2016, **52**, 5777-5787.

41.	S. Gonell, M. Poyatos, E. Peris, *Angew. Chem. Int. Ed.*, 2013, **52**, 7009-7013.

42.	S. Gonell, R. G. Alabau, M. Poyatos, E. Peris, *Chem.l Commun.*, 2013, **49**, 7126-7128.

43.	M. G. Organ, M. Abdel-Hadi, S. Avola, I. Dubovyk, N. Hadei, E. A. B. Kantchev, C. J. O'Brien, M. Sayah, C. Valente, *Chem. Eur. J.*, 2008, **14**, 2443-2452.

44.	J. P. Wolfe, S. Wagaw, S. L. Buchwald, *J. Am. Chem. Soc.*, 1996, **118**, 7215-7216.

45.	M. S. Driver, J. F. Hartwig, *J. Am. Chem. Soc.*, 1996, **118**, 7217-7218.

46.	P. G. Alsabeh, M. Stradiotto, *Angew. Chem. Int. Ed.*, 2013, **28**, 7242-7246

47.	G. M. Whitesides, M. Hackett, R. L. Brainard, J. P. P. M. Lavalleye, A. F. Sowinski, A. N. Izumi, S. S. Moore, D. W. Brown, E. M. Staudt, *Organometallics*, 1985, **4**, 1819-1830.

48.	M. N. Nadagouda, R. S. Varma, *Green. Chem.*, 2008, **10**, 859-862.

49.	G. Burzicki, A. S. Voisin-Chiret, J. S.-d. Oliveira Santos, S. Rault, *Tetrahedron*, 2009, **65**, 5413-5417.

50.	Q. Zhou, B. Zhang, L. Su, T. Jiang, R. Chen, T. Du, Y. Ye, J. Shen, G. Dai, D. Han, H. Jiang, *Tetrahedron*, 2013, **69**, 10996-11003.

51.	J. W. Tilley, S. Zawoiski, *J. Org. Chem.*, 1988, **53**, 386-390.

52.	B. Zhang, R. Chen, H. Jiang, Q. Zhou, F. Qiu, D. Han, R. Li, W. Tang, A. Zhong, J. Zhang, X. Yu, *Tetrahedron*, 2016, **72**, 2813-2817.

53.	P. F. H. Schwab, F. Fleischer, J. Michl, *J. Org. Chem.*, 2002, **67**, 443-449.

54.	S. T. Handy, T. Wilson, A. Muth, *J. Org. Chem.*, 2007, **72**, 8496-8500.

55.	M. Yoshizawa, M. Tamura, M. Fujita, *Science*, 2006, **312**, 251-254.

56.	C. Sicre, J. L. Alonso-Gómez, M. M. Cid, *Tetrahedron*, 2006, **62**, 11063-11072.

57. J. Nasielski, N. Hadei, G. Achonduh, E. A. B. Kantchev, C. J. O'Brien, A. Lough, M. G. Organ, *Chem. Eur. J.*, 2010, **16**, 10844-10853.

58. J. Ji, T. Li, W. H. Bunnelle, *Org. Lett.*, 2003, **5**, 4611-4614.

59. D. Guest, M.-T. Chen, G. J. Tizzard, S. J. Coles, M. L. Turner, O. Navarro, *Eur. J. Inorg. Chem.*, 2014, **2014**, 2200-2203.

60. I. Maluenda, M.-T. Chen, D. Guest, S. Mark Roe, M. L. Turner, O. Navarro, *Catal. Sci. Technol.*, 2015, **5**, 1447-1451.

61. J. Yang, L. Wang, *Dalton Trans.*, 2012, **41**, 12031-12037.

62. T. Wang, L. Liu, K. Xu, H. Xie, H. Shen, W.-X. Zhao, *RSC Adv.*, 2016, **6**, 100690-100695.